CO_2 Capture by Aqueous Absorption
Summary of 2nd Quarterly Progress Reports 2010

by Gary T. Rochelle

Supported by the Luminant Carbon Management Program

and the

Industrial Associates Program for CO_2 Capture by Aqueous Absorption

Department of Chemical Engineering

The University of Texas at Austin

July 31, 2010

Introduction

This research program is focused on the technical obstacles to the deployment of CO_2 capture and sequestration from flue gas by alkanolamine absorption/stripping and on integrating the design of the capture process with the aquifer storage/enhanced oil recovery process. The objective is to develop and demonstrate evolutionary improvements to monoethanolamine (MEA) absorption/stripping for CO_2 capture from coal-fired flue gas. The Luminant Carbon Management Program and the Industrial Associates Program for CO_2 Capture by Aqueous Absorption support 17 graduate students. These students have prepared detailed quarterly progress reports for the period April 1, 2010 to June 30, 2010. Also included are papers presented by Fred Closmann and Gary Rochelle at the Clearwater Clean Coal Conference in Florida in June, a paper presented by Eric Chen at the conference in Talloires, France, and a dissertation proposal by Qing Xu.

Conclusions

Thermodynamics and Rates

In 2-methylpiperazine with 0.33 mol CO_2/mol alkalinity at 40 °C, the unhindered monocarbamate, 4-carboxyl-2-methylpiperazine, is six times more concentrated than the mildly hindered monocarbamate, 1-carboxyl-2-methylpiperazine. The amount of dicarbamate is 3% of the original amine and very little bicarbonate was found in this loaded solution.

At CO_2 partial pressure of 0.1 kPa, 8 m 1,2-diamino-propane (MEDA) has an absorption rate about half that of 8 m PZ, but twice as great as that of 7 m MEA and 12 m EDA. However, as CO_2 partial pressure is increased to 0.5 kPa, CO_2 absorption in MEDA is approximately as fast as in MEA and EDA. Crystallization occurs in 8 m MEDA at CO_2 loading richer than 0.42 mol/mol alkalinity.

Solids precipitated at 40 ^oC from 6 m potassium glycinate at P^*_{CO2} greater than 2 kPA. The heat of CO_2 absorption is 69 kJ/mol, compared to 82 kJ/mol for MEA. The adjusted capacity is 25% less than 7 m MEA. The absorption rate is competitive with 7 m MEA at low loading, but becomes less attractive as CO_2 loading increases.

6 m potassium sarcosine has a low adjusted capacity of 0.27 mol CO_2/kg solvent and a low heat of CO_2 absorption (62 kJ/mol). Its CO_2 absorption rate is almost twice that of 7 m MEA.

The CO_2 solubility from 40 to 160 ^oC is represented well by the correlations:

$$\text{8 m 1MPZ: } \ln P_{CO_2} = 35.2 - \frac{10344}{T} - 6.4\alpha + 9741\frac{\alpha}{T}$$

$$\Delta H_{abs} = -R(-10344 + 9741\alpha) \quad (J/mol\ CO_2)$$

$$\text{8 m 2MPZ: } \ln P_{CO_2} = 39.8 - \frac{12554}{T} - 19.6\alpha + 14509\frac{\alpha}{T} - 8.1\alpha^2$$

$$\Delta H_{abs} = -R(-12554 + 14509\alpha) \quad (J/mol\ CO_2)$$

$$\text{4 m PZ/4 m 2MPZ: } \ln P_{CO_2} = 41.2 - \frac{12998}{T} - 27.0\alpha + 14684\frac{\alpha}{T} + 7.3\alpha^2$$

$$\Delta H_{abs} = -R(-12998 + 14684\alpha) \quad (J/mol\ CO_2)$$

$$\text{10 m DGA: } \ln P_{CO_2} = 28.1 - \frac{7572}{T} + 67.8\alpha - 25209\frac{\alpha}{T} - 115\alpha^2 + 50113\frac{\alpha^2}{T}$$

$$\Delta H_{abs} = -R(-7572 - 25209\alpha + 50113\alpha^2) \quad (J/mol\ CO_2)$$

In 8 m PZ-CO_2-H_2O the PZ/PZH^+ accounts for approximately 37 to 47% from 0.3 to 0.4 mol CO_2/equivalent PZ. PZ carbamate accounts for about 10% of the total PZ. Bicarbonate is only 3% of the total amine.

PZ volatility in 8 m PZ-CO_2-H_2O system is approximately 0.78 and 0.11 Pa at nominal lean and rich loading corresponding to ~500 Pa and 5,000 Pa at 40 ºC.

Modeling

The previous correlation which used a polytropic compression efficiency of 72% and an intercooler pressure drop of 0 kPa was roughly equivalent to a compressor with 80% efficiency and 20% pressure loss in each intercooler.

A 5 °C approach on the reboiler improved performance over a 10 °C approach by 1.0–1.2 kJ/mol CO_2 fairly equally for all configurations.

The lowest work requirement with the 1-stage flash using 8 m PZ was 34.7 kJ/mol CO_2 with a reboiler at 150 °C, a rich loading and 0.415, and a lean loading of 0.34.

A rich loading of 0.48 in 9 m MEA will require approximately the same absorber mass transfer area as a rich loading of 0.40 in 8 m PZ.

A new absorber model for 8 m PZ has been developed. It uses the 5deMayo v.1 thermodynamic framework and kinetics extracted from experimental work by Dugas (2009) using the WWC. The reported CO_2 flux data are matched with a ±20% deviation using the developed WWC model. Model results above 80 ^oC show a higher deviation from experimental data due to additional phenomena becoming predominant at these conditions, possibly the increase of diffusion effects of reactants and products.

Preliminary evaluation by the new Aspen Plus® model, 5deMayo v.1, of pilot plant results with 8 m PZ improved CO_2 removal from 67 to 90% with the addition of intercooling,

The critical L/G for 9 m MEA at our pilot plant conditions will be 17 gpm solvent at 350 cfm gas. At this L/G, intercooling should increase CO_2 removal from 75 to 92% with a lean loading of 0.35.

With both partial load boiler operation and partial load reboiler operation, there is a linear relationship between the optimum lean loading and the optimum steam rate.

With both partial load boiler operation and partial load reboiler operation, keeping the stripper pressure valve wide open and letting the stripper pressure swing is found to be the most profitable strategy.

At a CO_2 price of \$50/tCO_2, adding even an inflexible CO_2 capture system improves annual operating profits by at least 20%, with a venting-only flexible capture system adding another 3–6%. Adding a solvent storage system to a plant with flexible CO_2 capture improved annual operating profits by 12–14% compared to inflexible capture, but the capital costs of additional solvent inventory, storage tanks, and larger stripping/compression equipment must be accounted for to determine if the additional costs are justified.

CO_2 emissions are greater with flexible CO_2 capture, but emissions are still 75–82% lower than when no CO_2 capture system is available. CO_2 capture systems are utilized over 90% of the time when the base plant is operating in all flexible capture scenarios studied.

Solvent Management

At 175 ^{o}C, acidified PZ degraded at about half the rate of PZ with 0.3 CO_2 loading. Ethylenediamine was produced as with loaded solution, but no formate was produced.

At 175 °C, PZ with 0.1 loading degraded with formate and EDA production at about half the rate of solutions at 0.3 loading. The rate of formate production appears to be correlated with the estimated concentration of the species piperazine carbamate.

The use of glass cuvettes in the thermal degradation produced no significant effects on degradation rate or organic products. The cuvettes eliminated corrosion and accumulation of dissolved metals.

Formate production by oxidation increased from 4 to 19 mmol/kg over the course of nearly 600 hours at 55 and 70 °C.

100 mM Inh A is not effective at inhibiting oxidative degradation of 7 m MDEA at 90 °C.

Sparging with nitrogen reduced by 85% the production of formate and DEA in oxidation of 7 m MDEA with cycling from 55 to 120 ^{o}C.

When cycled from 55 to 120 °C with 98% O_2, 8 m PZ produced 0.046 mM formate/hr, compared to 0.31 mM/hr with 7 m MDEA. The apparent loss rate of PZ was 5%/week. EDA was produced at a rate of 0.17 mM/hr

When 7 m MDEA with 0.35 m quaternary amine (α = 0.2) was thermally degraded for four weeks at 150 °C, we detected the presence of monoethanolamine (MEA), diethanolethylamine, N,N'-dimethyl ethanamine (DMEA), and hydroxyethyl piperazine. We did not detect the secondary amine DEA or the amino acid bicine. We also observed 49 mM formate after 30 days.

At 40 to 70 ^{o}C, 50 mM Inh A reduced ammonia production from MEA oxidation by 86–93%. The activation energy of ammonia production was 86 kJ/mol without Inh A and 113 kJ/mol with 100 mM Inh A.

GC-MS identified imidazol, 1-(2-hydroxyethyl)-imidazol, and 2-oxazolidone as oxidation products of MEA.

Significant masses observed on LC-MS and MS-MS (direct infusion) in oxidatively degraded MEA samples include 128, 199, and 215. The collision induced dissociation (CID) mass spectra of the 128 and 199 compounds indicate that they may be substituted imidazols. The compound with molar mass 199 was the only product to exhibit a strong UV absorbance, and has a molecular formula of $C_8H_{14}N_3O_3$.

1. CO_2 Rates with Piperazine Derivatives *p. 13*

by Xi Chen

Quantitative ^1H and ^{13}C NMR studies were performed on 2-methylpiperazine(2MPZ)-CO_2-H_2O at 0.33 mol CO_2/mol alkalinity and 40 °C to investigate the speciation and better understand the reaction mechanism. Integration over spectrum peaks gives the relative concentration of different 2MPZ species. It was found that 63% of 2MPZ was converted to carbamate, 80% of which is 4-carboxyl-2-methylpiperazine.

8 m 1,2-diaminopropane (1-methyl-ethylenediamine, MEDA) at two lean CO_2 loadings (α = 0.35 and 0.42 mol/mol alkalinity) was tested using the Wetted Wall Column (WWC). Results show that it has a higher absorption rate than 7 m monoethanolamine (MEA) or 12 m ethylenediamine (EDA) at the lean condition, but has a slower rate as the loading was increased. At CO_2 loading higher than 0.42, precipitation occurs and no further measurement can be made.

2. CO_2 Rates with Amino Acids *p.28*

by Le Li

Two amino acid solvents, 6 m GlyK and 6 m sarcosine, were tested for their potential for CO_2 absorption during this quarter. The CO_2 solubility and absorption/desorption rates for these solvents were measured using the wetted wall column. 6 m GlyK was tested at three loading conditions (α: 0.33, 0.41, 0.45). A rich loading could not be reached since the 6 m GlyK solvent begins to precipitate around 0.5 CO_2 loading. The absorption rate for 6 m GlyK is competitive with 7 m MEA at low loading, but decreases quickly as CO_2 loading increases. The theoretically predicted capacity of 6 m GlyK is 75% of the capacity for 7 m MEA, and the theoretical heat of absorption at the rich loading condition for 6 m GlyK is 15% lower than 7 m MEA. Thus, GlyK solvents are not competitive with 7 m MEA based on the parameters tested. 6 m sarcosine was tested at six loading conditions (α: 0.2, 0.3, 0.36, 0.45, 0.49, 0.55). As a CO_2 absorption solvent, 6 m sarcosine is not attractive for its capacity or heat of absorption, having a lower value for both parameters compared to 7 m MEA and 6 m GlyK. The absorption rate of 6 m sarcosine makes it attractive, as it is significantly higher than 7 m MEA and both GlyK solvents at rich loading conditions. A literature review on amino acid solvents was also conducted this quarter, with a summary of the key articles reviewed included in this report.

3. CO_2 and Amine Volatility at High Temperature *p. 41*

by Qing Xu

In this quarter the total pressure was measured at 100–160 °C for CO_2 loaded 1-methylpiperazine (1MPZ), 2-methylpiperazine (2MPZ), piperazine/2MPZ (PZ/2MPZ), and Diglycolamine (DGA®). CO_2 partial pressure was derived from the total pressure data.

Based on the data at 40 to 160 °C, for each solvent an empirical model of CO_2 partial pressure was developed; the heat of absorption of CO_2 is given by the derivative of that expression. In the following equations P_{CO2} is in Pa, T is in K, R is the gas constant in J/mol·K, and α is the CO_2 loading.

For 7.7–8 m 1MPZ: $\ln P_{CO_2} = 35.2 - \frac{10344}{T} - 6.4\alpha + 9741\frac{\alpha}{T}$

$$\Delta H_{abs} = -R(-10344 + 9741\alpha) \quad (J / mol\ \mathrm{CO_2})$$

For 6.7–8 m 2MPZ: $\ln P_{CO_2} = 39.8 - \frac{12554}{T} - 19.6\alpha + 14509\frac{\alpha}{T} - 8.1\alpha^2$

$$\Delta H_{abs} = -R(-12554 + 14509\alpha) \quad (J / mol\ \mathrm{CO_2})$$

For 4 m PZ/4 m 2MPZ: $\ln P_{CO_2} = 41.2 - \frac{12998}{T} - 27.0\alpha + 14684\frac{\alpha}{T} + 7.3\alpha^2$

$$\Delta H_{abs} = -R(-12998 + 14684\alpha) \quad (J / mol\ \mathrm{CO_2})$$

For 9.6–10 m DGA®: $\ln P_{CO_2} = 28.1 - \frac{7572}{T} + 67.8\alpha - 25209\frac{\alpha}{T} - 115\alpha^2 + 50113\frac{\alpha^2}{T}$

$$\Delta H_{abs} = -R(-7572 - 25209\alpha + 50113\alpha^2) \quad (J / mol\ \mathrm{CO_2})$$

At the mid-loading where P_{CO2} is 1.5 kPa at 40 °C, the ΔH_{abs} is 69, 66, 66, and 73 kJ/mol CO_2 for 1MPZ, 2MPZ, PZ/2MPZ, and DGA®, respectively.

4. Amine Volatility *p. 51*

by Thu Nguyen

For 8 m PZ-CO_2-H_2O at either 27 ºC or 40 ºC, the PZ/PZH^+ species dominates at nominal lean loading and gradually decreases toward richer loading. This species accounts for approximately 0.37–0.47 of the total PZ concentration at the above conditions. The gradual decrease of free PZ results in decreasing amine volatility. PZ carbamate, on the other hand, is seen to increase with loading as more PZ reacts with CO_2. PZ dicarbamate is also present and accounts for ~0.1 of the total amine whereas its concentration is practically negligible in loaded 2 m PZ at similar conditions. Both bicarbonate and carbonate species are present in a ratio of ~0.03 moles of total CO_2 to total amine. This ratio remains approximately the same in loaded 2 m PZ.

PZ volatility in 8 m PZ-CO_2-H_2O is approximately 0.11 and 0.78 Pa at nominal lean and rich loading corresponding to ~500 Pa and 5,000 Pa at 40 ºC. The PZ apparent activity coefficient varies from ~0.001 to 0.02 for this system over the nominal range of loadings and absorber operating temperatures from 40–65 ºC. This coefficient increases with temperature due to PZ having an exothermic partial molar excess enthalpy heat of solution, but is found to decrease with either increasing loading or lower PZ concentration due to a decrease of free PZ in solution.

5. Modeling MDEA/PZ Thermodynamics p. 60

by Peter Frailie

The heat capacity, VLE, activity coefficient of CO_2, and unloaded volatility of 2, 5, 8, and 10 m PZ solutions were incorporated into Aspen Plus®. The model adequately predicts heat capacity and VLE data over significant loading and temperature ranges (0.20–0.40 loading and 40 ^oC–160 ^oC). Experimental data concerning speciation and high temperature unloaded PZ volatility still need to be collected and/or validated before they can be incorporated into a future model. The discrepancy between the Gibbs-Helmholtz and calorimetric heat of absorption predictions seems to have been minimized, though the reason for this discrepancy still is not completely understood. A similar model was constructed for MDEA that included unloaded MDEA volatility, VLE data for 4.52 m and 8.4 m MDEA, heat capacity for loaded solutions of 30–60 wt % MDEA, and CO_2 activity coefficient in loaded solutions at 25, 40, and 60 ^oC. Data for the unloaded MDEA/PZ blend have already been incorporated into the model, and loaded data will be regressed as soon as they are made available.

6. Modeling Stripper Performance for CO_2 Capture by Amines p. 77

by David Van Wagener

During this quarter, several tasks were addressed. First, the previous compressor correlation was compared against the compression work for more realistic values of compressor efficiency and intercooler pressure drop. A multi-stage compressor with a polytropic efficiency of 80% and a 20% pressure loss per intercooler was found to predict results similar to a 72% efficient compressor with no pressure drop in the intercoolers. Next, a 5 °C approach was specified for the reboilers of all previous results with MEA. This change improved the overall performance by 1.0–1.2 kJ/mol CO_2 fairly evenly for all configurations. Finally, the new PZ thermodynamic model was used to simulate a 1-stage flash. The equivalent work at 150 °C and the optimum loading of 0.34 was 34.7 kJ/mol CO_2, a 1.3 kJ/mol CO_2 improvement over 9 m MEA at its optimum. For future work, it was determined that an acceptable rich loading of 0.4 for PZ was equivalent to a rich loading of 0.48 for MEA because the log mean driving force in the absorber was double for MEA, indicating that both sets of conditions would require the same packing area since PZ demonstrates twice the reaction rate.

7. CO_2 Absorption Modeling Using Aqueous Amines p. 86

by Jorge M. Plaza

The new thermodynamic model for concentrated PZ, "5deMayo", was used to determine kinetic constants for 8 m PZ. A wetted wall column model was set up to extract kinetic constants from raw data reported by Dugas for 8 m PZ.

Once the kinetic framework was established, an absorber model was built for the November 2008 and summer 2010 pilot plant campaigns. It uses a FORTRAN subroutine to implement the Tsai interfacial area correlation and the viscosity correlation presented by Plaza.

The developed model was used for a preliminary evaluation of intercooling with 8 m PZ. Results show that intercooling may increase CO_2 removal as much as 34%.

The previously developed 9 m MEA model was used to determine potential conditions for the summer pilot plant campaign. Results are included in this report.

8. Optimum Design and Control of a 7 m MEA System p. 94

by Sepideh Ziaii

In the previous quarter, the integrated dynamic model of the absorber and stripper with MEA, created in Aspen Custom Modeler (ACM®), was combined with a first order approximation model of steam turbines in order to take into account steam pressure variation during dynamic operation.

In this quarter, the multi-variable steady state optimization tools of ACM® were implemented to maximize the profit of the 100 MW coal-fired power plant as the ratio of CO_2 selling price to electricity price varies. This steady state optimization gives the optimum design curves for lean loading and CO_2 removal versus price ratio.

In addition, implementing multi-variable dynamic optimization tools and running the simulation at dynamic mode enabled us to optimize the operation of the capture in response to two dynamic scenarios: partial steam load in flexible capture and partial boiler load operation. The results have shown that as the load varies, controlling L/G at the design value in the stripper and absorber can allow the plant to stay close to the optimum path and consequently the cost of employing an advanced multi-variable control system can be avoided.

9. Electric Grid-Level Implications of Flexible CO_2 Capture Operation p. 106

by Stuart Cohen, Department of Mechanical Engineering. Supported by the EPA STAR Fellowship Program and the Luminant Carbon Management Program

Co-supervised by Prof. Michael Webber

Flexible post-combustion absorption/stripping that vents carbon dioxide (CO_2) or stores rich solvent at partial- or zero-load can be used to vary power output in response to electricity prices and improve economic performance of a coal-fired facility with CO_2 capture. Optimization and deterministic models have been created and utilized to investigate profit maximizing behavior of a single 500 MW coal-fired facility in the Electric Reliability Council of Texas (ERCOT) grid under configurations with flexible CO_2 capture, inflexible CO_2 capture, or no CO_2 capture. Results are compared based on whether the plant operates reactively to the most recent posted price, uses a day-ahead price forecast, or has perfect knowledge of future electricity prices.

Assuming a price of US$50 per metric ton of CO_2, major conclusions are as follows:

- High costs without CO_2 capture allow net annual output to be greater with CO_2 capture than without, despite CO_2 capture energy requirements.
- Adding an inflexible CO_2 capture system improves annual operating profits by at least 20 % from the no-capture case.
- Compared to annual operating profits earned with inflexible CO_2 capture, venting-only flexible capture improves profits by 3–6%, and flexible capture with solvent storage improves profits by 12–14%.
- Venting CO_2 at high prices should be economical because it has negligible capital costs, but cash flow analysis is required to determine if the operating profit improvements with solvent storage justify the capital costs of additional solvent inventory, storage tanks, and larger stripping/compression equipment.

- Accurate price forecasting is necessary to plan solvent storage operation, but the economic benefits of venting-only flexible CO_2 capture can be achieved without accurate price forecasting.
- Ramp limits have only a minor effect on economic results, but ramp limits might be more important when considering ancillary service markets and detailed plant control concerns.
- CO_2 emissions are greater with flexible CO_2 capture, but emissions are still 75–82% lower than when no CO_2 capture system is available.

11. Measurement of Packing Liquid Phase Film Mass Transfer Coefficient *p. 128*

by Chao Wang

(also supported by the Process Science and Technology Center)

Packing is widely used in distillation, stripping, and scrubbing processes because of its relatively low pressure drop, good mass transfer efficiency, and ease of installation. Packing is being investigated for the post-combustion carbon capture process for these reasons. Research continues to focus on development of high performance packing, especially on minimizing pressure drop, maximizing mass transfer efficiency, and minimizing costs. The design of packed absorbers for carbon dioxide capture will require the reliable measurement and accurate prediction of the effective area a_e, gas and liquid film mass transfer coefficient k_G and k_L. My research is focused on the measurement of these important fundamental parameters for packings and construction of a mechanistic design model.

In the last quarterly report, the mass transfer data for three packings were presented. The $NaOH/CO_2$ was used for contact area measurement, $NaOH/SO_2$ for k_G measurement, and toluene/water for k_L measurement. In this report, these data are compared with literature data and published models to assist in verifying our data, refining our experimental methods, and developing improved models.

Among numerous mass transfer coefficient models, two are selected for comparison with our structured packing data and two to compare with our random packing data. They are the models by Rocha, Bravo, Billet, and Wagner. The model results compare favorably to our experimental data.

12. Pilot Plant Testing of Advanced Process Concepts using Concentrated Piperazine

by Dr. Eric Chen

Supported by the CO_2 Capture Pilot Plant Project and by NRGEnergy/DOE Contract)

Pilot plant testing of 8 m PZ in a two-stage heated flash with absorber intercooling is planned for early fall of 2010. A skid-mounted two-stage flash pilot unit will need to be fabricated and the absorber retrofitted for intercooling. In this reporting period, isometric piping drawings for the skid were completed based on the 3-D model. Material associated with the fabrication of the skid was ordered, which included flanges, pipe fittings, pipe, hand valves, check valves, pressure relief valves, gaskets, Swagelok fittings, studs, nuts, and washers.

Welding of the skid support structure was completed and the base assembly was hot-dipped galvanized. The top piping support sections were sandblasted/painted and bolted to the base assembly. The major process equipment (high pressure pump, cross-exchanger, two steam

heaters, and two gas-liquid separators) were set in place on the skid. Two welders were hired and certified for welding stainless and carbon steel pipe. All of the piping associated with the skid was first cut, fitted, and tacked. The welders have begun tack welding of the pipe lines and this is approximately 10% completed.

The instrument junction box and an externally mounted air-conditioner unit were procured and installed on the skid. Cable trays, controller mount tracks, and two Rosemount 848 temperature transmitters were installed inside the junction box. The six Fisher-Baumann control valves and the Micromotion F-100 coriolis flowmeter were procured. Emerson Process Management agreed to donate the Micromotion flowmeter, two Micromotion 7829 viscometers, five 3095 integral orifice flowmeters, two level transmitters, and the hardware and software associated with the Delta V process control system. The six control valves were purchased at a substantial discount through Emerson Process Management.

The absorber intercooler pump was procured and fabrication of the new collector plate was completed. An existing Alfa Laval M3-FG plate and frame heat exchanger will be used. A new Micromotion F-100 coriolis flowmeter was purchased. The pump, flowmeter, heat exchanger, and control valve were mounted to the small skid and installed on the second level of the SRP pilot plant structure.

Welding of the skid piping should be completed by mid-July. The piping will be pressure tested and insulated with foam glass. The instrumentation, cabling, conduit, and power supplies will then be installed on the skid. Once the insulation and instrumentation is complete, the skid will be set in place outside and the connected to the pilot plant. The piping and instrumentation tie-ins of the intercooler skid will also be completed.

Detailed reporting of this activity is limited to sponsors of the CO_2 Capture Pilot Plant Project and does not appear in this report to Luminant sponsors.

13. MDEA/PZ Degradation in Cycled Solvents *p. 138*

by Fred Closmann

(also supported by the Process Science & Technology Center)

7 m methyldiethanolamine (MDEA) was degraded in three separate experiments in the Integrated Solvent Degradation Apparatus (ISDA) during the quarter. We measured a formate production rate of 0.15 mM/hr in the ISDA with the thermal reactor maintained at 90 °C and 7 m MDEA dosed with 100 mM Inh A, which indicated that the oxidative degradation inhibitor was not effective at this temperature. When we utilized a headspace gas of 98% air/2% O_2 and maintained the thermal reactor at 90 °C, we measured a formate production rate of 0.04 mM/hr, compared to 0.12 mM/hr when we utilized a 98% O_2/2% CO_2 gas at comparable conditions. When we stripped dissolved oxygen from the solvent immediately downstream of the oxidative reactor using a 2 L/min N_2 gas purge in 7 m MDEA cycled from 55 to 120 °C in the ISDA, we reduced the formate production rate to 0.047 mM/hr. The rate without stripping was 0.31 mM/hr, indicating that stripping dissolved oxygen is a practical solution to reducing oxidative degradation in absorber/stripper configurations.

The formate production rate in 8 m piperazine (PZ) (0.3 moles CO_2/mole alk) was 0.05 mM/hr, compared to 0.31 mM/hr measured in 7 m MDEA when cycled from 55 to 120 °C. When we reduced the thermal reactor temperature to 90 °C, the formate production rate was 0.013 mM/hr

in 8 m PZ. We measured an ethylenediamine (EDA) production rate of 0.17 mM/hr in 8 m PZ, and a PZ loss rate of ~5%/wk.

When 7 m MDEA was treated with 0.35 m tetramethylammonium chloride (quat), loaded to 0.2 moles CO_2/mole alk, and thermally degraded at 150 °C for up to 30 days in the absence of oxygen in the thermal cylinder headspace, we detected monoethanolamine (MEA), diethanol ethylamine, and dimethylethanamine (DMEA). We did not detect bicine or diethanolamine (DEA), both of which are detected in cycling experiments, confirming that these are primarily oxidative degradation products of MDEA.

We improved our oxidative degradation model for the ISDA using a plug-flow reactor model, and estimated energies of activation (Ea) for the production of DEA, formate and bicine of 85,000, 91,000, and 100,000 kJ/mol*K.

14. Degradation of PZ, substituted PZ, and PZ analogs p. 155

by Stephanie Freeman

A solution of 8 m PZ containing 0.1 mole CO_2/mole alkalinity was degraded at 175 °C for 15 weeks to further explore the effect of CO_2 concentration. The solution lost 45% of the original amine compared to 5, 71, and 73% for the unloaded, 0.3 loading, and 0.4 loading, respectively, at the same conditions. The concentration of CO_2 has a direct impact on the rate of PZ degradation.

The production of total formate, the main degradation product, ranged from 16 mmol/kg in the unloaded solution to 251, 851, and 692 mmol/kg in the 0.1 loading, 0.3 loading, and 0.4 loading experiments.

Using an estimated speciation of 8 m PZ at 175 °C, it was determined that the production of formate was closely associated with the mole fraction of $PZCOO^-$, indicating this species is likely involved in the initial stages of the mechanism that produces formate and formyl amides such as N-formyl PZ. The degradation rate of PZ was closely related to the free PZ and H^+PZ mole fractions.

Glass cuvettes were used to eliminate contact between the amine solution and the interior surfaces of the stainless steel thermal cylinders. The degradation rate of 8 m PZ with 0.3 mole CO_2 per mole alkalinity was slightly reduced, losing only 66% of the initial amine compared to 71% in the traditional experimental setup after 15 weeks at 175 °C. The production of total formate was reduced from 708 mmol/kg to 538 mmol/kg in the cuvette experiment. No iron, nickel, or chromium was found in the solution.

15. Degradation of MEA and Other Amines p. 182

by Alex Voice

MEA was degraded in the high gas flow (HGF) apparatus at various temperatures and inhibitor concentrations. Addition of 50 mM Inh A resulted in 63–80% reduction in the rate of ammonia production. Addition of 100 mM Inh A resulted in 86–93% reduction in the rate of ammonia production. The activation energies for no inhibitor, 50 mM Inh A, and 100 mM Inh A were 86 kJ/mol, 102 kJ/mol, and 113 kJ/mol, respectively.

GC-MS was used to identify imidazol, 1-(2-hydroxyethyl)-imidazol, and 2-oxazolidone on GC-MS. A significant unknown product on the chromatogram was identified as trimethylamine, based on the closest library reference match.

Significant masses observed on LC-MS and MS-MS (direct infusion) in oxidatively degraded MEA samples include 128, 199, and 215. These masses did not correspond with any known degradation products. The collision induced dissociation (CID) mass spectra of the 128 and 199 compounds indicate that they may be substituted imidazols. The compound with molar mass 199 was the only product to exhibit a strong UV absorbance, and has a molecular formula of $C_8H_{14}N_3O_3$.

MEA, which was oxidized and then thermally degraded, showed similar MEA loss to thermal degradation of neat solutions. At the high temperature, some formamide was converted to formate. All oxalate products were converted to formate. Nitrite was completely consumed, but nitrate was stable.

Activation energy for ammonia production from MEA solutions in the presence of oxygen was 86–113 kJ/mol. Addition of 100 mM Inh A reduced the ammonia production rate by 93%. GC-MS was used to identify 1-(2-hydroxyethyl)- imidazole, 2-oxazolidone, and an unknown with mass spectrum similar to trimethylamine in oxidized MEA. Another product with molecular weight 199 was found to have the formula $C_8H_{13}N_3O_3$ using high-resolution mass spectrometry with electrospray ionization. The rate of MEA loss during thermal degradation was not affected by the presence of oxidation products.

16. Nitrosamine Formation in CO_2 Capture by Piperazine *p. 206*

by Mandana Ashouripashaki, Department of Civil Engineering
Cosupervised by Prof. Howard Liljestrand

Secondary amines in the presence of nitrite and nitrate ions, through a nitrosation reaction, can form carcinogenic products called nitrosamines. Nitrosation reactions have been known for over 150 years but their carcinogenic properties were first discovered in 1956 and since then there has been an explosion of interest in their chemistry and particularly in methods of destroying them. Piperazine (PZ) is an amine of interest in our study and nitrosation products of PZ are N-nitrosopiperazine and N-N, dinitrosopiperazine.

The available methods for detecting nitrosamines are not applicable for dinitrosopiperazine (DNPZ) because of its lack of volatility. In this quarter, standard dinitrosopiperazine which has been synthesized in the lab was injected directly to determine if DNPZ can be detected by mass spectrometry. We found that using a mixture of methanol and water as a solvent gave us the best result for the detection of DNPZ.

A method has been developed for quantifying DNPZ with liquid chromatography followed by mass spectrometry (LC-MS). The primary results are reported here.

17. Thermal Reclaiming *p. 231*

by Steven Fulk

In this quarter concentrated, loaded piperazine (PZ) solutions created last quarter using a simple heated-beaker evaporator were analyzed using a variety of techniques. Two solutions were created; the first solution was 8 m PZ with 0.3 molCO_2/mol alkalinity, and the second solution was 8 m PZ with 0.3 mol CO_2/mol alkalinity plus 250 mM formic acid. Total Inorganic Carbon (TIC) and cation chromatography analysis showed the solution containing formic acid had 1.4 mol PZ/kg solution and 0.02 mol CO_2/mol alkalinity less than the solution with no formic acid. The difference is hypothesized to be the formate/amine/formamide equilibrium reaction. Anion

chromatography showed less formate than predicted from a mass balance on the non-volatile species in the concentrated solution. Formamide reversal using NaOH is needed to confirm the hypothesis.

Goals for next quarter include performing three experiments. First, thermal degradation experiments using stainless steel bombs will analyze degradation characteristics of concentrated amine solutions. Second, liquid-liquid equilibrium experiments will be conducted on amines and inhibitor mixtures. Finally, a thermal reclaiming apparatus with continuous FTIR vapor sampling constructed this quarter will be used to reclaim aqueous amine solutions. Liquid and vapor samples will be analyzed for composition.

18. Amine Reclaiming by Solids Precipitation *p. 240*

by Humera Abdul Rafique

The solubility of potassium sulfate (K_2SO_4) in piperazine (PZ) solution increases with increasing loading because of a greater concentration of carbamate and protonated amine in the system. The solubility decreases with decrease in temperature. The solubility of K_2SO_4 is lower in PZ than in MEA when determined using the solid solubility experimental procedure, i.e., the solubility decreases in organic solutions with greater organic concentrations.

It has been determined that the solubility window for CO_2 in PZ solutions is between 0.3 and 0.46. In order to establish the loading limit of the PZ solutions, experiments are being carried out to determine the solubility of hydrated protonated piperazine carbamate by initially preparing the crystals and using the solid solubility method to determine the solubility.

Attachments:

CO_2 rates with PZ Derivatives

Quarterly Report for April 1– June 30, 2010

by Xi Chen

Supported by the Luminant Carbon Management Program

and the

Industrial Associates Program for CO_2 Capture by Aqueous Absorption

Department of Chemical Engineering

The University of Texas at Austin

July 1, 2010

Abstract

Quantitative ^{1}H and ^{13}C NMR studies were performed on 2-methylpiperazine(2MPZ)-CO_2-H_2O at 0.33 mol CO_2/mol alkalinity and 40 °C to investigate the speciation and better understand the reaction mechanism. Integration over spectrum peaks gives the relative concentration of different 2MPZ species. It was found that 63% of 2MPZ was converted to carbamate, 80% of which is 4-carboxyl-2-methylpiperazine.

8 m 1,2-diaminopropane (1-methyl-ethylenediamine, MEDA) at two lean CO_2 loadings (α = 0.35 and 0.42 mol/mol alkalinity) was tested using the Wetted Wall Column (WWC). Results show that it has a higher absorption rate than 7 m ethanolamine (MEA) or 12 m ethylenediamine (EDA) at the lean condition, but has a slower rate as the loading was increased. At CO_2 loading higher than 0.42, precipitation occurs and no further measurement can be made.

Introduction

WWC measurements show that 2MPZ or a blend of 2MPZ and PZ are promising solvents for CO_2 capture with their high CO_2 capacity and fast absorption rate. To correctly interpret and model the experimental data on thermo-equilibrium and mass transfer, speciation of CO_2-loaded amine solution via NMR was initiated last quarter. In this quarter, quantitative ^{1}H and ^{13}C NMR measurements were made to more rigorously determine the relative amount of different CO_2 related species in loaded 2MPZ solution.

An ethylenediamine derivative solvent, 1,2-diaminopropane (Figure 1), was tested with the WWC in this quarter.

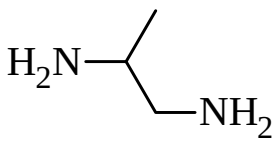

Figure 1: Molecular structure of 1,2-diaminopropane

Our previous study showed that EDA absorbs CO_2 at a rate similar to MEA. However, free EDA is almost completely depleted at rich loading and the rate becomes extremely slow. The methyl group substitution is expected to introduce steric hindrance to the adjacent amino groups, resulting in less stable carbamate. Thus more free amine may be available and make up for the lower reaction rate caused by steric hindrance. Higher cyclic capacity of CO_2 is also expected.

Experimental Methods

Experimental apparatus, procedures, and analytical methods for the WWC have been described in previous reports and will not be repeated here. 2MPZ (99%, AK Sci., Inc., Mountain View, CA), 1,2-propanediamine (99%, Acros Organics, Geel, Belgium), $^{13}CO_2$ (99.9%, Cambridge Isotope Laboratories, Inc, PA), and deionized water (Millipore, Direct-Q) were used in this study.

Since ^{13}C is only of 1.1% abundance in nature, 99.9% $^{13}CO_2$ was used for loading amine solution to enhance the signal in ^{13}C NMR spectrum. 1 wt % 1,4-Dioxane (99%, Acros) was added to each sample as the reference standard. 10 wt % D_2O (99.9%, Cambridge Isotope Laboratories, Inc, PA) was also added to enhance signal output. All samples were placed in NMR sample tubes (5.0 mm O.D. x 0.77 mm I.D. x 7 in. length, 300 mHz, yellow top WILMAD Labglass). To avoid any change of content, NMR tubes were thermally sealed before being submitted for NMR analysis by a spectrometer (Varian INOVA 500 MHz NMR Spectrometer) located in the Chemistry and Biochemistry Department in the University of Texas at Austin. To obtain spectrum at temperatures higher than room temperature, samples were kept in a water bath that is thermo-stated at a requested temperature for at least 1 hour prior to spectrum acquisition.

Results and Discussion

The molecular structures of different 2MPZ and CO_2 related species are shown in **Error! Reference source not found.**. The carbon and hydrogen atoms are labeled with numbers to differentiate them. Hydrogen atoms share the same number with the carbon that they attach to. The atom labeling is consistent with that used in the previous report.

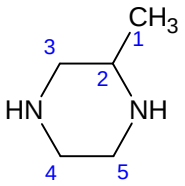

2MPZ

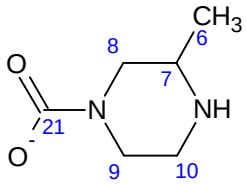

2MPZ-COO$^-$

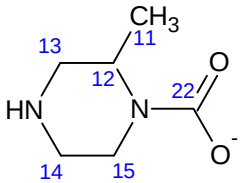

$^-$OOC-2MPZ

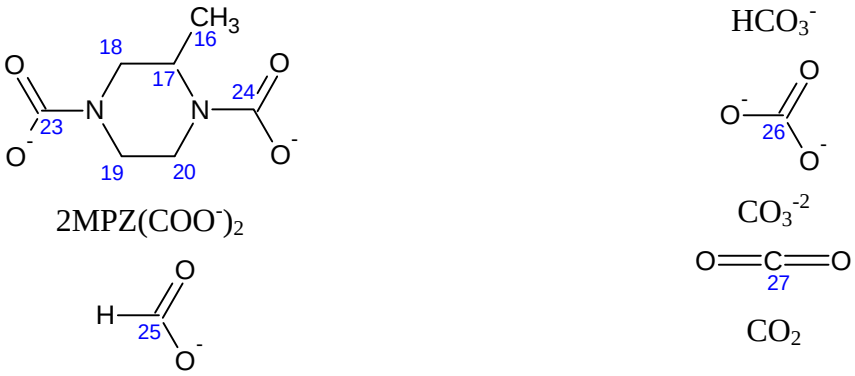

Figure 2: Molecular structure of different products from reactions between CO_2 and 2MPZ aqueous solution

Note that the products shown can also be in their protonated forms. Due to the rapid rate of mutual transformation, protonated and unprotonated products cannot be differentiated by the spectrometer used in this study. The methyl would cause steric hindrance on the neighboring amino group and make the formation of carbamate less energetically favored. Hence 4-carboxyl-2-methylpiperazine (2MPZ-COO^-) is expected to be the dominant carbamate form of 2MPZ.

The apparent composition in number of moles per kg H_2O of the NMR sample, which is determined gravimetrically from preparation of the sample, is shown in Table 1.

Table 1: Composition of the NMR sample

Component	Apparent concentration (mole/kg H_2O)
1,4-Dioxane	0.4278
D_2O	15.3608
2MPZ	8.0094
$C^{13}O_2$	5.7752

^{1}H spectrum at 40 °C

Quantitative proton NMR spectrum is shown in Figure 3. The peak at 3.5 ppm corresponds to the internal standard, 1,4-Dioxane. To quantitatively analyze the NMR data, the same methodology used by Hilliard (2008) is followed. In this method, a universal ratio is determined with the equation:

$$R_b = \frac{\varphi \cdot n_{ref}}{A_{ref}} \tag{1}$$

where:

R_b is the number of moles of dioxane/kg-H_2O per unit area;

φ is the number of active protons or carbons in dioxane;

n_{ref} is the experimental dioxane molality based on the batch solution, mol/kg H_2O;

A_{ref} is the experimental integrated area for the dioxane reference peak.

With the R_b calculated, the molality of other species in the same sample can be determined by the following equation:

$$n_i = \frac{A_i \cdot R_b}{\varphi} \tag{2}$$

where A_i and n_i are the experimental integrated peak area for species i and the number of active proton or carbons in species I, respectively. The calculated values of R_b and n_i are summarized along with peak ID. At the moment, most of the proton peaks cannot be assigned to the corresponding protons since they are not separated. Only those protons that have been definitely identified are shown in Table 2.

Table 2: Number of moles per kg H_2O of different protons determined from the amount of the internal standard (Dioxane)

Peaks	ID	# of H	ppm	A_{ref}	R_b
Dioxane	Ref	8	3.53	1.00	3.4221
				A_i	n_i
2MPZ/2MPZH$^+$	H1	3	1.0	6.48	7.3917
2MPZ/2MPZH$^+$	H4	1	2.4	0.95	3.2510

Based on the information from H4, the concentration of 2MPZ/2MPZH$^+$ is expected to be 3.25 m, which accounts for 41% of original 2MPZ. This means 59% of 2MPZ has been converted to carbamate at this CO_2 loading.

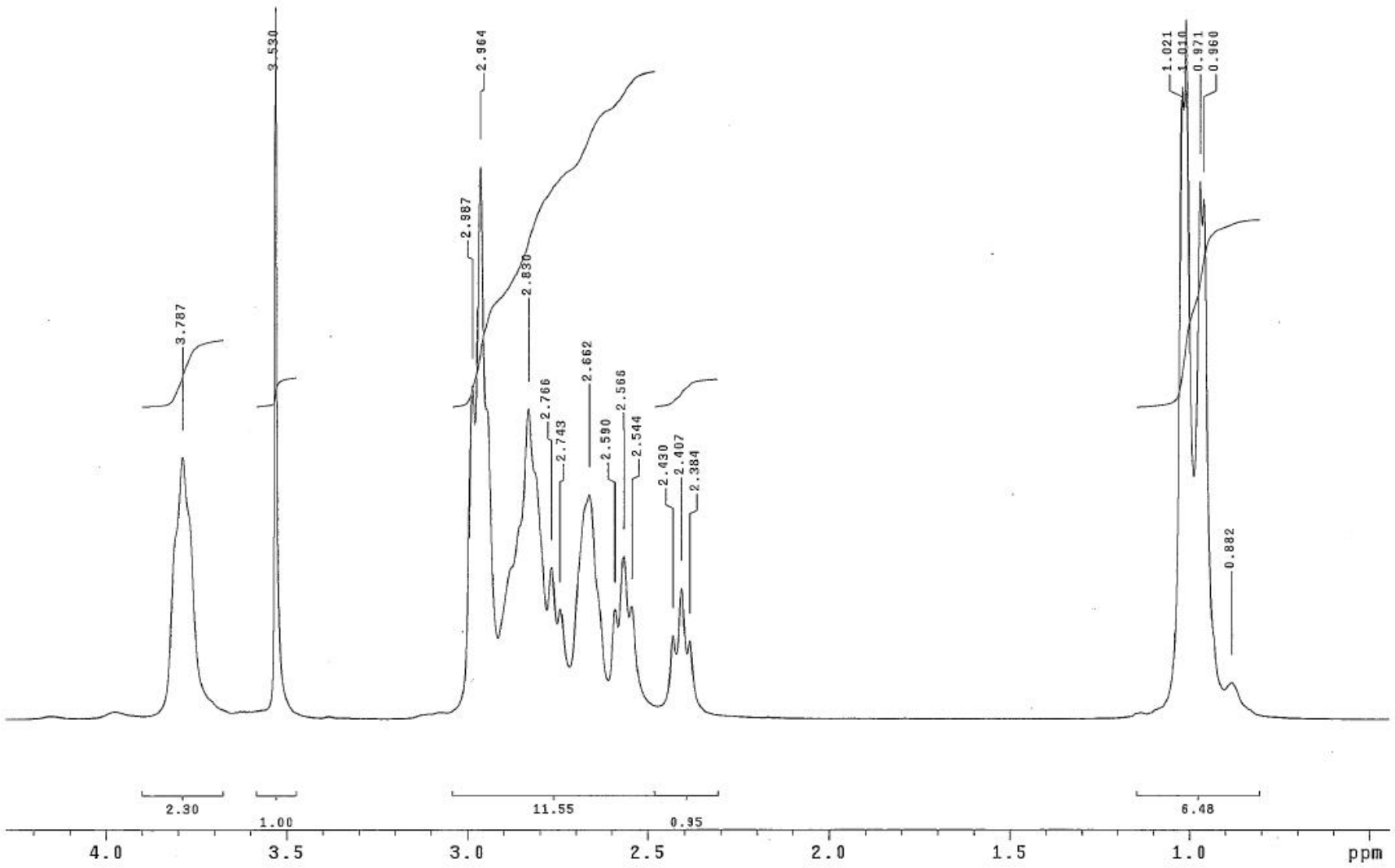

Figure 3: ^{1}H NMR Spectrum from 0 to 4 ppm for 8 m 2MPZ, α = 0.33 mol/mol alkalinity, T = 40 °C

^{13}C spectrum at 40 °C

Figure 4 presents the entire ^{13}C spectrum. **Error! Reference source not found.**–8 illustrate the zoom-in spectrum at different chemical shift regions. The corresponding numbers for different carbon peaks as well as peak areas are summarized in Table 3. The concentration of different species determined from R_b is also shown.

Table 3: Number of moles per kg H_2O of different carbon atoms determined from the amount of the internal standard (Dioxane)

Peaks	ID	Type of C	# of C	ppm	A_{ref}	R_b
Dioxane	Ref	C^{12}	4	66.500	1.00	1.7110
					A_i	n_i
2MPZ/2MPZH$^+$	C1	C^{12}	1	17.143	1.65	2.8232
	C2	C^{12}	1	49.439	1.81	3.0970
	C3	C^{12}	1	48.794	1.90	3.2510
	C4	C^{12}	1	42.837	1.86	3.1825
	C5	C^{12}	1	42.135	1.86	3.1825
2MPZ-COO$^-$/H2MPZ-COO$^-$	C6	C^{12}	1	16.238	2.18	3.7301
	C7	C^{12}	1	50.548	2.45	4.1921
	C8	C^{12}	1	48.463	2.62	4.4829
	C9	C^{12}	1	43.476	2.66	4.5514
	C10	C^{12}	1	41.645	2.47	4.2263
$^-$OOC-2MPZ/$^-$OOC-2MPZH$^+$	C11	C^{12}	1	-	-	-
	C12	C^{12}	1	-	-	-
	C13	C^{12}	1	-	-	-
	C14	C^{12}	1	-	-	-
	C15	C^{12}	1	-	-	-
2MPZ(COO$^-$)$_2$	C16	C^{12}	1	-	-	-
	C17	C^{12}	1	-	-	-
	C18	C^{12}	1	-	-	-
	C19	C^{12}	1	-	-	-
	C20	C^{12}	1	-	-	-
2MPZ-COO$^-$/H2MPZ-COO$^-$	C21	C^{13}	1	162.034	258.89	442.9728

$^{-}$OOC-2MPZ/$^{-}$OOC-2MPZH^{+}	C22	C^{13}	1	161.092	42.47	72.6681
2MPZ(COO^{-})$_2$	C23	C^{13}	1	162.605	17.21	29.4471
2MPZ(COO^{-})$_2$	C24	C^{13}	1	163.143	14.86	25.4261
HCO_3^{-}/ CO_3^{-2}	C25/C26	C^{13}	2	>164	8.86	7.5799
CO_2	C27	C^{13}	1	-	-	-

Note that there are no ^{13}C peaks found in the up field (0–54 ppm, Figure 7) for $^{-}$OOC-2MPZ/$^{-}$OOC-2MPZH^{+} or 2MPZ(COO^{-})$_2$, presumably because these species exist in very small amounts and ^{13}C is also not abundant enough on these natural carbons. All the $^{13}CO_2$ reacted with 2MPZ and formed carboxyl groups, so sharp peaks appear in the region of >160 ppm. The identification of the peak for HCO_3^{-}/ CO_3^{-2} is not positive. The three small peaks at the far down field (> 164 ppm) may also be due to the carbamate from impurity amines. For the moment, they are all considered as bicarbonate or carbonate, which should not significantly affect our conclusion since all of them are present in very small amounts compared to other species.

The concentration of ^{13}C-enriched species shown in Table 3 has to be further corrected. The amount of $^{-}$OOC-2MPZ/$^{-}$OOC-2MPZH^{+} can be determined either from C6 to C10 or C12. The two methods of calculation render a ratio which correlates the amounts determined from a normal carbon atom and enriched ^{13}C group. This number is in turn used to determine the amount of other carbamate species. The composition of 2MPZ- related or CO_2-related species calculated in this way is shown in Table 4. For any species that can be represented by multiple carbon peaks, the average value of the peak areas was used.

Table 4: Composition of the sample determined from NMR spectrum

Component	Concentration (mole/kg H_2O)	Percentage of the total 2MPZ (%)
2MPZ/2MPZH^{+}	3.107	37.4
2MPZ-COO^{-}/H2MPZ-COO^{-}	4.237	51.0
$^{-}$OOC-2MPZ/$^{-}$OOC-2MPZH^{+}	0.695	8.37
2MPZ(COO^{-})$_2$	0.262	3.16
HCO_3^{-}/ CO_3^{-2}	0.073	-
Total amount of 2MPZ	8.301	100.0
Total amount of CO_2	5.529	-
α (mol/mol alkalinity)	0.333	-

Although the total amount of 2MPZ and CO_2 determined from the NMR spectrum is slightly different from the nominal amount shown in Table 1, the deviation is only +3% and -4%, respectively. The results from the NMR spectrum will be used hereafter. It can be seen that at

CO_2 loading of 0.333, 51% of the original 2MPZ is in the form of 2MPZ-COO^-/H2MPZ-COO^-, while only 8% of 2MPZ is converted to $^-$OOC-2MPZ/$^-$OOC-2MPZH^+. The amount of 2MPZ$(COO^-)_2$ is only 3%. This agrees with the hypothesis that $^-$OOC-2MPZ is less stable than 2MPZ-COO^- because of the steric hindrance.

The amount of 2MPZ/2MPZH^+ determined from ^1H and ^{13}C spectra is different, namely, 41% vs. 37%, which is again in the expected error range.

^1H-^{13}C correlation at 40 °C

^1H-^{13}C correlation spectrum (Figure 8Figure 7) was also obtained to facilitate peak identification. The correlation between C2 and H2 or C7 and H7 distinguish themselves from the other s by forming single black dot. Each of other carbon atoms is found to interact with two hydrogen atoms, exhibiting two circles on the spectrum. This reflects the fact that each of these carbon atoms has two hydrogen atoms attached to it. Nonetheless, it is still difficult to identify all proton peaks.

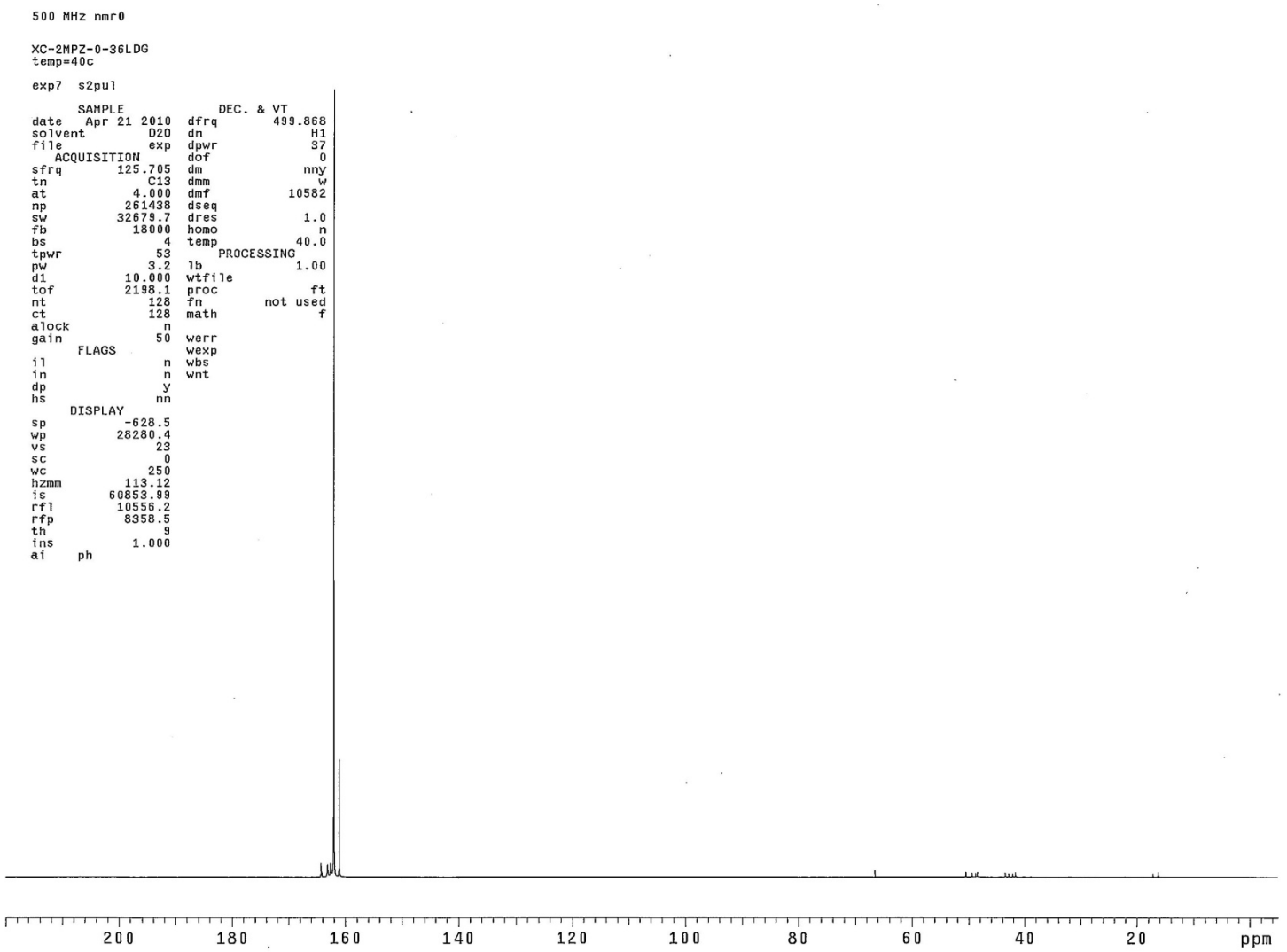

Figure 4: ^{13}C NMR Spectrum from 0 to 165 ppm for 8 m 2MPZ, α = 0.33 mol/mol alkalinity, T = 40 °C

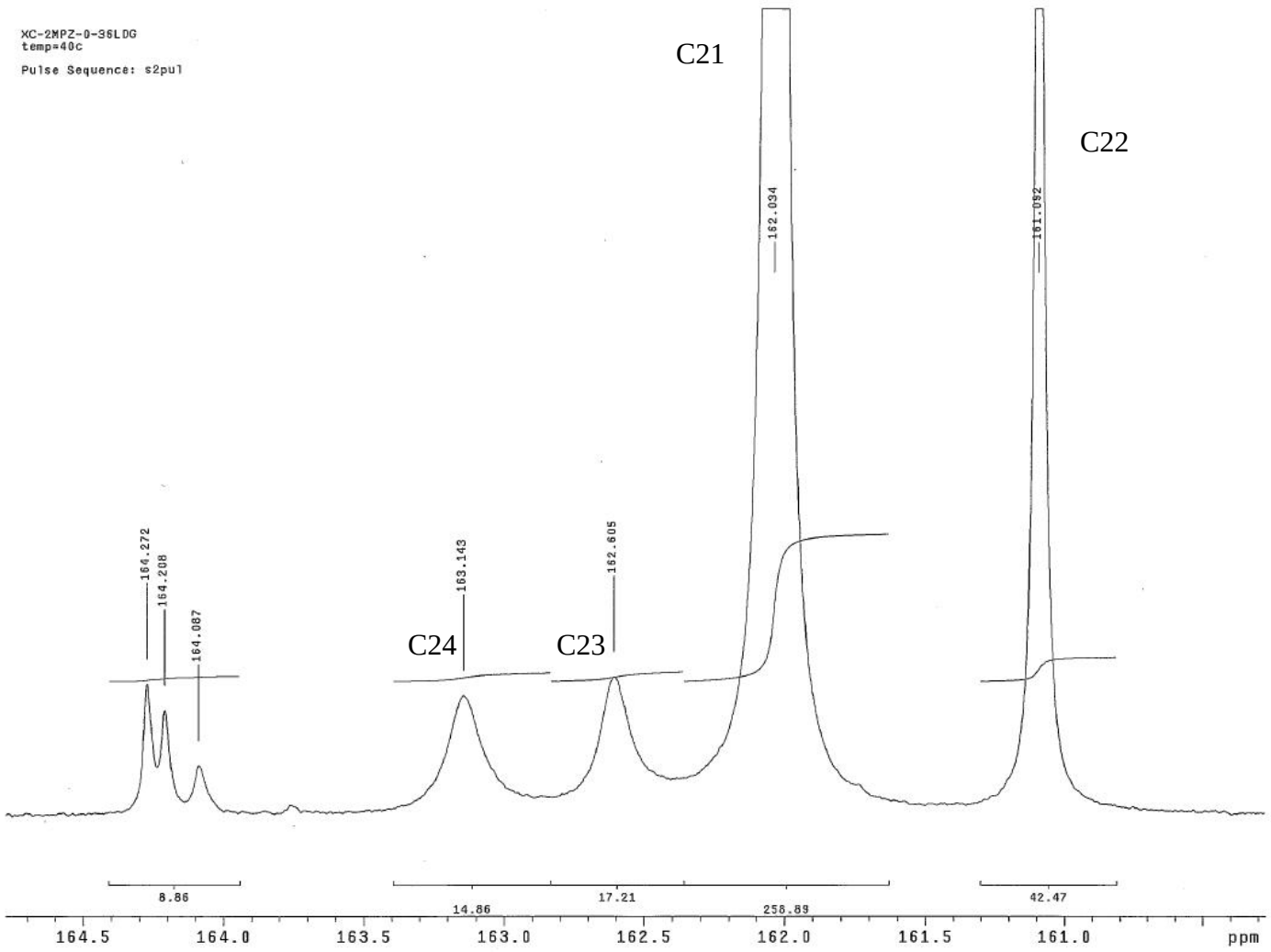

Figure 5: ^{13}C NMR Spectrum from 160 to 165 ppm for 8 m 2MPZ, α = 0.33 mol/mol alkalinity, T = 40 °C

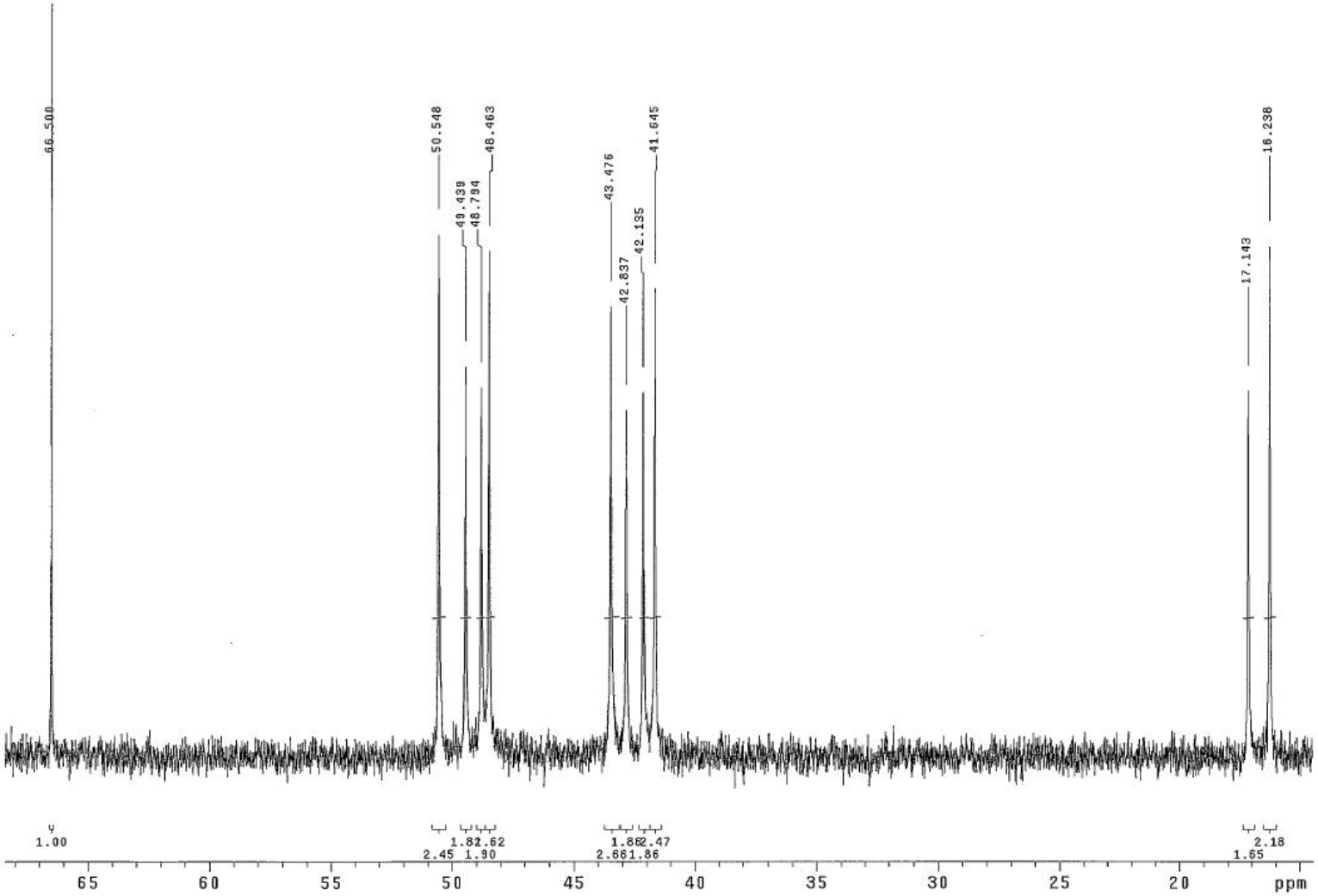

Figure 6: ^{13}C NMR Spectrum from 0 to 68 ppm for 8 m 2MPZ, α = 0.33 mol/mol alkalinity, T = 40 °C

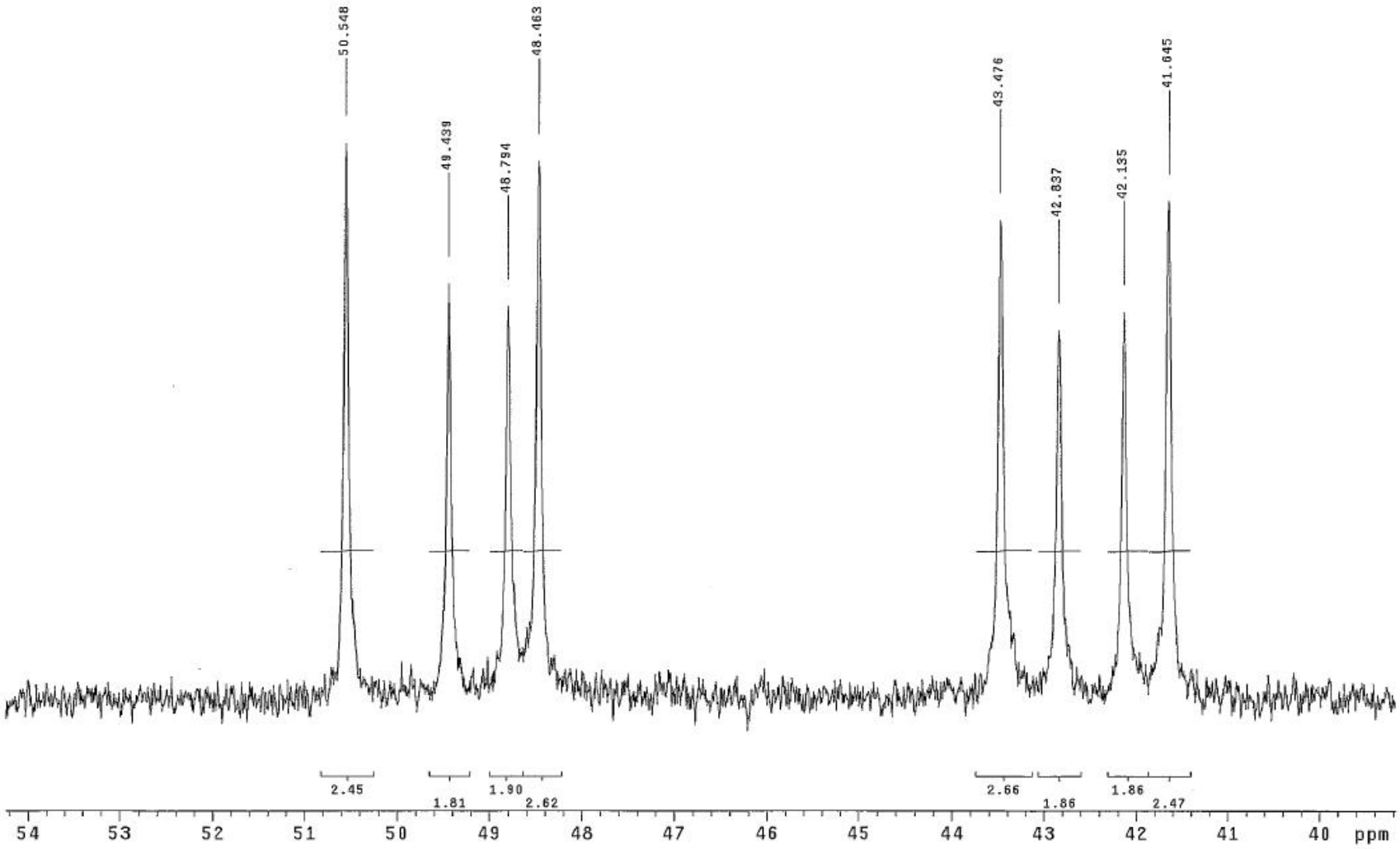

Figure 7: ^{13}C NMR Spectrum from 40 to 54 ppm for 8 m 2MPZ, α = 0.33 mol/mol alkalinity, T = 40 °C

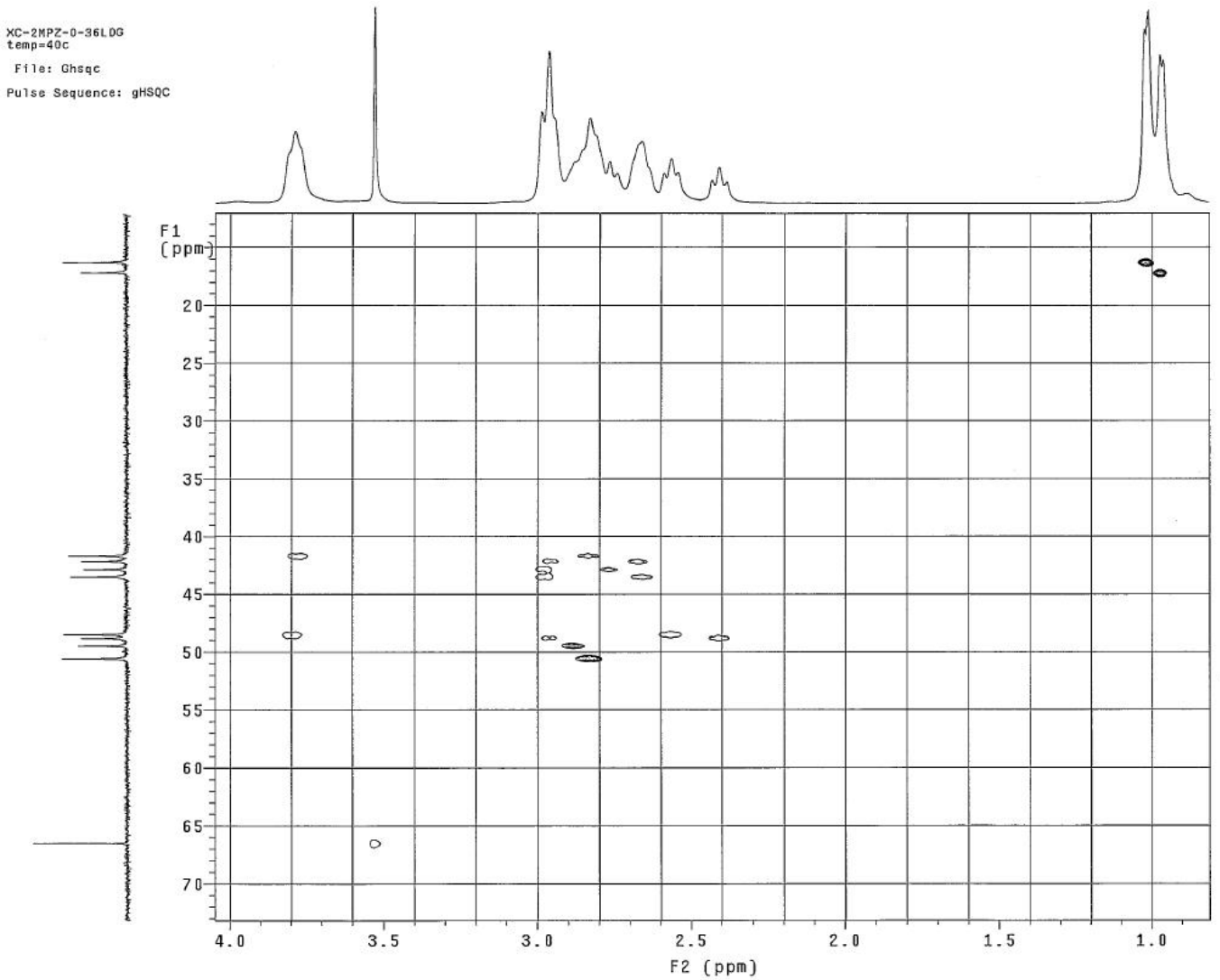

Figure 8: ^{1}H-^{13}C Correlation for 8 m 2MPZ, α = 0.33 mol/mol alkalinity, T = 40 °C

Absorption/Desorption rates in MEDA

In Figure 9, absorption/desorption rates for 8 m MEDA at 40, 60, 80, and 100 °C are compared with those of 12 m EDA, 7 m MEA, and 8 m PZ at 40 °C. At Lean CO_2 partial pressure of 0.1 kPa, CO_2 absorption in MEDA is faster than that in MEA and EDA, but slower than that in PZ. As CO_2 equilibrium partial pressure was increased to 0.5 kPa, the MEDA rate dropped to a value similar to that of EDA and MEA. It is thus inferred that the effect of methyl group is only significant at lean CO_2 loading, and diminishes as more CO_2 is absorbed.

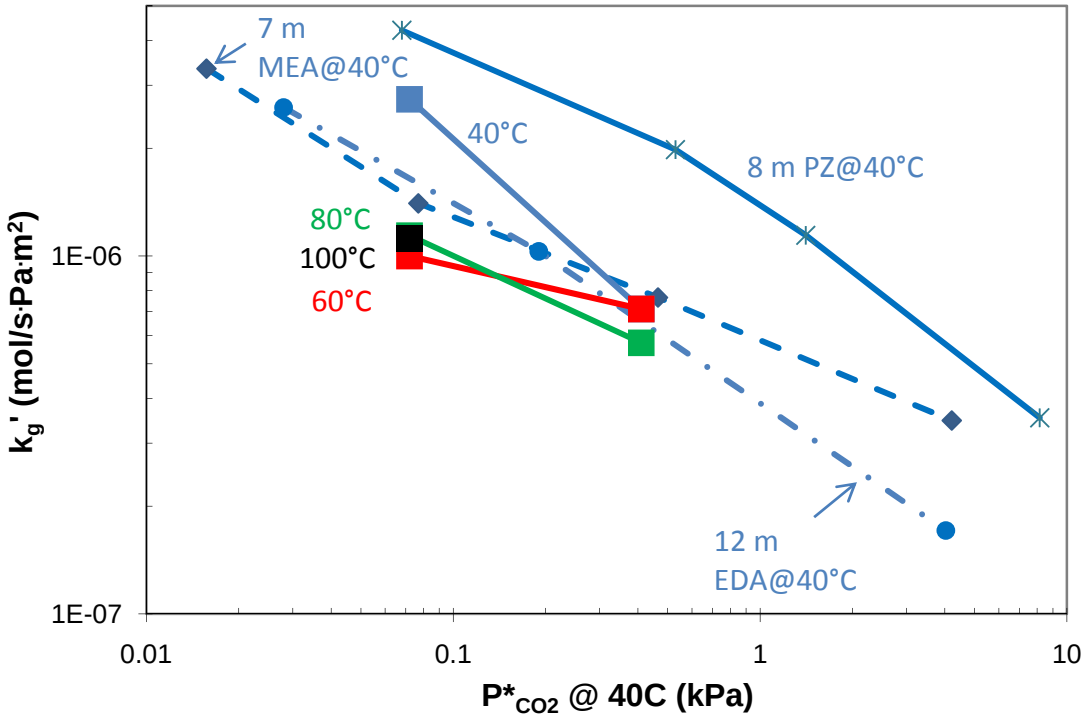

Figure 9: CO_2 mass transfer rate for 8 m 1,2-diaminopropane

Table 5: CO_2 solubility and kg' at different temperatures for 8 m MEDA

Temp (°C)	CO_2 Loading (mol/mol alka)	P_{CO2} (kPa)	kg' ($\times 10^7$mol/s·Pa·m^2)
40	0.357	0.07	27.4
40	0.417	0.41	7.1
60	0.357	0.63	10.0
60	0.417	3.57	7.1
80	0.357	4.07	11.4
80	0.417	16.5	5.7
100	0.357	21.5	11.2

Due to a crystallization problem at higher loading, experimental data were only obtained at two loadings for 8 m 1,2-diaminopropane solution. Consequently, heat of absorption and CO_2 capacity cannot be calculated. Compared at the same CO_2 loading, 8 m MEDA has a slightly higher CO_2 partial pressure than 12 m EDA. This is due to the lower stability of MEDA carbamate as was expected.

Conclusions

In 2-methylpiperazine aqueous solution at CO_2 loading of 0.33 mol/mol alkalinity and 40 °C, 4-carboxyl-2-methylpiperazine or its protonated form accounts for 51% of the original amine, while the amount of 1-carboxyl-2-methylpiperazine is only 1/6 of that of 4-carboxyl-2-methylpiperazine. The amount of dicarbamate is 3% of the original amine and very little bicarbonate was found in this loaded solution. The addition of the methyl group makes the formation of carbamate less likely on the neighboring amino group.

CO_2 solubility and absorption rate for 8 m 1,2-diaminopropane (MEDA) at two lean loadings were measured with the WWC. At CO_2 partial pressure of 0.1 kPa, 8 m MEDA has an absorption rate about half that of 8 m PZ, but twice as large as those of 7 m MEA and 12 m EDA. However, as CO_2 partial pressure is increased to 0.5 kPa, CO_2 absorption in MEDA is approximately as fast as that in MEA and EDA. Crystallization occurs in 8 m MEDA at CO_2 loading richer than 0.42 mol/mol alkalinity.

Future work

More quantitative ^{13}C NMR will be performed on 2MPZ loaded solution at CO_2 loading of 0.1 and 0.25 mol/mol alkalinity to determine the species distribution over a broader range of CO_2 loading. This information will be used for establishing a valid thermodynamic model for the 2MPZ-CO_2-water system.

Amine screening efforts will be continued on N-methyl-1,3-propanediamine (MAPA) and other PZ blends.

References

Hilliard MD. *A Predictive Thermodynamic Model for an Aqueous Blend of Potassium Carbonate, Piperazine, and Monoethanolamine for Carbon Dioxide Capture from Flue Gas.* The University of Texas at Austin. Ph.D. Dissertation. 2008;1083.

CO_2 Rates with Amino Acids

Quarterly Report for April 1 – June 30, 2010

by Le Li

Supported by the Luminant Carbon Management Program

and the

Industrial Associates Program for CO_2 Capture by Aqueous Absorption

Department of Chemical Engineering

The University of Texas at Austin

July 6, 2010

Abstract

Two amino acid solvents, 6 m GlyK and 6 m sarcosine, were tested for their potential for CO_2 absorption during this quarter. The CO_2 solubility and absorption/desorption rates for these solvents were measured using the wetted wall column. 6 m GlyK was tested at three loading conditions (α: 0.33, 0.41, 0.45). A rich loading could not be reached since the 6 m GlyK solvent begins to precipitate around 0.5 CO_2 loading. The absorption rate for 6 m GlyK is competitive with 7 m MEA at low loading but decreases quickly as CO_2 loading increases. The theoretically predicted capacity of 6 m GlyK is 75% of the capacity for 7 m MEA, and the theoretical heat of absorption at the rich loading condition for 6 m GlyK is 15% lower than 7 m MEA. Thus, GlyK solvents are not competitive against 7 m MEA based on all parameters tested. 6 m sarcosine was tested at six loading conditions (α: 0.2, 0.3, 0.36, 0.45, 0.49, 0.55). As a CO_2 absorption solvent, 6 m sarcosine is not attractive in terms of capacity or heat of absorption, having a lower value for both parameters when compared to 7 m MEA and 6 m GlyK. 6 m sarcosine is attractive in terms of absorption rate, which is significantly higher than 7 m MEA and both GlyK solvents at rich loading conditions. A literature review on amino acid solvents was also conducted this quarter, with a summary of the key articles reviewed included in this report.

Introduction

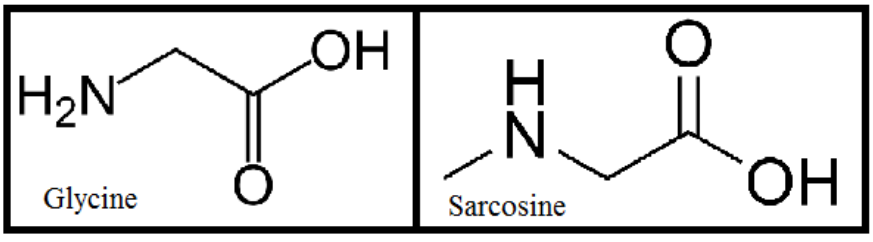

Figure 1: Chemical Structure of Glycine and Sarcosine

Amino acid solvents were investigated for CO_2 absorption using the wetted wall column during this quarter. The two solvents tested were 6 m glycine and 6 m sarcosine. The structures of these two amino acids are shown in Figure 1. Glycine was tested using the wetted wall column during the last quarter at a concentration of 3.55 m, which was chosen to ensure solvent

solubility upon CO_2 loading. Since 3.55 m is too low in concentration compared to the industry standard of 7 m MEA, glycine was tested again at the 6 m concentration. A new amino acid, sarcosine, was also tested this quarter at a concentration of 6 m. For both amino acids, the solvent was formulated by neutralizing the amino acid with an equimolar amount of KOH in water.

A brief background on amino acid solvents for CO_2 absorption was introduced in the last quarterly report, including basic chemistry, advantages, and unique characteristics. During this quarter, a comprehensive literature review was performed on amino acids as a solvent group. The scientific articles relevant to the application of amino acids solvents in CO_2 capture are summarized below.

Literature Review

Hook (1997)

This is the earliest published work which focuses on the screening of various amino acids for CO_2 absorption. The amino acids tested were: glycine, alanine, Alkazid M (N-methyl alanine), methylamino propionic acid, methyl-2 (methylamino) propionic acid, and 2-methyl-2-[2'(-hyroxyethyl)-1'-(amino)] propionic acid. Absorption and desorption experiments were conducted using laboratory scale apparatuses that are similar to a stirred cell setup. Only qualitative conclusions on the absorption/desorption rates were made from the experimental data, where the rates of the amino acid solvents are compared against the rates of MEA and AMP. All experiments were conducted using solvents at 2.5 M amino acid concentration. Crystallization upon CO_2 loading was observed for several amino acids at this concentration. The author proposed a relationship between the position of methyl groups and the crystallization behavior of the solvent.

University of Twente

The published works on amino acid solvents from The University of Twente are summarized in Table 1. The research efforts initially focused on the analysis of taurine solvents for CO_2 absorption. The majority of the data reported are physical properties of the solvents, which includes: density, viscosity, diffusivity of the solvent in water, critical CO_2 loadings, and solid precipitant analysis (Kumar, 2001; 2003). Conventional absorption/desorption experiments were conducted using only N_2O, directly measuring the diffusivity of N_2O, solubility of N_2O, and the physical mass transfer coefficient of N_2O into taurine solvents. All of the analysis regarding the solubility of CO_2 into taurine solvents was derived from applying the N_2O-CO_2 analogy to the N_2O. A CO_2-taurine reaction kinetics study was performed using a stirred cell apparatus, and the reaction rates were reported and the mechanism of the reaction analyzed (Kumar, 2003). The only other experiment reported where CO_2 was used as the absorbent gas was a membrane contactor study. While CO_2 absorption rate data was reported from this experiment, the measured values are specific for the conditions in a membrane fiber contactor (Kumar, 2002).

Table 1: Journal Publications on Amino Acid Solvents from the University of Twente

Amino Acid	Base	Concen (M)	Temperature (K)	α_{CO2}	Properties Analyzed	Author Year
Taurine Glycine	K	0.5–4	293–328 295	/	Solubility, diffusivity, density, viscousity, D_{NO2}	Kumar 2001
(N/A) Taurine	K	1.0 – 2	295	0–0.32	Absorption in membrane fiber contactor	Kumar 2002
Taurine	K	1.0 – 4	298	0–0.7	Critical loading for solubility; K_2CO_3 effect; kL·a of N_2O; solids analysis (^{13}C NMR)	Kumar 2003
Taurine Glycine	K	0.1 – 4	285, 295, 305 295	/	Reaction rate constant	Kumar 2003
Glycine	K	0.1-3	293–313	/	Density, viscosity, N_2O solubility, k_{app}	Portugal 2007
β-alanine, 6-aminohexanoic acid Taurine Glycine Methionine Phenylala-nine Glutamic acid Aspartic acid	/	/	293-353	/	Dissociation constant K, thermodynamic properties	Hamborg 2007
Taurine Glycine Sarcosine Proline	K	0 – 3	293–368	/	Solvent diffusion coefficient; diffusivity of N_2O	Hamborg 2008
Threonine	K	0.1 – 3	293–313	/	Density, viscosity, D_{N2O}, N_2O solubility, physical mass transfer coefficient, reaction kinetics	Portugal 2008
β-alanine, 6-aminohexanoic acid, Arginine, Aspartic acid, Glutamic acid, Methionine, Phenylalanine, Proline, Sarcosine	K	0.25-3.5	298–333	/	Density, viscosity, physical solubility of N_2O	Holst 2008
Alanine Sarcosine Proline Taurine	K, Na, Li	Saturation	293–313	/	Saturation concentration; conditions effecting solubility	Majchrowics 2009

Recent amino acid works at the University of Twente includes a major screening effort using a wide range of amino acids (Hamborg, 2007, 2008; Holst, 2008; Majchrowics, 2009). The reported properties for the amino acids are: solvent density, viscosity, solvent solubility, thermodynamic parameters, diffusivity of N_2O, and the physical solubility of N_2O. There were no experiments reported where CO_2 was used as the gas phase in these screening works. A more in-depth effort was invested in the analysis of two amino acids: glycine and threonine. The study of these two amino acid solvents was within the scope of the earlier taurine study. The data available for these solvents include: density and viscosity measurements, physical solubility of N_2O, and the kinetic rate analysis using a stirred cell reactor (Portugal, 2007, 2008).

Table 2: Journal Publications on Amino Acid Solvents from Various Research Institutes

Amino Acid	Base	Concentration	T(K)	α_{CO2}	Properties Analyzed	Year/Author/ Institution
Glycine	Na	10–50 wt %	303–353	/	Density, viscosity, surface tension, physical solubility, D_{N2O}, kinetics, $E_{Activation}$	2005-2007/ Lee/ Yonsei University
Glycine	K	1–3 (M)	303–323	/	Membrane wetting, mass transfer rate	2007/ Yan / Zhejiang Univ., China
Glycine	Na	10–30 wt %	298–353	0.5–3.5	Density, CO_2 solubility	2009/Harris/ Universiti Teknologi Petronas, Malaysia
Sarcosine	K, MAPA	3.5M 5M	313–353	0.1–0.6	CO_2 solubility, speciation	2010/Aronu/ NTNU

Other Works

Among other published amino acid works, glycine was studied by three research groups. Researchers at Yonsei University in South Korea conducted experiments very similar in scope to the studies at the University of Twente. The reported analyses include the measurement of physiochemical properties and the diffusivity and solubility of N_2O in glycine solvents. All of the reported CO_2 absorption data were generated using the N_2O analogy without performing experiments using CO_2 in the gas phase (Lee, 2005, 2006, 2007). The glycine studies at the Universiti Teknologi Petronas in Malaysia included direct CO_2 solubility measurements obtained using an equilibrium cell (Harris, 2009). Sarcosine is currently being studied at Norwegian University of Science and Technology, where the CO_2 solubility of loaded sarcosine solvents is measured in an equilibrium cell (Aronu, 2010).

While Tables 1 and 2 summarize the majority of the scientific publications on amino acid solvents, there are also industrial reports on various amino acid-based solvents. However, these

data are more difficult to procure and systematically summarize, and therefore have not been reviewed in an organized manner. It is obvious from the research that there have been very few experiments performed with amino acid solvents using CO_2 as the gas phase. A majority of the work done uses N_2O in the experiments and performs the N_2O analogy to report CO_2 solubility and diffusivity. There is a lack of absorption rate measurements among the available data for amino acid solvents, particularly at CO_2 loaded conditions.

Experimental Methods

The absorption rate measurements and CO_2 solubility data were obtained using the wetted wall column. The method is identical to that used by Dugas (2009).

Materials

Table 3: Materials Used for Potassium Glycinate Solvent Preparation

Chemical	Purity	Source
Glycine	98.50%	Fisher BioReagents
Sarcosine	98.00%	Acros Organics
Potassium Hydroxide	87.00%	Fisher Chemical
DDI Water	100.00%	Millipore, Direct-Q

Table 4: Chemical Species Present in 6 m Potassium Glycinate Initial Solution

Chemical Species	Mass (g)	Wt %
Glycine	472.9	25.2%
Potassium Hydroxide	354.2	18.87%
Water	1050.33	55.95%
GlyK (Salt)	719.76	38.34%

Table 5: Chemical Species Present in 6 m Potassium Sarcosine Initial Solution

Chemical Species	Mass (g)	Wt%
Sarcosine	534	29.315%
Potassium Hydroxide	336.63	18.48%
Water	892	48.97%
SarK (salt)	768.6	42.2%

All chemicals used in the preparation of the solvents are listed in Table 3. The amino acid solvents of 6 m glycine and 6 m sarcosine were prepared by mixing equimolar amounts of amino

acid with potassium hydroxide (KOH) in water. The mass of each species present in the initial 6 m glycine and 6 m sarcosine solutions is shown in Tables 4 and 5. Gaseous CO_2 (99.99%, Matheson Tri-Gas) was loaded into the initial solution to reach the lowest loading condition. More CO_2 were added to the solvent after each experiment to reach the next loading condition.

Results and Discussion

Solvent Solubility Observations

6 m GlyK is not soluble at room temperature at CO_2 loading of 0.5 and above. The solution becomes more soluble as temperature increases. However, a rigorous analysis has not been performed to outline the relationship between temperature, loading, and solubility for this solvent. It was also observed that at the 0.41 and 0.45 loading conditions, the solvent began to crystallize at 80 °C. The solid crystals disappeared after the solvent was heated to 100 °C for both loading conditions.

Absorption/Desorption Rates

The liquid mass transfer coefficient (k_g') was measured for the 6 m GlyK solution at 40 °C, 60 °C, 80 °C, and 100 °C for three CO_2 loading conditions below the solvent solubility limit. Figure 2 compares the 6 m GlyK results to the rates for 7 m MEA and 3.55 m GlyK. The 6 m GlyK solution has similar absorption rates as 7 m MEA and 3.55 m GlyK at the two lower loading conditions. The absorption rate for 6 m GlyK decreases much faster than 3.55 m GlyK and 7 m MEA as loading increases.

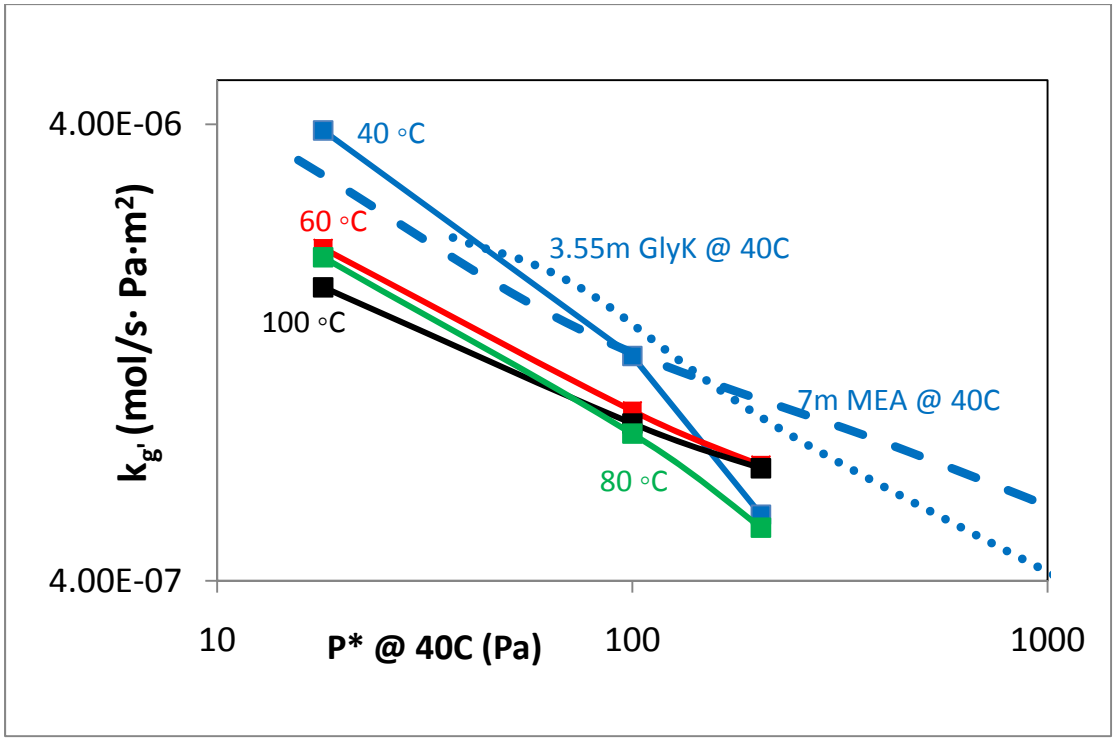

Figure 2: CO_2 Liquid Phase Mass Transfer Coefficient (k_g') for 6 m GlyK

6 m sarcosine solution was tested for absorption rates at 6 loading conditions. The measured k_g' values at the 4 high loading conditions are plotted in Figure 3 against the 7 m MEA results. 6 m

sarcosine shows competitive rate performance against 7 m MEA across the entire range of CO_2 loadings tested. The k_g' for 6 m sarcosine does not decrease at a significantly fast rate as observed for 6 m glycine.

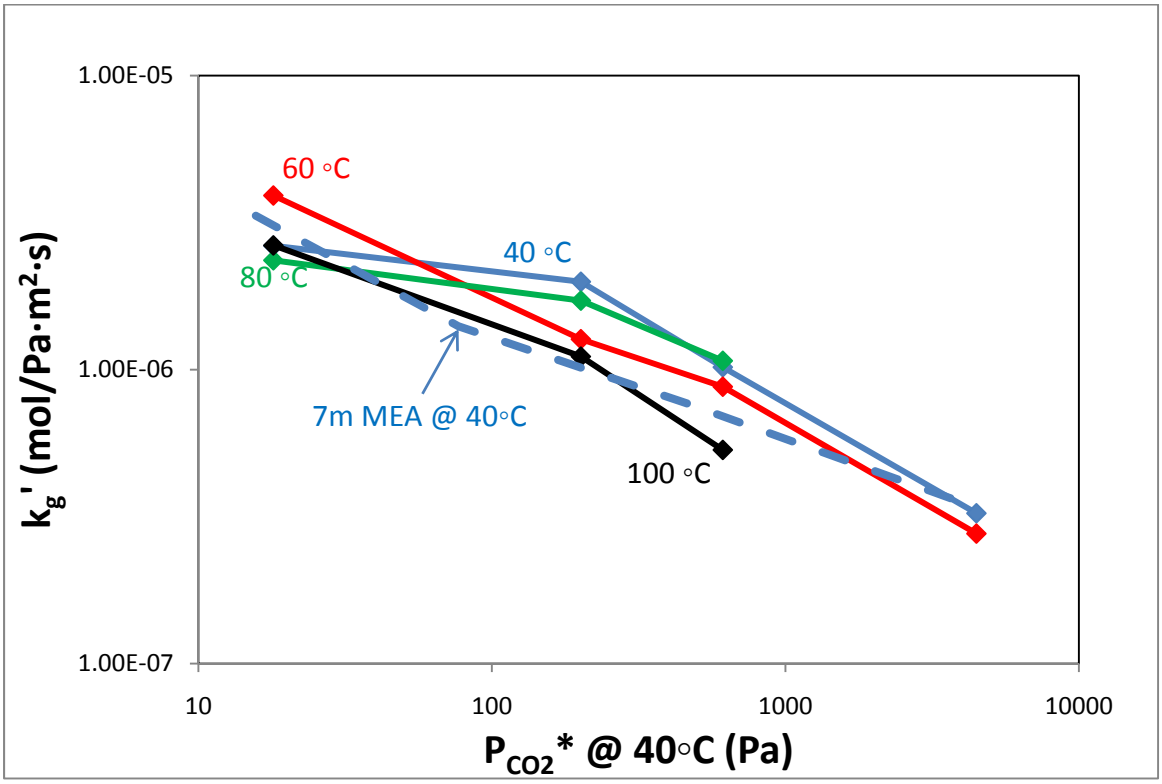

Figure 3: CO_2 Liquid Phase Mass Transfer Coefficient (k_g') for 6 m Sarcosine(K)

CO_2 Solubility

Since for primary and secondary amines the CO_2 solubility of the solvent is independent of amine concentration, the CO_2 solubility results for 3.55 m and 6 m GlyK were analyzed together. The CO_2 solubility results for 3.55 m GlyK were reported in the prevous quarterly report (Rochelle, 2010). The CO_2 equilibrium partial pressure for both GlyK systems taken at four temperatures and seven loading conditions are shown in Figure 4, where the filled data points are results from 3.55 m GlyK and the empty data points are 6 m GlyK data. To generate a thermodyanmic model for this solvent system which relates CO_2 equilibrium with CO_2 loading, the following semi-empirical equation is used:

$$\ln(P) = a + b/T + c \cdot \alpha + d \cdot \alpha / T + e \cdot \alpha^2 \quad (1)$$

The CO_2 partial pressures measured for both concentrations were regressed together to fit Equation 1. The four data points measured at the 4.8 loading for the 3.55 m GlyK solvent were left out of the regression analysis since they are potential outliers. The results of the regression analysis are shown as solid lines in Figure 4 and compared against the results for 7 m MEA at 40 °C and 100 °C (shown as dotted lines). It can be seen that the CO_2 equilibrium partial pressure for GlyK solvents is lower than for 7 m MEA across the loading range tested.

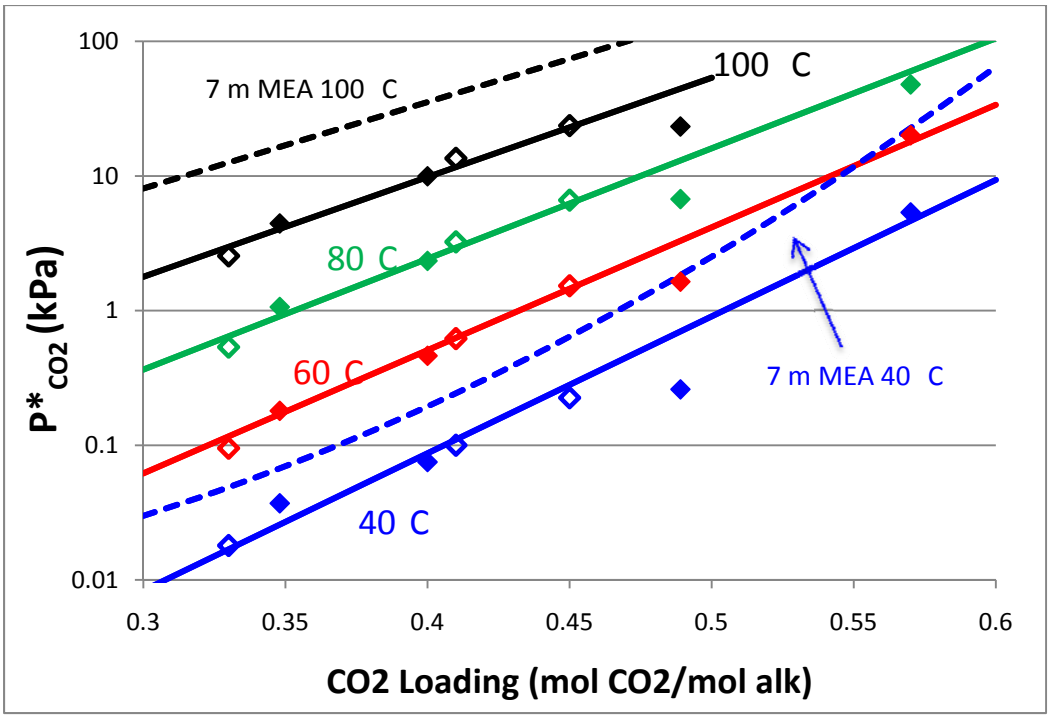

Figure 4: CO_2 Solubility Measured for GlyK

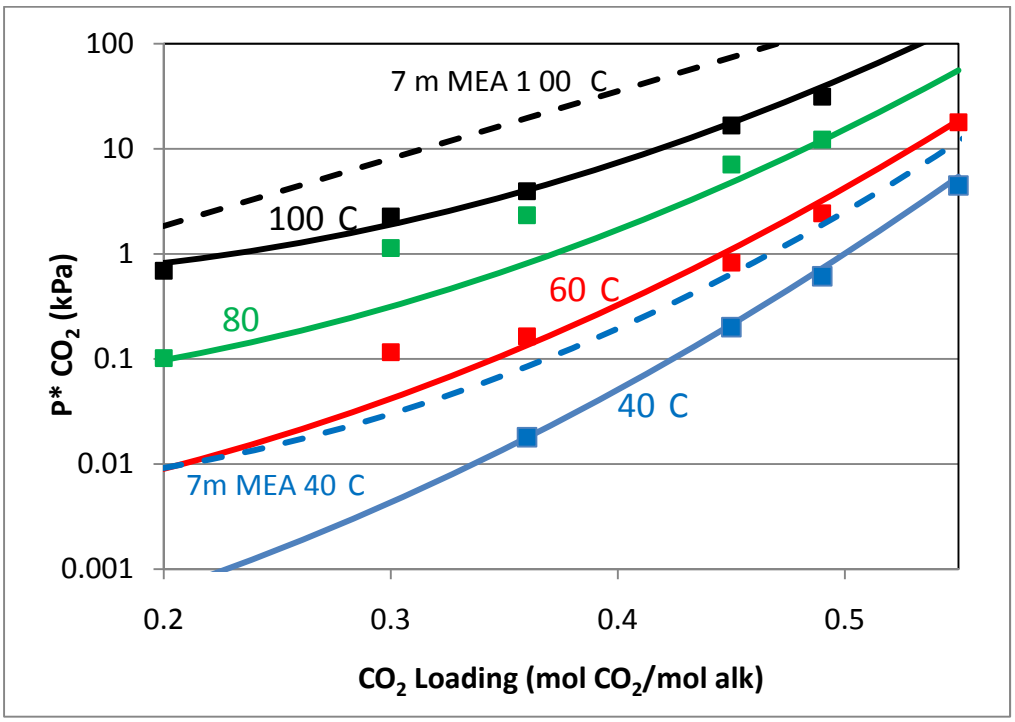

Figure 5: CO_2 Solubility Measured for 6 m Sarcosine(K)

The CO_2 solubility of 6 m sarcosine was measured at four temperatures and six loading conditions, the results are plotted on Figure 4 as solid data points. The measured equilibrium CO_2 partial pressure values at 80 °C are much higher than expected at the 0.3 and 0.36 loading

conditions. The data point taken at the 0.3 loading condition and 60 °C also has a much higher value than expected. This inconsistency can be explained by some equipment instabilities experienced during the experiment. Therefore, these three points were not included during the analysis of the data set. A thermodynamic model was generated for 6 m sarcosine by regressing the data set to fit the semi-empirical expression shown in Equation 1. The resulting equilibrium curves are shown in Figure 4 as the solid lines. The regressed model fits the measured data points well with the exception of the three inconsistent points mentioned earlier. The CO_2 equilibrium partial pressure for 6 m sarcosine is much lower than 7 m MEA across the entire loading range and temperature tested.

The experimentally measured values of k_g' and CO_2 partial pressures for 6 m GlyK are summarized in Table 6, and 6 m sarcosine results are shown in Table 7.

Table 6: CO_2 Solubility and k_g' Measured at Various Loading and Temperatures for 6 m Potassium Glycinate

Loading	Temperature	k_g'	P^*_{CO2}
(mol CO_2/mol alk)	(°C)	(X 10^7 mol/Pa·s·m^2)	(kPa)
0.33	40	38.79	0.018
0.41	40	12.43	0.1
0.45	40	5.58	0.204
0.33	60	21.40	0.095
0.41	60	9.42	0.62
0.45	60	7.16	1.531
0.33	80	17.58	0.536
0.41	80	8.84	3.243
0.45	80	7.06	6.619
0.33	100	20.45	2.549
0.41	100	8.40	13.529
0.45	100	5.23	23.675

Table 7: CO_2 Solubility and k_g' Measured at Various Loading and Temperatures for 6 m Potassium Sarcosine

Loading	Temperature	k_g'	P^*_{CO2}
(mol CO_2/mol alk)	(°C)	(X 10^7 mol /s· Pa·m^2)	(kPa)
0.36	40	26.40	0.018
0.45	40	19.91	0.201
0.49	40	10.20	0.612
0.55	40	3.25	4.477
0.3	60	64.83	0.116
0.36	60	39.10	0.164
0.45	60	12.69	0.826
0.49	60	8.75	2.43
0.55	60	2.77	17.877
0.2	80	78.90	0.102
0.3	80	46.19	1.136
0.36	80	23.56	2.33
0.45	80	17.17	7.096
0.49	80	10.72	12.26
0.2	100	87.16	0.691
0.3	100	50.94	2.266
0.36	100	26.48	3.947
0.45	100	11.08	16.699
0.49	100	5.33	31.295

CO_2 Capacity

The CO_2 capacity of a solvent is determined by taking the difference in loading between the CO_2 rich condition and the CO_2 lean condition. The rich and lean conditions for a solvent are the CO_2 loadings which correspond to CO_2 equilibrium partial pressures of 5 kPa and 0.5 kPa, respectively. The values of 5 kPa and 0.5 kPa were chosen for conventional amine solvents in order to ensure a proper driving force to remove 90% CO_2 from a coal fired power plant (12% CO_2). Amino acid solvents, however, exhibit unique characteristics that are different from conventional amines. Particularly, many amino acid solvents precipitate as the CO_2 loading increases, which greatly limits the operation of these solvents at high loading conditions. Also, the absorption rate and heat of absorption decreased significantly as CO_2 loading increased for the GlyK system (at both 3.55 m and 6 m concentrations). To overcome these operational disadvantages, the rich and lean loadings for amino acid solvents are redefined to CO_2 partial pressures of 1 kPa and 0.1 kPa. This new operation range corresponds to a much leaner CO_2 loading range, which not only allows amino acid solvents to operate under its solubility limit, it also maximizes the absorption rate and heat of absorption of the solvent. Since amino acid solvents should operate under this low CO_2 partial pressure range, they are potentially good candidate solvents for natural gas power plants, which typically have lower CO_2 concentrations in their flue gas.

Heat of Absorption

The heat of absorption for both the GlyK system and 6 m sarcosine are calculated by applying Equation 1 to the following thermodynamic relationship:

$$\Delta H_{Abs} = -R\frac{d\ln P}{d(1/T)} \tag{2}$$

The heat of absorption for both systems was calculated at the midpoint of the operating range (P^*_{CO2}=0.5 kPa), and the values reported in Table 8.

Table 8: Measured Properties of Tested Amino Acid Solvents for CO_2 Absorption

Solvent	Operation Range (P^*_{CO2} kPa)		Capacity (mol CO_2/kg Solution)	k_g' (40 °C) @ Rich Loading ($\times 10^7$ mol CO_2/s·Pa·m^2)	ΔH_{abs} (kJ/mol)
	Lean	Rich			
GlyK (3.55 m)	0.1	1	0.25	4.26	68.74 (@ P_{co2}=0.5kPa)
GlyK (6 m)	0.1	1	0.35*	N/A	68.74* (@ P_{co2}=0.5kPa)
SarK (6 m)	0.1	1	0.27	7.7	66.5 (@ P_{co2}=0.5kPa)
MEA 7 m (Dugas, 2009)	0.5	5	0.47	3.1	82 (@ P_{co2}=1.5kPa)

The measured key absorption parameters for both 6 m GlyK and 6 m sarcosine are summarized in Table 8 and compared against the values for 7 m MEA and 3.55 m GlyK. 6 m GlyK exhibits identical thermodynamic behavior to 3.55 m GlyK, which translates to a lower heat of absorption than 7 m MEA. The 6 m GlyK is expected to have a greater capacity than the 3.55 m solvent, but still not competitive with 7 m MEA. The 6 m GlyK system is limited by the solvent solubility. As a result, the reported heat of absorption and capacity are purely theoretical values, since the solvent cannot be operated at the rich loading condition. The absorption rate at rich loading is not reported for the 6 m GlyK due to this solubility limit of the solvent. 6 m sarcosine has a heat of absorption lower than both 7 m MEA and the GlyK. The capacity of 6 m sarcosine is also much lower than 7 m MEA. However, this solvent is the most attractive in terms of absorption rates, which double the rate for 7 m MEA and is much higher than 3.55 m GlyK.

Conclusions

6 m GlyK is not an attractive solvent for CO_2 absorption, mainly because it is limited by solubility upon CO_2 loading. A rich operation loading condition could not be reached before solids begin to precipitate, which occurred at a CO_2 loading of 0.5. GlyK at 6 m concentration shares the thermodynamic behavior of 3.55 m, which has a heat of absorption 15% lower than 7 m MEA. The capacity calculated for 6 m GlyK is 0.35 mol CO_2/kg solvent, which is 25% lower than 7 m MEA.

The absorption rate of the 6 m GlyK is competitive with 7 m MEA at low loadings, but becomes less attractive as CO_2 loading increases. 6 m GlyK is not comparable to 7 m MEA at rich loadings due to solubility limitations. Based on the observed solid precipitation behavior, it can be suggested that 6 m GlyK operate in the lean loading range.

6 m sarcosine as a CO_2 absorption solvent is not competitive in terms of heat of absorption and capacity. The heat of absorption is 20% lower than 7 m MEA and similar to the GlyK solvents.

At the typical rich loading, 6 m sarcosine absorbs CO_2 two times faster than 7 m MEA and 80% faster than GlyK. 6 m sarcosine is also superior to 6 m GlyK since it does not precipitate at high CO_2 loadings.

Future Work

The screening of various new amino acid solvents for CO_2 absorption will be continued during the next quarter. New amino acids as well as blends of various amino acids are candidates for this screening work. Also, efforts will be invested in changing the base used to neutralize the amino acid solvents and testing the effects of various salts on the CO_2 absorption performance of the solvents. A reliable analytical method for the testing of amino acid concentration in the solvent is yet to be developed, and efforts on this work will be continued during the next quarter.

References

Dugas RE. *Carbon dioxide absorption, desorption, and diffusion in aqueous piperazine and monoethanolamine.* The University of Texas at Austin. Ph.D. Dissertation. 2009.

Hamborg ES, Niederer JPM, Versteeg GF. "Dissociation Constants and Thermodynamic Properties of Amino Acids Used in CO_2 Absorption from (293 to 353) K." *J Chem Eng Data*. 2007;52:2491–2502.

Hamborg ES, van Swaaijj WPM, Versteeg GF. "Diffusivities in Aqueous Solutions of the Potassium Salt of Amino Acids." *J Chem Eng Data*. 2008;53:1141–1145.

Harris F, Kurnia KA, Mutalib MIA, Thanapalan M. "Solubilities of Carbon Dioxide and Densities of Aqueous Sodium Glycinate Solutions before and after CO_2 Absorption." *J Chem Eng Data*. 2009;54:144–147.

Holst JV, Kersten SRA, Hogendoorn KJA. "Physiochemical Properties of Several Aqueous Potassium Amino Acid Salts." *J Chem Eng Data.* 2008;53:1286–1291.

Hook, RJ. "An Investigation of Some Sterically Hindered Amines as Potential Carbon Dioxide Scrubbing Compounds." *Ind Eng Chem Res*. 1997;36:1779–1790.

Kumar PS, Hogendoorn JA, Feron PHM, Versteeg GF. "Density, Viscosity, Solubility, and Diffusivity of N_2O in Aqueous Amino Acid Salt Solutions." *J Chem Eng Data.* 2001;46:1357–1361.

Kumar PS, Hogendoorn JA, Feron PHM, Versteeg GF. "Equilibrium Solubility of CO_2 in Aqueous Potassium Taurate Solutions: Part 1. Crystallization in Carbon Dioxide Loaded Aqueous Salt Solutions of Amino Acids." *Ind Eng Chem Res.* 2003;42:2832–2840.

Kumar PS, Hogendoorn JA, Feron PHM, Versteeg GF. "Kinetics of the Reaction of CO_2 with Aqueous 2 Potassium Salt of Taurine and Glycine." *AIChE J.* 2006;49(1):203–213.

Kumar PS, Hogendoorn JA, Feron PHM, Versteeg GF. "New absorption liquids for the removal of CO_2 from dilute gas streams using membrane contactors." *Chem Eng Sci.* 2002;57:1639–1651.

Lee S, Song HJ, Maken S, Park JW. "Kinetics of CO_2 Absorption in Aqueous Sodium Glycinate Solutions." *Ind Eng Chem Res.* 2007;46:1578–1583.

Lee S, Choi SI, Maken S, Song HJ, Shin HC, Park JW, Jang KR, Kim JH. "Physical Properties of Aqueous Sodium Glycinate Solution as an Absorbent for Carbon Dioxide Removal." *J Chem Eng Data*. 2005;50:1773–1776.

Lee S, Song HJ, Maken S, Shin HC, Song HC, Park JW. "Physical Solubility and Diffusivity of N_2O and CO_2 in Aqueous Sodium Glycinate Solutions." *J Chem Eng Data*. 2006;51:504–509.

Majchrowicz ME, Brilman DWF, Groeneveld MJ. "Precipitation regime for selected amino acid salts for CO_2 capture from flue gases." *Energy Proc*. 2009;1:979–984.

Rochelle GT et al. "CO_2 Capture by Aqueous Absorption, First Quarterly Progress Report 2010." Luminant Carbon Management Program. The University of Texas at Austin. 2010.

Portugal AF, Derks PWJ, Versteeg GF, Magalhães FD, Mendes A. "Characterization of potassium glycinate for carbon dioxide absorption purposes." *Chem Eng Sci*. 2007;62:6534–6547.

Portugal AP, Magalhães FD, Mendes A. "Carbon dioxide absorption kinetics in potassium threonate." *Chem Eng Sci*. 2008;63:3493–3503.

Yan SP, Fang MX, Zhang WF, Wang SY, Xu ZK, Luo ZY, Cen KF. "Experimental study on the separation of CO_2 from flue gas using hollow fiber membrane contactors without wetting." *Fuel Proc Technol*. 2007;88:501–511.

CO_2 Solubility at 100–160 °C in Aqueous Amines

Quarterly Report for April 1 – June 30, 2010

by Qing Xu

Supported by the Luminant Carbon Management Program

and the

Industrial Associates Program for CO_2 Capture by Aqueous Absorption

Department of Chemical Engineering

The University of Texas at Austin

July 2, 2010

Abstract

In this quarter the total pressure was measured at 100–160 °C for CO_2 loaded 1-methyl-piperazine (1MPZ), 2-methyl-piperazine (2MPZ), piperazine (PZ)/2MPZ blend and diglycolamine (DGA®). CO_2 partial pressure was derived from the total pressure data.

Based on the data at 40 to 160 °C, for each solvent an empirical model of CO_2 partial pressure was developed; the heat of absorption of CO_2 is given by the derivative of that expression. In the following equations P_{CO2} is in Pa, T is in K, R is the gas constant in J/mol·K and α is the CO_2 loading.

For 7.7–8 m 1MPZ: $\ln P_{CO_2} = 35.2 - \frac{10344}{T} - 6.4\alpha + 9741\frac{\alpha}{T}$

$$\Delta H_{abs} = -R(-10344 + 9741\alpha) \quad (J/mol\ \mathrm{CO_2})$$

For 6.7–8 m 2MPZ: $\ln P_{CO_2} = 39.8 - \frac{12554}{T} - 19.6\alpha + 14509\frac{\alpha}{T} - 8.1\alpha^2$

$$\Delta H_{abs} = -R(-12554 + 14509\alpha) \quad (J/mol\ \mathrm{CO_2})$$

For 4 m PZ/4 m 2MPZ: $\ln P_{CO_2} = 41.2 - \frac{12998}{T} - 27.0\alpha + 14684\frac{\alpha}{T} + 7.3\alpha^2$

$$\Delta H_{abs} = -R(-12998 + 14684\alpha) \quad (J/mol\ \mathrm{CO_2})$$

For 9.6–10 m DGA®: $\ln P_{CO_2} = 28.1 - \frac{7572}{T} + 67.8\alpha - 25209\frac{\alpha}{T} - 115\alpha^2 + 50113\frac{\alpha^2}{T}$

$$\Delta H_{abs} = -R(-7572 - 25209\alpha + 50113\alpha^2) \quad (J/mol\ \mathrm{CO_2})$$

At the mid-loading where P_{CO2} is 1.5 kPa at 40 °C, the ΔH_{abs} is 69, 66, 66, and 73 kJ/mol CO_2 for 1MPZ, 2MPZ, PZ/2MPZ, and DGA®, respectively.

Introduction

For concentrated piperazine solution, thermal degradation is negligible up to 150 ºC (Freeman et al., 2008). Better energy performance may be obtained by increasing stripper temperature without degradation of PZ (Rochelle et al., 2008). Multi-stage flashes instead of a simple stripper show a better performance by flashing at elevated temperature. Some other configurations for stripping at elevated temperature also give better energy performance than the simple stripper (Rochelle et al., 2010).

For thermally resistant amines such as PZ, 1MPZ, 2MPZ, and DGA®, the stripper temperature can be increased; for amines with relatively high thermal degradation rates, for instance, MEA, stripper temperature is limited but the thermal reclaimer operating temperature is up to 150 ºC. Measurements of CO_2 solubility at high temperature expand the temperature range to 160 °C to get the temperature dependence of CO_2 solubility and the heat of absorption. The data are also important for the design of the high temperature processes.

Experimental Methods

Apparatus

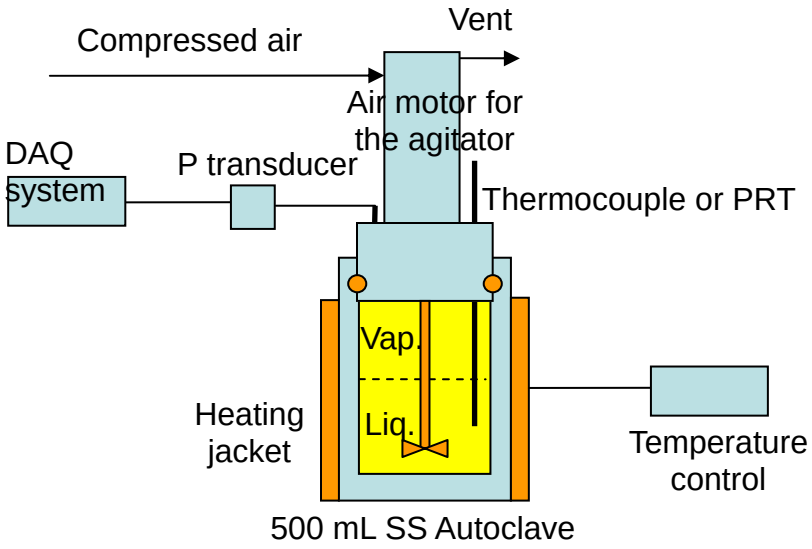

Figure 1: Total Pressure Measurement with an Autoclave

As shown in Figure 1, an autoclave (ZipperClave®, by Autoclave Engineers) was used as the equilibrium cell. Its designed operating range is up to 2000 psia and 232 ºC. The 500 mL pressure vessel is made of 316 SS stainless steel. Closure is effected by a resilient spring member inserted through a circumferential groove in the body and cover (Autoclave Engineers). A magnetic hollow shaft agitator (MAG075, MagneDrive II Series, by Autoclave Engineers) was used to get equilibrium without leaking to the atmosphere. It was driven by a compressed air motor (2AM-NCC-16, by Gast®). The agitator circulates both liquid and vapor phases.

Temperature was controlled by a Fuji Electric PXZ-4 temperature controller, with connection to a K-type thermocouple placed inside the thermal well of the autoclave.

A pressure transducer (Druck® PTX 611, 0-30 bar absolute) was connected to a signal converter and a data logger NI USB 6009; LabView® SignalExpress® software was used for data recording.

The pressure reading system was calibrated by a dead weight pressure tester (S/N 19189/278, by Budenberg Volumetrics, INC.).

Before each run, about 300 to 350 mL of the CO_2 loaded aqueous amine solution was prepared and added into the autoclave. To avoid the effects of O_2, N_2 was used to purge air and then the cell was sealed. Initial pressure and temperature readings were recorded for later data correction. Then the cell was heated. Data recording of pressure started at around 100 ºC and the intervals of the data points were 10 ºC. Liquid samples were collected before and after each experiment and analyzed by TIC and acid titration. The agitation rate varied from 1200 RPM to 1800 RPM.

Analyzing methods

Total Inorganic Carbon (TIC)

The concentration of CO_2 in solution was determined by TIC analysis. The liquid samples collected before and after each run were diluted by a factor of 100. About 10–15 μL diluted sample was injected into a CO_2 analyzer (Model 525, Horiba PIR 2000). Details can be found in Appendix B.2 of Hilliard's dissertation (2008).

Acid Titration

The total alkalinity of solution was determined by acid titration using a Metrohm-Peak 835 Titrando equipped with an automatic dispenser, Metrohm-Peak 801 stirrer, and 3M KCl pH probe. Details are available in Appendix A.3 of Hilliard (2008) and Appendix F of Sexton (2008).

Results and Discussion

Results Summary

In this period the total pressure over CO_2 loaded solutions was measured at 100–160 °C for 8 m 1MPZ, 6.7 and 7.6 m 2MPZ, 4 m 2MPZ/4 m PZ blend, and 10 m DGA®. CO_2 partial pressure was calculated by subtracting the partial pressure of N_2 and water from the total pressure. P_{water} was assumed following the Raoult's Law and P_{amine} was neglected. The calculation example is in Appendix 4 of Qing Xu's fourth quarterly report of 2008 (Rochelle et al., 2009a).

The liquid composition has been corrected for 100–160 °C data because the real CO_2 loading in the liquid phase is off from that measured at room temperature, and this difference becomes significant at high temperature and high loading.

All the experiments were performed by Mychal Zipper, an undergraduate research assistant, supervised by Qing Xu.

1MPZ

Table 1: Total Pressure and CO_2 Partial Pressure in 1MPZ

1MPZ(m)	T (ºC)	Loading in liq.	P_t (Pa)	P_{CO2} (Pa)	1MPZ(m)	T (ºC)	Loading in liq.	P_t (Pa)	P_{CO2} (Pa)
7.76	120	0.192	398641	224679	7.66	100	0.246	332583	243669
7.76	130	0.188	617272	380653	7.66	120	0.238	804441	630327
7.76	140	0.183	932039	615549	7.66	130	0.232	1154022	917197
7.76	150	0.178	1320142	903341	7.66	140	0.224	1605983	1289218
7.76	160	0.170	1822934	1281791	7.66	150	0.215	2161104	1743939

1MPZ(m)	T (°C)	Loading in liq.	P_t (Pa)	P_{CO2} (Pa)	1MPZ(m)	T (°C)	Loading in liq.	P_t (Pa)	P_{CO2} (Pa)
					7.66	160	0.205	2813830	2272216

There are 40–100 °C CO_2 solubility data from WWC experiments by Xi Chen (Chen et al., 2010). An empirical model was developed by regressing the low temperature data and the new high temperature data.

$$\ln P_{CO_2} = (35.2 \pm 0.7) - \frac{10344 \pm 234}{T} - (6.4 \pm 3.5)\alpha + (9741 \pm 1197)\frac{\alpha}{T} \quad (1)$$

According to the Gibbs-Helmholtz Equation, the heat of absorption can be derived from the empirical CO_2 partial pressure model.

$$\Delta H_{abs} = -R\frac{\partial \ln P_{CO_2}}{\partial(\frac{1}{T})} = -R(-10344 + 9741\alpha) \quad (J / mol\ CO_2) \quad (2)$$

Figure 2 gives the CO_2 partial pressure over 1MPZ from 40 to 160 °C at various loadings. The model fairly predicts the data.

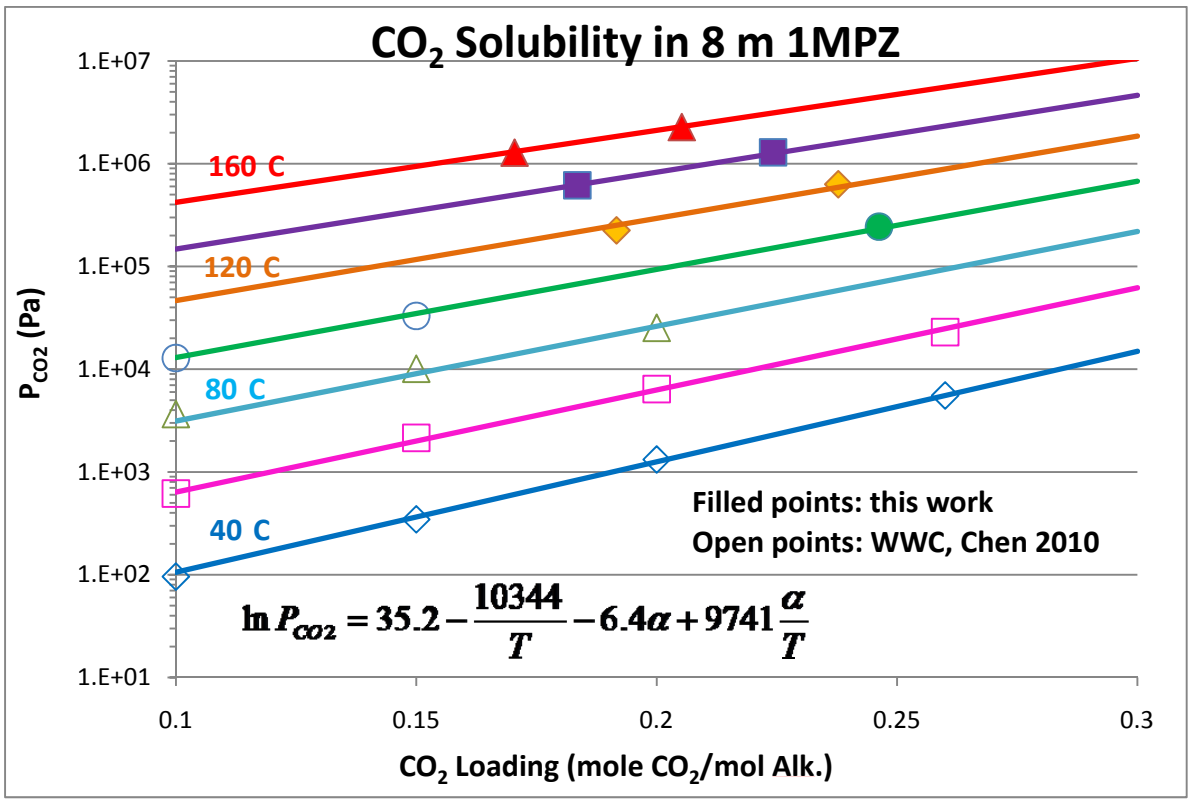

Figure 2: CO_2 Solubility in 1MPZ

2MPZ

Table 2: Total Pressure and CO_2 Partial Pressure in 2MPZ

2MPZ (m)	T (ºC)	Loading in liq.	P_t (Pa)	P_{CO2} (Pa)	2MPZ (m)	T (ºC)	Loading in liq.	P_t (Pa)	P_{CO2} (Pa)
7.61	120	0.279	319424	145028	6.69	100	0.389	295009	204635
7.61	130	0.276	499180	261970	6.69	120	0.379	748053	571081
7.61	140	0.272	766059	448779	6.69	130	0.372	1099721	859007
7.61	150	0.266	1133002	715160	6.69	140	0.363	1568603	1246637
7.61	160	0.258	1668020	1125526	6.69	150	0.353	2132920	1708905
					6.69	160	0.340	2819288	2268781

There are 40–100 °C CO_2 solubility data from WWC experiments by Xi Chen (Rochelle et al., 2010). An empirical model was developed by regressing the low temperature data and the new high temperature data.

$$\ln P_{CO_2} = (39.8 \pm 0.8) - \frac{12554 \pm 262}{T} - (19.6 \pm 3.2)\alpha + (14509 \pm 917)\frac{\alpha}{T} - (8.1 \pm 2.6)\alpha^2 \quad (3)$$

$R^2 = 0.9992$

According to the Gibbs-Helmholtz Equation, the heat of absorption can be derived from the empirical CO_2 partial pressure model.

$$\Delta H_{abs} = -R\frac{\partial \ln P_{CO_2}}{\partial(\frac{1}{T})} = -R(-12554 + 14509\alpha) \quad (J / mol\ CO_2) \quad (4)$$

Figure 3 gives the CO_2 partial pressure over 2MPZ from 40 to 160 °C at various loadings. The model predicts the data well.

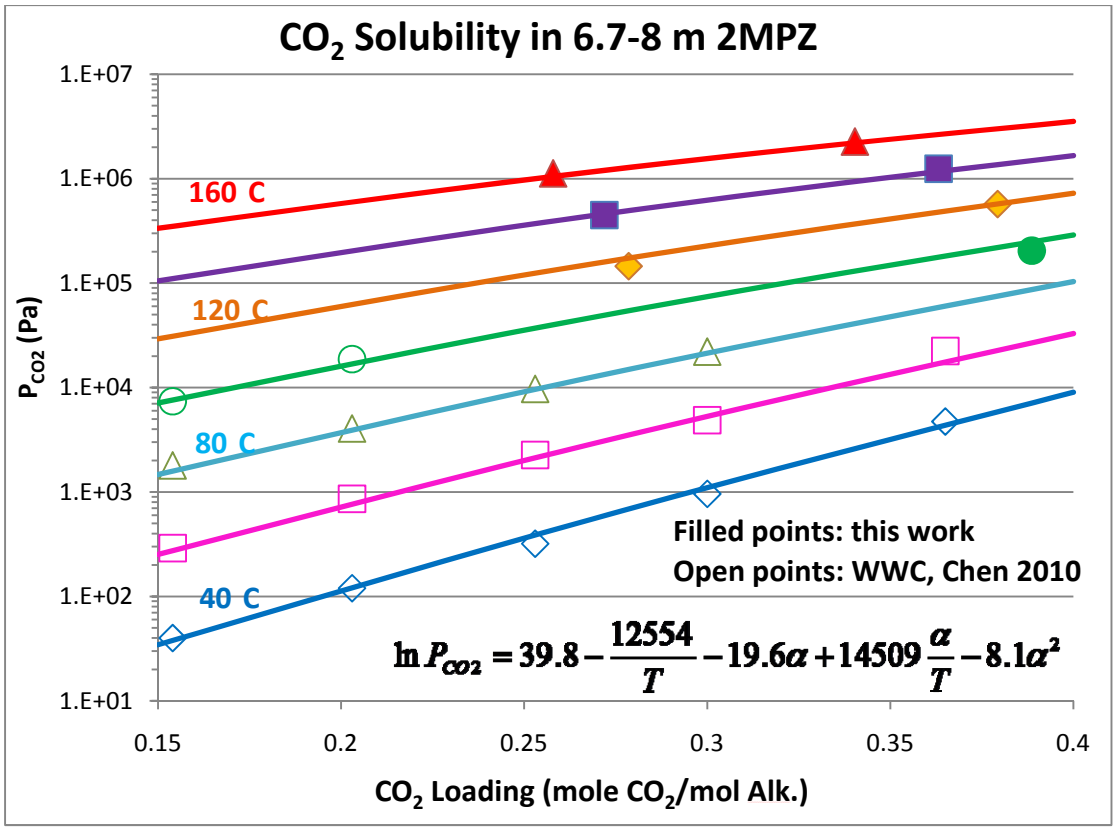

Figure 3: CO_2 Solubility in 2MPZ

PZ/2MPZ

Table 3: Total Pressure and CO_2 Partial Pressure in PZ/2MPZ

PZ/2MPZ (m)*	T (°C)	Loading in liq.	P_t (Pa)	P_{CO2} (Pa)	PZ/2MPZ (m)*	T (°C)	Loading in liq.	P_t (Pa)	P_{CO2} (Pa)
7.63	120	0.306	316326	141986	7.86	100	0.397	315289	226586
7.63	130	0.303	489101	251967	7.86	120	0.389	749728	576026
7.63	140	0.300	744288	427110	7.86	130	0.384	1073061	836796
7.63	150	0.295	1090637	672930	7.86	140	0.376	1517380	1201364
7.63	160	0.288	1553809	1011490	7.86	150	0.369	2001100	1584922
					7.86	160	0.359	2624063	2083730

*: PZ/2MPZ (m) is the total moles of PZ and 2MPZ per kg water. PZ and 2MPZ have approximately the same concentration.

There are 40–100 °C CO_2 solubility data from WWC experiments by Xi Chen (Rochelle et al., 2010). An empirical model was developed by regressing the low temperature data and the new high temperature data.

$$\ln P_{CO_2} = (41.2 \pm 0.8) - \frac{12998 \pm 238}{T} - (27.0 \pm 2.8)\alpha + (14684 \pm 746)\frac{\alpha}{T} + (7.3 \pm 2.4)\alpha^2 \quad (5)$$

According to the Gibbs-Helmholtz Equation, the heat of absorption can be derived from the empirical CO_2 partial pressure model.

$$\Delta H_{abs} = -R\frac{\partial \ln P_{CO_2}}{\partial(\frac{1}{T})} = -R(-12998 + 14684\alpha) \quad (J/mol\ CO_2) \tag{6}$$

Figure 4 gives the CO_2 partial pressure over PZ/2MPZ from 40 to 160 °C at various loadings. The model fairly predicts the data.

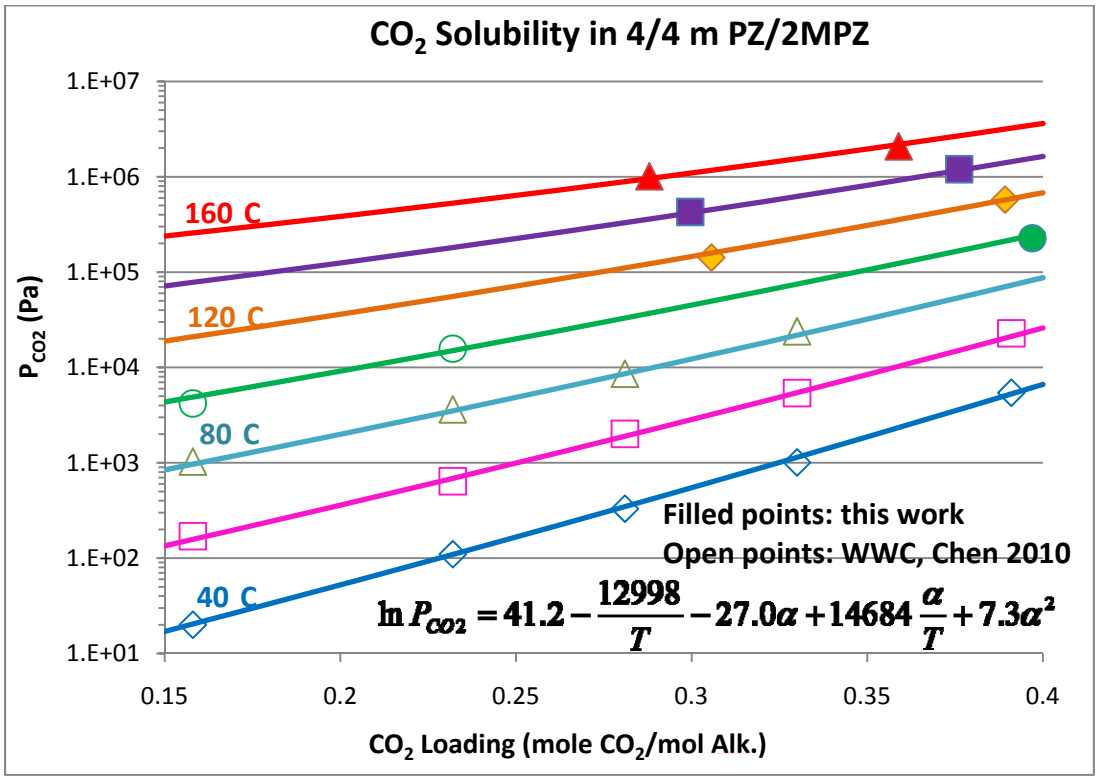

Figure 4: CO_2 Solubility in PZ/2MPZ

DGA®

Table 4: Total Pressure and CO_2 Partial Pressure in DGA®

DGA® (m)	T (°C)	Loading in liq.	P_t (Pa)	P_{CO2} (Pa)	DGA® (m)	T (°C)	Loading in liq.	P_t (Pa)	P_{CO2} (Pa)
9.55	100	0.410	143780	57390	9.60	100	0.488	442294	355970
9.55	120	0.402	421264	252093	9.60	120	0.473	900635	731592
9.55	130	0.396	647135	417032	9.60	130	0.463	1220248	990319
9.55	140	0.387	969565	661791	9.60	140	0.450	1636697	1329156
9.55	150	0.375	1380149	974826	9.60	150	0.437	2104106	1699089
9.55	160	0.361	1885160	1358919	9.60	160	0.421	2676015	2150173

There are 40–100 °C CO_2 solubility data from WWC experiments by Xi Chen (Rochelle et al.,

2009b). An empirical model was developed by regressing the low temperature data and the new high temperature data.

$$\ln P_{CO_2} = (28.1 \pm 1.3) - \frac{7572 \pm 376}{T} + (67.8 \pm 10.0)\alpha - (25209 \pm 3383)\frac{\alpha}{T} - (115 \pm 18)\alpha^2 + (50113 \pm 6361)\frac{\alpha^2}{T} \quad (7)$$

According to the Gibbs-Helmholtz Equation, the heat of absorption can be derived from the empirical CO_2 partial pressure model.

$$\Delta H_{abs} = -R\frac{\partial \ln P_{CO_2}}{\partial(\frac{1}{T})} = -R(-7572 - 25209\alpha + 50113\alpha^2) \quad (J/mol\ CO_2) \quad (8)$$

Figure 4 gives the CO_2 partial pressure over DGA® from 40 to 160 °C at various loadings. The model fairly predicts most of the data but over-predicts the 160 °C solubility.

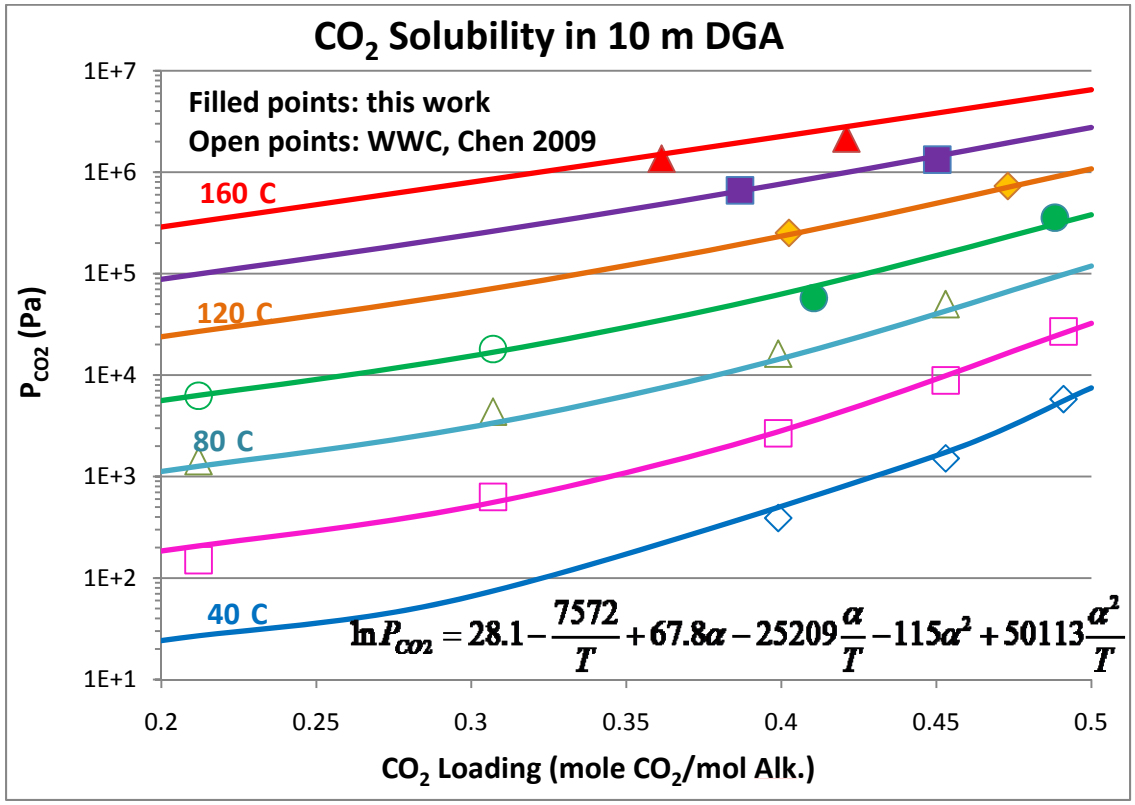

Figure 5: CO_2 Solubility in DGA®

Comparison of heat of absorption

Table 5 compares the heat of absorption of CO_2 in PZ, MEA, 1MPZ, 2MPZ, 2MPZ/PZ blend, and DGA®. The PZ and MEA empirical models are from previous regression work (Rochelle et al., 2010). The loadings are defined as moles of CO_2 per mole alkalinity. Therefore for MEA

and DGA®, the loading $\alpha = \frac{CO_2(mol)}{MEA\ or\ DGA(mol)}$; for PZ, 1MPZ, 2MPZ, and PZ/2MPZ, $\alpha = \frac{CO_2(mol)}{amine\ (mol)\cdot 2}$.

MEA and DGA® have the highest ΔH_{abs}, while PZ and PZ derivatives have similar ΔH_{abs}.

Table 5: Comparison of the heat of absorption of CO_2

Solvent	ΔH_{abs} (J/mol CO_2)	ΔH_{abs} (kJ/mol CO_2)*	Mid-loading**
3.5–13 m MEA	$-R(-12189+1130\alpha+12845\alpha^2)$	72±4	0.486
0.9–12 m PZ	$-R(-11011+4789\alpha+9765\alpha^2)$	67±2	0.357
7.7–8 m 1MPZ	$-R(-10344+9741\alpha)$	69±3	0.207
6.7–8 m 2MPZ	$-R(-12554+14509\alpha)$	66±3	0.314
4/4 m PZ/2MPZ	$-R(-12998+14684\alpha)$	66±3	0.341
9.6–10 m DGA®	$-R(-7572-25209\alpha+50113\alpha^2)$	73±3	0.447

*: The heat of absorption of CO_2 at mid-loading.
**: The loading where P_{CO2} is 1.5 kPa at 40 °C, calculated from the 40–160 °C empirical models.

Conclusions

In this quarter the total pressure was measured at 100–160 °C for CO_2 loaded 1MPZ, 2MPZ, PZ/2MPZ, and DGA®. CO_2 solubility data was generated from the total pressure and empirical models were developed. The empirical models predict the data. At 160 °C, CO_2 partial pressure is 12.8 and 22.7 bar over 0.17 and 0.21 loading 8 m 1MPZ, 11.3 bar over 0.26 loading 7.6 m 2MPZ, 22.7 bar over 0.34 loading 6.7 m 2MPZ, 10.1 and 20.8 bar over 0.29 and 0.36 loading 4 m PZ/4 m 2MPZ blend, 13.6 and 21.5 bar over 0.36 and 0.42 loading 10 m DGA®.

The heat of absorption was derived from the P_{CO2} empirical models. Among the screened 4 solvents as well as MEA and PZ, MEA and DGA® have the highest ΔH_{abs}, while PZ and PZ derivatives have similar lower ΔH_{abs}. At the mid-loading where P_{CO2} is 1.5 kPa at 40 °C, the ΔH_{abs} are 69, 66, 66, 73 kJ/mol CO_2 for 1MPZ, 2MPZ, PZ/2MPZ, and DGA, respectively.

Future Work

The following work is proposed for the next quarter:

Build up a single vapor pass VLE apparatus with an oil bath as the temperature control. Test the new apparatus and measure VLE for CO_2 loaded MEA and PZ. The scheme of the new apparatus is shown in Figure 6.

Repeat some of the total pressure measurements for CO_2 loaded PZ and MEA. Vary the amine concentration and the loading.

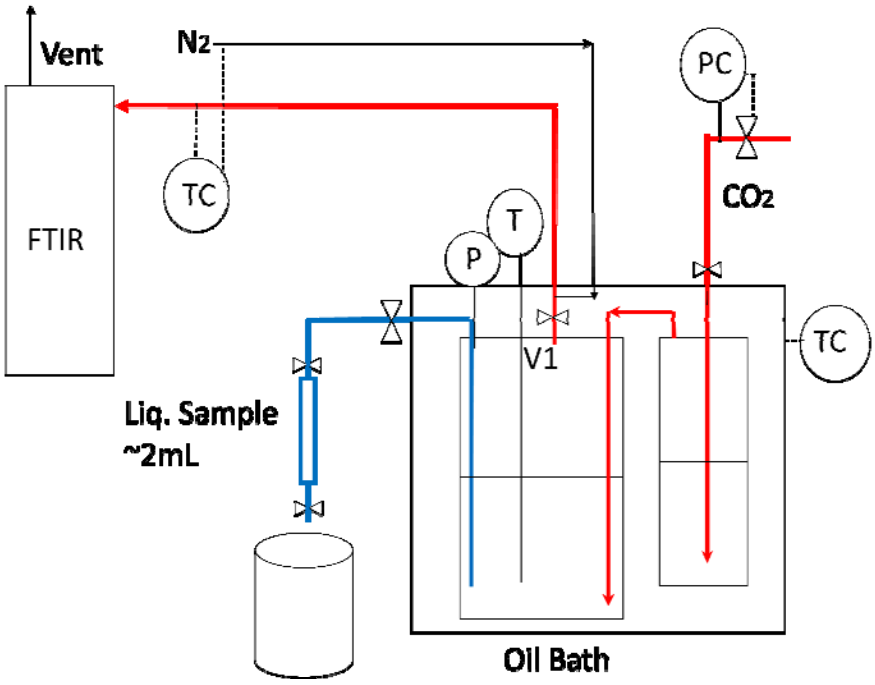

Figure 6: Scheme of the Single Vapor Pass VLE Apparatus with an Oil Bath

Red: vapor passing line; blue: liquid sampling line

References

Autoclave Engineers®, Zipperclave® 500&1000 mL stirred reactor, http://www.autoclaveengineers.com/ae_pdfs/SR_500_1000_Zip.pdf

Chen X, Rochelle GT. "Aqueous Piperazine Derivatives for CO_2 Capture: Accurate Screening by a Wetted Wall Column". *Chem Eng Res Des.* 2010, submitted.

DIPPR, 1998-Provo, UT: BYU DIPPR, Thermophysical Properties Laboratory, 1998-Version 13.0.

Freeman SA, Dugas R, Van Wagener D, Nguyen T, Rochelle GT. "Carbon dioxide capture with concentrated, aqueous piperazine." *GHGT-9*, Washington D.C. 2008.

Hilliard MD. *A Predictive Thermodynamic Model for an Aqueous Blend of Potassium Carbonate, Piperazine, and Monoethanolamine for Carbon Dioxide Capture from Flue Gas.* The University of Texas at Austin. Ph.D. Dissertation. 2008.

Rochelle GT et al. "CO_2 Capture by Aqueous Absorption, Third Quarterly Progress Report 2008." Luminant Carbon Management Program. The University of Texas at Austin. 2008.

Rochelle GT et al. "CO_2 Capture by Aqueous Absorption, Second Quarterly Progress Report 2009." Luminant Carbon Management Program. The University of Texas at Austin. 2009a.

Rochelle GT et al. "CO_2 Capture by Aqueous Absorption, Third Quarterly Progress Report 2009." Luminant Carbon Management Program. The University of Texas at Austin. 2009b.

Rochelle GT et al. "CO_2 Capture by Aqueous Absorption, Fourth Quarterly Progress Report 2009." Luminant Carbon Management Program. The University of Texas at Austin. 2010.

Sexton AJ. *Amine Oxidation in CO_2 Capture Processes*. The University of Texas at Austin. Ph.D. Dissertation. 2008.

Amine Volatility

Quarterly Report for April 1 – June 30, 2010

by Thu Nguyen

Supported by the Luminant Carbon Management Program

and the

Industrial Associates Program for CO_2 Capture by Aqueous Absorption

Department of Chemical Engineering

The University of Texas at Austin

July 1, 2010

Abstract

This progress report discusses two main experimental objectives of this past quarter: (1) speciation study of loaded 8 m PZ system as a function of loading and temperature, (2) volatility of loaded 8 m PZ system. 8 m PZ speciation was analyzed using NMR technique. 8 m PZ volatility measurement was made with a hot gas FTIR.

In 8 m PZ-CO_2-H_2O at either 27 ºC or 40 ºC, the PZ/PZH^+ species dominates at nominal lean loading and accounts for 0.37 to 0.47 of total PZ. At richer loading, PZ carbamate dominates with 0.43–0.53 of total PZ. PZ dicarbamate is found to exist at a fraction of ~0.1 of the total PZ present. Bicarbonate and carbonate species are the least prevalent in solution at a ratio of ~0.03 moles of total carbon to total PZ.

PZ volatility in 8 m PZ-CO_2-H_2O is approximately 0.11 and 0.78 Pa at nominal lean and rich loading corresponding to ~500 Pa and 5,000 Pa at 40 ºC. The PZ apparent activity coefficient varies from ~0.001 to 0.02 for this system over the nominal range of loading from 40 to 65 ºC.

Introduction

The first part of this report discusses NMR analysis for 8 m PZ-CO_2-H_2O systems with loadings of 0.25, 0.3, and 0.4 mol CO_2/equivalent PZ at 27 ºC and 40 ºC. The loadings of 0.3 and 0.4 mol CO_2/equivalent PZ are considered to be the nominal lean and rich loading for corresponding to about 500 and 5,000 Pa of CO_2 partial pressure. NMR analysis measures the ionic and molecular species in solution and provides understanding on how volatility changes with CO_2 loading. Temperature also drives speciation which, in turn, affects volatility. Amine concentration drives speciation as well, although it was not studied at this point. The speciation for loaded 8 m PZ-CO_2-H_2O includes PZ/PZH^+, $PZ(COO)^-$/$H^+PZ(COO)^-$, $PZ(COO)_2^-$, HCO_3^-/CO_3^{2-}. Note each individual species and its protonated form are not distinguished separately by NMR due to the fast exchange of the proton between the species and its protonated counterpart.

This report also presents the volatility of loaded 8 m PZ compared to 10 m PZ for nominal lean and rich loading from 40 ºC to 65 ºC. The apparent amine activity coefficient is given as a function of temperature, loading, and amine concentration. Any deviation of the apparent amine activity coefficient from 1 indicates non-ideal solution behavior.

Experimental Methods

Amine Volatility Measurements

Amine volatility was measured in a stirred reactor coupled with a hot gas FTIR analyzer (Fourier Transform Infrared Spectroscopy, Temet Gasmet Dx-4000) as shown in Figure 1.

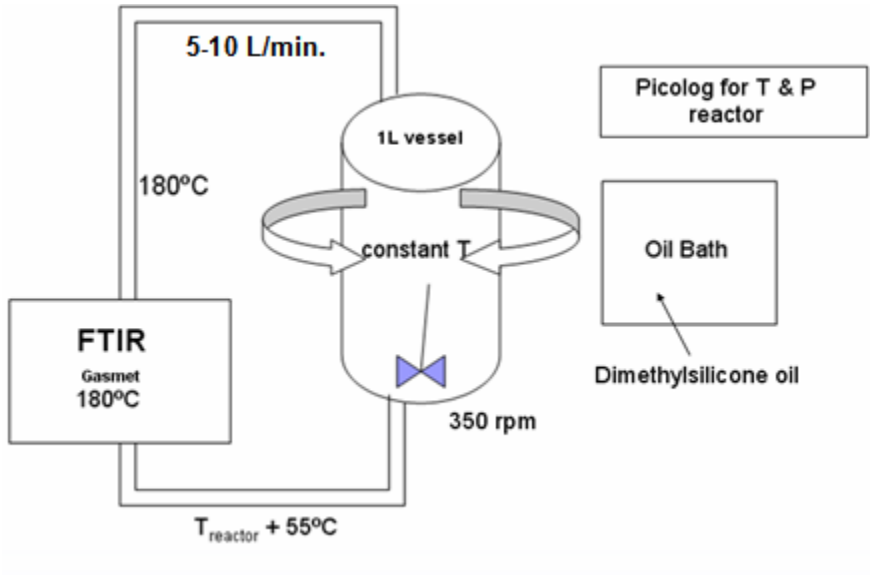

Figure 1: Amine Volatility Experimental Setup

The 1 L glass reactor was agitated at 350 rpm. Temperature in the reactor was controlled by circulating dimethylsilicone oil. The reactor was insulated with thick aluminum foil. Vapor from the headspace of the reactor, primarily 5–10 L/min., was circulated by a heated sample pump to the FTIR through a heated Teflon line. Both the line and analyzer were maintained at 180 ºC to prevent possible condensation or adsorption of amine. The FTIR measured amine, CO_2, and water concentration in the gas. After the gas passed through the FTIR, it was returned to the reactor through a heated line maintained ~55 ºC hotter than the reactor. It was determined that the 55 ºC difference was sufficient to ensure that the return gas does not upset the solution that is in equilibrium with the gas inside the reactor, and to prevent potential heat loss at the bottom of the reactor.

Amine Concentration

The amine concentration was determined by acid titration (Hilliard, 2008) with an automatic Titrando series titrator with an automatic equivalence point detection. A 300X diluted sample was titrated with 0.1 N H_2SO_4 to a pH of 2.4. The amount of acid needed to reach the equivalence point at a pH of 3.9 was used to calculate the total amine concentration.

Loading Verification

The loadings of solutions are verified by using Total Inorganic Carbon (TIC) analysis. The samples are diluted in H_2O and subsequently dissolved in 30 wt % H_3PO_4 to release aqueous carbon-containing products. The CO_2 is carried by an N_2 stream to an infrared detector which analyzes and reports the CO_2 composition as voltage. The resulting voltage peaks are integrated

and correlated to CO_2 concentrations using a 1000 ppm inorganic carbon standard made from a mixture of potassium carbonate and potassium bicarbonate (Ricca Chemical, Pequannock, NJ).

NMR Preparation and Analysis

A batch amine-water solution, roughly 5–10 g, is prepared and subsequently mixed with 1 wt % of 1,4-dioxane and roughly 10 wt % of deuterium oxide. Dioxane serves as an internal reference, while the deuterium oxide acts as a resonance lock for field stabilization to prevent the NMR signal of the sample from being swamped by that of the solvent. The solution is then loaded with $^{13}CO_2$ (99% purity, Cambridge Isotopes Laboratory) using a mini glass sparging apparatus until the desired loading is achieved. Next, the loaded solution is transferred into an NMR tube (Wilmad glass, 5 mm OD x 0.77 mm ID) which is then sealed thermally. The NMR analysis is performed with a Varian INOVA 500 MHZ NMR Spectrometer with variable temperature control. Samples at 40 °C and 60 °C are conditioned by heating for at least 1 hour in a water bath at the temperature of interest prior to NMR analysis.

Theory

Amine Volatility in Loaded Amine-H_2O-CO_2

For loaded amine-water-CO_2, the amine volatility is interpreted as the amine apparent activity coefficient. From the Modified Raoult's Law this quantity is computed as follows:

$$\gamma_{amine} = P_{amine} / (x_{amine} * P°_{amine}) \quad (2)$$

where:

γ_{amine} is the symmetric activity coefficient of the amine
P_{amine} is the partial pressure of the amine in the gas
x_{amine} is the liquid phase mole fraction of the amine
$P°_{amine}$ is the vapor pressure of the amine at a given temperature.

NMR

In NMR the structure and functional groups of a molecule contribute to the way the molecule will behave when placed in a magnetic field. An NMR spectrum is a plot of the absorbance energy by a molecule as a function of the frequency. This frequency has units of PPM relative to the operating frequency of the NMR spectrometer and is commonly referred to as the chemical shift, δ. In this section, the molecular structure for each species present in this study has been identified and the active nuclei (proton or carbon) for each molecule have been labeled accordingly, as shown in Figures 2–8.

Proton NMR

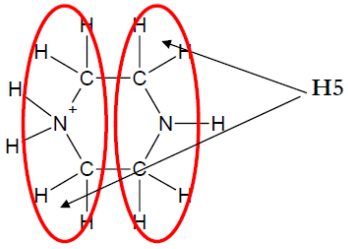

Figure 2: Molecular structure and Active Proton Nuclei of PZ and PZH^+

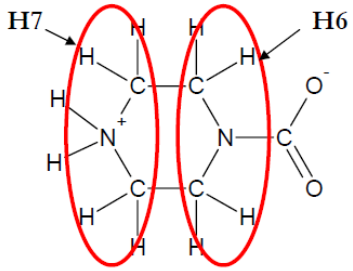

Figure 3: Molecular structure and Active Proton Nuclei of $PZCOO^-$ and H^+PZCOO^-

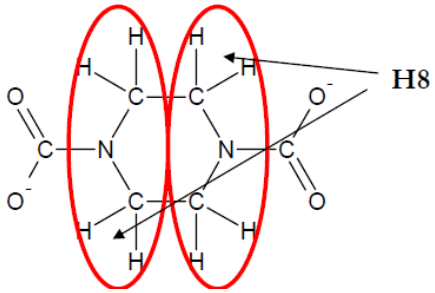

Figure 4: Molecular structure and Active Proton Nuclei of $PZ(COO^-)_2$

^{13}C NMR

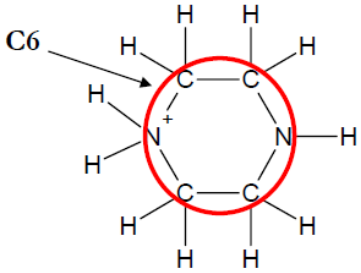

Figure 5: Molecular Structure and Active Carbon Nuclei of PZ and PZH^+

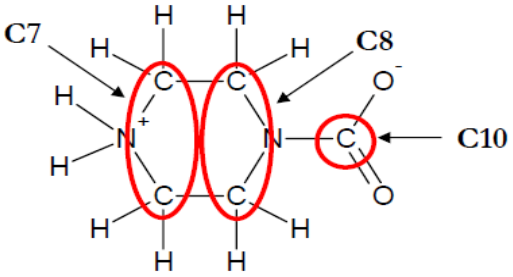

Figure 6: Molecular Structure and Active Carbon Nuclei of $PZCOO^-$ and H^+PZCOO^-

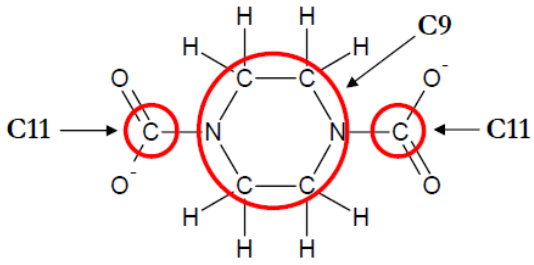

Figure 7: Molecular Structure and Active Carbon Nuclei of $PZ(COO^-)_2$

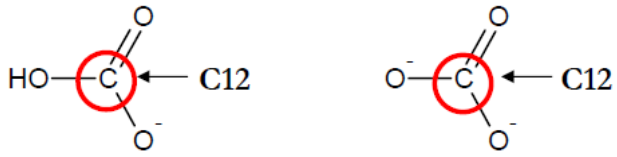

Figure 8: Molecular Structure and Active Carbon Nuclei of HCO_3^- and CO_3^{2-}

Data

Table 1: NMR Speciation Results for Loaded 8 m PZ-CO_2-H_2O

		Fraction of Total Amine			
Loading	**T (°C)**	**PZ/PZH^+**	**$PZ(COO)^-/H^+$**	**$PZ(COO)_2^-$**	**HCO_3^-/CO_3^{2-}**
0.38	40	0.465	0.460	0.075	0.025
0.30	40	0.467	0.438	0.095	0.026
0.23	40	0.563	0.370	0.066	-
0.38	27	0.365	0.534	0.100	0.026
0.30	27	0.471	0.430	0.099	-

loading is defined as moles of CO_2/equivalent of PZ

Table 2: Volatility and CO_2 Solubility for Loaded 8 m PZ-CO_2-H_2O System

PZ (m)	**T (°C)**	**Loading**	**P_{PZ} (Pa)**	**P_{CO2} (Pa)**	**P_{H2O} (Pa)**	**γ_{PZ}**
8.17	40	0.260	1.28	115	5762	0.0093
8.17	45	0.260	2.25	172	7252	0.0122
8.17	50	0.260	3.59	349	9338	0.0147
8.17	55	0.260	5.89	513	11921	0.0184
8.17	60	0.260	8.33	707	14703	0.0200
8.17	65	0.260	11.12	1120	18677	0.0208
7.96	40	0.293	0.78	410	5889	0.0059
7.96	45	0.293	1.30	599	7486	0.0073
7.96	50	0.293	2.22	944	9583	0.0094
7.96	55	0.293	3.42	1331	12378	0.0110
7.96	60	0.293	5.58	1844	15572	0.0138

7.96	65	0.293	8.07	3031	19365	0.0155
7.96	70	0.293	11.94	4051	24556	0.0180
7.93	40	0.395	0.11	8187	5918	0.0008
7.93	45	0.395	0.16	11737	7595	0.0009
7.93	50	0.395	0.29	15979	9765	0.0013
7.93	55	0.395	0.56	20121	12428	0.0019
7.93	60	0.395	1.09	23968	15486	0.0028
7.93	65	0.395	1.95	28308	20319	0.0038

loading is defined as moles of CO_2/equivalent of PZ

Results

NMR Speciation for 8 m PZ-CO_2-H_2O at Nominal Loading

Figure 9 shows the NMR speciation of 8 m PZ-CO_2-H_2O at 40 ºC over a range of nominal lean and rich loading. These results are also compared to those of 2 m PZ-CO_2-H_2O at 27 ºC to illustrate speciation differences due to changes in temperature and amine concentration (Hilliard, 2008).

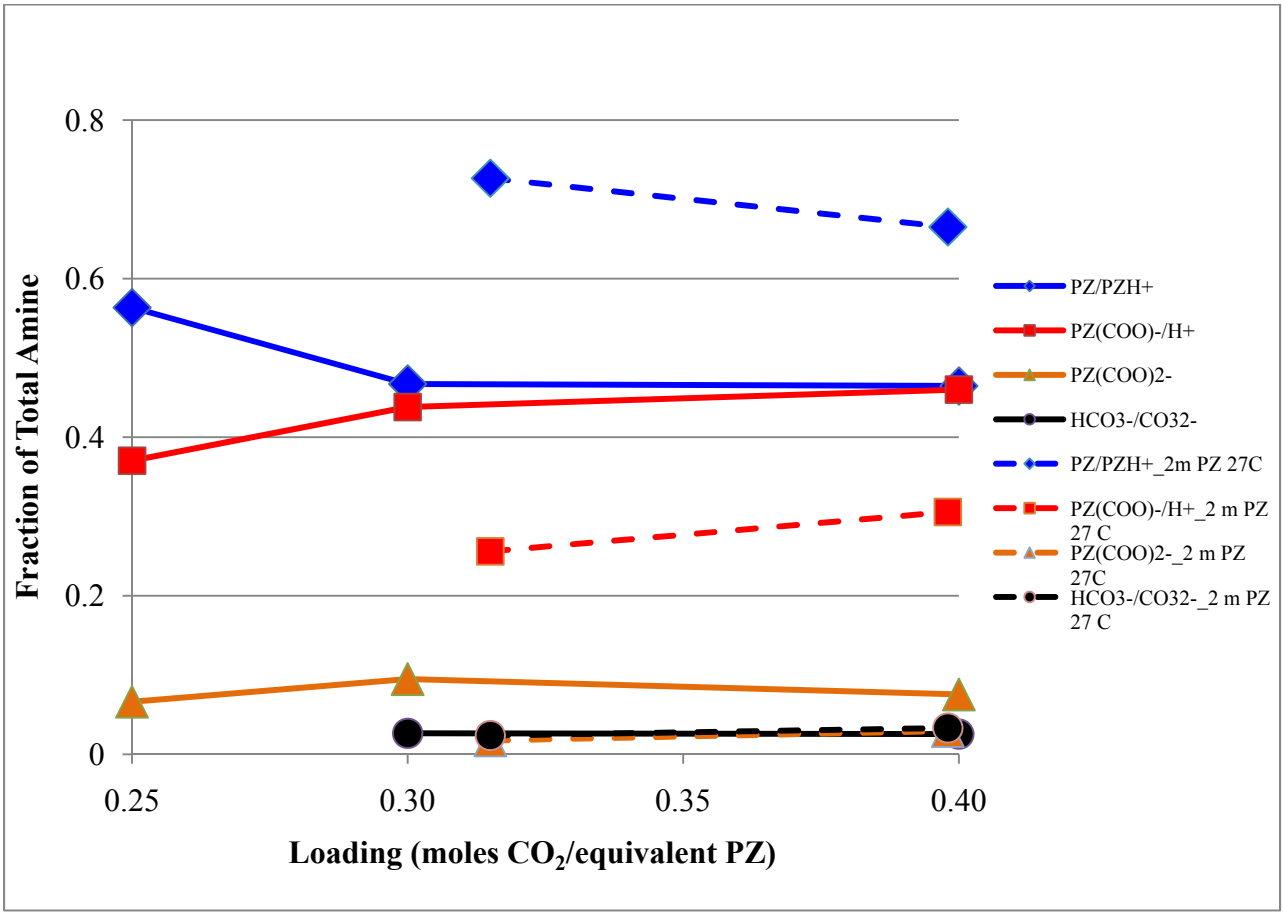

Figure 9: NMR Speciation of Loaded 8 m PZ at 40 ºC versus Loaded 2 m PZ at 27 ºC

For both PZ systems, PZ/PZH^+ is the dominant species, followed by $PZ(COO)^-/H^+$ over the loading range depicted. As CO_2 loading is increased, the concentration of free/protonated PZ decreases as more PZ carbamate is formed. This speciation behavior is responsible for PZ volatility decreasing as loading is increased. $PZ(COO)_2^-$ comprises a very small fraction of the total amine in a loaded 8 m PZ system whereas its presence is practically negligible in loaded 2 m PZ system. HCO_3^-/CO_3^{2-} species is the least prevalent species in both systems and is present at negligible fraction.

Figure 10 presents the speciation of loaded 8 m PZ system compared to that of 2 m PZ at 27 ºC.

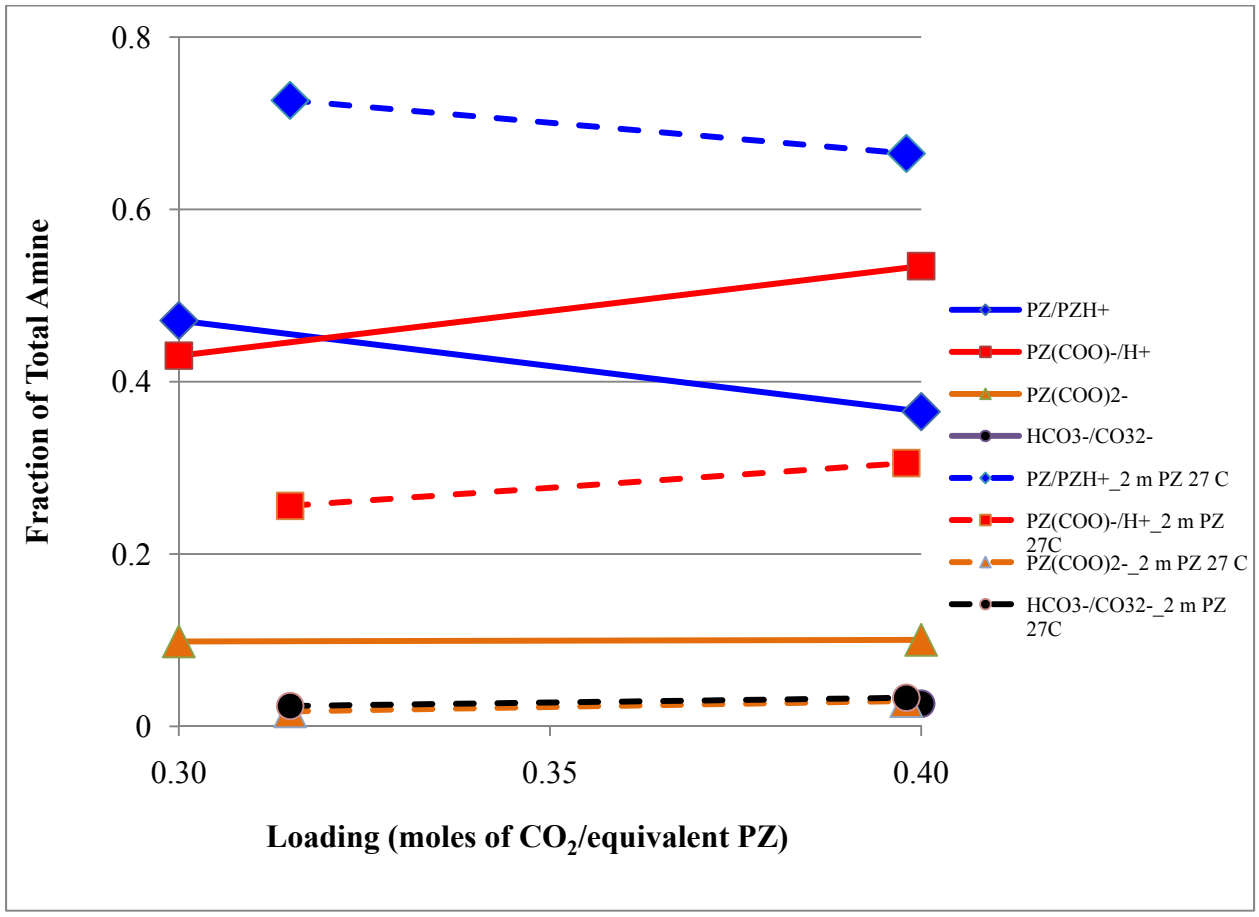

Figure 10: NMR Speciation of Loaded 8 m PZ versus Loaded 2 m PZ at 27 ºC

As loading is increased, the amount of free and protonated PZ species in both systems decreases as more PZ carbamate is being generated. In a loaded 8 m PZ system, the amount of PZ dicarbamate is much more appreciable than in a loaded 2 m PZ system. Both bicarbonate and carbonate species are present in negligible amounts in both loaded systems.

PZ Volatility in 8 m PZ-CO_2-H_2O System

Figure 11 shows the volatility of PZ expressed as the apparent PZ activity coefficient in 8 m PZ-CO_2-H_2O. This parameter is compared to that of 10 m PZ-CO_2-H_2O over the same range of temperature and loading.

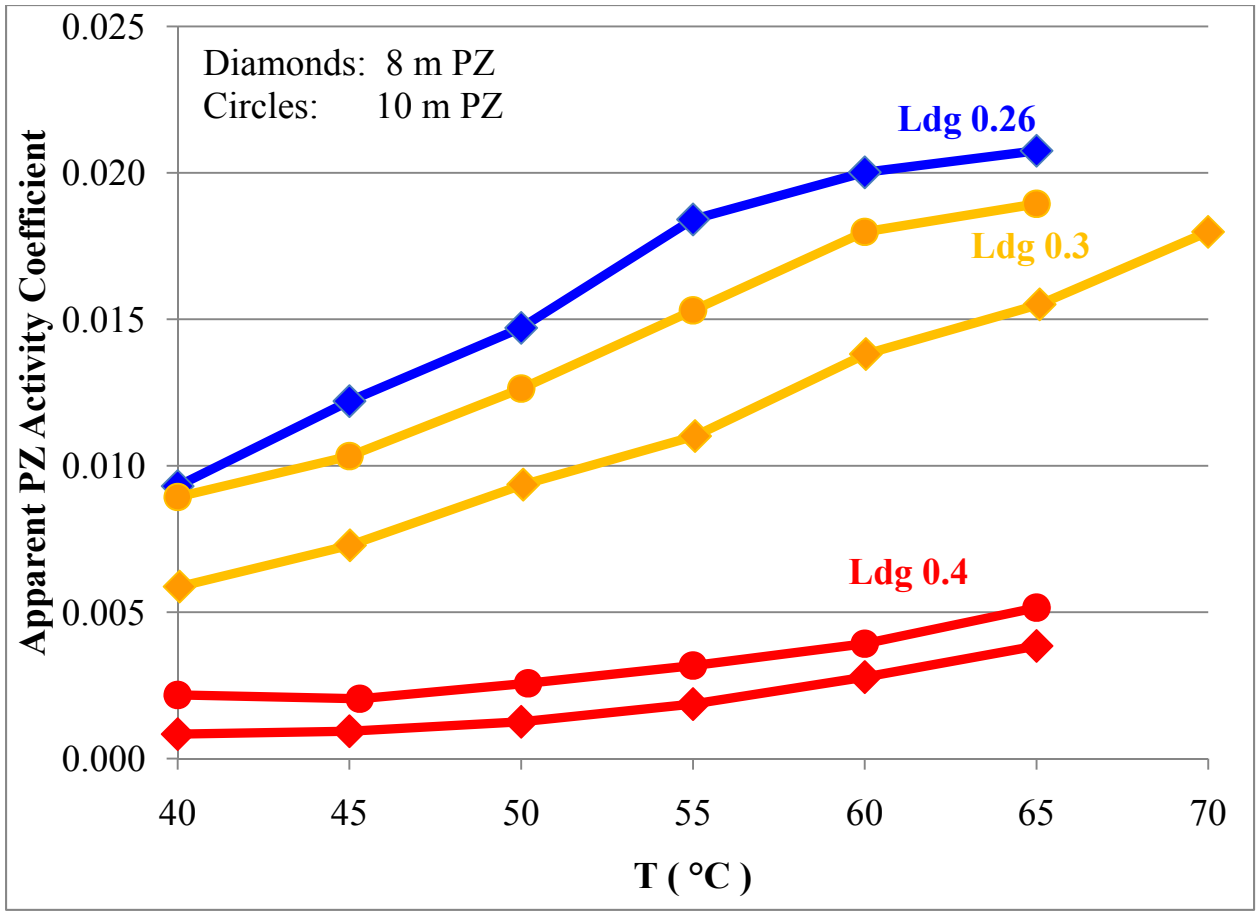

Figure 11: PZ Volatility in 8 m PZ-CO_2-H_2O System versus 10 m PZ-CO_2-H_2O System

In both 8 m and 10 m PZ-CO_2-H_2O, the amine apparent activity coefficient increases with temperature. This is due to PZ having an exothermic partial molar excess enthalpy heat of solution. Also, at a given temperature and amine concentration, PZ activity coefficient is found to decrease toward zero with greater loading. As more CO_2 is introduced into solution at higher loadings, more PZ is being consumed leaving less free amine available. Also, at a given temperature and loading, the apparent PZ activity coefficient is greater for 10 m PZ than 8 m PZ. With 10 m PZ, there is more free amine present in solution compared to 8 m PZ.

Conclusion

For 8 m PZ-CO_2-H_2O at either 27 ºC or 40 ºC, the PZ/PZH^+ species dominates at nominal lean loading and gradually decreases toward richer loading. This species accounts for approximately 0.37–0.47 of the total PZ concentration at the above conditions. The gradual decrease of free PZ results in decreasing amine volatility. PZ carbamate, on the other hand, is seen to increase with loading as more PZ reacts with CO_2. PZ dicarbamate is also present and accounts for ~0.1 of the total amine whereas its concentration is practically negligible in loaded 2 m PZ at similar conditions. Both bicarbonate and carbonate species are present in a ratio of ~0.03 moles of total CO_2 to total amine. This ratio remains approximately the same in loaded 2 m PZ.

PZ volatility in 8 m PZ-CO_2-H_2O system is approximately 0.11 and 0.78 Pa at nominal lean and rich loading corresponding to ~500 Pa and 5,000 Pa at 40 ºC. The PZ apparent activity

coefficient varies from ~0.001 to 0.02 for this system over the nominal range of loadings and absorber operating temperatures from 40–65 ºC. This coefficient increases with temperature due to PZ having an exothermic partial molar excess enthalpy heat of solution, but is found to decrease with either increasing loading or lower PZ concentration due to a decrease of free PZ in solution.

Future Work

In the next quarter, we will measure the C_p of the 7 m MDEA/2 m PZ blend at nominal lean and rich loadings from 40120 ºC. NMR analysis will be performed for loaded 8 m PZ at 5 ºC to fully explore the effects of temperature on speciation. NMR will also be obtained for the MDEA/PZ blend. CO_2 solubility and amine volatility will be measured for the 5 m MDEA/5 m PZ blend at nominal loadings and absorber operating temperatures. Finally, an attempt will be made to model the existing volatility, NMR, and C_p data in Aspen Plus® to construct a robust thermodynamic framework for MDEA-PZ.

References

Hilliard MD. *A Predictive Thermodynamic Model for an Aqueous Blend of Potassium Carbonate, Piperazine, and Monoethanolamine for Carbon Dioxide Capture from Flue Gas.* The University of Texas at Austin. Ph.D. Dissertation. 2008.

Modeling MDEA/PZ Thermodynamics

Quarterly Report for April 1 – June 30, 2010

by Peter Frailie

Supported by the Luminant Carbon Management Program

Department of Chemical Engineering

The University of Texas at Austin

July 1, 2010

Abstract

The goal of this study is to evaluate the performance of an absorber/stripper operation that utilizes the MDEA/PZ blended amine. Before analyzing unit operations and process configurations, the thermodynamic framework for the blended amine must be satisfactorily constructed. The approach used in this study is first to construct separate MDEA and PZ models that can later be reconciled via cross parameters to accurately model the MDEA/PZ blended amine. This study is currently in the process of developing the MDEA/PZ model based on thermodynamic and kinetic data. Separate MDEA and PZ models have been finished that accurately predict VLE, heat capacity, unloaded amine volatility, CO_2 activity coefficient, and heat of absorption. The goals for the next quarter are to finalize the MDEA/PZ thermodynamic and kinetic models and to begin designing an absorption/stripping process.

Introduction

The removal of CO_2 from process gases using alkanolamine absorption/stripping has been extensively studied for several solvents and solvent blends. An advantage of using blends is that the addition of certain solvents can enhance the overall performance of the CO_2 removal system. A disadvantage of using blends is that they are very complex compared to a single solvent, thus making them much more difficult to model.

This study will focus on a blended amine solvent containing piperazine (PZ) and methyldiethanolamine (MDEA). Previous studies have shown that this particular blend has the potential to combine the high capacity of MDEA with the attractive kinetics of PZ (Bishnoi, 2000). These studies have supplied a rudimentary Aspen Plus®-based model for an absorber with MDEA/PZ. The report also makes the recommendation that more kinetic and thermodynamic data must be acquired concerning the MDEA/PZ blend before the model can be significantly improved. Three researchers in the Rochelle lab have been acquiring these data, and they are currently being incorporated into the model. One of the major goals of this study will be to improve the supplied Aspen Plus® absorber model with up-to-date thermodynamic and kinetic data. Another major goal of this study will be to make improvements to the MDEA and PZ thermodynamic models, which should simplify the construction of the blended amine model.

Methods and Discussion

During the past quarter the PZ and MDEA thermodynamic models were finished, and significant progress was made in regressing the thermodynamics and kinetics of the MDEA/PZ blend. What follows is a description of the sequential regression used to develop each of the models, as well as a brief discussion of each of the incorporated data sets.

PZ Thermodynamic Model

PZ/H_2O Regression

The first set of data incorporated into the PZ thermodynamic model was unloaded amine volatility measured by Nguyen (Rochelle, 2009) and Xu (Rochelle, 2010). Figure 1 compares the experimental data and the Aspen Plus® predictions for low (Nguyen) and high (Xu) temperature PZ volatility in unloaded solutions of 2, 5, 8, and 10 m PZ.

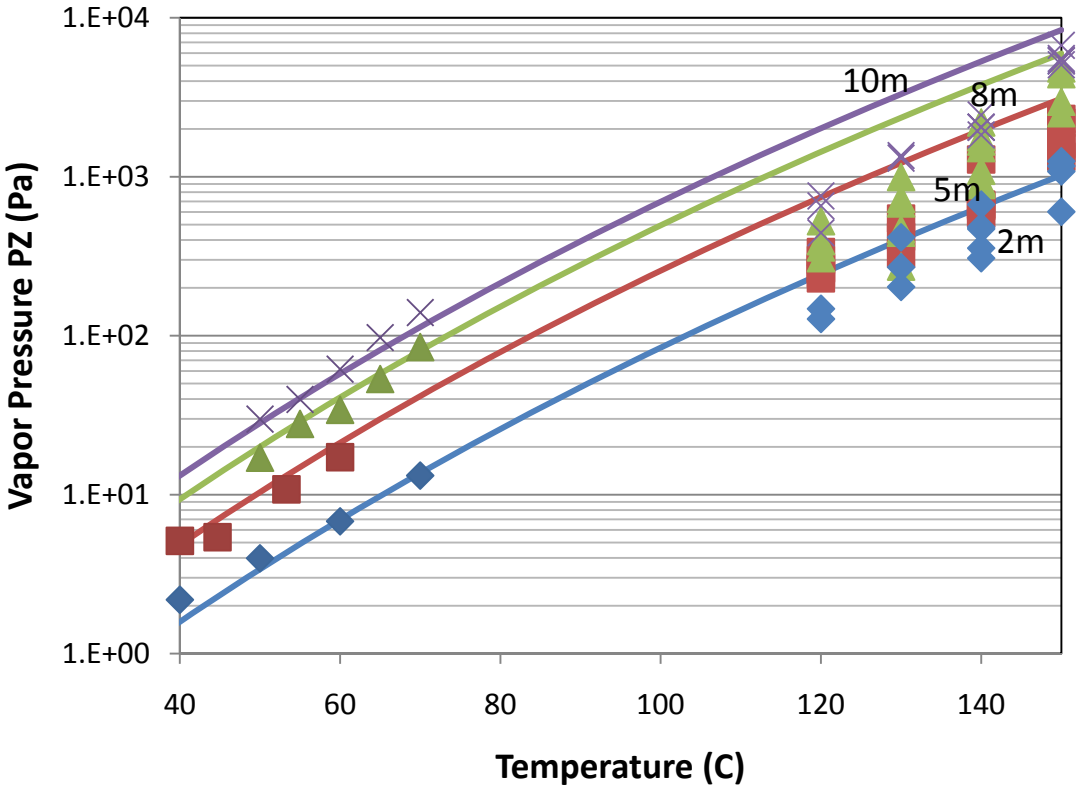

Figure 1: PZ volatility as a function of temperature for 2, 5, 8, and 10 m unloaded solutions between 40 °C and 150 °C

It should be noted that the high temperature data were not included in the regression. The apparatus used to measure the high temperature volatility data is relatively new, and the experimentalist collecting these data has expressed concern over its accuracy. Until the accuracy of the high temperature volatility data can be validated, only the low temperature data will be used in the regression.

This model treats PZ as a Henry's component. The parameters used to fit unloaded PZ volatility are ideal gas heat capacity, infinite dilution activity coefficients, and Henry's constant in water. Table 1 reports all of the parameters and their standard deviations.

Table 1: Parameters used to regress unloaded PZ volatility

Parameter	Species	Std. Dev.	Units
CPIG/1	PZ	1.24E5	J/kmol.K
CPIG/2	PZ	350	J/kmol.K
NRTL/1	PZ/H_2O	0.10	N/A
NRTL/1	H_2O/PZ	1.78	N/A
NRTL/3	PZ/H_2O	0.0178	N/A
Henry/1	PZ/H_2O	0.963	N/A
Henry/2	PZ/H_2O	311.2	K

PZ/H_2O/CO_2 Regression

Rather than regress the ΔG_{form}, ΔH_{form}, and $C_{P,aq}$ of PZH^+ to fit VLE and loaded heat capacity data, they were manually adjusted to fit pKa data for PZ between 20 ^oC and 80 ^oC (Hetzer, 1968). Figure 2 compares the Aspen Plus® predictions and experimental data for the pKa of PZ.

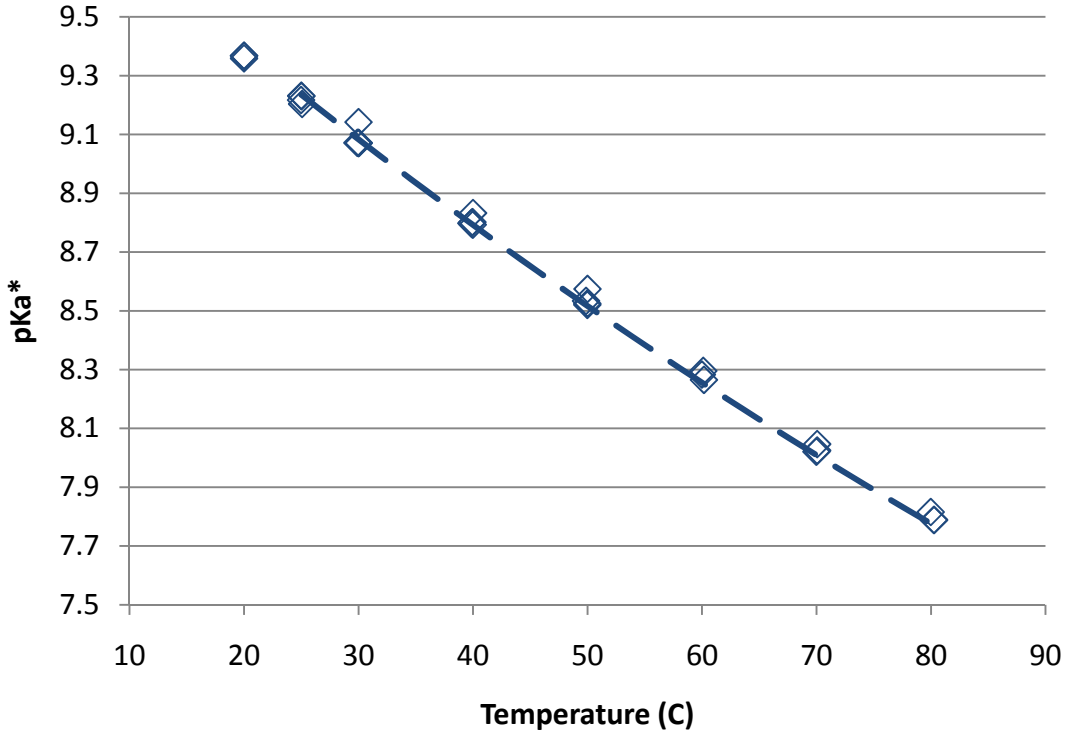

Figure 2: Aspen Plus® predictions (line) and experimental data (points) for pKa* of unloaded PZ between 25 ^oC and 80 ^oC

It should be noted that the pKa values in the literature had to be converted from a symmetric to an asymmetric activity coefficient reference state. The method for accomplishing this conversion can be found in Hilliard (2008).

The next regression included VLE and heat capacity for 2, 5, 8, 10, and 12 m loaded PZ solutions between 40 °C and 160 °C. Figure 3 compares the experimental data and the Aspen Plus® predictions for 8 m PZ VLE between 40 °C and 160 °C.

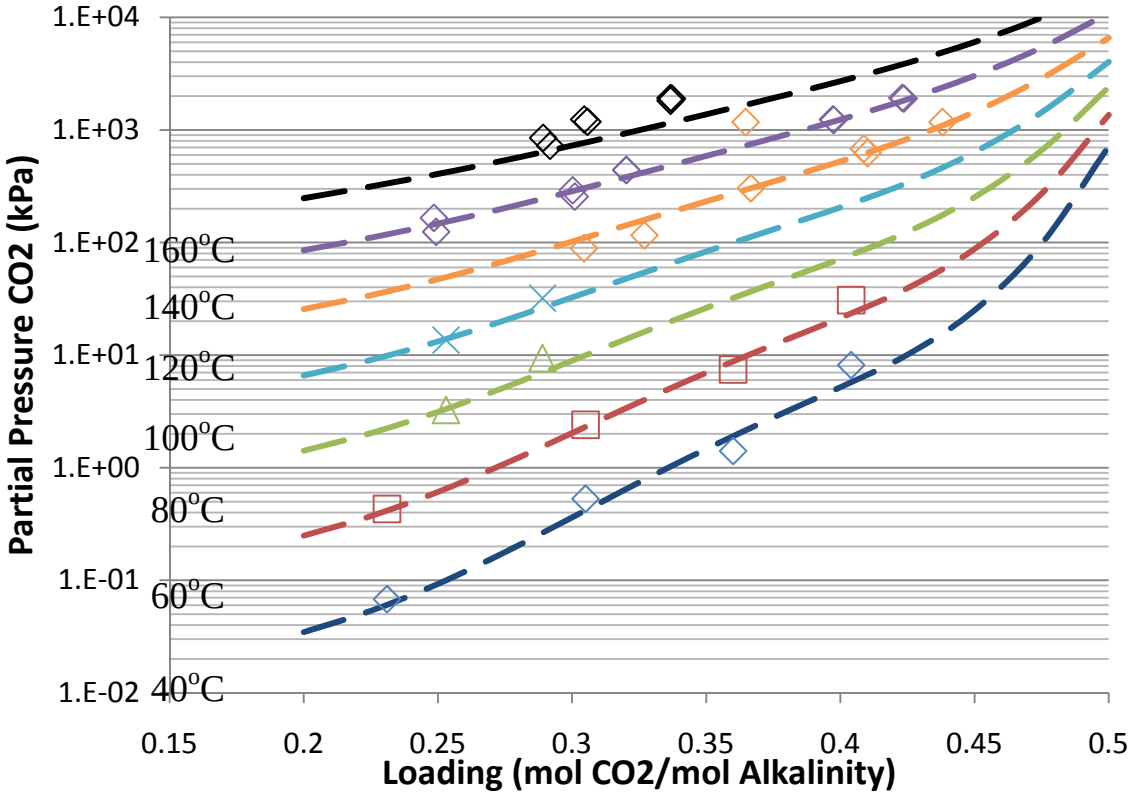

Figure 3: Experimental (points) and Aspen Plus® predictions (lines) for VLE of loaded 8 m PZ solution between 40 °C and 160 °C

All VLE data used in the regression were collected by experimentalists in the Rochelle group. Data above 100 °C were collected by Qing Xu (Rochelle, 2010), and data at 100 °C and below were collected by Ross Dugas (2009). It should be noted that the data above 100 °C were not explicitly regressed in Aspen Plus®. Because the data exhibit so much scatter, the least squares regression would have a tendency to overweight the importance of thse data. While Aspen Plus® allows users to adjust the relative weightings of data sets, it was much more precise to regress points predicted by Xu than to adjust the weighting arbitrarily to compensate for the scatter.

Figure 4 compares the experimental data (Freeman, 2008) and the Aspen Plus® predictions for 8 m PZ heat capacity between 40 °C and 150 °C at loadings of 0.21, 0.29, and 0.40.

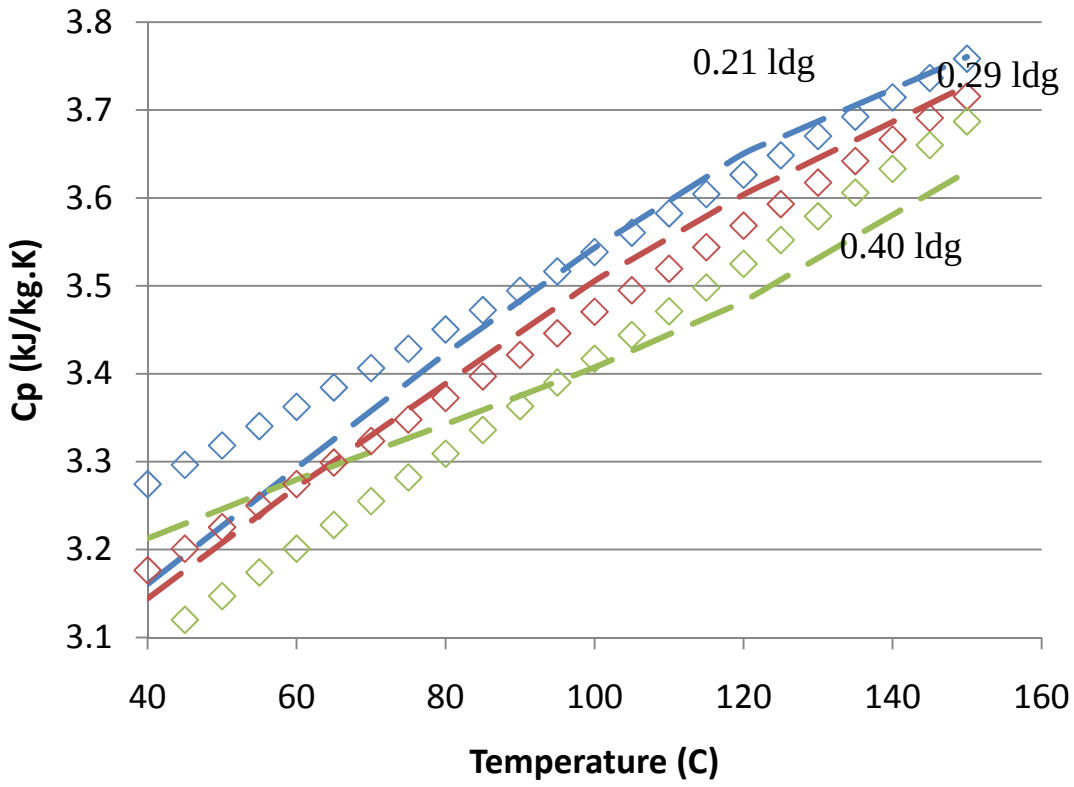

Figure 4: Experimental (points) and Aspen Plus® predictions (lines) for heat capacity of 8 m PZ solution between 40 °C and 150 °C at loadings of 0.21, 0.29, and 0.40 mol CO_2 per mol alkalinity

The dashed lines in Figure 4 do not represent the results of the Aspen Plus® regression, but rather the results of a separate calorimetric analysis. When Aspen Plus® regresses heat capacities it does not take into account the heat associated with potential changes in speciation. While this is not an issue with simple amines such as MDEA, PZ/H_2O/CO_2 mixtures are very complex, thus making it necessary to account for changes in speciation when calculating heat capacity.

Figure 5 compares the experimental data (Freeman, 2008) and the Aspen Plus® predictions for loaded 8 m PZ volatility between 40 °C and 60 °C.

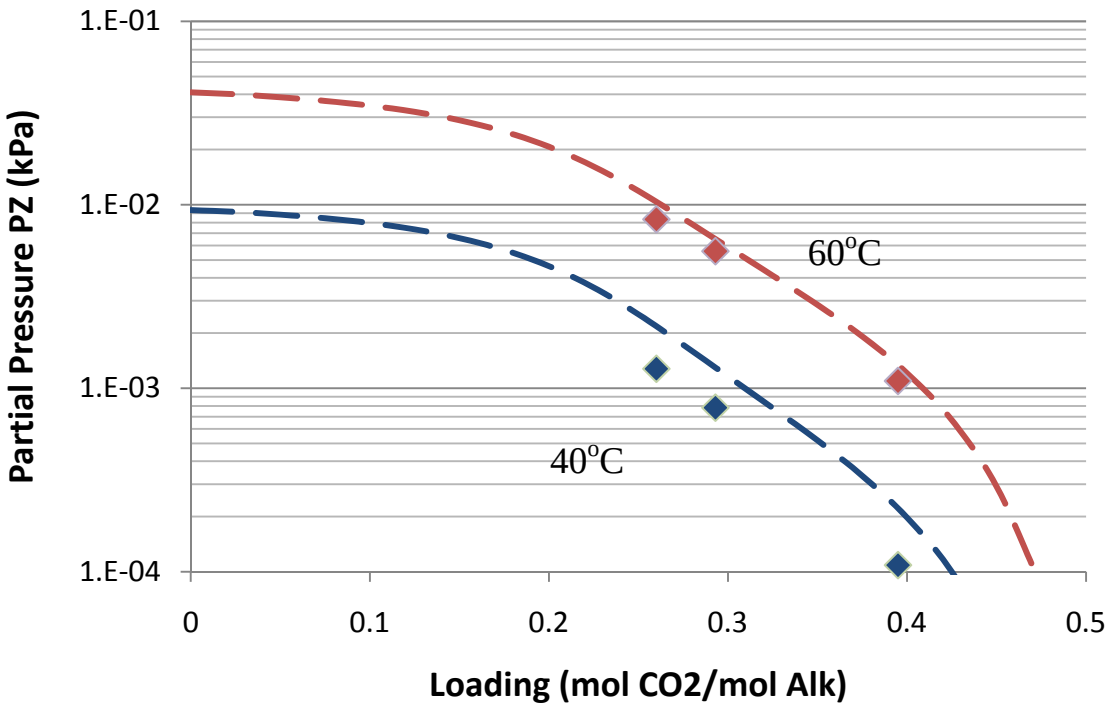

Figure 5: Experimental (points) and Aspen Plus® predictions (lines) for volatility of loaded 8 m PZ solution between 40 °C and 60 °C

In addition to the data sets shown above, VLE data sets for 2, 5, and 12 m solutions and heat capacity data sets for 2, 5, and 10 m solutions were included in the Aspen Plus® regression. Over similar temperature ranges the Aspen Plus® predictions adequately fit the experimental data.

The model also needs to predict speciation and heat of absorption data adequately. Though these data sets were not directly regressed in Aspen Plus®, they were periodically checked to ensure reasonable results. Figure 6 shows the speciation of an 8 m PZ solution at 40 °C as a function of loading.

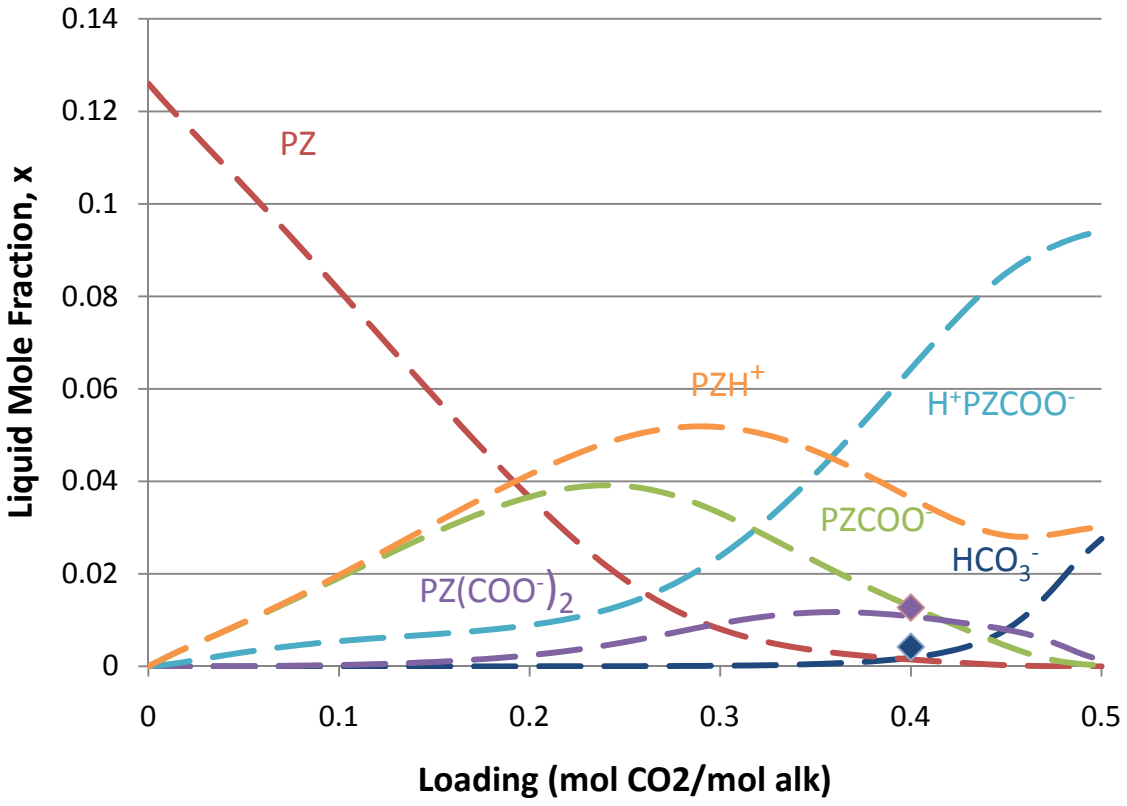

Figure 6: Aspen Plus® predictions (lines) and NMR data (points) of speciation as a function of loading for an 8 m PZ solution at 40 °C

Though there is very little speciation data with which to validate this result, preliminary NMR measurements for a solution at 0.4 loading suggest that this prediction is accurate. Because the speciation data could not be regressed directly, certain parameters had to be adjusted manually to fit the data. The only species that had to be adjusted was bicarbonate. Because bicarbonate concentration is relatively low through the operational loading range (0.3–0.42), adjusting these parameters did not significantly affect other properties (e.g., VLE, volatility, heat capacity, etc.).

Figure 7 compares the experimental (Rochelle, 2008) and the Aspen Plus® predictions for the heat of absorption of CO_2 as a function of loading for an 8 m PZ solution between temperatures of 60 °C and 100 °C.

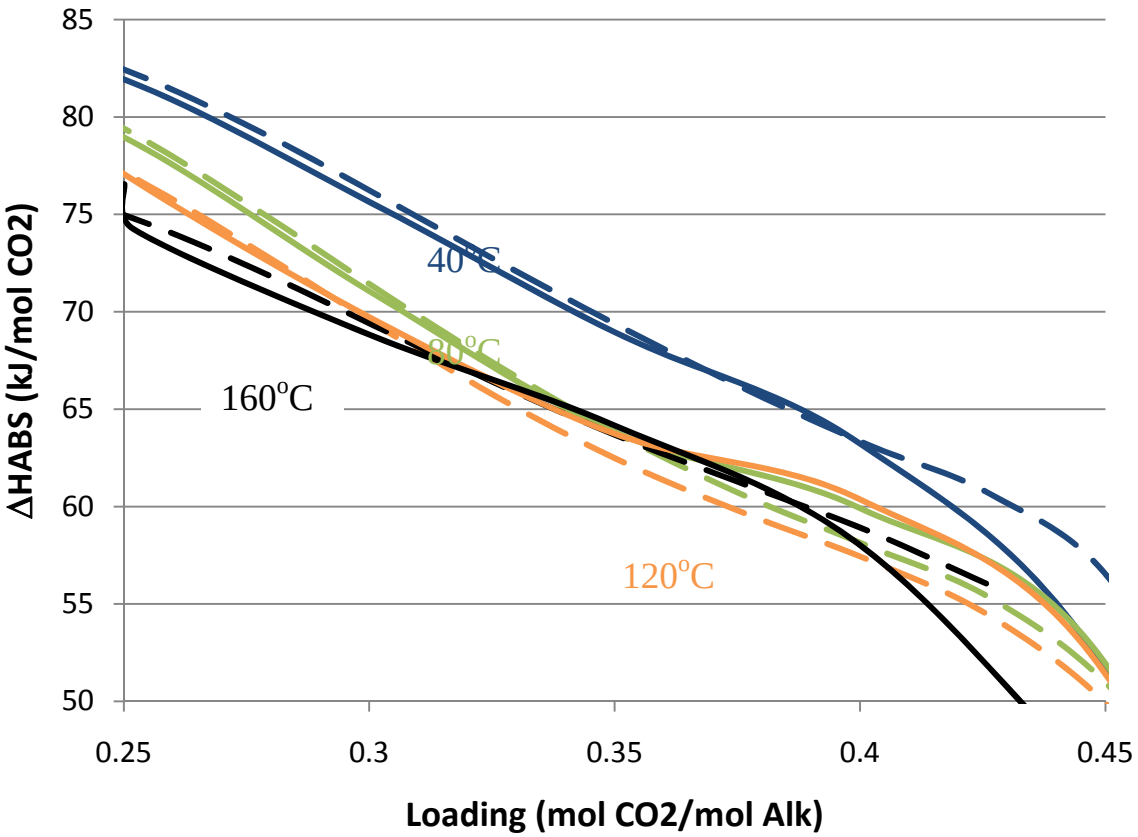

Figure 7: Comparison of Gibbs-Helmholtz (dashed lines) and calorimetric (solid lines) predictions for heat of absorption of loaded 8 m PZ solution between 40 °C and 160 °C

There are two ways of expressing the heat of absorption in Aspen Plus®. One way is by applying the Gibbs-Helmholtz equation to the VLE predictions, and the other way is to run a sensitivity analysis to determine the enthalpy change that occurs when a modicum of CO_2 is absorbed. Theoretically, these two methods should predict similar values for the heat of absorption, but this has not always been the case. While the reason for this discrepancy is still not fully understood, both methods are predicting mostly consistent heats of absorption for each amine in this report.

Finally, using a FORTRAN subroutine supplied by Aspentech the activity coefficient of CO_2 was regressed for loaded solutions between 25 °C and 60 °C. Figure 8 compares the Aspen Plus® predictions and experimental points (Svendsen, 2009) for the activity coefficient of CO_2 in a loaded 8 m PZ solution.

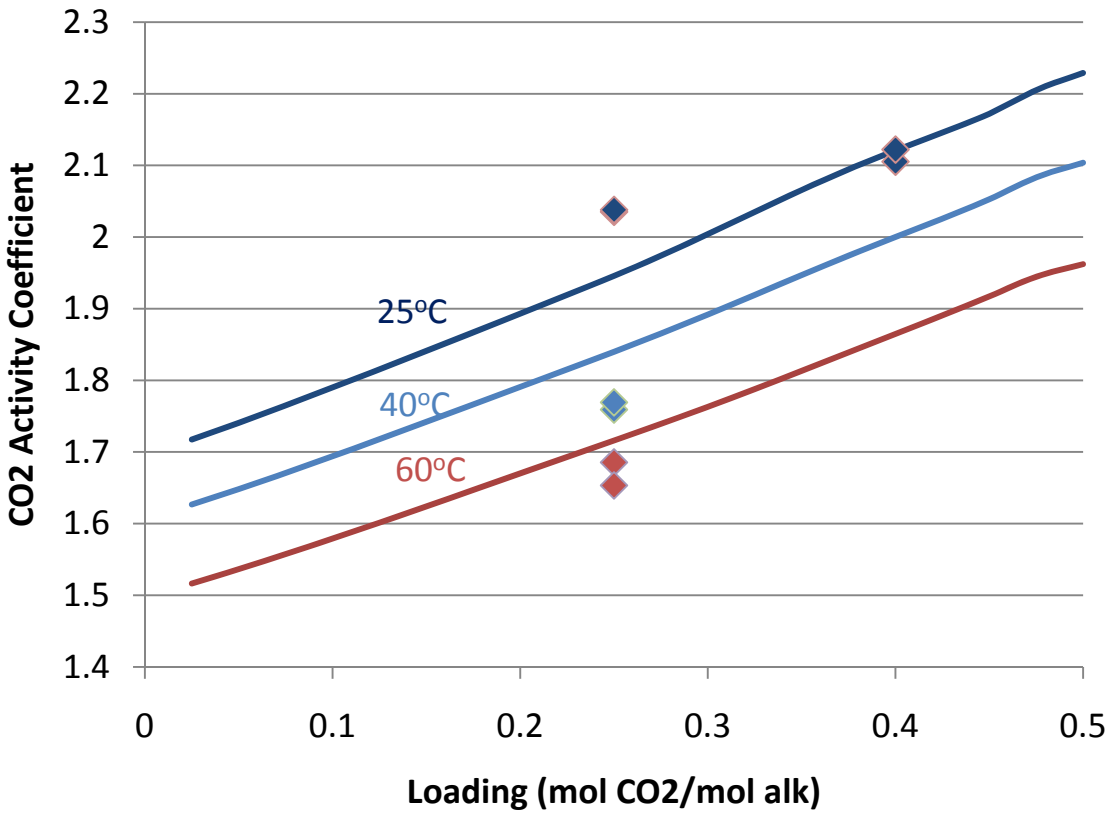

Figure 8: Aspen Plus® predictions (lines) and experimental data (points) for the activity coefficient of CO_2 in a loaded 8 m PZ solution

MDEA Thermodynamic Model

MDEA/H_2O Regression

The MDEA thermodynamic model was developed using the same procedure employed for the development of the PZ thermodynamic model. Just as with PZ, MDEA was modeled as a Henry's component. MDEA volatility data (Kim, 2008; Nguyen, 2009) were incorporated by regressing MDEA Henry's constant in water, ideal gas heat capacity, and infinite dilution activity coefficient. Figure 9 compares experimental data and the Aspen Plus® predictions between 40 °C and 100 °C for unloaded MDEA solutions, and Table 2 reports the regressed parameters and their standard deviations.

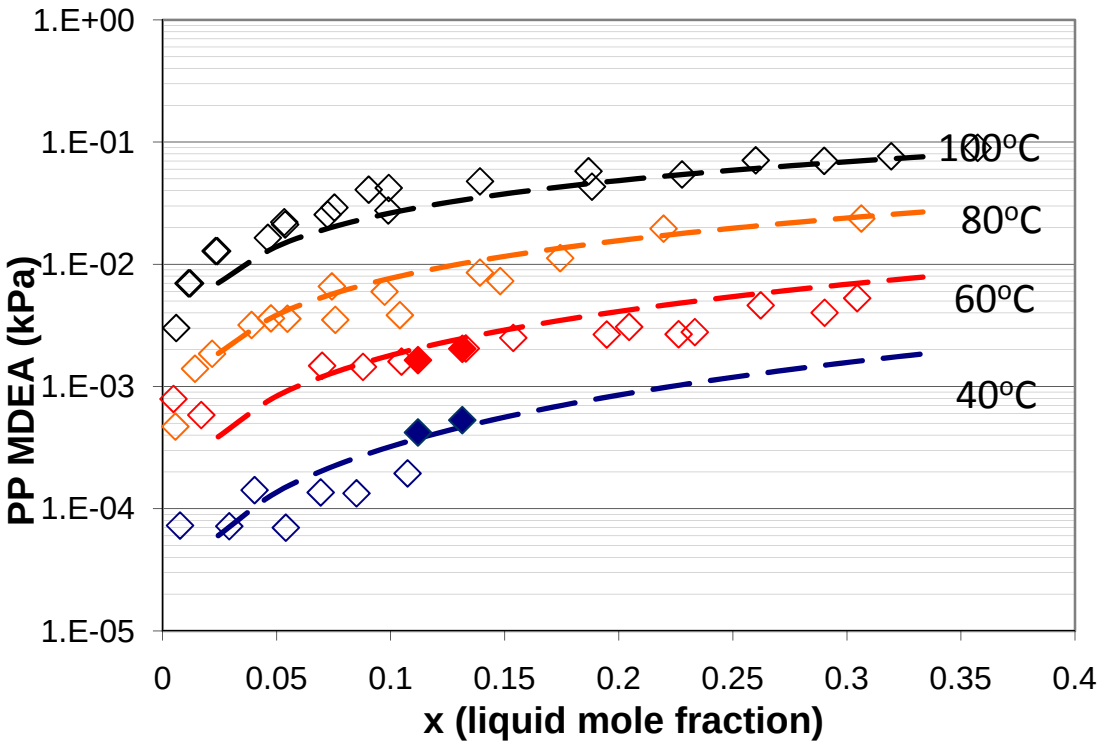

Figure 9: Aspen Plus® predictions (lines) and experimental data from Kim et al. (open points) and Nguyen (filled points) for unloaded MDEA volatility between 40 °C and 100 °C

Table 2: Parameters used to regress unloaded MDEA volatility

Parameter	Species	Std. Dev.	Units
CPIG/1	MDEA	4.17E4	J/kmol.K
CPIG/2	MDEA	128	J/kmol.K
NRTL/1	MDEA/H_2O	0.251	N/A
NRTL/1	H_2O/MDEA	0.487	N/A
NRTL/2	MDEA/H_2O	58.7	K
NRTL/2	H_2O/MDEA	132	K
Henry/1	MDEA/H_2O	39.7	N/A
Henry/2	MDEA/H_2O	1239	K
Henry/3	MDEA/H_2O	6.77	N/A
Henry/4	MDEA/H_2O	0.01	K^{-1}

MDEA/H_2O/CO_2 Regression

The pKa of MDEA was fit by adjusting the ΔG_{form}, ΔH_{form}, and $C_{P,aq}$ of the protonated species ($MDEAH^+$). Figure 10 compares the Aspen Plus® predictions and experimental data (Hamborg, 2007) for the pKa of PZ.

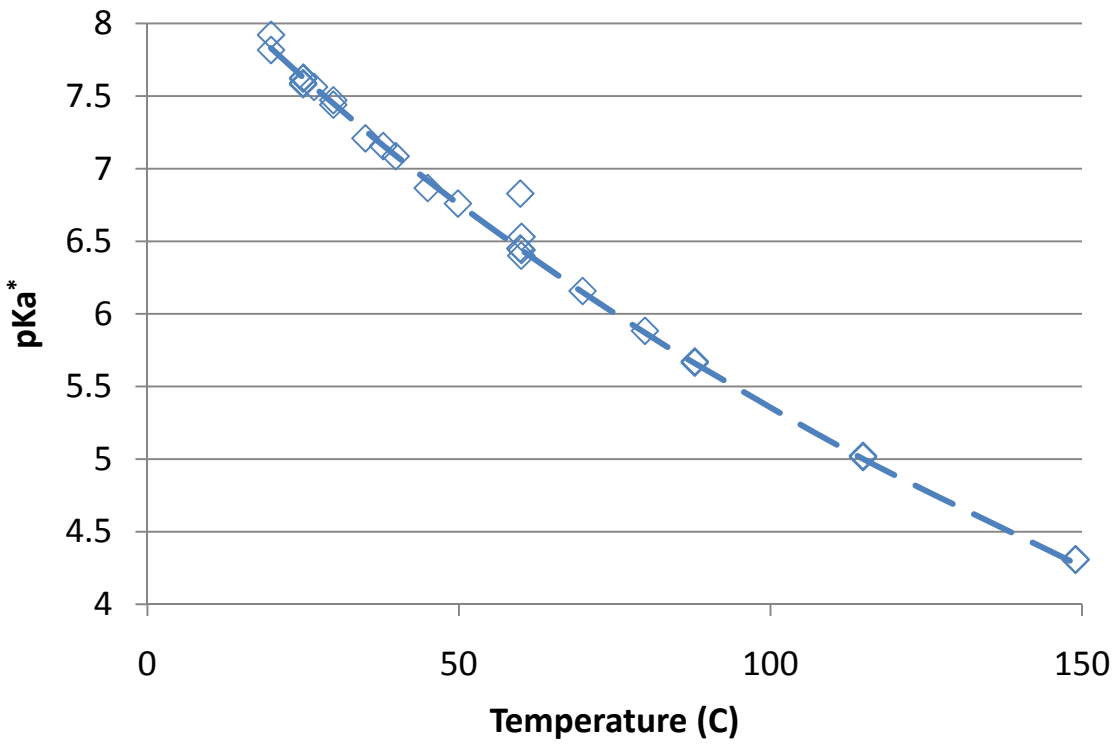

Figure 10: Comparison of Aspen Plus® predictions (line) and experimental data (points) for pKa* of unloaded MDEA between 20 °C and 150 °C

The next regression included VLE data for 4.52 m and 8.4 m MDEA between loadings of 0.001 and 0.7 mol CO_2/mol alkalinity from 25 °C to 120 °C, as well as heat capacity for 30–60 wt % MDEA solutions between loadings of 0.0 and 0.5 at 25 °C. Figure 11 compares the Aspen Plus® predictions and experimental data (Jou, 1982; Jou, 1993) for 4.52 m and 8.4 m MDEA VLE from a loading of 0.001 to 0.7 between 25 °C and 120 °C.

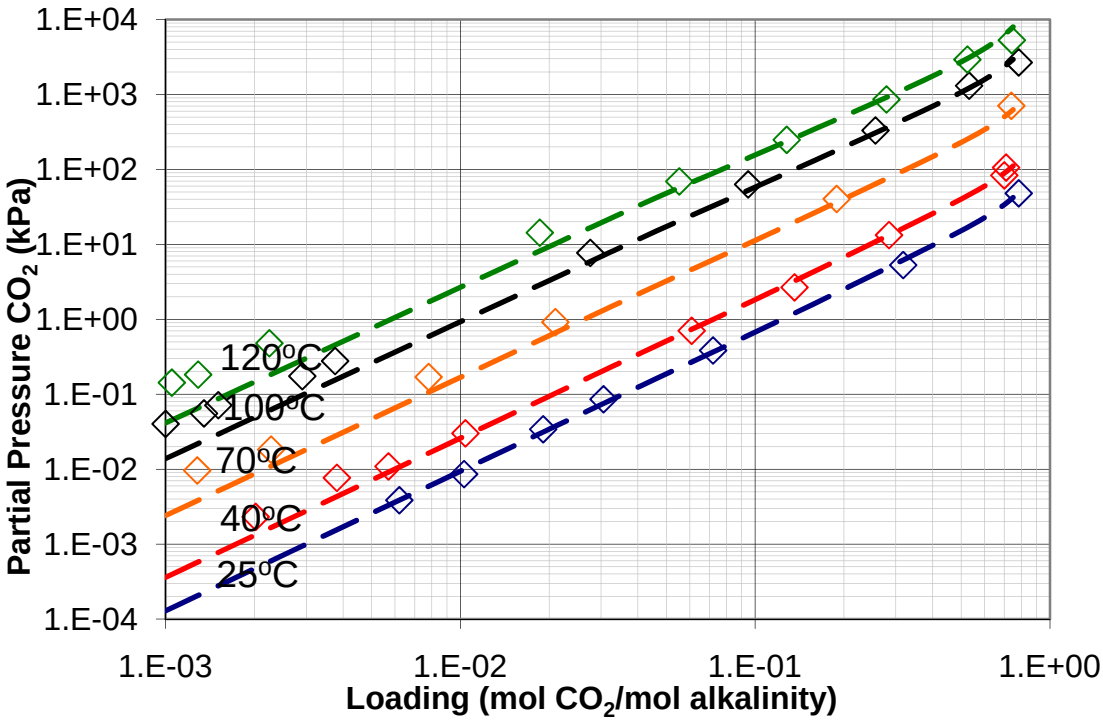

Figure 11: Experimental (points) and Aspen Plus® predictions (lines) for VLE of loaded 8.4 m MDEA solution between 25 °C and 120 °C

Figure 12 compares the Aspen Plus® predictions and experimental data (Weiland, 1997) for loaded MDEA heat capacity at 25 °C.

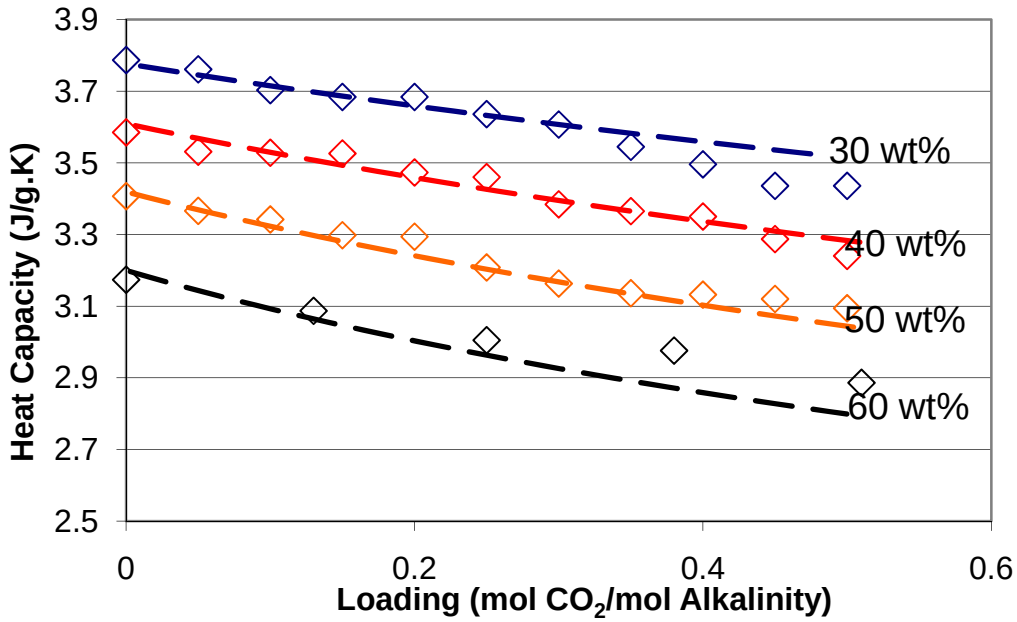

Figure 12: Experimental (points) and Aspen Plus® predictions (lines) for heat capacity of loaded MDEA solutions at 25 °C

Both the Gibbs-Helmholtz equation and a calorimetric analysis were used to calculate the ΔH_{ABS} for 8.4 m MDEA. Figure 13 compares the predicted values for ΔH_{ABS} using the two methods.

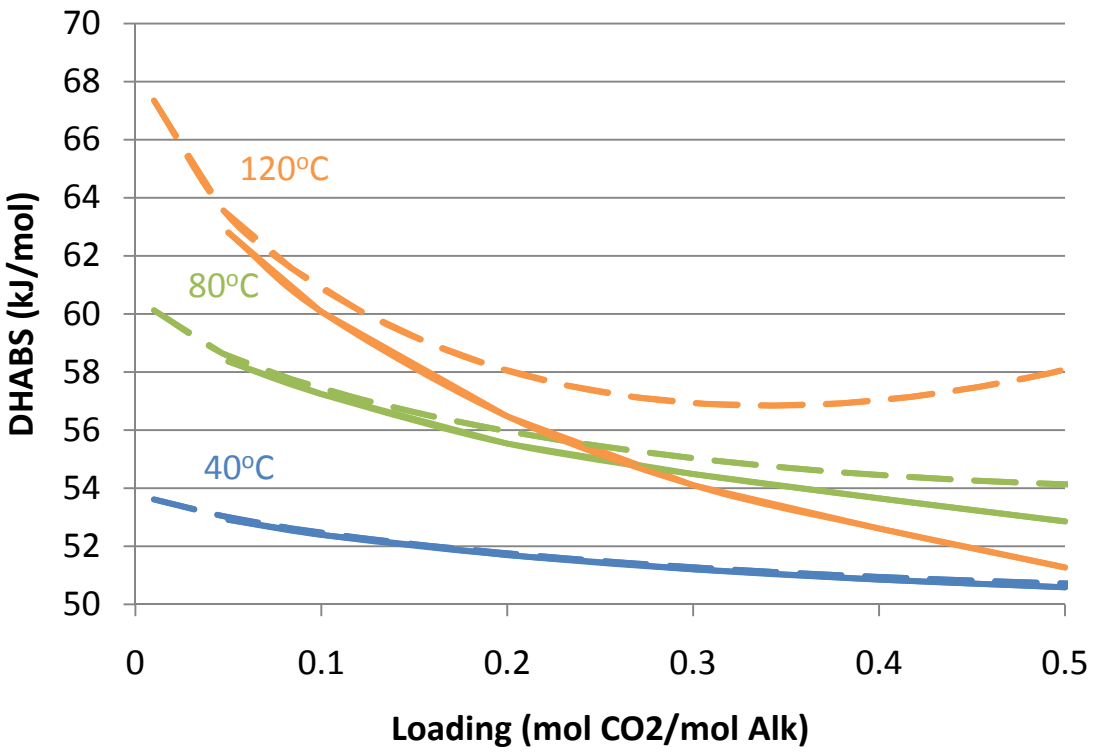

Figure 13: Comparison of Gibbs-Helmholtz (dashed lines) and calorimetric (solid lines) predictions for heat of absorption of loaded 8.4 m MDEA solution between 40 °C and 120 °C

Finally, the activity coefficient of CO_2 in loaded solutions was fit manually by adjusting certain molecule-molecule and cation-anion tau parameters. Figure 14 compares Aspen Plus® predictions and experimental values (Rinker, 1997) for the activity coefficient of CO_2 in loaded solutions.

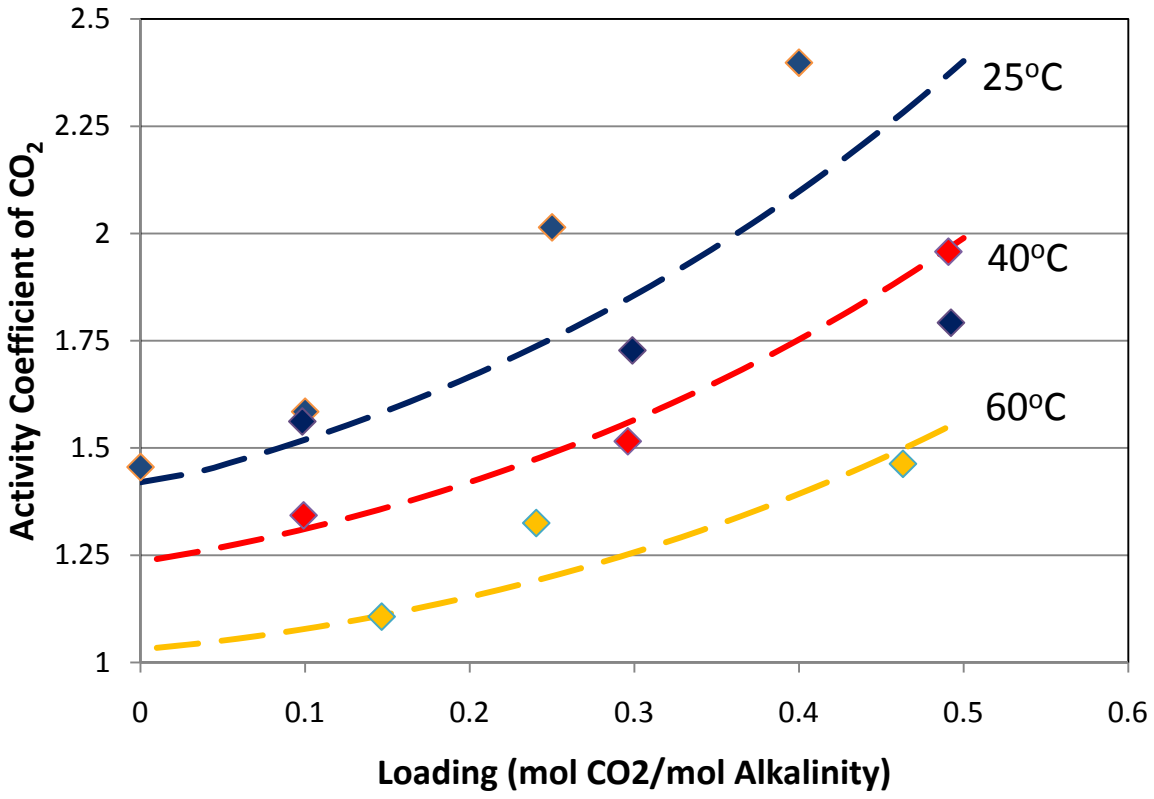

Figure 14: Comparison of Aspen Plus® predictions (lines) and experimental data (points) for the activity coefficient of CO_2 in a loaded MDEA solution

MDEA/PZ Thermodynamic Model

When regressing thermodynamic parameters for the blended amine, only cross-parameters [e.g., NRTL parameters for MDEA-PZ, tau parameters for MDEA/($MDEAH^+$, $PZCOO^-$)] may be modified. This ensures that the model can accurately predict performance of MDEA, PZ, and the MDEA/PZ blend.

MDEA/PZ/H_2O Regression

Unloaded blend volatility was regressed by adjusting the MDEA-PZ NRTL parameters. Table 3 reports the regressed parameters and their standard deviations, and Figure 15 compares the Aspen Plus® predictions and experimental values (Nguyen, 2009).

Table 3: Parameters used to fit MDEA/PZ volatility

Parameter	Species	Std. Dev.	Units
NRTL/1	MDEA/PZ	0.0454	N/A
NRTL/1	PZ/MDEA	0.0579	N/A

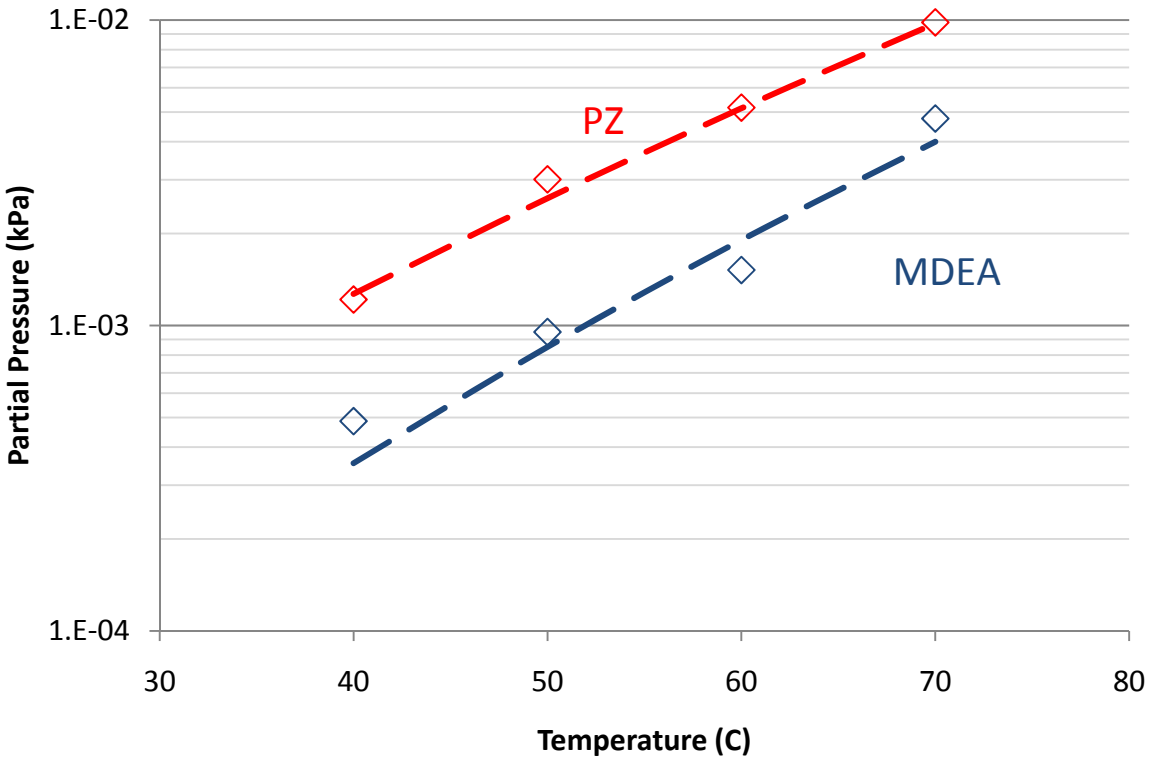

Figure 15: Comparison of Aspen Plus® predictions (lines) and experimental data from Nguyen (points) for unloaded MDEA/PZ volatility between 40 °C and 70 °C

MDEA/PZ/H_2O/CO_2 Regression

Currently the amount of loaded blend data is quite limited. The only VLE data available are for 7 m MDEA/2 m PZ and 5 m MDEA/2 m PZ at temperatures less than or equal to 100 °C, and the only loaded heat capacity data are currently being validated. As data are collected they will be incorporated into this thermodynamic model.

Conclusions

The heat capacity, VLE, activity coefficient of CO_2, and unloaded volatility of 2, 5, 8, and 10 m PZ solutions were incorporated into Aspen Plus®. The model adequately predicts heat capacity and VLE data over significant loading and temperature ranges (0.20–0.40 loading and 40 °C–160 °C). Experimental data concerning speciation and high temperature unloaded PZ volatility still need to be collected and/or validated before they can be incorporated into a future model. The discrepancy between the Gibbs-Helmholtz and calorimetric heat of absorption predictions seems to have been minimized, though the reason for this discrepancy still is not completely understood. A similar model was constructed for MDEA that included unloaded MDEA volatility, VLE data for 4.52 m and 8.4 m MDEA, heat capacity for loaded solutions of 30–60 wt % MDEA, and CO_2 activity coefficient in loaded solutions at 25, 40, and 60 °C. Data for the unloaded MDEA/PZ blend have already been incorporated into the model, and loaded data will be regressed as soon as they are made available.

Future Work

Finishing the MDEA/PZ model is the top priority for this next quarter. This will include regressing data for MDEA/PZ/H_2O/CO_2 solutions and constructing a wetted wall column in Aspen Plus® to fit kinetic data for the 7 m MDEA/2 m PZ and 5 m MDEA/2 m PZ blends. The goal for this next quarter will be to finalize the MDEA/PZ model and begin modeling absorption/stripping processes.

References

Bishnoi S. *Carbon Dioxide Absorption and Solution Equilibrium in Piperazine Activated Methyldiethanolamine*. The University of Texas at Austin. Ph.D. Dissertation. 2000.

Dugas RE. *Carbon Dioxide Absorption, Desorption, and Diffusion in Aqueous Piperazine and Monoethanolamine*. The University of Texas at Austin. Ph.D. Dissertation. 2009.

Freeman SA, Dugas RE, Van Wagener DH, Nguyen T, Rochelle GT. CO_2 "Capture with Concentrated, Aqueous Piperazine." *GHGT-9*. Washington, DC: Elsevier, 2008.

Hamborg ES, Niederer JPM, Versteeg GF. "Dissociation Constants and Thermodynamic Properties of Amino Acids Used in CO_2 Absorption from (293 to 353) K." *J. Chem Eng Data*. 2007;52:2491–2502.

Hetzer HB, Robinson RA, Bates RG. "Dissociation Constants of Piperazinium Ion and Related Thermodynamic Quantities from 0 to 50°." *J Phys Chem.* 1968;72(6):2081–2086.

Hilliard MD. *A Predictive Thermodynamic Model for an Aqueous Blend of Potassium Carbonate, Piperazine, and Monoethanolamine for Carbon Dioxide Capture from Flue Gas*. The University of Texas at Austin. Ph.D. Dissertation. 2008:133–135.

Jou FY, Mather AE, Otto FD. "Solubility of hydrogen sulfide and carbon dioxide in aqueous methyldiethanolamine solutions." *Ind Eng Chem. Process Des Dev.* 1982;21(4):539–544.

Jou FY, Carroll JJ, Mather AE Otto FD. "The Solubility of Carbon Dioxide and Hydrogen Sulfide in a 35 wt % Aqueous Solution of Methyldiethanolamine." *Can J Chem Eng.* 1993;71:264–268.

Kim I, Svendsen HF, Borresen E. "Ebulliometric Determination of Vapor-Liquid Equilibria for Pure Water, Monoethanolamine, N-Methyldiethanolamine, 3-(Methylamino)-propylamine, and Their Binary and Ternary Solutions." *J Chem Eng Data*. 2008;53:2521–2531.

Nguyen T. Personal communication. July 20, 2009.

Rochelle GT et al. "CO_2 Capture by Aqueous Absorption, Second Quarterly Progress Report 2008." Luminant Carbon Management Program. The University of Texas at Austin. 2008.

Rochelle GT et al. "CO_2 Capture by Aqueous Absorption, Third Quarterly Progress Report 2009." Luminant Carbon Management Program. The University of Texas at Austin. 2009.

Rochelle GT et al. "CO_2 Capture by Aqueous Absorption, Fourth Quarterly Progress Report 2009." Luminant Carbon Management Program. The University of Texas at Austin. 2010.

Rinker EB, Ashour SS, Sandall OC. "Physical Property Data Important in Modeling H_2S and CO_2 Absorption into Aqueous DEA, MDEA and Blends of DEA and MDEA." *Gas Processors Association*. RR-158. December 1997.

Svendsen HF. Personal communication. November 11, 2009.

Weiland RH, Dingman, JC, Cronin DB. “Heat Capacity of Aqueous Monoethanolamine, Diethanolamine, N-Methyldiethanolamine, and N-Methyldiethanolamine-Based Blends with Carbon Dioxide.” *J Chem Eng. Data.* 1997;42:1004–1006.

Modeling Stripper Performance for CO_2 Capture by Amines

Quarterly Report for April 1 – June 30, 2010

by David Van Wagener

Supported by the Luminant Carbon Management Program

and the

Industrial Associates Program for CO_2 Capture by Aqueous Absorption

Department of Chemical Engineering

The University of Texas at Austin

July 31, 2010

Abstract

During this quarter, several tasks were addressed. First, the previous compressor correlation was compared against the compression work for more realistic values of compressor efficiency and intercooler pressure drop. A multi-stage compressor with a polytropic efficiency of 80% and a 20% pressure loss per intercooler was found to predict results similar to a 72% efficient compressor with no pressure drop in the intercoolers. Next, a 5 °C approach was specified for the reboilers of all previous results with MEA. This change improved the overall performance by 1.0–1.2 kJ/mol CO_2 fairly evenly for all configurations. Finally, the new PZ thermodynamic model was used to simulate a 1-stage flash. The equivalent work at 150 °C and the optimum loading of 0.34 was 34.7 kJ/mol CO_2, a 1.3 kJ/mol CO_2 improvement over 9 m MEA at its optimum. For future work, it was determined that an acceptable rich loading of 0.4 for PZ was equivalent to a rich loading of 0.48 for MEA because the log mean driving force in the absorber was double for MEA, indicating that both sets of conditions would require the same packing area since PZ demonstrates twice the reaction rate.

Introduction

Work in previous quarters addressed the effect of increasing process complexity in the stripper on its energy efficiency. 9 m MEA had been selected as the solvent for the analysis since a robust solvent model was available for Aspen Plus®. Additionally, the solvent was a concentrated form of the industry standard, 7 m MEA. The higher concentration had been previously used in a pilot plant campaign and verified to be a workable solvent for CO_2 capture (Plaza et al., 2010). The complexity analysis demonstrated a clear improvement in the efficiency of the stripper with higher complexity configurations. The quantitative definition of complexity was somewhat arbitrary, so the different types of complexity that were added resulted in an inexact improvement trend. However, the most important improvement was found to be using interheating in the middle of a stripping column. This improvement alone resulted in the best performance.

Now that MEA has been thoroughly analyzed, the relative performance of piperazine (PZ) will be investigated. Concentrated PZ has shown promise as a competitive amine solvent for CO_2 capture. In comparison with 7 m MEA, it has twice the effective reaction rate (k_g'), slower oxidative degradation, higher resistance to thermal degradation, twice the CO_2 capacity, and slightly improved amine volatility. One of the only apparent negative qualities of PZ is its lower heat of absorption, which has been previously shown to reduce the stripper efficiency (Oyenekan, 2007). However, PZ can be run up to 150 °C in the stripper, whereas MEA could only be safely run at maximum of 120 °C to avoid substantial thermal degradation. It was uncertain whether the ability to run at high temperature would more than offset the low heat of absorption, but initial estimates indicated that the ability to run 30 °C higher would make PZ a more competitive solvent. The average heat of absorption of concentrated PZ is approximately 65 kJ/mol CO_2, compared to MEA whose average heat of absorption is approximately 80 kJ/mol CO_2.

A model for concentrated PZ in Aspen Plus® (5deMayo.v.1) has been finalized by Plaza and Frailie. Like previous models, it accurately predicts VLE and heat capacity of the solvent, but it also addresses previous imperfections in the amine volatility and heat of absorption predictions. The model is robust for process simulations, and it will be used for stripper simulations in concurrence with absorber simulations by Plaza.

Methods and Results

Compressor Efficiency & Intercooling Pressure Drop

A correlation was previously developed for the compression work of a water saturated CO_2 stream exiting a stripper. The correlation was derived using several assumptions: the minimum number of compression stages was used to yield a compression ratio no greater than 2; the final pressure was 150 bar; the inlet pressure was 0.8-20 bar; the compressor polytropic efficiency was 72%; and the intercoolers had no pressure drop. The compressor efficiency and intercooler pressure drop would be highly variable depending on the type of compressor used, so the effect of these two variables on the compression work was inspected.

The direct effect of compressor efficiency and intercooling pressure drop was straightforward and obvious: improved compressor efficiency reduced the overall compressor work, and more pressure drop in the intercoolers resulted in higher overall compression work. The effect of these two variables was more significant at low inlet pressures where there were more compression stages and a greater overall change in pressure. Next, instead of specifying pressure drop as a constant for each stage, it was defined as a function of the inlet pressure for each specific intercooler. In a real process the coolers would most likely be designed in this fashion to achieve an equal relative impact on the streams between each stage. Additionally, although a polytropic efficiency of 72% was initially specified, a more realistic value would be 80%. This increased efficiency was evaluated with two levels of intercooler pressure drop, defined by the following equation:

$$\Delta \boldsymbol{P_n} = \boldsymbol{\varepsilon} \cdot \boldsymbol{P_{inlet,n}} \quad (1)$$

where ε was the fraction of the inlet pressure lost in intercooler *n*. Values of 0, 0.1, and 0.2 were used for ε. These results are shown in Figure 1, compared against the original correlation with 72% polytropic efficiency and no pressure drop in the intercoolers.

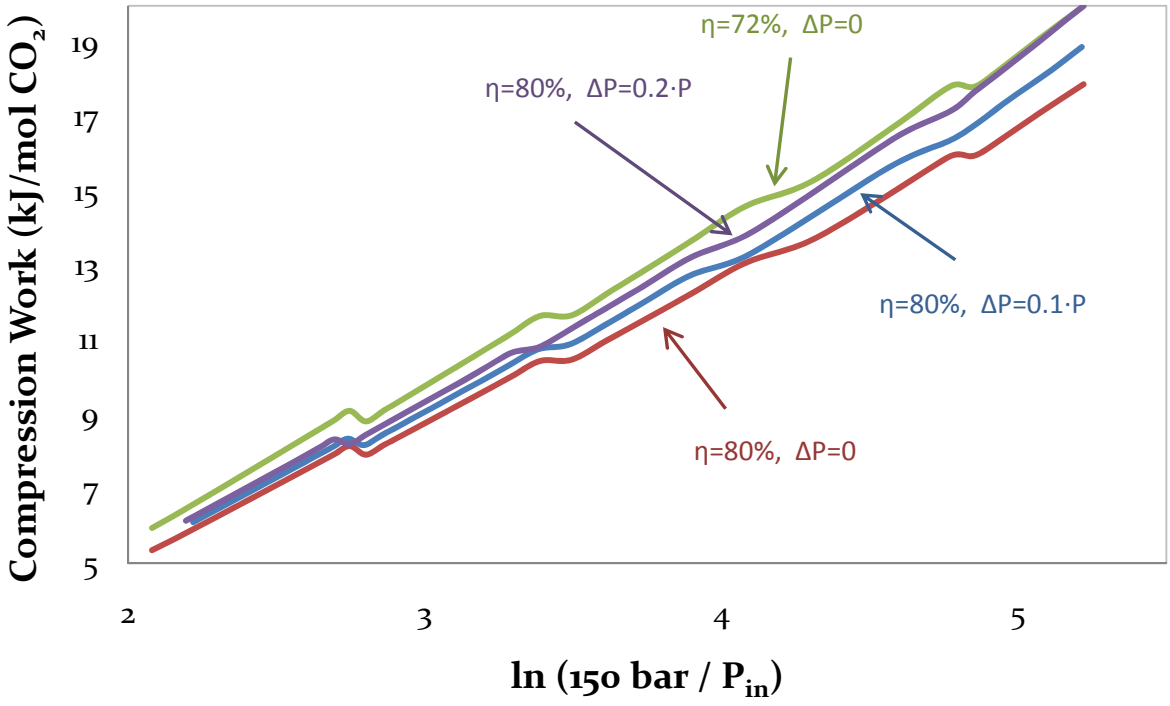

Figure 1: Compressor Work for Various Conditions

The case with 80% polytropic efficiency and 20% pressure loss in each intercooler predicted compression work closest to the original correlation conditions, and it also represented an acceptable real case scenario.

Complexity Modeling

In previous work, the effect of configuration complexity on stripper performance was investigated using 9 m MEA as the solvent. A number of specifications were set to maintain similarities between the different cases and allow for a fair comparison between the process arrangements. Following the assumptions of previous work by Van Wagener and Oyenekan, a 5 °C approach was specified on the cross exchanger but a 10 °C approach was specified on the reboiler. A 5 °C approach should be attainable for both exchangers, so the complexity calculations were reevaluated using a 5 °C approach on the reboiler. This change only affected the calculation of the equivalent work of the steam usage, stemming from the heat duty and reboiler temperature.

$$W_{eq} = \sum_{i=1}^{n_{reboilers}} 0.75 * Q_i \left(\frac{T_i + 5K - T_{sink}}{T_i + 5K} \right) + W_{pumps} + W_{comps} \qquad (2)$$

Updated work requirements of selected configurations running at 100 °C, 110 °C, and 120 °C are in Table 1, Table 2, and Table 3, respectively. The improvement from using a 10 °C reboiler approach was fairly consistent between the various configurations, lean loadings, and temperatures. The optimum lean loadings did not change. Of the listed configurations, the average improvements were 1.19 kJ/mol CO_2 at 100 °C, 1.06 kJ/mol CO_2 at 110 °C, and 1.01

kJ/mol CO_2 at 120 °C (table of individual improvements not shown). As with the results using a reboiler with a 10 °C approach, these calculations consistently held the following assumptions:

- Rich loading of 0.5, corresponding to an equilibrium CO_2 partial pressure of 5 kPa at 40 °C
- Rich pump achieved stripper vessel pressure and added 50 kPa for frictional losses and 250 kPa for gravitational losses to top of a column (where applicable)
- 5 °C cold side approach on main cross exchanger
- CO_2 compression to 150 bar
- CO_2 compression work was calculated with the correlation; assumed precooling/intercooling to 40 °C with water knockout, and maintained a compression ratio no greater than 2 with a minimum number of compression stages.

Table 1: Performance of Stripper Configurations at 100 °C

Configuration	**Equivalent Work (kJ/mol CO_2)**		
Lean loading →	*0.30*	*0.37*	*Optimum*
1-Stage flash	50.1	41.5	37.0
Simple Stripper	39.0	37.5	36.9
Stripper with adiabatic lean flash	37.9	36.9	36.0
2-Stage flash	44.5	37.9	35.1
2-Stage Multi-pressure, packed top	-	36.5	35.2
3-Stage flash	42.5	36.6	34.5
Double matrix, packed LP top	38.2	36.0	35.0
4-Stage flash	41.4	35.9	34.2

Table 2: Performance of Stripper Configurations at 110 °C

Configuration	**Equivalent Work (kJ/mol CO_2)**		
Lean loading →	*0.30*	*0.37*	*Optimum*
1-Stage flash	45.9	38.4	35.7
Simple Stripper	36.9	35.6	35.1
Stripper with adiabatic lean flash	37.0	35.1	34.5
2-Stage flash	40.6	35.2	33.9
2-Stage Multi-pressure, packed top	36.1	34.3	33.8
3-Stage flash	38.7	34.2	33.4
Double matrix, packed LP top	36.3	33.9	33.4
4-Stage flash	37.7	33.8	33.3

Table 3: Performance of Stripper Configurations at 120 °C

Configuration	Equivalent Work (kJ/mol CO_2)		
Lean loading →	*0.30*	*0.37*	*Optimum*
1-Stage flash	42.1	36.1	34.9
Simple Stripper	35.7	34.2	34.0
Stripper with adiabatic lean flash	35.5	33.6	33.6
2-Stage flash	37.3	33.7	33.5
2-Stage Multi-pressure, packed top	34.5	33.2	33.2
3-Stage flash	35.8	33.2	33.1
Double matrix, packed LP top	34.1	32.4	32.4
Interheated Column	33.5	32.5	32.5
4-Stage flash	35.0	33.0	33.0

This new equivalent work calculation method using a 5 °C approach on the reboiler will be the standard for upcoming continued work on the stripper. At the respective optimum lean loading of each configuration, the improvement from the base case simple stripper is only 1.5 kJ/mol CO_2 at 120 °C, yet reducing the steam temperature by 5 °C improved the equivalent work by 1.0–1.2 kJ/mol CO_2. Even though the smaller temperature approach would require a larger reboiler, the investment would surely be worthwhile compared to the improvement by more drastically increasing the process complexity.

Piperazine Modeling

The new, completed Aspen Plus® thermodynamic model for concentrated PZ was cleaned up for easier use and file exchange. Extraneous components from previous regressions (MEA, PZ solids, etc.) were eliminated, and the parameter forms were consequently cleaned out for the missing components. Other files that were deleted to reduce the file size included data sets, regression sets, and sensitivity sets. The Aspen Plus® backup file (.bkp file) initially transferred with altered parameters for an unknown reason, but this was remedied by cleaning up the original completed model again, and the property predictions were checked to ensure that the correct model would be used.

The previous pilot plant campaign with concentrated PZ will eventually be used to validate the thermodynamic model, but only the 1-stage flash has been modeled. As a first check of the model, the 1-stage flash was simulated with 8 m PZ for 90 °C–150 °C in 10 °C increments (except 100 °C). As in the MEA analysis, the rich loading was held constant; an equilibrium CO_2 partial pressure of 7.5 kPa at 40 °C was used, corresponding to a loading of 0.415. Since PZ has a reaction rate with CO_2 approximately twice that of MEA, it is assumed that PZ will require a lower driving force in the absorber and could therefore attain a higher equilibrium partial pressure in the rich stream. The predictions of the equivalent work for this analysis are displayed in Figure 2. Similar to the results for 9 m MEA, the work requirement decreased with increasing temperature in the evaluated temperature range. Additionally, the optimum lean loading, denoted by the minimum of each curve, decreased with increasing stripper temperature. This would benefit the absorber to increase the CO_2 reaction rate on the lean end and reduce the possibility of a lean pinch. At 150 °C the equivalent work at the optimum lean loading of 0.34 was 34.7 kJ/mol CO_2, which was an improvement compared to the lowest equivalent work of 36.0 kJ/mol CO_2 using a 1-stage flash with 9 m MEA.

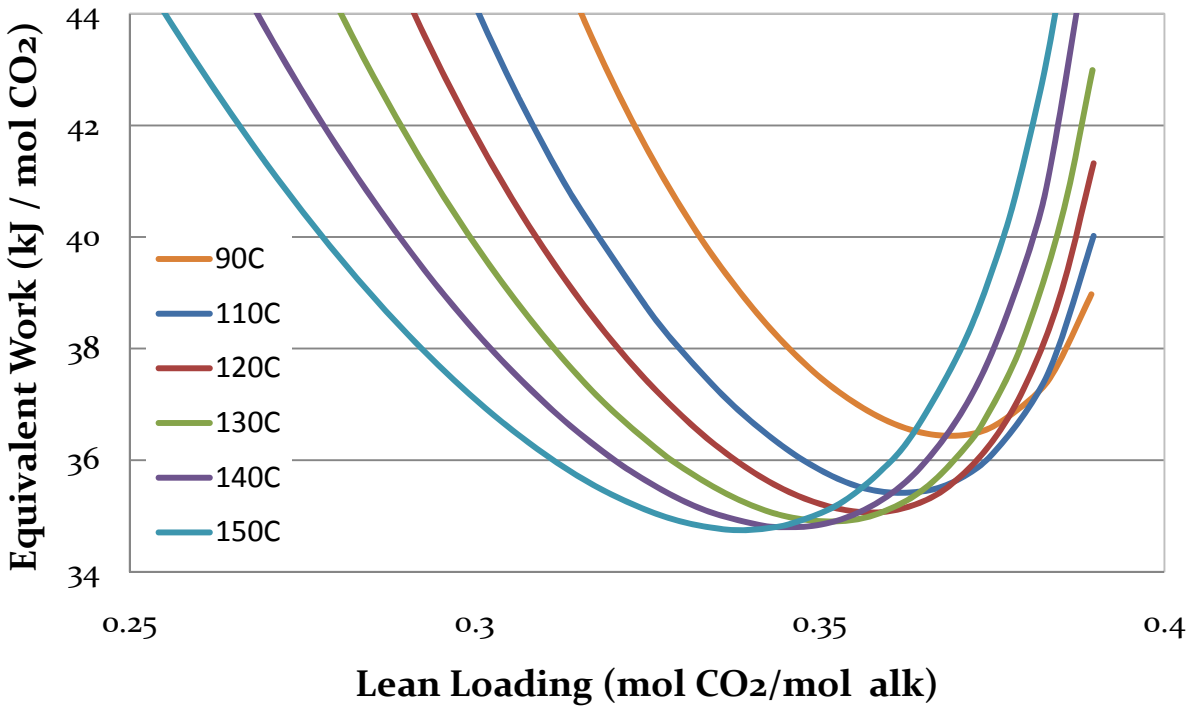

Figure 2: 1-Stage Flash Performance with PZ

A point worth noting with these preliminary PZ results is the similarity in the trend in the effect of increasing reboiler temperature and increasing complexity with MEA (Figure 3). By increasing temperature or complexity, the equivalent work decreased with diminishing return, and the optimum lean loading also went down. These effects were most likely observed in both cases due to the approach to reversibility. This fact can easily be recognized for the complexity case since increasing the number of flash stages made the process more reversible, by the definition of reversibility. This improvement reached a limit as the number of steps approached a large number. In the case of increasing the reboiler temperature, the process became more reversible because the CO_2 desorbed at a higher pressure when stripping at higher temperature. This was essentially "thermal compression", using less intensive pump work to achieve the high stripper pressure instead of compressing the large-volume vapor in the same pressure range. Eventually higher temperature would result in increasing equivalent work due to the significant energy required for pump work which was not captured from the returning high-pressure lean solvent.

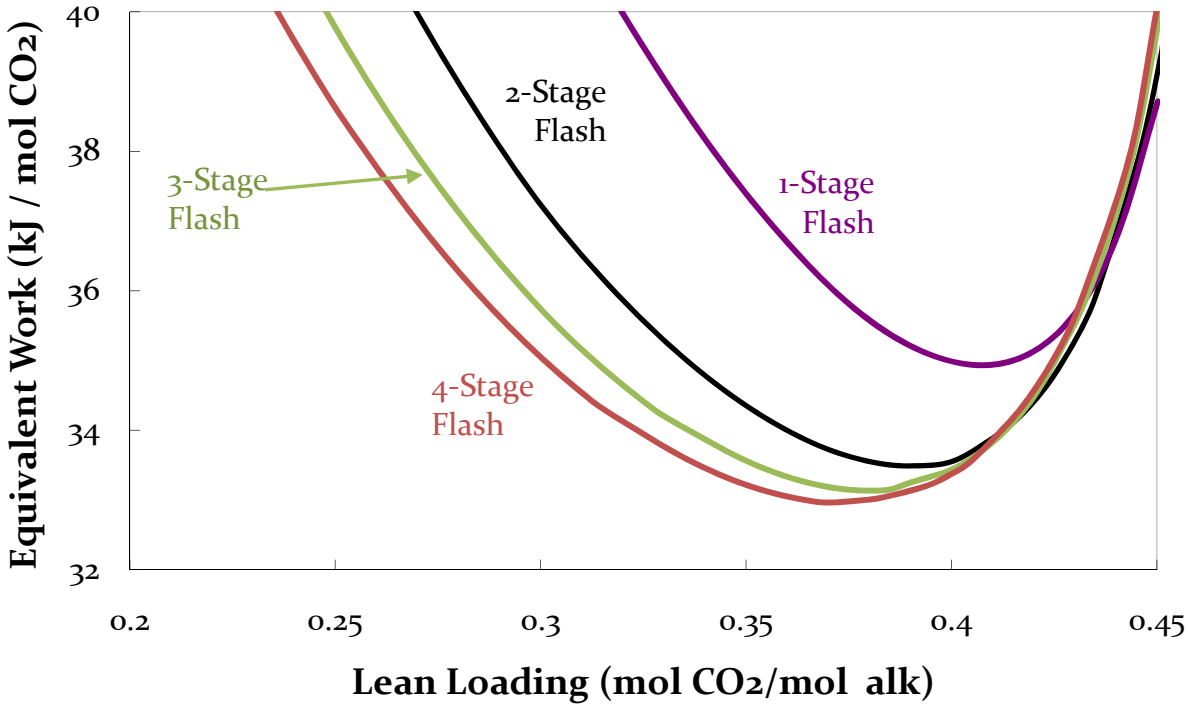

Figure 3: Increasing Complexity Effect with 9 m MEA in Multi-Stage Flash

For future analysis with PZ, the rich loading of 0.415 will not be used. This rich a loading may not be possible to achieve in the absorber. To make the simulation more conservative, a rich loading corresponding to 5 kPa of CO_2 partial pressure at 40 °C will be used. Additionally, a new rich loading for MEA will be evaluated with relevant configurations and temperatures. In this quarter, the new rich loading for MEA was determined based on a 5 kPa rich loading for PZ. Since PZ has approximately twice the reaction rate with CO_2, an appropriate rich/lean loading set for MEA was found which provides twice the driving force of a 5 kPa/0.5 kPa rich/lean loading set for PZ. First, rate data (Dugas, 2009) for MEA and PZ were individually correlated into equation form:

$$\ln k'_{g,MEA} = -0.40 \cdot lnP^* - 14.35 \quad (3)$$

$$\ln k'_{g,PZ} = -0.42 \cdot lnP^* - 13.44 \quad (4)$$

These correlations predicted the effective mass transfer coefficient in mol/s-Pa-m^2 as a function of the equilibrium partial pressure of the solvent in kPa. Using these equations and an assumed 90% removal of CO_2, a set of rich and lean loadings could be calculated for MEA or PZ when given a set of loadings for the other solvent. A log mean flux between rich and lean was calculated for each solvent as a basis for matching the fluxes.

$$N_{CO_2} = \left[k'_g \cdot \left(P_{g,CO_2} - P^*_{l,CO_2}\right)\right]_{LM} \quad (5)$$

As shown in Tables 4 and 5 below, the loadings for a PZ solvent were calculated to match the flux of an MEA solvent with loadings of 5 kPa/0.5 kPa. Similarly, the loadings for an MEA solvent were calculated to match the flux of a PZ solvent with loadings of 5 kPa/0.5 kPa. In the

future, it is expected that the lower loadings will be used for each solvent. MEA will be recalculated for a rich loading of 0.48, and a rich loading of 0.40 will be used for PZ. Also, it is expected that new loadings could be calculated to account for any overstripping/understripping that may result at the optimum lean loading. More specifically, using the PZ rich loading of 0.4 and an optimum lean loading of interest, a fair lean loading for the comparable MEA case will be one that yields an average flux in the absorber equal to the PZ case.

Table 4: P^* sets for MEA and PZ (kPa)

MEA		PZ	
Rich	Lean	Rich	Lean
5.0	0.50	8.4	0.84
1.5	0.15	5.0	0.50

Table 5: Loading Sets for MEA and PZ

MEA		PZ	
Rich	Lean	Rich	Lean
0.50	0.45	0.42	0.33
0.48	0.40	0.40	0.31

Conclusions

- The previous correlation which used a polytropic compression efficiency of 72% and an intercooler pressure drop of 0 kPa was roughly equivalent to a compressor with 80% efficiency and 20% pressure loss in each intercooler.
- A 5 °C approach on the reboiler improved performance over a 10 °C approach by 1.0–1.2 kJ/mol CO_2 fairly equally for all configurations.
- A new Aspen Plus® thermodynamic model for concentrated PZ was used to simulate a 1-stage flash.
- The lowest work requirement with the 1-stage flash using 8 m PZ was 34.7 kJ/mol CO_2 and used a reboiler at 150 °C, a rich loading and 0.415, and a lean loading of 0.34.
- A correlation was developed for k_g', and log mean driving forces in the absorber were calculated to determine acceptable rich loadings for each solvent which recognize the faster reaction rate of PZ.
- A rich loading of 0.48 in MEA assumes roughly equivalent mass transfer area as a rich loading of 0.40 in PZ.

Future Work

The PZ model will be evaluated with other configurations which proved beneficial for 9 m MEA. Additionally, a 5 °C approach on the reboiler will be enforced for these calculations as well as the 1-stage flash calculations. 120 °C and 150 °C will be temperatures of interest for this analysis since they are the ceiling temperatures of MEA and PZ, respectively. 120 °C will be investigated with PZ to determine if there is any benefit of running concentrated PZ in a process configured to run with MEA. Also, the new suggested rich loadings of 0.48 and 0.40 for MEA and PZ will be used to truly compare the performance of the two solvents.

The pilot plant campaign from November 2008 which used concentrated PZ will be used to validate the Aspen Plus® thermodynamic model and more thoroughly analyze the performance in the campaigns.

References

Dugas RE. *Carbon Dioxide Absorption, Desorption, and Diffusion in Aqueous Piperazine and Monoethanolamine.* Ph.D. Dissertation. The University of Texas at Austin. 2009.

Oyenekan BA. Alternative stripper configurations for CO_2 capture by aqueous amines. *AIChE J.* 2007;53(12):3144–3154.

Plaza JM, Van Wagener DH, Rochelle GT. "Modeling CO_2 capture with aqueous monoethanolamine." *Int J Greenhouse Gas Control.* 2010;4(2):161–166.

Modeling CO_2 Absorption Using Aqueous Amines

Quarterly Report for April 1 – June 30, 2010

by Jorge M. Plaza

Supported by the Luminant Carbon Management Program

and the

Industrial Associates Program for CO_2 Capture by Aqueous Absorption

Department of Chemical Engineering

The University of Texas at Austin

July 1, 2010

Abstract

The new thermodynamic model for concentrated PZ, "5deMayo", described by Frailie in this report was used to determine kinetic constants for 8 m PZ. A wetted wall column model was set up as described in Rochelle et al. (2010) to extract kinetic constants from raw data reported by Dugas (2009) for 8 m PZ.

Once the kinetic framework was established, an absorber model was built for the November 2008 and the summer 2010 pilot plant campaigns. It uses a FORTRAN subroutine to implement the Tsai (2008) interfacial area correlation and the viscosity correlation presented by Plaza (Rochelle et al., 2009).

The developed model was used for a preliminary evaluation of intercooling with 8 m PZ. Results show that intercooling may increase CO_2 removal as much as 34%.

Additionally, the previously developed 9 m MEA model was used to determine potential conditions for the summer pilot plant campaign. Results are included in this report.

PZ Kinetics Development

The "5deMayo"' thermodynamic framework was used to set up a wetted wall column (WWC) model to obtain kinetic constants for 8 m PZ. The WWC was implemented as described in Rochelle et al. (2010). Table 1 shows the kinetic expressions included in the 8 m PZ model. The values for the bicarbonate formation reaction (Equations 3a and 3b) determined by Plaza (Rochelle et al., 2010) were adjusted to maintain consistency with the new thermodynamic framework.

Table 1: Kinetic expressions used in the PZ model

Reaction	Rate Expression	
$2\,PZ + CO_2 \rightarrow PZH^+ + PZCOO^-$	$r = k_1 a_{PZ} a_{CO_2} a_{PZCOO^-}$	(1a)
$PZH^+ + PZCOO^- \rightarrow 2\,PZ + CO_2$	$r = \frac{k_1}{K_{PZCOO^-}} \frac{a_{PZH^+} a^2_{PZCOO^-}}{a_{PZ}}$	(1b)

$2\,PZCOO^- + CO_2 \rightarrow PZ(COO^-)_2 + H^+PZCOO^-$	$r = k_2 a^2_{PZCOO^-} a_{CO_2}$	(2a)
$PZ(COO^-)_2 + H^+PZCOO^- \rightarrow 2\,PZCOO^- + CO_2$	$r = \frac{k_2}{K_{PZ(COO^-)_2}} a_{H^+PZCOO^-} a_{PZ(COO^-)_2}$	(2b)
$PZCOO^- + CO_2 + H_2O \rightarrow HCO_3^- + H^+PZCOO^-$	$r = k_3 a_{PZCOO^-} a_{CO_2}$	(3a)
$HCO_3^- + H^+PZCOO^- \rightarrow PZCOO^- + CO_2 + H_2O$	$r = \frac{k_3}{K_{HCO_3^-}} \frac{a_{H^+PZCOO^-} a_{HCO_3^-}}{a_{H_2O}}$	(3b)
$PZ + H^+PZCOO^- \leftrightarrow PZH^+ + PZCOO^-$	Equilibrium*	(4)

*Reaction 4 is included as an equilibrium reaction.

In the earlier work (Rochelle et al., 2010) the rate constants were adjusted to match K_G. In this work, the rate constants were adjusted to match the measured values ofCO_2 flux (N_{CO2}) with desorption and absorption data from Dugas (2009). Appendix A shows the data selected to extract kinetic constants. CO_2 flux in the WWC was calculated as follows:

$$N_{CO_2} = \frac{n^{in}_{CO_2} - n^{out}_{CO_2}}{A_{intf}} \quad (5)$$

where: n is the mole flow of CO_2 in and out of the WWC, and
A_{intf} is the interfacial area of the WWC.

Results match reported flux data within 20% for 40, 60, and 80 °C as seen in Figure 1. However, deviation increases for 100 °C. This might be related to other phenomena taking a larger role in the absorption/desorption process such as the diffusion of reactants and products.

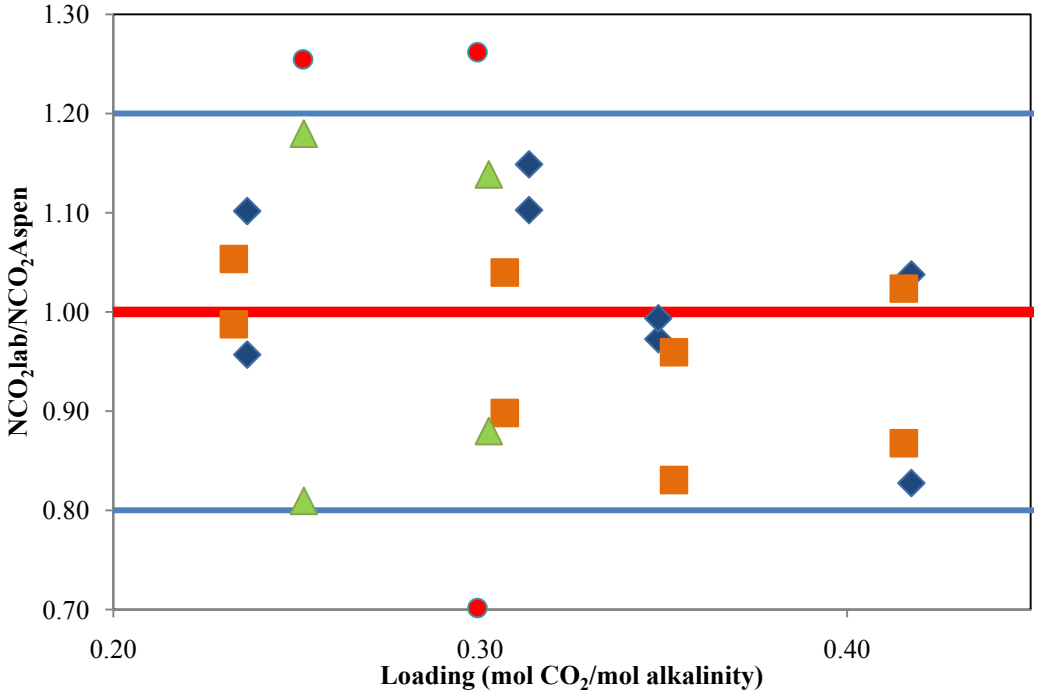

Figure 1: Ratio between carbon dioxide flux obtained in the lab and using the Aspen Plus® WWC model. (♦) 40 °C, (■) 60 °C, (▲) 80 °C, (●) 100 °C

8 m PZ Absorber Model

The "5deMayo" thermodynamic framework and the obtained kinetic constants were used to build an absorber model for 8 m PZ. Figure 2 shows the conditions for the model.

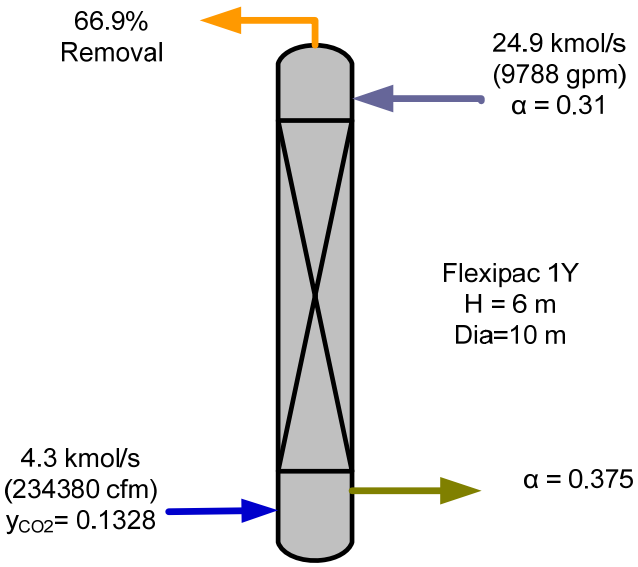

Figure 2: 8 m PZ CO_2 Absorber model conditions

The resulting temperature and CO_2 mass transfer profiles (Figure 3) suggest that intercooling may improve the performance of this system. The mass transfer pinch is located near the temperature bulge similar to the cases in Plaza et al. (2009). Intercooling in the middle of the column to 40 ^{o}C (Figure 4) breaks the pinch allowing the absorber to reach 90% removal with a rich loading of 0.398.

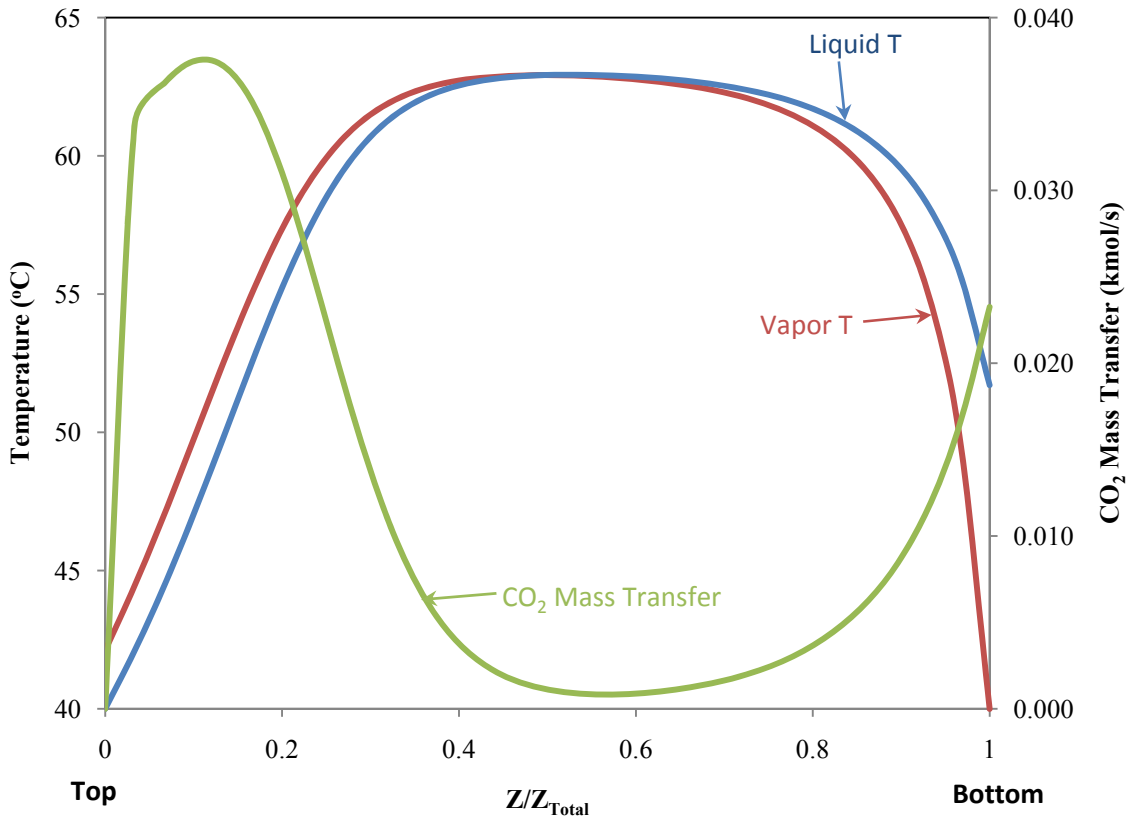

Figure 3: Temperature and CO_2 Mass Transfer Profiles for an absorber with 8 m PZ without intercooling, lean loading = 0.31, rich loading = 0.375, 66.9% CO_2 removal

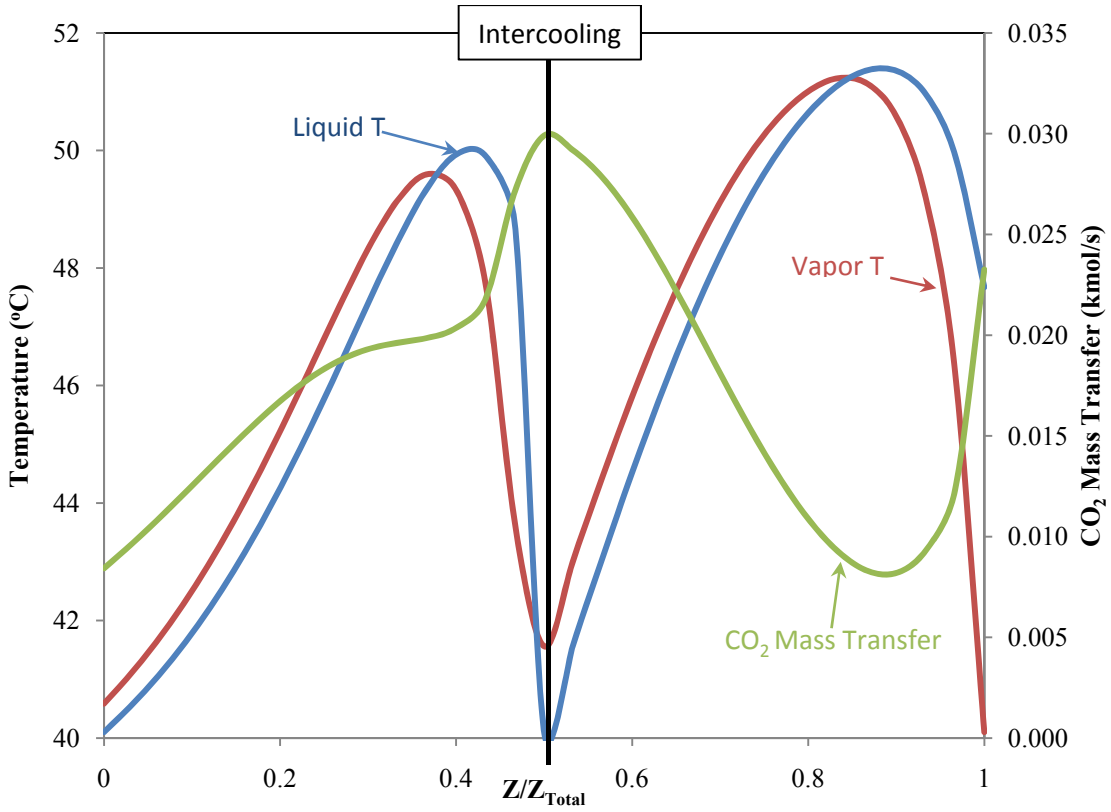

Figure 4: Temperature and CO_2 Mass Transfer Profiles for an Intercooled Absorber with 8 m PZ

Summer 2010 Pilot Plant Campaign

The summer 2010 pilot plant campaign will demonstrate the performance of 8 m PZ and process concepts such as intercooling and the two-stage flash. This campaign will use two 3.05 m beds of the novel packing Raschig Super-Pak 250 (RSP250). This packing was added to the absorber model It will be implemented in the absorber model using the interfacial area by Tsai (2008). Since this packing is a hybrid between structured and random packing, the required channel dimensions for the Tsai correlation are not available (base, side, and height) so the specific area reported for RSP250 was used as an approximation to the wetted perimeter in the Tsai correlation:

$$L_p = A_{sp} = \frac{4S}{Bh} \tag{6}$$

where: L_p is the packing wetted perimeter.
A_{sp} is specific area of the packing (for RSP250 it is 250 m^2/m^3)
S is the packing channel side (m)
B is the base of the packing channel (m)
h is the height of the packing channel (m)

The base (B) and height (h) of the packing channel were taken from Flexipac 1Y and the side (S) was calculated to match A_{sp} for RSP250.

The summer campaign will also include runs for 9 m MEA with and without intercooling. Using the previously developed MEA model (Plaza et al., 2010), the critical L/G has been determined (Figure 5) and the conditions for the MEA runs were proposed to compare the performance of intercooling for this solvent. Table 2 presents the proposed process conditions and the expected results.

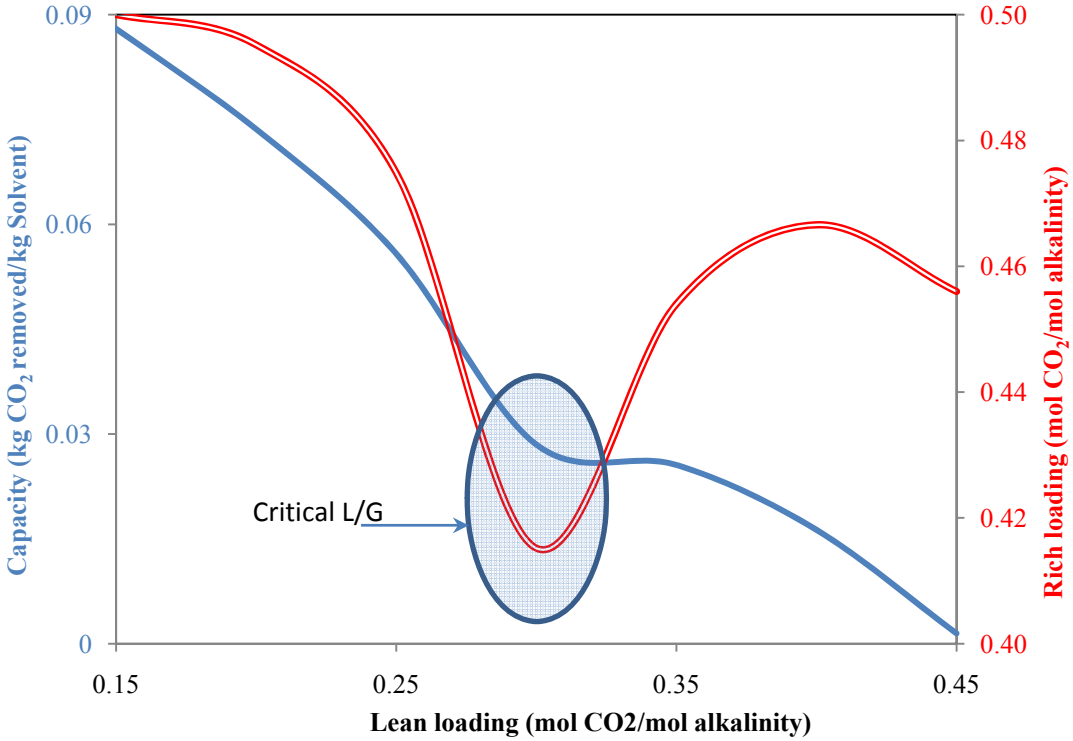

Figure 5: Critical L/G determination using change in solvent capacity and rich loading with respect to lean loading. 9 m MEA. 90% CO_2 removal with 6.1 m of RSP250 packing. Diameter 0.427 m

Table 2: Proposed Pilot Plant Conditions. 9 m MEA. 6.1 m RSP250. Diameter 0.427 m, intercooling of liquid to 40 ^oC at middle, 12% inlet CO_2

Run*	Lean Solvent (gpm)	Gas Flow (cfm)	Lean Ldg (mol CO_2/mol alkalinity)	Rich Ldg	CO_2 Removal %	Intercooling
1	17	350	0.300	0.42	90.0	NO
2	17	350	0.350	0.451	75.2	NO
3	17	350	0.300	0.430	97.8	YES
4	17	350	0.350	0.470	91.8	YES
5	11	350	0.300	0.470	81.6	NO
6	11	350	0.294	0.481	90.0	YES
7	9.38	500	0.200	0.493	90.0	YES
8	9.38	500	0.200	0.490	88.9	NO

9	15	500	0.287	0.468	90.0	YES
10	15	500	0.287	0.455	83.3	NO

*Runs 1–4 have been specified in the critical L/G region.

Conclusions

A new absorber model for 8 m PZ has been developed. It uses the 5deMayo v.1 thermodynamic framework and kinetics extracted from experimental work by Dugas (2009) using the WWC. The reported CO_2 flux data are matched with a ±20% deviation using the developed WWC model (Figure 1). Model results above 80 ^oC show a higher deviation from experimental data due to additional phenomena becoming predominant at these conditions, possibly the increase of diffusion effects of reactants and products.

Preliminary evaluation of 8 m PZ using the developed model shows that intercooling may improve considerably the performance of an absorber. Intercooling to 40 ^oC in the middle of the column generated an increase in CO_2 removal of 34%.

The study of the critical L/G for the 9 m MEA runs in the summer 2010 pilot plant campaign showed similar behavior to that observed by Plaza (2009) for K^+/PZ. At the left of the critical L/G (ldg<0.30) the improvement due to intercooling is marginal. However around the critical L/G region (ldg ≈ 0.30) intercooling offers an improvement as high as 10% in removal.

Future Work

The PZ absorber interface for the developed model will be analyzed to optimize segment number and position. Currently the maximum number of segments possible (50) has been used. This variable will be fine tuned before model reconciliation and validation using data from the November 2008 pilot plant campaign.

The validated and reconciled model will be used to generate conditions to be run in the summer 2010 pilot plant campaign.

The validated MEA and PZ models will be used to study and compare intercooling using each solvent. Results will be compared and applied to improve on the critical L/G equation proposed in Plaza et al. (2009).

References

Dugas RE. *Carbon Dioxide Absorption, Desorption and Diffusion in Aqueous Piperazine and MEA.* The University of Texas at Austin. Ph.D. Dissertation. 2009.

Plaza JM, Chen E, Rochelle GT. "Absorber Intercooling in CO_2 Absorption by Piperazine Promoted Potassium Carbonate." *AIChE J.* 2009;56(4):905–914.

Plaza JM, Van Wagener DH, Rochelle GT. "Modeling CO_2 capture with aqueous monoethanolamine." *Int J Greenhouse Gas Control.* 2010;4(2):161–166.

Rochelle GT, et al. "CO_2 Capture by Aqueous Absorption, Third Quarterly Progress Report 2009." Luminant Carbon Management Program. The University of Texas at Austin; 2009.

Rochelle GT, et al. "CO_2 Capture by Aqueous Absorption, Fourth Quarterly Progress Report 2009." Luminant Carbon Management Program. The University of Texas at Austin. 2010.

Tsai R, Seibert AF, Eldridge B, Rochelle GT. "Influence of Viscosity and Surface Tension on the Effective Mass Transfer Area of Structured Packing." *Energy Proc.* 2008;1:1197–1204.

Appendix A: Regressed data set

Table A-1: WWC selected data for extraction of CO_2 kinetic data

No.	Temperature (^oC)	Loading (mol CO_2/mol Alkalinity)	PCO_2 (Pa)	Flux (mol/s-m^2)
1	40	0.237	0	$-1.07*10^{-4}$
2		0.237	180	$1.88*10^{-4}$
3		0.313	0	$-6.66*10^{-4}$
4		0.313	1500	$1.07*10^{-3}$
5		0.349	0	$-8.72*10^{-4}$
6		0.349	2400	$5.62*10^{-4}$
7		0.4175	0	$-1.99*10^{-3}$
8	40	0.417	11500	$8.18*10^{-4}$
9	60	0.233	0	$-7.67*10^{-4}$
10		0.233	1150	$1.15*10^{-3}$
11		0.307	0	$-2.75*10^{-3}$
12		0.307	4000	$1.46*10^{-3}$
13		0.353	0	$-3.57*10^{-3}$
14		0.353	11000	$1.55*10^{-3}$
15		0.415	0	$-7.14*10^{-3}$
16		0.415	58000	$6.26*10^{-3}$
17	80	0.252	0	$-5.85*10^{-3}$
18		0.252	7500	$4.94*10^{-3}$
19		0.302	0	$-9.22*10^{-3}$
20		0.302	20000	$8.45*10^{-3}$
21	100	0.252	0	$-1.58*10^{-2}$
22		0.252	30000	$7.01*10^{-3}$
23		0.299	0	$-2.07*10^{-2}$
24		0.299	75000	$1.86*10^{-2}$

Optimization of Design and Operation in MEA Plant

Quarterly Report for April 1 – June 30, 2010

by Sepideh Ziaii Fashami

Supported by the Luminant Carbon Management Program

and the

Industrial Associates Program for CO_2 Capture by Aqueous Absorption

Department of Chemical Engineering

The University of Texas at Austin

July 5, 2010

Abstract

In the previous quarter, the integrated dynamic model of the absorber and stripper with MEA, created in Aspen Custom Modeler (ACM)®, was combined with a first order approximation model of steam turbines in order to take into account steam pressure variation during dynamic operation.

In this quarter, the multi-variable steady state optimization tool of the ACM® was implemented to maximize the profit of the 100 MW coal-fired power plants as the ratio of CO_2 selling price to electricity price varies. This steady state optimization gives the optimum design curves for lean loading and CO_2 removal versus price ratio.

In addition, implementing multi-variable dynamic optimization tools and running the simulation at dynamic mode enabled us to optimize the operation of the capture in response to two dynamic scenarios: partial steam load in flexible capture and partial boiler load operation. The results have shown that as the load varies, controlling L/G at the design value in the stripper and absorber can lead the plant to stay close to the optimum path and consequently the cost of employing an advanced multi-variable control system can be avoided.

Introduction

Dynamic modeling of a process is a helpful tool that is commonly used not only for analyzing the dynamic behavior and designing simple control strategies but also for optimizing the operation of the plant in response to possible disturbances. However, this powerful tool has not been previously implemented for optimizing the operation and control of the aqueous absorption plant. In the few works found on dynamic modeling in available literature (Kvamsdal et al., 2009; Ziaii et al., 2009), the dynamic simulation of absorption/stripping with MEA was only used to investigate the dynamic behavior of the system in response to the partial load operational scenarios. No method was implemented to optimize the operation of the plant during transitional operations.

In this work, first, the steady state optimization tool of ACM® was used for detailed design of the capture by maximizing the total power plant profit as the ratio of the CO_2 to electricity prices changes by running the steady state model of the capture with design specifications. Second, the dynamic optimization tool was tied with dynamic simulation of the MEA plant which is initially designed at a specific optimum design point to find optimized set point paths for the solvent rate and the steam rate for two partial load operation scenarios. This optimization maximized the power plant profit at the time when the new steady state is reached by optimizing the final values of the solvent rate, steam rate, and stripper top pressure. The first scenario represents the variation that may happen in the electricity or CO_2 market conditions and the second one represents the variation of the boiler load that directly affects the operation of the capture.

Analytical Methods

As explained in the first quarterly report of 2010, the fully integrated model of the MEA system was created in an ACM® flow sheet. The whole model consists of the dynamic model of the absorber and stripper, steady state models of the heat exchangers, steady state performance curves of multi-stage compressor and a first order-approximated model of a three-stage steam turbine.

The case study that we discuss in this report is a base case with 7 m MEA in a 100 MW coal-fired power plant. The main design specifications are fixing the maximum flooding at 80% to determine the column diameter, 120 °C as the design reboiler temperature, 10 °C temperature approach for the reboiler, and 5 °C temperature approach for the cross heat exchanger. The absorber contains 15 m of Mellapak 250Y packing and the stripper contains 10 m of the same packing (Figure 1).

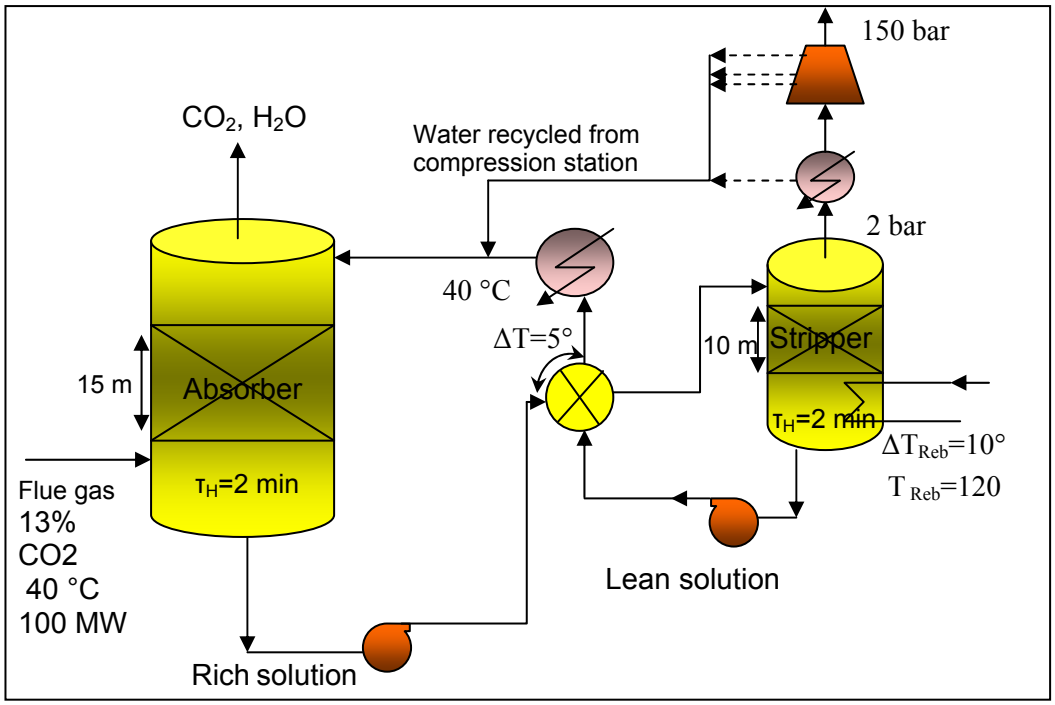

Figure 1: Absorption/stripping process flow sheet with design specification

The steady state and dynamic optimization done in this work uses power plant profit ($/day) as the objective function. Equation 1 gives the formulation of this objective function:

$$Profit(\$/hr) = Elec.Price(\$/kWh) \times Elect.gen.(kW) + CO_2\ Price(\$/ton) \times removedCO_2(ton/hr) \quad (1)$$

where the electricity generation is the energy, which can be generated by steam in the power cycle, minus total lost work due to CO_2 capture.

Equation 2 calculates total lost work in a CO_2 capture plant:

$$W_{lost} = 0.75 Q_{Reb}\left(\frac{T^{sat}(P_{ext}) - T_{sink}}{T^{sat}(P_{ext})}\right) + W_{comp} + W_{pumps} \quad (2)$$

It is assumed that the total energy generated by steam is only a function of total steam rate in the steam cycle and varies proportional to that variable. The influence of other factors, such as steam turbine inlet/outlet conditions, is neglected.

Obviously, this objective function only represents the trade off between the work lost and amount of CO_2 removed. It does not reflect the influence of capital cost of the power cycle and capture on the profit.

Steady State Optimization

We implemented the FEASOPT optimization method in ACM® and ran it with the steady state model of a MEA plant in the steady state running mode to maximize the profit by optimizing the lean loading and CO_2 removal at the same time. Other independent process variables were set at their design specification as shown in Figure 1. Optimization was carried out for different values of the ratio of CO_2 price to the electricity price ranging from 2 to 7($/ton CO_2)/(cents/kWh)). This steady state optimization provides optimum design curves for lean loading and removal as a function of price ratio. The results are shown in Figures 3, 4, 6, 7, and 8 and the explanation is in the discussion section.

Dynamic Optimization

The purpose of implementing dynamic optimization was to find optimum operational curves for manipulated variables to maximize the power plant profit. The capture was initially designed at the optimum point obtained from above discussed design optimization where the price ratio is 2.6 and associated optimum removal and lean loading are 90.1% and 0.225 respectively.

The dynamic optimization procedure maximizes the objective function when the new steady state is reached by running the model of the process in the dynamic mode and getting the final values of process variables in response to a specific disturbance in each iteration. The dynamic simulation of our system cannot be carried out unless we replace design specifications by dynamic specifications. Important dynamic specs in our system are listed in Table 1:

Table1: Variable specifications for dynamic simulation and optimization

	Free	Fixed
Columns	Flood factor	Dc
Heat exchangers	ΔT	Area and overall heat

Reboiler	ΔP T_{Reb}	transfer coefficient Kv (Kv= ΔP/F)
Valves	ΔP	Cv
Compressor and pumps	Moving on the general constant speed performance curve	
Sumps	τ_{liq}	

As shown in Figure 2, there are four valves in the flow sheet that can be used for control purposes. The valve on the lean solution is manipulated to control the level in the reboiler. The other three valves regulate the steam, solvent, and the vapor rate at the top of the stripper. The operating curves provided by dynamic optimization only give the optimum final values of the controlled variables so that they can be used only to establish a set point. With the current optimization in this work, controller tuning parameters are not optimized.

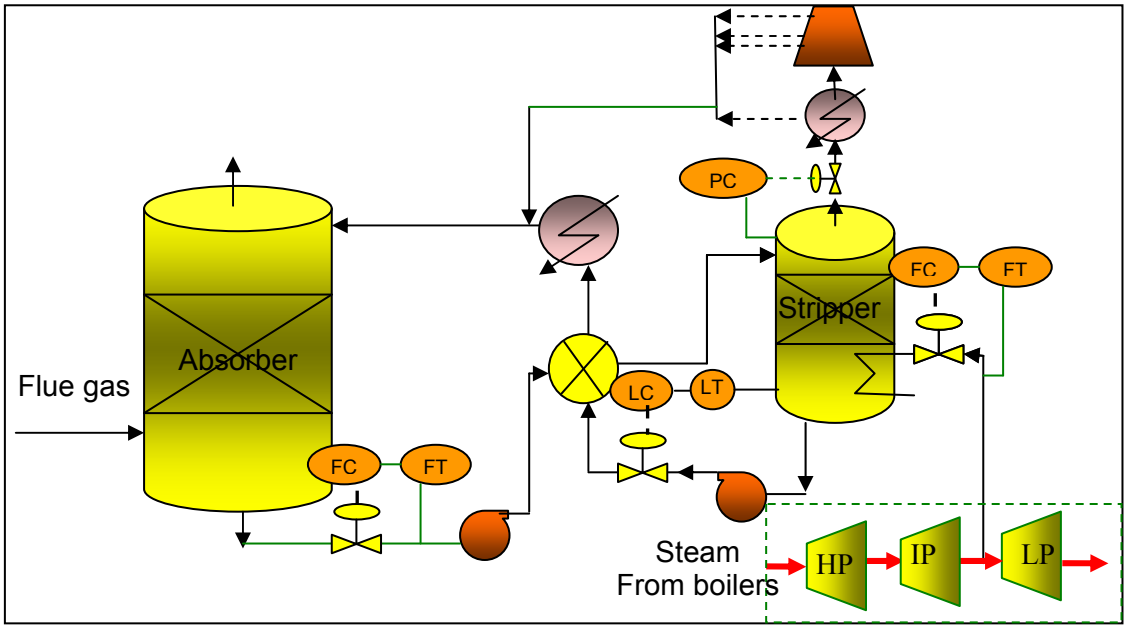

Figure 2: Absorption/stripping process flow sheet with control valves

This analysis implemented the FEASOPT method to do multi-variable dynamic optimization and ultimately optimized the set point paths of steam rate, solvent rate, and stripper pressure over a range of variations in disturbances for two dynamic scenarios:

1. Partial steam load operation in flexible capture: this allows recovery of some or all of the energy required for solvent regeneration and CO_2 compression to increase power output under appropriate electricity market conditions. In this scenario, the model is optimized in response to the price ratio variation over a range of 2 to 5.
2. Partial boiler load operation: an upstream disturbance exposing capture specifically in a variable load power plant. It is simulated by making the same percentage changes in both flue gas rate and power cycle steam rate simultaneously. In this work the boiler load is reduced up to 70% of the full load.

Results and discussion

Optimization in Response to the Price Ratio Variation

As discussed in the previous section, the steady state optimization was performed to optimize design variables (lean loading and CO_2 removal) for different values of price ratios. Then dynamic optimization was carried out for a case study designed at a specific point on the optimum design curve (price ratio = 2.6, removal = 90.1%, lean loading = 0.225) to find the optimum operating curve as the price ratio varies. This means that if the controller set point moves on the operating curve as the price ratio varies, we can make the highest profit at the new steady state condition. Therefore, this level of optimization does not optimize the dynamic characteristics and cannot give any information about the behavior of the system during the transition time. Where the dynamic performance of the system is concerned, we should have carried out a dynamic optimization with another objective function which may include weighted terms of the difference between the optimum set points and controlled variables and/or a term representing the reaching time to find the fastest and shortest path to the new operating condition. Figures 3, 4, 6, and 7 indicate both optimum design curve and operating curve found for some of the important process variables.

Figure 3 illustrates the design and operating curves of CO_2 penetration versus price ratio. CO_2 penetration is defined as the fraction of the CO_2 in the flue gas that is released to the atmosphere. It is formulated as follows:

$$CO_2\,penetration = 1 - CO_2\,removal \tag{3}$$

As shown in Figure 3, as the price ratio increases, meaning that the CO_2 price increases or electricity price decreases, the plant should be designed at higher level of removal. For low price ratios (2–3) the rate of the reduction is much higher relative to the higher price ratios. The design curve shows a big change around price ratio = 2.1, which means that there are two local optima around this point, at 53% and 70% removal. The minimum number shown on x axis is 2, because at this point the value of CO_2 becomes zero and at a price ratio lower than 2, the use of CO_2 capture has no value. The optimum operating curve deviates from the design curve specifically when the new price ratio is higher than the initial price ratio because of using different specifications in steady state and dynamic simulation (listed in Table1). Even at the design point (price ratio = 2.6) the optimum operating point does not lie on the design curve because for design optimization the level of the liquid in the absorber sump is not optimized but fixed based on 2-minute liquid hold-up time, while for operation optimization the liquid level is a free variable and is optimized to minimize the energy consumption associated with the rich solution pump. Therefore, the initial absorber sump level and consequently other variables such as solvent circulation rate, lean loading, and removal are not identical for design and initial operating condition.

Figure 4 indicates how the optimum lean loading varies with price ratio for both design and operating cases. No significant deviation is seen between the design and operating curves for lean loading for the selected case study.

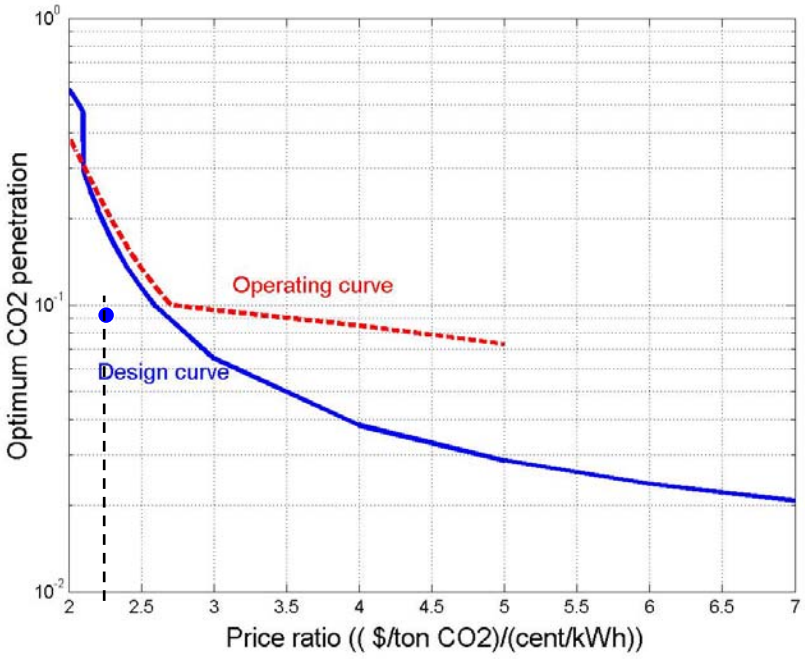

Figure 3: Optimum design curve and optimum operating curve of CO_2 penetration versus the ratio of CO_2 price to electricity price, H_{abs}=15m, H_{strip} = 10m, cross heat exchanger ΔT_{design} = 5 °C, reboiler ΔT_{design} = 10 °C, reboiler T_{design} = 120 °C, s_{umps} = 2 min, operating curve obtained for the plant designed at price ratio = 2.6 (removal = 90.1% and lean loading = 0.225)

Considering the design curve, at medium and high price ratios where the system is designed at removal higher than 70%, the optimum lean loading is lower than 0.25, while at low level of removal (≤ 53%), optimum lean loadings are greater than 0.39. Figure 5 illustrates how the optimum lean loading moves from low to high as the level of removal increases. Comparing the equivalent work curve of 90% removal to 70% and 53%, we can see that at lower removal the minimum part of the curve is very flat so that the global minimum can easily change from low to high as the removal varies slightly. That is why the optimum lean loading changes significantly around price ratio = 2.1.

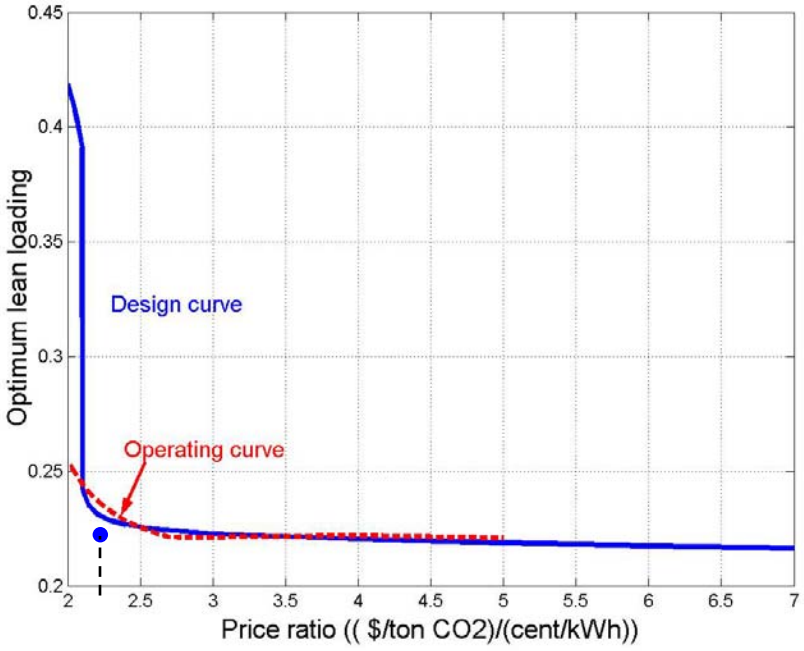

Figure 4: Optimum design curve and optimum operating curve of lean loading versus the ratio of CO_2 price to electricity price, H_{abs} = 15m, H_{strip} = 10m, cross heat exchanger ΔT_{design} = 5 °C, reboiler ΔT_{design} = 10 °C, reboiler T_{design} = 120 °C, τ_{sump} = 2 min, operating curve obtained for the plant designed at price ratio = 2.6 (removal = 90% and lean loading 0.225)

Figure 6, representing optimum solvent rate versus price ratio, shows such a jump at this specific point. However, there is no jump seen for optimum steam rate (see Figure 7). One of the variables that were optimized during dynamic optimization is pressure at the top of the stripper. The results suggest that in order to stay on maximum profit and minimum energy lost, the pressure valve should be kept wide open and the stripper pressure should be allowed to drop as the steam rate reduces.

Looking at optimization results for different process variables can help us to determine a better control strategy for a dynamic scenario and find the best control variables. This method would be more helpful if an advanced multi-variable control method is no longer used and just a simple SISO multi-loop scheme is desired. For example, if we look at the plot sketching optimum solvent rate versus steam rate (Figure 8), a linear relation is observed between these variables. Both variables are normalized to their design value. Although the slope of the line deviates slightly from one, we can set a ratio control on the steam rate and solvent rate and still stay close to the optimum path. By using this control strategy in practice, the number of decision variables that should be optimized through a real time optimization is reduced and consequently convergence time of optimization decreases.

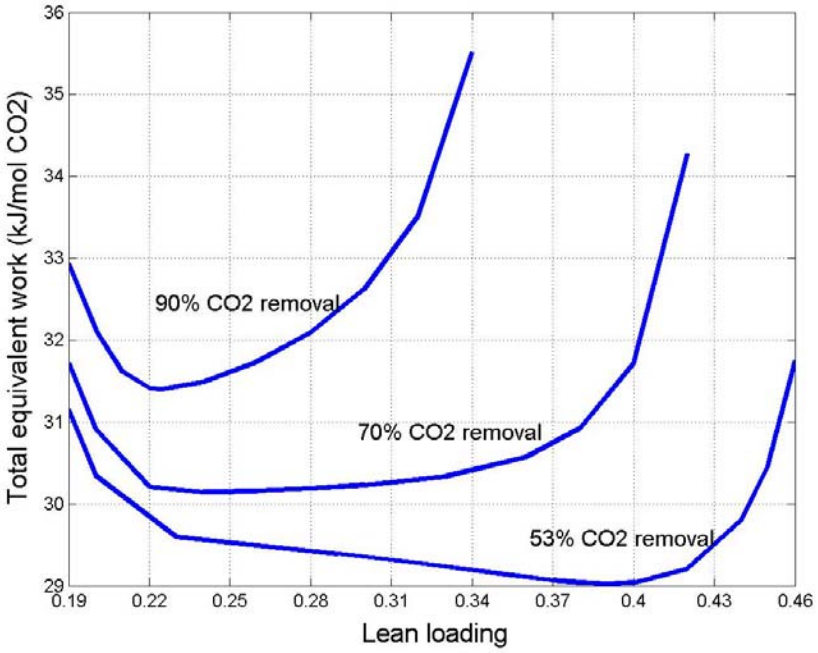

Figure 5: Capture total lost work versus lean loading, H_{abs} = 15m, H_{strip} = 10m, cross heat exchanger ΔT_{design} = 5 °C, reboiler ΔT_{design} = 10 °C, reboiler T_{design} = 120 °C

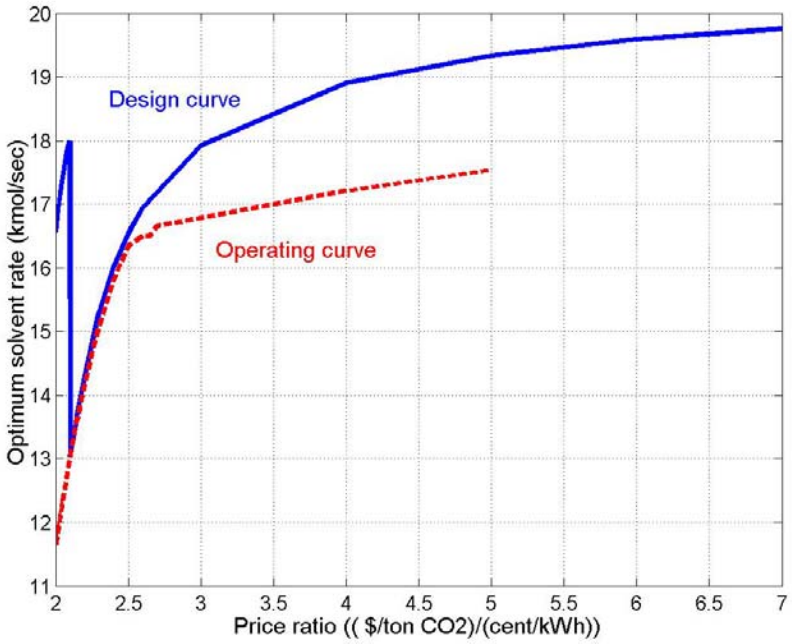

Figure 6: Optimum design curve and optimum operating curve of solvent flow rate versus the ratio of CO_2 price to electricity price, H_{abs} = 15m, H_{strip} = 10m, cross heat exchanger ΔT_{design} = 5°C, reboiler ΔT_{design} = 10 °C, reboiler T_{design} = 120 °C, τ_{sump} = 2 min, operating curve obtained for the plant designed at price ratio = 2.6 (removal= 90% and lean loading = 0.225)

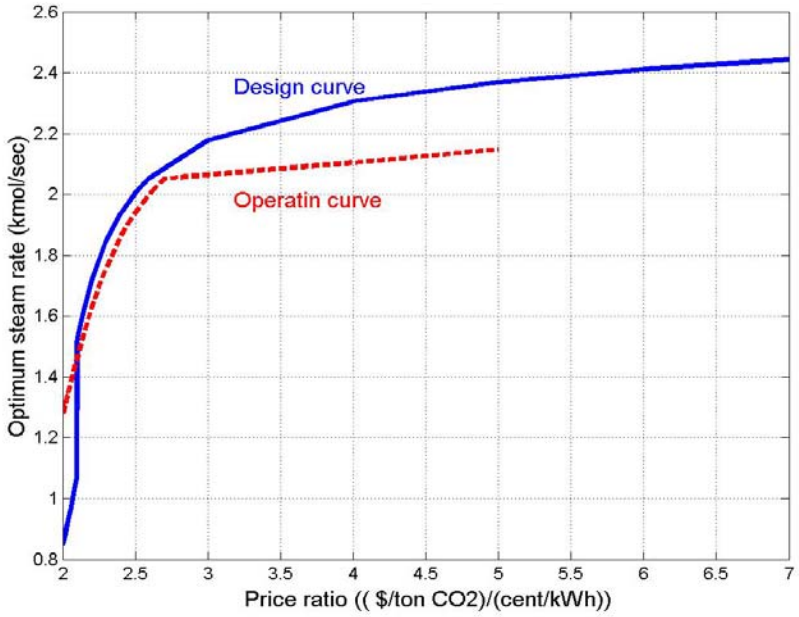

Figure 7: Optimum design curve and optimum operating curve of steam flow rate versus the ratio of CO_2 price to electricity price, H_{abs} = 15m, H_{strip} = 10m, cross heat exchanger ΔT_{design} = 5 °C, reboiler ΔT_{design} = 10 °C, reboiler T_{design} = 120 °C, τ_{sump} = 2 min, operating curve obtained for the plant designed at price ratio = 2.6 (removal = 90% and lean loading = 0.225)

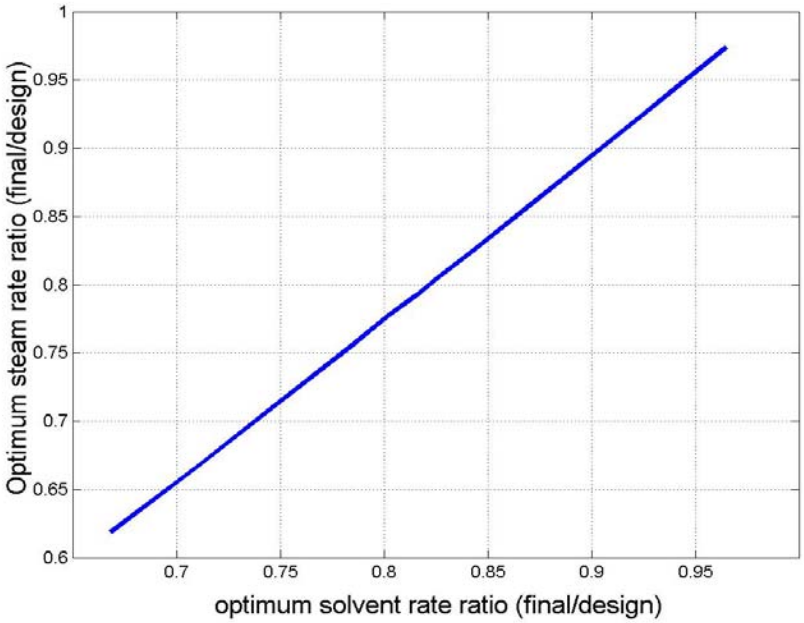

Figure 8: Optimum operating curve of steam flow rate versus solvent flow rate for the plant designed at price ratio = 2.6 (removal = 90% and lean loading = 0.225) with design specifications: H_{abs} = 15m, H_{strip} = 10m, cross heat exchanger ΔT_{design} = 5 °C, reboiler ΔT_{design} = 10 °C, reboiler T_{design} = 120 °C, τ_{sump} = 2 min

Optimization in Response to the Partial Boiler Load Operation

As mentioned in dynamic optimization in the analytical methods section, in variable load power plant boilers may be operated at a reduced load due to with reduced power demand and this would affect the operation of the absorber and stripper. When the boiler load decreases, the flow of flue gas directed to the absorber and total steam rate entering the first stage of steam turbine decreases. Changing total steam rate in the power cycle influences the stripper operation by changing the rate and the pressure of extracted steam entering the reboiler. In the simulation of this operation, we assumed that both flue gas rate and total steam rate vary proportionally to the boiler load.

The simulation and optimization of this dynamic scenario is performed for the plant designed initially at 90.1% removal and 0.225 lean loading. Similar to the partial steam load operation, optimizing the pressure shows that keeping the pressure valve always wide open and letting the stripper pressure drop with decreasing steam rate would be the most energy efficient and profitable strategy for partial boiler load operation.

As Figure 9 indicates, optimum steam rate and solvent rate vary linearly with the boiler load. The deviation of the slope of the solvent rate from 1 is slightly more than steam rate. Since the deviation of slopes of solvent and steam rates are not significant, by placing a ratio control loop between flue gas rate, steam rate, and solvent rate the plant may stay close to the optimum path without spending too much for real-time optimization expenses.

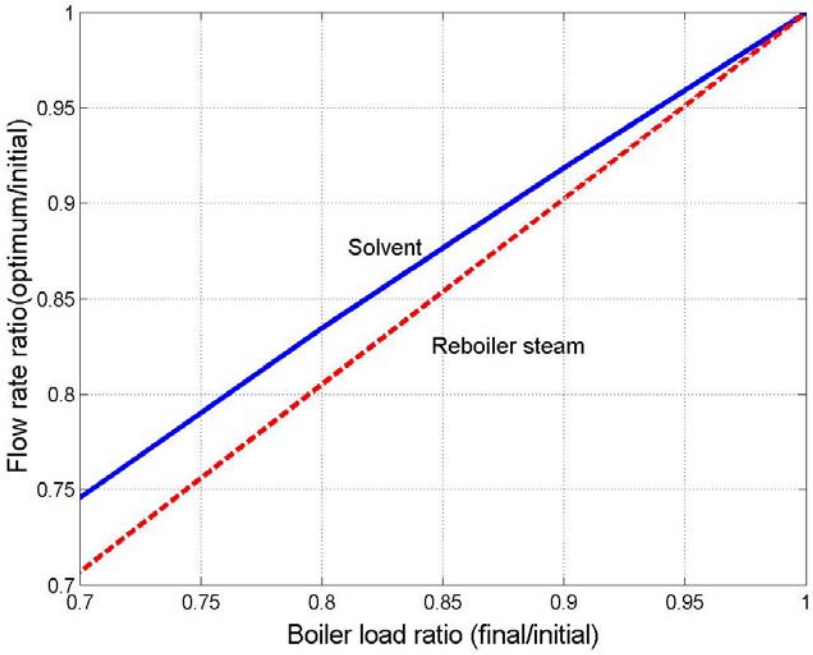

Figure 9: Optimum steam rate and solvent rate (normalized by initial rates) versus normalized boiler load, H_{abs} = 15m, H_{strip} = 10m, cross heat exchanger ΔT_{design} = 5 °C, reboiler ΔT_{design} = 10 °C, reboiler T_{design} = 120 °C, τ_{sump} = 2 min, operating curve obtained for the plant designed at price ratio = 2.6 (removal = 90% and lean loading = 0.225)

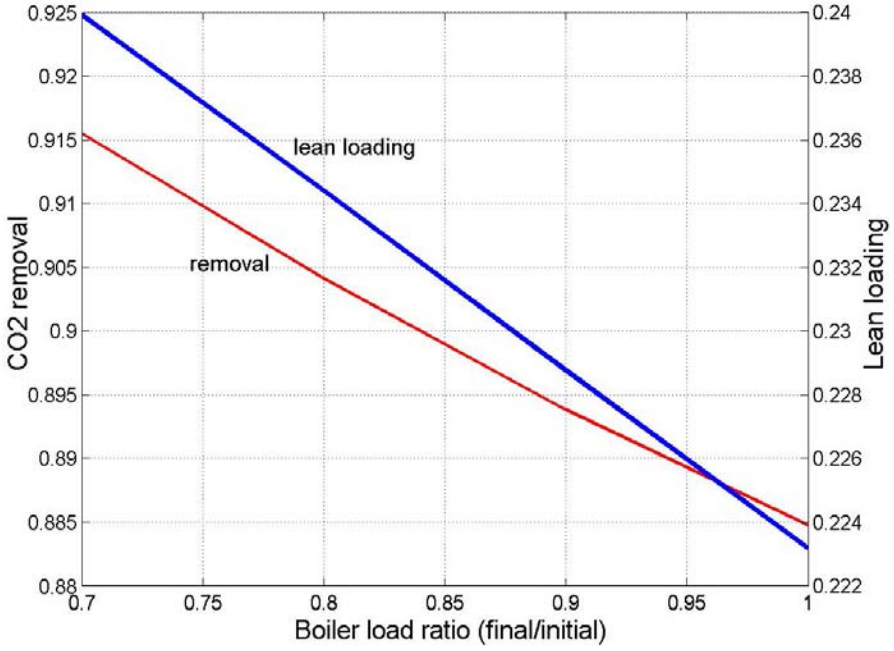

Figure 10: Optimum CO_2 removal and lean loading versus normalized boiler load, H_{abs} = 15m, H_{strip} = 10m, cross heat exchanger ΔT_{design} = 5 °C, reboiler ΔT_{design} = 10 °C, reboiler T_{design} = 120 °C, τ_{sump} = 2 min, operating curve obtained for the plant designed at price ratio = 2.6 (removal = 90% and lean loading = 0.225)

Optimum CO_2 removal and lean loading changes linearly with boiler load (Figure 10). As shown in Figure 10, both optimum removal and lean loading increase as boiler load decreases. Since the rich loading goes up as the inlet CO_2 flow rate increases and L/G decreases in the absorber, lean loading goes up slightly although the stripper L/G rate is almost constant.

From a process control perspective, the current results indicate that keeping L/G constant in both absorber and stripper is a control strategy that enables the plant to run close to the optimum path during variable load operation of the boiler.

Conclusions

1) The dynamic model of the absorption/stripping process was integrated with the first order approximation model of the power plant steam turbines. By doing so, the variation of steam pressure at the IP/LP crossover point is taken into account in dynamic simulation.

2) Power plant profit was maximized by implementing the multi-variable steady state optimization tools of ACM® for the capture model design specifications. Lean loading and removal simulation were optimized at different values of price ratio (CO_2 price/electricity price) for design purposes. Results show that:

    a. when the price ratio is between 2.1 and 7, the plant should be designed for removal between 70% and 98% and lean loading in the range of 0.22–0.25.

    b. The jump observed at a price ratio of 2:1 represents the appearance of two local optimum points for lean loading and removal.

c. For a price ratio lower than 2:1, the plant should be designed at high lean loading (≥ 0.39).

3) Two operational scenarios were dynamically simulated: partial reboiler steam load and partial boiler load operations. By implementing the multi-variable dynamic optimization tools of ACM® to maximize profit , solvent rate, steam rate, and stripper pressure were optimized. The results show that:

   a. For reboiler steam partial load operation, surprisingly, a linear relationship exists between the optimum solvent rate and reboiler steam rate with the line slope very close to 1.

   b. For boiler partial load operation, a linear relationship exists between the optimum solvent rate and reboiler steam rate with the boiler load. The slope of the line is relatively close to 1.

   c. For both scenarios, keeping the pressure valve wide open and letting the stripper pressure swing is found to be the most profitable strategy.

   d. This significant observation leads to a practical application in which the ratio control between the solvent rate and steam rate in scenario 1 and ratio control between the solvent rate, steam rate, and flue gas rate in scenario 2 can be proposed as optimum strategies in response to the associated disturbances.

Future Work

For the next quarterly report, we plan to investigate the effects of controllers tuning parameters on the energy performance during the transition time. We will also evaluate the effects of the liquid hold-up time in column sumps on the dynamic performance to see if any additional solvent inventory is required.

References

Kvamsdal HM, Jakobsen JP, Hoff KA. "Dynamic Modeling and Simulation of a CO_2 Absorber Column for Post-Combustion CO_2 Capture". *Chem Eng & Proc*. 2009;48:135–144.

Rochelle GT et al. "CO_2 Capture by Aqueous Absorption, First Quarterly Progress Report 2010." Luminant Carbon Management Program. The University of Texas at Austin. 2010.

Ziaii S, Cohen SM et al. "Dynamic operation of amine scrubbing in response to electricity demand and pricing." *GHGT-9*. Washington, DC. 2008.

Electric Grid-Level Implications of Flexible CO_2 Capture Operation

Quarterly Report for April 1 – June 30, 2010

by Stuart Cohen

Supported by the EPA STAR Fellowship Program and the
Luminant Carbon Management Program

Department of Chemical Engineering
The University of Texas at Austin

July 3, 2010

Abstract

Flexible post-combustion absorption/stripping that vents carbon dioxide (CO_2) or stores rich solvent at partial- or zero-load can be used to vary power output in response to electricity prices and improve economic performance of a coal-fired facility with CO_2 capture. Optimization and deterministic models have been created and utilized to investigate profit maximizing behavior of a single 500 MW coal-fired facility in the Electric Reliability Council of Texas (ERCOT) grid under configurations with flexible CO_2 capture, inflexible CO_2 capture, or no CO_2 capture. Results are compared based on whether the plant operates reactively to the most recent posted price, uses a day-ahead price forecast, or has perfect knowledge of future electricity prices.

Assuming a price of U.S. $50 per metric ton of CO_2, major conclusions are as follows:

- High costs without CO_2 capture allow net annual output to be greater with CO_2 capture than without, despite CO_2 capture energy requirements.
- Adding an inflexible CO_2 capture system improves annual operating profits by at least 20% from the no-capture case.
- Relative to annual operating profits earned with inflexible CO_2 capture, venting-only flexible capture improves profits by 3–6%, and flexible capture with solvent storage improves profits by 12–14%.
- Venting CO_2 at high prices should be economical because it has negligible capital costs, but cash flow analysis is required to determine if the operating profit improvements with solvent storage justify the capital costs of additional solvent inventory, storage tanks, and larger stripping/compression equipment.
- Accurate price forecasting is necessary to plan solvent storage operation, but the economic benefits of venting-only flexible CO_2 capture can be achieved without accurate price forecasting.
- Ramp limits have only a minor effect on economic results, but ramp limits might be more important when considering ancillary service markets and detailed plant control concerns.
- CO_2 emissions are greater with flexible CO_2 capture, but emissions are still 75–82% lower than when no CO_2 capture system is available.

Introduction to Flexible CO_2 Capture

Flexible operation of a post-combustion amine absorption and stripping system entails varying the liquid and vapor flow rates in the stripping and/or absorption systems in order to choose the most economical CO_2 capture operating point for current electricity market conditions. During partial- or zero-load CO_2 capture, some or all of the steam being used for solvent regeneration would be redirected back to the power cycle to increase electrical output. The resulting decrease in CO_2 flow out of the stripper also reduces energy requirements for CO_2 compression. Solvent flow to the absorber and stripper and flue gas flow to the absorber could also be modulated for efficient system operation.

Flexible CO_2 capture could allow the plant operator to increase power output when electricity prices are high if additional electricity sales offset any increase in CO_2 emissions costs under a CO_2 regulatory framework (Ziaii et al., 2008). In addition, operating CO_2 capture at zero-load during annual peak electricity demand can eliminate the need to spend billions of dollars to replace generation capacity lost when CO_2 capture operates at full-load (Cohen et al., 2010).

There are two general concepts for a flexible CO_2 capture system using amine absorption/stripping. One concept reduces the energy requirements of solvent stripping and CO_2 compression while allowing CO_2 removal rates to fall. Figure 1 displays one such configuration, where the steam and rich solvent flow rates to the stripper are reduced equally and simultaneously during partial- or zero-load operation (Ziaii et al., 2008). At partial-load, rich solvent that is not sent to the stripper is recycled to the absorber, so CO_2 removal rates in the absorber will decrease as solvent becomes saturated with CO_2. Zero-load could involve recirculating all solvent through the absorber, or the CO_2 capture system could be bypassed completely. This design's primary disadvantage is increased CO_2 emissions and any associated CO_2 costs.

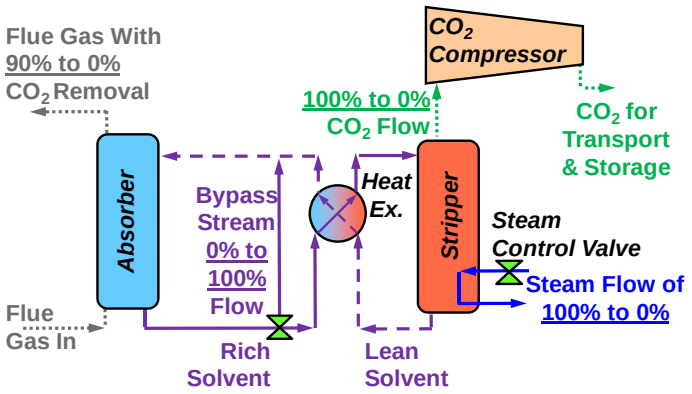

Figure 1: Simultaneously reducing steam and rich solvent flow to the stripper allows increased output but at the expense of additional CO_2 emissions.

Another flexible CO_2 capture concept uses large solvent storage tanks to maintain high CO_2 removal when stripping and compression systems operate at partial- or zero-load (Figure 2) (Chalmers and Gibbins, 2007). When electricity prices are high, the plant may operate in net "storage mode" with stripping and compression at partial- or zero-load while absorber load remains high by receiving lean solvent from one storage reservoir and depositing rich solvent into another. Net "regeneration mode" is then utilized when electricity prices are low; stripping

and compression systems return to a higher load to treat the current process stream and the stored rich solvent. To treat both current stream and stored solvent, stripping and compression systems must be larger and require more total energy than a CO_2 capture system without solvent storage. Maintaining high CO_2 removal keeps operating costs down during net storage mode, but any operating profit improvement must be weighed against the capital cost of solvent inventory, storage tanks, and larger stripping and compression equipment. Maintenance requirements will require the ability to bypass the CO_2 capture system, so a facility with solvent storage system would likely maintain the option to vent additional CO_2 when necessary or desired. Additional details on this concept are in the 2nd Quarterly Report of 2009 (Rochelle et al., 2009a).

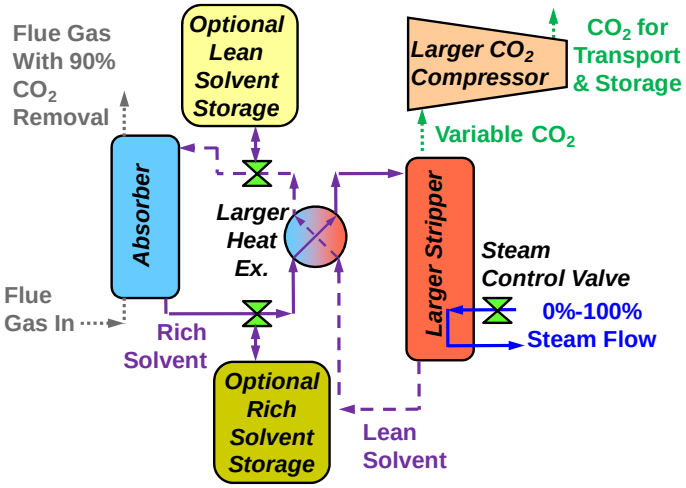

Figure 2: Including solvent storage incurs significant capital costs but allows continued high CO_2 removal at partial- and zero-load.

Flexible Capture in Response to Volatile Electricity Prices

Most of my previous work has focused on flexible post-combustion absorption/stripping in response to peak electricity demand and electricity prices set by the marginal cost of the most expensive plant dispatched at a given time. Due to market realities such as strategic bidding and transmission congestion, prices do not necessarily equal the marginal cost of the most expensive plant dispatched; historical prices patterns are much more complex and volatile (Hagi and Tafreshi, 2007). Flexible CO_2 capture is cited for its usefulness in taking advantage of short-lived electricity price spikes, but little quantitative valuation appears in the literature (Chalmers and Gibbins, 2007). My 4th Quarterly Report of 2009 and presentation in the January 2010 Rochelle Group Research Review introduced a preliminary valuation of flexible CO_2 capture in response to historical electricity prices and ancillary services (Rochelle et al., 2009b). To improve on the rigor of that work, my focus this quarter has been on creating plant-level models that analyze how a single plant can maximize its profits using flexible capture in response to volatile electricity prices.

The Importance of Price Foreknowledge

Volatile electricity prices are inherently difficult to predict, so a realistic assessment of flexible CO_2 capture operation must consider the degree to which future electricity prices are known. Optimizing plant operation using historical electricity prices might yield the most profitable operating strategy, but doing so implies perfect foreknowledge of electricity prices. Perfect

foreknowledge is obviously unreasonable, but while highly irregular price spikes remain difficult to predict, day-ahead prices excluding these outliers can be predicted fairly well using a wide variety of statistical time series and intelligent systems models (Li et al., 2005). The most successful models have achieved mean square error of 5–7 U.S. dollars per megawatt-hour ($/MWh) and mean absolute percent error of 10–12% (Li et al., 2005; 2007). Without any forecasting ability, the plant must react to the most recent price signal. Under this reactive mode of operation, price posting procedures are particularly important. Whether prices are posted at the beginning or end of the pricing interval directly affects the ability to profitably operate in response to changes in price, and different markets might follow different procedures.

Methodology

Deterministic and optimization models are created and employed to maximize profits at a single coal-fired power plant by choosing the electrical output and CO_2 capture load in each pricing interval, consistent with the assumed degree of price foreknowledge. The plant is assumed to be operating in the Electric Reliability Council of Texas (ERCOT) market. Though changes in electrical output at large coal-fired facilities could influence electricity price, this analysis assumes the plant is a price-taker. Rigorous electricity price prediction is beyond the scope of this work, so historical ERCOT prices are used as input. Annual CO_2 emissions, operating costs, operating profits, and capacity factors can then be calculated from optimal power output and CO_2 capture load.

The models are used to compare results for the same facility with flexible CO_2 capture that must vent additional CO_2 at partial- or zero-load (Figure 1), flexible capture with solvent storage (Figure 2), inflexible CO_2 capture, or no CO_2 capture. Under all degrees of price foreknowledge, an inflexible CO_2 capture system must treat all the flue gas produced in a given time interval, and a plant without CO_2 capture incurs no costs associated with CO_2 capture.

No Price Foreknowledge

With no electricity price foreknowledge, any change in operating point will be chosen strictly based on the most recent posted electricity price. A deterministic model created using MATLAB software calculates electrical output and CO_2 capture load in the no foreknowledge case for plant configurations without CO_2 capture, with inflexible CO_2 capture, and with flexible CO_2 capture that must vent additional CO_2 at partial- or zero-load. The solvent storage configuration is not applicable for a scenario with no price foreknowledge because some future price prediction is required to reasonably plan when to operate in net storage or regeneration mode.

CO_2 capture will only operate commercially under a regulatory regime that incurs a cost per quantity of CO_2 emitted. In the ERCOT grid, electricity prices are most commonly set by natural gas-fired plants, so the existence of a CO_2 regulatory scheme is imposed by adding the emissions costs of an average ERCOT gas-fired facility to historical electricity in each interval. Low electricity prices are not likely set by natural gas-based facilities, but the same adjustment is used under the assumption that doing so will not significantly change the resulting dispatch.

Calculated marginal costs are then used to find the minimum price to justify turning the base plant on and the minimum price to justify reducing CO_2 capture load. CO_2 capture will not operate at all unless marginal costs are lower at full-load CO_2 capture than at partial- or zero-load capture, so CO_2 capture load is not reduced for high electricity prices unless additional electricity sales offset additional CO_2 emissions costs. Assuming marginal costs decrease monotonically as

CO_2 capture load increases, this threshold electricity price is calculated using Equation 1 below. As a simplifying approximation, base plant performance is assumed constant across output quantities. The base plant and capture system will turn off completely if the electricity price is below the lowest available marginal cost less any average fixed costs of CO_2 capture. The cost model includes costs of fuel, CO_2 emissions, base plant variable operation and maintenance, solvent makeup, caustic makeup for solvent reclaiming, waste disposal of solvent degradation products, CO_2 transport and storage, and additional water use for the CO_2 capture system.

$$P_R = \frac{C_{\min} Q_{\min} - C_{\max} Q_{\max}}{Q_{\min} - Q_{\max}}$$

$P_R =$ threshold price above which to reduce capture load ($/MWh)

$C =$ marginal cost ($/MWh) (1)

$Q =$ net output (MW)

Subscripts: max = full-load CO_2 capture, min = minimum-load CO_2 capture

The model uses these price thresholds to determine the electrical output and CO_2 capture load over all pricing intervals. For flexible CO_2 capture systems, a nonzero minimum capture load and capture system ramp rate can be specified. Capture load is defined as the flow ratio of steam extracted in the current interval to the steam extracted when stripping CO_2 from all the rich solvent coming from an absorber treating the full flue gas flow of a base plant at maximum output (the steam flow with full-load inflexible CO_2 capture). For instance, if 50% of the low pressure (LP) steam is extracted for 100% load CO_2 capture, 25% of the low pressure steam is extracted for 50% load CO_2 capture. To maintain focus on CO_2 capture operation versus base plant operation, minimum output and ramp limits for the base power plant are not considered, nor are startup and shutdown costs. Because power system ramp limits are not included, the CO_2 capture system may operate at any load during an interval when the base plant turns on or prior to an interval when the base plant turns off.

Profits are calculated for two cases: 1) prices are posted at the beginning of each interval, so operation in the current interval is based on price in that interval; 2) prices are posted at the end of each interval, so operation in the current interval is based price in the previous interval.

Perfect Price Foreknowledge

An optimization model created using GAMS software finds the profit maximizing operating conditions given perfect foreknowledge using the adjusted historical electricity prices. The model is formulated as a mixed-integer linear program (MILP) with decision variables that include base plant power output, binary commitment to indicate whether the plant is on or off, and fractional load of the absorber and stripper. Stripper load is equivalent to the "capture load" definition in the previous section and establishes the load on all stripping and compression systems. Absorber load is the ratio of fractional CO_2 removal in the current interval to the maximum design CO_2 removal and determines the load of all components involved in CO_2 absorption. Absorber load could be modulated by varying flue gas or lean solvent flow rates and properties, but this analysis assumes that flue gas flow remains constant and absorber load decreases due to rich solvent recycle and the resulting increase in lean loading.

The model includes constraints on minimum and maximum base plant power output, absorber load, and stripper load, as well as ramp limits on the fractional change in absorber or stripper

load per pricing interval. Because the flue gas flow and amount of steam available for solvent stripping decreases with base plant power output, the maximum absorber and stripper load is limited by the base plant power output. Additional concerns such as ramp limits on base plant power output and startup costs are not included at this time to maintain consistency with the previous case of no price foreknowledge.

Venting Only: In the venting-only configuration, absorber and stripper load can be no greater than 100% and must be equal at all times.

Solvent Storage: If solvent storage is available, absorber and stripper load are decoupled. The absorber can continue to remove CO_2 from incoming flue gas while stripper load is reduced if the absorber is supplied by stored lean solvent, and solvent exiting the absorber is sent to a rich solvent storage tank. Assuming the stripping and compression systems are built to handle the current process stream and stored rich solvent, stripper load can exceed 100%. Maximum stripper load will likely be constrained either by the size of the stripping and compression equipment or by the maximum quantity of low pressure steam that can be extracted from the power cycle. The preliminary results below neglect limits on equipment size and assume that all low pressure steam could be extracted for stripping if desired, so the maximum stripper load is the inverse of the fraction of steam extracted at 100% load (i.e. if 40% steam is extracted at 100% load, the maximum stripper load is 250%).

Another decision variable when using a solvent storage system is the quantity of CO_2 currently held in rich solvent storage for later stripping and compression. The maximum quantity of CO_2 stored is limited by the solvent absorption capacity (difference between rich and lean loading), solvent physical properties, and the size of the storage facility. A CO_2 flow balance relates the change in quantity of CO_2 stored at a given time, where the quantities of CO_2 absorbed or stripped in a given interval are calculated from the absorber and stripper loads (Equation 2).

$$
\begin{aligned}
& l_t = l_{t-1} + CO_{2_{abs,t}} - CO_{2_{str,t}} \\
& l = \text{ CO}_2 \text{ level} \\
& CO_{2_{abs}} = \text{ CO}_2 \text{ absorbed} \\
& CO_{2_{str}} = \text{ CO}_2 \text{ stripped} \\
& t = \text{ pricing interval index}
\end{aligned}
\tag{2}
$$

Day-Ahead Price Forecasting

To simulate operation in response to day-ahead price forecasts, a set of pseudo-forecasted prices is created by removing outliers from and smoothing actual historical prices. Outliers are removed based on standard deviation from a moving average, and price data without outliers are smoothed using a Savitzky-Golay polynomial filter. Outlier removal and smoothing parameters are adjusted until they achieve a mean square error of $9.01/MWh and mean absolute percent error of 8.6% when compared to historical data without outliers. These quantities are judged reasonably close to values achieved using the most accurate day-ahead price forecasting models available.

The optimization model described in the Perfect Foreknowledge section is used with the pseudo-forecasted prices to determine optimal operation under the forecasted prices. Actual profits are then calculated using historical electricity prices.

If a facility with solvent storage can only plan its operation one day in advance, it might require that the quantity of CO_2 stored in rich solvent to start each day at a specific value. This value was calculated by finding the average quantity of CO_2 stored at the beginning of the day over an entire year with perfect price foreknowledge and no ramp limits on the CO_2 capture system. Seasonal variations in the starting CO_2 level were not considered. Any day-ahead forecasting case with solvent storage is then constrained such that the stored CO_2 level must return to the starting CO_2 level at the beginning of each day.

Base Case Input Parameters

Table 1 includes major input parameters that are kept constant across all studies described below. Base plant performance is an average across coal-fired power plants in ERCOT (USEPA, 2007). The CO_2 capture system uses a baseline 30 wt % monoethanolamine (MEA) solvent with energy performance, CO_2 removal, and design capacity typical of simulations completed by the Rochelle group (Ziaii et al., 2008; Oyenekan, 2006; USNETL, 2007). Solvent storage capacity is chosen to allow four hours with the absorber at full-load and the stripper at zero-load when starting with an empty rich storage tank. This quantity of storage is on the order of that suggested by other authors (Haines and Davison, 2009). Coal prices in Texas have been 1.5–2 U.S. dollars per million British thermal units ($/MMBTU) since the late 1990s, and the base CO_2 price is chosen as a relatively low price relative to that necessary for CO_2 capture investment (USEIA, 2010; USNETL, 2007).

Table 1: Base case input parameters for the power plant, capture system, and electricity market[1]

Parameter	Units	Value
Base Plant		
Maximum output	MW	500
CO_2 emissions rate	tCO_2/MWh	1.03
Heat rate	MMBTU/MWh	10.8
CO_2 Capture System		
Solvent		30 wt % MEA
Maximum CO_2 removal	Fractional	0.9
Energy required per unit CO_2 captured	MWh/tCO_2	0.269
Fraction of LP steam extracted for full-load capture	Fractional	0.4
Solvent capacity (rich minus lean loading)	$molCO_2$/molMEA	0.12
Solvent Storage System		
Volume of rich and lean storage tanks	m^3	66,400
Electricity Market		
Coal price	$/MMBTU	1.5
CO_2 price	$/$tCO_2$	50

[1] Units: tCO_2 = metric ton of CO_2, MW = megawatt, m^3 = cubic meters

CO_2 emissions rate of average ERCOT gas-fired plant	tCO_2/MWh	0.52

All studies use historical ERCOT electricity prices in each 15-minute pricing interval in 2008.

In addition to varying the degree of price foreknowledge and the existence of a solvent storage system, all scenarios are studied without a ramp limit on the CO_2 capture system and with a 2%/min. (100% in 50 min.) ramp limit. Ramp limits are equivalent for the absorber and stripper and are the same for ramping up or down. A 2%/min. ramp limit is considered a near worst-case scenario because steam redirection back to the LP turbine could likely occur much faster (Lucquiaud et al., 2008).

Results & Discussion

Operation with Venting-Only Configuration

The three panels of Figure 3 demonstrate typical modes of operation in the venting-only flexible CO_2 capture configuration under three scenarios: no ramp limit (Panel A), 2%/min. ramp limit with no price foreknowledge (Panel B), 2%/min. ramp limit with perfect price foreknowledge (Panel C). Without a ramp limit, there are no inter-temporal constraints. Optimal operation in each interval is possible regardless of price foreknowledge, so operation is the same as with perfect knowledge.

To illustrate all possible operating modes, each panel displays fractional base plant load and CO_2 capture load for January 5/6 and June 12/13, 2008. Base plant load is defined as the fraction of gross power output in the current interval to maximum output (500 MW), so it does not account for the energy requirements of CO_2 capture.

The base plant and CO_2 capture system turns off below an electricity price of $52/MWh, the marginal cost at full-load CO_2 capture, or it would earn negative profits. This market condition occurs in several intervals, especially those between interval 84 and 132. Above $136/MWh, additional electricity sales at partial- or zero-load CO_2 capture offset any added CO_2 emissions costs. There are several times after interval 240 when the price exceeds this threshold and capture load drops as much as possible within any ramping constraints. Operation is similar regardless of the degree of price foreknowledge, suggesting that any economic benefits of a venting-only flexible capture system can be realized with minimal price forecasting ability.

In the absence of startup/shutdown costs and base plant ramp limits, the base plant can switch between full- and zero-load regardless of the duration of a low price period. In an actual plant, this practice is unrealistic due to thermal loads, process stability, maintenance concerns, and cost, so further developments of the model will include startup/shutdown costs and base plant ramp limits. These changes will eliminate the rapid on/off cycling seen in Figure 3.

General operating behaviors will be the same in the day-ahead forecasting case as with perfect price foreknowledge, but plants will operate in response to the forecasted price curve rather than actual historical prices.

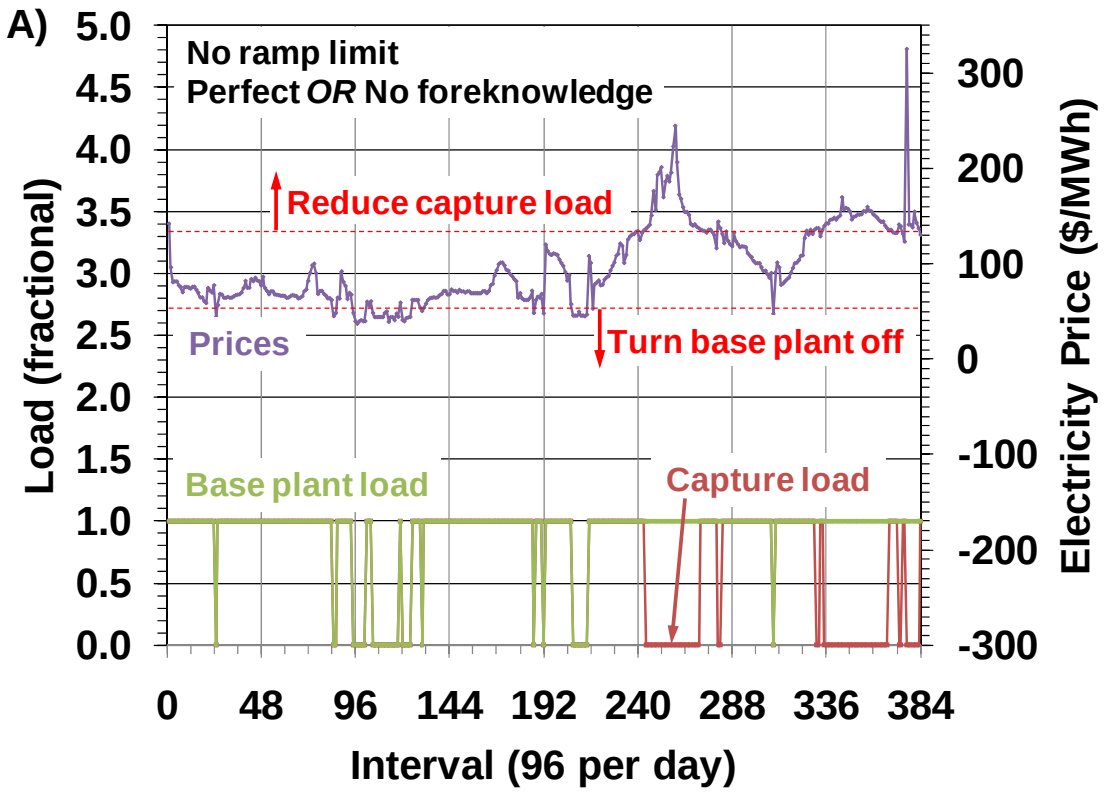
A)
No ramp limit
Perfect *OR* No foreknowledge
Reduce capture load
Turn base plant off
Prices
Base plant load
Capture load
Load (fractional)
Electricity Price ($/MWh)
Interval (96 per day)
5.0
4.5
4.0
3.5
3.0
2.5
2.0
1.5
1.0
0.5
0.0
300
200
100
0
-100
-200
-300
0
48
96
144
192
240
288
336
384

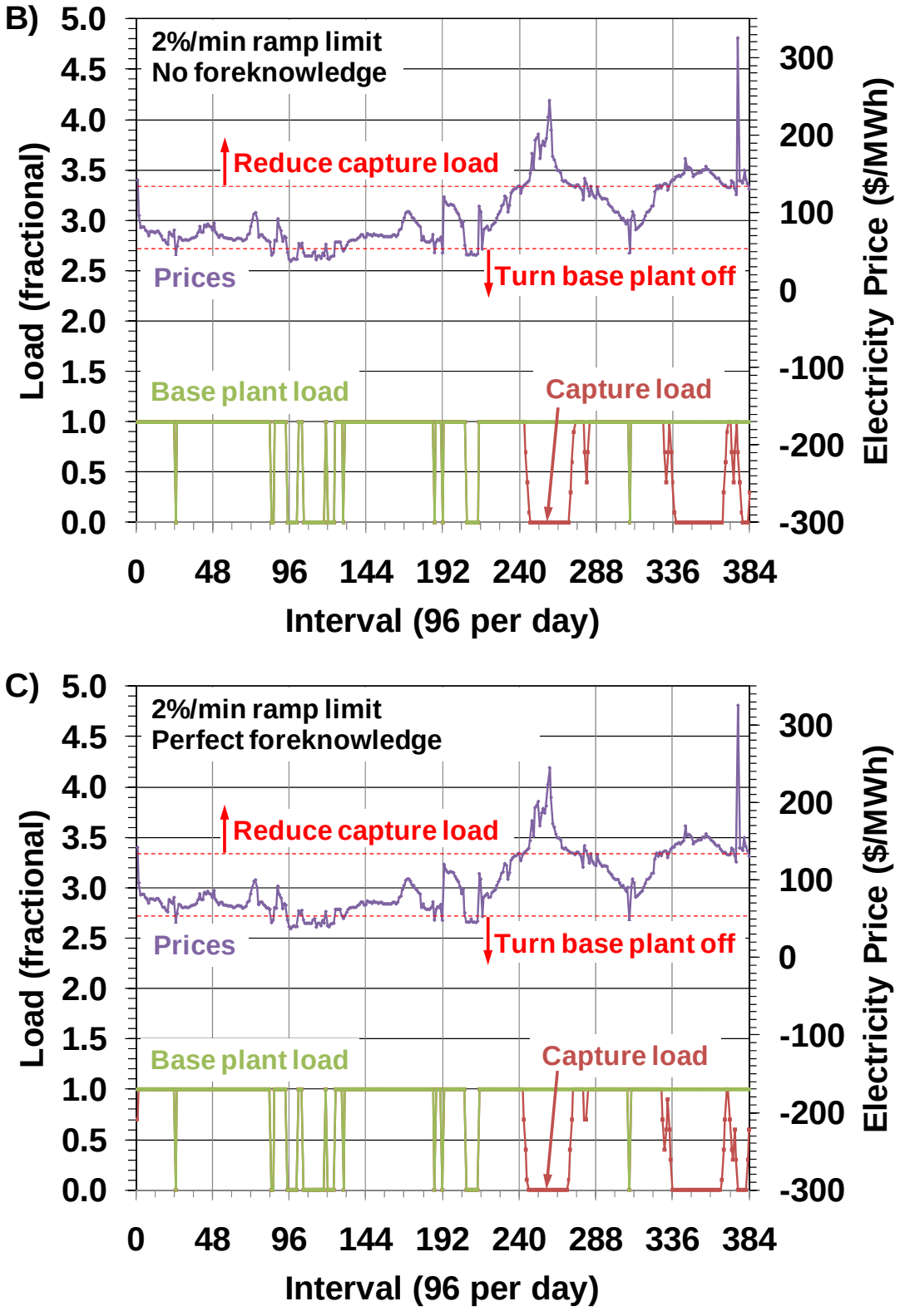

Figure 3: A plant with a venting-only flexible CO_2 capture system operates similarly regardless of the degree of price foreknowledge or existence of ramp limits.

Operation with Solvent Storage

Some prediction of future prices is necessary with a solvent storage system to reasonably plan the intervals when the plant should store rich solvent, regenerate stored solvent, or possibly even vent additional CO_2. Operational planning is particularly difficult with ramp limits on the CO_2 capture system and when planning to incur higher marginal costs to regenerate stored solvent during low electricity price intervals when high costs could incent the plant to turn off completely. Therefore, only the perfect knowledge and day-ahead forecast cases are considered with solvent storage.

Figure 4 illustrates operating regimes for a power plant with a flexible CO_2 capture system and solvent storage. When the stripper load exceeds the absorber load, CO_2 is being stripped from current process stream and stored rich solvent, so more CO_2 is stripped than absorbed. If the stripper load is below the absorber load, more CO_2 is being absorbed than stripped, so the excess rich solvent must be sent to storage. The absorber and stripper load could also be reduced simultaneously below the base plant load to vent additional CO_2, possibly during high price intervals when the rich storage tank is full or overall profits are improved by reserving storage capacity for a later time.

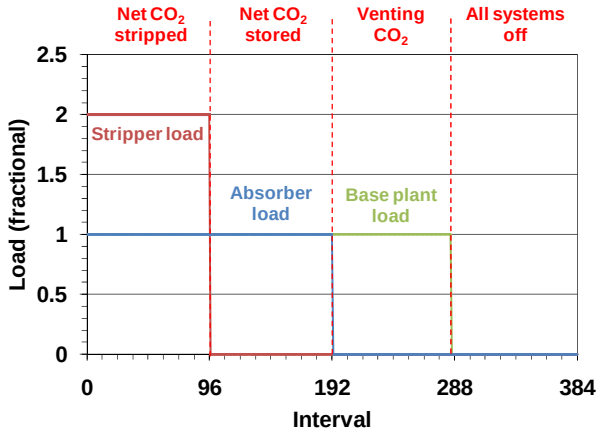

Figure 4: Relative absorber, stripper, and base plant load defines four different operating regimes for a facility that uses flexible CO_2 capture with solvent storage.

Figure 5 shows base plant, absorber, and stripper load for January 5/6 and June 12/13 when solvent storage is available and there is perfect price foreknowledge. There is no ramp limit for Panel A and a 2%/min. ramp limit for Panel B. In both panels, there are many transition periods between net CO_2 regeneration and net CO_2 storage when prices are low and high relative to prices in neighboring intervals. Maximum stripper load is 250% if all LP steam is extracted. A stripping and compression system 2.5 times the size of that required for an inflexible system would be capital intensive, so future work will quantify the costs and benefits of solvent storage under different assumptions of storage and equipment size.

All systems turn off when prices are very low, such as between intervals 96 and 125. With ramping constraints, there are also several instances when all systems turn off for a single interval because the mathematical formulation of the ramping constraint allows for the capture ramp limit to be ignored when the base plant turns on or off. This behavior will be eliminated by adding startup/shutdown costs and base plant ramp limits.

There are times between intervals 252–276 and after interval 336 when high prices and storage limitations justify reducing both absorber and stripper load and allowing additional CO_2 emissions. There are also a few times after interval 360 when absorber load is below stripper load to allow all stored solvent to be regenerated by the final interval, which is specified as a constraint in the model.

Without ramp limitations, stripper operation is very erratic and characterized by rapid shifts between zero- and full-load that would likely be undesirable from an operation and maintenance standpoint. When a ramp limit is imposed, behavior is considerably smoother; however, the large size of stripping and compression equipment relative to storage capacity still allows for many storage cycles per day.

Figure 6 provides another representation of solvent storage operation by plotting, across all intervals, the quantity of CO_2 stored in rich solvent for later regeneration. Again, Panel A displays results without ramp limits, while Panel B shows data with a 2%/min. capture system ramp limit. As indicated by Figure 5, rapid cycling occurs between 0 tCO_2 and the maximum of 1856 tCO_2.

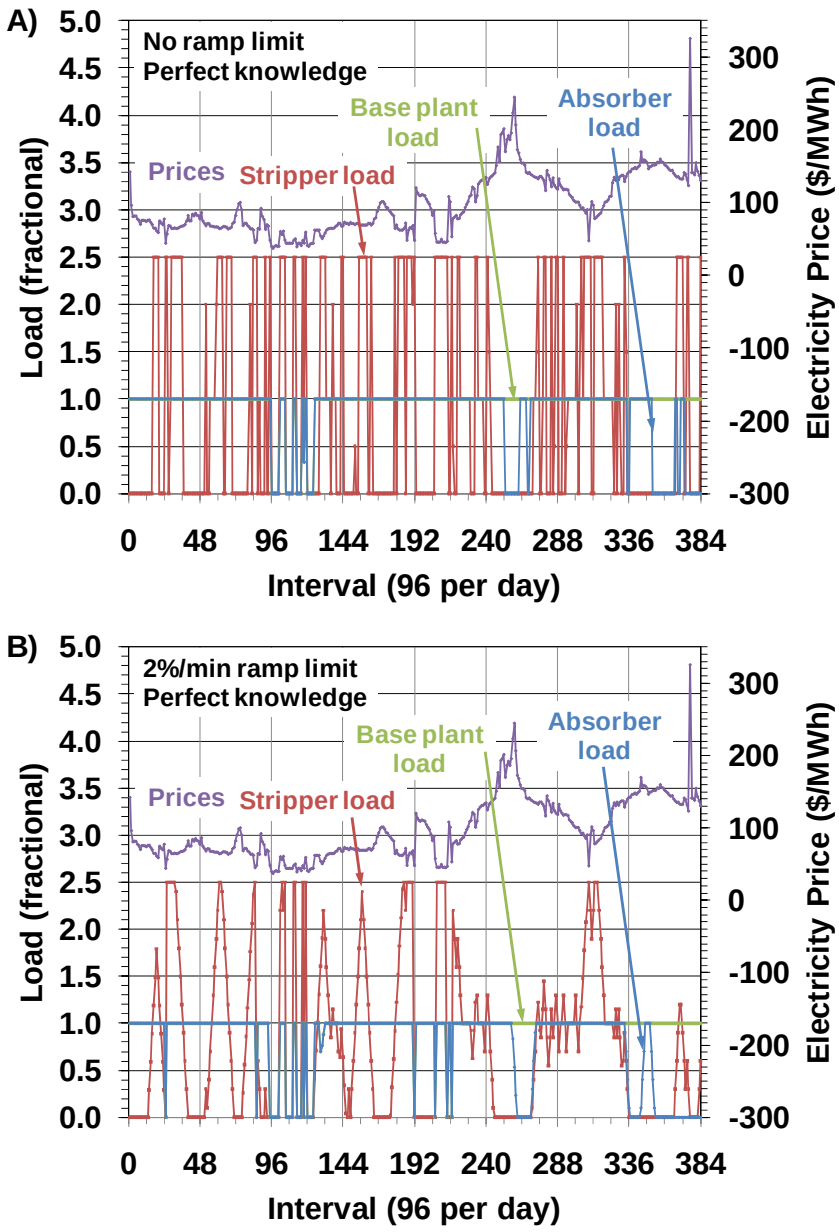

Figure 5: A plant with flexible CO_2 capture and solvent storage may choose to rapidly cycle stripping and compression systems if the equipment is large enough.

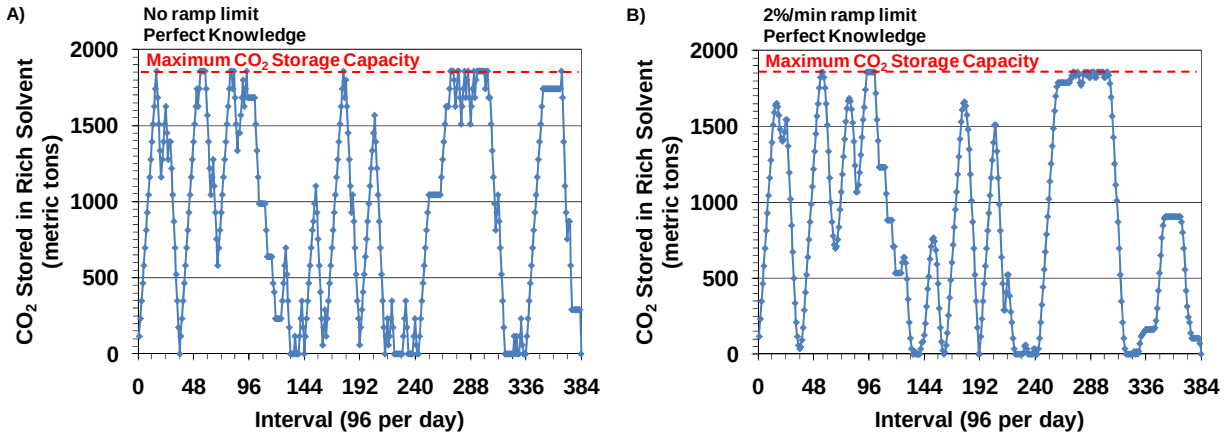

Figure 6: The amount of CO_2 stored in rich solvent over time demonstrates patterns of cycling the solvent storage system.

The fundamental behaviors of a facility with solvent storage are the same using the pseudo-forecasted electricity prices as with historical prices, but the starting CO_2 level for each day must be specified. Figure 7 shows the annual mean CO_2 level in each of the 96 pricing intervals in a day assuming perfect price foreknowledge and no CO_2 capture load ramp limits. The upper and lower quartile levels are also shown. On average, there is net CO_2 regeneration between 0:00 and 7:30, and net CO_2 storage through the daytime and evening hours. The high frequency behavior at upper and lower storage limits occurs because there are no ramping constraints to damp such behavior. Based on these data, the starting CO_2 level for each day is set to 1450 tCO_2 in any day-ahead forecasting scenarios with solvent storage.

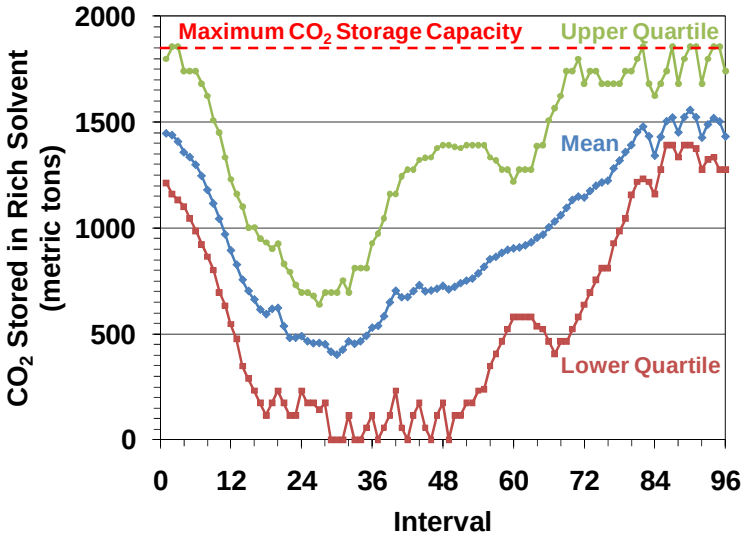

Figure 7: The annual mean, upper quartile, and lower quartile quantity of CO_2 stored in each interval indicate the average daily operation of the solvent storage system.

Comparison of Annual Performance

Data tables display aggregate results for different plant and CO_2 capture configurations with no price foreknowledge (Table 2), perfect foreknowledge (

Table 3), and day-ahead forecasting (Table 4). Flexible CO_2 capture scenarios are compared to scenarios without CO_2 capture and with an inflexible CO_2 capture system that must process all flue gas produced in a given interval.

Operation: Depending on the type of CO_2 capture system and the degree of price foreknowledge, net electric output to the grid is 2.6–13.7% greater with CO_2 capture than without, despite the energy requirements of CO_2 capture. The \$50/tCO_2 price is high enough for a coal-fired plant without CO_2 capture to be dispatched far less than if CO_2 capture systems are installed, hence the base plant capacity factor of around 60% without CO_2 capture compared to over 80% for CO_2 capture cases. Net electrical output and overall CO_2 capture capacity factors are greatest with solvent storage due to the capability to increase power output without major CO_2 emissions costs. The degree to which overall CO_2 capture capacity factor is lower than base plant capacity factor reflects the amount of time additional CO_2 is vented at reduced absorber load, but flexible CO_2 capture systems still remain on over 90% of the time when the base plant is operating. For each CO_2 capture scenario, output is greatest with day-ahead forecasting because smoothing and outlier removal produces higher prices in some low price intervals when the plant would otherwise choose not to operate. The existence of a 2%/min ramp limit has only a minor effect on aggregate plant operation, suggesting that economic and environmental performance is not sensitive to CO_2 capture ramp limitations.

CO_2 Emissions: Annual CO_2 emissions with inflexible CO_2 capture are approximately 86% lower than without CO_2 capture. CO_2 emissions are 1.25–1.82 times greater with flexible systems relative to inflexible systems, but flexible CO_2 capture scenarios still achieve emissions reductions of 75–82% from the no-capture case. In fact, higher base plant capacity factors when CO_2 capture is available allow for more CO_2 to be captured in CO_2 capture scenarios than is emitted in no-capture scenarios.

Total CO_2 emissions data are reflected in relative average CO_2 emissions rates; though the emissions rate with full-load CO_2 capture is 0.137 tCO_2/MWh, average emissions rates for flexible systems range from 0.222–0.244 tCO_2/MWh with venting-only flexible capture and 0.163–0.172 tCO_2/MWh with solvent storage. There is slightly more CO_2 venting with perfect price foreknowledge because the plant can take advantage of random high price spikes, though CO_2 emissions are slightly greater with day-ahead forecasting than perfect foreknowledge when solvent storage is available.

Economics: Due to the \$50/tCO_2 emissions cost, using an inflexible CO_2 capture system reduces total operating costs by 23–26% and increases total operating profits by 20–25% relative to the no-capture case. Costs are greater with flexible capture than with inflexible capture because flexible capture systems sometimes choose higher cost operating points in order to earn greater overall profits.

Relative to an inflexible capture system, venting-only flexible capture increases operating profits by 3.6–6.3% depending on ramp limit, price foreknowledge, and price posting procedures. If prices are posted at the beginning of each price interval, it appears more profitable to operate a venting-only system in response to posted prices rather than to plan operations based on day-ahead price forecasts. Even an inflexible CO_2 capture facility will likely be designed to allow bypass during maintenance outages, so providing the option for venting-only flexible capture should not incur major costs aside from minimal extra pipes and valves and some additional operation and maintenance cost. Therefore, the operating profit improvements with venting-only

flexible capture are likely justified, though further economic analysis is required for a more definitive assessment.

A flexible CO_2 capture system with solvent storage earns 12–14% operating profit increase over the inflexible scenario, though at the expense of significant capital costs for solvent inventory, storage tanks, and stripping/compression equipment 2.5 times larger than with an inflexible system. Cash flow analysis will identify if these operating profit improvements justify the incremental capital costs of solvent storage. Limiting the size of the stripping/compression system will reduce the operating profit improvements as well as capital costs, so sensitivity of any cash flow calculation to both storage capacity and stripping/compression equipment size must be assessed to provide detailed recommendations about the value of solvent storage.

In most plant configurations and price foreknowledge conditions, profits are lower when a conservative capture ramp limit is imposed, but differences are slight. Price foreknowledge significantly improves profits with solvent storage, but a venting-only configuration performs as well if not better with limited price forecasting ability. For the venting-only configuration, profits are approximately the same with day-ahead forecasting as with price reactive operation if prices are posted at the end of each pricing interval.

Table 2: Aggregate annual results with no electricity price foreknowledge[2]

Parameter	Units	Venting, No ramp limit	Venting, 2%/min ramp limit	Inflexible Capture	No Capture
Total Output to Grid	TWh	2.782	2.777	2.705	2.637
Total CO_2 Emitted	$MtCO_2$	0.6564	0.6401	0.3717	2.719
Total CO_2 Captured	$MtCO_2$	3.060	3.077	3.345	0
Total Operating Cost	million USD	$153.02	$152.43	$142.22	$193.01
Total Operating Profits - Prices Posted at Start	million USD	$135.33	$133.52	$127.62	$105.09
Total Operating Profits - Prices Posted at End	million USD	$131.18	$130.45	$125.85	$101.34
Capture Capacity Factor When Base Plant is On	fractional	0.9149	0.9198	1	0
Capture Capacity Factor - Overall	fractional	0.7509	0.7549	0.8208	0
Base Plant Capacity Factor	fractional	0.8208	0. 8208	0.8208	0.6005
Average CO_2 Emissions Rate	tCO_2/MWh	0.2360	0.2305	0.1374	1.0312

[2] Units: TWh = terawatt-hour, $MtCO_2$ = million metric ton of CO_2

Table 3: Aggregate annual results with perfect electricity price foreknowledge

Parameter	Units	Venting, No ramp limit	Venting, 2%/min ramp limit	Storage, No ramp limit	Storage, 2%/min ramp limit	Inflexible Capture	No Capture
Total Output to Grid	TWh	2.782	2.785	2.956	2.896	2.705	2.637
Total CO_2 Emitted	$MtCO_2$	0.6564	0.6781	0.4816	0.4947	0.3717	2.719
Total CO_2 Captured	$MtCO_2$	3.061	3.035	3.551	3.448	3.345	0
Total Operating Cost	million USD	$153.22	$153.88	$157.74	$155.10	$142.83	$193.01
Total Operating Profits	million USD	$135.33	$134.98	$145.61	$144.06	$127.20	$105.09
Capture Capacity Factor When Base Plant is On	fractional	0.9149	0.9078	0.9322	0.9662	1	0
Capture Capacity Factor - Overall	fractional	0.7509	0.7446	0.8713	0.8459	0.8208	0
Base Plant Capacity Factor	fractional	0.8208	0.8199	0.8905	0.8706	0.8208	0.6005
Average CO_2 Emissions Rate	tCO_2/MWh	0.2360	0.2435	0.1629	0.1708	0.1374	1.0312

Table 4: Aggregate annual results with day-ahead electricity price forecasting

Parameter	Units	Venting, No ramp limit	Venting, 2%/min ramp limit	Storage, No ramp limit	Storage, 2%/min ramp limit	Inflexible Capture	No Capture
Total Output to Grid	TWh	2.858	2.857	2.970	2.929	2.789	2.612
Total CO_2 Emitted	$MtCO_2$	0.6369	0.6358	0.5044	0.5034	0.3833	2.693
Total CO_2 Captured	$MtCO_2$	3.196	3.197	3.540	3.482	3.450	0
Total Operating Cost	million USD	$156.51	$156.47	$158.97	$156.90	$147.26	$191.16
Total Operating Profits	million USD	$130.94	$130.88	$141.65	$141.30	$125.99	$101.76
Capture Capacity Factor When Base Plant is On	fractional	0.9265	0.9268	0.9255	0.9680	1	0
Capture Capacity Factor - Overall	fractional	0.7842	0.7844	0.8685	0.8543	0.8464	0
Base Plant Capacity Factor	fractional	0.8464	0.8464	0.8931	0.8800	0.8464	0.5948
Average CO_2 Emissions Rate	tCO_2/MWh	0.2229	0.2225	0.1698	0.1719	0.1374	1.0312

Conclusions

Optimization and deterministic models have been created and utilized to study profit maximizing behavior of a single coal-fired facility with flexible CO_2 capture under varying degrees of electricity price foreknowledge. The models can be used to consider a flexible CO_2 capture system that must vent additional CO_2 at partial- or zero-load or one that uses solvent storage to maintain high CO_2 removal when CO_2 capture load is reduced.

At a CO_2 price of \$50/tCO_2, net annual output is greater with CO_2 capture than without, despite CO_2 capture energy requirements. Without a way to defray CO_2 emissions costs, the base plant will operate far less often. Adding even an inflexible CO_2 capture system improves annual operating profits by at least 20% under the conditions studied, with a venting-only flexible capture system adding another 3–6%. Since the incremental cost of venting-only flexible CO_2 capture is expected to be small, venting-only flexible capture is expected to be economically desirable under these conditions. Adding a solvent storage system to a plant with flexible CO_2 capture improved annual operating profits by 12–14% compared to inflexible capture, but the capital costs of additional solvent inventory, storage tanks, and larger stripping/compression equipment must be accounted for to determine if the additional costs are justified.

With venting-only flexible CO_2 capture, economic benefits can be achieved without accurate price forecasting, but price forecasting is important to effectively plan the operation of a solvent storage system. Solvent storage is useful for improving profits across a wide range of electricity prices, but operation must be planned carefully to account for ramp limits and the dilemma of low electricity prices at times when the plant has high marginal costs necessitated by the need to regenerate stored rich solvent. Despite the availability of a solvent storage system, venting CO_2 when electricity prices are high might be desirable to reserve rich solvent storage capacity for a later time.

Ramp limits have only a minor effect on aggregate economic results, but this finding might not be true when considering ancillary service markets and detailed power plant control concerns.

CO_2 emissions are greater with flexible CO_2 capture, but emissions are still 75–82% lower than when no CO_2 capture system is available. CO_2 capture systems are utilized over 90% of the time when the base plant is operating in all flexible capture scenarios studied.

Future Work

The model used for this report will be made more realistic by adding startup/shutdown costs and ramp rate limits on the base power plant. For the solvent storage configuration, a limit on the size of stripping and compression equipment will be used to set the maximum stripper load rather than assuming that all low pressure steam could be extracted and used in an extremely large stripping/compression system.

Sensitivity studies will investigate the effect of capture ramp limit, CO_2 price, and solvent storage capacity on performance, economic, and environmental metrics. These studies will seek limiting parameter values required to make flexible CO_2 capture economically or environmentally attractive.

Cash flow analysis will be used to weigh any operating profit benefits with capital or annual maintenance costs. This analysis is especially pertinent to a capital intensive solvent storage system, whose incremental costs are likely far greater than those associated with venting-only flexible CO_2 capture.

References

Chalmers H, Gibbins J. “Initial evaluation of the impact of post-combustion capture of carbon dioxide on supercritical pulverised coal power plant part load performance.” *Fuel*. 2007;86:2109–2123.

Cohen SM, Rochelle GT, Webber ME. “Turning CO_2 Capture On & Off in Response to Electric Grid Demand: A Baseline Analysis of Emissions and Economics.” *ASME Journal of Energy Resources Technology*. 2010;132.

Hagi HV, Tafreshi SMM. “An Overview and Verification of Electricity Price Forecasting Models.” *The 8th International Power Engineering Conference*. Singapore, 2007.

Haines MR, Davison JE. “Designing Carbon Capture power plants to assist in meeting peak power demand.” *9th International Conference on Greenhouse Gas Control Technologies.* Washington DC, 2009.

Li G, Liu CC, Lawaree J, Gallanti M, Venturini A. “State-of-the-art of electricity price forecasting.” *CIGRE/IEEE PES International Symposium*. 2005.

Li G, Liu CC, Mattson C, Lawaree J. “Day-Ahead Electricity Price Forecasting in a Grid Environment.” *IEEE Transactions on Power Systems.* 2007;22:266–274.

Lucquiaud M, Chalmers H, Gibbins J. “Capture-ready supercritical coal-fired power plants and flexible post-combustion CO_2 capture.” *9th International Conference on Greenhouse Gas Control Technologies*. Washington, DC, 2008.

Oyenekan B. *Modeling of Strippers for CO_2 capture by Aqueous Amines.* The University of Texas at Austin. Ph.D. Dissertation. 2006; 291.

Rochelle GT, et al. “CO_2 Capture by Aqueous Absorption, Second Quarterly Progress Report 2009.” Luminant Carbon Management Program, The University of Texas at Austin. 2009a.

Rochelle GT, et al. “CO_2 Capture by Aqueous Absorption, Fourth Quarterly Progress Report 2009.” Luminant Carbon Management Program, The University of Texas at Austin. 2009b.

USEIA. Electric Power Annual with data for 2008. Washington, DC, USDOE. 2010.

USEPA. Emissions & Generation Resource Integrated Database (eGRID). *eGRID2006_Version_2_1*. 2007.

USNETL. Cost and Performance Baseline for Fossil Energy Plants. *Bituminous Coal and Natural Gas to Electricity*. J. M. Klara. 2007;1.

Ziaii S, Cohen SM, Rochelle GT, Webber ME. “Dynamic operation of amine scrubbing in response to electricity demand and pricing”. *9th International Conference on Greenhouse Gas Technologies*. Washington, DC, 2008.

Measurement of Packing Effective Area and Mass Transfer Coefficients

Quarterly Report for April 1 – June 30, 2010

by Chao Wang

Supported by the Luminant Carbon Management Program,
Industrial Associates Program for CO_2 Capture by Aqueous Absorption
and the Process Science and Technology Center

Department of Chemical Engineering
The University of Texas at Austin

July 1, 2010

Abstract

Packing is widely used in distillation, stripping, and scrubbing processes because of its relatively low pressure drop, good mass transfer efficiency, and ease of installation. Packing is being investigated for the post-combustion carbon capture process for these reasons. Research continues to focus on development of high performance packing, especially on minimizing pressure drop, maximizing mass transfer efficiency, and minimizing costs. The design of packed absorbers for carbon dioxide capture will require the reliable measurement and accurate prediction of the effective area a_e, gas and liquid film mass transfer coefficient k_G and k_L. My research is focused on the measurement of these important fundamental parameters for packings and construction of a mechanistic design model.

In the last quarterly report, the mass transfer data for three packings were presented. The $NaOH/CO_2$ was used for contact area measurement, $NaOH/SO_2$ for k_G measurement, and toluene/water for k_L measurement. In this report, these data are compared with literature data and published models to assist in verifying our data, refining our experimental methods, and developing improved models.

Among numerous mass transfer coefficient models, two are selected for comparison with our structured packing data and two to compare with our random packing data. They are the models by Rocha, Bravo, Billet, and Wagner. The model results compare favorably to our experimental data.

Modeling work

In this quarter, work focused on data verification and model development. Four models were chosen to compare with our work, including the Billet and Schultes model and the Rocha, Bravo, and Fair model for structured packing, and the Bravo and Fair model and the Wagner model for random packings.

Rocha developed a semi-experimental model based on hundreds of previous experimental results (Rocha et al., 1996). The test systems include cyclohexane/n-hexane, o/p-xylenes, ethylbenzene/styrene, methanol/ethanol, chlorobenzene/ethylbenzene and i-butane/n-butane. The packings included in the data bank are Flexipac 2Y, Gempak 2A, Gempak 2 AT, Intalox 2T, Maxpak, Sulzer BX, Mellapak 250 Y, Mellapak 350 Y, Mellapak 500 Y, etc.

The gas phase mass transfer coefficient is represented as:

$$\frac{k_G S}{D_g} = 0.054\left(\frac{(U_{ge} + U_{Le})\rho_g S}{\mu_g}\right)^{0.8}\left(\frac{\mu_g}{D_g \rho_g}\right)^{0.33} \tag{1}$$

The effective gas and liquid velocities are described as:

$$U_{ge} = \frac{U_{gs}}{\varepsilon(1 - h_L)\sin\theta} \tag{2}$$

$$U_{Le} = \frac{U_{Ls}}{\varepsilon h_L \sin\theta} \tag{3}$$

for the above equations,

D_g is the gas phase diffusion coefficient,
μ_g is the gas viscosity,
ρ_g is gas density,
ε is the packing void fraction,
h_L is the fractional liquid holdup,
U_{gs} and U_{Ls} are the gas and liquid superficial velocities, and
θ is the packing corrugation angle.

The experimental data and the data predicted by Rocha's k_G model are compared in Figure 1. Structured packing data for the Mellapak 2X, Flexipac 1.6 Y HC, and Raschig Super Ring 250 are presented. From this figure, we can see that our experimental data agrees with the Rocha model. Data for Flexipac and RSP fits better with Rocha than data for Mellapak 2X. The exponent for k_G over u_G given by Rocha is 0.8 which is close to our experimental exponent, which is 0.83 for Mellapak 2X, 1.00 for Flexipak 1.6 Y HC, and 0.81 for RSP 250.

The k_L experimental data and the data predicted by the Rocha k_L model are compared in Figure 2. Since the Mellapak 2X k_L data is not good and needs to be repeated, it is not included. From Figure 2, we can see that the experimental data for k_L also fits well with Rocha.

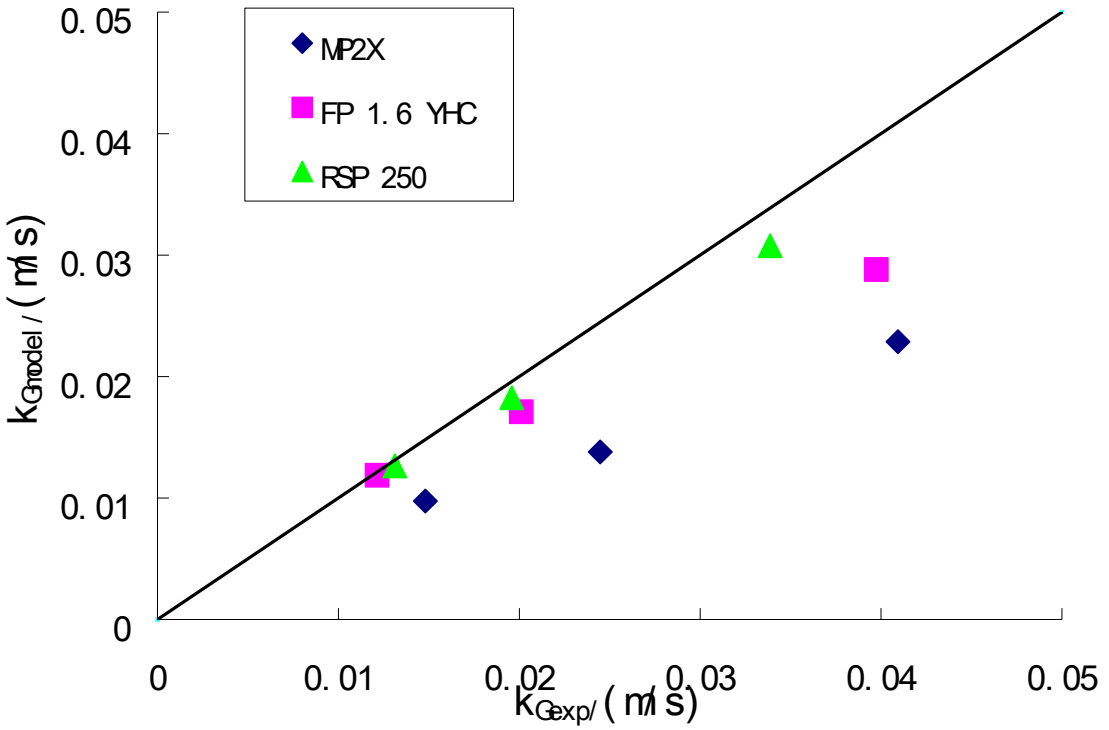

Figure 1: Comparison of k_G experimental data and literature model (Rocha et al.)

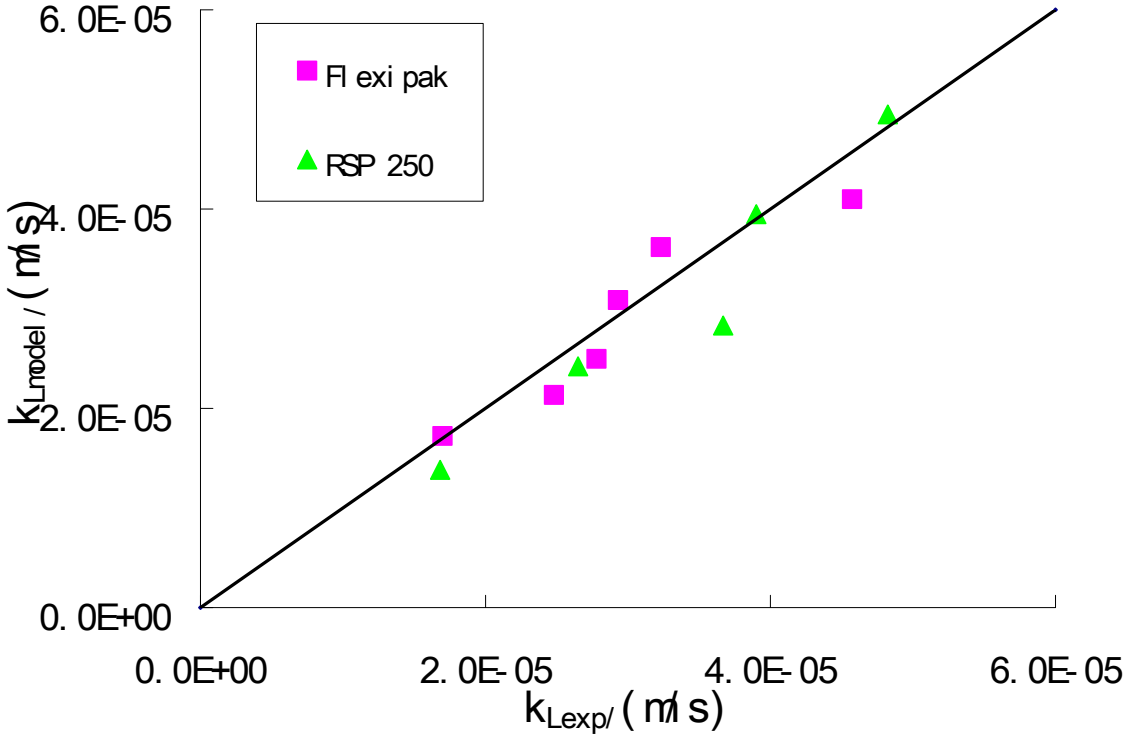

Figure 2: Comparison of experimental k_L data and literature model (Rocha et al.)

The Bravo et al. (1985) model is based on structured packings and experimental data produced by the Separations Research Program at The University of Texas at Austin (UT/SRP). The packings measured are gauze-type structured packings. The test systems include o/p xylenes, ethylbenzene/styrene, methanol/ethanol, and ethylene/propylene glycols.

The model uses effective gas and liquid velocities instead of superficial velocities. The effective velocities are expressed as:

$$U_{g,eff} = \frac{U_{gs}}{\varepsilon \sin\theta} \tag{4}$$

$$U_{L,eff} = (3\Gamma / 2\rho_L)(\rho_L{}^2 g / 3\mu_L \Gamma)^{0.333} \tag{5}$$

where:

Γ=L/(PA$_t$), k$_G$/(s*m perimeter)
A$_t$ = tower cross section area, m^2
P = available perimeter, m/m^2 tower cross section

The gas side mass transfer coefficient is based on extensive earlier investigation of wetted wall columns and is expressed in the form of a Sherwood number:

$$N_{Sh} = 0.0328(N_{\mathrm{Re}})^{0.77}(N_{Sc})^{0.333}$$

Where: N$_{Sh}$= Sherwood number for gas,
= k$_G$d$_{eq}$/D$_G$ for distillation
N$_{Re}$= Reynolds number for gas,
Defined for the present geometry as (d$_{eq}\rho_G\mu_G$)(U$_{g,eff}$+U$_{L,eff}$)
N$_{Sc}$= Schmidt number for gas,
= μ_G/ρ_GD$_G$

The liquid side mass transfer coefficient model chosen for this study is based on film penetration theory, as first proposed by Higbie (1935):

$$k_L = 2(D_L / \pi t)^{0.5} \tag{6}$$

where the exposure time t is taken as the residence time for liquid flow between corrugation changes (i.e., length S). Thus,

$$k_L = 2[D_L U_{L,eff} / (\pi S)]^{0.5} \tag{7}$$

A comparison of experimental data with predicted k$_G$ by Bravo et al. is shown in Figure 3. Compared to the Rocha model, the Bravo prediction shows more deviation from the experimental data. In general, the Bravo model under-predicts the experimental data. The Rocha model may provide better comparison since it is based on a larger set of structured packing data.

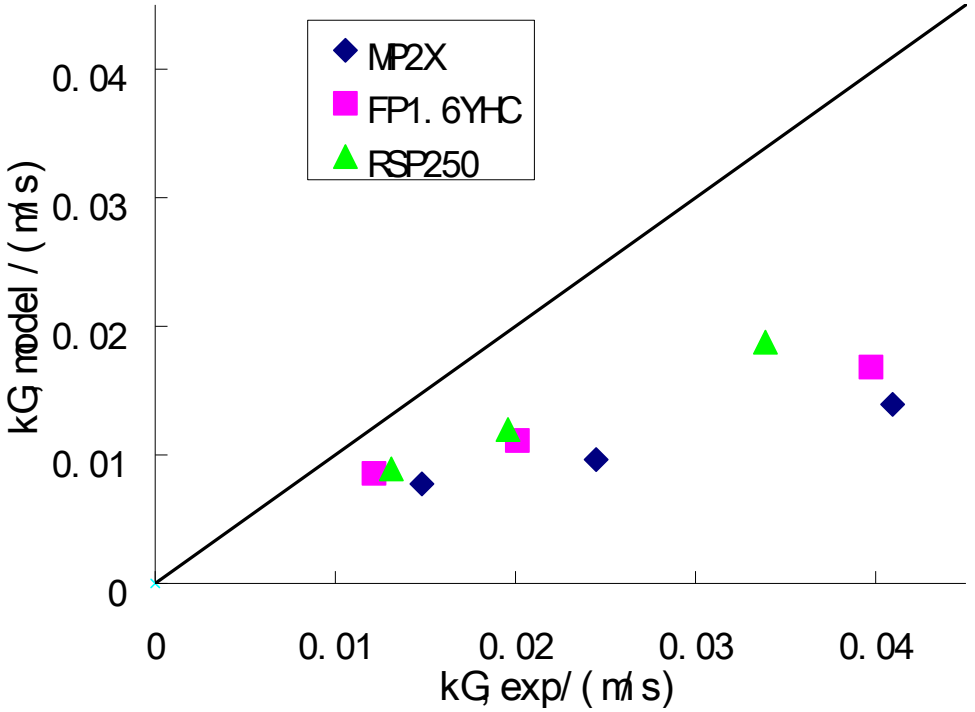

Figure 3: Comparison of experimental k_G data and literature model (Bravo et al.)

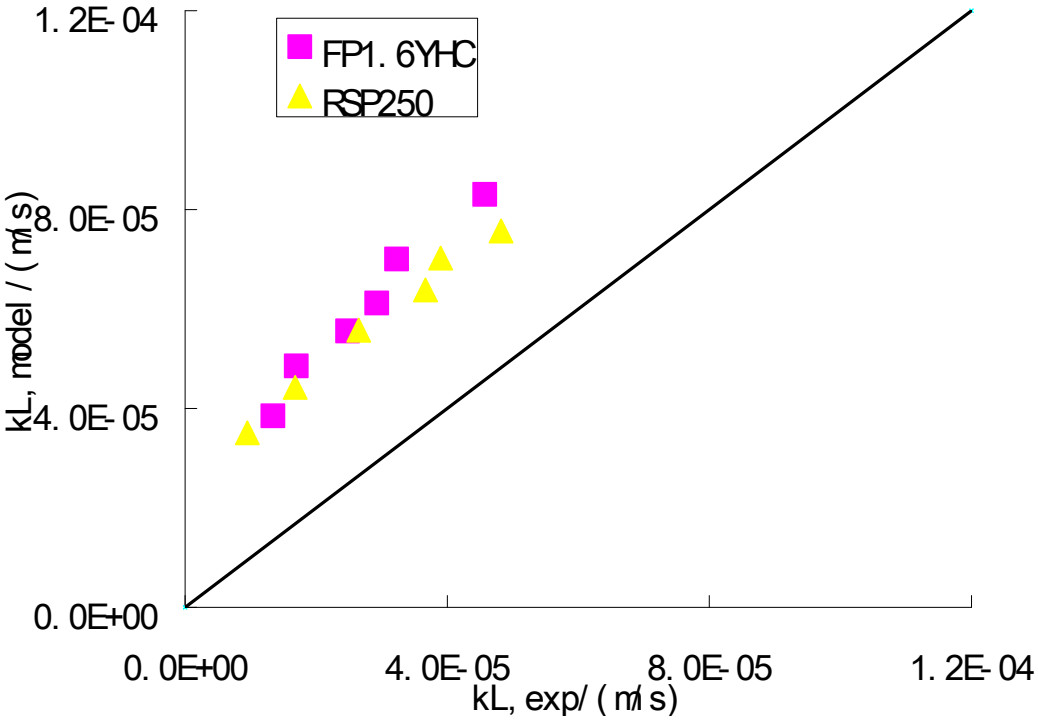

Figure 4: Comparison of experimental k_L data and literature model (Bravo et al.)

The Billet and Schultes model (1993) is another well publicized mass transfer coefficient model that is focused on random packing. The experimental test system used in this research includes

ammonia-air/water, ammonia-propane/water, ammonia-freon 12/water, sulphur dioxide-air/water, sulphur dioxide-oxygen/water, acetone-air/water, methanol-air/water, ethanol-air/water, carbon dioxide-air/1 molal NaOH in water. The packings tested include metal pall rings, plastic pall rings, ceramic pall rings, plastic ralu rings, plastic NOR PAC rings, metal NOR PAC rings, plastic hi-flow rings, and ceramic raschig rings, among others.

The equation for gas side mass transfer coefficient is:

$$k_G a = C_G \frac{1}{(\varepsilon - h_L)^{1/2}} \frac{a^{3/2}}{l_\tau^{1/2}} D_G \left(\frac{u_G}{a \nu_G}\right)^{3/4} \left(\frac{\nu_G}{D_G}\right)^{1/3} \left(\frac{a_P}{a}\right) \tag{8}$$

where C_G is a packing coefficient;

l_τ is the characteristic length of the flow path, $l_\tau = 4\varepsilon/a$;

ν is the kinetic velocity.

The equation for liquid side mass transfer coefficient is:

$$k_L a = C_L \left(\frac{g}{\nu_L}\right)^{1/6} \left(\frac{D_L}{l_\tau}\right)^{1/2} a^{2/3} u_L^{1/3} \left(\frac{a_P}{a}\right) \tag{9}$$

where C_L is the packing coefficient for liquid side mass transfer coefficient.

A comparison of experimental k_G data with the predicted k_G by Billet and Schultes k_G model is provided in Figure 5. From the parity plot, the data predicted by the Billet and Schultes model are in good agreement with our experimental data. However, the model tends to over-predict the packing performance. A possible reason for this could be that Billet and Schultes did not study packings similar to those used in our study. The exponent provided by Billet and Schultes for k_G prediction is 0.75 which is close to our experimental exponent of 0.98.

The experimental data and predicted k_L of Billet and Schultes are compared in Figure 6. The values predicted by Billet's model under-predict the experimental k_L data at low liquid rates and then over-predict at high liquid velocities. One possible explanation is the exponent on the liquid velocity is 0.5 for the Billet and Schultes model while our experimental data suggest the exponent is 0.77. Overall, the k_L prediction is in good agreement with the experimental data.

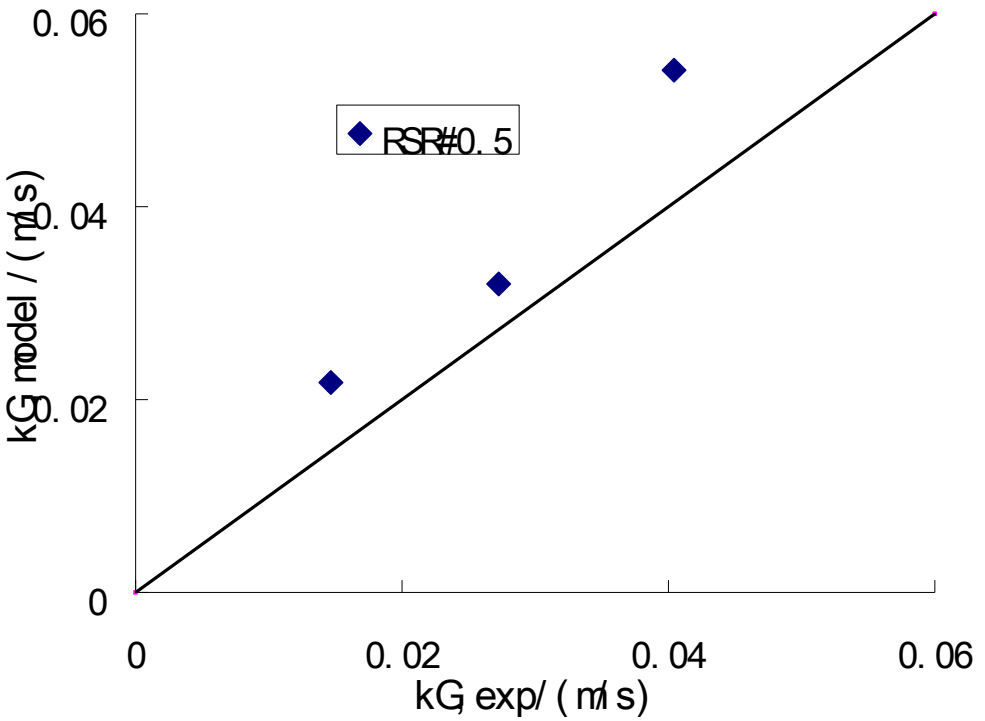

Figure 5: Comparison of experimental k_G data and Billet and Schultes model

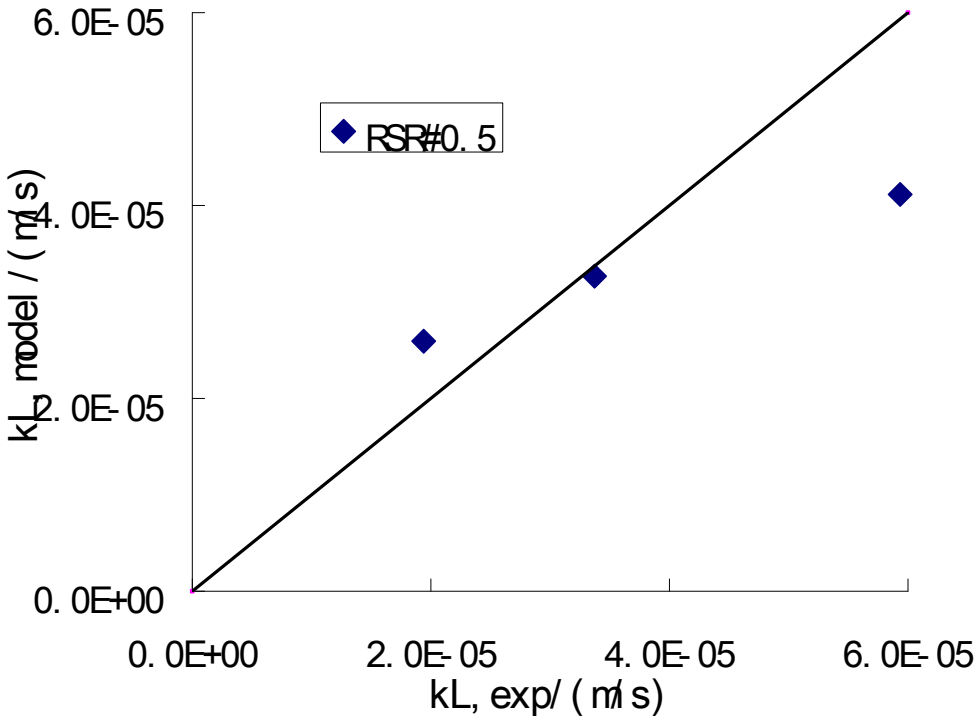

Figure 6: Comparison of experimental k_L data and Billet and Schultes model

Another model for random packing is proposed by Wagner et al. (1997). This model is focused on the newer "high-efficiency" random packings: IMTP, CMR, Fleximax, and Nutter. These

packings are of the high void fraction, through-flow type and have become quite popular for new designs as well as for retrofits. The model is based on an earlier data bank from the laboratories of Fractionation Research, Inc. and the Separations Research Program (SRP) at the University of Texas at Austin. The only packing parameter used in this model is C_{pk}, a packing coefficient which is specific to each packing. The equation for k_G is:

$$k_G = \frac{1}{C_{pk}}\left[\frac{4D_G u_G}{\pi Z(\varepsilon - h)}\right]^{0.5} \tag{10}$$

where C_{pk} is packing coefficient,
D_G is gas phase diffusivity,
h is operation hold-up and ε is packing void fraction.
The equation for k_L is:

$$k_L = \frac{1}{C_{pk}}\left[\frac{4D_L u_L}{\pi Z h}\right]^{0.5} \tag{11}$$

where C_{pk} is packing coefficient,
D_L is liquid phase diffusivity,
h is operation hold-up.

Figure 7 compares the actual experimental data with the predicted k_G. In general, the predicted k_G is 15–45% higher than the experimental data. A possible reason could be that the packing coefficient in Wagner's paper is based on random packings.

Figure 8 shows a comparison of the Wagner et al. k_L model with experimental data. The k_L results predicted by Wagner's model show some deviation from the experimental data. Results show that the Wagner et al. k_L model is less accurate than the Billet and Schultes model.

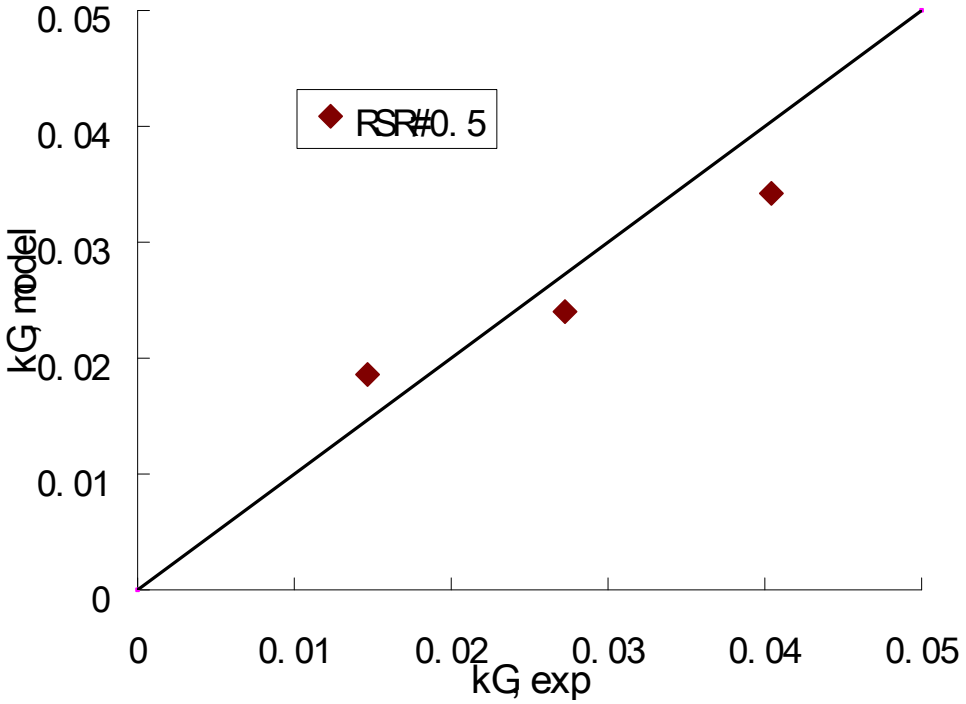

Figure 7: Comparison of experimental k_G data and Wagner et al. model

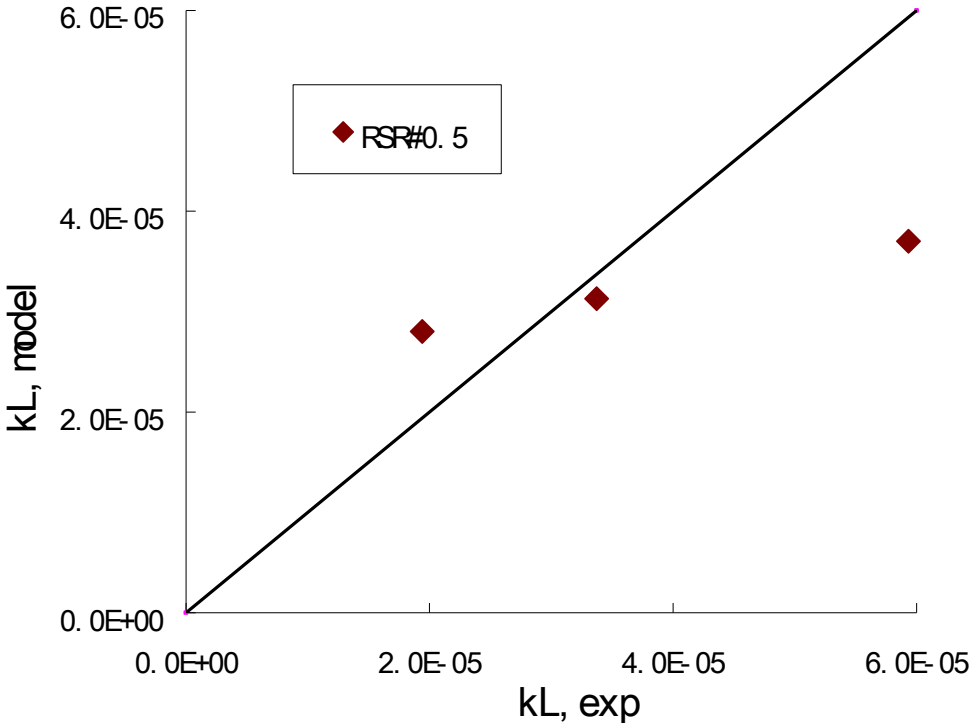

Figure 8: Comparison of experimental k_L data and Wagner et al. model

Conclusions

Gas and liquid side film mass transfer coefficients are compared among experimental data and literature models in this quarterly report.

1. For structured packing, Rocha's model fits in with our experimental data better than the Bravo model. All the data is within 30% deviation for Rocha. The k_G data predicted by Bravo is less than experiment value and the k_L data predicted by Bravo is greater.
2. For random packing, the two models by Billet and Schultes and Wagner et al. both predict our experimental data well. For the liquid side mass transfer coefficient, at high liquid flow rate, both of those models' value is less than the experiment value.
3. Since we are just beginning this series of experiments, our experimental method is far from perfect. It needs to be refined and more data are needed to judge the models.

Future Work

Future work will be focused on analyzing experimental data and obtaining new data in the next quarter.

We will repeat hold-up experiments for Flexipac 1.6 Y HC and repeat FP's k_La measurement using 10 feet of packing. We will also repeat k_La measurement for Mellapak 2X using 10 feet of packing.

The next new packing to be studied is the Raschig Super Ring # 0.7, a metal random packing. We will measure pressure drop, liquid hold-up, mass transfer effective area, and gas and liquid

mass transfer coefficient for that. We may also study the plastic 1-inch Pall ring and the metal 1-inch Pall ring in the next quarter pending availability of the equipment.

References

Billet R, Schultes M. "Predicting Mass Transfer in packed columns." *Chem Eng Technol.* 1993;16:1–9.

Bravo JL, Rocha JA, Fair JR. "Mass transfer in gauze packings." *Hydrocarbon Processing.* 1985;64:91–95.

Rocha JA, Bravo JL, Fair, JR. "Distillation Columns Containing Structured Packings: A Comprehensive Model for Their Performance.2. Mass-Transfer Model." *Ind Eng Chem Res.* 1996;35:1660–1667.

Wagner I, Stichlmair J, Fair JR. "Mass Transfer in Beds of Modern, High-Efficiency Random Packings." *Ind Eng Chem Res.* 1997;36:227–237.

MDEA/PZ Degradation in Cycled Solvents

Quarterly Report for April 1 – June 30, 2010

by

Fred Closmann

Supported by the Luminant Carbon Management Program

and

Industrial Associates Program for CO_2 Capture by Aqueous Absorption

Department of Chemical Engineering

The University of Texas at Austin

July 8, 2010

Abstract

7 m methyldiethanolamine (MDEA) was degraded in three separate experiments in the Integrated Solvent Degradation Apparatus (ISDA) during the quarter. We measured a formate production rate of 0.15 mM/hr in the ISDA with the thermal reactor maintained at 90 °C and 7 m MDEA dosed with 100 mM Inh A, which indicated that the oxidative degradation inhibitor was not effective at this temperature. When we utilized a headspace gas of 98% air/2% O_2 and maintained the thermal reactor at 90 °C, we measured a formate production rate of 0.04 mM/hr, compared to 0.12 mM/hr when we utilized a 98% O_2/2% CO_2 gas at comparable conditions. When we stripped dissolved oxygen from the solvent immediately downstream of the oxidative reactor using a 2 L/min N_2 gas purge in 7 m MDEA cycled from 55 to 120 °C in the ISDA, we reduced the formate production rate to 0.047 mM/hr. The rate without stripping was 0.31 mM/hr, indicating that stripping dissolved oxygen is a practical solution to reducing oxidative degradation in absorber/stripper configurations.

The formate production rate in 8 m piperazine (PZ) (0.3 moles CO_2/mole alk) was 0.05 mM/hr, compared to 0.31 mM/hr measured in 7 m MDEA when cycled from 55 to 120 °C. When we reduced the thermal reactor temperature to 90 °C, the formate production rate was 0.013 mM/hr in 8 m PZ. We measured an ethylenediamine (EDA) production rate of 0.17 mM/hr in 8 m PZ, and a PZ loss rate of ~5%/wk.

When 7 m MDEA was treated with 0.35 m tetramethylammonium chloride (quat), loaded to 0.2 moles CO_2/mole alk, and thermally degraded at 150 °C for up to 30 days in the absence of oxygen in the thermal cylinder headspace, we detected monoethanolamine (MEA), diethanol ethylamine, and dimethyl ethanamine (DMEA). We did not detect bicine or diethanolamine (DEA), both of which are detected in cycling experiments, confirming that these are primarily oxidative degradation products of MDEA.

We improved our oxidative degradation model for the ISDA using a plug-flow reactor model, and estimated energies of activation (Ea) for the production of DEA, formate and bicine of 85, 91, and 100 kJ/mol*K.

Introduction

During the 2nd Quarter 2010, we continued degradation experiments with 7 m MDEA at a loading of 0.1 moles CO_2/mole alkalinity in the ISDA in order to understand system behavior and the role of dissolved and entrained oxygen on solvent degradation. Three experiments with this solvent (C-14, C-15 and C-18) were completed during the quarter. Experiments C-16 and C-17 were conducted in the quarter with 8 m PZ at a loading of 0.3 moles CO_2/mole alkalinity.

Samples from each experiment were analyzed for heat stable salts (HSS) using anion chromatography, amine (MDEA) and amine degradation products with cation functionality using cation chromatography, amino acids using separation and electrochemical detection on a Dionex ICS-3000 system, alkalinity using acid titration, and total inorganic carbon (TIC) using infrared detection (IR). A subset of samples was analyzed using chromatography (gas and IC) followed by mass spectrometry (MS). However, note that a malfunction with the infrared spectrometer (IR) linked to our TIC instrument late in the quarter prevented measurement of CO_2 loading in experiments C-17 and C-18 prior to reporting time.

For experiment C-18, the ISDA was modified through the installation of an 8" tall by 1.25" diameter glass column in place of the glass bubble removal chamber; N_2 gas was sparged in this modified tube to strip dissolved oxygen from the solvent as it passed through this chamber and exited to the positive displacement pump. C-18 was performed to test our ability to remove dissolved oxygen before the solvent entered the cross-exchanger and reduce oxidative degradation. C-18 was the only experiment conducted with the bubble chamber modified for stripping of dissolved oxygen.

Two thermal degradation experiments were conducted in the quarter. Thermal No. 13 was conducted with 7 m DEA at loadings of 0 and 0.2 moles CO_2/mole alkalinity. All sample cylinders were placed in the 150 °C oven and the total duration of the experiment was 13 days. Thermal No. 14 included 7 m MDEA with and without 0.35 m quaternary methyl ammonium chloride (quat) at loadings of 0 and 0.2 moles CO_2/mole alkalinity, with all sample cylinders placed in the 150 °C oven. All Thermal No. 14 sample cylinders were charged with solvent in a sealed glove bag under a N_2 gas atmosphere to ensure that no oxygen was present in the headspace of the sample cylinders before sealing the cylinders.

For the oxidative degradation model, the evaluation of ISDA data to extract degradation product formation rates was modified in the quarter to normalize data to a standard across each experiment. The standard chosen for evaluation of rates was the slope of the line for degradation product concentration versus time at the point in time where 2% of total alkalinity loss occurred. For example, in experiment C-12, a loss of 2% of measured alkalinity occurred at approximately 30 hours into the experiment. Rates of degradation product formation were all interpreted at the 30-hour mark for this experiment. For experiment C-6, 2% alkalinity loss occurred at approximately 14.3 hours. This standard was chosen to provide uniform evaluation of data used as inputs to the oxidative degradation model discussed later in this report. This standard will be used for all data sets from the ISDA in future.

Cycling (ISDA) Experiments (In-Depth) Discussion

A summary of the degradation rates measured for each of the ISDA experiments is listed in Table 1. Data tables for experiments C-14 through C-18 are included at the end of this quarterly report as Tables A-1 through A-10. The experimental data are arranged in Table 1 to allow

evaluation of results in sequential manner as opposed to chronological order, and include data from past experiments. All cycling experiments were conducted with either 7 m MDEA at an initial loading of 0.1 moles CO_2/mole alkalinity, or 8 m PZ at an initial loading of 0.3 moles CO_2/mole alkalinity; both conditions approximately match the CO_2 solubility condition at 55 °C for the 2 kPa CO_2 gas provided to the oxidative reactor headspace. The solvent in all experiments included the stainless steel metals mix (0.4 mM Fe, 0.1 mM Cr, and 0.05 mM Ni), with metals added as dissolved metal salts. The experimental setup typically includes a headspace gas of 98% O_2/2% CO_2 at a flow rate of 100 ml/min.

Formate is the primary heat stable salt observed when MDEA is degraded in the ISDA with oxygen present. From cation chromatography, we observe and quantify DEA in all experiments. DEA comprises the majority of cation products in degraded MDEA. Of the amino acids, we continue to identify and quantify bicine and glycine in cycled MDEA as an oxidative degradation product using chromatography with electrochemical detection (Dionex AAA-Direct Method).

Table 1: ISDA Experimental Results Summary (7 m MDEA, Ldg = 0.1)

Expt	T_{th} (°C)	Stir Rate (rpm)	Purge Gas	Other Conditions	Alk Loss (mM/hr)	MDEA Loss (mM/hr)	DEA Prod Rate (mM/hr)	Formate Prod (mM/hr)	Formate w/ Hydrolysis (mM/hr)	Bicine (mM/hr)	Glycine (mM/hr)
C-8	120	1440	N_2/CO_2	SS metals; bubble vessel	1.7	1.9	0	0.013	0.001	0	0
C-9	120	0	N_2/CO_2	SS metals; bubble vessel	3	4.1	0	0.007	0.002	0	0
C-13	120	1440	Air/CO_2	SS metals; bubble vessel	0.76	0.24	0.37	0.084	0.08	0.061	0.001
C-14	90	1440	Air/CO_2	SS metals; bubble vessel	0.76	0.22	0.08	0.044	0.058	0.062	~0
C-18	120	1440	O_2/CO_2	SS metals; mod bubble vessel with N_2 purge	0.74	0	0.39	0.047	0.044	0.088	0.01
C-4	120	520	O_2/CO_2	SS metals	2.8	3.4	NM	0.17	0.15	NM	NM
C-5	120	1000	O_2/CO_2	SS metals; bubble removal	4.3	8.5	NM	0.37	0.57	NM	NM
C-1	120	1440	O_2/CO_2		5.2	8.8	NM	0.59	0.98	0.48	0.001
C-2	55	1440	O_2/CO_2		1.4	~0.0	NM	0.0052	~0	~0	~0
C-15	90	1440	O_2/CO_2	SS metals; BR, Inh A	1.82	2.37	~0	0.15	0.23	0.27	0.004
C-7*	120	1440	O_2/CO_2	SS metals; BR, Inh A	5.4	5	1.8	0.22	0.29	0.35	~0
C-3	55	1440	O_2/CO_2	SS metals	1.5	0.9	0	0.0018	0.01	0.05	0
C-11	80	1440	O_2/CO_2	SS metals; bubble vessel	1.3	0.91	0	0.034	0.057	0.11	0
C-12	90	1440	O_2/CO_2	SS metals; bubble vessel	2.5	2.87	1.55	0.12	0.15	0.13	0.006
C-10	100	1440	O_2/CO_2	SS metals; bubble vessel	3	3.9	1.64	0.17	0.29	0.22	0.007
C-6	120	1440	O_2/CO_2	SS metals; bubble vessel	5.3	4.6	2.56	0.31	0.34	0.34	0.007

Experiment C-14

Experiment C-14 was conducted with an oxidative reactor headspace gas composition of 98% air/2% CO_2 and a thermal reactor temperature of 90 °C to measure the extent of degradation at a reduced oxygen concentration (~20%). In the previous quarter, C-13 was conducted with a headspace gas of 98% air/2% CO_2 with a thermal reactor temperature of 120 °C; the results of C-13 and C-14 are compared directly to each other, as presented in Table 1.

The MDEA (cation IC) and alkalinity loss rates were approximately the same for C-13 and C-14, at 0.76 and 0.22–0.24 mM/hr, respectively. However, the degradation product formation rates differed, as demonstrated by reduced DEA, formate, and total formate (including amides) production rates in C-14 where the thermal reactor was maintained at 90 °C, resulting in reduced oxidation rates. One exception was the bicine production rate, which was approximately 0.06 mM/hr in both experiments. When compared to the results for C-12, also conducted with a thermal reactor temperature of 90 °C, the results of C-14 indicate that the MDEA and alkalinity

loss rates were an order of magnitude less than in C-12. The degradation product formation rates were approximately 40% of those measured in C-12, with the exception of DEA (5%), reflecting that only 20% of the oxygen used in C-12 was present in oxidative reactor headspace in C-14.

Experiment C-15

Experiment C-15 was conducted with a thermal reactor temperature of 90 °C, a purge gas of 98% O_2/2% CO_2, and 100 mM Inh A. This experiment was conducted to allow direct comparison to the results of C-12 which was conducted at similar conditions without Inh A. The alkalinity and MDEA loss rates were reduced approximately 25%, and no DEA was produced in C-15. However, the formate, total formate (including amides), and bicine production rates actually increased over C-12 where no Inh A was utilized, indicating that the inhibitor was not effective at reducing overall oxidative degradation at these cycling conditions. Figure 1 presents the results of the two experiments conducted with Inh A to date, and their counterparts without Inh A. These comparisons indicate that Inh A is generally not effective at reducing oxidative degradation over the temperature range of 90 to 120 °C.

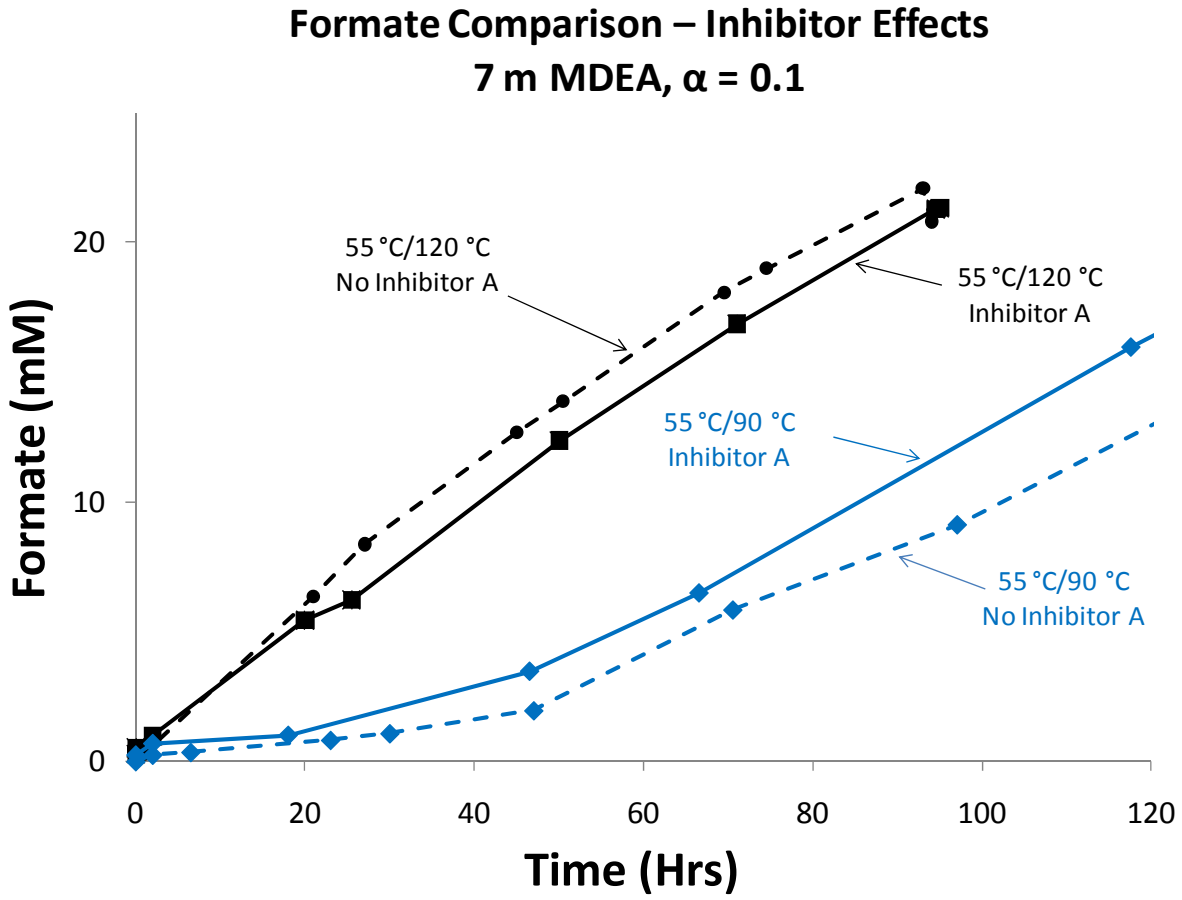

Figure 1: Inhibitor A Comparisons (7 m MDEA, Ldg = 0.1)

Experiments C-16 and C-17

Experiments C-16 and C-17 were performed with 8 m PZ at thermal reactor temperatures of 120 and 90 °C, respectively. All other conditions were the same, including the standard oxidative reactor temperature of 55 °C. Experiment C-19 was begun before the quarter ended, but

terminated due to mechanical limitations with the gear-driven pump in maintaining the necessary pressure to operate the thermal reactor at 130 °C with 8 m PZ at a loading of 0.3 moles CO_2/mole alkalinity. Pressures in excess of 80 psig were experienced, whereas the gear pump/magnetic drive used in the apparatus is rated to 75 psig.

As listed in Table 2, when the thermal reactor temperature was reduced from 120 to 90 °C, the alkalinity and PZ loss rates were reduced from 1.2 and 1.1 mM/hr to 0.12 and 0.11 mM/hr, respectively. The formate production rates were 0.046 and 0.013 mM/hr, respectively, at 120 and 90 °C. For comparison, the formate production rate in MDEA at a thermal reactor temperature of 120 °C was measured as 0.31 mM/hr in C-6 (Figure 2). Figure 2 also presents formate concentrations in 8 m PZ degraded in the low-gas apparatus at 55 °C; the rate of formate production in the low-gas system was an order of magnitude lower than in the ISDA (0.004 mM/hr). The rates of production of total formate, which includes the amide of formate, were approximately 2.8 X the rates of production of formate alone in both 8 m PZ experiments (C-16 and C-17). The ratios of total formate to formate production in 7 m MDEA at comparable conditions were 1.1 to 1.25, indicating that more amide is formed in 8 m PZ than in 7 m MDEA.

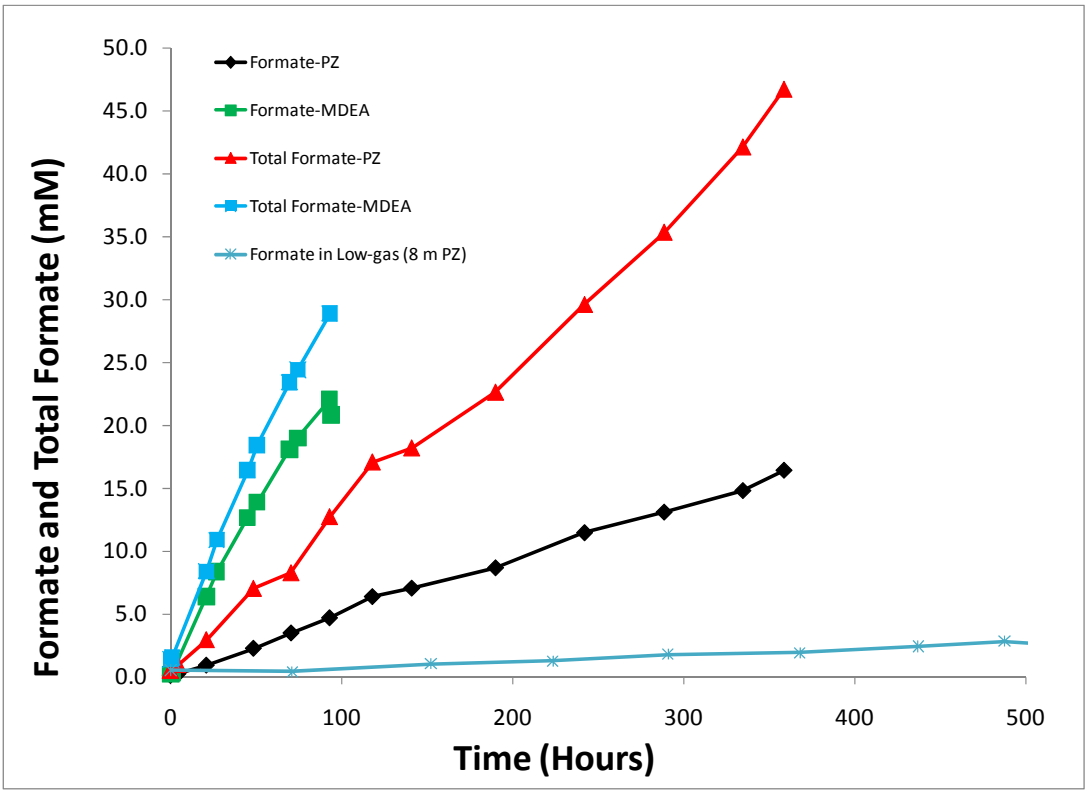

Figure 2: Formate/Total Formate - 8 m PZ, Ldg = 0.3 Cycled from 55 to 120 °C

We measured ethylenediamine (EDA) production rates of 0.07 and 0.17 mM/hr at thermal reactor temperatures of 90 and 120 °C, respectively, in 8 m PZ. These rates are 65 and 15% of the PZ loss rates at 90 and 120 °C, respectively. The amino acid bicine was not detected in degraded PZ samples, whereas we consistently detect bicine in degraded MDEA; we detected glycine at a concentration of 6.6 mM after 359 hours of cycling 8 m PZ to 120 C in C-16.

Table 2: ISDA Degradation Rates/Ratios (8 m PZ, Ldg = 0.3)

Expt	T_{th} (°C)	Stir Rate (rpm)	Purge Gas	Other Conditions	Alk Loss (mM/hr)	PZ Loss (mM/hr)	EDA Prod Rate (mM/hr)	Formate Prod (mM/hr)	Formate w/ Hydrolysis (mM/hr)	Bicine (mM/hr)	Glycine (mM)
C-16	120	1440	O_2/CO_2	SS metals; bubble vessel	1.2	1.1	0.17	0.046	0.130	0	0.013
C-17	90	1440	O_2/CO2	SS metals; bubble vessel	0.12	0.11	0.07	0.013	0.038	0	0.003

Figure 3 presents the concentration of PZ, alkalinity, and PZ degradation products with time in C-16, which cycled the solvent from 55 to 120 °C. Of the degradation products, EDA comprised the greatest concentration, at ~60 mM after 350 hours of cycling. Total formate (including n-formyl amide) was measured at nearly 50 mM after 350 hours. Finally, the measured PZ loss rate was approximately 5%/wk.

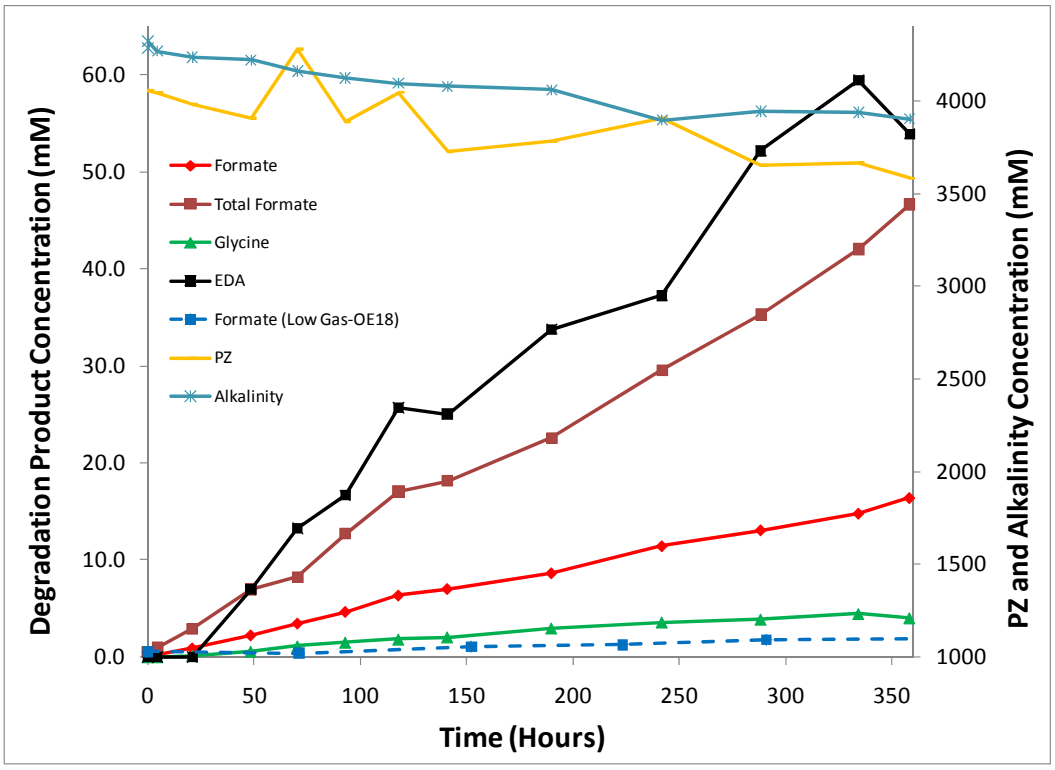

Figure 3: PZ and Degradation Products - 8 m PZ, Ldg = 0.3 Cycled from 55 to 120 °C

Experiment C-18

The ISDA was modified for dissolved oxygen removal from the solvent in experiment C-18. An 8" tall by 1.25" diameter glass column was installed in place of the glass bubble removal chamber. Solvent passed through this chamber as before, but a fritted stone was installed at three-quarters of full depth and N_2 was passed through the stone at a nominal rate of 2 L/min in order to strip dissolved oxygen from the solvent as it passed through this modified bubble removal chamber and exited to the positive displacement pump. All other conditions of the system were maintained the same as those in experiment C-6 to allow direct comparison of degradation data; C-18 was performed to test our ability to remove dissolved oxygen before the solvent entered the cross-exchanger and reduce oxidative degradation.

The alkalinity loss rate measured with stripping in C-18 was an order of magnitude less than that measured in C-6 (0.74 vs. 5.3 mM/hr). Any loss in MDEA concentration in C-18 was undetectable by cation chromatography. Formate and total formate production rates in C-18 were approximately 15% of the comparable rates measured in C-6 where stripping was not implemented (Figure 4). The DEA production rate was measured as 0.39 mM/hr when we stripped dissolved oxygen, compared to 2.56 mM/hr in experiment C-6. In general, experiment C-18 demonstrated that dissolved oxygen can be stripped from the solvent before it is pumped to the cross exchanger, effectively reducing the rate of oxidative degradation. We reduced the oxidation product formation rates to levels comparable to those measured when the thermal reactor was maintained at 80 °C.

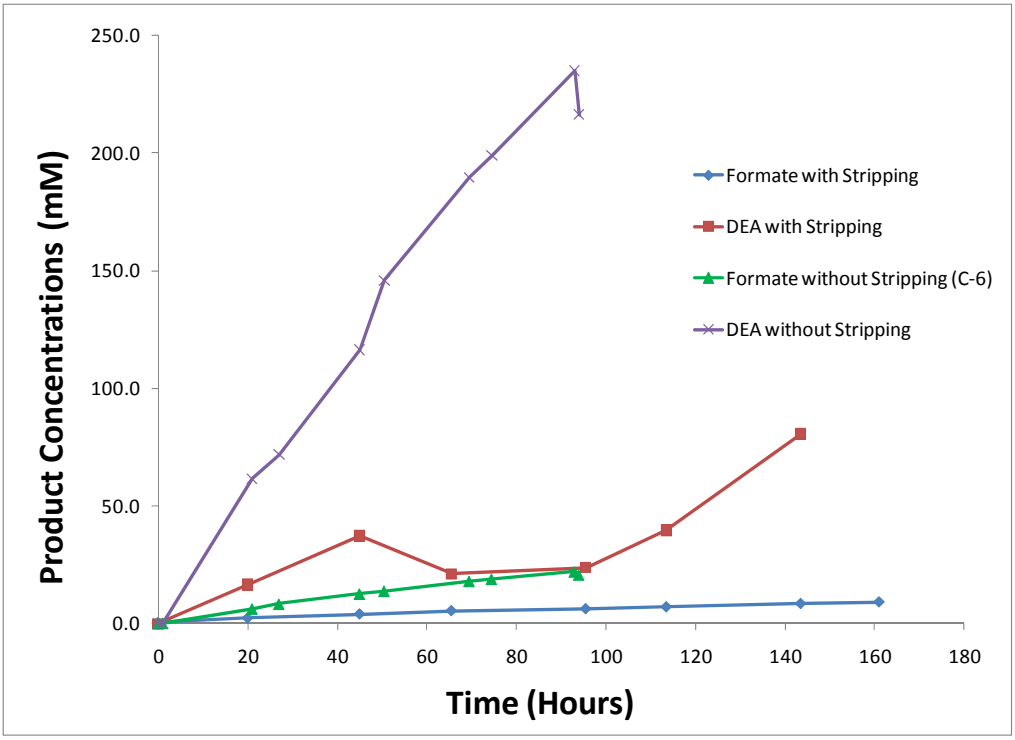

Figure 4: Formate and DEA Concentration Comparisons
7 m MDEA Cycled from 55 to 120 °C with/without Stripping

Oxidative Degradation Model

We continued the development of an oxidative degradation model based on data collected from the ISDA over a range of thermal reactor temperatures (55 to 120 °C). The purpose of the model is to predict the rates of oxidative degradation that can be expected in a solvent in the heat exchanger and piping entering the top of the steam stripper, as these are the most likely locations for oxygen to be present at higher temperatures. A simple rate law relationship using the Arrhenius equation over-predicts oxidation rates at temperatures above 100 °C, we believe due to complete consumption of dissolved oxygen in the ISDA in the thermal reactor. Our oxidative model is intended to correct for the depletion of dissolved oxygen at the higher temperatures.

The basis for the model is that solvent degradation in the ISDA behaves as an isothermal plug flow reactor (PFR), with an approximation that all oxidative degradation occurs in the thermal

reactor at the higher temperatures; rates of degradation product formation over the temperature range 55 to 80 °C are relatively low compared to 90 °C and above, indicating that degradation processes are negligible in solvent when not passing through the thermal reactor.

We utilized a factor (S) to relate the amount of degradation product formed to the amount of oxygen consumed per pass of solvent through the system, using Henry's Law to relate dissolved oxygen in the solvent to that in the gas phase in contact with the solvent in the oxidative reactor.

$$k = k_o * \exp\left[-\frac{E_a}{R}\left(\frac{1}{T}-\frac{1}{T_o}\right)\right]$$

Arrhenius

$$S = \left[\frac{\Delta \mathrm{Pr}od}{\Delta O_2}\right]$$

$$\Delta[Prod] = S \cdot P_{O_2} \cdot Q \cdot t \cdot \frac{1 - e^{-\left(\frac{k \cdot V_{TR}}{Q}\right)}}{H_{O_2} \cdot V_{tot}}$$

Plug Flow Model

Using degradation product formation rates over the temperature range of 55 to 120 °C, we regressed values of activation energy (E_a), rate constant (k_o), and S for formate, DEA and bicine formed in the system. As a starting point, we chose the measured values of k_o at 90 °C for each component based on the knowledge that dissolved oxygen was not completely consumed at this temperature in the ISDA.

We estimated k_o, E_a and S for the three components as listed in Table 3. The model currently provides values for each parameter within an expected range for DEA and formate, but does not provide expected values for bicine using engineering judgment. For example, the S-value for bicine was regressed to 4,848, which indicates an extremely large (~4,900 mole/mole) ratio of bicine produced to oxygen consumed. However, the k_o and E_a values regress to values within an expected range. Further, k_o for bicine is three orders of magnitude lower than for DEA and five orders of magnitude lower than for formate, reflecting the greater tendency for MDEA to degrade to DEA and formate than to bicine. The activation energies for all three compounds regressed to a value of 85= to 100 kJ/mol*K.

Table 3: Regressed Model Parameters for the ISDA (7 m MDEA, Ldg = 0.1)

DEA Values		Bicine		Formate	
ko	0.0559	ko	2.29E-05	ko	2.6330
Ea	85054	Ea	100000	Ea	90998
S	16.72	S	4848.20	S	0.10

Figure 5 presents the measured and predicted product formation rates vs. 1/T (K) for the components formate and bicine based on the regressed E_a and k_o. We have also presented the measured rates for DEA as well as formate in the low-gas reactor. The predicted rates for k_o approximately match the measured values at higher temperatures for formate, but slightly over-

predict at the lower temperature. For bicine, the match is poor at all but the highest temperatures, which is expected based on the regressed value for S (~4,900). In general, the model provides a better fit for formate than was provided by using a simple rate-law model based on Arrhenius. We believe the model is compensating for the complete consumption of dissolved oxygen at the higher temperatures in the ISDA.

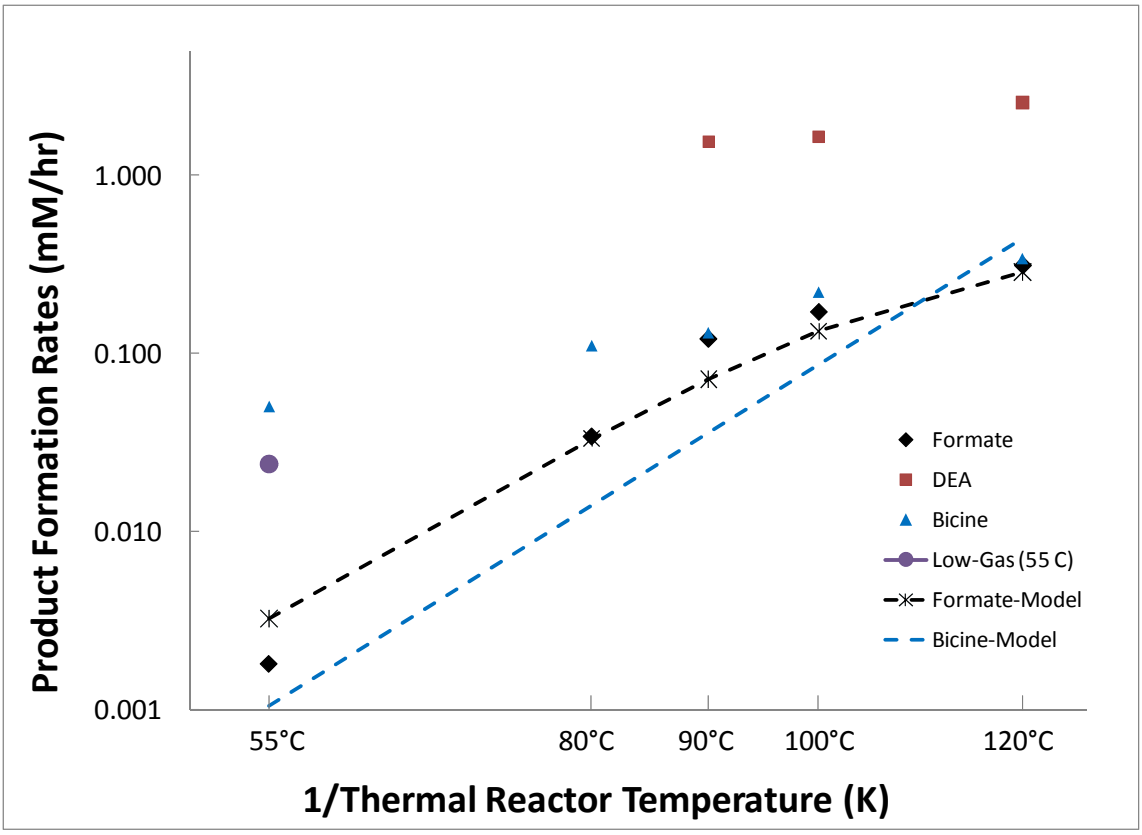

Figure 5: Oxidative Model - Predicted vs. Measured Concentrations

Degradation Mechanisms and Thermal Experiments

We recently completed Thermal No. 13 and Thermal No. 14 experiments using Swagelok sample cylinders for investigation of thermal degradation of solvents. Thermal No. 13 included 7 m diethanolamine (DEA) at loadings of 0 and 0.2 moles CO_2/mole alkalinity degraded at 150 °C for up to two weeks in forced convection ovens. In Thermal No. 14, we reacted 7 m MDEA with 0.35 m tetramethylammonium chloride and loaded the solution to 0.2 moles CO_2/mole alkalinity. This solvent was thermally degraded at 150 °C for up to four weeks.

Thermal No. 13

In Thermal No. 13, we confirmed the presence of 1-methyl piperazine in degraded 7 m DEA (α = 0.2) after only two days of degradation at 150 °C in both loaded and unloaded solutions. We also made a possible confirmation of dimethyl piperazine in the loaded solution degraded for 13 days at 150 °C. Unlike the results of Blanc et al. (1982), we did not observe hydroxyethyl piperazine (HEP) with cation chromatography. However, we did observe as much as 42 mM formate after 13 days. We analyzed for amino acids, but only detected bicine, and at concentrations at the low end of our standard curve (1 ppm).

Thermal No. 14

In Thermal No. 14, we combined a quaternary amine (tetramethylammonium chloride) with MDEA and loaded the solvent to determine the effect of the quat on initiation of arm-switching reactions in the solvent. After loading the solution with 0.2 moles CO_2/mole alk, the solvent was placed in sample cylinders under a nitrogen gas blanket in a glove bag to eliminate oxygen in the headspace of the sample cylinders. Sample cylinders were placed in forced convection ovens at 150 °C for up to a month.

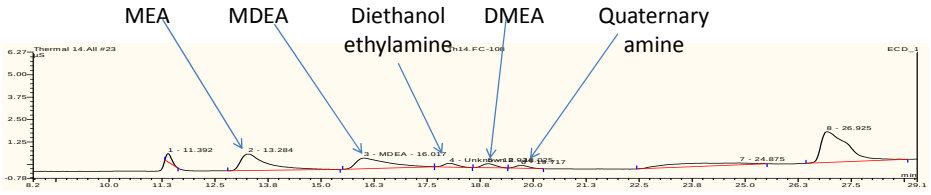

Figure 6: Thermal No. 14: MDEA + Quat Degraded at 150 °C for 26 days

After 26 days of degradation at 150 °C, we confirmed the presence of monoethanolamine (MEA), diethanolethylamine, N,N'-dimethyl ethanamine (DMEA), and hydroxyethyl piperazine (Figure 6). These results are similar to those of Bedell (2010). However, we did not detect amino acids in degraded solutions. Bedell reported as much as 0.11 M bicine when starting with 4.2 M MDEA degraded in a microcalorimeter with a starting partial pressure of oxygen of 0.55 MPa. We did not measure appreciable concentrations of bicine in our experiment due to the absence of oxygen in the sample cylinder headspace; the only oxygen available to the solvent was that oxygen dissolved into the sample upon placement into the cylinder. DEA was also not detected in Thermal No. 14 samples, further indicating that DEA is primarily an oxidative degradation product of MDEA, as evidenced by its presence in cycled 7 m MDEA from the ISDA. We did measure formate at approximately 49 mM in a Thermal No. 14 sample degraded for 30 days.

In general, Thermal No. 14 results, including the observation of disproportionation reaction products, are consistent with those of other researchers. However, the observation of MEA at high relative concentrations in our reaction solutions was not anticipated and cannot be explained by simple arm-switching reactions wherein methyl groups from the quat would exchange with hydroxyethyl groups from MDEA to result in other products (i.e., DMEA).

Conclusions

Cycling experiment C-15 with 7 m MDEA indicated that 100 mM Inh A is not effective at inhibiting oxidative degradation at 90 °C. The measured formate production rate was 0.15 mM/hr versus 0.12 mM/hr without Inh A. Figure 1 of this report presents the formate concentrations from four experiments conducted to date in the ISDA with 7 m MDEA, and

generally supports the conclusion that Inh A is not effective in slowing oxidative degradation in the cycled solvent at 90 and 120 °C.

In cycling experiment C-18, we modified our system to strip dissolved oxygen from the solvent immediately after exiting the oxidative reactor and prior to pumping to the cross-exchanger, by sparging N_2 gas at ~2 L/min through a modified bubble removal vessel. We successfully reduced the formate and total formate production rates to 0.047 and 0.044 mM/hr, respectively, when we stripped oxygen and cycled to 120 °C. The measured rates for formate and total formate production were 0.31 and 0.34 mM/hr, respectively, without stripping. We also reduced the DEA production rate from 2.6 to 0.4 mM/hr through stripping. The practical implication of these results is that we can reduce or eliminate oxidative degradation in an absorber/stripper system by implementing gas stripping before the solvent is pumped to the heat exchanger. The problem of oxidative degradation of solvents in scrubbing of post-combustion flue gas streams was addressed by Chakravarti (2001) in the development of an approach to remove O_2 from rich amine streams in CO_2 scrubbing systems in service for treatment of flue gases.

We degraded 8 m PZ in two experiments in the ISDA this quarter, and reported lower formate production than measured in comparable cycling experiments with 7 m MDEA. We measured a formate production rate of 0.046 mM/hr when we cycled 8 m PZ (α = 0.3 moles CO_2/mole alk) from 55 to 120 °C, versus a rate of 0.31 mM/hr when we cycled 7 m MDEA (α = 0.3 moles CO_2/mole alk) at comparable conditions. However, as presented in Figure 2 of this report, we observed five times as much formate production when we cycled 8 m PZ to 120 °C than in a low-gas experiment at 55 °C with this solvent. Of the degradation products in cycled PZ, EDA was measured at the greatest concentration, at nearly 60 mM after approximately 360 hours of cycling. We measured a PZ loss rate of 5%/wk when we cycled to 120 °C in the thermal reactor in C-16.

The oxidative degradation model was improved through the development of a plug flow reactor model to correct for oxidative degradation behavior with each pass of solvent through the system. Model improvements were necessary to account for complete consumption of dissolved oxygen at the higher experimental temperatures (>100 °C). Experimental data (C-3, C-6, C-10, C-11, and C-12) were normalized to a 2% alkalinity loss standard. With these standardized rates, the prediction of k_o for formate and DEA improved with the model over the predicted values provided by the simple rate-law oxidative model. The model does not provide a reasonable value of the stoichiometric coefficient (S) for bicine. One possible explanation is that bicine is not a direct oxidation product of MDEA, but instead, a product of another MDEA degradation product.

Two thermal degradation experiments were completed in the quarter. In Thermal No. 13, we degraded 7 m DEA (α = 0.2) at 150 °C for 13 days and detected the presence of methyl-piperazine and dimethyl piperazine, and as much as 42 mM formate. We detected very little bicine after two weeks of degradation. In Thermal No. 14, we degraded 7 m MDEA with 0.35 m quaternary amine (α = 0.2) for four weeks at 150 °C, and detected the presence of monoethanolamine (MEA), diethanolethylamine, N,N'-dimethyl ethanamine (DMEA), and hydroxyethyl piperazine. Of importance, we did not detect the presence of the secondary amine DEA or the amino acid bicine, both of which are oxidative degradation products; Thermal No. 14 sample cylinders were sealed under a nitrogen gas blanket. However, we measured formate at approximately 49 mM in a sample thermally degraded at 150 °C for 30 days. We also

observed formate in Thermal No. 13 samples (42 mM after 13 days). The observation of formate in both the Thermal No. 13 and Thermal No. 14 samples further supports the idea that formate production will occur in a primarily reduced environment (without oxygen), with the formate carbon potentially originating from the carbon in CO_2.

Future Work

Work planned for the 3rd Quarter 2010 will include the completion of one additional cycling experiment (C-20) with 7 m MDEA. C-20 will entail dosing 7 m MDEA with 200 mM formate at the beginning of the experiment to understand whether formate is in competition with MDEA for dissolved oxygen as the solvent oxidatively degrades. We will observe trends in the formate and MDEA concentrations; should formate consume oxygen and degrade at the outset of the experiment, we anticipate that this will inhibit MDEA oxidation until the formate is consumed.

After obtaining a pump capable of delivering a higher differential pressure to the solvent, we will complete one more cycling experiment with 8 m PZ (α = 0.3 moles CO_2/mole alk) with the thermal reactor temperature set to 130 °C; this experiment was initiated in the last quarter but abandoned due to insufficient pressure delivery with the existing pump.

Cycling experiments with 7 m MDEA/2 m PZ will be initiated in the third quarter to understand the degradation of this blend in the ISDA. The initial experiment will entail cycling the solvent from 55 to 120 °C for up to three weeks to obtain baseline data on how this solvent degrades in the system. Subsequent experiments will be performed with the thermal reactor set at temperatures other than 120 °C; based on Aspen Plus® modeling, at a loading of 0.14 moles CO_2/mole alk, the total pressure (absolute) of the solvent will not exceed 4 bar at 130 °C, allowing us to operate the ISDA in its current configuration at this temperature. The 0.14 loading was chosen to be in equilibrium with the purge gas utilized in these experiments at 55 °C, which has a partial pressure of 2 kPA CO_2.

A thermal degradation experiment will be started in August which will be a repeat of Thermal No. 7. We will thermally degrade 7 m MDEA/2 m PZ at loadings of 0, 0.1, and 0.25 moles CO_2/mole alk at temperatures of 120, 135, and 150 °C to better understand the degradation potential and pathways in the blend. It is anticipated that sample cylinders will be placed in the ovens for degradation for up to eight weeks to gain an understanding of the degradation potential of the blend at all three temperatures. In Thermal No. 7, we determined that PZ loss was nearly complete after only 25 days at 150 °C in a similar experiment. In the repeat experiment, we will measure the concentration of heat stable salts, amino acids, and amines using cation IC.

We will continue to improve the oxidative degradation model for degradation of MDEA in the ISDA which is based on plug flow reactor behavior in the thermal reactor; the model will be useful for estimating rates of oxidative degradation at the hot side of the cross exchanger. We have regressed k_o, E_a, and S values for formate and DEA that fall within anticipated limits, but the regressed values for bicine production do not currently match anticipated results. The predicted rate (k_o) for formate provides a closer approximation to measured rates than was provided by a simple rate law (Arrhenius).

Finally, we will continue working with IC-MS and GC-MS methods to identify degradation products in degraded MDEA, PZ, and the blend.

References

Bedell S, Worley CM, Darst K, Simmons K, The Dow Chemical Company. "Thermal and Oxidative Disproportionation in Amine Degradation - O_2 Stoichiometry and Mechanistic Implications." Submitted to *Int. J. Greenhouse Gas Control*, September, 2009.

Blanc C, Grall, Demarais, Societe Nationale Elf Aquitaine, "The Part Played by Degradation Products in the Corrosion of Gas Sweetening Plants Using DEA and MDEA", Gas Conditioning Conference, 1982.

Chakravarti S, Gupta A. "Carbon Dioxide Recovery Plant". Patent Appl. No. 09/774,031. Filed January 31, 2001.

Table A-1
Cycling Experiment C-14
Solvent: 7 m MDEA, Ldg = 0.1 moles CO_2/mole alkalinity
Amendments: 0.4 mM Fe/0.1 mM Cr/0.05 mM Ni; 98 % Air/2 % CO_2
Conditions: 55 °C/90 °C
Conducted: March/April 2010

		Amine Concentration					Heat Stable Salts Concentrations				Amino Acids	
Sample No.	Degradation Time (hr)	MDEA (Tit) (m)	MDEA (Cations) (mM)	α_{act} (moles CO_2/mole alk)	Corrected (m)	DEA (mM)	Formate (mM)	Glycolate (mM)	Oxalate (mM)	Sulfate (mM)	Bicine (mM)	Glycine (mM)
C-14-0	0	6.54	3480.5	0.104	6.55	0.3	0.14	0.00	0.44	1.40	0.00	0.00
C-14-1	3	6.55	3391.3	0.103	6.55	3.5	0.48	0.00	0.57	1.40	0.00	0.00
C-14-2a	19	6.53	3396.8	0.092	6.53	5.2	0.69	0.19	0.43	1.26	0.00	0.00
C-14-2b	19	6.53	3463.7	0.095	6.53	1.6	0.55	0.20	0.28	1.28	0.00	0.00
C-14-2c	19	6.57	3369.0	0.090	6.57	0.0	0.54	0.19	0.40	1.20	0.00	0.00
C-14-2.avg	19		3409.8			0.0	0.60	0.19	0.37	1.25	0.00	0.00
C-14-3	42.5	6.51	3709.2	0.076	6.52	12.9	1.06	0.57	0.34	1.26	0.12	0.00
C-14-4	66.5	8.64	3322.6	0.072	8.62	5.2	1.99	1.06	0.25	1.68	0.29	0.00
C-14-5	91	6.40	3394.8	0.049	6.42	2.8	3.47	1.71	0.54	1.23	2.76	0.00
C-14-6	121.5	6.40	3508.0	0.036	6.42	0.5	5.07	2.24	0.73	1.27	3.95	0.00
C-14-7	143.5	6.35	3485.3	0.043	6.37	23.3	6.24	2.56	0.80	1.37	5.78	0.00
C-14-8a	163	6.21	3386.5	0.035	6.22	52.9	6.95	2.81	0.82	1.24	7.02	0.00
C-14-8b	163	6.23	3386.9	0.036	6.25	27.5	7.35	2.88	0.89	1.58	5.57	0.00
C-14-8c	163	6.18	3316.2	0.043	6.20	10.9	6.93	2.85	0.87	1.20	7.21	0.00
C-14-8.avg	163		3363.2			0.0	7.08	2.85	0.86	1.34	6.60	0.00
C-14-9sp	164	6.26	3328.1	0.041	6.29	48.4	7.00	2.90	0.80	1.24	7.43	0.00
C-14-10sp	187	6.21	6920.5	0.040	6.23	884.2	8.37	3.14	1.05	1.36	7.73	2.07
C-14-11sp	210.5	6.21	7061.0	0.033	6.23	920.2	9.47	3.46	1.30	1.34	10.93	4.24
C-14-12sp	234.5	6.29	3343.8	0.030	6.30	2.5	10.09	4.22	1.39	1.60	12.91	0.00
C-14-13sp	263.5	6.14	3489.8	0.033	6.16	3.7	12.55	4.03	1.42	1.20	17.15	0.00
C-14-14sp	305.5	6.03	3774.5	0.033	6.05	52.3	14.75	4.66	1.69	1.23	20.88	0.00

Table A-2
Cycling Experiment C-14 (Hydrolyzed Samples)
Solvent: 7 m MDEA, Ldg = 0.1 moles CO_2/mole alkalinity
Amendments: 0.4 mM Fe/0.1 mM Cr/0.05 mM Ni; 98 % Air/2 % CO_2
Conditions: 55 °C/90 °C
Conducted: March/April 2010

		Amine Concentration					Heat Stable Salts Concentrations				Amino Acids	
Sample No.	Degradation Time (hr)	MDEA (Tit) (m)	MDEA (Cations) (mM)	α_{act} (moles CO_2/mole alk)	Corrected (m)	DEA (mM)	Formate (mM)	Glycolate (mM)	Oxalate (mM)	Sulfate (mM)	Bicine (mM)	Glycine (mM)
C-14-0+NaOH	0	6.54	3571.8	0.104	6.55	0.0	1.3	0.0	0.8	1.8	0.0	0.0
C-14-1+NaOH	3	6.55	3712.2	0.103	6.55	0.0	1.4	0.1	0.8	1.8	0.0	0.0
C-14-2a+NaOH	19	6.53	3738.5	0.092	6.53	0.0	1.5	0.3	0.6	1.8	0.0	0.0
C-14-2b+NaOH	19	6.53	3697.5	0.095	6.53	0.0	1.5	0.3	0.6	1.7	0.0	0.0
C-14-2c+NaOH	19	6.57	3861.8	0.090	6.57	0.0	1.5	0.2	0.6	1.8	0.0	0.0
C-14-2.avg	19		3765.9			0.0	1.5	0.3	0.6	1.8	0.0	0.0
C-14-3+NaOH	42.5	6.51	3838.5	0.076	6.52	0.0	1.9	0.6	0.5	1.7	0.0	0.0
C-14-4+NaOH	66.5	8.64	2036.6	0.072	8.62	0.0	3.1	1.2	0.8	1.9	1.4	0.0
C-14-5+NaOH	91	6.40	3815.4	0.049	6.42	0.0	5.2	1.9	0.7	1.6	1.8	0.0
C-14-6+NaOH	121.5	6.40	3665.6	0.036	6.42	0.0	7.5	2.4	0.9	1.7	4.2	0.0
C-14-7+NaOH	143.5	6.35	3590.0	0.043	6.37	0.0	8.7	2.6	1.0	1.7	5.9	0.0
C-14-8a+NaOH	163	6.21	3791.0	0.035	6.22	0.0	9.8	2.9	1.5	1.8	7.8	0.0
C-14-8b+NaOH	163	6.23	3897.5	0.036	6.25	0.0	10.0	2.9	1.3	2.0	7.6	0.0
C-14-8c+NaOH	163	6.18	12036.6	0.043	6.20	130.1	9.8	3.1	1.2	2.0	7.4	0.0
C-14-8.avg	163		6575.0			0.0	9.9	3.0	1.3	1.9	7.6	0.0
C-14-9sp+NaOH	164	6.26	18034.1	0.041	6.29	201.4	11.4	3.1	1.1	2.2	7.8	5.6
C-14-10sp+NaOH	187	6.21	12189.4	0.040	6.23	159.0	13.0	3.4	1.3	2.1	10.1	5.9
C-14-11sp+NaOH	210.5	6.21	5155.4	0.033	6.23	60.8	12.8	3.3	1.6	2.0	11.9	0.0
C-14-12sp+NaOH	234.5	6.29	5225.2	0.030	6.30	67.7	14.6	3.9	1.5	2.1	13.7	0.0
C-14-13sp+NaOH	263.5	6.14	4489.1	0.033	6.16	0.0	17.6	4.3	1.9	2.0	17.2	0.0
C-14-14sp+NaOH	305.5	6.03	4095.2	0.033	6.05	63.7	18.3	4.4	2.0	2.2	21.6	0.0

Table A-3
Cycling Experiment C-15
Solvent: 7 m MDEA, Ldg = 0.1 moles CO_2/mole alkalinity
Amendments: 0.4 mM Fe/0.1 mM Cr/0.05 mM Ni; 100 mM Inh A; 98 % O_2/2 % CO_2
Conditions: 55 °C/90 °C
Conducted: April 2010

		Amine Concentration					Heat Stable Salts Concentrations				Amino Acids	
Sample No.	Degradation Time (hr)	MDEA (Tit) (m)	MDEA (Cations) (mM)	α_{act} (moles CO_2/mole alk)	Corrected (m)	DEA (mM)	Formate (mM)	Glycolate (mM)	Oxalate (mM)	Sulfate (mM)	Bicine (mM)	Glycine (mM)
C-15-0	0	6.31	3552.9	0.1	6.32	0.00	0.23	0.08	0.21	1.28	0.00	0.00
C-15-1	2	6.22	3475.9	0.098	6.23	0.00	0.64	0.11	0.33	1.50	0.00	0.00
C-15-2	18	6.21	3403.5	0.08	6.22	0.00	0.95	0.50	0.22	1.26	0.49	0.00
C-15-3	46.5	6.02	3446.1	0.07	6.03	0.00	3.28	1.75	0.36	1.15	6.15	0.00
C-15-4	66.5	5.86	3408.6	0.065	5.88	0.00	6.14	2.91	0.89	1.47	8.39	0.00
C-15-5	117.5	5.65	3378.7	0.056	5.66	0.00	15.12	5.32	1.64	1.46	23.20	0.19
C-15-6	137.5	5.56	3114.5	0.063	5.57	0.00	18.32	5.49	2.22	1.41	48.46	3.49
C-15-7	163.5	5.43	3118.1	0.041	5.44	0.00	25.09	6.87	3.11	1.38	42.29	0.49

Table A-4
Cycling Experiment C-15 (Hydrolyzed Samples)
Solvent: 7 m MDEA, Ldg = 0.1 moles CO_2/mole alkalinity
Amendments: 0.4 mM Fe/0.1 mM Cr/0.05 mM Ni; 100 mM Inh A; 98 % O_2/2 % CO_2
Conditions: 55 °C/90 °C
Conducted: April 2010

		Amine Concentration					Heat Stable Salts Concentrations				Amino Acids	
Sample No.	Degradation Time (hr)	MDEA (Tit) (m)	MDEA (Cations) (mM)	α_{act} (moles CO_2/mole alk)	Corrected (m)	DEA (mM)	Formate (mM)	Glycolate (mM)	Oxalate (mM)	Sulfate (mM)	Bicine (mM)	Glycine (mM)
C-15-0+NaOH	0	6.31	2862.7	0.1	6.32	0.00	0.00	0.00	0.35	1.82	0.00	0.00
C-15-1+NaOH	2	6.22	2699.2	0.098	6.23	0.00	2.60	0.35	0.33	1.86	0.00	0.00
C-15-2+NaOH	18	6.21	2583.7	0.08	6.22	0.00	3.14	0.54	0.87	2.15	0.00	0.00
C-15-3+NaOH	46.5	6.02	5954.0	0.07	6.03	0.00	6.89	2.10	0.72	1.86	4.88	0.42
C-15-4+NaOH	66.5	5.86	5647.7	0.065	5.88	0.00	10.18	3.17	1.57	2.11	8.57	0.00
C-15-5+NaOH	117.5	5.65	5735.8	0.056	5.66	0.00	24.11	5.69	3.41	2.06	31.42	2.09
C-15-6+NaOH	137.5	5.56	5021.7	0.063	5.57	0.00	32.55	6.57	4.63	2.32	40.32	2.22
C-15-7+NaOH	163.5	5.43	5585.6	0.041	5.44	0.00	36.65	7.44	6.15	2.28	55.23	3.25

Table A-5
Cycling Experiment C-16
Solvent: 8 m PZ, Ldg = 0.3 moles CO_2/mole alkalinity
Amendments: 0.4 mM Fe/0.1 mM Cr/0.05 mM Ni; 98 % O_2/2 % CO_2
Conditions: 55 °C/120 °C
Conducted: April/May 2010

		Amine Concentration					Heat Stable Salts Concentrations				Amino Acids	
Sample No.	Degradation Time (hr)	PZ (Tit) (m)	PZ (Cations) (mM)	α_{act} (moles CO_2/mole alk)	Corrected (m)	EDA (mM)	Formate (mM)	Glycolate (mM)	Oxalate (mM)	Sulfate (mM)	Bicine (mM)	Glycine (mM)
C-16-0	0	7.59	4013.3	0.316	7.58	0.0	0.10	0.00	0.00	1.03	0.00	0.00
C-16-0B	0	7.66	4056.4	0.318	7.70	0.0	0.09	0.00	0.00	0.31	0.00	0.00
C-16-1	4.5	7.52	4043.1	0.329	7.57	0.0	0.21	0.02	0.00	1.01	0.00	0.00
C-16-2	21	7.39	3981.2	0.319	7.46	0.0	0.89	0.15	0.01	0.97	0.00	0.15
C-16-3	48.5	7.35	3907.2	0.321	7.43	7.0	2.23	0.31	0.04	1.00	0.00	0.58
C-16-4	70.5	7.16	4276.5	0.317	7.25	13.3	3.46	0.33	0.08	1.03	0.00	1.12
C-16-5	93	7.03	3889.8	0.304	7.12	16.7	4.66	0.35	0.11	0.95	0.00	1.50
C-16-6	118	6.93	4045.2	0.296	7.03	25.7	6.35	0.41	0.21	0.93	0.00	1.82
C-16-7	141	6.89	3727.3	0.301	7.00	25.0	7.02	0.47	0.23	0.90	0.00	2.05
C-16-8	190	6.83	3781.5	0.296	6.94	33.8	8.64	0.53	0.40	0.93	0.00	2.96
C-16-9	242	6.37	3904.8	0.295	6.52	37.3	11.43	0.53	0.73	1.06	0.94	3.59
C-16-10	288.5	6.50	3650.3	0.289	6.63	52.2	13.07	0.62	1.04	0.95	1.35	3.88
C-16-11	334.5	6.47	3666.0	0.285	6.61	59.5	14.79	0.49	1.58	0.93	1.70	4.45
C-16-12	358.5	6.38	3580.9	0.286	6.52	53.9	16.40	0.79	1.92	0.94	1.82	4.01

Table A-6
Cycling Experiment C-16 (Hydrolyzed Samples)
Solvent: 8 m PZ, Ldg = 0.3 moles CO_2/mole alkalinity
Amendments: 0.4 mM Fe/0.1 mM Cr/0.05 mM Ni; 98 % O_2/2 % CO_2
Conditions: 55 °C/120 °C
Conducted: April/May 2010

		Amine Concentration					Heat Stable Salts Concentrations				Amino Acids	
Sample No.	Degradation Time (hr)	PZ (Tit) (m)	PZ (Cations) (mM)	α_{act} (moles CO_2/mole alk)	Corrected (m)	EDA (mM)	Formate (mM)	Glycolate (mM)	Oxalate (mM)	Sulfate (mM)	Bicine (mM)	Glycine (mM)
C-16-0+NaOH	0	7.59	4345.3	0.316	7.58	0.0	0.46	0.00	0.01	0.53	0.00	0.00
C-16-0B+NaOH	0	7.66	4194.7	0.318	7.70	0.0	0.48	0.00	0.02	1.40	0.00	0.00
C-16-1+NaOH	4.5	7.52	4405.6	0.329	7.57	0.0	0.93	0.48	0.01	1.20	0.00	0.00
C-16-2+NaOH	21	7.39	4558.1	0.319	7.46	0.0	2.91	0.16	0.06	1.22	0.00	0.00
C-16-3+NaOH	48.5	7.35	4286.6	0.321	7.43	0.0	6.99	0.20	0.13	1.23	0.00	0.84
C-16-4+NaOH	70.5	7.16	3130.9	0.317	7.25	0.0	8.23	0.18	0.27	1.75	0.00	1.21
C-16-5+NaOH	93	7.03	4180.9	0.304	7.12	0.0	12.69	0.30	0.30	1.20	0.00	1.97
C-16-6+NaOH	118	6.93	4019.9	0.296	7.03	0.0	17.03	0.35	0.44	1.29	0.00	2.75
C-16-7+NaOH	141	6.89	4007.6	0.301	7.00	0.0	18.15	0.30	0.51	1.17	0.85	3.12
C-16-8+NaOH	190	6.83	4220.5	0.296	6.94	25.2	22.57	0.32	0.77	1.18	0.98	3.94
C-16-9+NaOH	242	6.37	3995.5	0.295	6.52	40.4	29.55	0.00	1.34	1.20	1.22	5.12
C-16-10+NaOH	288.5	6.50	3873.5	0.289	6.63	43.6	35.29	0.00	1.94	1.09	1.54	5.60
C-16-11+NaOH	334.5	6.47	3930.0	0.285	6.61	65.8	42.06	0.00	2.67	1.16	1.99	5.94
C-16-12+NaOH	358.5	6.38	NM	0.286	6.52	NM	46.65	0.00	3.91	1.38	2.45	6.64

Table A-7
Cycling Experiment C-17
Solvent: 8 m PZ, Ldg = 0.3 moles CO_2/mole alkalinity
Amendments: 0.4 mM Fe/0.1 mM Cr/0.05 mM Ni; 98 % O_2/2 % CO_2
Conditions: 55 °C/90 °C
Conducted: May/June 2010

		Amine Concentration					Heat Stable Salts Concentrations				Amino Acids	
Sample No.	Degradation Time (hr)	PZ (Tit) (m)	PZ (Cations) (mM)	α_{act} (moles CO_2/mole alk)	Corrected (m)	EDA (mM)	Formate (mM)	Glycolate (mM)	Oxalate (mM)	Sulfate (mM)	Bicine (mM)	Glycine (mM)
C-17-0	0	NM	3616.9	NM	NM	0.0	0.31	0.00	0.01	0.22	0.00	0.00
C-17-1	4	NM	3672.6	NM	NM	0.0	0.21	0.00	0.01	0.85	0.00	0.00
C-17-2	21.5	NM	3739.6	NM	NM	0.0	0.48	0.00	0.01	0.82	0.00	0.00
C-17-3	45	NM	3580.8	NM	NM	0.0	1.09	0.00	0.01	0.83	0.00	0.07
C-17-4	69	NM	3700.2	NM	NM	0.0	1.32	0.00	0.02	0.87	0.00	0.17
C-17-5	93	NM	3838.8	NM	NM	7.9	1.72	0.00	0.03	0.83	0.00	0.23
C-17-6	120	NM	3605.5	NM	NM	11.0	2.10	0.00	0.03	0.86	0.00	0.30
C-17-7	165	NM	3697.4	NM	NM	10.6	2.69	0.00	0.05	0.79	0.00	0.47
C-17-8	216	NM	3530.9	NM	NM	13.9	3.20	0.00	0.07	0.88	0.00	0.51
C-17-9	261	NM	3661.6	NM	NM	18.7	3.53	0.00	0.10	0.84	0.00	0.54
C-17-10	313	NM	3634.3	NM	NM	23.2	4.43	0.00	0.12	1.31	0.00	0.73
C-17-11	358	NM	3666.4	NM	NM	21.0	5.07	0.00	0.16	0.95	0.00	0.80
C-17-12	413	NM	3622.9	NM	NM	30.5	5.72	0.00	0.20	1.08	0.00	1.13
C-17-13	429	NM	3644.2	NM	NM	32.9	6.38	0.00	0.21	1.84	0.00	1.22

Table A-8
Cycling Experiment C-17 (Hydrolyzed Samples)
Solvent: 8 m PZ, Ldg = 0.3 moles CO_2/mole alkalinity
Amendments: 0.4 mM Fe/0.1 mM Cr/0.05 mM Ni; 98 % O_2/2 % CO_2
Conditions: 55 °C/90 °C
Conducted: May/June 2010

		Amine Concentration					Heat Stable Salts Concentrations				Amino Acids	
Sample No.	Degradation Time (hr)	PZ (Tit) (m)	PZ (Cations) (mM)	α_{act} (moles CO_2/mole alk)	Corrected (m)	EDA (mM)	Formate (mM)	Glycolate (mM)	Oxalate (mM)	Sulfate (mM)	Bicine (mM)	Glycine (mM)
C-17-0 + NaOH	0	NM	4514.8	NM	NM	0.0	0.70	0.25	0.00	0.67	0.00	0.00
C-17-1 + NaOH	4	NM	4561.9	NM	NM	0.0	0.83	0.46	0.00	1.20	0.00	0.00
C-17-2 + NaOH	21.5	NM	4241.4	NM	NM	22.8	1.19	0.34	0.03	0.98	0.00	0.00
C-17-3 + NaOH	45	NM	4466.3	NM	NM	0.0	3.19	0.27	0.06	1.38	0.00	0.00
C-17-4 + NaOH	69	NM	4429.3	NM	NM	0.0	3.82	0.17	0.13	1.07	0.00	0.19
C-17-5 + NaOH	93	NM	4416.3	NM	NM	0.0	5.74	0.21	0.13	2.26	0.00	0.38
C-17-6 + NaOH	120	NM	4354.0	NM	NM	0.0	6.92	0.17	0.20	1.08	0.00	0.66
C-17-7 + NaOH	165	NM	4351.2	NM	NM	0.0	6.96	0.18	0.19	1.08	0.00	0.72
C-17-8 + NaOH	216	NM	4091.7	NM	NM	0.0	9.01	0.17	0.20	1.13	0.00	0.89
C-17-9 + NaOH	261	NM	4098.8	NM	NM	10.3	10.54	0.22	0.31	1.35	0.00	1.05
C-17-10 + NaOH	313	NM	4348.5	NM	NM	15.7	12.60	0.23	0.37	1.40	0.00	1.31
C-17-11 + NaOH	358	NM	4296.4	NM	NM	24.1	14.91	0.30	0.46	1.08	0.00	1.53
C-17-12 + NaOH	413	NM	4100.2	NM	NM	30.8	17.17	0.19	0.43	2.37	0.00	1.84
C-17-13 + NaOH	429	NM	4140.3	NM	NM	21.4	0.00	0.25	0.61	1.14	0.00	1.97

Table A-9
Cycling Experiment C-15
Solvent: 7 m MDEA, Ldg = 0.1 moles CO_2/mole alkalinity
Amendments: 0.4 mM Fe/0.1 mM Cr/0.05 mM Ni; 100 mM Inh A; 98 % O_2/2 % CO_2
Conditions: 55 °C/90 °C
Conducted: June 2010

		Amine Concentration					Heat Stable Salts Concentrations				Amino Acids	
Sample No.	Degradation Time (hr)	MDEA (Tit) (m)	MDEA (Cations) (mM)	α_{act} (moles CO_2/mole alk)	Corrected (m)	DEA (mM)	Formate (mM)	Glycolate (mM)	Oxalate (mM)	Sulfate (mM)	Bicine (mM)	Glycine (mM)
C-18-0	0	6.30	3002.1	NM	6.30	0.00	0.35	0.10	0.00	0.63	0.00	0.00
C-18-1	20	6.50	3515.8	NM	6.50	16.62	2.36	0.99	0.02	0.72	0.87	0.45
C-18-2	45	6.23	3274.4	NM	6.23	37.36	4.08	2.44	0.05	0.74	2.72	0.58
C-18-3	65.5	6.56	3559.0	NM	6.56	21.10	5.47	3.31	0.09	0.57	4.09	0.77
C-18-4	95.5	6.40	3373.8	NM	6.40	23.75	6.33	4.32	0.13	0.62	6.17	1.00
C-18-5	113.5	6.17	3801.2	NM	6.17	39.70	7.12	4.96	0.16	0.57	7.69	1.05
C-18-6	143.5	6.13	3348.5	NM	6.13	80.55	8.54	6.12	0.22	0.58	10.37	1.33
C-18-7	161	5.99	3456.1	NM	5.99	NM	9.25	6.57	0.26	0.71	11.93	1.49

Table A-10
Cycling Experiment C-15 (Hydrolyzed Samples)
Solvent: 7 m MDEA, Ldg = 0.1 moles CO_2/mole alkalinity
Amendments: 0.4 mM Fe/0.1 mM Cr/0.05 mM Ni; 100 mM Inh A; 98 % O_2/2 % CO_2
Conditions: 55 °C/90 °C
Conducted: June 2010

		Amine Concentration					Heat Stable Salts Concentrations				Amino Acids	
Sample No.	Degradation Time (hr)	MDEA (Tit) (m)	MDEA (Cations) (mM)	α_{act} (moles CO_2/mole alk)	Corrected (m)	DEA (mM)	Formate (mM)	Glycolate (mM)	Oxalate (mM)	Sulfate (mM)	Bicine (mM)	Glycine (mM)
C-18-0+NaOH	0	6.30	3474.3	NM	6.30	0.00	2.02	0.58	0.01	1.07	0.00	0.00
C-18-1+NaOH	20	6.50	3578.9	NM	6.50	7.42	3.16	1.67	0.03	1.07	1.21	0.77
C-18-2+NaOH	45	6.23	3890.8	NM	6.23	31.62	5.38	3.25	0.08	1.05	2.56	1.02
C-18-3+NaOH	65.5	6.56	3907.7	NM	6.56	31.40	6.38	4.01	0.12	1.06	3.82	1.10
C-18-4+NaOH	95.5	6.40	3949.7	NM	6.40	29.06	7.94	4.95	0.17	1.18	5.94	1.31
C-18-5+NaOH	113.5	6.17	5041.0	NM	6.17	53.24	9.19	5.68	0.21	1.25	7.63	1.40
C-18-6+NaOH	143.5	6.13	3272.1	NM	6.13	62.84	10.38	6.67	0.27	1.10	10.52	1.75
C-18-7+NaOH	161	5.99	3485.4	NM	5.99	93.17	10.83	6.83	0.27	1.06	11.94	1.92

Thermal Degradation and Oxidation of Concentrated Piperazine (PZ)

Quarterly Report for April 1 – June 30, 2010

by Stephanie A. Freeman

Supported by the Luminant Carbon Management Program

and the

Industrial Associates Program for CO_2 Capture by Aqueous Absorption

Department of Chemical Engineering

The University of Texas at Austin

July 1, 2010

Abstract

A solution of 8 m PZ containing 0.1 mole CO_2 per mole alkalinity was degraded at 175 °C for 15 weeks to further explore the effect of CO_2 concentration. The solution lost 45% of the original amine compared to 5, 71, and 73% for the unloaded, 0.3 loading, and 0.4 loading, respectively, at the same conditions. The concentration of CO_2 has direct impact on the rate of PZ degradation.

The production of total formate, the main degradation product, ranged from 16 mmol/kg in the unloaded solution to 251, 851, and 692 mmol/kg in the 0.1 loading, 0.3 loading, and 0.4 loading experiments.

Using an estimated speciation of 8 m PZ at 175 °C, it was determined that the production of formate was closely associated with the mole fraction of $PZCOO^-$, indicating this species is likely involved in the initial stages of the mechanism that produces formate and formyl amides such as N-Formyl PZ. The degradation rate of PZ was closely related to the free PZ and H^+PZ mole fractions.

Glass cuvettes were used to eliminate contact between the amine solution and the interior surfaces of the stainless steel thermal cylinders. The degradation rate of 8 m PZ with 0.3 mole CO_2 per mole alkalinity was slightly reduced, losing only 66% of the initial amine compared to 71% in the traditional experimental setup after 15 weeks at 175 °C. The production of total formate was reduced from 708 mmol/kg to 538 mmol/kg in the cuvette experiment. No iron, nickel, or chromium was found in the solution.

Acidified 8 m PZ (containing only free PZ and H^+PZ) degrades slowly, losing only 34% of the initial amine compared to 71% in the 8 m PZ with 0.3 mole CO_2 per mole alkalinity over 15 weeks at 175 °C. The acidified PZ generated ethylenediamine (EDA) as the only major degradation product. In CO_2 loaded PZ solutions, formyl amides, formate, and EDA are all usually found to be major products. The degradation of acidified PZ indicates a separate mechanism creates EDA through H^+PZ while CO_2-containing species are responsible for participating in the mechanism that creates formate and formyl amides.

PZ oxidation does increase with temperature, as expected, as evidenced by the increased production of degradation products. Total formate production increased from 4 to 19 mmol/kg over the course of nearly 600 hours at 55 and 70 °C. As with previous oxidation work, PZ loss was difficult to assess due to fluctuations in the data most likely caused by changes in the overall water balance.

Introduction

Concentrated aqueous piperazine (PZ) is being investigated as a possible alternative to 30 wt % (or 7 m) MEA in absorber/stripper systems to remove CO_2 from coal-fired power plant flue gas (Freeman et al., 2009). PZ solutions are subject to oxidation and thermal degradation, as previously shown at 5 and 8 m PZ (see previous quarterly reports). The kinetics of CO_2 absorption are faster in concentrated PZ (Cullinane and Rochelle, 2006; Dugas and Rochelle, 2009). The capacity of concentrated PZ is greater than that of MEA, while the heat of absorption and volatilities are comparable (Freeman et al., 2009).

This quarter was focused on continuing thermal degradation and oxidation experiments. Two experiments (TE22 and TE23) that concluded last quarter but were not analyzed in time to make the previous quarterly report are discussed here. Three experiments on PZ concentration and CO_2 loading in 8 m PZ (TE32, TE33, TE34) concluded this quarter, but only the results for TE34 were analyzed in time for this report. Two experiments (TE10 and TE11) continued through the quarter with periodic sampling. Seven new thermal experiments (TE35 through TE41) were started this quarter and will finish in the third and fourth quarters of 2010 and first quarter of 2011. The third experiment in the newly redesigned oxidation reactor was completed and the results are reported here (OE19). Mass spectrometry continued on experimental samples in an effort to identify new degradation products.

Analytical Methods

Total Inorganic Carbon Analysis (TIC)

Quantification of CO_2 loading was performed using a total inorganic carbon analyzer. In this method, a sample is acidified with 30 wt % H_3PO_4 to release the CO_2 present in solution (Hilliard, 2008). The CO_2 is carried in the nitrogen carrier gas stream to the detector. PicoLog software was used to record the peaks produced from each sample. A calibration curve was prepared at the end of each analysis using a TIC standard mixture of K_2CO_3 and $KHCO_3$. The TIC method quantifies the CO_2, CO_3^{-2}, and HCO_3^- present in solution. These species are in equilibrium in the series of reactions shown below in Equation 1.

$$CO_3^{2-} + 2H^+ \leftrightarrow HCO_3^- + H^+ \leftrightarrow H_2CO_3 \leftrightarrow CO_2 + H_2O \quad (1)$$

Acidification of the sample shifts the equilibrium toward CO_2 which bubbles out of solution and is detected in the analyzer.

Acid pH Titration

Titration with 0.2 N H_2SO_4 was used to determine the concentration of amines in experimental samples. The automated Titrando apparatus (Metrohm AG, Herisau, Switzerland) was used for this method. A known mass of sample was diluted with water and the autotitration method was then used. The Titrando titrates the sample with acid while monitoring the pH. The equivalence points are recorded. The equivalence point around a pH of 3.9 corresponds to basic amine species in solution (Hilliard, 2008). The test is not sensitive to the type of amine, so if PZ has

degraded to ethylenediamine (EDA), the titration test will detect the sum of contributions from the species.

Anion IC

The anion IC was used to determine the concentration of glycolate, acetate, formate, chloride, nitrite, sulfate, oxalate, and nitrate in experimental samples. A Dionex ICS-3000 instrument with AS15 IonPac column, 4-mm Anionic Self-Regenerating Suppressor (ASRS), carbonate removal device (CRD), and carbonate removal from eluent generation was used as previously described by Sexton using a linear KOH eluent concentration (Sexton, 2008). No major modifications have been made to the method in this quarter.

Cation IC

The cation IC was used to determine the concentration of PZ and ethylenediamine (EDA) in experimental samples. A Dionex ICS-2500 instrument with CS17 IonPac column with 4-mm Cationic Self-Regenerating Suppressor (CSRS) was used as previously described by Sexton with a linear increase of methanesulfonic acid (MSA) concentration in the eluent (Sexton, 2008). No major modifications have been made to the method in this quarter.

NaOH Treatment for Amides

An analytical test for the formation of amides was developed by Sexton and has been included in the results shown here. Experimental samples were treated with 5 N NaOH (in equal gravimetric amounts) and allowed to sit overnight. The anion IC analytical method was then used to quantify increases in the concentrations of analytes as compared to the original samples (Sexton, 2008). In most cases, the main increases were in the production of formate and oxalate following NaOH treatment.

The addition of strong base reverses the amide formation reaction that has occurred during the experiment. As an example, the formation of N-formylPZ (FPZ) is shown in Equation 2 below:

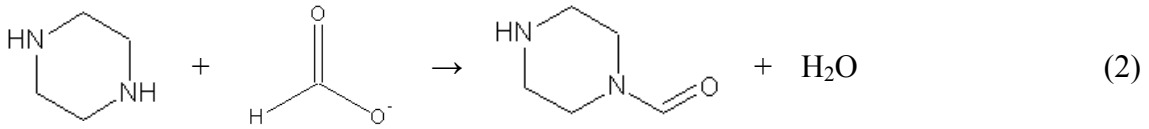

(2)

(PZ) (Formate) (N-formylPZ)

The addition of NaOH hydrolyzes the bond between the amine group and the carbon of the formyl group to reverse the reaction. In this way, the free formate created from reversing this reaction can be used to identify the formate bound as N-formylPZ. The same process can be used to identify the oxalate amine of PZ.

Inductively-Coupled Plasma Optical Emission Spectrometry (ICP-OES)

The concentration of multiple elements was measured using a Varian 710-ES Axial Inductively-Coupled Plasma Optical Emission Spectrometer (Varian Inc., Palo Alto, CA). The ICP-OES is effective for measuring the concentration of multiple analytes (heavy metals and other elements) simultaneously in a single dilution. The system is controlled through ICP Expert II Software. Samples are prepared by first making the desired dilution (10 – 1000X) and then adding 1% concentrated HNO_3. Each sample needs to be approximately 10 mL in volume and created in a plastic vial. An autosampler holds all the standards and samples to be run and each is pumped to

the glass, concentric spray chamber, or nebulizer, where an argon stream nebulizes the sample and it is sent directly to the plasma flame. The molecules break down in the plasma into their atoms and lose electrons, giving off optical wavelengths characteristic to each element. The emitted wavelengths are then sent to the solid state CCD detector. The plasma is created by electromagnetic induction, or time-varying magnetic fields, and creates energy that breaks down argon, the carrier or rarefield gas. The plasma flame is stable and maintained at 7000 K.

For each element of interest, the four wavelengths with the highest intensity of absorption are measured and one argon wavelength is used as a background measurement. A separate calibration curve is made for each wavelength and the final concentration reported for each element is the average of the calibrated concentration of all four wavelengths. ICP-OES allows for quick analysis of multiple metals in solution, which is especially useful for samples that corroded stainless steel (Fe, Cr, and Ni), or low gas flow experiments where multiple metals and tracers have been added (Fe, Cr, Ni, Cu, V, K, or Na).

Cation IC – Mass Spectrometry (MS)

Mass spectrometry (MS) with cation IC is used to help identify unknown peaks on cation IC chromatography or other unknown cations in solution. A Thermo Finnigan TSQ MS is attached to a Dionex ICS-2500 IC with an IonPac CS17 analytical column (4 x 250 mm), IonPac CG17 guard column (4 x 50 mm), Dionex AS40 autosampler, and 4-mm CSRS is used as described above. The main modification is that the suppressor does not run in regeneration mode, the outlet analyte stream is sent to the MS and an additional water stream is added into the suppressor using N_2 gas.

After separation on the cation IC column, the sample stream enters the MS, which uses electrospray ionization (ESI) to ionize the molecules in solution. The ions then enter the mass analyzer in the first quadrant of the MS, which sorts ions based on their mass-to-charge ratio (m/z) using an electric field. The standard conditions used are a range of 50–300 m/z. There is a 2.2 minute delay in the resolution of the cation IC chromatogram and the MS spectrum that is taken into account while analyzing data. Direct injections can also be performed to analyze samples without separation in the CS17 column. In this mode, more parameters can be controlled such as capillary temperature, sheath gas pressure, auxiliary gas pressure, and electrospray voltage. This is useful in tuning the instrument and performing CID on standard solutions.

Results and Discussion

Amide Reversal Qualification

The amide reversal was developed in our group by Sexton in order to quantify amides using anion IC (Sexton, 2008). The amide reversal was based on work by Koike and colleagues on analyzing diethanolamine (DEA) (Koike et al., 1987). The rate at which amides reverse has been under some debate within our group. Sexton developed his method primarily for use with degraded monoethanolamine (MEA) and N-formyl MEA is not readily available from chemical suppliers for purchase. N-formyl PZ, on the other hand, is readily available so a quantification of the time needed for full reversal can be performed.

A solution was created by spiking 8 m PZ α=0.3 with 100 mM of N-Formyl PZ (FPZ) (1-Piperazine-carboxaldehyde, Acros Organics, CAS 7755-92-2). The standard alkaline treatment

using 5 N NaOH was performed as described above. The time of the initial treatment was recorded for each sample. The NaOH treatment was then diluted 50X (to achieve 100X total dilution) at pre-prescribed time points and the time of dilution was recorded. It was assumed during the experiment that the dilution to 100X effectively quenched the amide reversal process. The treatment time discussed in this section is the time between the initial treatment with NaOH and the time of dilution to 100X.

The samples were analyzed using Anion IC and Cation IC to determine the concentration of formate and PZ released from the alkaline treatment of the FPZ. The PZ increase was difficult to quantify since I was looking for an increase of 100 mmol/kg above the background concentration of 4400 mmol/kg PZ. The formate concentration, however, was a great indicator of the completion of the amide reversal. The concentration of formate found in each sample was compared to the expected concentration based on the initial spike of formate. A percentage recovered was calculated as shown in Equation 3.

$$\%\ \text{Recovered} = \frac{[\text{Formate}]}{[\text{Formate}_{\text{expected}}]} \times 100 \qquad (3)$$

The experiment was first performed with a spike of 100 mmol/kg FPZ and then twice with a spike of 200 mmol/kg FPZ. The increase in the concentration of FPZ was intended to allow the PZ recovery to be observed. The percent formate recovered for each of the three experiments is plotted in Figure 1 below. Surprisingly, all three experiments showed a stable recovery of over 100% of the spiked FPZ. Each experiment ended up at between 111 and 115%. This was not expected, but repeatable. One explanation is that a portion of the molecules in the FPZ provided by Acros are dehydrated, yielding an average molecular weight that is slightly higher than the actual molecular weight of FPZ. If that were the case, each experiment would have been spiked with more FPZ than intended and more formate would have been recovered than expected. This possibility will be investigated in the next quarter by attempting to identify the purity of the FPZ based on the concentration of FPZ and the recovery of both formate and PZ.

Despite the unexpected recovery characteristics, the other objective of this experiment was to determine the time needed for full reaction of any amides in solution. It is clear from all three experiments that the maximum recovery is achieved within the first 5 hours. The standard procedure at this point is to allow NaOH treated samples to react overnight, and this appears to be sufficient for PZ-based amides. The next step in this analysis will be to spike degraded PZ with FPZ and perform the same experiment. It is very likely that the reversal will proceed more slowly in degraded solvent since there are more constituents and more types of molecules that may be reacting. Now that PZ is being cycled by Fred Closmann, larger quantities of degraded PZ are available for this experiment. The results of this planned experiment will be reported next quarter.

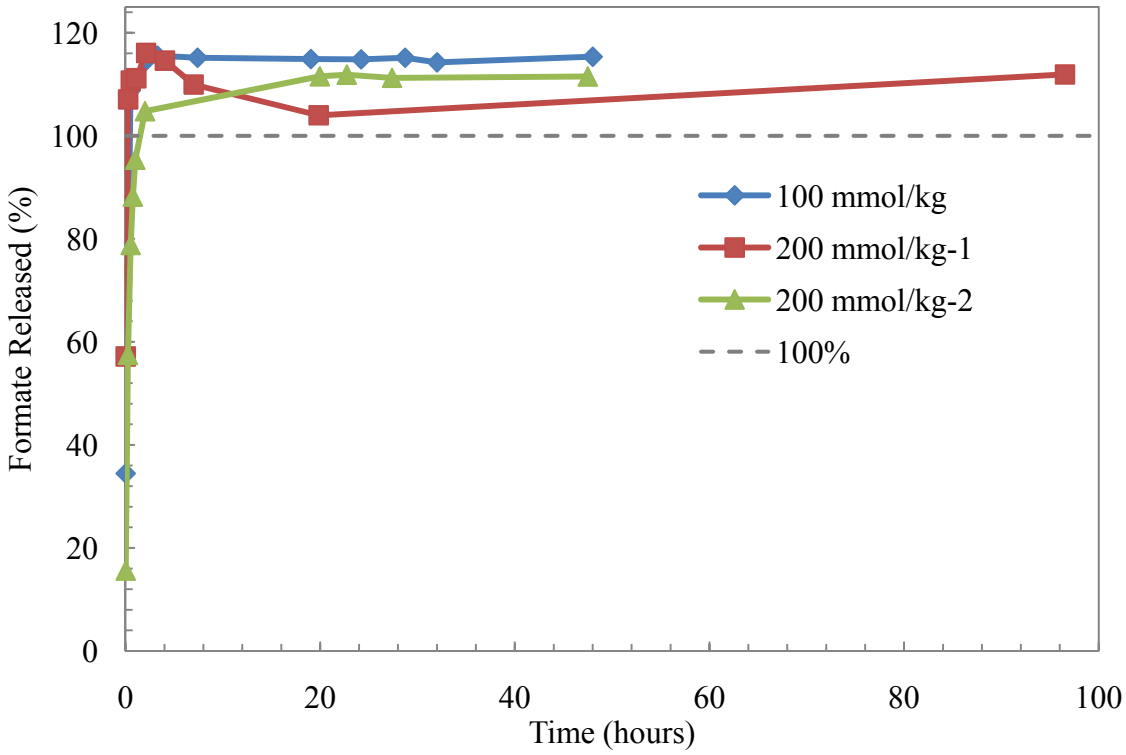

Figure 1: Formate Recovered During Alkaline Amide Reversal of FPZ

Thermal Degradation

Eight thermal degradation experiments concluded this quarter and the analytical results are discussed below for six of them. An experiment looking at the impact of H^+PZ on thermal degradation of PZ was concluded last quarter and is discussed in relation to CO_2 concentration effects (TE23). An experiment further investigating the effect of CO_2 concentration on thermal degradation is discussed in relation to previous data (TE34). The results of an experiment investigating the use of glass cuvettes to prevent the amine solution from contacting the internal metal surfaces of the thermal cylinders are also reported (TE22).

Thermal Degradation of Acidified 8 m PZ (TE23)

The contribution of the various PZ species in solution to the overall degradation of 8 m PZ is not clear. Numerous species are present in solution in the presence of CO_2 including free PZ, $PZCOO^-$, H^+PZ, H^+PZCOO^-, $PZ(COO^-)_2$, and other species at negligible concentrations. It has been shown previously that in the absence of CO_2, very little degradation occurs in concentrated PZ (Rochelle, 2010a). The addition of CO_2 to 8 m PZ produces CO_2-containing species ($PZCOO^-$, H^+PZCOO^-, and $PZ(COO^-)_2$) as well as protonated PZ (H^+PZ). In an attempt to isolate the effect of H^+PZ on the degradation pathway(s) of PZ, a PZ solution with H^+PZ, but without any CO_2 species was degraded. The reaction of CO_2 and PZ produces both $PZCOO^-$ and H^+PZ, so PZ was acidified with a sulfuric acid to produced only H^+PZ without $PZCOO^-$.

An 8 m PZ solution acidified with 0.3 mole H^+ per mole alkalinity was thermally degraded at 175 °C for 15 weeks in order to assess the contribution of H^+PZ to the overall degradation of PZ. The concentration profiles for PZ and the observed degradation products are shown below in Figure 2. Very low levels of formate, formyl amides, acetate, and acetyl amides were quantified

for this experiment while EDA was the dominant degradation product. As formate and total formate are the traditional markers for thermal degradation, the presence of EDA as the main degradation product appears to indicate a difference in the way that H^+PZ participates in the degradation process.

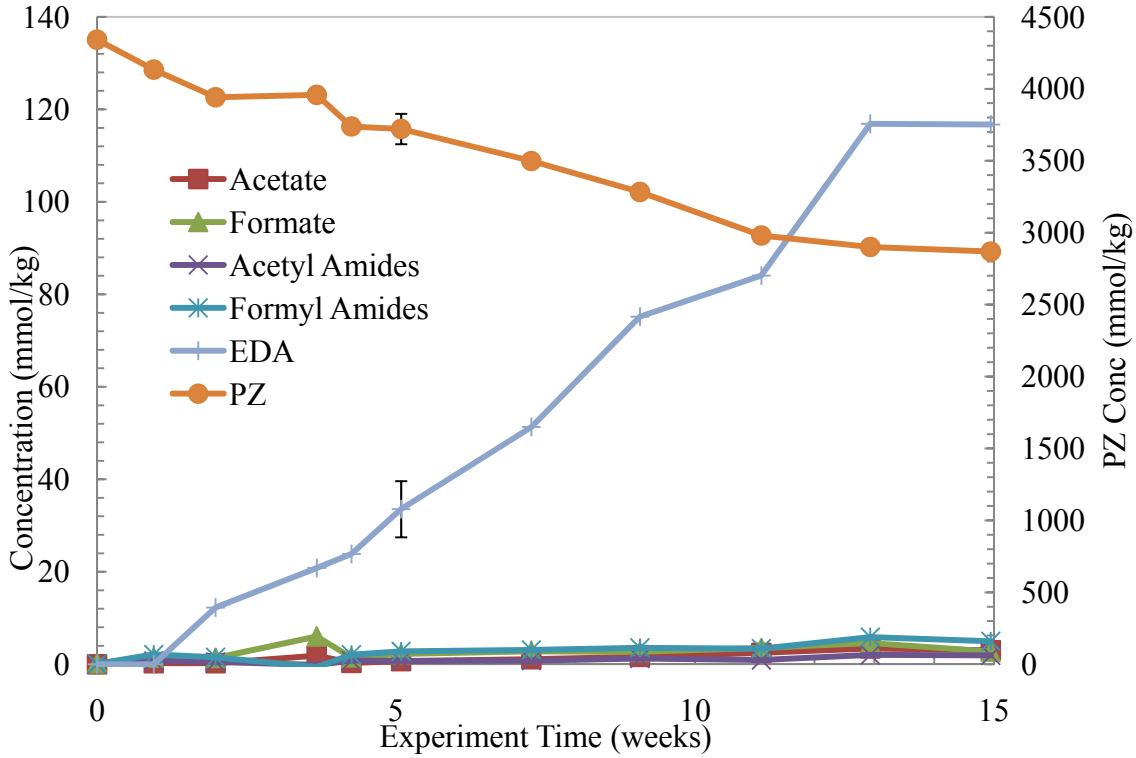

Figure 2: Concentration Profiles for Acidified 8 m PZ Degraded at 175 °C for 15 weeks

To further explore the differences in the behavior of this acidified experiment, the loss of PZ is compared in Figure 3 among this experiment, an unloaded experiment, and two traditional, loaded experiments. The loss of PZ in the acidified experiment lies between the unloaded and 0.3 loading experiments. H^+PZ does catalyze degradation of PZ without CO_2-containing species, but not quite as fast as when both protonated and carbamate species are present.

The production of total formate in these experiments is compared in Figure 4. The formate results are striking in that essentially no formate was produced in the H^+PZ experiment. This matches closely the unloaded experiment where negligible formate was produced as well. This observation suggests that the mechanism of H+PZ does not lead to the production of formate while it does produce significant amounts of EDA. This also provides more evidence for the hypothesis made previously that CO_2 is reduced directly to produce formate (Rochelle, 2010a). It still is not clear in which form the CO_2 resides when it is converted to formate. It could be in the form of free CO_2, $PZCOO^-$, H^+PZCOO^- when converted to formate. The presence of formyl amides also suggests the need to determine which is truly produced first, formate or formyl amides. It is possible that $PZCOO^-$ is reduced in place to yield N-Formyl PZ which is then converted readily to free formate. The true sequence of reactions is not clear, but the evidence from this acidified PZ experiment further suggests that formate is not directly formed from PZ (i.e., the carbon of formate does not come from the PZ backbone).

One experiment that can shed light on this mechanistic issue is the use of $^{13}CO_2$ in a loaded PZ solution. As discussed last quarter, a solution of 8 m PZ loaded with $^{13}CO_2$ will be degraded in the third quarter of 2010 and the NMR analysis of these samples should be able to determine if the formate produced comes from the CO_2 or the PZ.

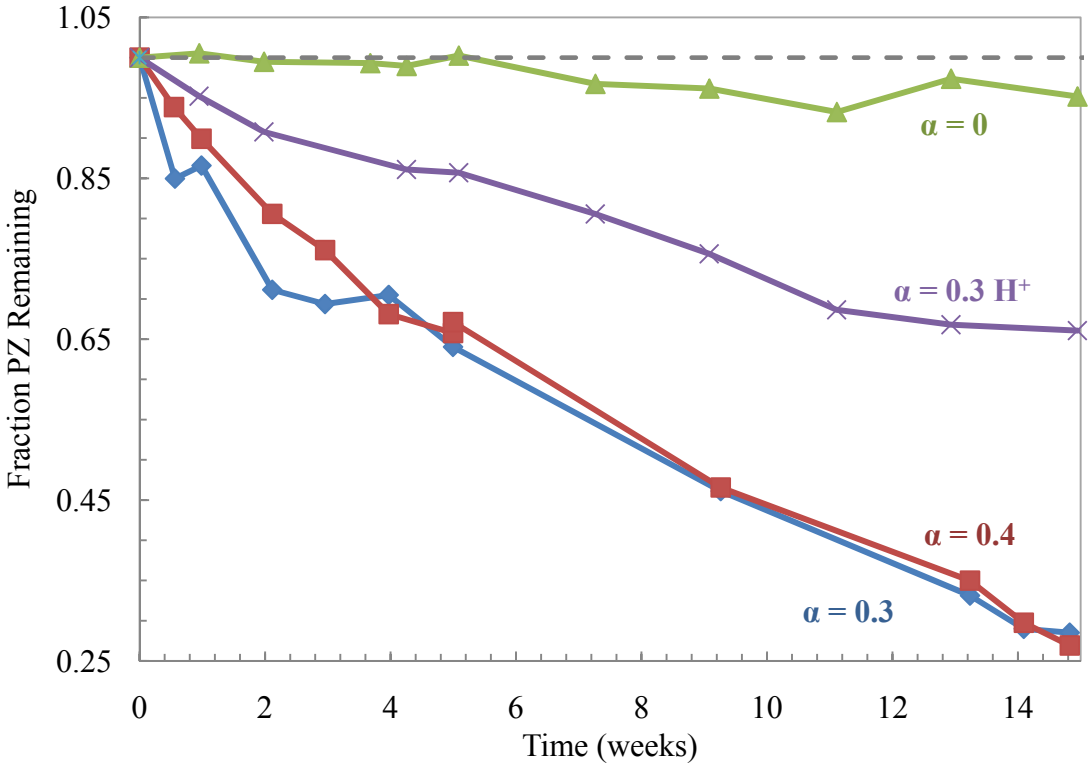

Figure 3: Comparison of PZ loss for Varying CO_2 Concentrations and Acidified PZ at 175 °C

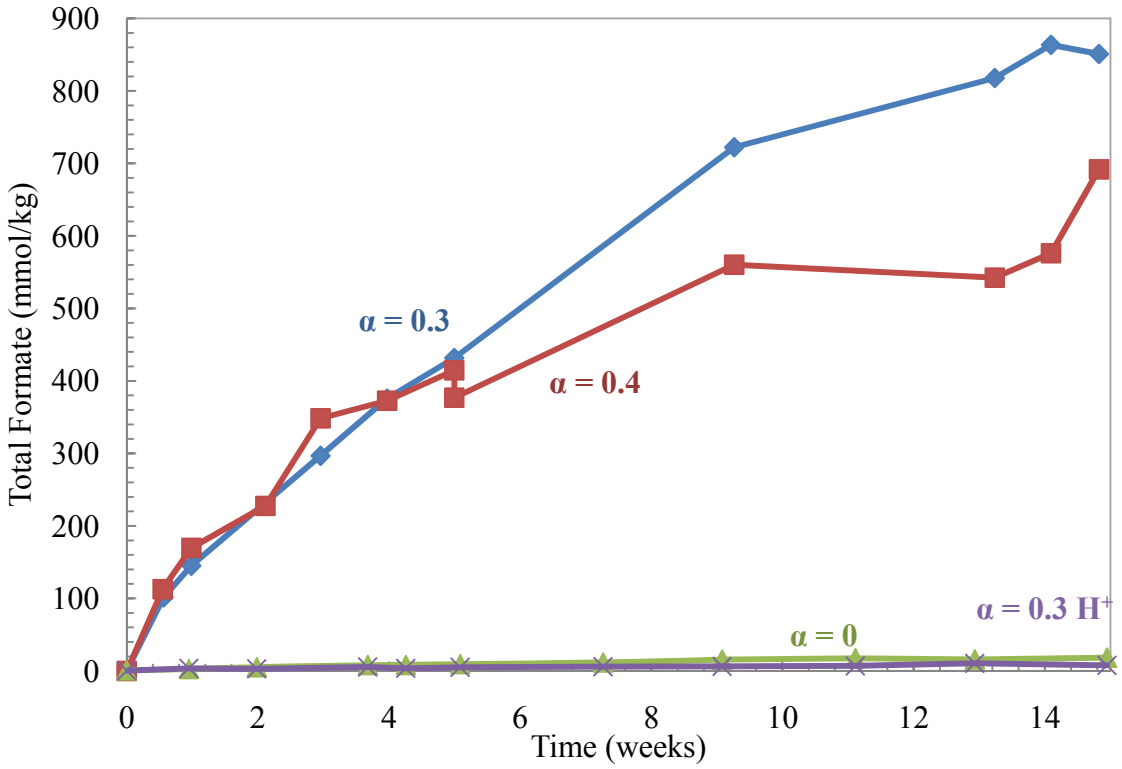

Figure 4: Comparison of Total Formate Production for Varying CO_2 Concentrations and Acidified PZ at 175 °C

Ideally, the complementary experiment could be completed where only CO_2 species are present without H^+PZ. Using potassium carbonate or potassium bicarbonate to create carbamate species poses a serious solubility problem in the presence of PZ. Only species at very low PZ concentration (less than 2 m PZ) could be conceived and it was decided that this concentration would not be able to provide directly comparable data.

Thermal Degradation of 8 m PZ with Low Loading (α = 0.1) (TE34)

Previous experiments have been conducted on the effect of CO_2 loading on the degradation of concentrated PZ (Rochelle, 2009; Rochelle, 2010b). The difference between a loading of 0.3 and 0.4 mole CO_2 per mole alkalinity was not clearly defined. It was determined that the speciation at these loadings may be too similar or have contrasting effects on degradation rates and the production rate of degradation products. Therefore, an experiment at a significantly lower loading, 0.1 mole CO_2 per mole alkalinity, was conducted. The samples from this experiment (TE34) were analyzed using the standard analytical techniques.

The concentration profiles for PZ and the degradation products are shown below in Figure 5. The primary degradation products quantified in this experiment were EDA, formyl amides, and formate, as with PZ degradation at other CO_2 concentrations. The concentrations of formyl amides and formate have similar concentration profiles as found previously with PZ degradation at higher CO_2 concentrations. The impact of these results is best understood in light of the rates of degradation in experiments with varying CO_2 concentrations.

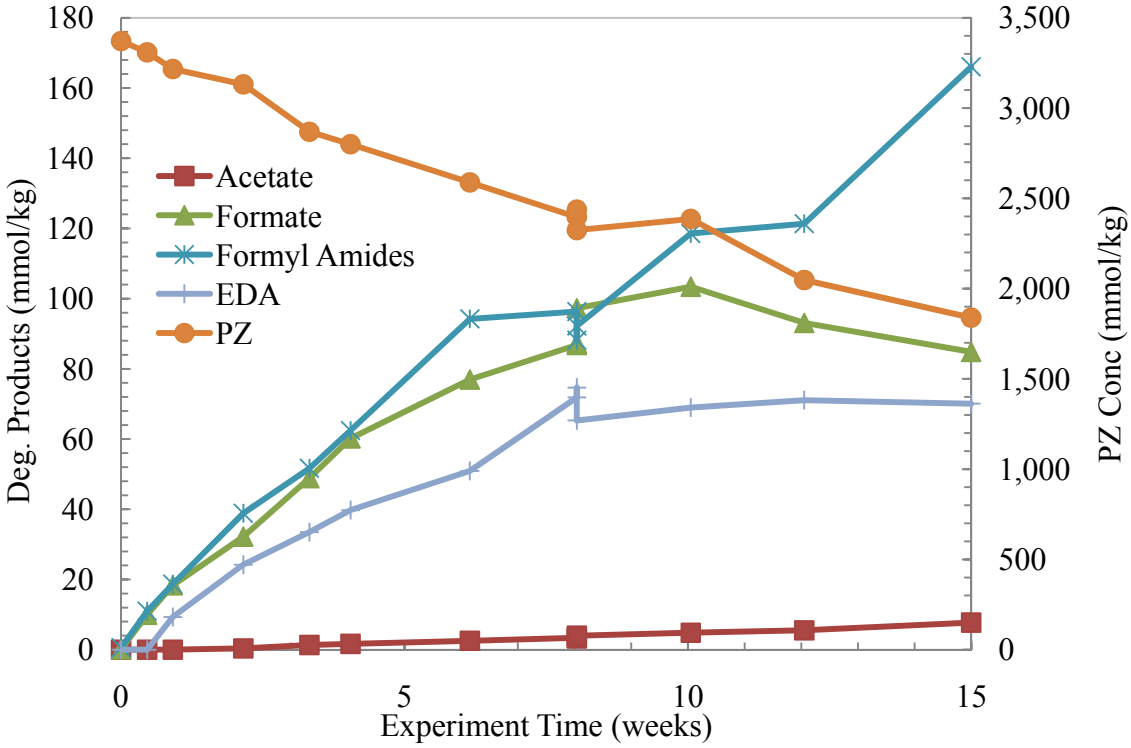

Figure 5: Concentration Profile for 8 m PZ, α = 0.1 at 175 °C for 15 weeks (TE34)

Effect of Loading on Thermal Degradation of PZ

With the completion of a thermal degradation experiment with low loading, the effect of CO_2 concentration on the thermal degradation of PZ can be further explored. As shown in the previous section, 8 m PZ with a loading of 0.1 mole CO_2 per mole alkalinity does demonstrate thermal degradation at 175 °C. Data for the degradation of 8 m PZ with 0, 0.3, and 0.4 moles CO_2 per mole alkalinity have been presented previously (Rochelle, 2010a; Rochelle, 2010b). A comparison of these new data with previous data provides further insight into the overall effect of CO_2 concentration.

The rate of PZ loss for thermal degradation experiments ranging from a loading of 0 to 0.4 moles CO_2 per mole alkalinity is compared in Figure 6. The rate of PZ loss for the experiment with 0.1 mole CO_2 per mole alkalinity fell between that of 0 and 0.4 loading, indicating that the degradation rate is dependent on CO_2 concentration. It was previously suggested that since the PZ loss rates for 0.3 and 0.4 loading were similar, it was just the presence of CO_2, not CO_2 concentration, which increased the rate of degradation over that of the unloaded solution. The concentration of total formate is compared in Figure 7. The production of total formate for the 0.1 loading experiment also fell between the formate concentrations in the unloaded and 0.3 and 0.4 loaded cases.

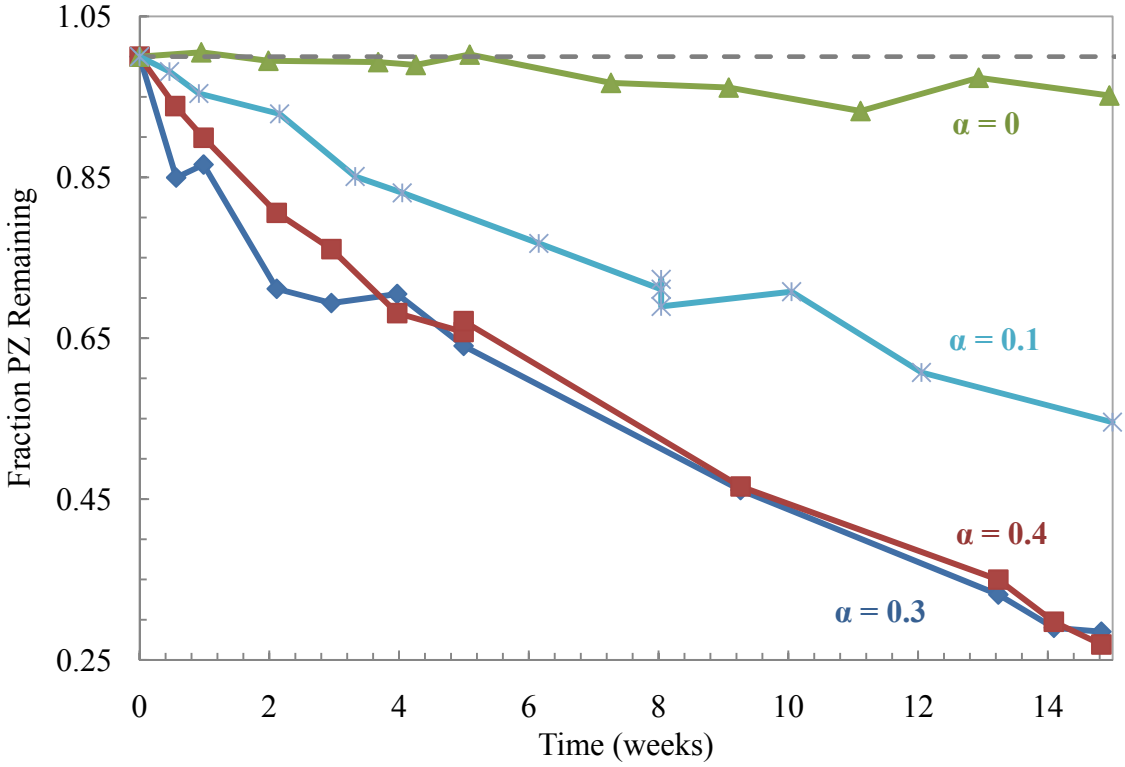

Figure 6: Comparison of PZ loss for Varying CO_2 Concentrations at 175 °C

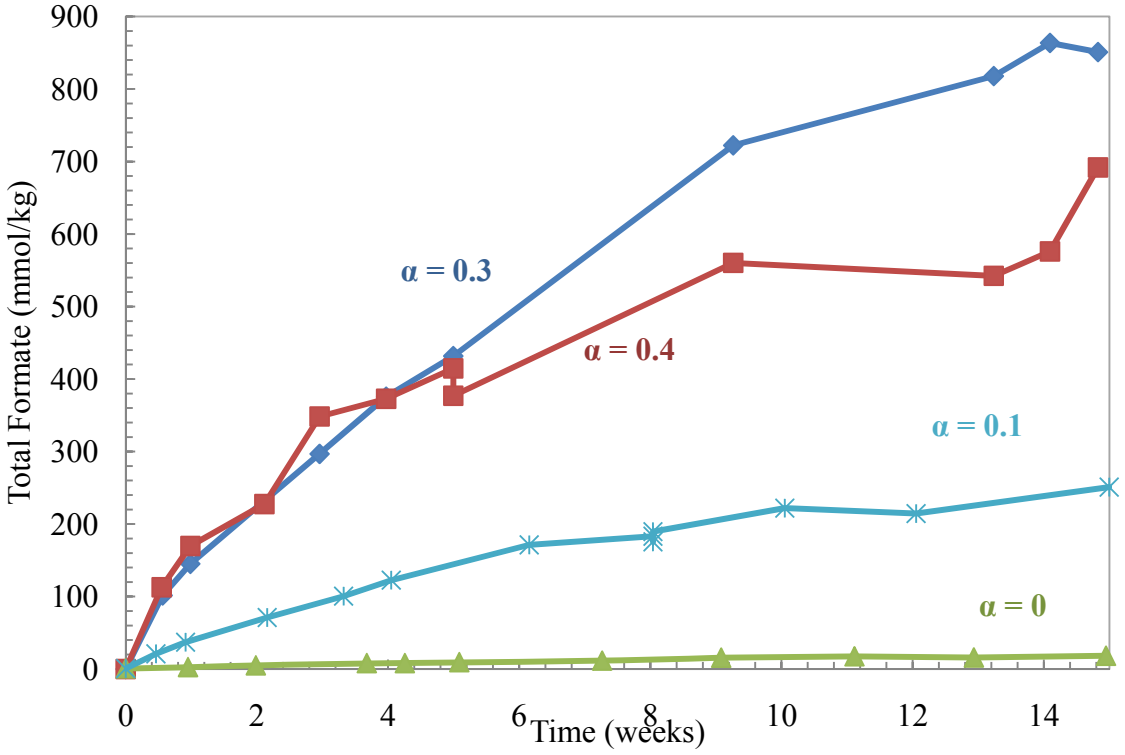

Figure 7: Comparison of Total Formate Production for Varying CO_2 Concentrations at 175 °C

It is expected that both the rate of PZ loss and production of degradation products would increase with increased CO_2 loading. This is based on previous observations of different amine solvents (Davis, 2009). However, in concentrated PZ, the behavior is not as straightforward in the 0.3 and 0.4 loading experiments. The rate of PZ loss is essentially the same between the two experiments while the 0.3 loading experiment actually produced more total formate than the 0.4 loading experiment. The most straightforward explanation is that the rates in PZ solutions are highly dependent on speciation, which is more varied than other amines previously studied such as MEA. There also appears to be a maximum in each rate, both PZ loss and formate production, that may occur in between 0.3 and 0.4 loading.

The speciation of a loaded PZ solution has never been measured at 175 °C directly, but modeling of PZ solutions using data at lower temperatures can predict the high temperature behavior. Peter Frailie has developed a thermodynamic Aspen Plus® e-NRTL framework for loaded PZ that includes speciation predictions to high temperatures (Frailie, this report). The estimated speciation for 8 m PZ at 175 °C is shown in Figure 8. The major species are free PZ, $PZCOO^-$, H^+PZ, H^+PZCOO^-, $PZ(COO^-)_2$, and HCO_3^-. The concentrations of free CO_2, CO_3^-, and $H_2^{+2}PZ$ are negligibly small and are not included in the figure. The balance of all the mole fractions is water at every point along the curve.

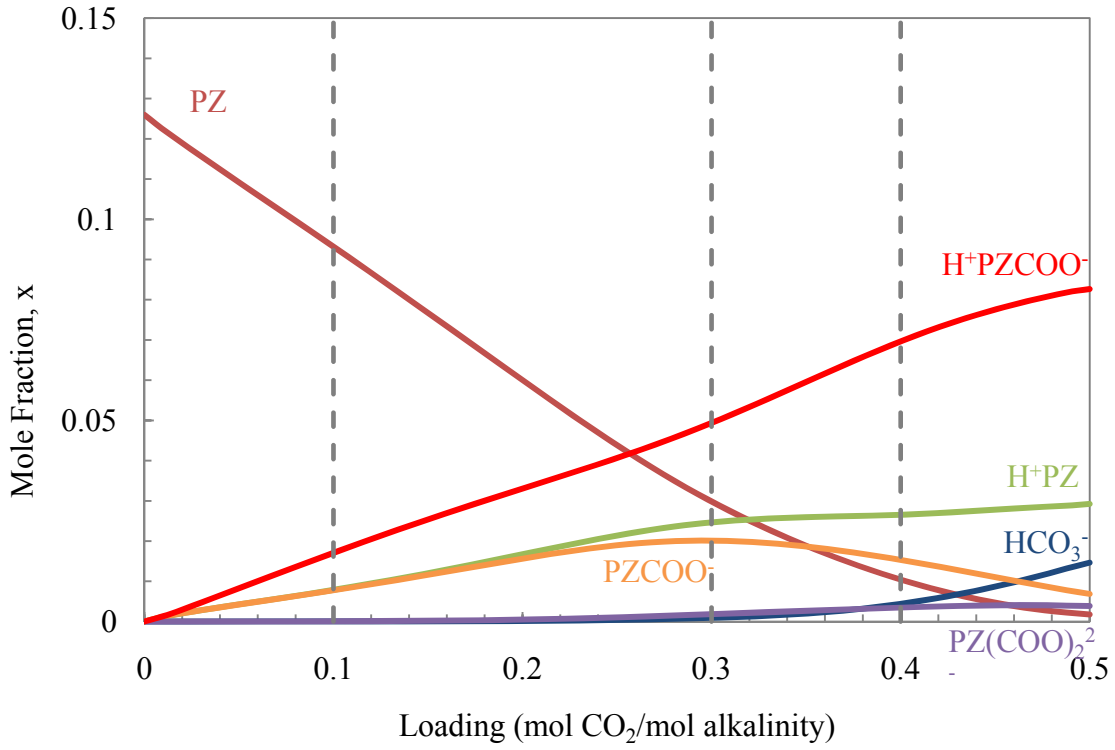

Figure 8: Estimated Speciation of 8 m PZ at 175 °C (Frailie, this report)

In unloaded solution, all the PZ is in the form of free PZ. At a loading of 0.1 mole CO_2 per mole alkalinity, the CO_2 in solution has reacted with PZ to create equimolar amounts of H^+PZ and $PZCOO^-$ with H^+PZCOO^- at twice the concentration of either. As the loading is increased to 0.3, the H^+PZCOO^- and H^+PZ both increase steadily while the $PZCOO^-$ begins to taper off and free

PZ steadily decreases. At a loading of 0.4 mole CO_2 per mole alkalinity, H^+PZCOO^- is the dominant species in solution with H^+PZ and $PZCOO^-$ as secondary species.

The total formate production and rate of PZ loss can now be analyzed in light of the estimated speciation at the experimental temperature of 175 °C. The mole fractions for the dominant species in solution at the four loadings of interest are shown in Table 1 below.

Table 1: Species Mole Fraction in 8 m PZ Estimated at 175 °C

	Species Mole Fraction			
CO_2 Loading (mol/mole alk)	0	0.1	0.3	0.4
H_2O	0.874	0.874	0.872	0.866
PZ	0.126	0.090	0.029	0.010
H^+PZ	0	0.0086	0.0249	0.0266
$PZCOO^-$	0	0.0085	0.0201	0.0152
H^+PZCOO^-	0	0.0187	0.0503	0.0701
$PZ(COO^-)_2$	0	0.0001	0.0019	0.0035
HCO_3^-	0	0	0.0009	0.0045

The total formate concentrations in the experiments at four different loadings were discussed in Figure 7 above. There appeared to be a discrepancy in that the formate concentration was higher in the 0.3 loading experiment compared to the 0.4 loading case. The assumption was that formate was linearly or exponentially related to the total CO_2 concentration. If the specific species in solution are analyzed individually, it appears there is an explanation.

In Figure 9 below, the total formate concentration after 15 weeks of degradation at 175 °C is compared with the estimated mole fraction of four different species. In panel A, the formate is compared to the sum of the mole fraction of all CO_2-containing species. That includes free CO_2, HCO_3^-, $PZCOO^-$, H^+PZCOO^-, and double the concentration of $PZ(COO^-)_2$. In panels B, C, and D, the formate concentration is compared directly to the mole fraction of $PZCOO^-$, H^+PZCOO^-, and free CO_2, respectively. Panels A, C, and D demonstrate the basis of the discrepancy observed in Figure 4. In these cases, the concentration of formate does not seem associated with the species compared in each case. On the other hand, Panel B appears to demonstrate that there is a strong correlation between the mole fraction of PZCOO- and the total formate produced in a degradation experiment. Both the formate concentration and PZCOO- concentration are lower in a 0.4 loading experiment than a 0.3 loading experiment.

This result suggests that the mechanism responsible for the creation of formate is controlled by the presence or reaction of PZCOO-. Most likely, the reaction of PZCOO- into an intermediate is the starting point of a thermal degradation mechanism that results in formate and N-Formyl PZ or formyl amides. This result also confirms that protonated PZ is not involved in the production of formate, as is hypothesized in the preceding section on acidified PZ degradation.

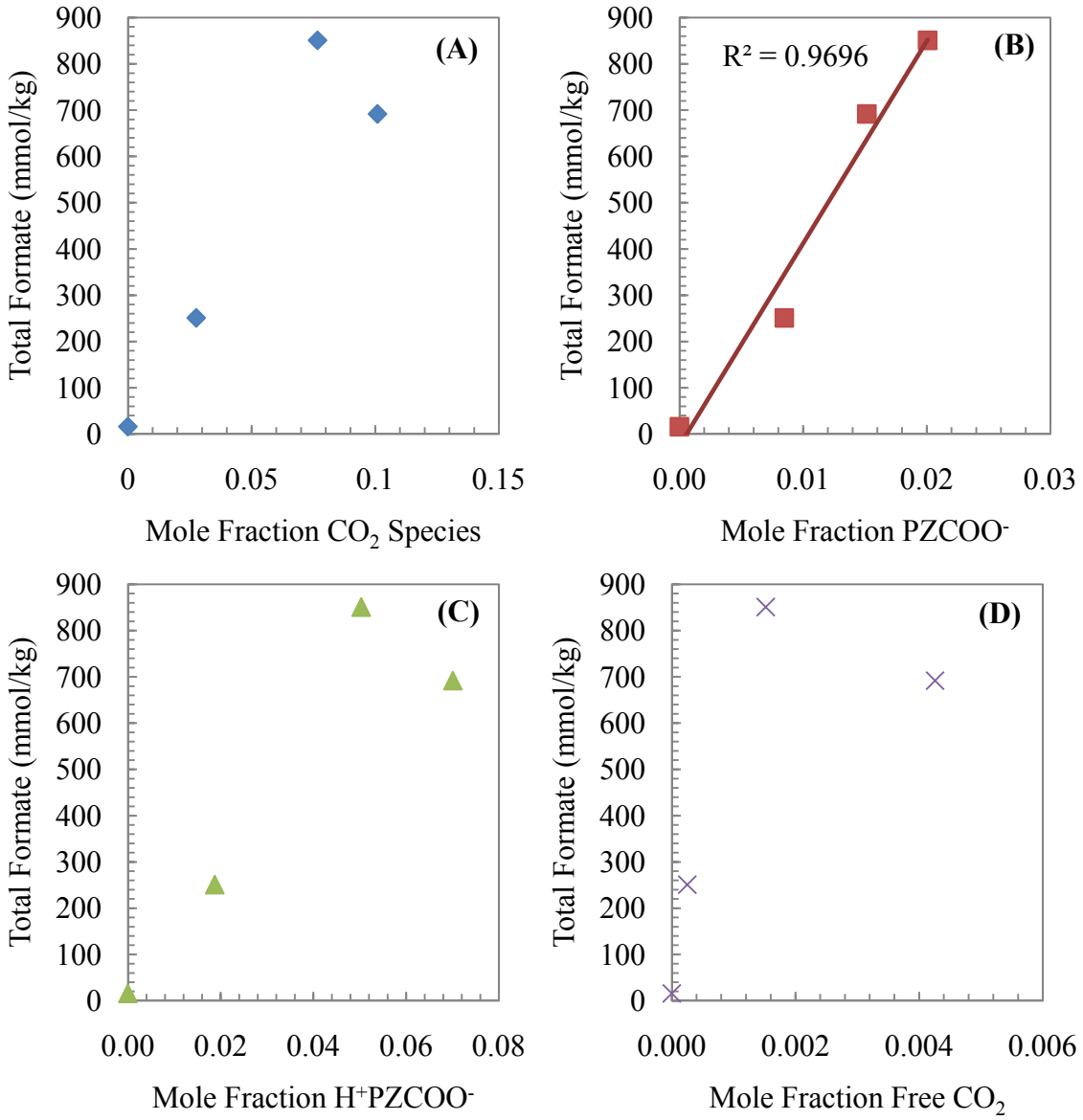

Figure 9: Relationships Between Total Formate and Mole Fraction of (A) Sum of CO_2 Species, (B) $PZCOO^-$, (C) H^+PZCOO^-, and (D) Free CO_2

For the rate of PZ degradation, the relationship between degradation and the speciation is not as straightforward as the production of total formate. The PZ degradation rate, reported as the logarithm of the percent PZ remaining after 15 weeks at 175 °C, is compared to the mole fraction of specific species in solution in Figure 10 below. In panel A, the rate is compared to the sum of mole fractions of PZ species in solution. This includes free PZ, H^+PZ, $PZCOO^-$, H^+PZCOO^-, and $PZ(COO^-)_2$. In panels B, C, D, and E, the rate is compared to the mole fractions of free PZ, H^+PZ, $PZCOO^-$, and H^+PZCOO^-, respectively. Both free PZ and H^+PZ appear to have a strong, but opposite, correlation with the degradation rate of PZ. These results are expected as the amount of free PZ should decrease with loading and H^+PZ should increase. The H^+PZ is assumed to be a highly reactive species that is present in high concentration based on the speciation presented above. It also may be expected that the loss of PZ would not be directly

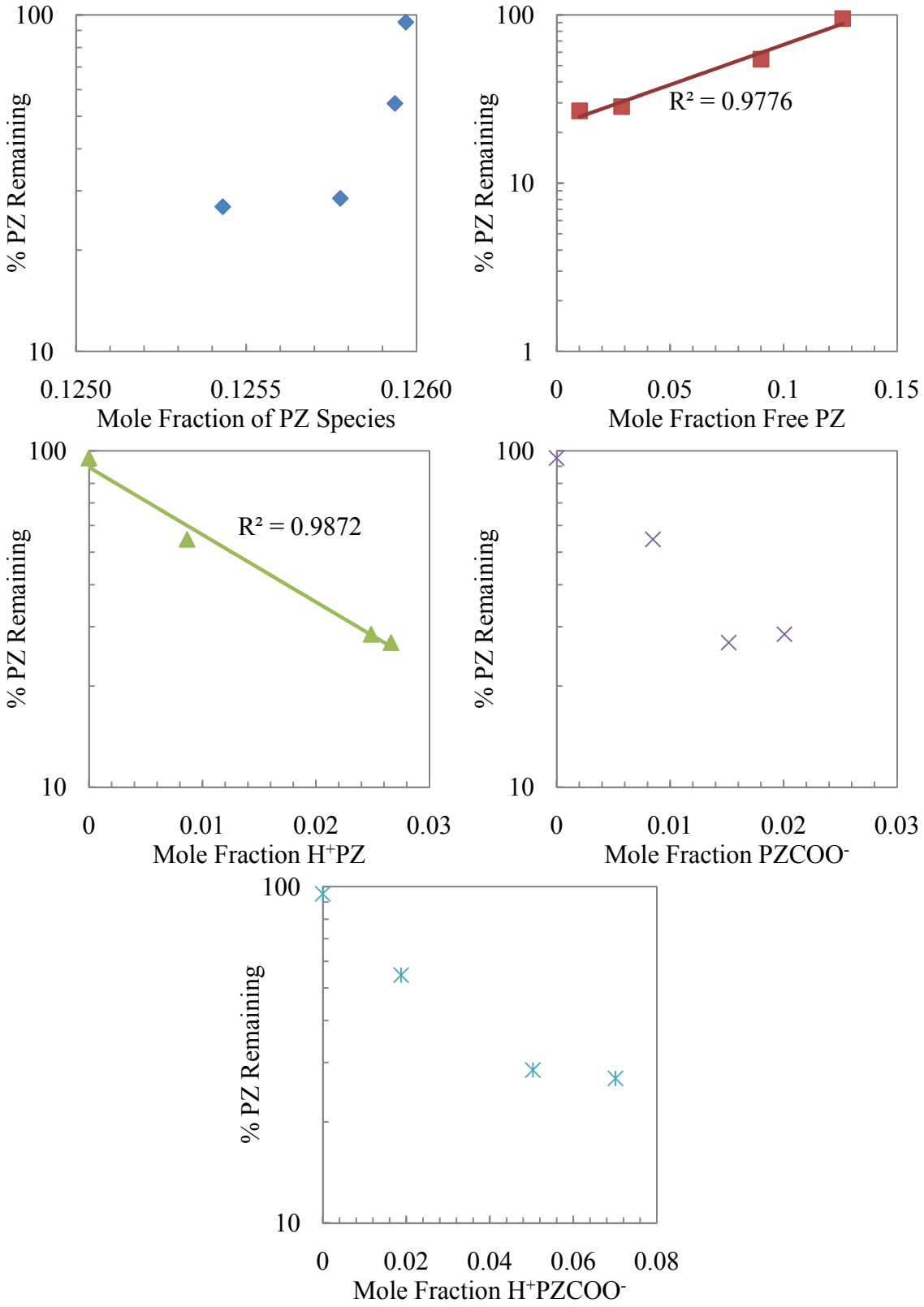

Figure 10: Relationships Between PZ Degradation and Mole Fraction of (A) Sum of PZ Species, (B) Free PZ, (C) H^+PZ, (D) $PZCOO^-$, and (E) H^+PZCOO^-

related to the CO_2-containing species since they appear to actively participate in the formation reactions for formate and formyl species. The zwitterion, H^+PZCOO^-, would not be expected to actively catalyze the production of either product, formate or EDA, or loss of amine since both active alkaline sites are consumed with a proton or CO_2 molecule already, reducing the pKa of the molecule.

Thermal Degradation of 8 m PZ with Glass Inserts (α = 0.3) (TE22)

During the 5th Trondheim Conference on Carbon Capture, Transport, and Storage (TCCCS), the idea of using glass inserts in our thermal degradation experiments was discussed with Aslak Einbu of SINTEF (Einbu, 2009). Their thermal degradation efforts were utilizing our basic design of stainless steel thermal cylinders, but Einbu had had success with using glass cuvettes to line the cylinders and prevent the amine solution from coming into contact with the metal surfaces. His observation was that this prevented the solution from corroding the cylinders and prevented the leaching of metal catalysts into solution. In an effort to investigate his findings, an experiment was set up using small glass cuvettes inserted into our thermal cylinders.

With this new experimental protocol, 8 m PZ with a loading of 0.3 mole per mole alkalinity was degraded at 175 °C for 15 weeks. The concentration profiles for PZ and the degradation products are shown below in Figure 11. EDA, formate, formyl amides, acetate, and acetyl amides were the main degradation products observed and quantified.

The concentrations of PZ and total formate are compared in Figure 12 for this experiment and a comparable experiment in the absence of glass cuvette inserts (TE12). Both were 8 m PZ with a loading of 0.3 mole CO_2 per mole alkalinity degrade at 175 °C for 15 weeks. The hypothesis for this experiment was that without having the amine solution in contact with the stainless steel inner walls of the cylinder, less metal would be leached into solution providing less catalyst for degradation. The concentration profiles indicate that less degradation did occur in the glass cuvette experiment. The PZ loss was slightly reduced while the concentration of total formate, a standard indicator for thermal degradation of PZ, was reduced. The difference is not drastic, with the glass cuvette experiment losing 66.1% of the original amine compared with 71.5% of the baseline experiment. Also, the cuvette experiment produced only 538 mmol/kg of total formate after 15 weeks while the baseline experiment produced 709 mmol/kg of total formate.

The observations of Einbu appear to be confirmed with our experimental conditions and concentrated PZ. One point of interest is the appearance of the degraded solutions. Einbu observed that solutions degraded in the glass cuvettes did not attain the dark, brownish coloring typical of degraded amine solutions while still achieving similar levels of degradation. The color has traditionally been attributed to both the presence of metals and colorized degradation products. The PZ experiment (TE22) reported here did not show that effect. The PZ degraded in the glass cuvettes appeared exactly the same as previously degraded PZ using the standard thermal cylinder protocol. It is important to note, however, the differences between the experimental protocol for the glass cuvette experiments at SINTEF and my work. The cuvettes used in this experiment did not reach the top of the thermal cylinder when placed inside. That is to say, the cuvettes were too short for our standard thermal cylinders and the top of the cuvette was approximately 2 cm from the top of the cylinder. Therefore, less solution could fit in the cuvette than a traditional experiment (7 mL vs. 10 mL). The extra headspace in the cylinder could have contributed to the differences seen in Figure 12. The CO_2 concentration in the solution would have been slightly different as the high temperature would vaporize solution and

drive CO_2 into the headspace. Analysis of the samples with ICP-OES showed that there were negligible concentrations of iron, nickel, and chromium in solution indicating that the solution was maintained separately from the stainless steel side walls of the solution. Therefore, the color of the solution must be from the degradation products alone. This may indicate that the dark color seen in traditional experiments is primarily from the degradation products, with little contribution from the low metals concentrations usually found.

Analysis of Metals in Thermally Degraded Solutions

Prior thermal degradation experiments were analyzed this quarter for their concentration of stainless steel metals: iron, nickel, and chromium. The experiments analyzed included TE16 (8 m 2-MPZ, α = 0.3 moles CO_2 per mole alkalinity), 17 (4 m PZ + 4 m 2-MPZ, α = 0.3), 21 (8 m PZ, α = 0), 22 (8 m PZ, α = 0.3 in glass), 23 (8 m PZ , α = 0.3 mole H^+ per mole alkalinity), 24 (8 m HomoPZ, α = 0.3), 25 (8 m Pyrrolidine (Pyr), α = 0.3), 26 (8 m Piperidine (PD), α = 0.3), and 27 (8 m Hexamethyleneimine (HexaMI), α = 0.3).

The concentrations of iron, chromium, and nickel for each experiment are shown below in Figures 13 through 20. No metals were detected in TE22 in any significant quantity (8 m PZ, α = 0.3 in glass).

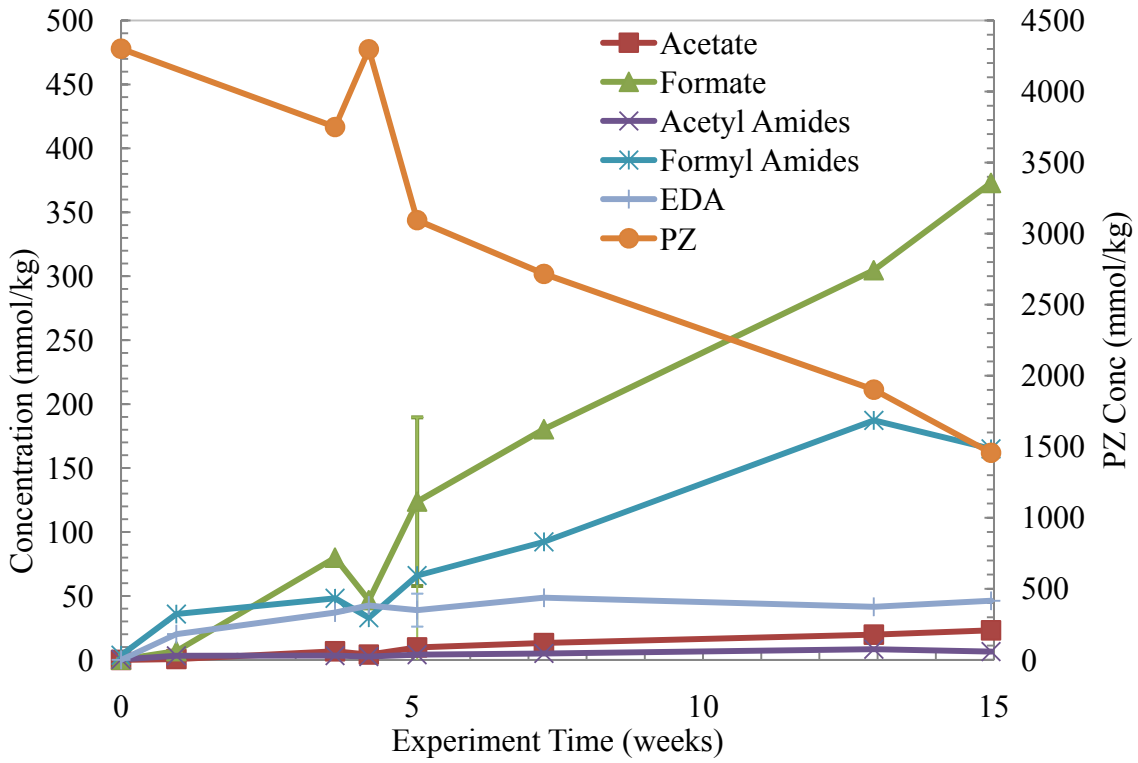

Figure 11: Concentration Profiles for 8 m PZ Thermal Degraded at 175 °C for 15 weeks with Glass Cuvette Inserts (TE22)

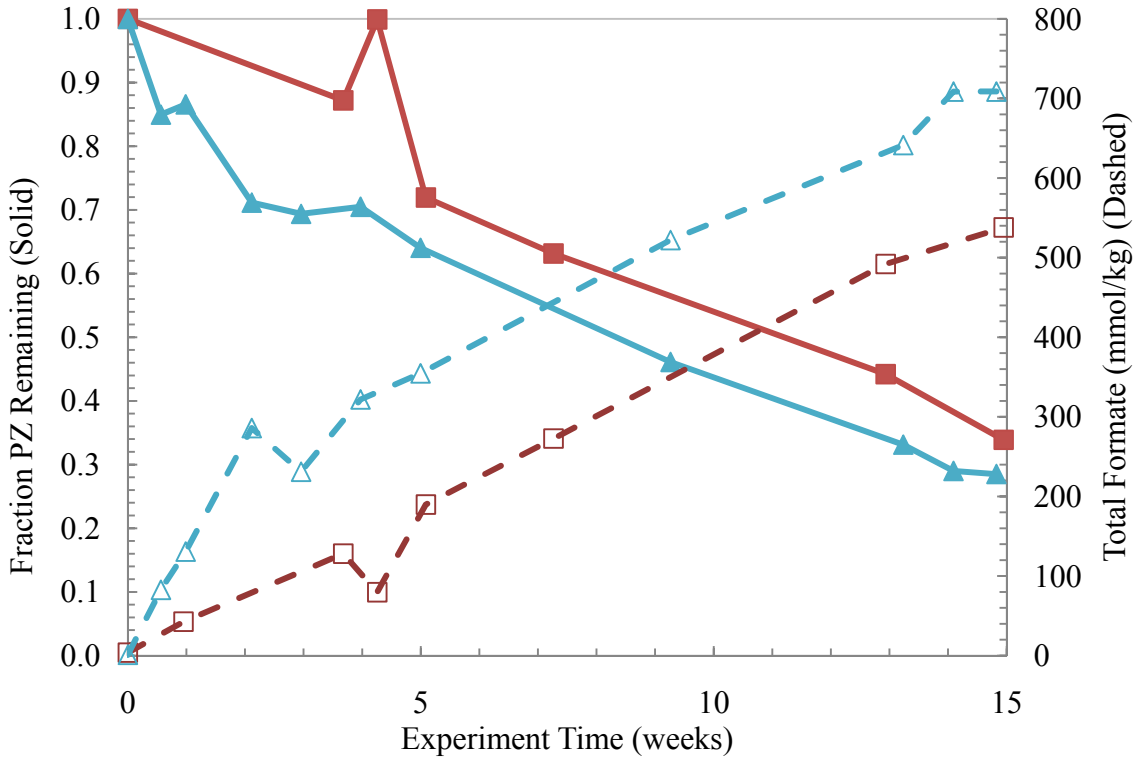

Figure 12: Comparison of Degradation of 8 m PZ at 175 °C With (Squares) and Without (Triangles) Glass Cuvette Inserts. Solid: Fraction PZ Remaining, Dashed: Total Formate

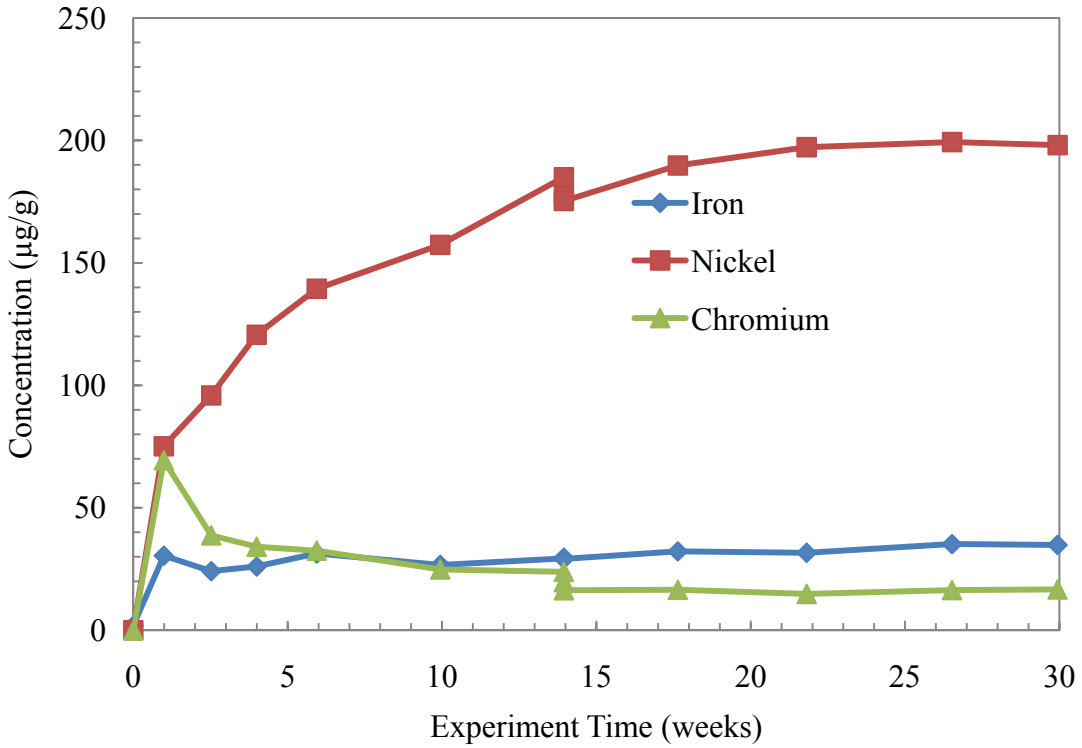

Figure 13: Concentration of Metals in 8 m 2-MPZ Thermally Degraded at 150 °C for 30 weeks (TE16)

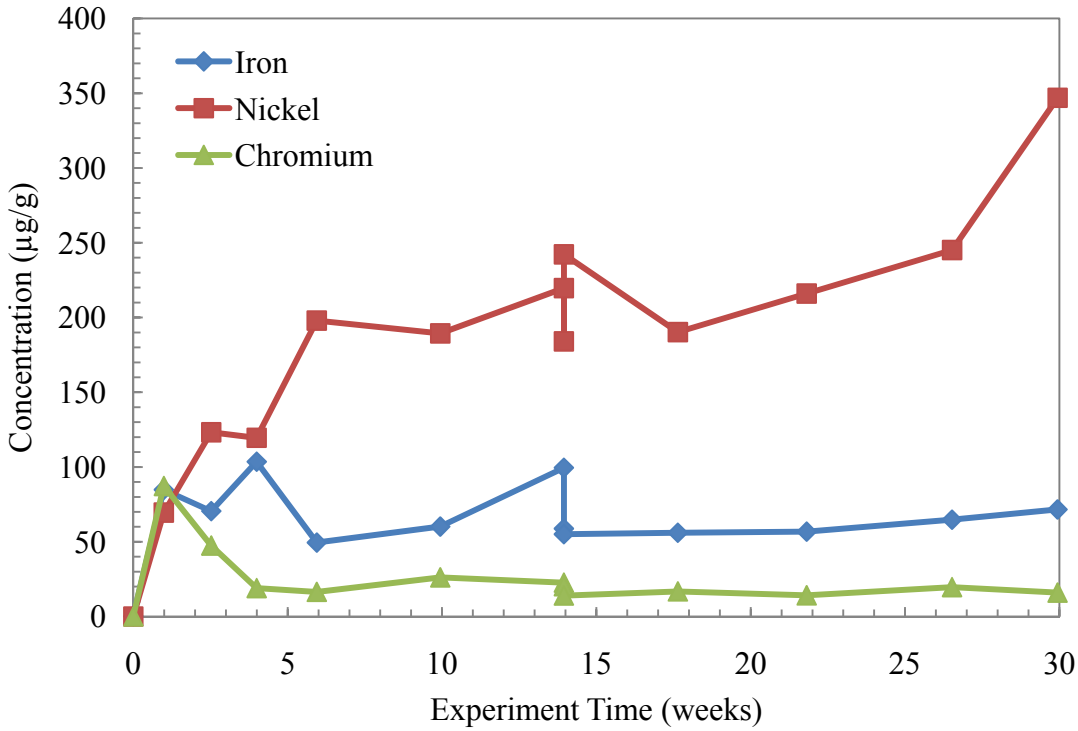

Figure 14: Concentration of Metals in 4 m PZ + 4 m 2-MPZ Thermally Degraded at 150 °C for 30 weeks (TE17)

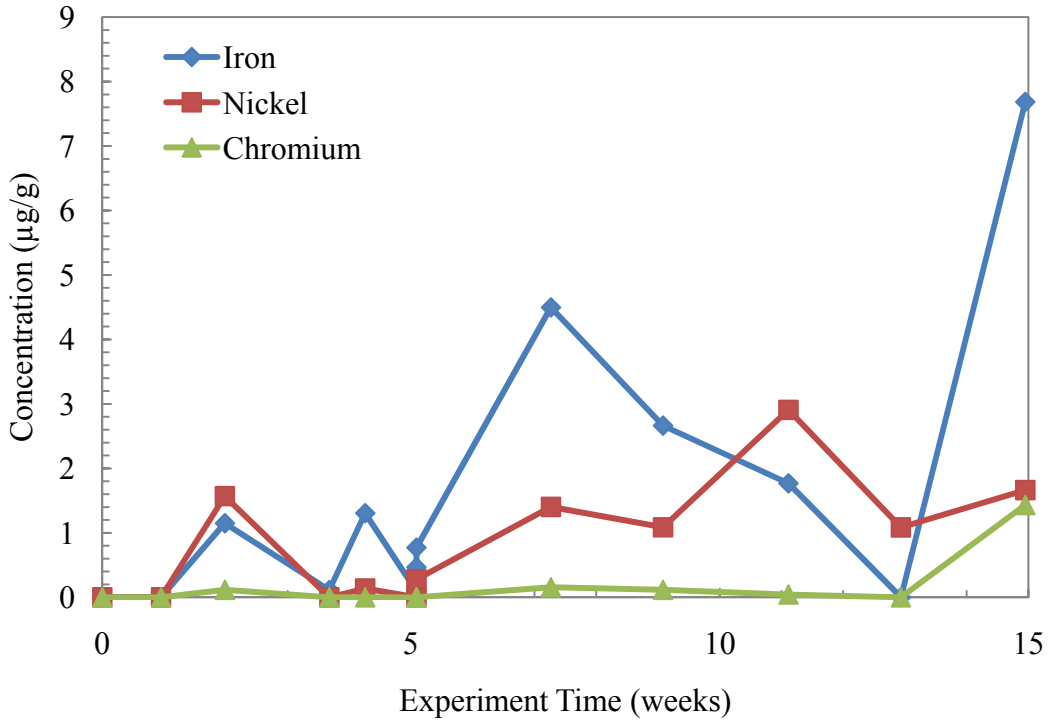

Figure 15: Concentration of Metals in 8 m PZ (α = 0) Thermally Degraded at 175 °C for 15 weeks (TE21)

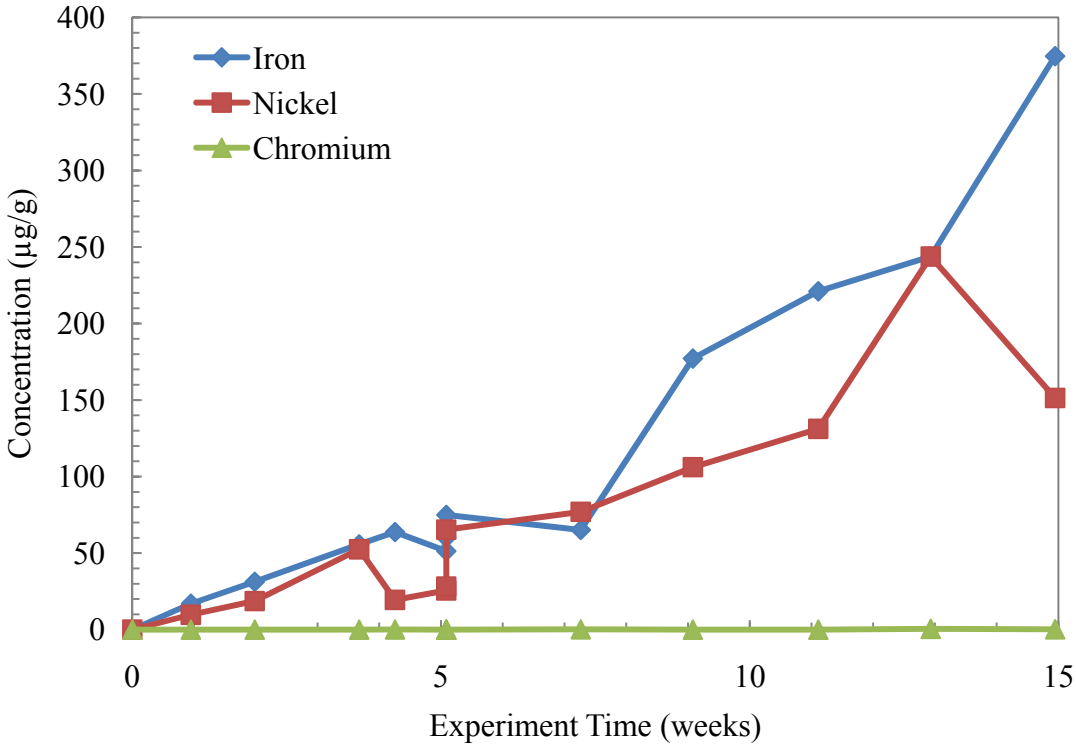

Figure 16: Concentration of Metals in 8 m PZ (α = 0.3 Mole H^+ per Mole Alkalinity) Thermally Degraded at 175 °C for 15 weeks (TE23)

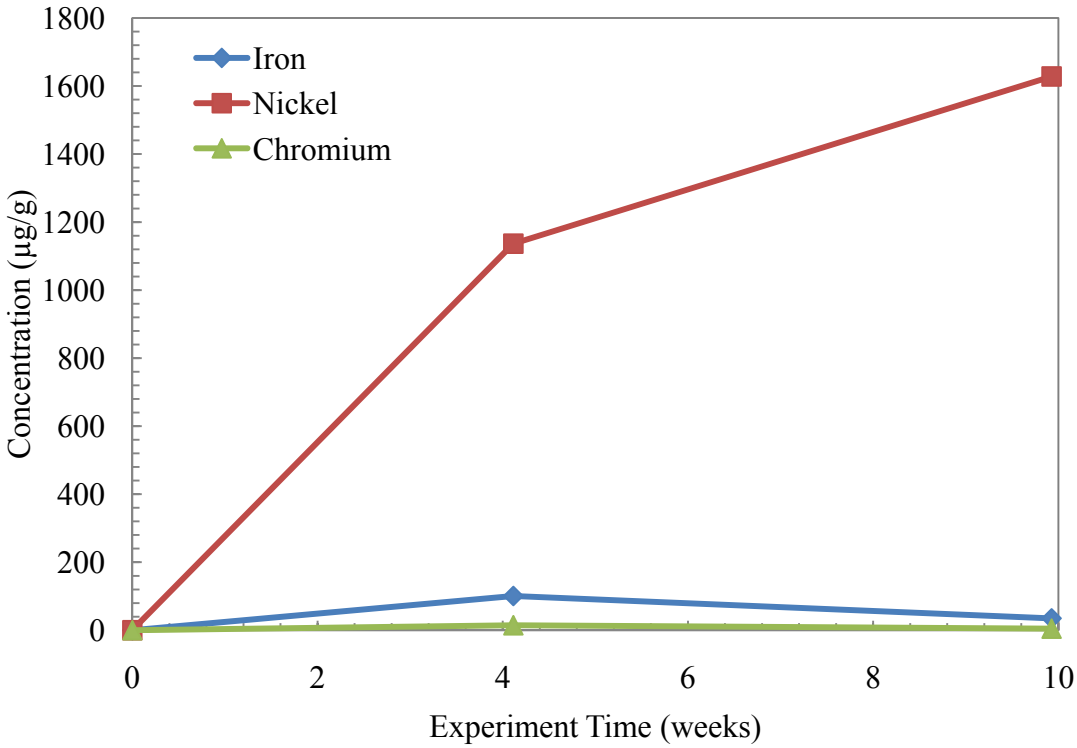

Figure 17: Concentration of Metals in 8 m HomoPZ (α = 0.3) Thermally Degraded at 175 °C for 15 weeks (TE24)

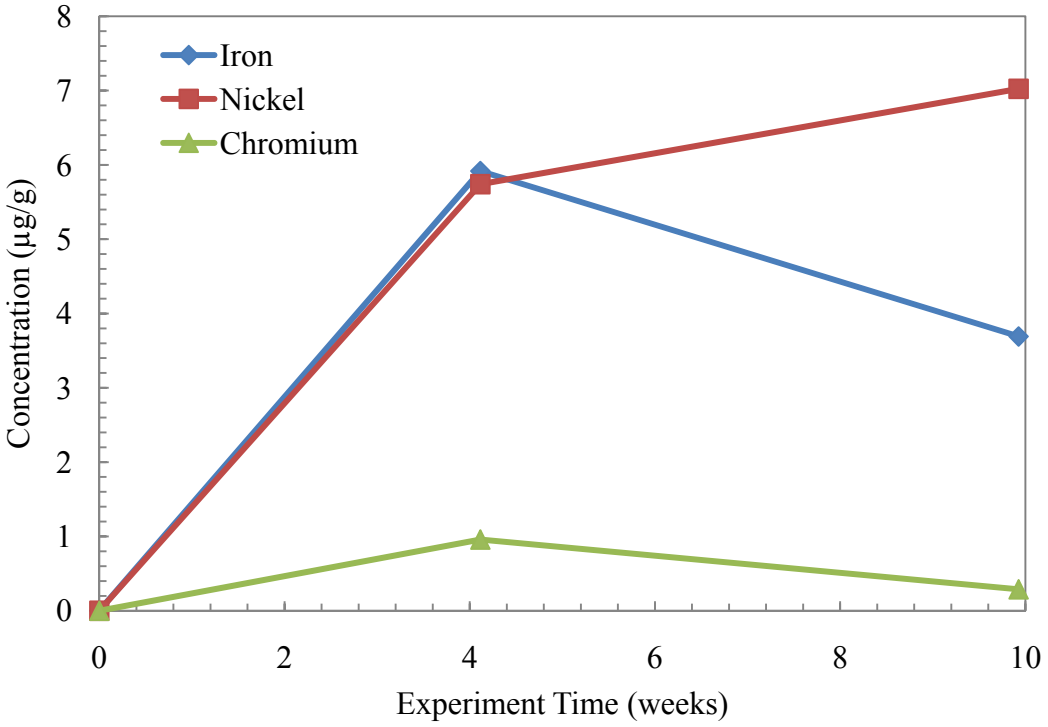

Figure 18: Concentration of Metals in 8 m Pyr (α = 0.3) Thermally Degraded at 175 °C for 15 weeks (TE25)

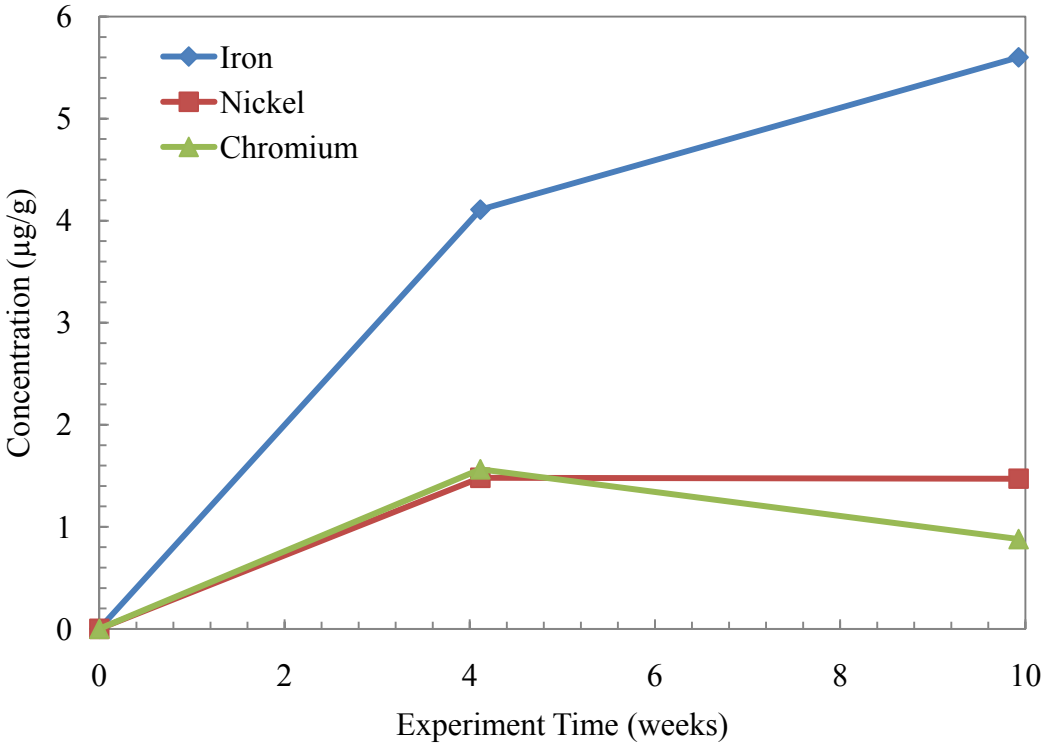

Figure 19: Concentration of Metals in 8 m PD (α = 0.3) Thermally Degraded at 175 °C for 15 weeks (TE26)

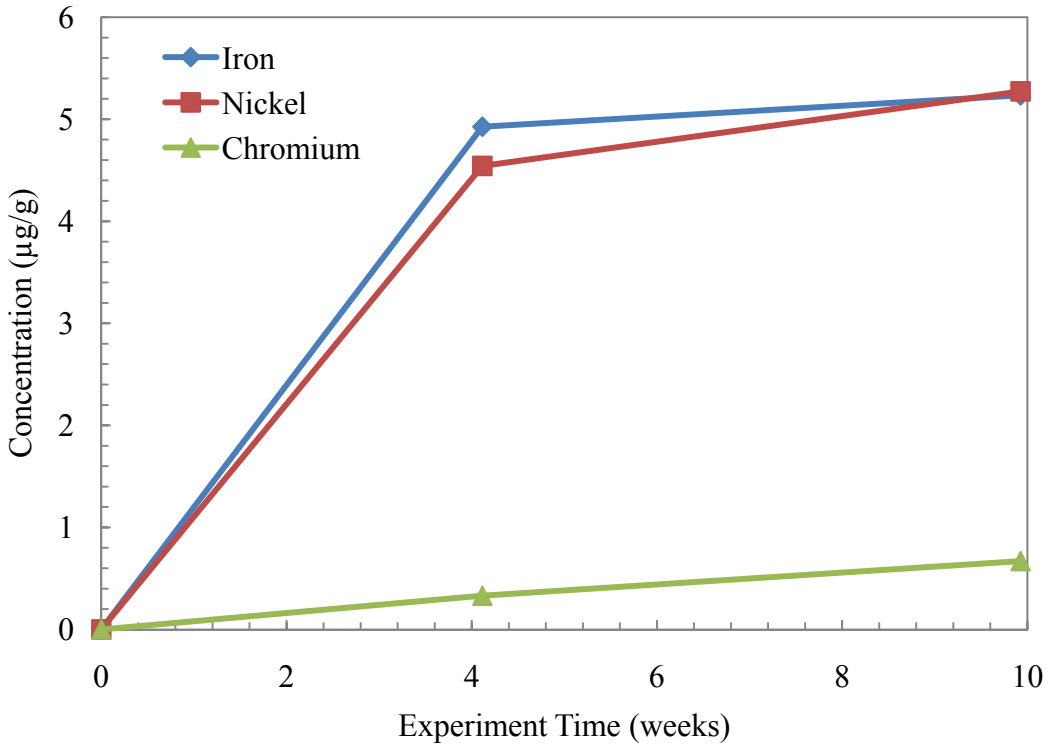

Figure 20: Concentration of Metals in 8 m HexaMI (α = 0.3) Thermally Degraded at 175 °C for 15 weeks (TE27)

Oxidative Degradation

OE19 – Stainless Steel Metals at 70 °C in the TOR

One oxidation experiment was completed this quarter on 8 m PZ. This experiment was the first to be performed at 70 °C. The water bath used for the Teflon Oxidation Reactor (TOR) was converted to an oil bath to achieve and maintain the high temperature of the reactor. The standard concentrations of stainless steel metals were used (0.4 mM Fe^{2+}, 0.1 mM Cr^{3+}, and 0.05 mM Ni^{2+}). The intention of this experiment was to increase the temperature in an attempt to increase the oxidation rate of concentrated PZ. Previous oxidation experiments, in the absence of copper, degrade very slowly and make it difficult to measure true degradation outside of analytical instrument error and water balance error.

The TOR was used to degrade 8 m PZ for nearly 600 hours at 70 °C with 2% CO_2/98% O_2 fed at 100 mL/min. The concentration profiles for PZ and the most abundant degradation products are shown below in Figure 21. EDA was not detected and formate, formyl amides, and acetate were the only degradation products detected and quantified. Overall, little PZ was lost from solution, only 2.84% over the 600 hours, or less than 0.005%/hr in this experiment.

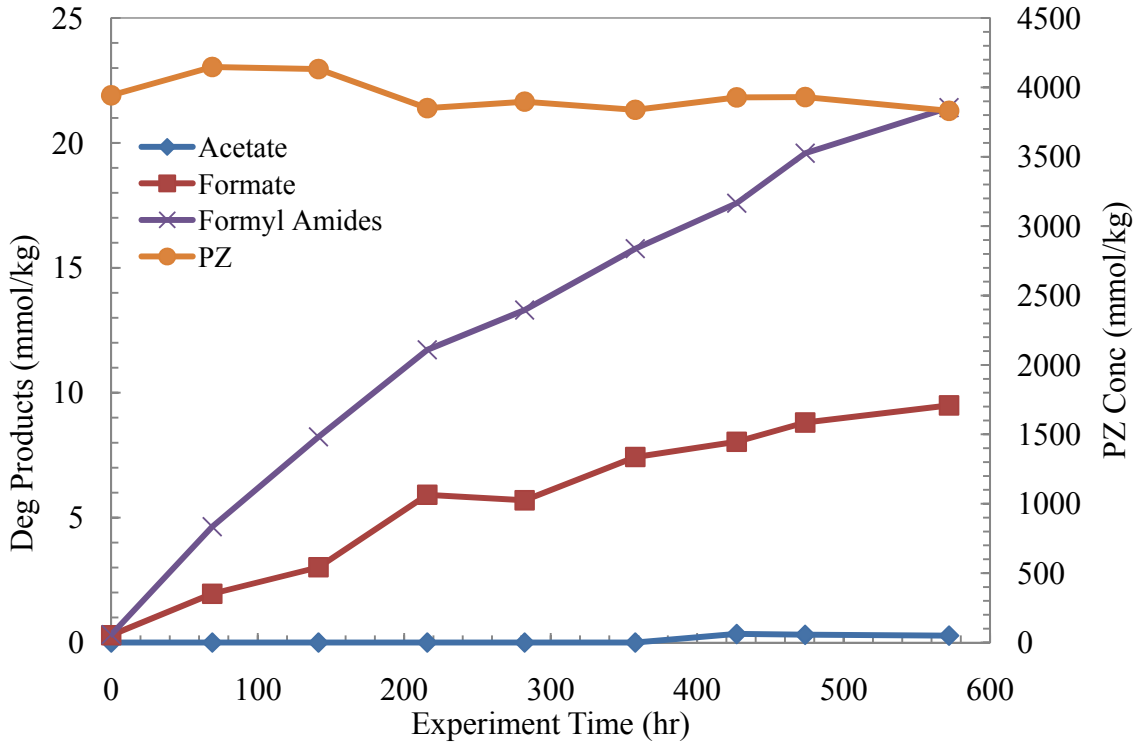

Figure 21: Concentration Profiles for Oxidation of 8 m PZ in the TOR at 70 °C

Temperature Induced Oxidation of PZ

With one high temperature experiment complete, the effect of temperature on oxidation can begin to be established. Only two temperatures, 55 and 70 °C, have so far been investigated, but the rates of PZ loss and degradation product creation can be analyzed at this point to determine if further temperature studies are warranted.

The PZ, formyl amide, and formate concentrations are compared for OE18 and OE19 in Figure 22. Both experiments were performed in the TOR with 8 m PZ and 2% CO_2/98% O_2 fed at 100 mL/min and agitated at 1400 rpm. The only difference was that the reactor temperature was 55 °C for OE18 and 70 °C for OE19.

The increased oxidation temperature noticeably increased the production of both formate and total formate. The loss of PZ is more convoluted due to issues with the water balance. The 70 °C experiment did lose a slightly higher fraction of PZ overall, but the difference between the experiments is not significant. The production of degradation products is always a more telling indicator of degradation in low-gas flow (LGF) or TOR experiments.

For simplification, only the PZ and total formate concentrations are shown in Figure 23. This total formate value simplifies the behavior of formate and formyl amides and gives an estimate of the 'total' degradation products produced in each experiment. From this figure, it is clear that the higher temperature experiment produced more degradation products and it is, therefore, assumed that more oxidation occurred in this experiment.

Another useful comparison for TOR oxidation experiments is the foaminess coefficient. The foaminess coefficient has been reported previously for various solvents and the procedure is

described in detail in published material (Chen et al., 2010; Thitakamol and Veawab, 2007). The production of foam in amine solvents is assumed to be caused by the presence of degradation products. The foaminess coefficient itself has no real intrinsic significance, but is a way to compare the tendency to foam between solvents in the same laboratory on the same apparatus. Since PZ concentration is an unreliable indicator of PZ oxidation due to the water balance issues, foaminess can provide additional insight into the overall amount of degradation products present.

The foaminess coefficient for OE18 and OE19 was tested for the final solution after the completion of each experiment. The foaminess coefficients calculated are compared in Table 2 to those of neat PZ and two highly oxidized PZ solutions (OE2 and OE5) in order of increasing foaminess. Data for neat PZ, OE2, and OE5 are taken from previous work by Xi Chen (Chen et al., 2010). The reactor type is indicated to differentiate between experiments performed in the newer Teflon Oxidation Reactor (TOR) or the original low-gas flow reactor (LGF).

The two newest experiments (OE18 and OE19) both have a higher foaminess coefficient than neat PZ, as would be expected for solutions that have been oxidized for any amount of time. Neither coefficient is close to the heavily degraded PZ solutions (OE2 and OE5) which both have foaminess coefficients greater than 300 10^{-3} m^2-s. Comparing just the two most recent experiments (OE18 and OE19), the foaminess does increase in the higher temperature experiment, indicating the presence of more degradation products overall.

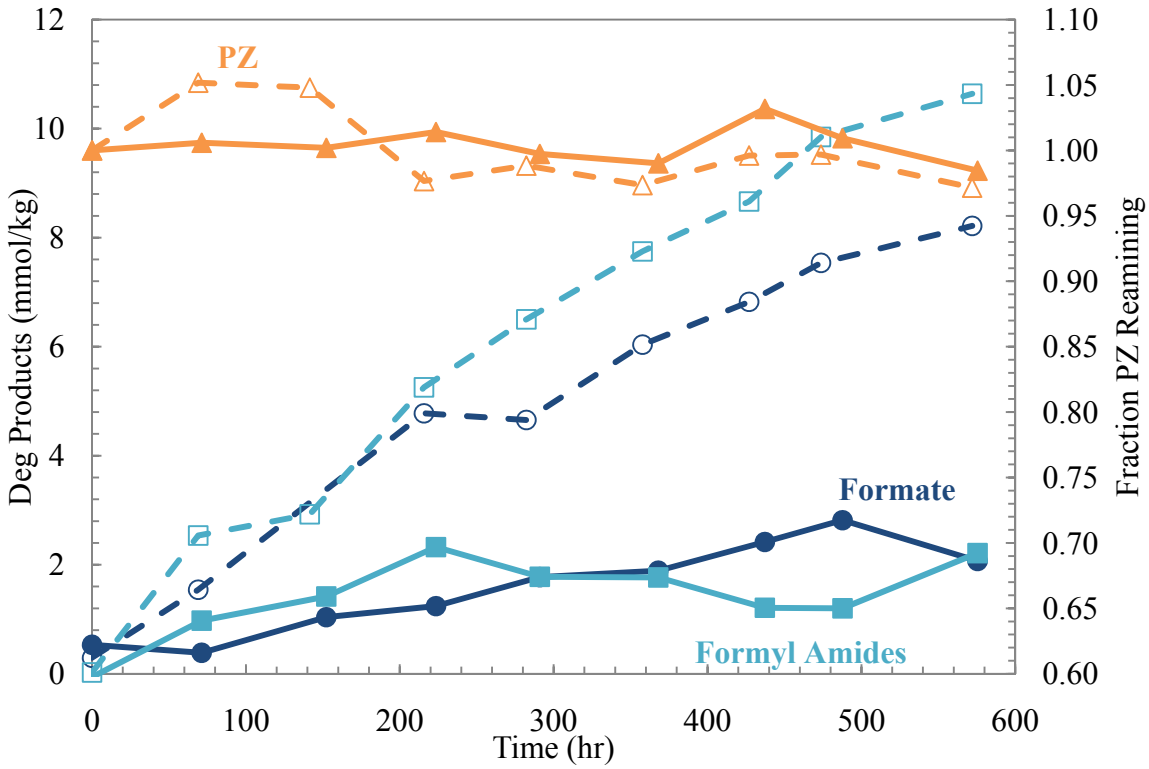

Figure 22: Comparison of Oxidation at 55 °C (Solid Lines) and 70 °C (Dashed Lines) for 8 m PZ in TOR

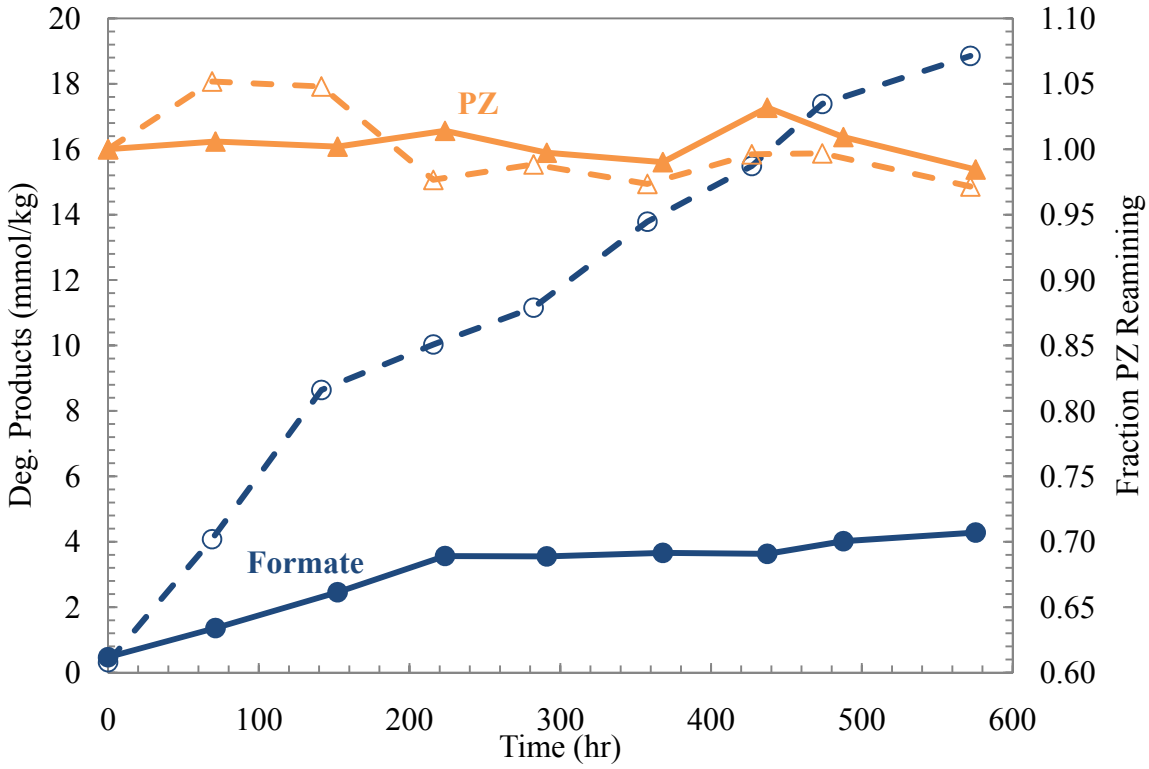

Figure 23: Comparison of PZ and Total Formate for Oxidation at 55 °C (Solid Lines) and 70 °C (Dashed Lines) for 8 m PZ in TOR

Table 2: Comparison of Foaminess Coefficients for Oxidized PZ

Expt	Solvent	CO_2 Loading (mol/mol alk)	Additives (mM)	Reactor	Foaminess Coefficient (10^{-3} m^2-s)	Foam Stability (s)
-	8 m PZ	0.3	-	-	78.8	29
OE18	8 m PZ	0.3	0.4 Fe^{2+}, 0.1 Cr^{3+}, 0.05 Ni^{2+}	TOR	117	45
OE19	8 m PZ	0.3	0.4 Fe^{2+}, 0.1 Cr^{3+}, 0.05 Ni^{2+}	TOR	195	35
OE5	8 m PZ	0.3	0.4 Fe^{2+}	LGF	>300	
OE2	10 m PZ	0.3	4.0 Cu^{2+}	LGF	303.5	>300

Conclusions

The effect of CO_2 loading on the thermal degradation of PZ was further explored this quarter with the completion of a low loading experiment. PZ was degraded slower than higher loadings and faster than the unloaded PZ experiments, as expected. The experiment containing 0.1 mole CO_2 per mole alkalinity lost 45% of the original amine compared to 5, 71, and 73% for the unloaded, 0.3 loading, and 0.4 loading, respectively, after 15 weeks at 175 °C. The concentration of CO_2 is further confirmed to directly relate to the rate of PZ degradation. The

production of the main degradation product, total formate, also speaks to the relationship of CO_2 to degradation. The production of total formate ranged from 16 mmol/kg in the unloaded solution to 251, 851, and 692 mmol/kg in the 0.1 loading, 0.3 loading, and 0.4 loading experiments. CO_2 was previously hypothesized as the carbon source for the formate degradation products found in PZ degradation and these results seem to back up that hypothesis.

Using an estimated speciation of 8 m PZ at 175 °C, it was determined that the production of formate was closely associated with the mole fraction of $PZCOO^-$, indicating this species is likely involved in the initial stages of the mechanism that produces formate and formyl amides such as N-Formyl PZ. The degradation rate of PZ was closely related to the free PZ and H^+PZ mole fractions.

The use of glass cuvettes to eliminate contact between the amine solution and the interior surfaces of the stainless steel thermal cylinders met with limited success. The overall degradation rate of 8 m PZ with 0.3 mole CO_2 per mole alkalinity was slightly reduced, losing only 66% of the initial amine compared to 71% in the traditional experimental setup after 15 weeks at 175 °C. The production of the main degradation product was reduced from 708 mmol/kg total formate in the traditional experiment to 538 mmol/kg total formate in the cuvette experiment. The presence of the cuvette did not prevent the coloration of the solution observed after degradation. No iron, nickel, or chromium was present in quantifiable concentrations using ICP-OES, further indicating that the coloration of the solutions is due to the production of unidentified degradation products.

Acidified 8 m PZ (containing only free PZ and H^+PZ) degrades slowly, losing only 34% of the initial amine compared to 71% in the 8 m PZ with 0.3 mole CO_2 per mole alkalinity over 15 weeks at 175 °C. The acidified PZ generated EDA as the only major degradation product. In CO^2 loaded PZ solutions, formyl amides, formate, and EDA are all usually found to be major products. The degradation of acidified PZ indicates a separate mechanism creates EDA through H^+PZ while CO_2-containing species ($PZCOO^-$, H^+PZCOO^-, $PZ(COO^-)_2$) are responsible for participating in the mechanism that creates formate and formyl amides.

PZ oxidation does increase with temperature, as expected, as evidenced by the increased production of degradation products. Total formate production increased from 4 to 19 mmol/kg over the course of nearly 600 hours at either 55 or 70 °C. As with previous oxidation work, PZ loss was difficult to assess due to fluctuations in the data most likely caused by changes in the overall water balance.

Future Work

The amide reversal process will be evaluated in a degraded PZ solvent obtained from the Integrated Solvent Degradation Apparatus (ISDA). The solution will be spiked with N-formyl PZ and the rate at which the alkaline amide reversal proceeds will be quantified through formate production. It is expected that the reaction will proceed slower than neat PZ due to the complexity of the mixture.

In the next quarter, at least two thermal degradation experiments will reach completion and the samples will be analyzed. Degradation of 8 m Morpholine and 8 m Hexamethylenediamine (HMDA) at 175 °C was started this quarter and will be completed in August 2011.

An experiment exploring the role of CO_2 in the generation of formate species will be started and concluded in the next quarter. An 8 m PZ solution containing 0.3 mole CO_2 per mole alkalinity

as $^{13}CO_2$ will be created and degraded for up to 6 weeks. The results will be analyzed using NMR in an attempt to observe that formate generated during degradation is the result of the CO_2. In this case, I believe that the formate will contain ^{13}C, which will show increased peaks on the ^{13}C NMR analysis. This will confirm that formate generated during degradation does not come from the carbons contained in the PZ backbone. It is possible that the formate peaks will overlap with the peaks from PZ, $PZCOO^-$, or H^+PZCOO^- and the results will be inconclusive.

PZ oxidation will continue to be investigated in the TOR. High temperature experiments will be the focus of future efforts in order to get oxidized PZ solutions in a timely fashion. An additional TOR may be created to increase the number of experiments that are possible before the end of my experiments. Planned experiments include spiking with formate and N-formyl PZ to determine the effect on the formate/formyl amide equilibrium.

References

Chen X, Freeman SA, Rochelle GT. "Foaming Behavior of Amine Solutions Used for CO_2 Capture with Different Additives." *Int. J. Greenhouse Gas Control*. 2010; Submitted.

Cullinane JT, Rochelle GT. "Kinetics of carbon dioxide absorption into aqueous potassium carbonate and piperazine." *Ind Eng Chem Res*. 2006;45(8):2531–2545.

Davis J. *Thermal Degradation of Aqueous Amines Used for Carbon Dioxide Capture*. The University of Texas at Austin. Ph.D. Dissertation. 2009:278.

Dugas RE, Rochelle GT. "Absorption and desorption rates of carbon dioxide with monoethanolamine and piperazine." *Energy Proc*. 2009;1(1):1163–1169.

Einbu A. Use of Glass Cuvettes in Thermal Cylinders to Reduce Metal Contamination. SA Freeman, Personal Communication. 2009.

Freeman SA, Dugas R, Van Wagener DH, Nguyen T, Rochelle GT. "Carbon dioxide capture with concentrated, aqueous piperazine." *Int. J.Greenhouse Gas Control*. 2010;4(2):119–124.

Hilliard MD. *A Predictive Thermodynamic Model for an Aqueous Blend of Potassium Carbonate, Piperazine, and Monoethanolamine for Carbon Dioxide Capture from Flue Gas*. The University of Texas at Austin. Ph.D. Dissertation. 2008:1083.

Koike L, Barone JS, Godinho OES, Aleixo LM, Reis FDM, Fernandes EC, Barbosa JB. "N-Formyldiethanolamine - A New Artifact in Diethanolamine Solutions." *Chem Ind.* 1987;(17):626–627.

Rochelle GT et al. "CO_2 Capture by Aqueous Absorption, Third Quarterly Progress Report 2009." Luminant Carbon Management Program. The University of Texas at Austin. 2009.

Rochelle GT et al. "CO_2 Capture by Aqueous Absorption, First Quarterly Progress Report 2010." Luminant Carbon Management Program. The University of Texas at Austin. 2010a.

Rochelle GT et al. "CO_2 Capture by Aqueous Absorption, Fourth Quarterly Progress Report 2009." Luminant Carbon Management Program. The University of Texas at Austin. 2010b.

Sexton AJ. *Amine Oxidation in CO_2 Capture Processes*. The University of Texas at Austin. Ph.D. Dissertation. 2008:262.

Thitakamol B, Veawab A. "Foaming Behavior in CO_2 Absorption Process Using Aqueous Solutions of Single and Blended Alkanolamines." *Ind Eng Chem Res*. 2007;47:216–225.

Degradation of MEA and Other Amines

Quarterly Report for April 1 – June 30, 2010

by Alexander K. Voice

Supported by the Luminant Carbon Management Program

and the

Industrial Associates Program for CO_2 Capture by Aqueous Absorption

Department of Chemical Engineering

The University of Texas at Austin

July 10, 2010

Abstract

MEA was degraded in the high gas flow (HGF) apparatus at various temperatures and inhibitor concentrations. Addition of 50 mM Inh A resulted in 63–80% reduction in the rate of ammonia production. Addition of 100 mM Inh A resulted in 86–93% reduction in the rate of ammonia production. The activation energies for no inhibitor, 50 mM Inh A, and 100 mM Inh A were 86 kJ/mol, 102 kJ/mol, and 113 kJ/mol, respectively.

GC-MS was used to identify imidazol, 1-(2-hydroxyethyl)-imidazol, and 2-oxazolidone on GC-MS. A significant unknown product on the chromatogram was identified as trimethylamine based on the closest library reference match.

Significant masses observed on LC-MS and MS-MS (direct infusion) in oxidatively degraded MEA samples include 128, 199, and 215. These masses did not correspond with any known degradation products. The collision induced dissociation (CID) mass spectrums of the 128 and 199 compounds indicate that they may be substituted imidazols. The compound with molar mass 199 was the only product to exhibit a strong UV absorbance, and has a molecular formula of $C_8H_{13}N_3O_3$.

MEA, which was oxidized and then thermally degraded, showed similar MEA loss to thermal degradation of neat solutions. At the high temperature, some formamide was converted to formate. All oxalate products were converted to formate. Nitrite was completely consumed, but nitrate was stable.

Introduction

Ammonia is produced from the oxidative fragmentation of monoethanolamine (MEA) into two formaldehydes and one ammonia, or one hydroxyacetaldehyde and one ammonia (Figure 1).

Initiation

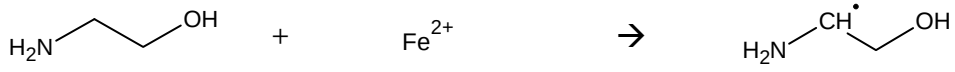

Propagation

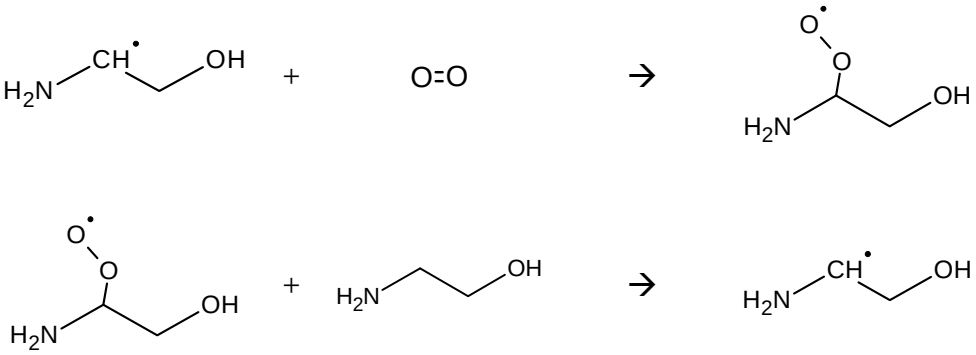

ammonia production

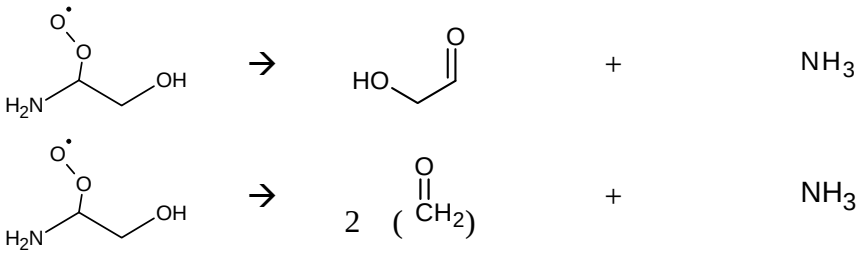

Figure 1: Oxidative Fragmentation Chain Reaction Mechanism

Aldehydes can go on to react with ammonia or MEA in solution to form the corresponding imine (Figure 2).

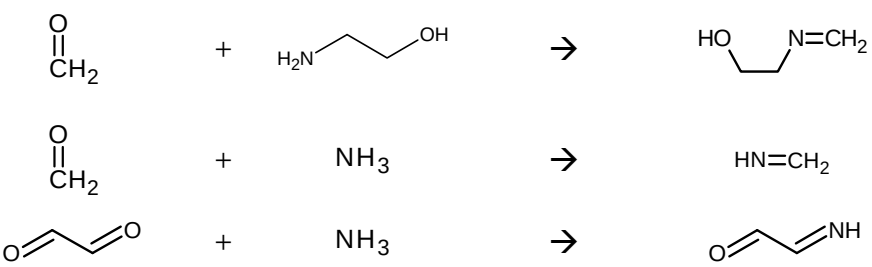

1-(2-hydroxyethyl)-methylimine	
methylimine	
Iminoacetaldehyde	

Figure 2: Condensation of Imines from Aldehydes and Amines

Imines can go on to form imidazols which are relatively stable to oxidation (Figure 3).

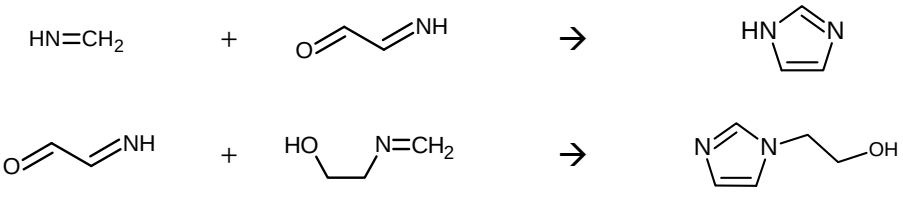

Imidazol	
1-(2-hydroxyethyl)-imidazol	

Figure 3: Condensation of Imidazols from Imines

Some products can undergo further oxidation and hydrolysis in solution (Figure 4).

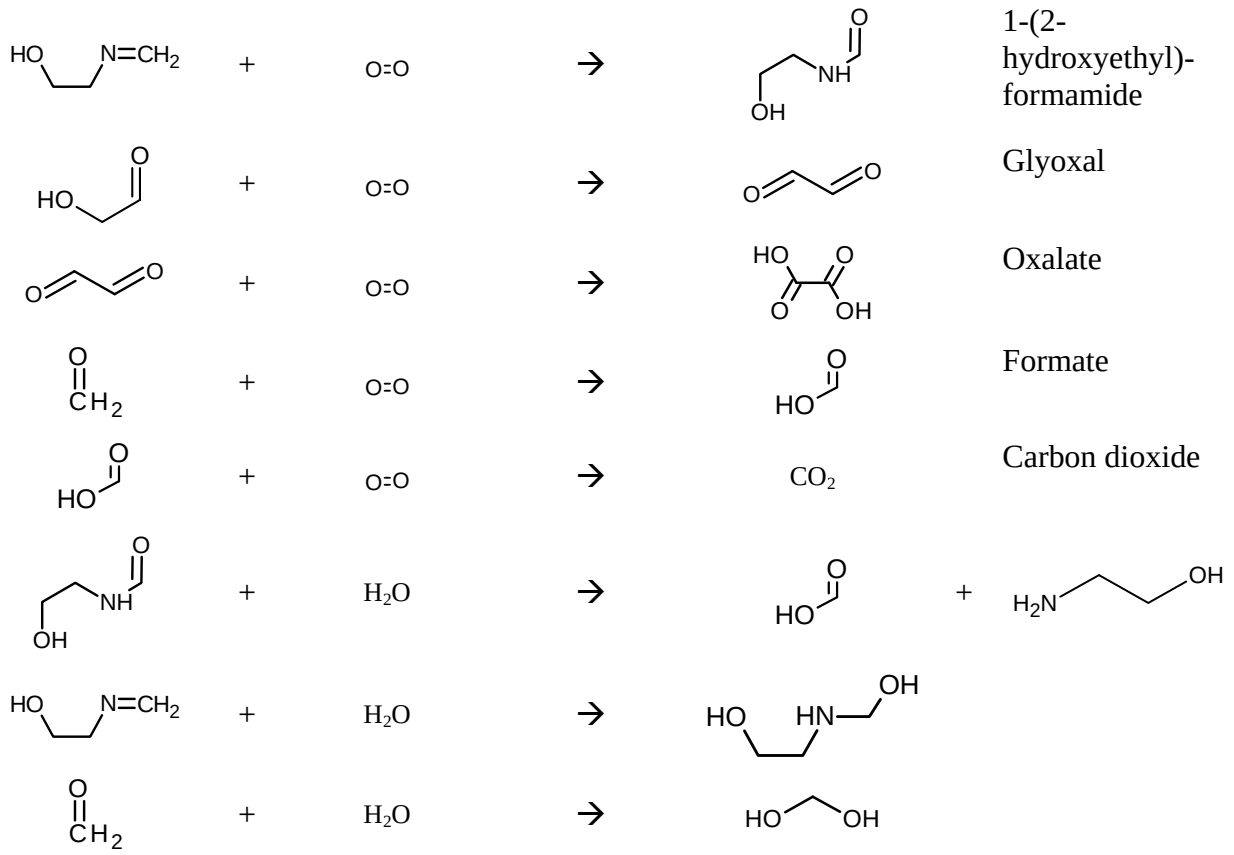

Figure 4: Oxidation and Hydrolysis of Degradation Products in Solution

Significant work has been done to assess ammonia rates for MEA in the presence of oxygen, iron, and copper. Goff (2005) found that copper was a potent catalyst for ammonia production in MEA systems. In addition, Goff found that ammonia production was enhanced by higher oxygen partial pressure, higher MEA concentration, and vigorous agitation. Low loading (0.15) experiments had the highest rates of ammonia production, while high loading (0.4) experiments had the lowest rates of ammonia production and zero loading was in the middle. Goff concluded that MEA oxidation was mass transfer controlled. Goff did not study the effect of temperature on ammonia production (all experiments were conducted at 55 °C).

Sexton (2008) conducted enhanced oxidation experiments by vigorously agitating MEA solutions in the presence of 98% oxygen, 2% CO_2, and various catalysts and inhibitors at 55 °C. Sexton quantified six significant new degradation products, 1-(2-hydroxyethyl)-formamide (HEF), 1-(2-hydroxyethyl-oxalamide, N,N'-di(2-hydroxyethyl)-oxalamide, 1-(2-hydroxyethyl)-imidazol (HEI), nitrate, and nitrite, as well as several heat stable salts (primarily formate and oxalate), which had been previously identified (Rooney, 1998). These new products allowed Sexton to close the material balance by 67% and 90% (for carbon and nitrogen, respectively) in the example below (Figure 5). Structures of significant new products are given in Figure 6.

Table 1: Summary of Low Gas Experiment by Sexton 9/07

MEA Initial (mol/kg)	4.512
MEA Final (mol/kg)	2.836

MEA Consumed (mol/kg)	1.676
Catalyst	1 mM Fe
Temperature	55 °C
Gas Rate	100 cc/min
Gas Composition	98%O_2/2%CO_2
Time (days)	20.67

Table 2: Mass Balance for Sexton 9/07

Major Products	Concentration (mol/kg)	Nitrogen (mol/kg)	Carbon (mol/kg)
HEI	287	574	1435
HEF	383	383	1149
Nitrate	42	42	0
Nitrite	89	89	0
NH3	33	33	0
Formate	144	0	144
Oxalate	10	0	20
Oxalamide*	44	0	264
MEA Consumed	1676	1676	3352
Lost		555	340
Lost %		33%	10%

*Sexton did not quantify the mono- and di- oxalamide separately. The di-amide is the dominant species and a primary product, therefore this species is used for the atom balance

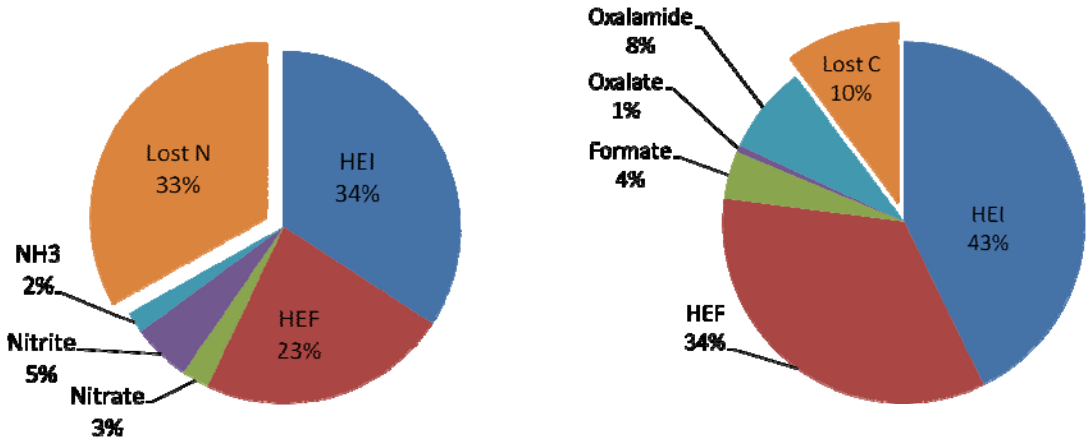

Figure 5: Nitrogen and Carbon Balances for Sexton 9/07

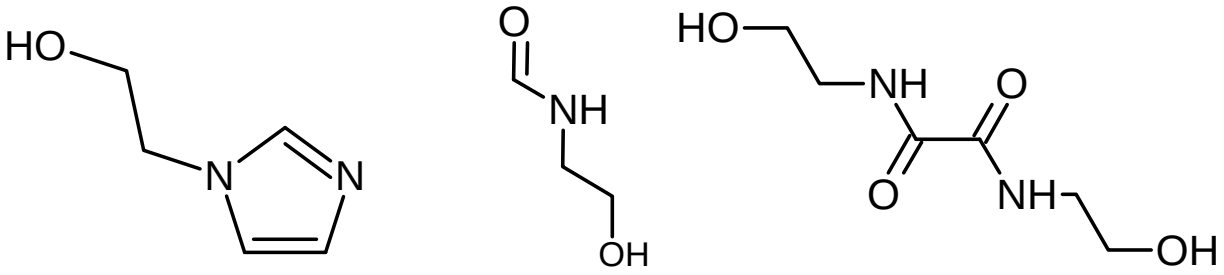

1-(2-hydroxyethyl)-imidazole 1-(2-hydroxyethyl)-formamide N,N'-dihydroxyethyl-oxalamide

Figure 6: Structures of Some New Degradation Products Identified by Sexton (2008)

Experimental Methods

MEA was degraded oxidatively in the high gas flow and low gas flow apparatuses. Products were analyzed by cation chromatography, anion chromatography, titration (H_2SO_4), total inorganic carbon (H_3PO4 evolution), total organic carbon (combustion), total nitrogen (combustion), LC-MS, and GC-MS. These techniques have been described in detail in previous work

Degradation Apparatus

The HGF apparatus is a semi-batch glass jacketed reactor, containing a vigorously agitated batch liquid phase and continuously sparged gas phase. Gas is continuously analyzed by FTIR for ethanolamine, water, CO_2, ammonia, and N_2O. These are the only gaseous components observed during MEA degradation. A summary of experimental conditions is provided in Table 1.

Table 3: HGF Experiment Summary

Solution volume	350 mL
Dry gas rate	5 SLPM
Gas composition	98% dry air, 2% CO_2
Agitation rate	1400 RPM
Measuring interval	5 minutes

The actual gas rate is determined by including the moisture content (measured by the FTIR) and gas temperature at each measuring interval. The ammonia rate (reported in mmol/kg/hr) is determined by normalizing the ammonia gas rate by the solution mass, taken as the average between the initial and final mass

The low gas flow (LGF) apparatus is similar to the high gas flow apparatus with the following exceptions. The gas is introduced to the headspace of the reactor, rather than sparged. The gas rate is 100 mL/min and the composition is 98% O_2/2% CO_2. The gas is saturated with water prior to entering the reactor; gas leaving the reactor is not analyzed. Thermal degradation of an oxidized MEA solution was carried out in a 2" SS316 pipe reactor with 500 mL volume and Swagelok end caps for sampling.

Analytical Methods

GC-MS and LC-MS methods were used to analyze degraded MEA samples.

Table 4: Summary of Analytical Methods

Instrument	*Column*	*Flowrate*	*Temperature*	*Mobile Phase*
GC-MS	Restek: Stabilwax	30 mL/min	100–320 °C	He
GC-MS	Restek: Rxi-5sil MS	30 mL/min	100–320 °C	He
LC-UV-MS	Phenomenex: Luna 3µm silica	500 ul/min	RT	2-16%H2O in ACN
LC-UV-MS	Shimadzu: C18	500 ul/min	RT	2-20%ACN in H2O

Results

Ammonia Production Rates in the HGF Apparatus

Ammonia production rates for 7 m MEA and other amines were evaluated in the high gas flow apparatus. Figure 1 shows a sample plot for the ammonia production rate over time in a 7 m MEA solution at three temperatures. The rate is evaluated at steady state.

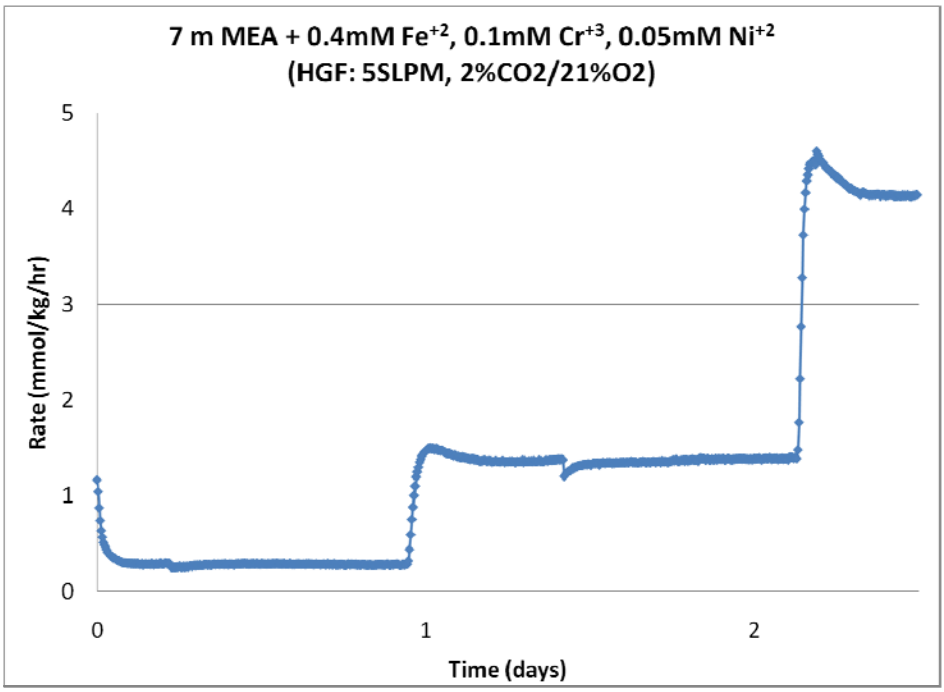

Figure 6: Sample plot for determination of ammonia production rates in the HGF apparatus. Data for 7 m MEA with 0.4 mM Fe, 1 mM Cr, 0.05 mM Ni at 40 °C, 55 °C, and 70 °C

Figure 2 shows a sample plot for the ammonia production rate at 70 °C. The system does not reach a clear steady state at 70 °C due to high volatility losses from the solution and strong dependence of ammonia production on MEA concentration. The system goes through an initial

burst phase where dissolved ammonia is stripped out (first 20–30 minutes), followed by a slow decrease as MEA is stripped out, continuously lowering the ammonia rate over several days. The rate for 70 °C is evaluated immediately following the burst phase.

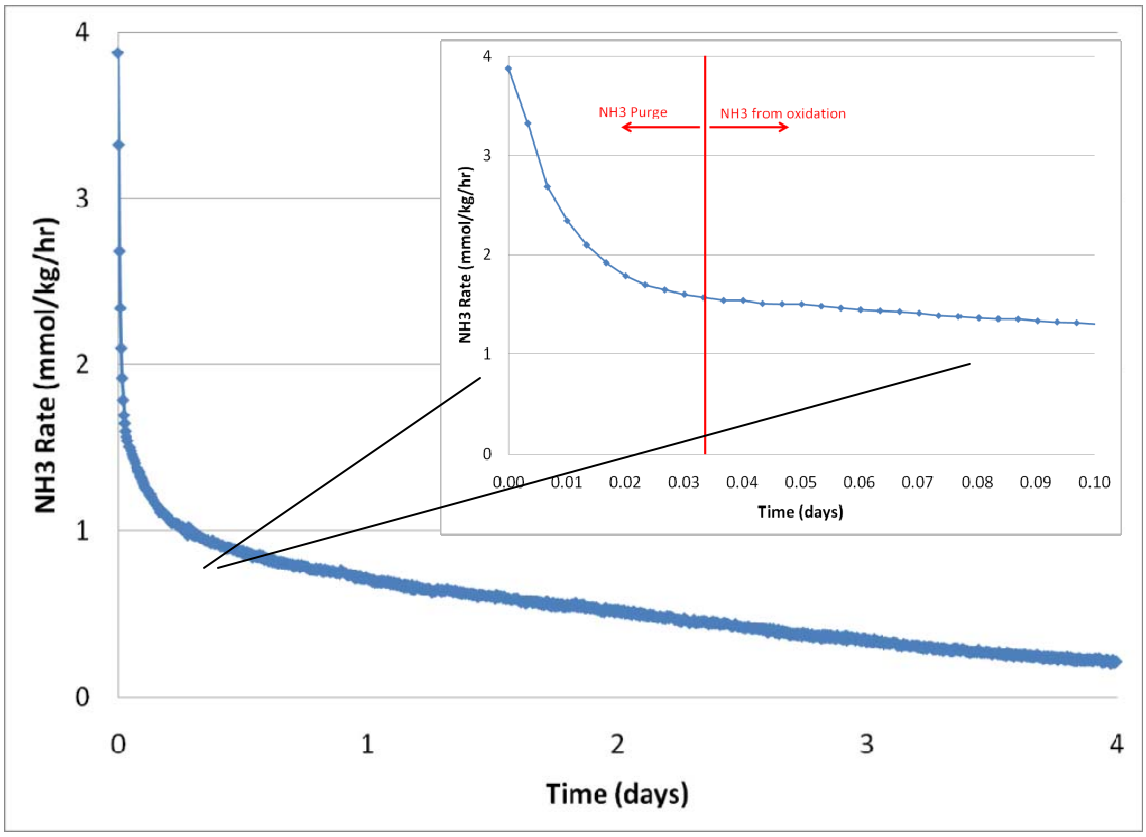

Figure 7: Sample plot for determination of ammonia production rates in the HGF apparatus. Data for 7 m MEA with 50 mM Inh A and 0.4 mM Fe, 0.1 mM Cr, 0.05 mM Ni at 70 °C. The red line indicates a transition from NH3 purging to NH3 production.

Ammonia rates are reported in Figure 8 at two concentrations of Inh A (50 mM, and 100 mM) in the presence of 0.4 mM Fe, 0.1 mM Cr, and 0.05 mM Ni. Each system was exposed to three temperatures (40 °C, 55 °C, 70 °C), which reflects the temperature bulge in a typical absorber (Plaza, 2010). Addition of 10 mM of Inh A appeared to increase the ammonia rate, although this result may reflect some experimental error and should be investigated further. The rates for ammonia production from 7 m MEA are compared with those for 17.7 (65 % wt) DGA®. DGA® did not produce any significant ammonia at 40 °C or 55 °C. At 70 °C the rate increased slowly for several days before reaching steady state. Addition of 100 mM Inh A appeared to increase the rate of ammonia production from the DGA® solution.

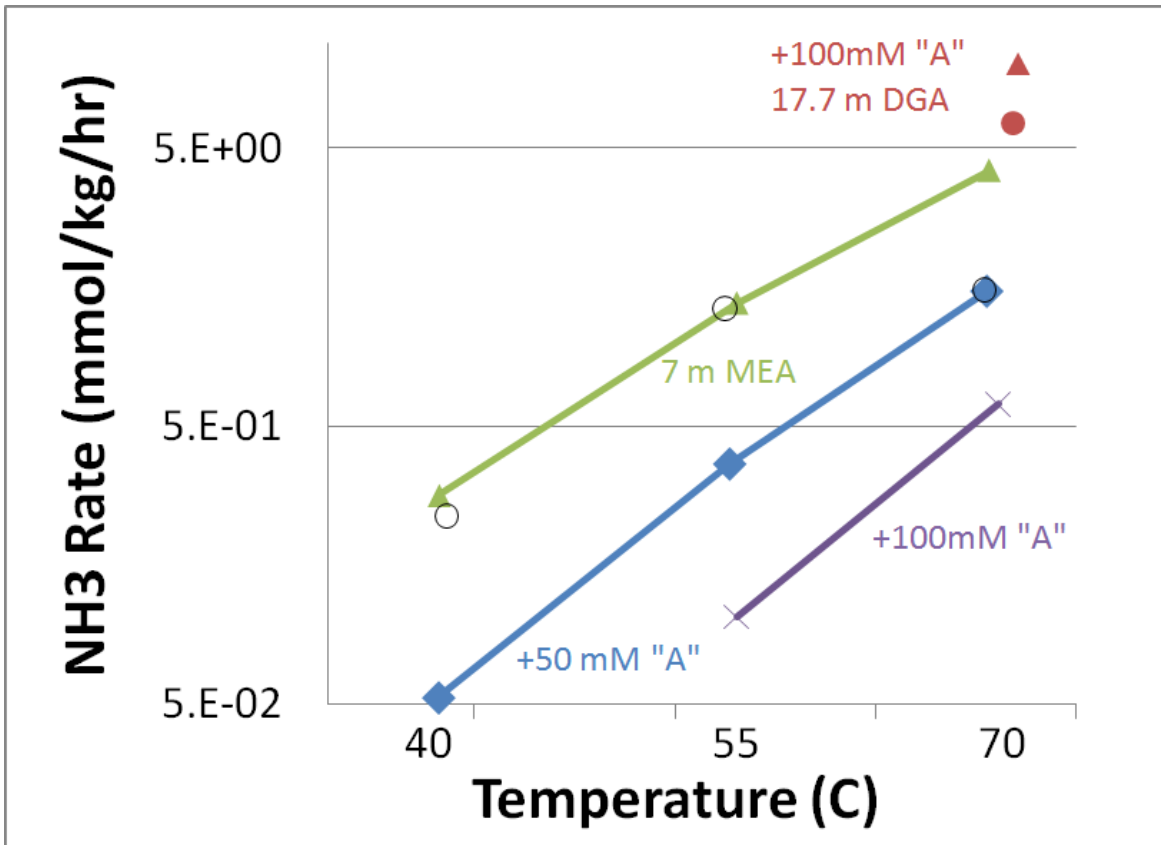

Figure 8: Ammonia rates for 7 m MEA at various temperatures and inhibitor concentrations in the HGF apparatus. Catalyst 0.4 mM Fe, 0.1 mM Cr, 0.05 mM Ni.

Table 5: Activation Energies of Ammonia Production

Inhibitor A added	Activation Energy (J/mol)
0	8.60E+04
50	1.02E+05
100	1.13E+05

Ammonia rates for various MEA concentrations at three temperatures are reported in Figure 9. An increase in MEA concentration appears to have a greater than first order effect on the rate of ammonia production (Figure 10). Ammonia rates are also plotted as a function of inhibitor concentration in Figure 11.

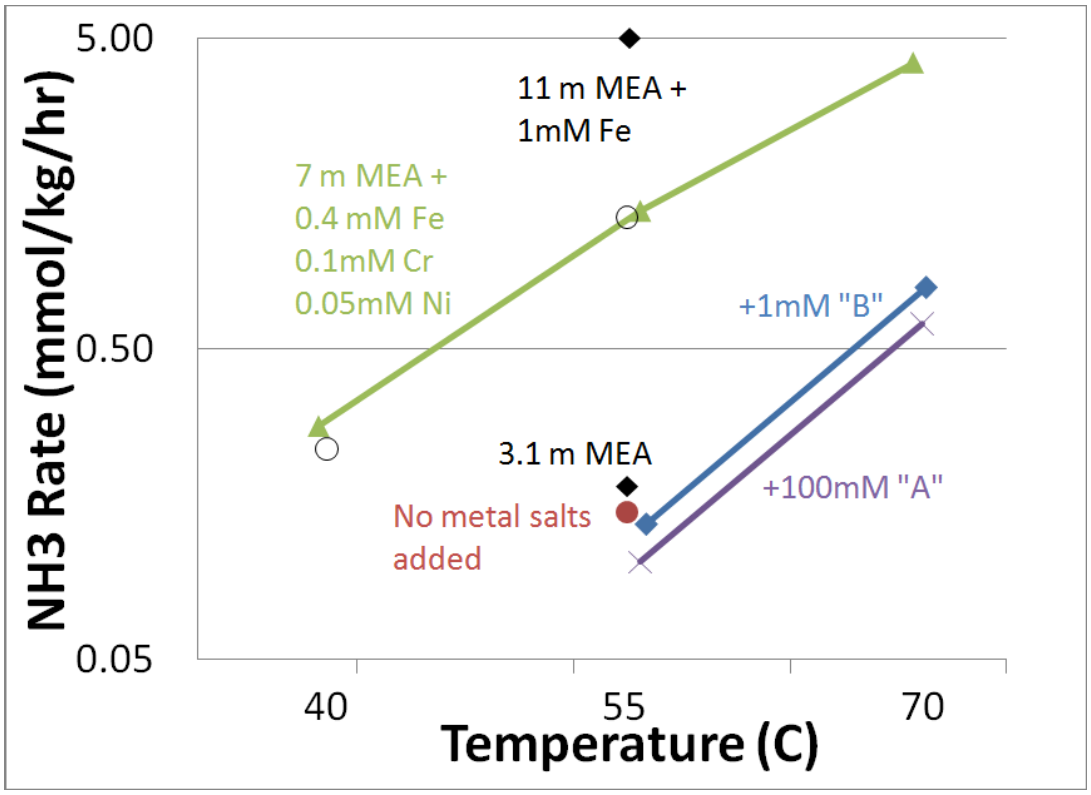

Figure 9: Ammonia rates for 7 m MEA at various temperatures and inhibitor concentrations in the HGF apparatus. Catalyst 0.4 mM Fe, 0.1 mM Cr, 0.05 mM Ni. For Inh B, the initial steady state rate is given.

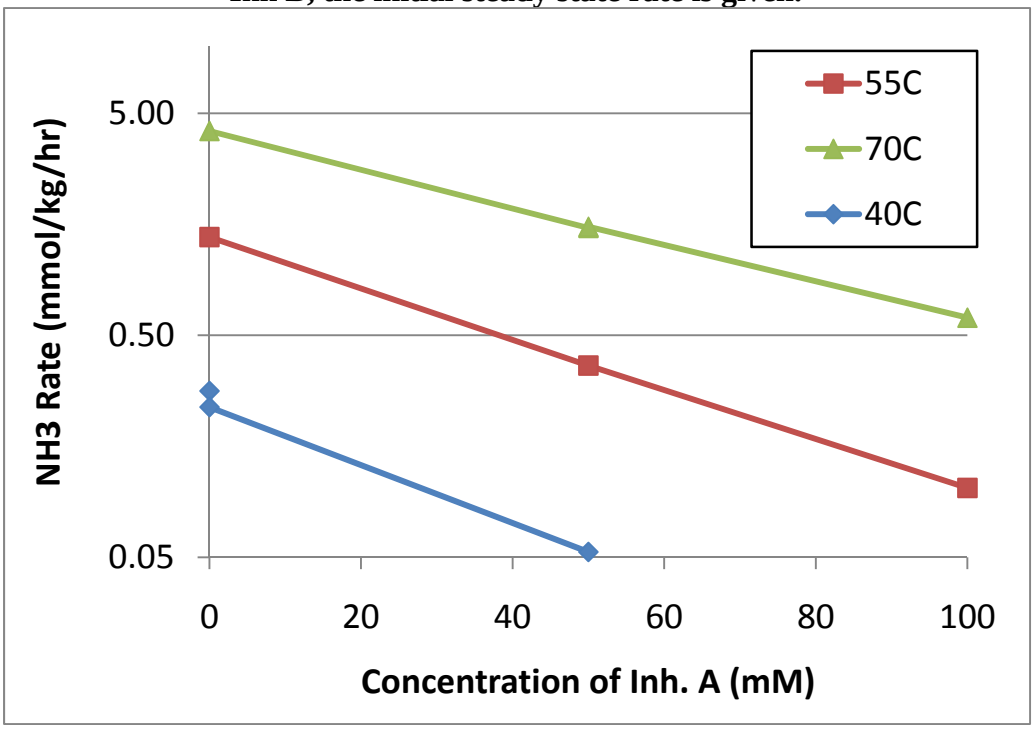

Figure 4: Ammonia rates for 7 m MEA at various temperatures and inhibitor concentrations in the HGF apparatus. Catalyst 0.4 mM Fe, 0.1 mM Cr, 0.05 mM Ni.

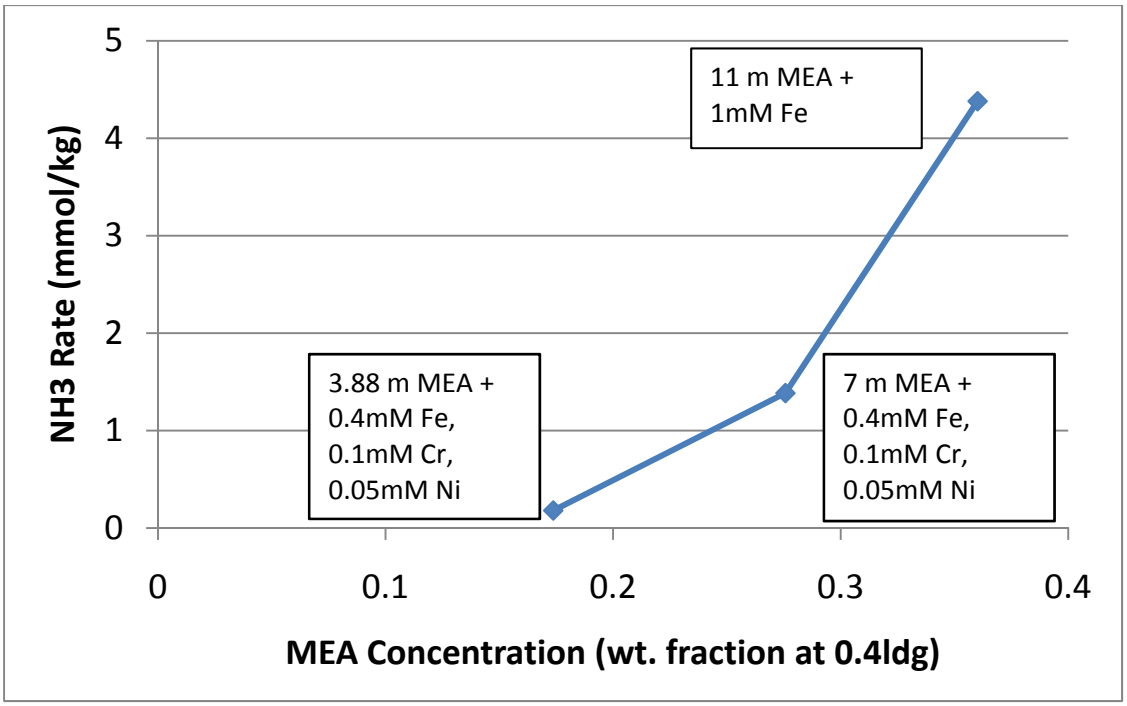

Figure 10: Ammonia rates for various MEA concentrations at 55 °C in the HGF apparatus.

A second inhibitor, Inhibitor B, was also evaluated at a concentration of 1 mM. The inhibitor had a strong effect initially at 55 °C and 70 °C (Figure 9). However, after several hours at 70 °C, this inhibitor began to act as a catalyst and substantially increased the degradation rate (Figure 11). This effect was attributed to a change in the active species in solution. The inhibitor may have changed oxidation states, or formed some complex at the higher temperature. Reduction of the temperature back to 55 °C decreased the rate, although it remained above the base case with no inhibitor. Finally, the rate for 7 m MEA with no metals added is also reported. This demonstrates that addition of a small amount of metal salts to the system can have a significant effect on the ammonia rate. Since industrial systems are assumed to contain trace amounts of metal, this rate is not of practical importance in industry.

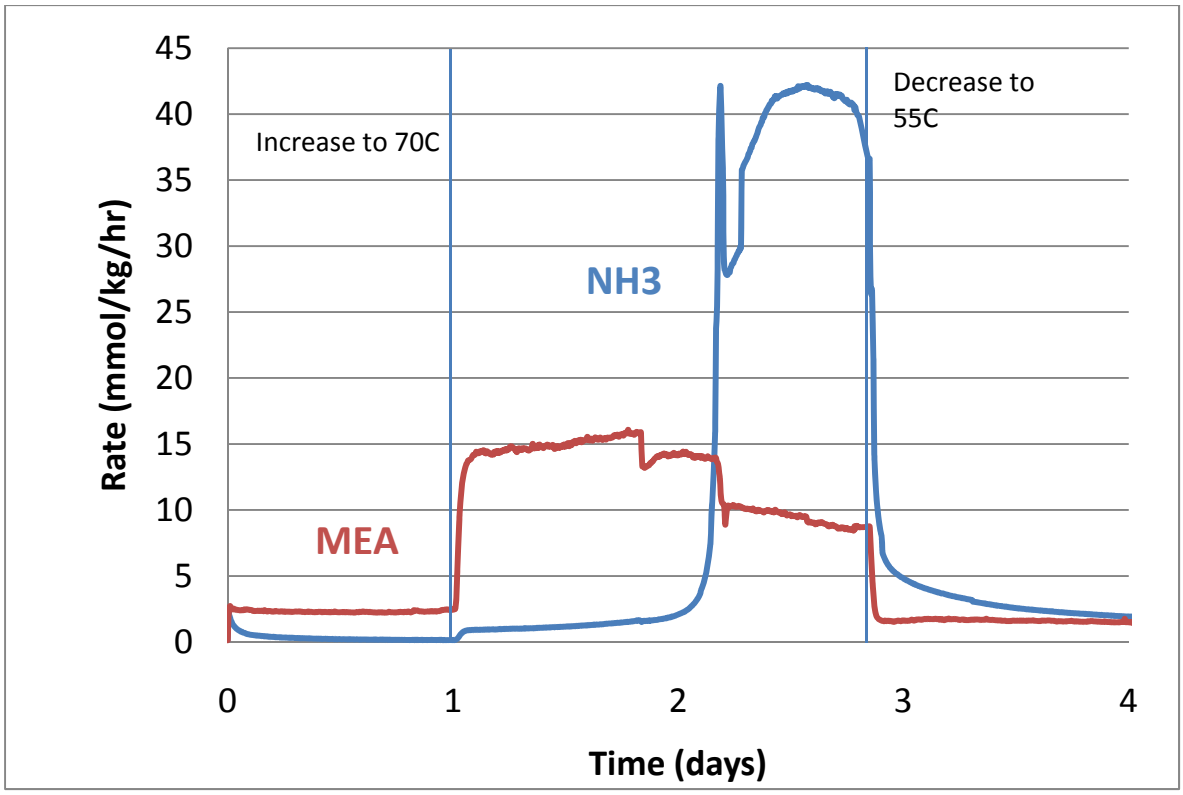

Figure 11: Ammonia Production from 7 m MEA + 1 mM Inh B at 55 °C and 70 °C in the HGF apparatus

Ammonia rates reported previously (Rochelle, 2010a, 2010b) are plotted in Figure 12 for comparison.

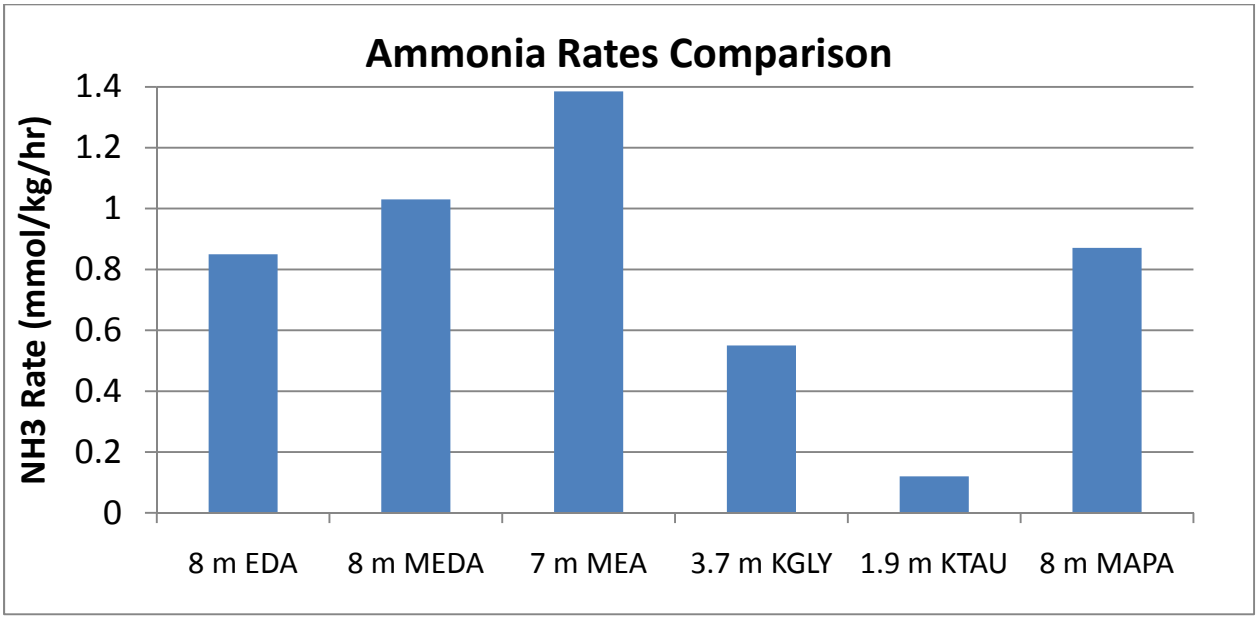

Figure 12: Ammonia Rates for Selected Amines at 55 °C. Other amines tested that did not produce significant amounts of ammonia at 55 °C include: 8 m PZ, 7 m MDEA, 4.8 m AMP, 17.7 m DGA®, and 8 m 1-MPZ.

Table 6: Ammonia Production from 7 m MEA in the HGF apparatus in the presence of 0.4 mM Fe, 0.1 mM Cr, 0.05 mM Ni at various temperatures and inhibitor concentrations

Inhibitor	*Temperature*	*NH3*
--	40.2	0.28
--	40.6	0.24
--	55.5	1.38
--	69.7	4.16
50 mM A	40.2	0.05
50 mM A	55.1	0.37
50 mM A	69.5	1.52
50 mM A	69.4	1.54
100 mM A	55.5	0.10
100 mM A	70.2	0.60

Table 7: Ammonia production rates from various solutions in the HGF apparatus in the presence of metals

Amine	*Concentration (m)*	*NH3 Rate (mmol/kg/hr)*	*Catalyst*
EDA	8	0.85	1 mM Fe
MEDA	8	1.03	1 mM Fe, 0.5 mM Cr, 0.25 mM Ni
K+Gly	3.66	0.55	1 mM Fe
K+Tau	1.9	0.12	1 mM Fe
MAPA	8	0.87	0.4 mM Fe, 0.1 mM Cr, 0.05 mM Ni
MEA	3.88	0.18	1.8 mM Fe, 0.02 mM Ni
MEA	7	1.38	0.4 mM Fe, 0.1 mM Cr, 0.05 mM Ni
MEA	11	4.38	1 mM Fe
PZ, 1-MPZ, MDEA, AMP, DGA®	various	<0.10	1 mM Fe

Liquid Phase Analysis of High Gas Flow Experiments

Initial and final samples of the liquid phase from each experiment were analyzed for the presence of MEA, total nitrogen, total organic carbon, total inorganic carbon, and heat stable salts. These

results are reported in Table 8. "Amine" indicates the amine loss (MEA in all cases except DGA®) calculated by the difference in amine concentration by cation chromatography with methane sulfonic acid elution. "Alkalinity" is the difference in total alkalinity between the initial and final samples by sulphuric acid titration. "NH_3" and "Volatile" are the total amounts of NH_3 and volatile amine detected by the FTIR analyzer over the course of the experiment. Formate, oxalate, nitrate, and nitrite are all detected by anion chromatography with sodium hydroxide elution. All amounts are in units of mmol/kg.

Table 8: Liquid phase analysis of high gas experiments

Experiment	*Amine*	*Alkalinity*	*NH3*	*Volatile*	*Formate*	*Oxalate*	*Nitrate*	*Nitrite*
10 mM A	814	828	201	336	9	1	7	7
50 mM A	648	579	78	692	4	0	2	2
50 mM A r2	1218	1230	56	1174	13	3	2	2
0 mM A	266	153	8	15	1	0	0	1
0 mM A r2	569	501	145	430	23	6	3	7
100 mM A	259	172	12	329	0	0	0	0
1 mM B	1932	1901	833	694	340	33	1	4
DGA®	1955	1804	624	611	255	52	8	14

Product Identification

LCMS Chromatograms

Chromatograms are provided for a sample of degraded MEA, which was oxidized in the LGF apparatus at 55°C in the presence of 98%O_2/2%CO_2 for two weeks. The sample was run using HILIC-mode chromatography (Figure 13) and standard reverse-phase chromatography (Figure 14). Table 8 provides a list of peak retention times.

Table 9: Retention Times for Masses Observed on LCMS

M+H	C18 Ret. Time	3um Silica Ret. Time	ESI MS-MS Major Peaks
200	11.09	7.27	182, 157, 139, 113, 69
129	3.88	24.00	85, 69, 111
113	13.92	21.37	69, 45, 81, 54
83		2.64	
151		2.12	
216	8.12	17.94	
62	3.47	24.82	44, 45, 43

The compound with parent m+h = 200 was analyzed by high resolution mass spectrometry. The exact mass was determined to be 200.1033 which likely corresponds to a compound with the formula $C_8H_{14}N_3O_3^+$ (mass = 200.10297). The unprotonated compound would have one fewer protons and a mass of 199. Other masses were too light to be observed on the high-res instrument.

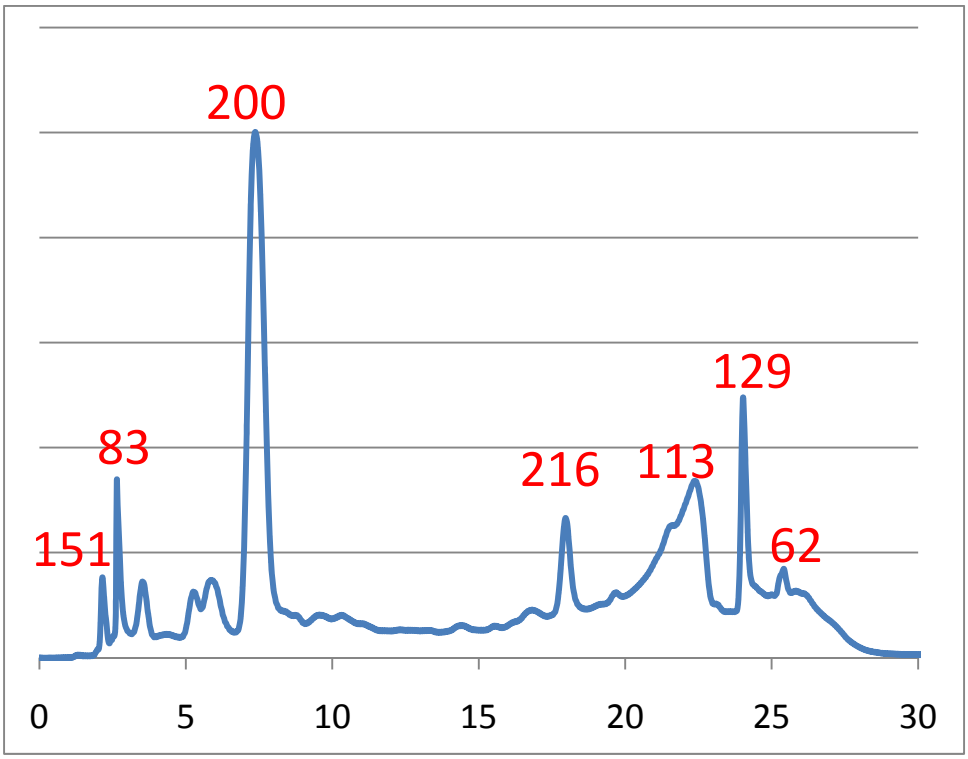

Figure 13: LC-UV chromatogram using 3um Silica Column

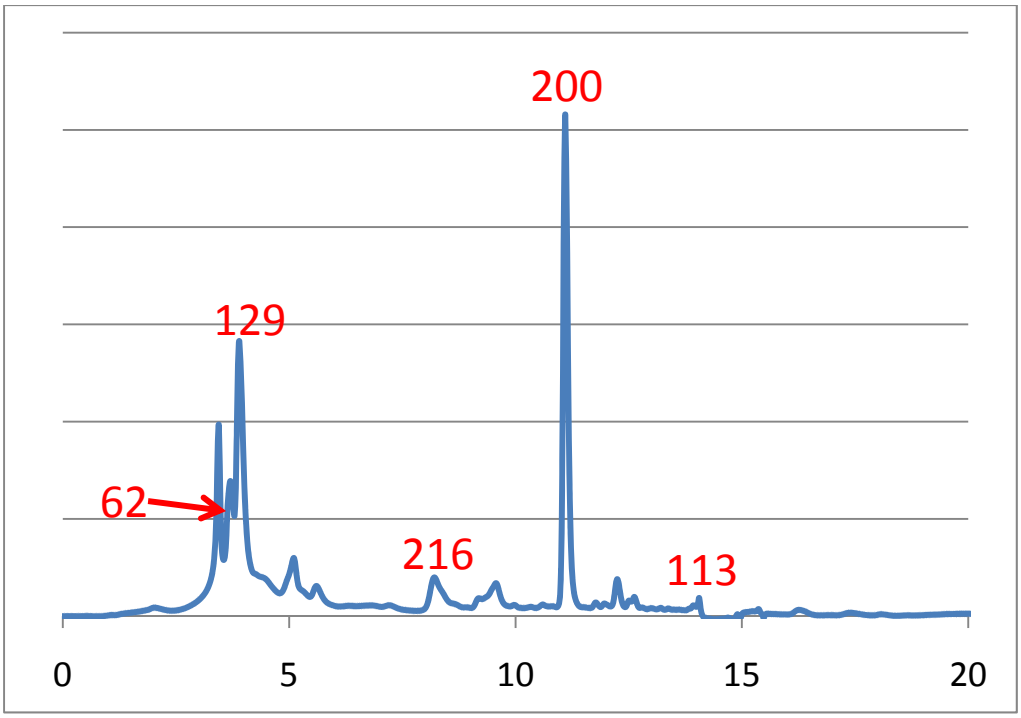

Figure 14: LC-UV chromatogram using C18 Column

Direct infusion to an MS-MS system using a syringe pump was used to identify m+h peaks in a degraded MEA sample (Figure 15). Table 9 provides a summary of the mass spectra collected for major peaks using collision induced dissociation.

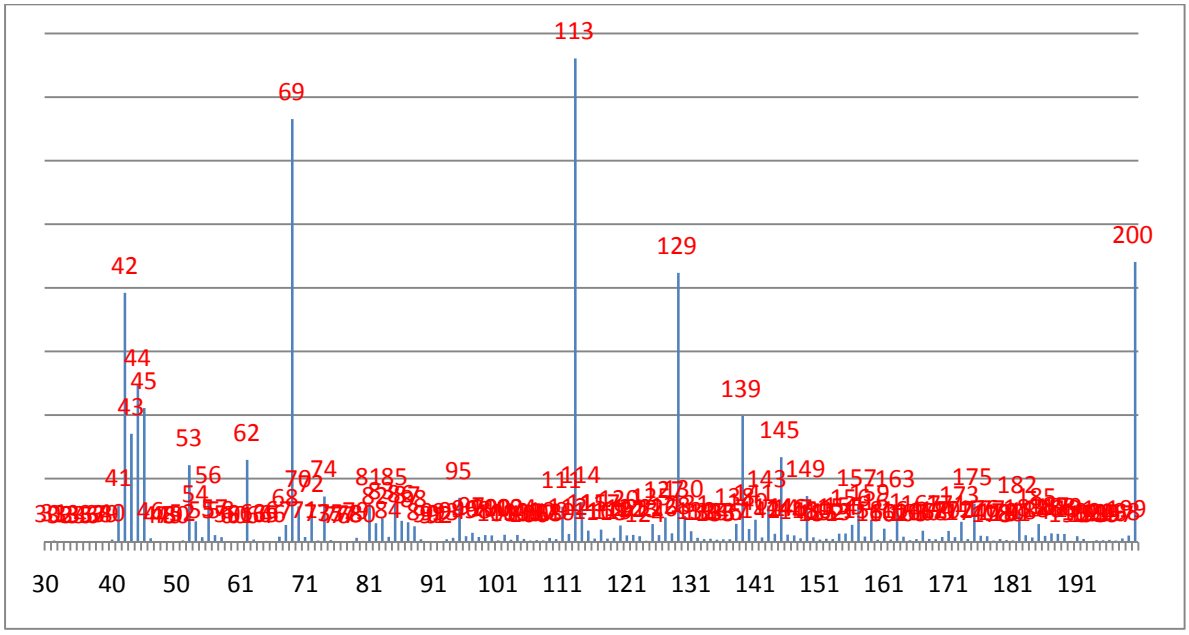

Figure 15: Syringe Infusion of Oxidatively Degraded MEA

Table 10: Mass Spectrum Peaks of Selected Peaks in Oxidatively Degraded MEA produced using ESI MS-MS (CID)

Parent m+h	Major fragments	Suspected Compound
129	111, 85, 69, 83, 45, 72, 56	hydroxyethyl imidazolone
113	69, 45, 42, 81, 54	hydroxyethyl imidazol
62	45, 44, 43	ethanolamine
200	157, 139, 182, 138, 113, 69	substituted imidazol
90	73, 55, 43, 45, 58	MEA-formate ester OR MEA-formate amide
87	44, 70, 85, 42	piperazine
145		hydroxyethyl piperazine
85	68, 67, 41, 40	imidazolone
139	95, 121, 68, 69, 79, 54, 42	substituted imidazol

GCMS Chromatograms:

Chromatograms for 3 different samples analyzed on two different columns are provided. Tables 10 and 11 provide an overview of the samples analyzed and the peaks observed. The largest degradation products (1–3) are observed for all three samples (Figures 16–21).

The Inh A sample has significantly lower levels of all degradation products. The high gas/11 m MEA sample has a higher MEA peak and smaller product peaks than the low gas/7 m sample, but larger product peaks than the Inh A/low gas sample. The high oxygen concentration in the low gas apparatus enhances degradation of the amine.

Table 11: GCMS Peak Summary

Peak #	Non-polar RT (min)	Polar RT (min)	Possible Compound	Parent Mass
1	21.10	5.39	trimethylamine	59
2	21.75	6.15	2-oxazolidone	87
3	23.19	8.62	1-(2-hydroxyethyl)-imidazole	112
4		6.20	ethanolamine	61
5	17.67		imidazole	68

Table 12: Summary of Samples Analyzed

Amine	Apparatus	Catalyst Added	Inhibitor	MEA Loss (%)
7 m MEA	LGF	0.4 mM Fe, 0.1 mM Cr, 0.05 mM Ni	none	35
11 m MEA	HGF	1 mM Fe	none	15
7 m MEA	LGF	0.4 mM Fe, 0.1 mM Cr, 0.05 mM Ni	100 mM Inh A	<5

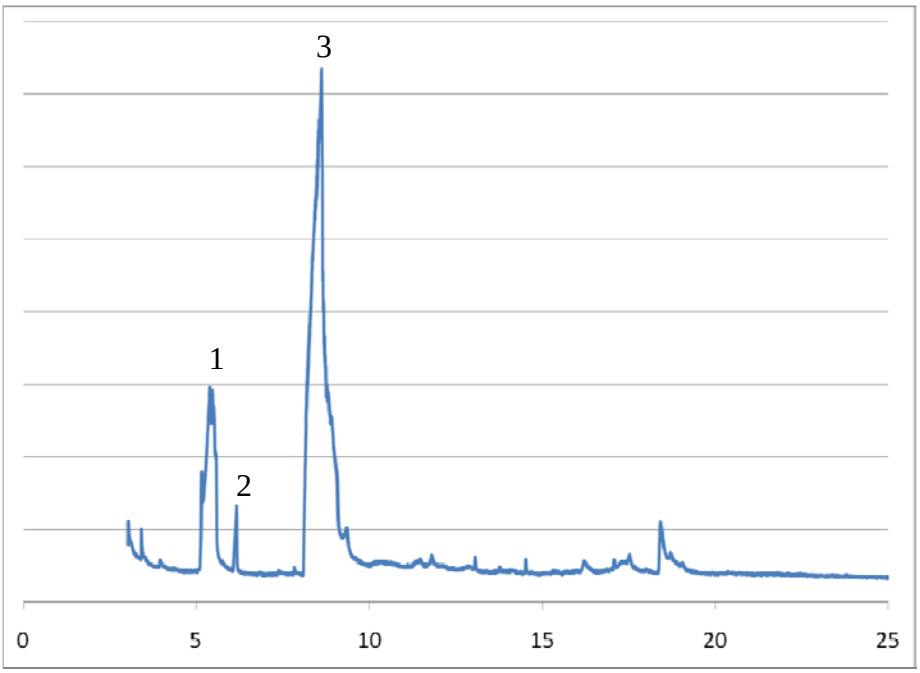

Figure 16: GC-MS chromatogram using poly-siloxane column for MEA degraded in the low gas apparatus

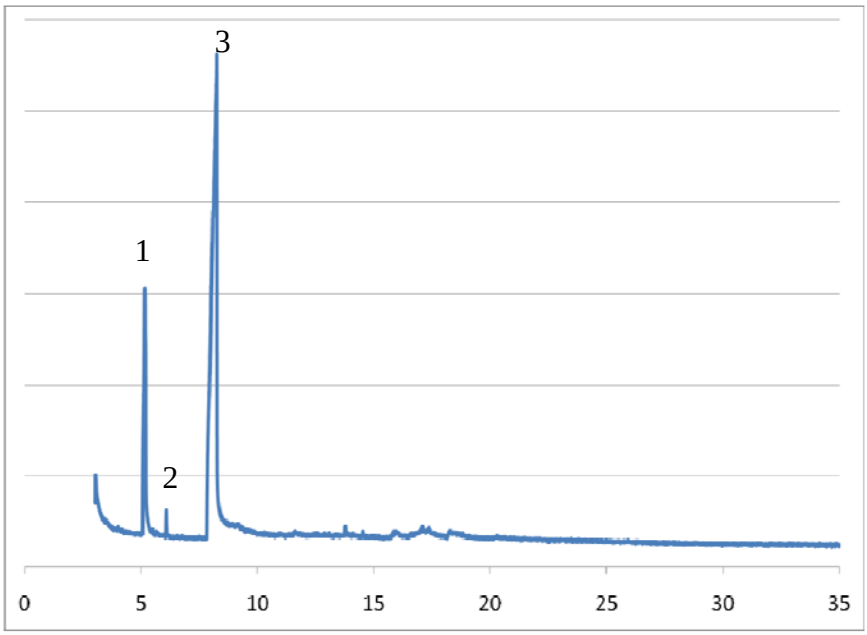

Figure 17: GC-MS chromatogram using poly-siloxane column for MEA degraded in the high gas apparatus

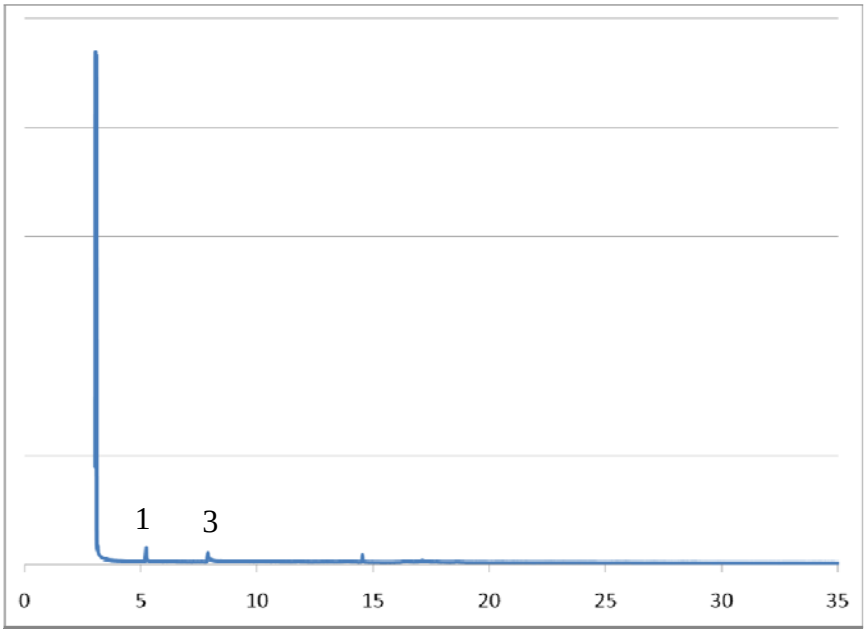

Figure 18: GC-MS chromatogram using poly-siloxane column for MEA degraded in the low gas apparatus with Inh A

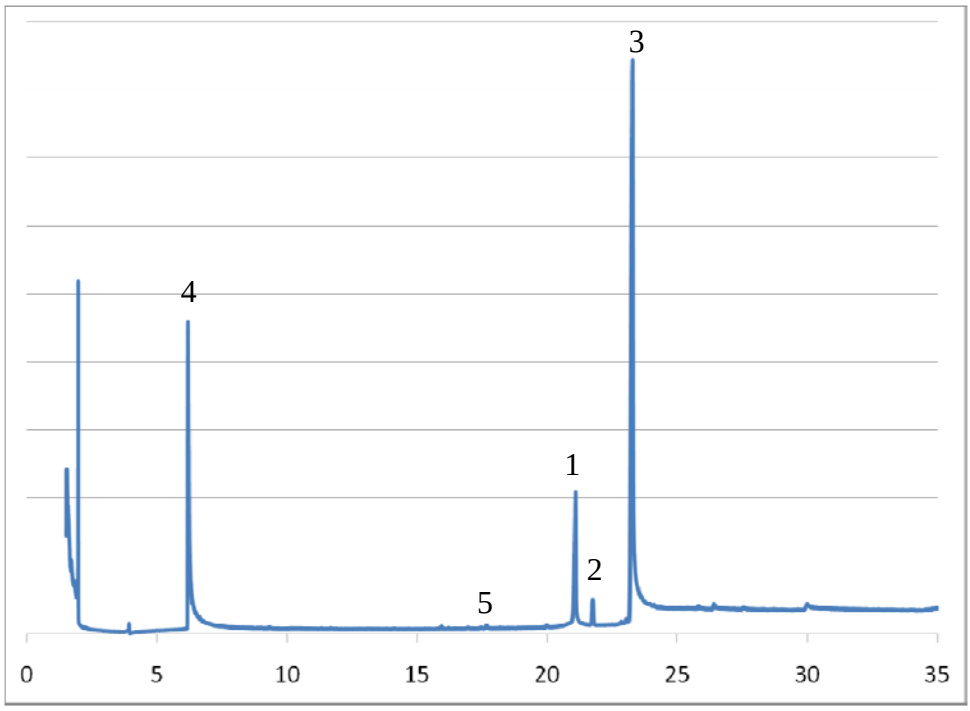

Figure 19: GC-MS chromatogram using Stabilwax column for MEA degraded in the low gas apparatus

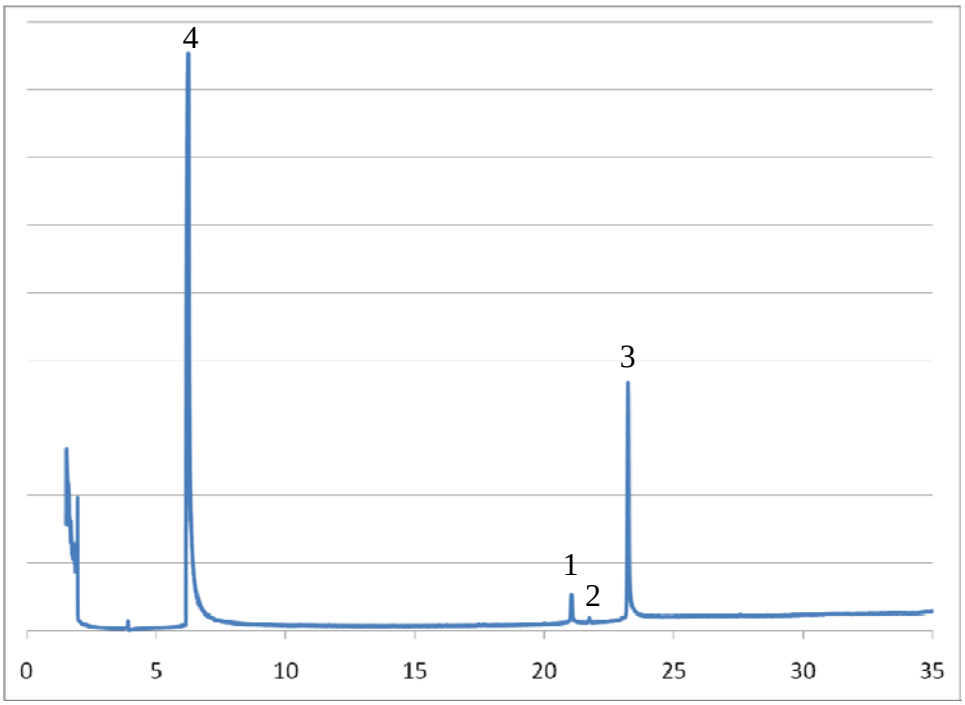

Figure 20: GC-MS chromatogram using Stabilwax column for MEA degraded in the high gas apparatus

Table 13: Summary of Peaks Observed on GC-MS

m+h	Suspected Compound	GC Retention Times (min)
60	trimethylamine	5.39, 21.10
62	ethanolamine	6.20
69	imidazole	17.67
85	1,3-dihydro-imidazolone	
88	2-oxazolidone	6.15, 21.75
113	1-(2-hydroxyethyl)-imidazole	8.62, 23.19

Cyclic Degradation

MEA was sequentially degraded oxidatively and thermally. The results confirmed that MEA loss during thermal degradation at 135 °C (as measured by cation chromatography) is not affected by prior oxidation (Figure 21).

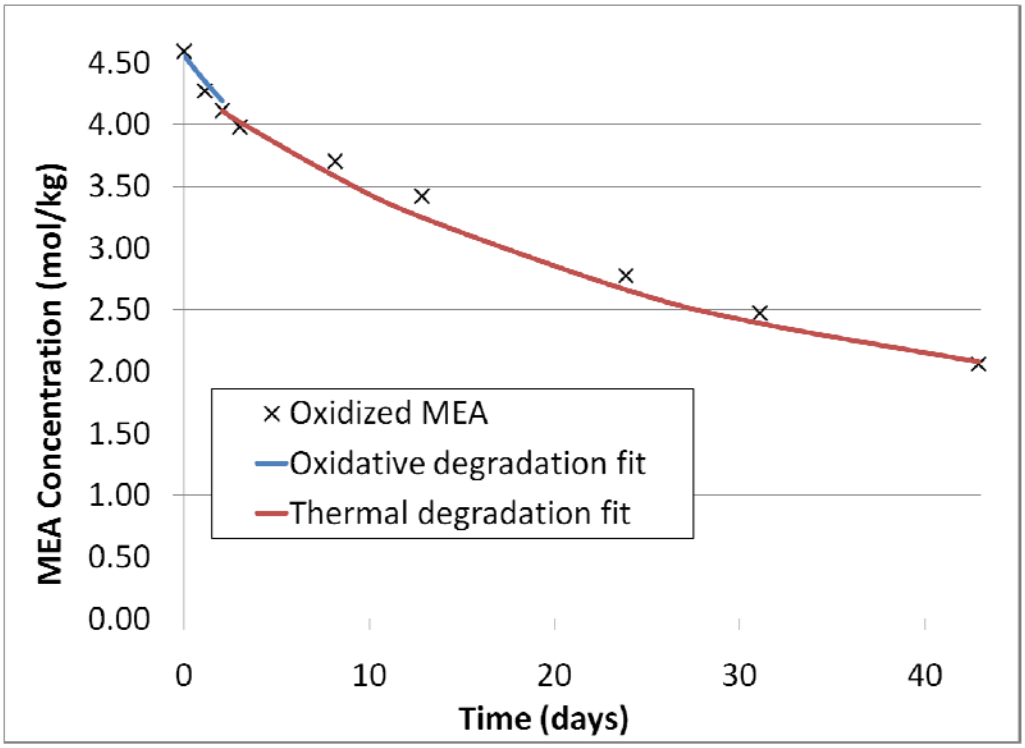

Figure 21: Thermal degradation of an oxidized 7 m MEA solution. Oxidation: LGF, 2% CO_2/98% O_2, 100 mL/min, 55 °C. Thermal degradation: 135 °C. The red and blue lines are the expected concentrations for neat solutions based on previous work (Davis, 2009; Rochelle, 2010).

Concentrations of some oxidation products were also monitored during oxidative and thermal degradation. At 135 °C, formamide was converted to formate until both species reached equilibrium (Figure 22).

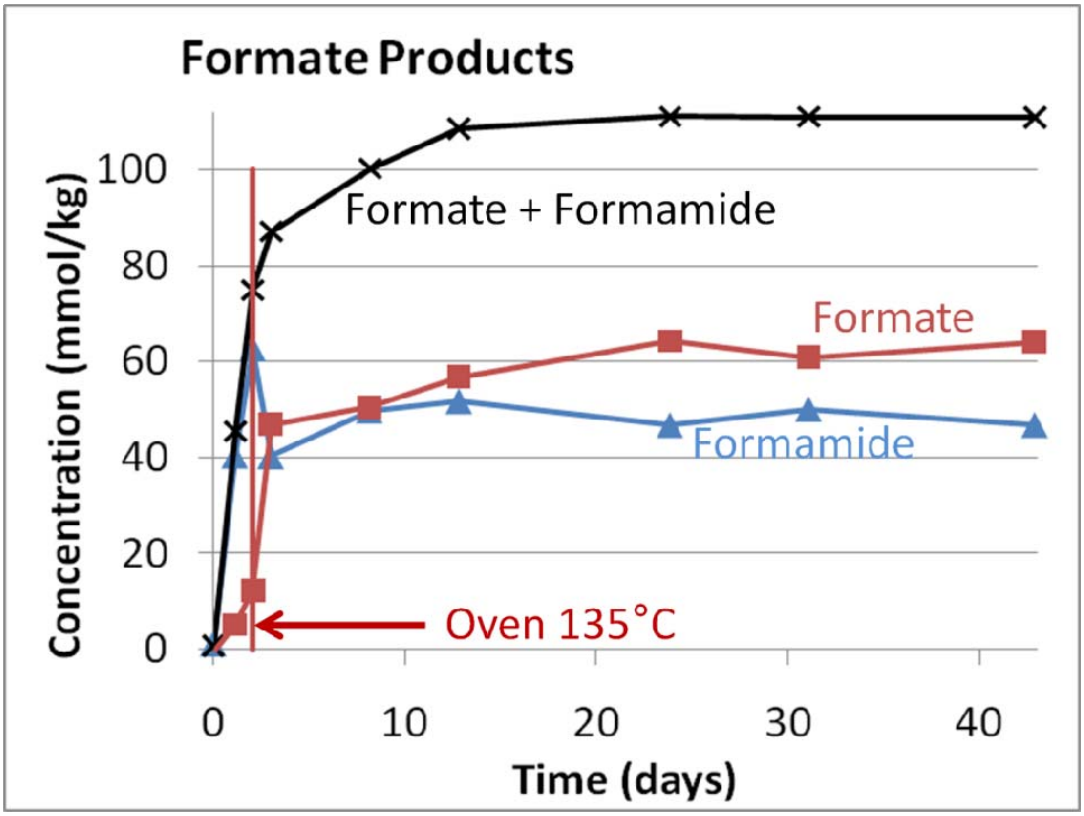

Figure 22: Fate of formate products of oxidation at high temperature. Oxidation: LGF, 2% CO_2/98% O_2, 100 mL/min, 55 °C. Thermal degradation: 135 °C.

Oxalamide was converted to oxalate, which was, in turn, converted to formate (Figure 23).

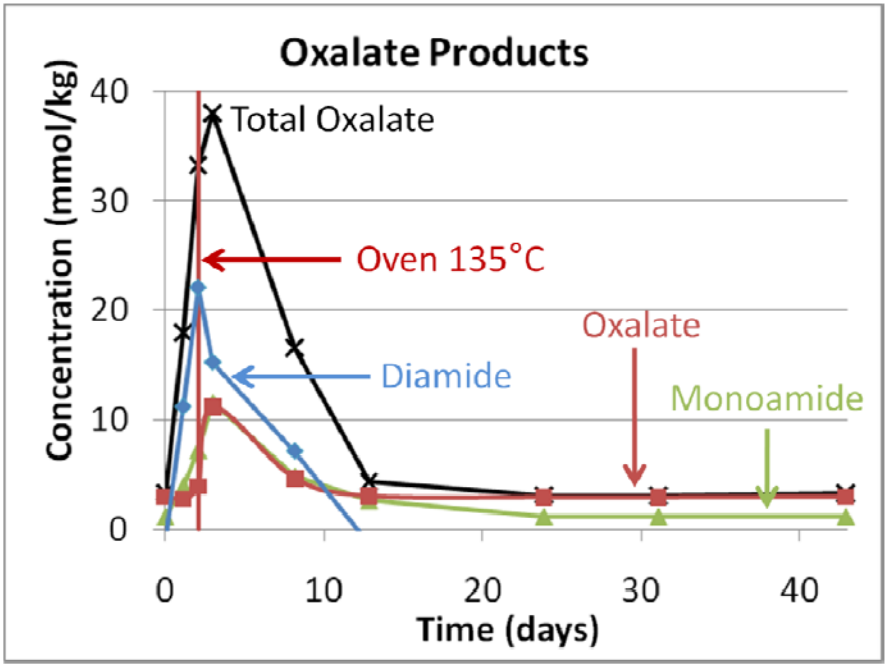

Figure 23: Fate of oxalate products of oxidation at high temperature. Oxidation: LGF, 2% CO_2/98% O_2, 100 mL/min, 55 °C. Thermal degradation: 135 °C.

Nitrate was stable at 135 °C, but nitrite disappeared after less than 24 hours (Figure 24).

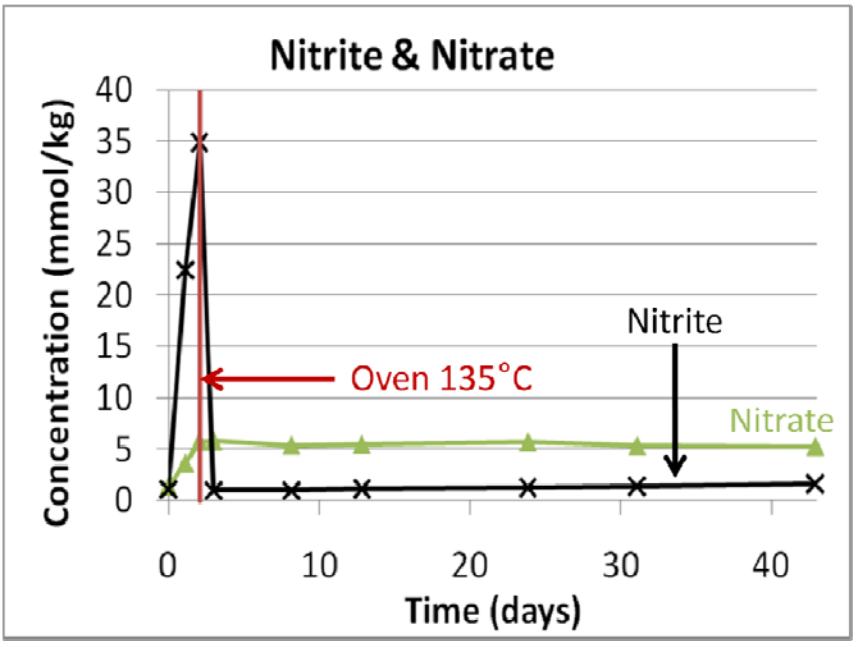

Figure 24: Fate of nitrate and nitrite at high temperature. Oxidation: LGF, 2% CO_2/98% O_2, 100 mL/min, 55 °C. Thermal degradation: 135 °C.

The nitrite likely reacted with MEA to form ethylene glycol and molecular nitrogen (1).

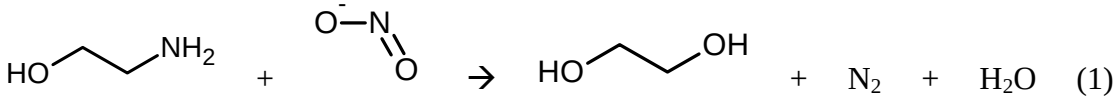

Additional details of this experiment are provided in Tables 12 and 13.

Table 14: Concentrations of heat stable salts during successive oxidation and thermal degradation. Oxidation: LGF, 2% CO_2/98% O_2, 100 mL/min, 55 °C. Thermal degradation: 135 °C.

Time	Formate	Oxamate	Nitrite	Oxalate	Nitrate	Formamide	Oxalamide	Temp
0.00	-0.4	1.2	1.1	3.0	1.4	1.2	-0.8	55
1.13	5.1	4.0	22.5	2.8	3.6	40.3	11.2	55
2.06	12.3	7.3	34.8	3.9	5.7	62.7	22.1	55
3.00	46.8	11.6	1.0	11.2	5.8	40.2	15.3	135
8.16	50.4	4.8	1.0	4.6	5.4	49.8	7.1	135
12.83	56.8	2.6	1.1	3.0	5.4	51.8	-1.3	135
23.85	64.3	1.2	1.3	2.9	5.6	46.8	-1.0	135
31.08	60.9	1.2	1.4	2.9	5.3	50.1	-1.0	135
42.89	64.1	1.2	1.6	3.0	5.3	46.8	-0.9	135

Table 15: Concentrations of MEA, alkalinity, and total inorganic carbon (TIC) during successive oxidation and thermal degradation. Oxidation: LGF, 2% CO_2/98% O_2, 100 mL/min, 55 °C. Thermal degradation: 135 °C.

Time	MEA (mol/kg)	Alkalinity (mol/kg)	TIC (mol/kg)
0.00	4.593	4.166	1.947
1.13	4.272	4.034	1.835
2.06	4.111	3.801	1.714
3.00	3.979	3.899	1.757
8.16	3.702	3.736	1.756
12.83	3.421	3.517	1.672
23.85	2.778	3.228	1.438
31.08	2.473	2.959	1.343
42.89	2.063	2.621	1.289

Future Work

Future work will focus on developing analytical (LC and GC) methods for identifying and quantifying unknowns in degraded samples, as well as further study of ammonia rates in the HGF apparatus.

References

Goff G. *Oxidative Degradation of Aqueous Monoethanolamine in CO_2 Capture Processes: Iron and Copper Catalysis, Inhibition, and O_2 Mass Transfer*. The University of Texas at Austin. Ph.D. Dissertation. 2005.

Plaza JP, Chen E, Rochelle GT. Absorber intercooling in CO_2 absorption by piperazine-promoted potassium carbonate. *AIChE J*.2010;56(4):905–914.

Rochelle GT et al. "CO_2 Capture by Aqueous Absorption, Fourth Quarterly Progress Report 2009". Luminant Carbon Management Program. The University of Texas at Austin. 2010a.

Rochelle GT et al. "CO_2 Capture by Aqueous Absorption, First Quarterly Progress Report 2010". Luminant Carbon Management Program. The University of Texas at Austin. 2010b.

Rooney PC, DuPart MS, Bacon TR. "Oxygen's Role in Alkanolamine Degradation". *Hydroc Proc*. Int. Ed. 1998;77(7):109–113.

Sexton A. *Amine Oxidation in CO_2 Capture Processes*. The University of Texas at Austin. Ph.D. Dissertation. 2008.

Nitrosamine Formation in CO_2 Capture by Piperazine

Quarterly Report for April 1 – June 30, 2010

by Mandana Ashouripashaki

Supported by the Luminant Carbon Management Program

and the

Industrial Associates Program for CO_2 Capture by Aqueous Absorption

Department of Chemical Engineering

The University of Texas at Austin

July 5, 2010

Abstract

Secondary amines in the presence of nitrite and nitrate ions, through a nitrosation reaction, can form carcinogenic products called nitrosamines. Nitrosation reactions have been known for over 150 years but their carcinogenic properties were first discovered in 1956 and since then there has been an explosion of interest in their chemistry and particularly in methods of destroying them. Piperazine (PZ) is an amine of interest in our study and nitrosation products of PZ are N-nitrosopiperazine and N-N, dinitrosopiperazine.

The available methods for detecting nitrosamines are not applicable for dinitrosopiperazine (DNPZ) because of its lack of volatility. In this quarter, standard dinitrosopiperazine that has been synthesized in the lab was injected directly to determine if DNPZ can be detected by mass spectrometry. We found that using a mixture of methanol and water as a solvent gave us the best result for the detection of DNPZ.

A method has been developed for quantifying DNPZ with liquid chromatography followed by mass spectrometry (LC-MS). The primary results are expressed in the current report.

Introduction

The kinetics of PZ demonstrates that it is an effective promoter for carbon dioxide removal from gas streams. The rate constant is an order of magnitude higher than a primary amine (Bishnoi, 2000), but the reaction between PZ and nitrite or NOx may cause nitrosopiperazine formation.

The purpose of this research is to develop the analytical methods for detecting, measuring, and also monitoring nitrosamines, especially dinitrosopiperazine, in CO_2 capture using PZ.

The methodology for nitrosopiperazine analysis includes several steps: sample collection, extraction, detection, measuring, and determination of nitrosopiperazine.

To determine nitrosamine production in CO_2 capture, a method will be necessary that can work in alkaline solution. This research will develop a method to detect dinitrosopiperazine using a

combination of mass spectrometry and HPLC in non-biological conditions and in both liquid and gas phases.

Standard pure dinitrosopiperazine solution is required to calibrate the instrument, and this is not available for purchase so it was synthesized using the USP 24 2000 method. This method uses PZ citrate ($2C_6H_8O_7$, 3C4H10N2) and sodium nitrite ($NaNO_2$) in presence of hydrochloric acid (HCl).

During the past two quarters the nitrosation reaction of PZ citrate and PZ at different pH values have been examined. Results were in a maximum pH range between 2 and 4. As expected, there was no evidence of nitrosamine in a high pH or alkaline environment, but according to the literature (Keefer and Roller, 1973; Kunisaki and Hayashi, 1978), aldehydes can catalyze a nitrosation reaction in an alkaline medium. Therefore a qualitative study on the reaction between PZ and piperazine citrate with sodium nitrite in the presence of different concentrations of formaldehyde at a temperature range of 20–98 °C has been done to observe the effect of aldehyde concentration and temperature on nitrosation reaction.

The investigation started with direct injection of a solution of dinitrosopiperazine in methanol as suggested by Attalla et al. (2010) but further experiments led us to change the solvent to a mixture of water and methanol to achieve better detection of DNPZ. Methanol must be used because DNPZ is not soluble in water. DNPZ is first dissolved in methanol then diluted by water and injected into the MS.

A method of establishing the calibration curve and sensitivity for DNPZ by liquid chromatography-mass spectrometry (LC-MS) is under investigation.

Theory of nitrosation reaction

The most regularly used reagent for nitrosation is nitrous acid, generated in aqueous acid solution from a nitrite salt, typically sodium nitrite. Nitrous acid exists in aqueous solution in equilibrium with dinitrogen trioxide $\boldsymbol{N_2O_3}$, Equation 1, an effective nitrosating species which can be observed as nitrosonioum nitrite Equation 2.

$$2HNO_2 \rightleftarrows N_2O_3 + H_2O \quad (1)$$

$$N_2O_3 + Amine \rightarrow {}^{+}Amine - NO + NO_2^- \quad (2)$$

The rate equation, Equation 3, has been established for a range of amines.

$$Rate = k[HNO_2]^2[A] \quad (3)$$

This is the rate equation expected for rate limiting attack by an equilibrium concentration of N_2O_3 on amine, and the third order rate constant k in Equation 3 is given by$k_2k_{\mathbf{N_2O_3}}$, where k_2 is the second order rate constant for N_2O_3 attack and $k_{\mathbf{N_2O_3}}$ is the equilibrium constant for N_2O_3formation.

In a CO_2 capture plant using PZ, the pH of the system is high, so the acidic condition which promotes formation of N_2O_3 as a most important nitrosation reagent is not available but there are some sources of nitrate and nitrite ions in different sections of the plant. There are some reports of nitroso-compound formation from inorganic nitrates. Normally a nitrite ion has no

capacity for effecting nitrosation. However, in the presence of some carbonyl group containing catalysts, nitrosation can be achieved in neutral and basic solution.

Catalysts include formaldehyde, chloral, benzaldehyde derivatives, and pyridox. Reaction 4 is particularly effective for the conversion of secondary amines to nitrosamines.

$$\begin{aligned} &R_2NH + R'CHO \overset{OH^-}{\longleftrightarrow} R_2N^+ = CHR' + \mathrm{H_2O} \\ &R_2N^+ = CHR' + NO_2^- \rightarrow R_2N - CHR'ONO \\ &R_2N - CHR'ONO \rightarrow R_2NNO + R'CHO \end{aligned} \qquad (4)$$

Product formation was efficient with the formation of an iminium ion intermediate, which reacts with nitrite ions giving a dialkilamino nitrite ester which breaks down rapidly and intramolecularly to give nitrosamine and regenerate the catalyst. This pathway has been suggested for the reaction of secondary amines with solid sodium nitrite in halogenated solvents (Roller et al., 1980).

In the previous quarter, nitrosamine formation from piperazine citrate and piperazine in acidic medium was investigated and the effect of formaldehyde on nitrosation reaction of piperazine citrate in absorber temperature range has been examined. In this quarter the effect of catalytic property of formaldehyde on piperazine nitrosation in the temperature range of 20–98 C has been demonstrated.

Experimental Methods

The fundamental procedure for all experiments follows USP 24 for nitrosation reaction of piperazine citrate.

Nitrosation reaction of piperazine citrate and piperazine in presence of formaldehyde

A solution of 2 gram PZ and piperazine citrate with 10 ml of sodium nitrite (1/2 V) was prepared. pH of the solutions have been measured by pH meter, which are listed in Table 1. At the experimental condition there was no evidence of any reaction between these reagents, but by adding formaldehyde and changing the pH, a nitrosation reaction began. Experiments were conducted with different concentrations of formaldehyde (various pH) and in temperature ranges of 20–60 °C for piperazine citrate nitrosation and 20–98 °C for nitrosation of piperazine. Results are shown in Tables 2 and 3 and Figures 1 and 2.

These reactions have been investigated because there is some evidence of aldehyde in amine degradation products, and aldehyde can be an intermediate product of the reaction between CO_2 and monoethanolamine (MEA).

Table 1: The reaction conditions for nitrosation of piperazine citrate and piperazine in presence of formaldehyde

		Sodium Nitrate ***(5 M)***	***pH*** **"**In starting point of reaction**"**	***Formaldehyde*** ***37%***	***Temperature***
Piperazine citrate	***2 gr*** ***(6.2 mmole)***	***50 mmole***	***8.2***	***0-200 mmole***	***20–60 °C***
Piperazine	***2 gr*** ***(23.5 mmole)***	***50 mmole***	***10.45***	***0-270 mmole***	***20–98 °C***

Direct injection of dinitrosopiperazine (DNPZ) to Mass Spectrometry

Mass Spectrometry (MS) is an analytical technique for determination of the elemental composition of a sample or molecule. The instrument consists of three main sections:

1. Ion source which converts gas phase sample molecules into ions;
2. Mass analyzer that sorts the ions by their masses by applying electromagnetic fields;
3. Detector, which measures the value of an indicator quantity and provides data for calculating the abundances of each ion present.

Here is a short explanation of the keywords that appear later in this report;

Direct Injection: Using the syringe pump that can be connected directly to the ion source to provide a steady state introduction of sample or tuning and calibrating solution.

Fragmentation: Breaking molecules to specific ions. Fragmentation pattern has led to mass spectra being used as "fingerprints" for identifying compounds.

According to the suggested method (Atalla et al., 2010) for detecting dinitrosopiperazine, samples of 0.00007–0.7 mmol dinitrosopiperazine per ml methanol have been injected to MS directly to see if MS can detect it. The mass spectrum diagram is shown in Figure 3.

When there was not any evidence of DNPZ in mass spectrum of above injections, water was added to the solution and in this case DNPZ could be detected by MS. To obtain more accurate results, the fragmentation method has been run with results shown in Figures 4, 5, 6, and 7.

For quantifying DNPZ, an LC-MS system has been used; the method of measurement was developed by employing a reverse phase column.

Solutions of 500 ppm piperazine (PZ), dinitrosopiperazine (DNPZ), and (DNPZ + PZ) in 80% methanol (MeOH) and 20% water have been injected to the LC-MS, and primary results are shown in Figures 8–16.

Results

Catalytic effect of formaldehyde on nitrosation reaction

Tables 2 and 3 show the results of nitrosation reaction of piperazine citrate and piperazine in the presence of formaldehyde (different pH). At acidic conditions, amine is protonated and NO^-, a nitrosating reagent, is released form nitrite. Therefore it is expected that nitrite ion with piperazine will react to N-Nitrosopiperazine and N, N–Dinitrosopiperazine. This reaction will not happen at alkaline conditions without catalysis by formaldehyde.

pH of solution has been measured by a pH meter in each batch of experiments. In the absence of formaldehyde, reaction mixture of PZ has a pH of 10.45 which is in alkaline range but by adding formaldehyde, pH goes down. The formaldehyde volume in solution was increased step by step to 20 ml giving a final a pH of 8.55. The same steps were conducted for nitrosation of piperazine citrate.

Data from the experiments are tabulated in Tables 2 and 3, and in Figures 1 and 2.

Table 3: The effect of formaldehyde concentration on nitrosation reaction between piperazine citrate and sodium nitrite at different temperatures

pH of the Solution	*Nitrosation reaction products yield (mole DNPZ/mole PZ)*			
	20 °C	*40 °C*	*50 °C*	*60 °C*
8.2	*0*	*0*	*0*	*0*
6.18	*0.56*	*0.59*	*0.45*	*0.4*
5.91	*0.76*	*0.77*	*0.62*	*0.52*
5.69	*0.57*	*0.53*	*0.44*	*0.42*
5.33	*0.93*	*0.66*	*0.52*	*0.49*
4.75	*0.53*	*0.61*	*0.49*	*0.43*
4.4	*0.43*	*0.41*	*0.38*	*0.31*
4.0	*0.0*	*0.0*	*0.47*	*0.0*

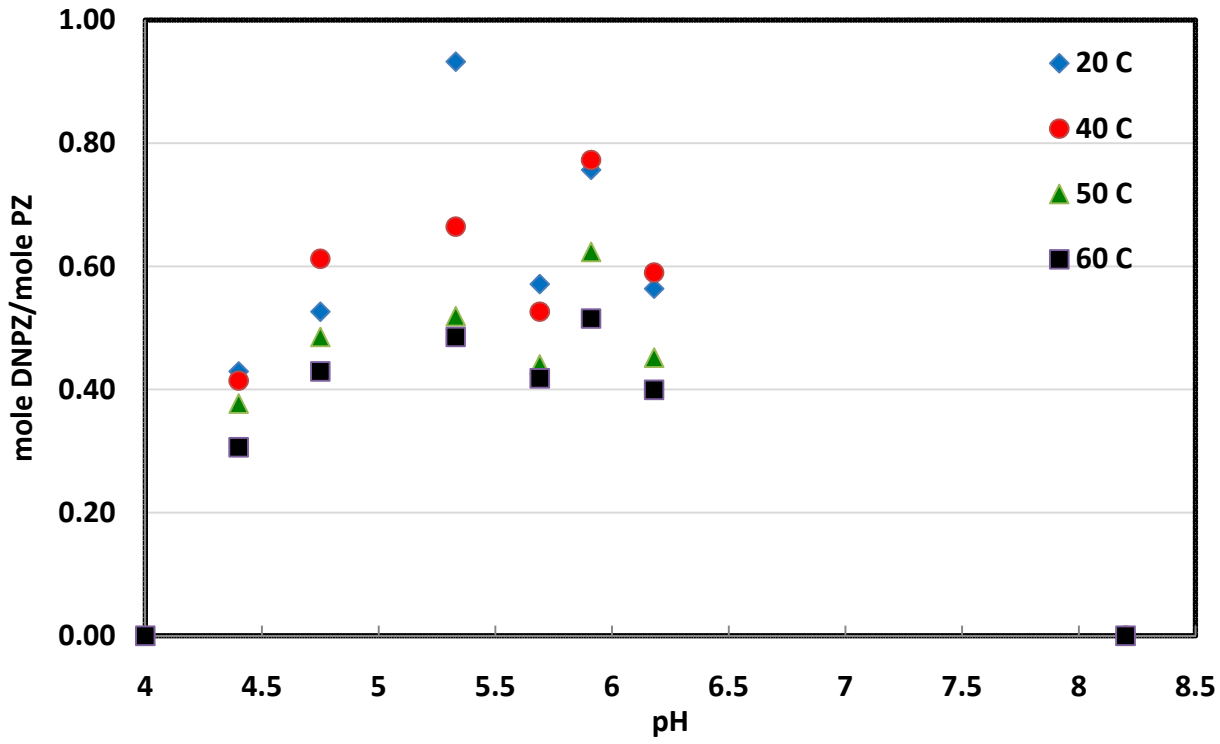

Figure 1: Nitrosation reaction of piperazine citrate according to formaldehyde concentration at different temperature

Previous reports showed that there is no evidence of piperazine citrate nitrosation where the pH is greater than 4. This new result shows that formaldehyde has a catalytic effect on the reaction and nitrosation occurs at a pH greater than 4.

Figure 1 shows a comparison between nitrosation reaction products when piperazine citrate has been used in the presence of different quantities of formaldehyde (different pH).

Temperature effect on nitrosation reaction has been investigated and the result has been demonstrated in Figure 1. At low temperature (20 °C) the reaction efficiency is more than at other temperatures, and as the temperature increases the efficiency of the nitrosation reaction decreases. It was also observed that at higher temperatures more time is required for starting the reaction.

Table 3: The effect of formaldehyde concentration on nitrosation reaction between piperazine and sodium nitrite at different temperatures

pH of the Solution	*Nitrosation reaction products yield (mole DNPZ/mole PZ)*				
	20 °C	*40 °C*	*60 °C*	*80 °C*	*98 °C*
10.45	*0*	*0*	*0*	*0*	*0*
10.21	*0.6*	*0.81*	*0.64*	*0.6*	*0.62*
10.17	*0.9*	*0.94*	*0.94*	*0.94*	*0.94*
10.06	*0.7*	*0.68*	*0.81*	*0.62*	*0.77*
9.98	*0.7*	*0.62*	*0.56*	*0.43*	*0.85*
9.65	*0.8*	*0.72*	*0.62*	*0.31*	*0.53*
9.51	*0.7*	*0.6*	*0.36*	*0.34*	*0.25*
9.33	*0.5*	*0.58*	*0.47*	*0.24*	*0.28*
9.12	*0.6*	*0.36*	*0.45*	*0.39*	*0.25*
8.96	*0.6*	*0.31*	*0.23*	*0.26*	*0.21*
8.8	*0.5*	*0.35*	*0.25*	*0.17*	*0.12*
8.71	*0.4*	*0.21*	*0.13*	*0.13*	*0.12*
8.55	*0.3*	*0.21*	*0.11*	*0.08*	*0.05*
8.0	*0.0*	*0.0*	*0.0*	*0.0*	*0.0*

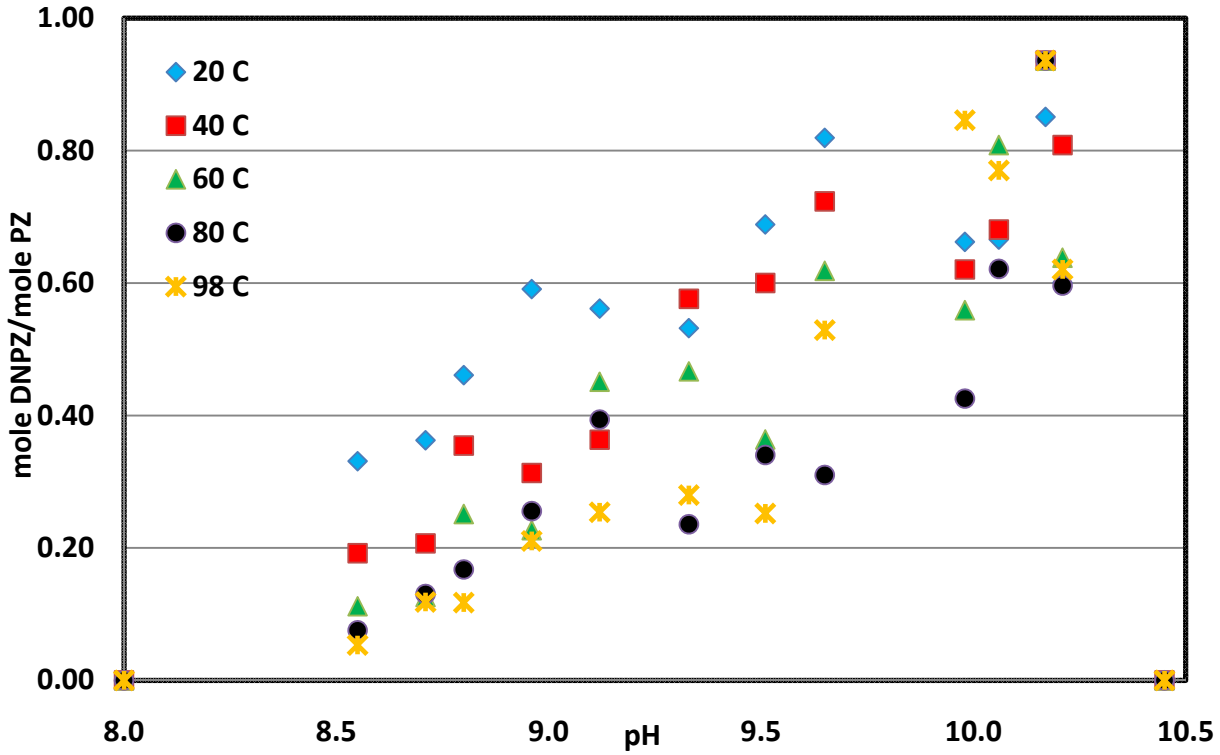

Figure 2: Nitrosation reaction of piperazine in different concentrations of formaldehyde at different temperature

According to the previous reports, nitrosation of piperazine could not happen at a pH greater than 8, an alkaline environment, but the new results show that at a high pH and in very strong basic medium formaldehyde can catalyze a nitrosation reaction of PZ.

Figure 2 shows a comparison between nitrosation reaction products when PZ has been used in the presence of different quantities of formaldehyde (different pH). These observations have been demonstrated before for some secondary amines and amino acids (Mirvish, 1970, 1975; Lijinsky and Keefer, 1970), and this research shows the same movement for piperazine nitrosation.

Temperature effect on nitrosation reaction has been investigated and the result has been demonstrated in Figure 2. At low temperature (20 °C) the reaction efficiency is more than other temperatures and increasing the temperature decreases the efficiency of nitrosation reaction. It is also observed that at a higher temperature more time is required for starting the reaction.

Direct injection of Dinitrosopiperazine to Mass Spectrometry (MS)

Samples of 0.00007–0.7 mmol of dinitrosopiperazine per ml of methanol have been injected to MS directly to see if MS can detect it. The mass spectrum diagram is shown in Figure 3.

Mass spectrometry shows the mass per charge of molecules and their relative abundance. For dinitrosopiperazine we are looking for m/z = 145 because the molecular weight of dinitrosopiperazine is 144 and by protonating with one hydrogen atom, the mass of ion will be 145.

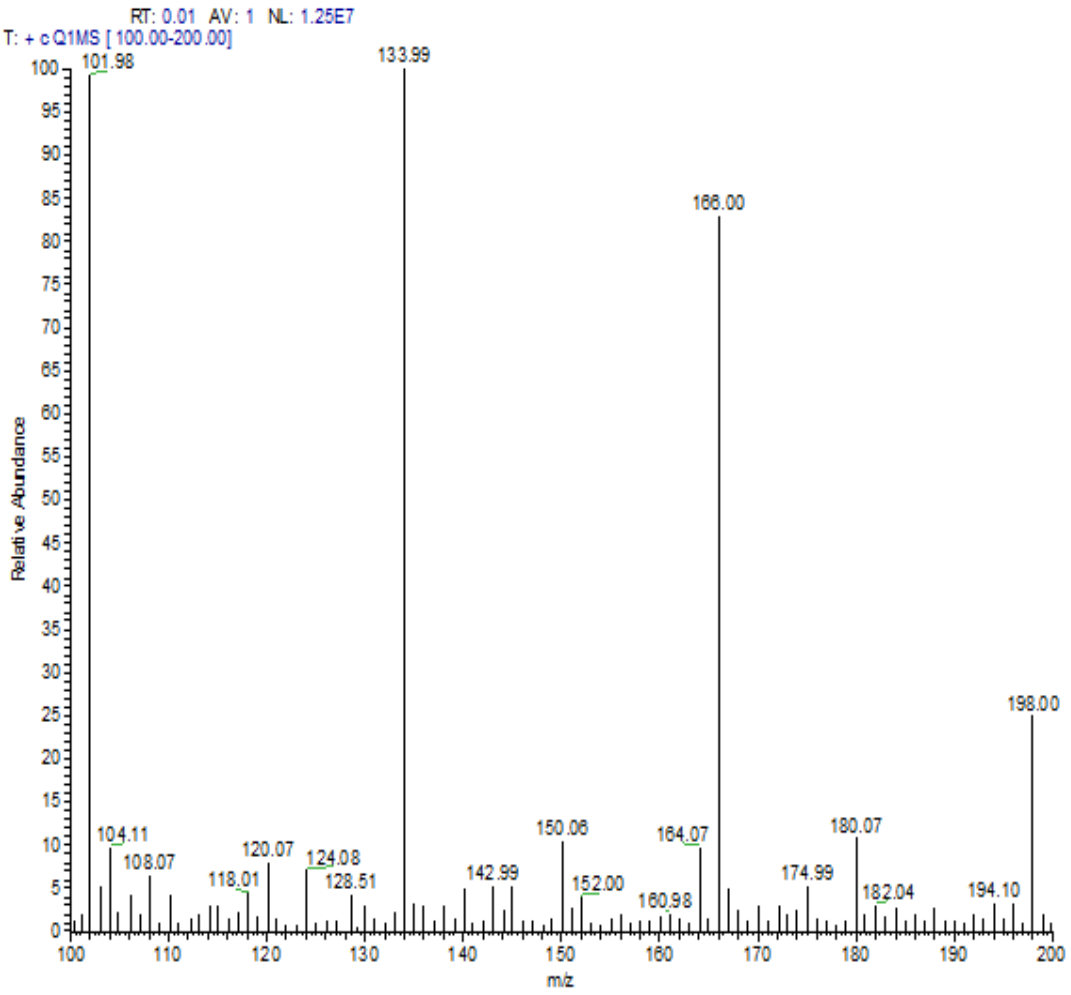

Figure 3: Mass spectrum of a sample of dinitrosopiperazine and methanol (relative abundance in terms of m/z)

Figure 3 shows the typical mass spectrum of samples that have been injected into the MS. All sample results were almost the same and in this report just one of them that was a common spectrum in most of the runs, has been described. There is no evidence of m/z equals to 145.

When water was added to the solutions (2 part methanol and one part water) and new samples injected to the MS, surprisingly, mass spectrum showed a peak at m/z of 145 which is dinitrosopiperazine (Figure 4).

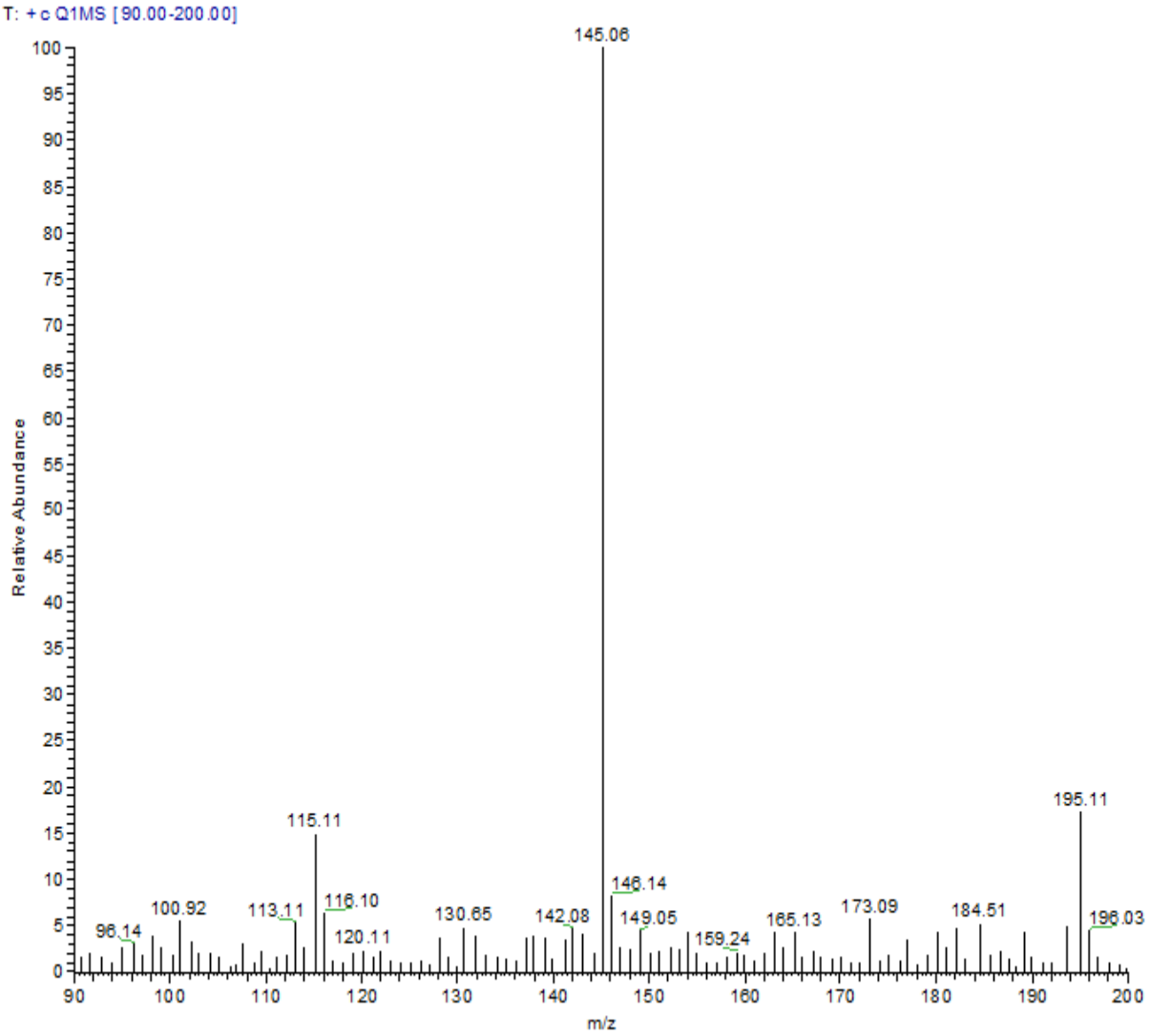

Figure 4: Mass spectrum of a sample of dinitrosopiperazine in methanol and water (Relative abundance in terms of m/z)

Rather than a big peak of dinitrosopiperazine, there is a small amount of mononitrosopiperazine in the injected sample as shown in Figure 4. m/z of 116.1 represents the molecular weight of mononitrosopiperazine which is 115.

When there is very small amount of a molecule in a sample or more than one molecule with the same molecular weight may exist, the fragmentation method has been used to confirm the detection of a specific molecule. By using fragmentation, an extremely small quantity of a component is recognizable.

Figures 4, 6, and 7 show the fragmentation steps of dinitrosopiperazine to 2 ions with m/z of 85.1 and 56.15.

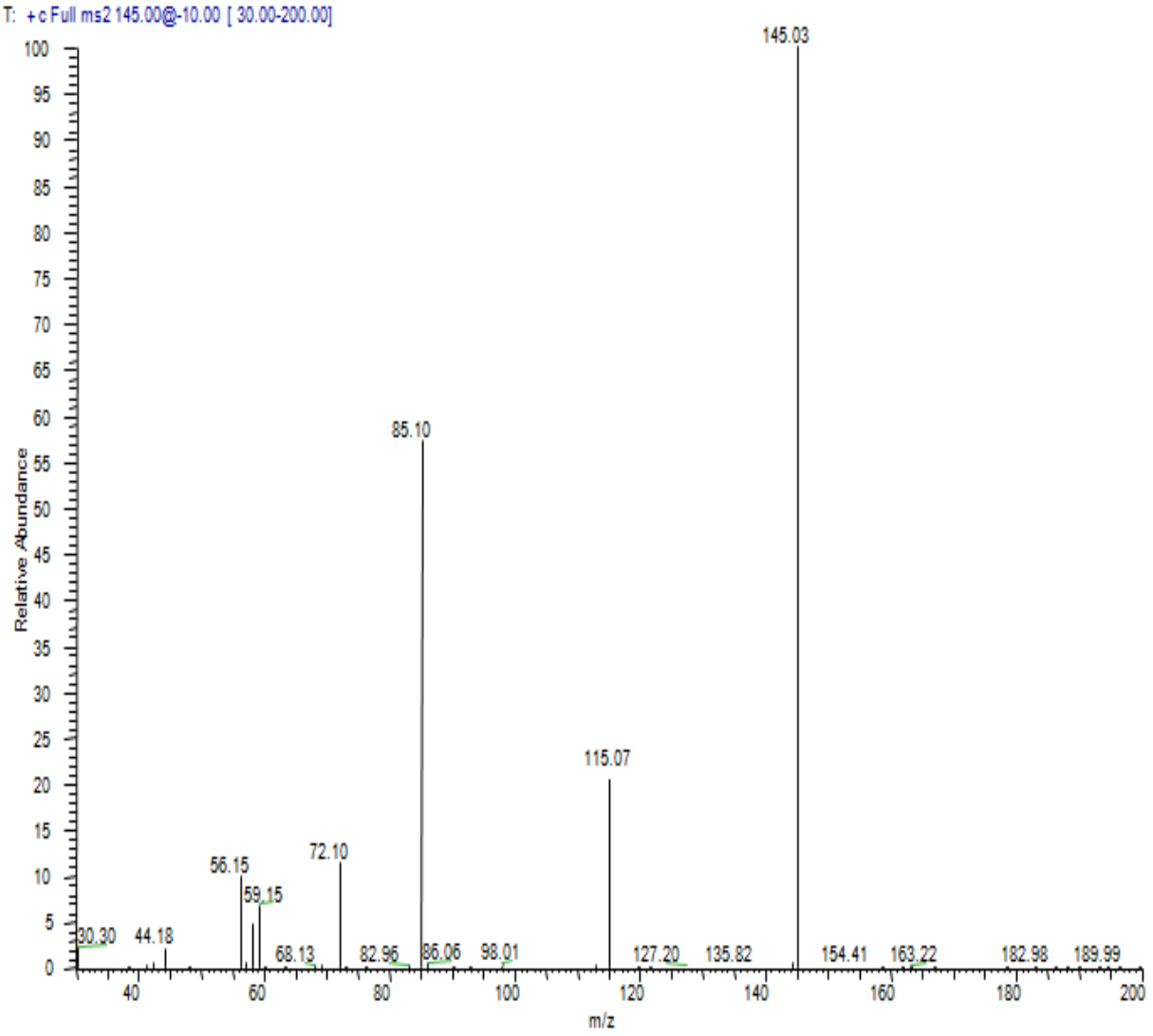

Figure 5: Mass spectrum of fragmentation of a sample of dinitrosopiperazine in methanol and water by collision energy of 10. (Relative abundance in terms of m/z)

With a collision energy of 10, Figure 5 shows dinitrosopiperazine fragments with the appearance of just one ion at a m/z of 85.1. With a collision energy of 20, DNPZ fragments to m/z of both 85.1 and 56.15, as shown in Figure 6.

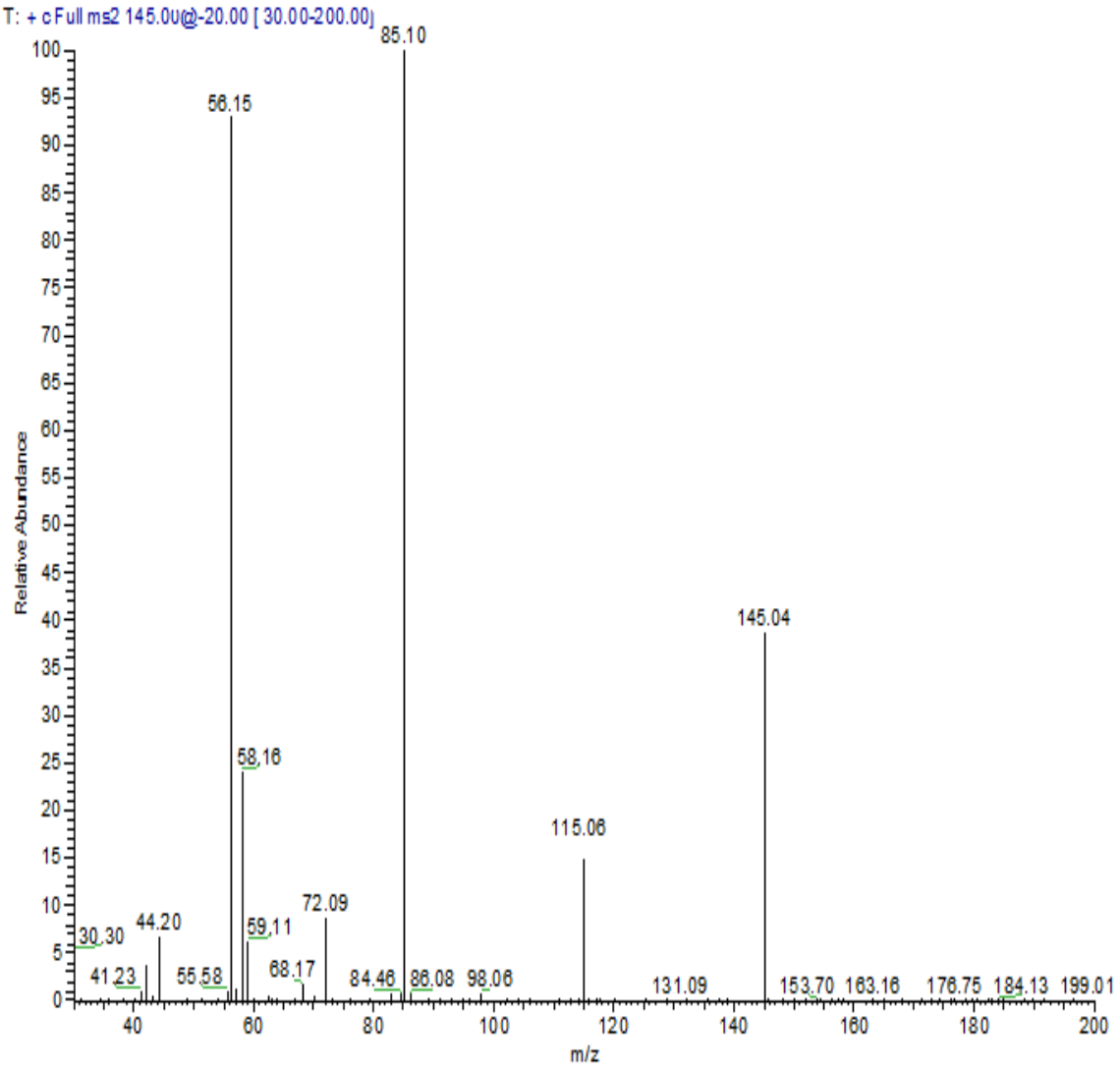

Figure 6: Mass spectrum of fragmentation of a sample of dinitrosopiperazine in methanol and water by collision energy of 20. (Relative abundance in terms of m/z)

Collision energy of 20 breaks almost 40% of the DNPZ, so the collision energy has been increased one more step, to 30. Figure 7 shows that with collision energy of 30 almost all DNPZ is broken to ions with m/z of 85.1 and 58.15.

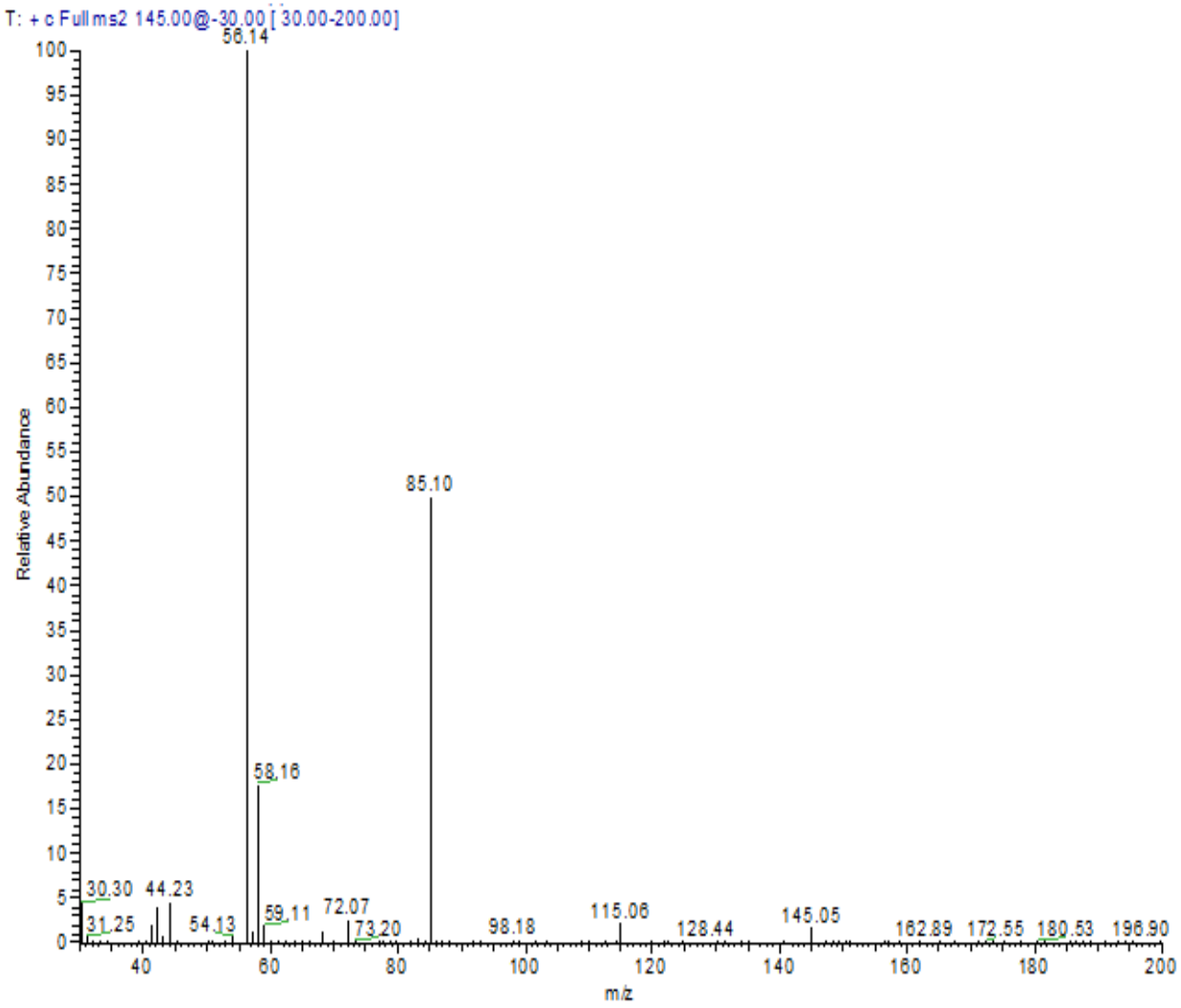

Figure 7: Mass spectrum of fragmentation of a sample of dinitrosopiperazine in methanol and water by collision energy of 30. (Relative abundance in terms of m/z)

Quantifying Dinitrosopiperazine by Liquid chromatography and Mass Spectrometry (LC-MS)

After detection of DNPZ by MS, an LC-MS system was used to quantify the concentration of DNPZ in different solutions. The investigative method is under development but for a start, solutions of DNPZ, PZ, and DNPZ+PZ in 80% methanol and 20% water have been applied to LC-MS using a reverse phase column. The primary results are shown in the following figures.

All samples have been applied to LC-MS and then chromatograms divided to three part of mass ranges, 145–145.2 for DNPZ, 116–116.2 for MNPZ, and 87–87.2 for PZ. Figures 8, 9, 10, 11, 12, 13, 14, 15, and 16 show the respective results.

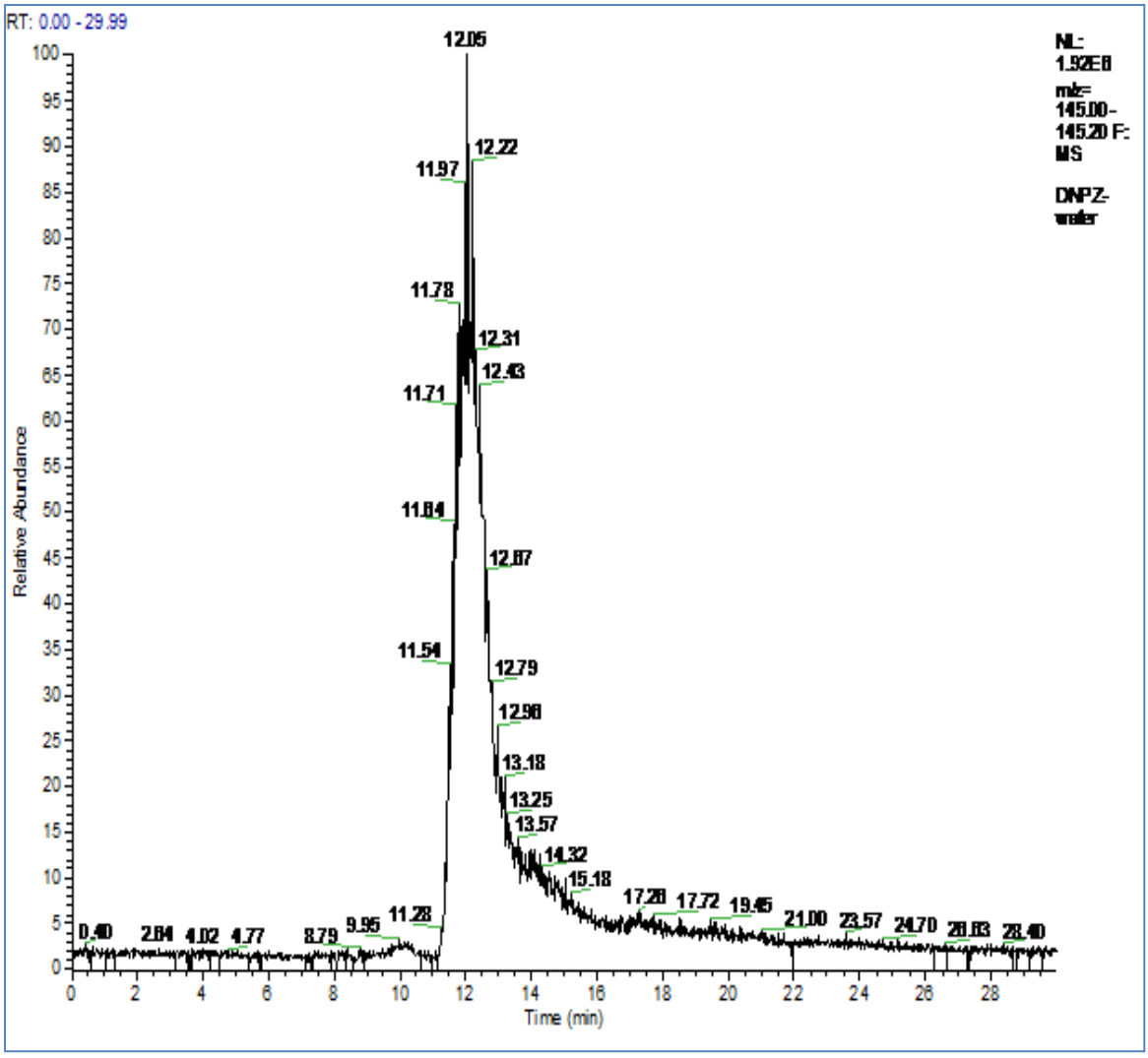

Figure 8: Chromatogram of a sample of dinitrosopiperazine in methanol and water analyzed by LC-MS

Figure 8 shows the chromatogram of DNPZ analysis by LC-MS when the mass range of detection is between 145 and 145.2 for DNPZ. The vertical axis presents relative abundance and the horizontal axis shows retention time.

DNPZ comes out at 12.05 minutes with a high relative abundance while there are other components with mass close to DNPZ, and considerably lower relative abundance, around it.

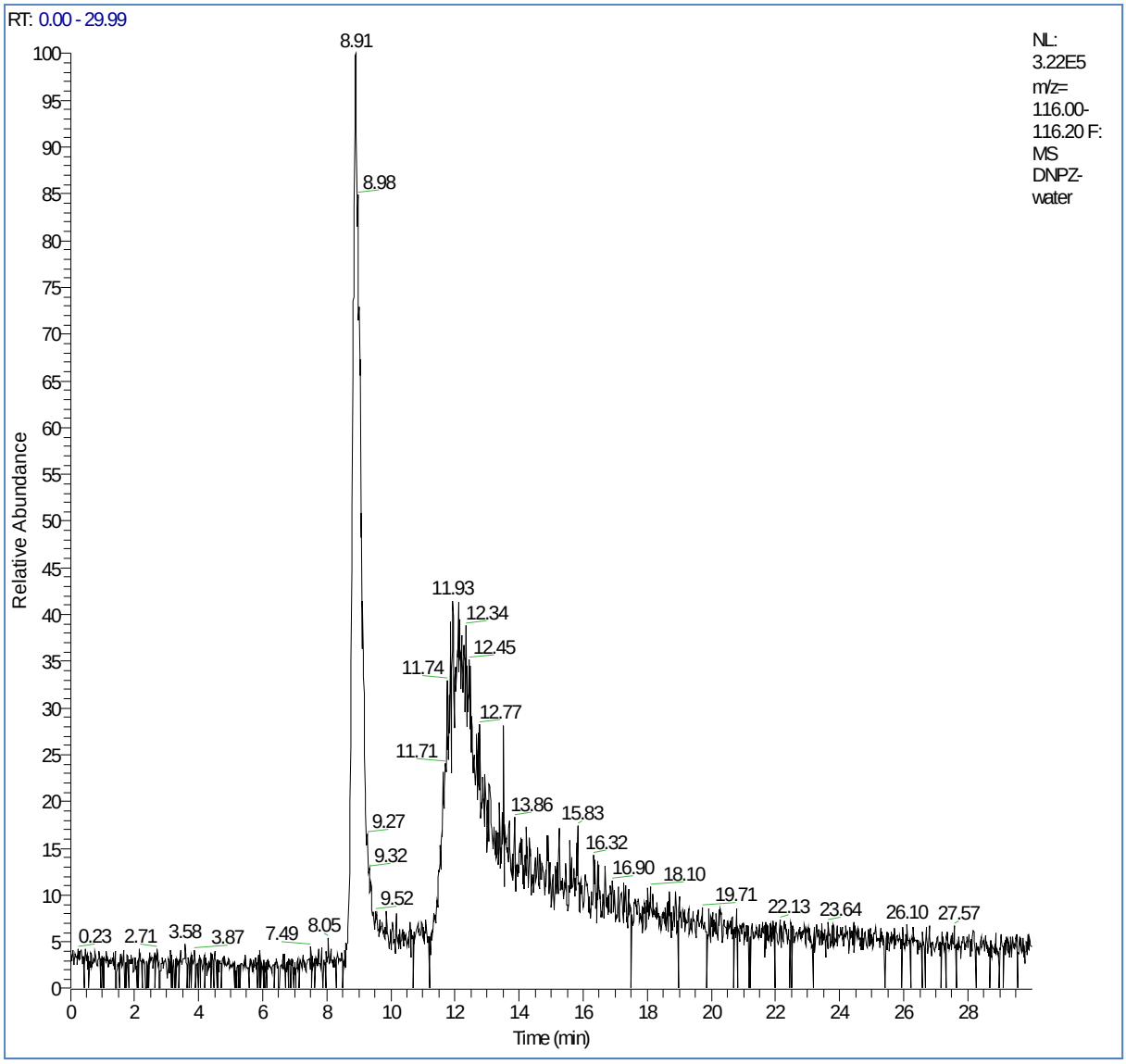

Figure 9: Chromatogram of a sample of dinitrosopiperazine in methanol and water analyzed by LC-MS in mass range of MNPZ (116)

Figure 9 shows that MNPZ can be produced when DNPZ is dissolved in methanol and water. Its retention time is around 8.9 minutes.

Figure 10 shows the amount of PZ that can be found in a DNPZ sample and it is not that much. Therefore LC-MS could be a good method to quantify DNPZ, although more investigations to obtain calibration curves and sensitivity of measurement are needed.

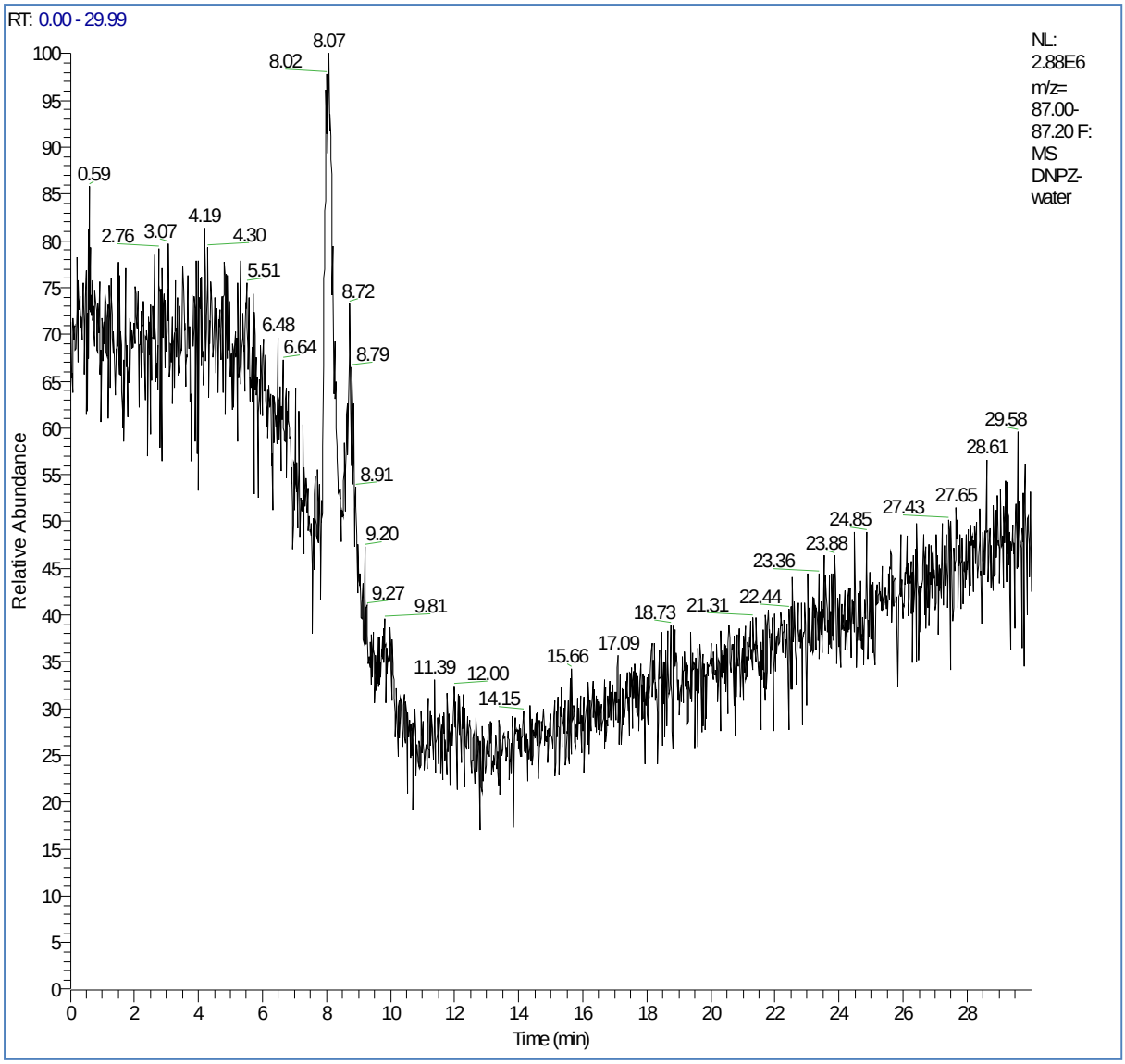

Figure 10: Chromatogram of a sample of dinitrosopiperazine in methanol and water analyzed by LC-MS in mass range of PZ (87)

The following two chromatograms show the response of LC-MS to a solution of piperazine (PZ) in methanol and water.

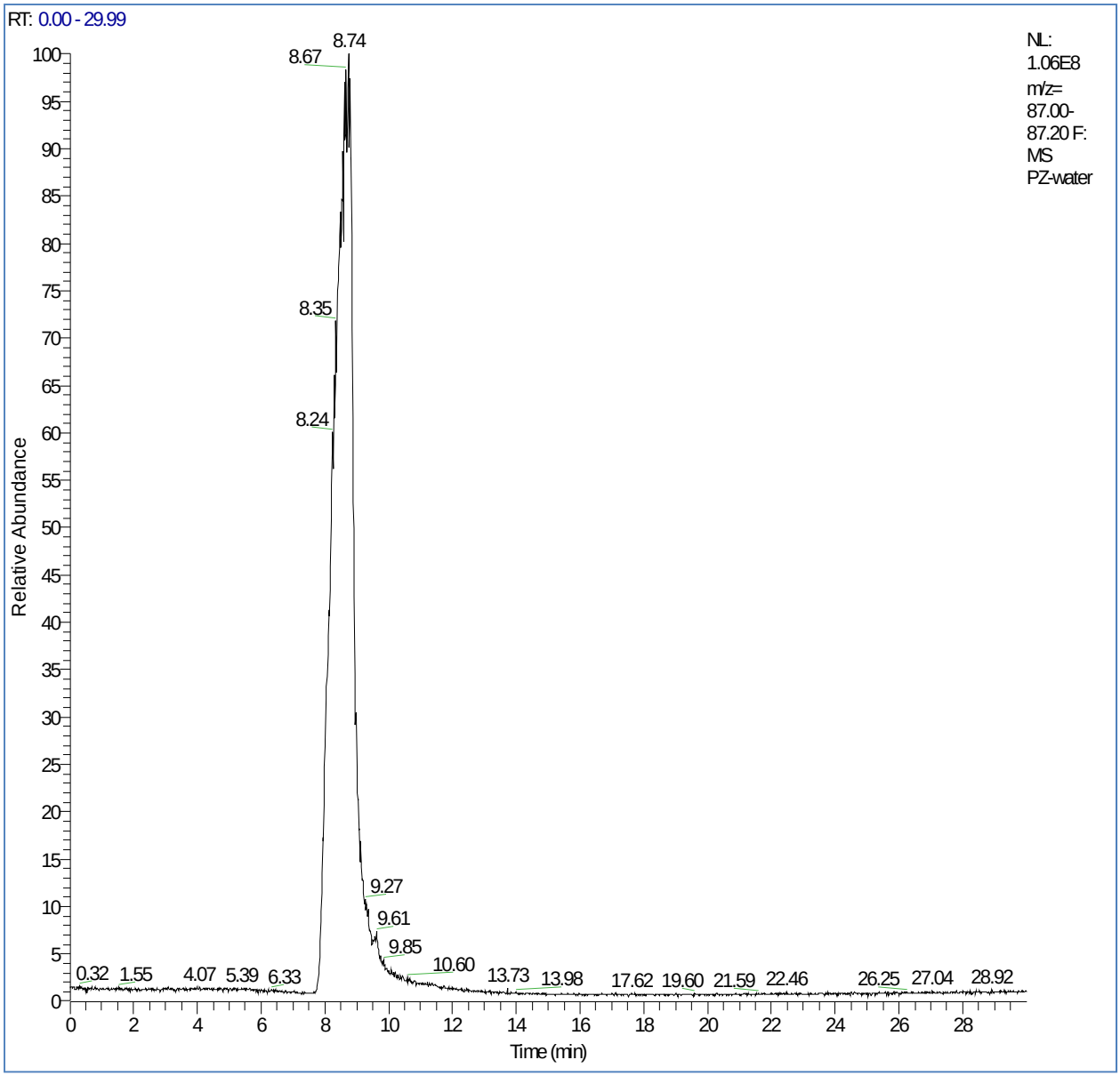

Figure 11: Chromatogram of a sample of piperazine in methanol and water analyzed by LC-MS in mass range of PZ (87)

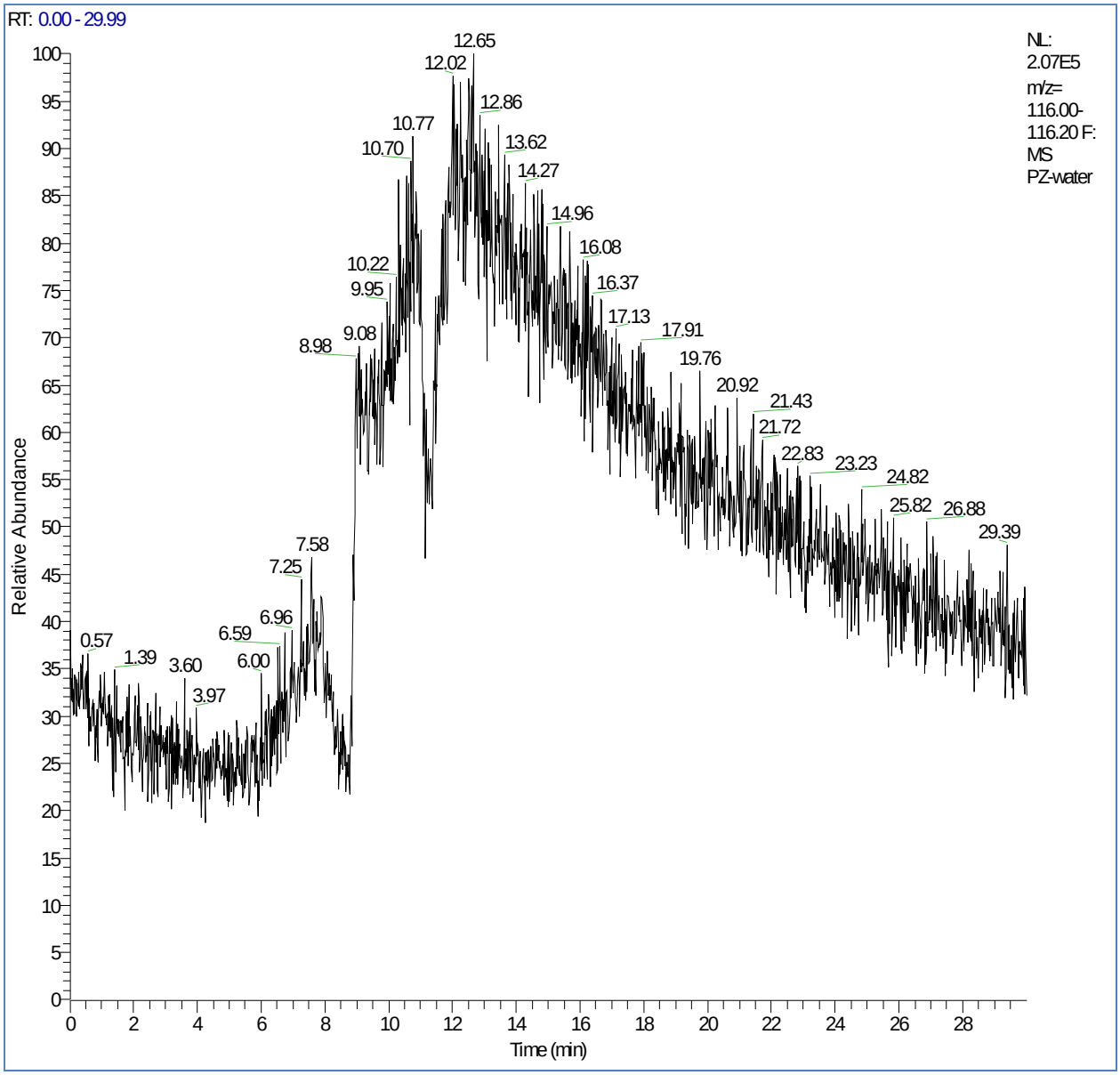

Figure 12: Chromatogram of a sample of piperazine in methanol and water analyzed by LC-MS in mass range of MNPZ (116)

The following three chromatograms demonstrate when an equal concentration of DNPZ and PZ in methanol and water is analysed by LC-MS. As noted there is some MNPZ rather than PZ and DNPZ in the LC-MS analysis.

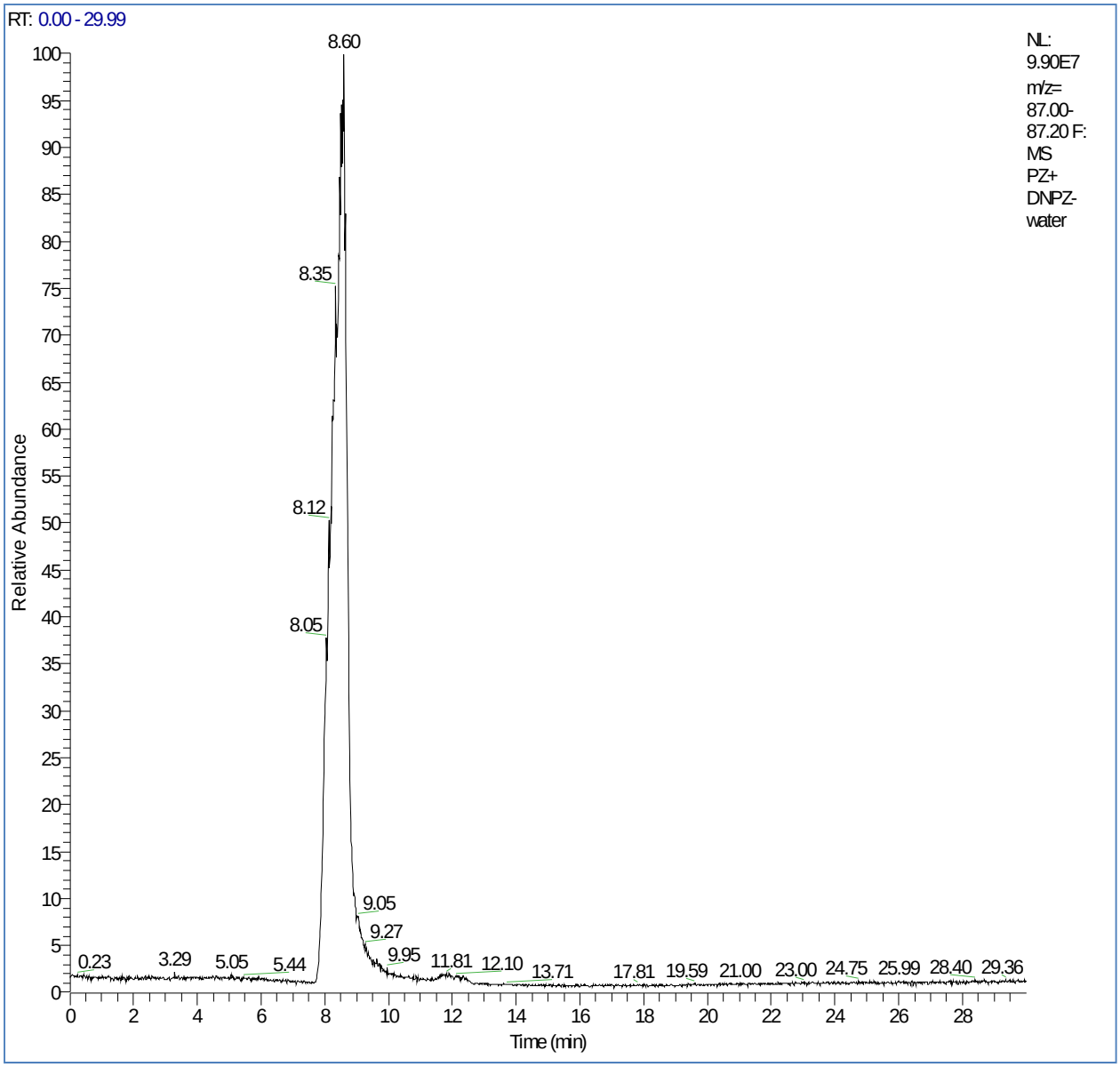

Figure 13: Chromatogram of a sample of piperazine and dinitrosopiperazine in methanol and water analyzed by LC-MS in mass range of PZ (87)

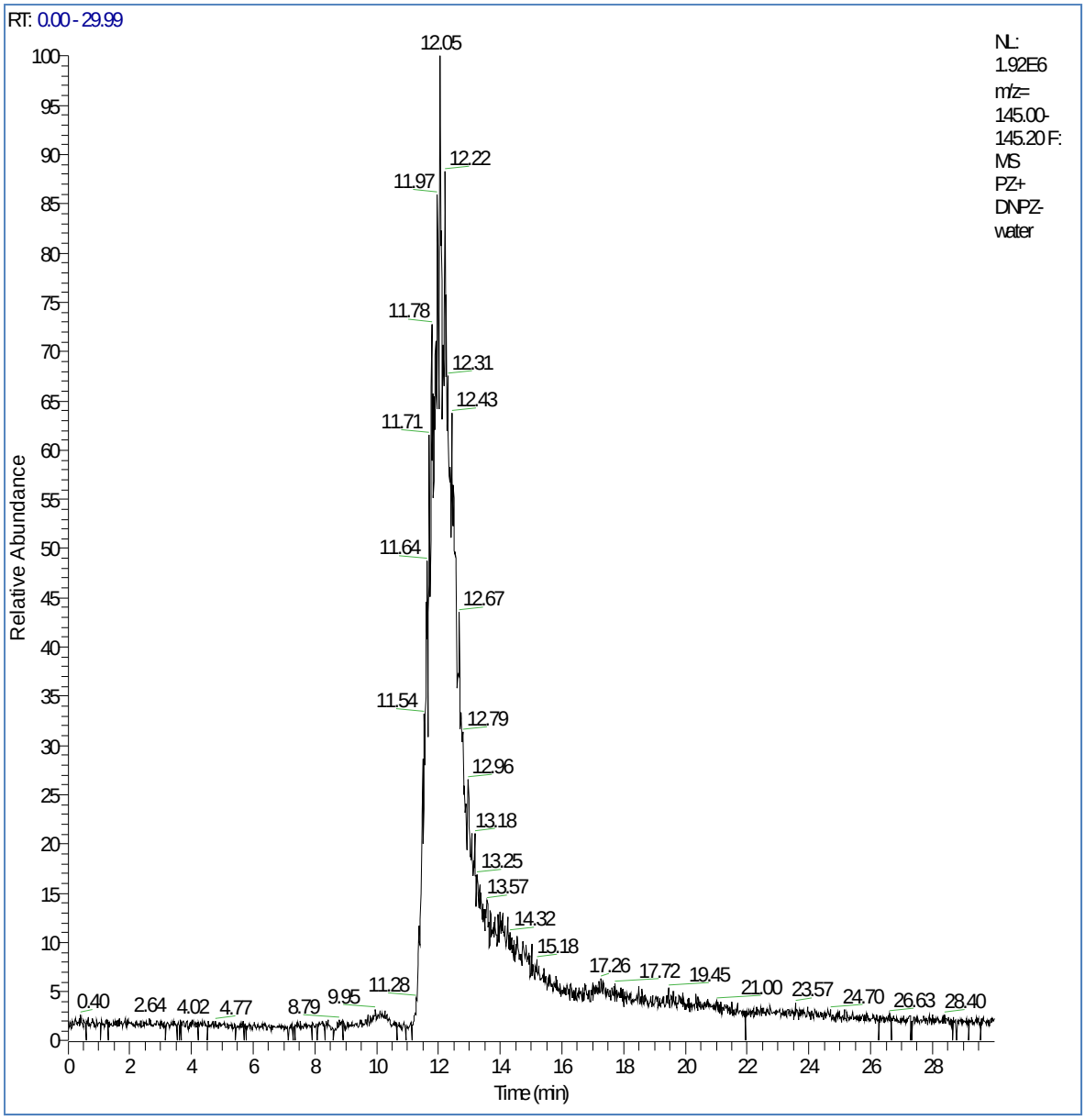

Figure 14: Chromatogram of a sample of piperazine in methanol and water analyzed by LC-MS in mass range of DNPZ (145)

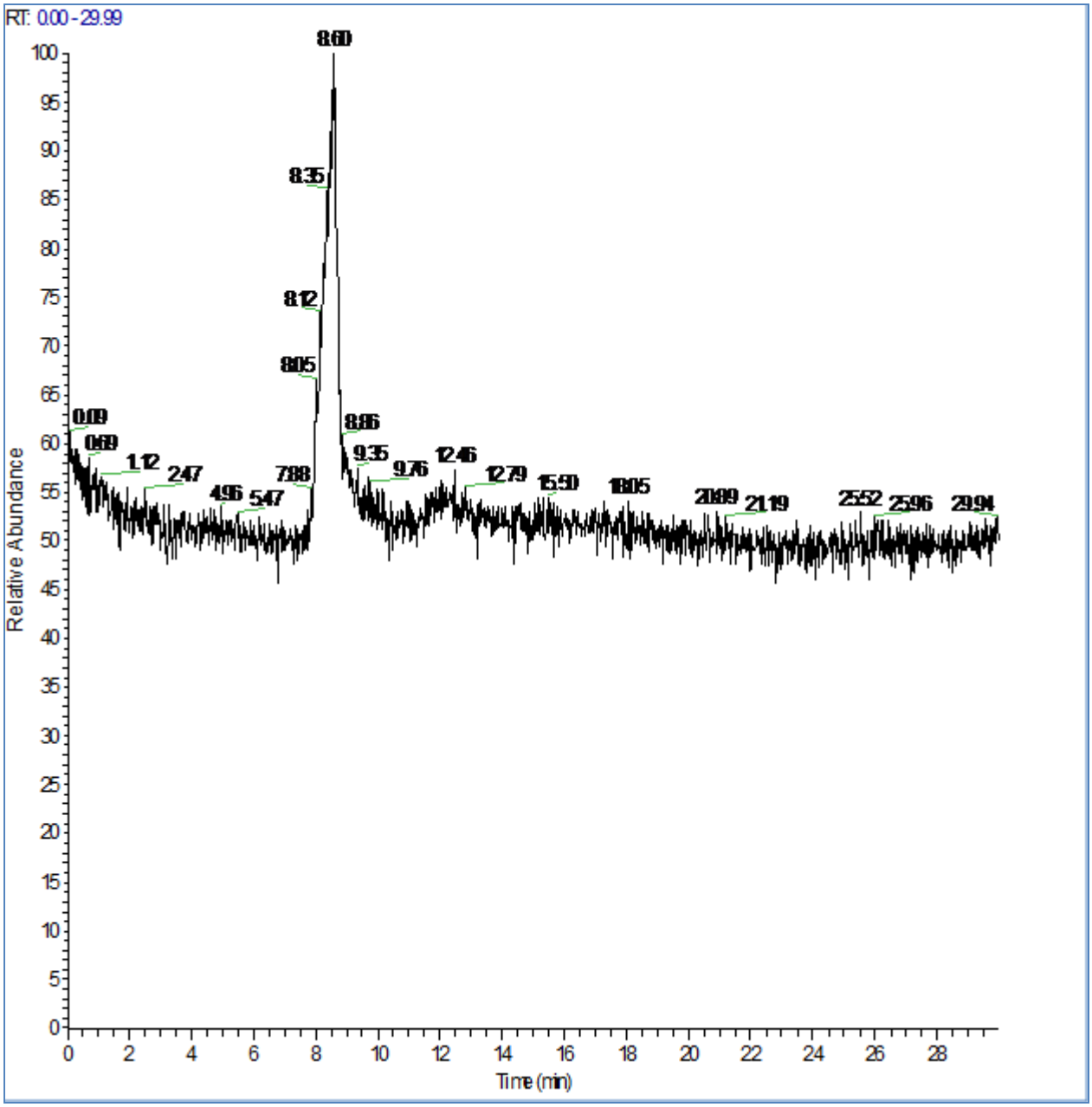

Figure 15: Chromatogram of a sample of piperazine in methanol and water analyzed by LC-MS in mass range of MNPZ (116)

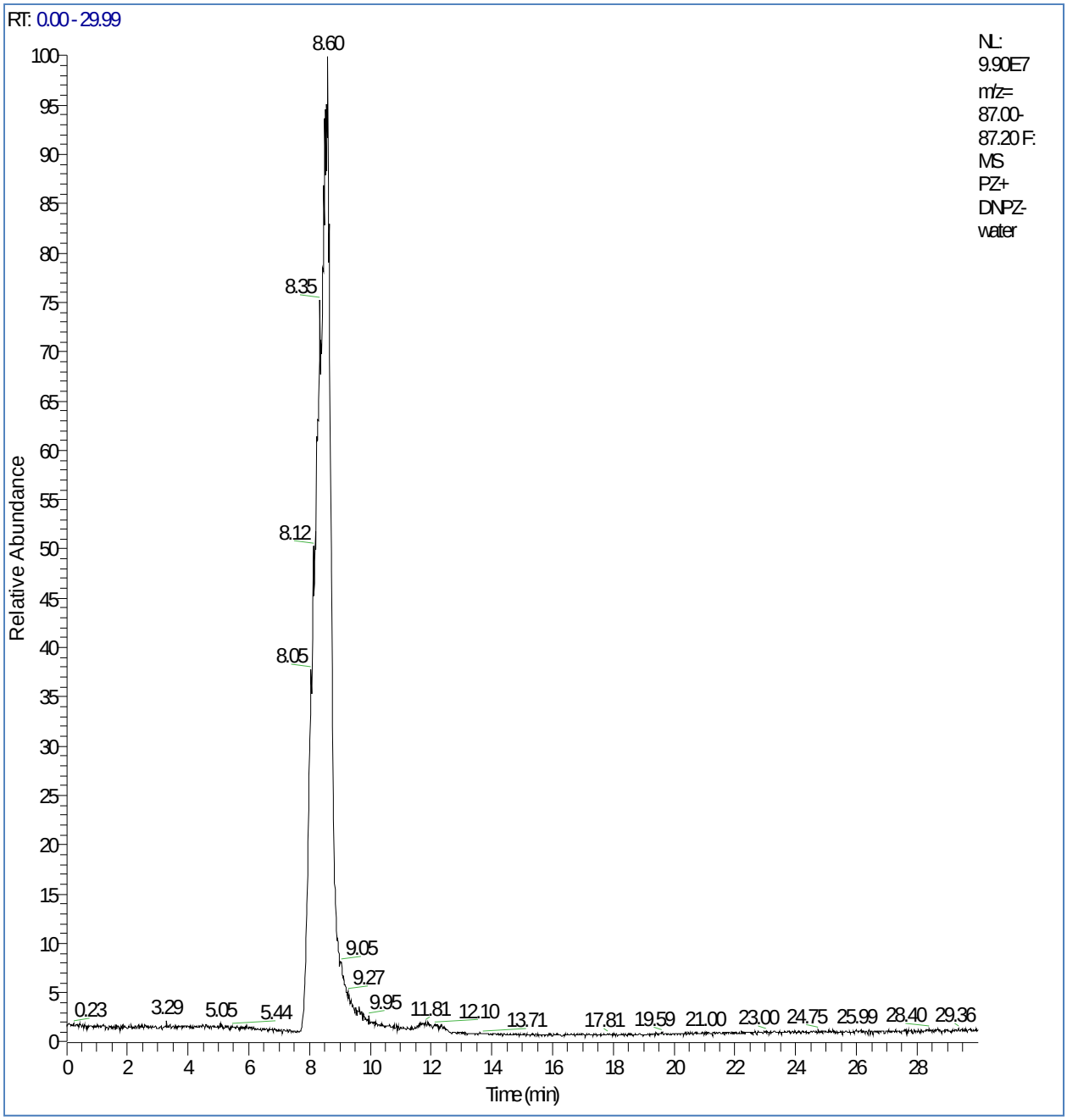

Figure 16: Chromatogram of a sample of piperazine in methanol and water analyzed by LC-MS in mass range of PZ (87)

Discussion

Results show the catalytic effect of formaldehyde on nitrosation reaction of piperazine and piperazine citrate with sodium nitrite in an alkaline environment. Formaldehyde decreases the pH of the solution and also it reacts with piperazine to form an intermediate ion which can react with a nitrite ion very easily and produces an unstable ester that breaks fast and produces nitrosopiperazine and formaldehyde.

The optimum pH for maximizing nitrosation product is around 10 and 6 for piperazine and piperazine citrate nitrosation, respectively. Reducing pH toward the neutral decreases the nitrosation rate.

Direct injection of dinitrosopiperazine solution in methanol and water is the best method for DNPZ detection by MS. Fragmentation of DNPZ under different collision energy breaks DNPZ with m/z of 145 to two ions with m/z of 85.1 and 56.14. LC-MS has been used to analyze DNPZ itself and also in a mixture with PZ.

Conclusions

Nitrosating of piperazine and piperazine citrate will not happen without the presence of formaldehyde in an alkaline solution, and by increasing temperature nitrosation will decrease. Excess amounts of formaldehyde will decrease nitrosation. Maximum production of nitrosamine from the reaction between piperazine and piperazine citrate with sodium nitrite at the experimental condition is in the pH range of 9.5–10.2 and 5.5–6, respectively, in the presence of formaldehyde.

Higher reaction temperatures move the maximum reaction rate to a lower pH range; however nitrosation reaction starting time is longer at higher temperatures.

MS detects dinitrosopiperazine and by collision energy of 30 breaks DNPZ to two identifying ions which help to identify DNPZ in very small quantities. DNPZ can be measured by LC-MS using a reverse phase column, but more runs are needed for calculating calibration curves and sensitivity of analysis.

Future Work

Next quarter will focus on developing a proper method for measuring DNPZ, especially in alkaline solution and real conditions of a CO_2 capture plant.

We will also investigate a reaction mechanism for nitrosation reaction of loaded piperazine from analysis of amine and nitrate and nitrite ions.

For further work, this research is going to focus on CO_2 capture conditions in liquid phase in the absorber and stripper to see the effect of degradation products on nitrosation reactions.

References

Attalla M, Azzi M. “Environmental impact of Atmospheric Emissions from Amine-based Post-Combustion CO_2 Capture.” Presented in *NILU, 2010.*

Keefer LK, Roller PP. "N-Nitrosation by Nitrite Ion in Neutral and Basic Medium." *Science*, 1973;181:1245–47.

Kunisaki N, Hayashi M. "Formation of N-Nitrosamines from Secondary Amines and Nitrite by Resting Cells of Escherichia coli B." *Applied and environmental microbiology*, 1978;37(2):279–282.

Lijinsky W, Keefer L, Loo J. "The preparation and properties of some nitrosamino acids." *Tetrahedron*, 1970;26:5137.

Mirvish S. "Formation of N-nitroso compounds chemistry kinetics and in-vivo occurrence." *Toxical Appl Pharmacol*, 1975;3(1):325.

Mirvish S, Wallcave L, Eagen M. "Ascorbate-Nitrite Reaction: Possible Means of Blocking the Formation of Carcinogenic N-Nitroso Compounds." *Science*, 1972;177(4043):65–68.

Osterdahl BG, Bellander B. "Determination of n-mononitrosopiperazine and n,n′-dinitrosopiperazine in human urine, gastric juice and blood." *J. Chromatogr*. 1983;278:71.

Roller PP, Keefer LK, Slavin BW. “N-Nitroso compounds: Analysis, Formation and Occurance.” IRAC Publication 31, Lyon, 1980;119.

United States Pharmacopeia XXIV. National Formulary 19, Rockville, USP Convention, Washington; 2000; 1341 & 2235.

Thermal Reclaiming of Aqueous Amines

Quarterly Report for April 1 – June 30, 2010

by Steven Fulk

Supported by the Luminant Carbon Management Program

and the

Industrial Associates Program for CO_2 Capture by Aqueous Absorption

Department of Chemical Engineering

The University of Texas at Austin

July 2, 2010

Abstract

In this quarter, concentrated, loaded piperazine (PZ) solutions created last quarter using a simple heated-beaker evaporator were analyzed using a variety of techniques. Two solutions were created; the first solution was 8 m PZ with 0.3 mol CO_2/ mol alkalinity, and the second solution was 8 m PZ with 0.3 mol CO_2/ mol alkalinity plus 250 mM formic acid. Total Inorganic Carbon (TIC) and cation chromatography analysis showed the solution containing formic acid had 1.4 mol PZ/kg solution and 0.02 mol CO_2/ mol alkalinity less than the solution with no formic acid. The difference is hypothesized to be the formate/amine/formamide equilibrium reaction. Anion chromatography showed less formate than predicted from a mass balance on the non-volatile species in the concentrated solution. Formamide reversal using NaOH is needed to confirm the hypothesis.

Goals for next quarter include performing three experiments. First, thermal degradation experiments using stainless steel bombs will analyze degradation characteristics of concentrated amine solutions. Second, liquid-liquid equilibrium experiments will be conducted on amines and inhibitor mixtures. Finally, a thermal reclaiming apparatus with continuous FTIR vapor sampling constructed this quarter will be used to reclaim aqueous amine solutions. Liquid and vapor samples will be analyzed for composition.

Introduction

Alkanolamines have been used to treat acid gases since 1930 (GPSA, 2004). Since the inception of the acid gas treating process, the need to develop new solvents to increase system capacity and optimization to meet economic and environmental concerns has become increasingly important. Though new and better solvents have been and are continually being developed to meet some of these demands, issues regarding process contaminants have remained and are becoming increasingly problematic. System contaminants pose a number of problems, specifically, the cost of solvent make-up and reduced system capacity due to amine degradation, waste disposal costs, equipment corrosion, and environmental concerns relating to greenhouse gas and nitrosamine emissions.

Pollutants can enter into acid gas treating systems by generation within the process or through the transport of material into the system. Contaminants generated within the process include oligomers of amines from thermal degradation, amine fragments from oxidative degradation, and metals from corrosion. Pollutants that flow into the system include flue gas impurities, fly ash metals, and user additives such as oxidation inhibitors, corrosion inhibitors, and antifoaming agents. Degradation products can lead to heat stable salt and amide formation, which bind usable amine causing solvent loss; therefore, whatever reclaiming technology is chosen, conversion of heat stable salts and amides back to useable amine must be considered.

Many methods to remove contaminants, or reclaim, have been developed. Reclaiming methods include filtration and adsorption, thermal reclaiming, ion exchange, electrodialysis, foam fractionation, and sulfate crystallization. Each system operates by a different separation principle, and thus each process will have inherent advantages and disadvantages.

Thermal reclaiming separates components from process streams based on volatility. In flue gas treatment, a small slip-stream from the bottom of the stripper column is sent to a kettle where the temperature is increased causing volatile components to exit at the top and solids and non-volatiles to accumulate in the bottom of the still. Unlike other reclaiming techniques, thermal reclaiming can remove nearly any type of process contaminant as long as it is less volatile than the amine. Since the separation is somewhat non-selective, bound amine in the form of heat stable salts and amides will be lost. Pretreatment with caustic solution can reverse amide formation and free any amine bound in a salt. Thermal reclaiming returns roughly 85–95% of usable amine (Cummings et al., 2007).

In this quarter, evaporated solutions simulating thermal reclaiming were analyzed to determine their concentrations and compared with the original, unconcentrated solutions.

Experimental Methods

Apparatus

The apparatus used this quarter consists of a 250 mL beaker, a ½" x 4', 140 W, 45 V, Glas-Col heat tape with a Cole-Parmer 11 amp, 120 V, 60 Hz solid-state power controller, a Mettler-Toledo PB5001 mass balance, and a 250 °C thermometer. The beaker was placed on a cork stopper to prevent charring the mass balance. A diagram of the apparatus can be seen in the previous quarterly report (Rochelle et al., 2009).

Procedures

Evaporation experiments began by securing the heating tape to the beaker on top of the mass balance in a vent hood and allowing the mass reading to reach a steady value. After the balance reading was stable, the balance was tared and approximately 100 mL of solution was added to the beaker. The mass and the temperature of the solution were recorded and then the power supply was turned on. The solution was allowed to vaporize continuously until a certain mass concentration was met. Mass and temperature measurements were recorded every five minutes. As a note of caution, the vaporizing solution should be kept in a closed vent hood to prevent amine vapors from entering the laboratory area which can lead to accidental inhalation.

Once the solution met the mass concentration value, pre-heated 2 mL bulb pipettes were used to extract hot, concentrated solutions which were transferred to pre-weighed 15 mL dram vials.

The concentrated sample solutions were then diluted to a dilution factor of 10x to prevent crystallization on cooling to room temperature.

Analytical Methods

Dilutions

Many of the analytical methods and sampling techniques performed this quarter required dilutions to achieve the desired concentration ranges or to prevent crystallization of the sampled material. Dilutions are performed gravimetrically by weighing a sample in a beaker, taring the balance, and weighing an amount of water added to the sample. The solution is then stirred and transferred to the appropriate vial. As a means of quantifying dilution, this report will use the term "dilution factor" which is calculated as follows:

$$\text{Dilution Factor} = \frac{\text{Mass of Sample} + \text{Mass of Added Water}}{\text{Mass of Sample}} \quad (1)$$

For this work, a dilution factor will be reported by an "x" following the value of the dilution factor. For example, a solution that is 100x diluted contains one part of the original sample for every 100 parts of the diluted solution by mass.

Total Alkalinity (Acid Titration)

The total alkalinity of solutions was determined by titration with 0.2 N H_2SO_4 using a Metrohm-Peak 835 Titrando with an auto-dispenser. In this method, a sample of known mass is diluted by water in a tall-profile titration beaker. The diluted solution is then titrated with acid and the pH of the solution is recorded. Once titration is complete, the volume of acid used to reach the equivalence point, nominally a pH of 3.9, is used to calculate the total alkalinity of the solution. Acidic titration is not selective for any particular specie and therefore reports the total alkalinity of the solution regardless of the mix of components displaying alkaline behavior.

Typical sample masses and dilution factors for acid titration are 0.2 g and 300x, respectively. Due to the concentrated nature of the samples collected, the sample mass was altered to a nominal value of 1 g of a 10x diluted solution to prevent wasting large quantities of acid and consequently overflowing the titration beakers, and to keep the volume of added acid in the same range as other experimentalists for comparison.

For a more detailed description of the Total Alkalinity procedure, please see Appendix A.3 of Hilliard (2008).

Total Inorganic Carbon Analysis (TIC)

The Total Inorganic Carbon analysis was used to quantify CO_2 loading in samples. Generally, a sample of known mass is injected into a port containing 30 wt % H_3PO_4 where the sample is acidified and CO_2 is given off according to the following equilibrium equations:

$$HCO_3^- + H_2O \leftrightarrow H_3O^+ + CO_3^{2-} \quad (2)$$

$$CO_2 + 2H_2O \leftrightarrow H_3O^+ + HCO_3^- \quad (3)$$

The CO_2 is then carried by a nitrogen stream to a Horiba PIR 2000 CO_2 analyzer where voltage response versus time data is sent to a computer for tabulation. A plot of voltage versus time for a given experimental run reveals a series of peaks corresponding to sample injections. The area of a given injection peak provides a means of calculating the amount of CO_2 contained in a sample

when compared to injections of a carbon standard. The carbon standard used for this analysis technique was a buffered K_2CO_3/$KHCO_3$ 1000 ppm by mass standard.

Injection volume depends on the concentration of CO_2 in the sample; consequently, the dilution factor of the sample plays a role in fine-tuning injection volumes to fall in the appropriate voltage range of the CO_2 analyzer. A dilution factor of 100x was found to be appropriate with starting (8 m PZ) solutions, so the sample size of the concentrated solution with a dilution factor of 10x was adjusted to meet the appropriate mass dilution factor. Once the solutions were diluted properly, the injection volumes were adjusted to achieve a voltage response of 0.5V. The injection volume of samples ranged from 25–45 μL. After all of the samples were injected in triplicate, five different volumes of the 1000 ppm by mass carbon standard were injected with a voltage response range encompassing all of the sample responses to create a calibration curve. The calibration curve was then used to calculate the moles of CO_2 contained in a sample. CO_2 concentration information given by TIC used in conjunction with amine concentration information from cation chromatography allows calculation of loading (moles CO_2/mol alkalinity) of the samples.

For a more detailed description of the TIC procedure, see Appendix B.2–B.7 of Hilliard (2008).

Cation Chromatography

Cation chromatography was performed this quarter using a Dionex ICS-2500 IC with an auto-sampler and a gradient pump providing a linear eluent concentration profile using methanesulfonic acid to quantify the amount of PZ in sample solutions. A detailed description of the cation chromatograph and procedures is described in Section 3.2 of the dissertation by Sexton (2008).

Due to the concentrated composition of the samples collected this quarter, the nominal dilution factor of 10,000x for the cation chromatography method was increased to 20,000x so that the amount of PZ contained in the diluted sample would fall within the 10–75 ppm by mass range of the PZ standards.

Anion Chromatography

Anion chromatography was carried out using a Dionex ICS-3000 IC with a KOH eluent to determine the quantity of anions such as formate, acetate, glycolate, oxalate, sulfate, nitrate, nitrite, and chloride found in the sample solutions. A detailed description of this method and procedures is described in Section 3.1 of the dissertation by Sexton (2008).

The nominal dilution factor of 100x was adjusted in a similar manner to that described for cation chromatography. A dilution factor of 500x was found to be satisfactory for concentrated solutions.

Results

Two different solutions were evaporated this quarter. The first solution was an 8 m PZ solution with a loading of 0.3 moles of CO_2 per mole of alkalinity. The second solution was an 8 m PZ solution with a loading of 0.3 moles of CO_2 per mole of alkalinity with the addition of 0.25 moles of formic acid per liter of solution to mimic a degraded solution. Table 1 shows the Total Alkalinity, Total Inorganic Carbon, and Cation Chromatography results for each solution. Note that each solution has a beginning (non-evaporated) sample and a concentrated sample entry.

Table 1: Total Alkalinity, TIC, and Cation IC Summary Table

Solution	Sample Type	Alkalinity (mol/kg sol.)	PZ (Cation) (mol/kg sol.)	CO_2 (TIC) (mol/kg sol.)	Loading (mol CO_2/ mol alk.)
8 m PZ, α = 0.3	Starting Solution	4.15	4.45	2.59	0.29
	91% Conc.	7.54	7.76	2.93	0.19
8 m PZ, α = 0.3 250 mM FA	Starting Solution	4.04	4.07	2.50	0.30
	89% Conc.	6.95	6.37	2.18	0.17

Freeman et al. showed that thermal degradation rates of 8 m PZ with 0.3 mol CO_2/ mol alkalinity lose about 0.44% and 8.0% amine per week at 150 and 175 °C (Freeman et al., 2010). Since a typical evaporation experiment lasted two hours, thermal degradation products were not analyzed. Furthermore, Sexton reports that the oxidative degradation rates for PZ are below 0.25 mM per hour even in the presence a strong oxidation catalyst such as copper (Sexton, 2008). Because degradation products were considered negligible for the experiments performed, only the second solution, 8 m PZ, α = 0.3, 250 mM formic acid, was analyzed by anion chromatography for formate. The results from the anion chromatograph can be seen in Table 2.

Table 2: Anion IC Summary Table

Solution	Sample Type	Formate (Anion) (mol/kg sol.)
8 m PZ, α = 0.3 250 mM FA	Starting Solution	0.21
	89% Conc.	0.66

Discussion

Table 1 illustrates that the addition of formic acid to a loaded PZ solution changes its thermodynamic behavior. This alteration can be seen in the difference in the concentration of PZ as well as in loading. Calculating a mass balance on the non-volatile species provides insight into these differences and is illustrated in Table 3. Expected values indicate what the concentration of that species should be based on the mass concentration of 89% and assuming that no non-volatiles (formate, N-formylpiperazine) leave the evaporating solution. The PZ difference column is the difference in measured PZ between the two solutions evaporated.

Table 3: Mass balance on the 8 m PZ, α = 0.3, 250 mM formic acid solution

Formate (mol/kg sol.)	Expected Formate (mol/kg sol.)	Difference (mol/kg sol.)	Formamide (mol/kg. sol)	Expected Formamide (mol/kg sol.)	PZ Difference (mol/kg sol.)
0.66	1.79	1.13	0.028	0.242	1.39

Using the above mass balance, it is hypothesized that the difference in ending PZ concentration is due to the equilibrium relationship between the amine, carboxylic acid, amide, and water.

$$\text{Amine} + \text{Carboxylic Acid} \leftrightarrow \text{Amide} + \text{Water} \quad (4)$$

Due to the dehydration of the solution, the concentrations of all of the species in equilibrium will increase; however, the effect of the increase of the amine and carboxylic acid concentrations will outweigh the increase in the amide concentration, which will shift the reaction to the right, creating more amide.

Verifying this point, addition of the expected formamide (formamide formed in preparing the initial solution) and the formate loss, a value of 1.37 mol/kg solution, yields a nearly identical value as the difference in PZ between the two solutions.

This hypothesis needs to be tested using the basic amide reversal technique outlined in Section 3.1.3 of Sexton (2008).

Future Work

Thermal Degradation

In the flue gas treating system, concentrated PZ at high temperatures is likely to be found in the thermal reclaimer and in hold-up areas. The concentrated solutions created in this quarter were roughly 66 wt % PZ or about 22 m; therefore, it would be advantageous to perform thermal degradation experiments on concentrated PZ solutions.

In the next quarter, thermal degradation experiments will be carried out on approximately 22 m PZ solutions at 175 °C. Stainless steel cylinders with Swagelok® end caps will be used for these experiments. The cylinders will be filled with solution, sealed, and placed in forced convection ovens. Cylinders will be taken out of the ovens and the solutions inside will be analyzed using the techniques discussed in this report. The results obtained will be compared with other thermal degradation rates for less concentrated PZ solutions.

Liquid-Liquid Equilibrium

Reclamation is a process that separates and recycles desired components used in amine scrubbing from undesired impurities. The desired species include amines, water, and user additives such as corrosion inhibitors or oxidation inhibitors. Corrosion inhibitors and oxidation inhibitors are often non-volatile species, meaning that they are likely to be thrown out with the reclaimer residue; therefore it would be economically beneficial to find some way of removing the inhibitors before thermal reclamation. A separation process before thermal reclaiming will allow the plant to recycle inhibitors while reducing the overall load on the thermal reclaimer, and consequently the reclaimer heat duty.

The slip-stream that is sent to the reclaimer will be a concentrated solution containing water, amine, degradation and corrosion products, and an assortment of ions. Due to the non-idealities of such a solution, it is likely that phase separation will occur. Phase separation of a mixture will occur when the stability requirement at constant temperature, pressure, and total number of moles shown below is not met (Sandler, 2006).

$$d^2G > 0 \tag{5}$$

The limits of the stability criteria, or when $d^2G = 0$, defines the binodal curve for the solution and as a result, the boundary for phase separation. For the solution under consideration, this binodal curve will likely define the liquid-liquid equilibrium boundary.

In the next quarter, a liquid-liquid equilibrium apparatus, shown in Figure 1 below, will be used to determine the boundaries of any liquid phase separations. The apparatus will consist of a 100 mL jacketed beaker circulated with a Lauda E-100 Ecoline Staredition water bath. The beaker will be plugged with a rubber stopper with a thermometer port and an upper sample port. The jacketed beaker will also have a lower sample port. The entire beaker system will be placed on a Corning model PC 220 Laboratory Stirrer/Hot plate to provide magnetic stirring of the liquid mixture.

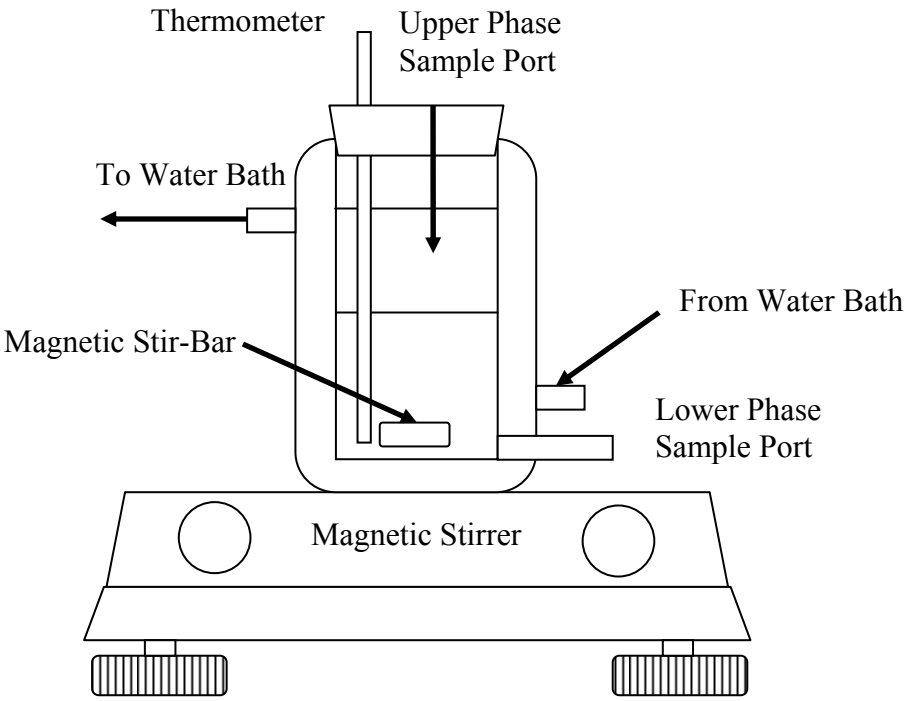

Figure 1: Liquid-liquid equilibrium apparatus

The experimental procedure will consist of adding small additions of crystalline amine to premade solutions of either corrosion or oxidation inhibitors. The solution will then be stirred for a period of time until it reaches equilibrium state, then the stirrer will be turned off and the solution will be allowed to settle to determine if phase separation has occurred. This procedure will be repeated until a phase separation occurs.

Reclaiming Apparatus

In this quarter, a thermal reclaiming apparatus, shown in Figure 2 below, with liquid and vapor sampling was designed and built. The reclaimer body is a 350 mL stainless steel Parr-Instruments 1108 Oxygen Bomb Calorimeter sealed with a 2-1/2" inner diameter FEP coated silicone o-ring. The calorimeter head is equipped with three ports; a liquid sampling line, a low-noise K-type thermocouple with miniature connector (model GKMQ-SS-125-U-12 by Omega®), and a vapor sampling line. The calorimeter assembly will be submerged in a Thermo Scientific® Digital One oil bath to regulate the reclaimer temperature. The vapor sampling line has a Druck® PTX-611 (0-3 bar absolute) pressure transducer. The signal from the pressure transducer is sent to a current-to-voltage signal converter before it is sent to a NI USB 6009 data logger using LabView® SignalExpress software to read the pressure of the reclaimer during

experimental runs. The vapor sampled during experimentation will be sent via a heated line at 180 °C to a Gasmet™ DX-4000 FTIR gas analyzer with Calcmet® software.

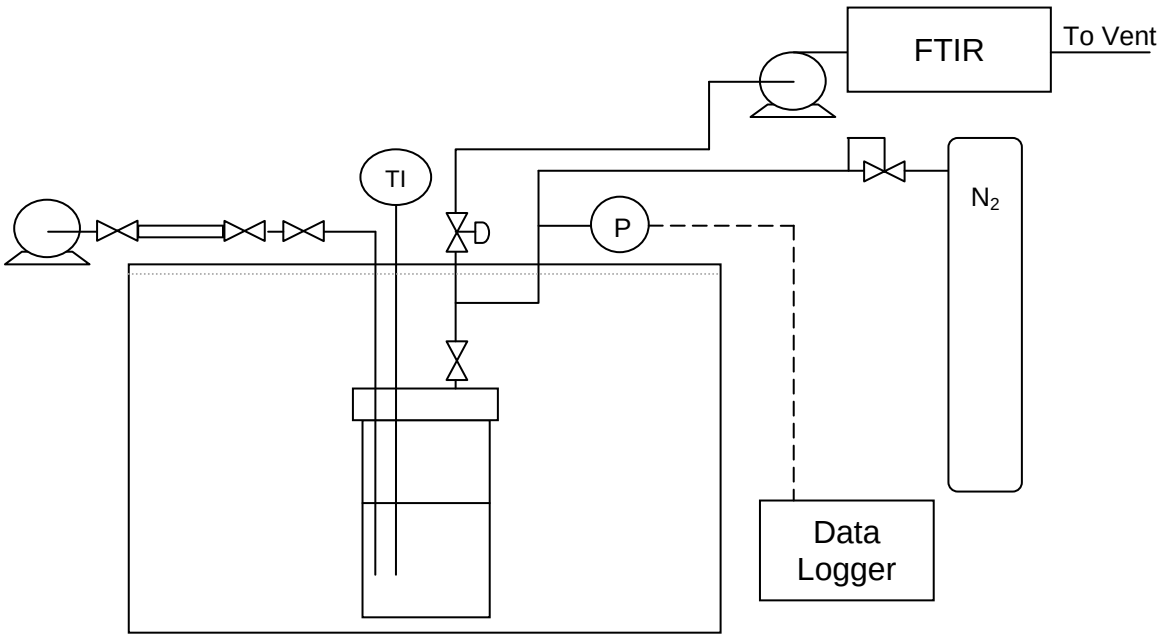

Figure 2: Thermal reclaiming apparatus with continuous vapor sampling

Experiments will begin by filling the calorimeter with a pre-weighed amount of loaded amine solution. The top of the calorimeter will be sealed and then submerged in the oil bath where the temperature will be increased. Once the desired temperature is reached, the vapor sampling line will be opened and the FTIR will continuously read the vapor sample coming off the top of the calorimeter. After the vapor sampling line is opened, a liquid sample will be taken using a sample pump and a stainless steel quick-disconnecting sample tube. The liquid sample will then be transferred to a glass sample vial and later analyzed using the analytical techniques discussed earlier. As vapor is sampled off the calorimeter, the solution inside will increase in non-volatile concentration, which will result in decreasing vapor production. Once a minimum vapor rate is achieved, the temperature of the oil bath will be increased and the sampling procedure will repeat.

References

Cummings AL, Smith GD, Nelsen DK. “Advances in Amine Reclaiming – Why There’s No Excuse to Operate a Dirty Amine System.” *Laurance Reid Gas Conditioning Conference.* 2007.

Freeman SA, Dugas R, Van Wagener DH, Nguyen T, Rochelle GT. “Carbon Dioxide Capture with Concentrated Aqueous Piperazine.” *IJGGC*. 2009;4:(2).

Hilliard MD. *A Predictive Thermodynamic Model for an Aqueous Blend of Potassium Carbonate, Piperazine, and Monoethanolamine for Carbon Dioxide Capture from Flue Gas.* The University of Texas at Austin. Ph.D. Dissertation. 2008.

Kohl A, Nielsen R. *Gas Purification.* 5th ed. Houston, TX: Gulf Publishing Company; 1997.

NGPSA. *Engineering Data Book.* Tulsa, OK; Natural Gas Processors Suppliers Association (NGPSA). 2004.

Rochelle GT et al. "CO_2 Capture by Aqueous Absorption, Third Quarterly Progress Report 2009." Luminant Carbon Management Program. The University of Texas at Austin. 2009.

Rochelle GT et al. "CO_2 Capture by Aqueous Absorption, First Quarterly Progress Report 2010." Luminant Carbon Management Program. The University of Texas at Austin. 2010.

Sandler SI. *Chemical, Biochemical, and Engineering Thermodynamics*. 4th ed. Hoboken, NJ: John Wiley & Sons, Inc.; 2006.

Sexton A. *Amine Oxidation in CO_2 Capture Processes*. The University of Texas at Austin. Ph.D. Dissertation. 2008.

Solvent Reclaiming by Solids Precipitation

Quarterly Report for April 1 – June 30, 2010

by Humera Abdul Rafique

Supported by the Luminant Carbon Management Program

and the

Industrial Associates Program for CO_2 Capture by Aqueous Absorption

Department of Chemical Engineering

The University of Texas at Austin

July 7, 2010

Abstract

The solubility of potassium sulfate (K_2SO_4) in piperazine (PZ) solution increases with increasing loading because of a greater concentration of carbamate and protonated amine in the system. The solubility decreases with decrease in temperature. The solubility of K_2SO_4 is lower in PZ than in MEA when determined using the solid solubility experimental procedure, i.e., the solubility decreases in organic solutions with greater organic concentrations.

It has been determined that solubility window for CO_2 in PZ solutions is between 0.3 and 0.46 (Freeman, 2008). In order to fully determine the loading limit of the PZ solutions, experiments are being carried out to determine the solubility of hydrated protonated piperazine carbamate by initially preparing the crystals and using the solid solubility method to determine the solubility.

Introduction

This quarter, analyses were completed of the previous experiments on potassium sulfate solid solubility in 8 m PZ at 0.3 and 0.4 CO_2 loading. The experiments were performed to determine the solubility of K_2SO_4 in aqueous PZ.

Figure 1 shows the solvent reclaiming system as modeled by Xu (2008) for an MEA absorption/stripping amine reclaiming system. A slip stream of the hot lean feed from the stripper is flashed though a three-stage flash system. Here CO_2 and H_2O are evaporated until the pressure in the system falls to 0.1 atmosphere.
Water is condensed in the precooler and intercoolers of the compressor. KOH is then fed to crystallize the sulfate present in the system. The K_2SO_4 solids are removed in the separator and the amine is returned to the absorption/stripping process (Xu, 2008). It is expected that a PZ absorption/stripping system will require a similar reclaiming system. The number of flash stages needed for a PZ system will be determined when enough data are collected using solid solubility experiments.

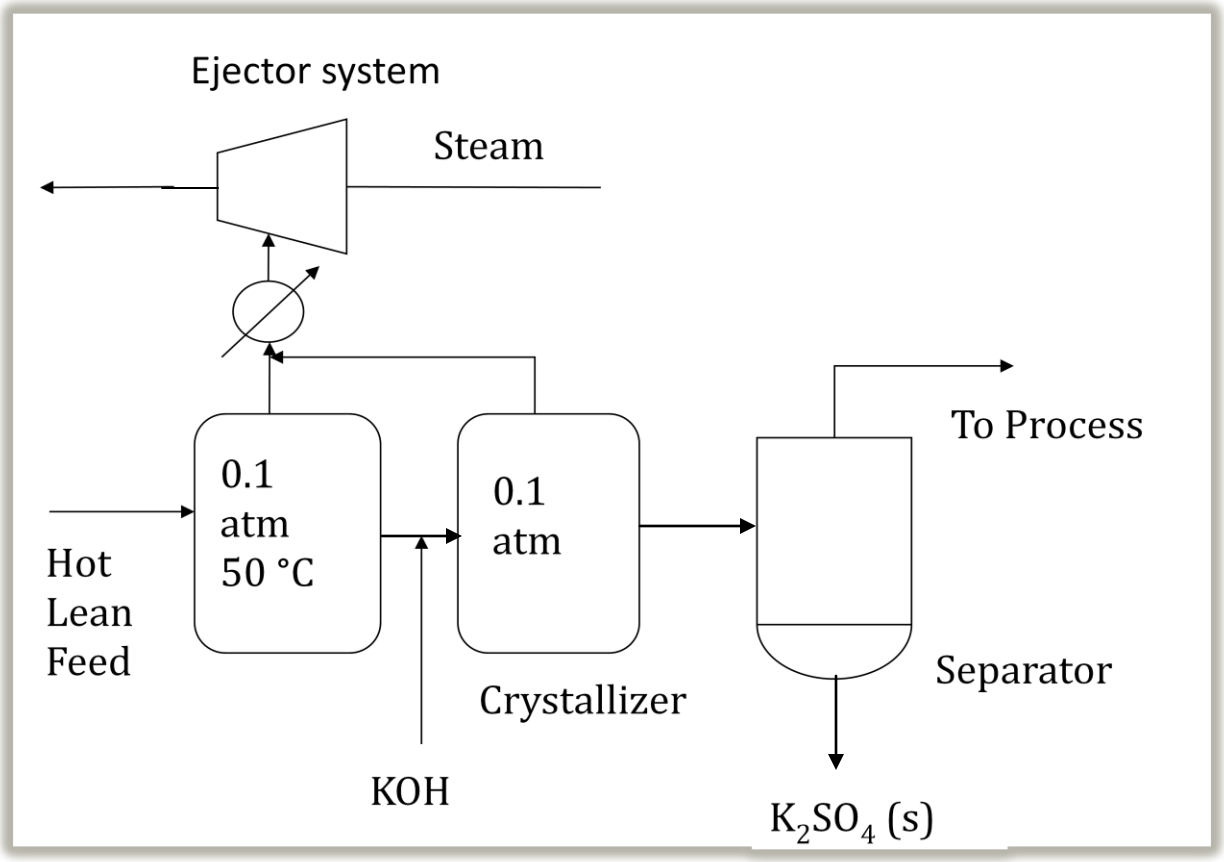

Figure 1: Solvent reclaiming system as predicted by Xu (2008) for MEA reclaiming

This quarter additional experiments were performed on the solubility of piperazine containing solids in piperazine solutions. This is a continuation of Freeman's work on classifying PZ solutions of various concentrations as either soluble or insoluble, depending on whether crystallization occurred after the PZ solution was loaded with CO_2.

Since PZ has been shown to be a useful amine for CO_2 removal through absorption/stripping, experiments are being carried out to better understand the solubility window that exists for PZ solutions in as a function of concentration, and CO_2 loading (Rochelle et al., 2008).

Experimental Methods

The three solid solubility experiments carried out last quarter to calculate the solubility of K_2SO_4 were as follows:
Experiments 1 and 2 – Solid Solubility of K_2SO_4 in 8 m PZ with a CO_2 loading of 0.3.
Experiment 3 – Solid Solubility of K_2SO_4 in 8 m PZ with a CO_2 loading of 0.4.

The temperature of the solution varied between room temperature and 80 °C. Solution was sampled using a filtered syringe and diluted in DDI water to prevent K_2SO_4 crystallization. Experimental samples were analyzed for K^+, SO_4^{-2}, CO_2, and PZ concentrations in the cation chromatograph, anion chromatograph, and TIC.

Analytical Methods

The concentration of K^+ and PZ in the samples was analyzed using a cation chromatograph. CO_2 concentration in solution was determined using a Total Inorganic Carbon (TIC) Analyzer, and the SO_4^{-2} concentration was analyzed using an anion chromatograph.

Cation Chromatography: The cation IC was used to determine the concentration of K^+ and PZ in experimental samples. A Dionex ICS-2500 with a CS17 IonPac column with 4-mm Cationic Self-Regenerating Suppressor (CSRS) was used as previously described by Sexton (2008) with a linear increase of methanesulfonic acid (MSA) concentration in the eluent.

Anion Chromatography: The anion IC was used to determine the concentration of SO_4^{-2} in the experimental samples. A Dionex ICS-3000 instrument with AS15 IonPac column, 4-mm Anionic Self-Regenerating Suppressor (ASRS), carbonate removal device (CRD), and carbonate removal from eluent generation was used as described by Sexton (2008).

Total Inorganic Carbon Analyzer: Quantification of CO_2 loading was performed using a total inorganic carbon analyzer. In this method, a sample is acidified with 30 wt % H_3PO_4 to release the CO_2 present in solution (Hilliard, 2008). The CO_2 is carried in the nitrogen carrier gas stream to the detector. PicoLog software was used to record the peaks produced from each sample. A calibration curve was prepared at the end of each analysis using a TIC standard mixture of K_2CO_3 and $KHCO_3$. The TIC method quantifies the CO_2, CO_3, and HCO_3 present in solution. These species are in equilibrium in the series of reactions shown below:

$$CO_3^{-2} + 2H^+ \leftrightarrow HCO^{-3} + H^+ \leftrightarrow H_2CO_3 \leftrightarrow CO_2 + H_2O \quad (1)$$

Acidification of the sample shifts the equilibrium toward CO_2 which bubbles out of solution and is detected in the analyzer (Rochelle et al., 2010). The TIC analysis helps identify whether loss of CO_2 was prevalent at higher temperatures of the experiment.

Results and Discussion

K_2SO_4 solid solubility experiments - The results from the analytical methods employed above were tabulated in Tables 1, 2, and 3 below.

Table 1: Solid Solubility of K_2SO_4 in 8 m PZ with CO_2 loading = 0.3

T (°C)	K^+ (mmol/kg)	PZ (mmol/kgsol)	SO_4^{-2} (mmol/kgsol)	CO_2 (mmol/kgsol)
21	74	2151	33	32
30	111	1869	47	29
40	171	2485	68	36
50	198	2465	87	39
60	191	2301	104	36
70	192	2185	122	34
80	246	2728	133	39

Table 2: Solid Solubility of K_2SO_4 in 8 m PZ with CO_2 loading = 0.3 (experiment 2)

T (°C)	K^+ (mmol/kg)	PZ (mmol/kgsol)	SO_4^{-2} (mmol/kgsol)	CO_2 (mmol/kgsol)
21	38	2116	27	31
30	94	2311	37	46
40	134	2565	57	35
50	164	3034	85	38
60	177	2938	90	38
70	108	1384	46	22
80	232	3525	115	45

Table 3: Solid Solubility of K_2SO_4 in 8 m PZ with CO_2 loading = 0.4

T (°C)	K^+ (mmol/kg)	PZ (mmol/kgsol)	SO_4^{-2} (mmol/kgsol)	CO_2 (mmol/kgsol)
30	133	2867	57	40
40	181	2939	81	39
50	250	3801	119	47
60	233	3121	132	39
70	290	3543	137	44
80	242	2881	117	37

The concentration of K^+ (Figure 2) and SO_4^{-2} (Figure 3) measured by the cation chromatograph and anion chromatograph respectively, was plotted against the inverse of temperature for all three experiments. The solubility of K_2SO_4 in water (Söhnel, 1985) for varying temperatures was also plotted in the same figure to compare the solubility of salt in the two different media. Plotted on the same curves were the K_2SO_4 solubility results for 7 m and 11 m MEA at 0.3 and 0.4 loading obtained from Xu (2008).

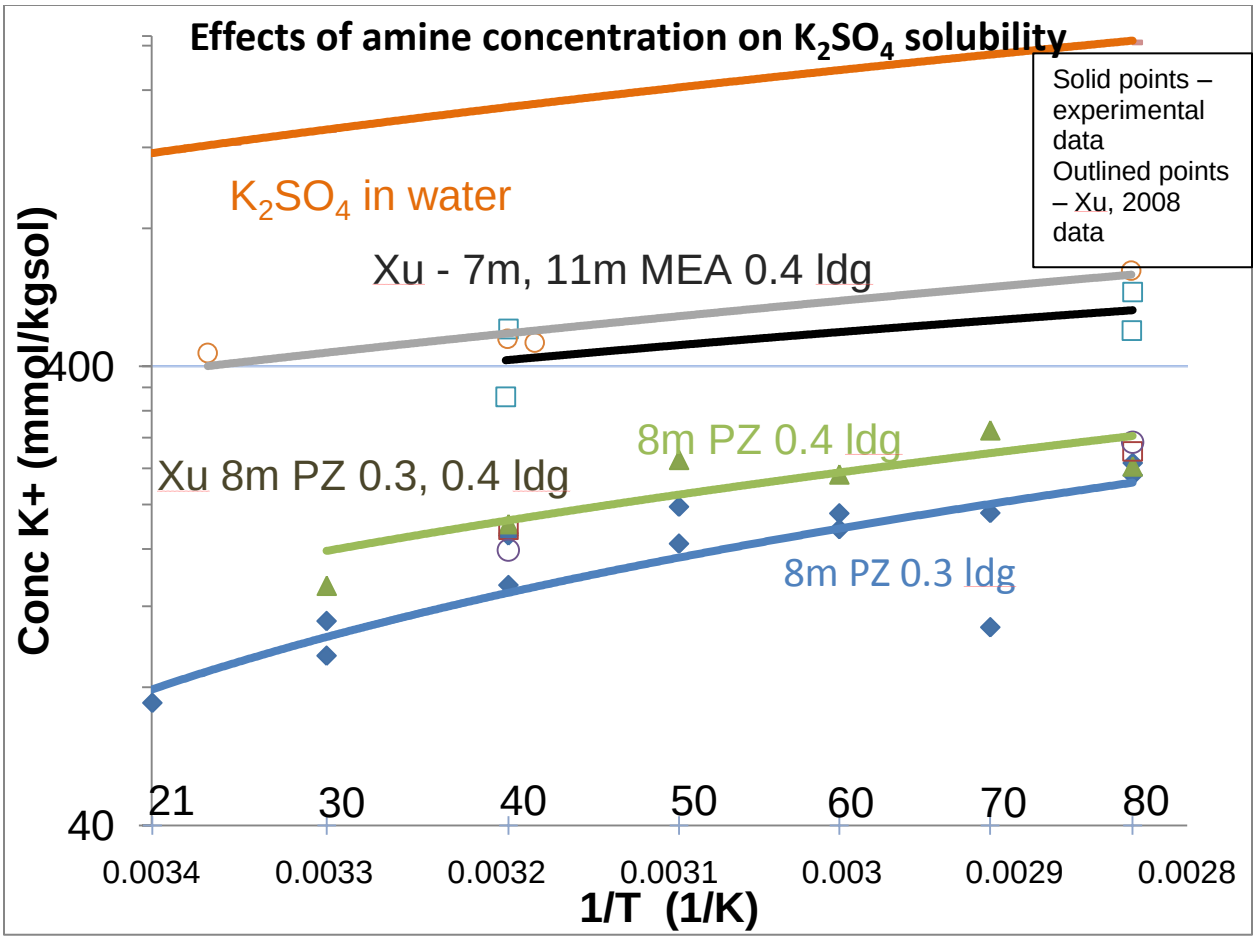

Figure 2: Concentration of Potassium in 8 m PZ saturated to K_2SO_4

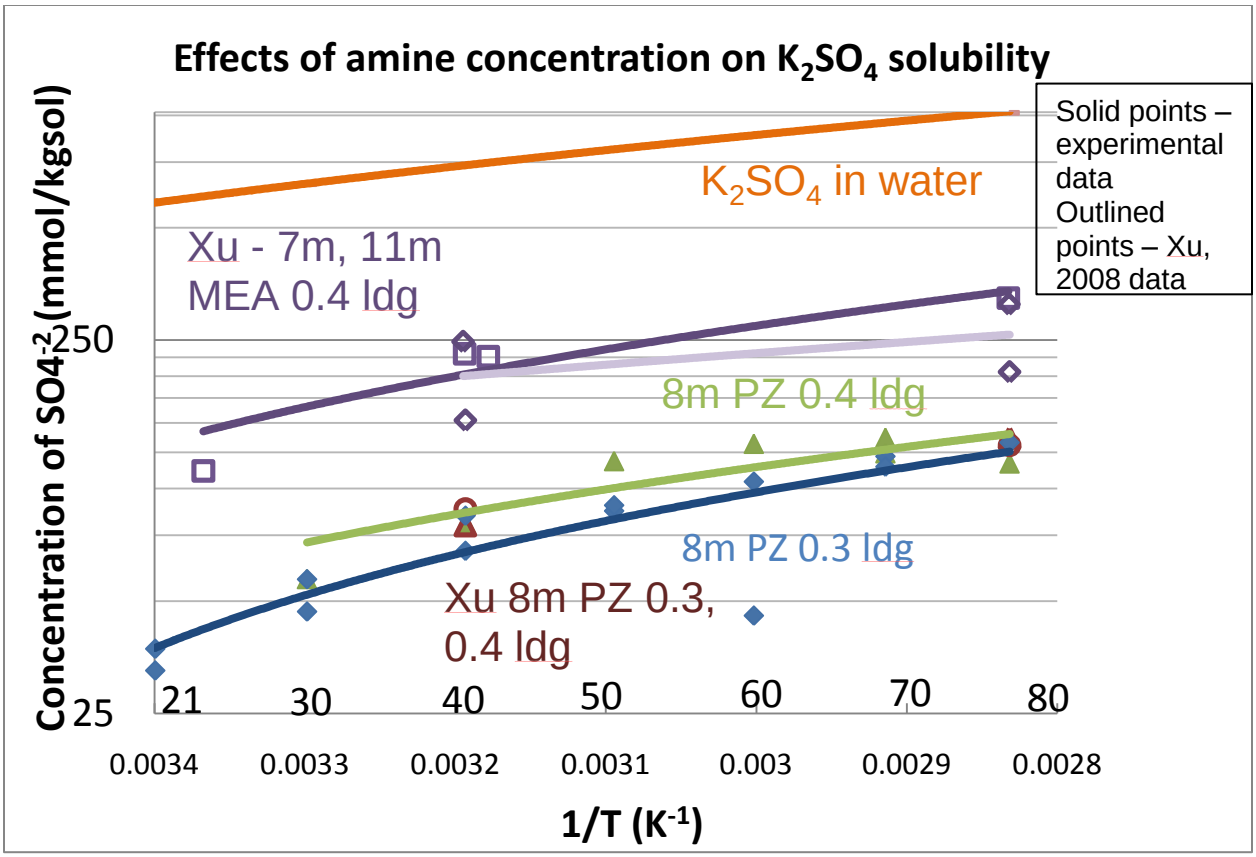

Figure 3: Concentration of Sulfate in 8 m PZ solutions

Figures 2 and 3 both show that the solubility of K_2SO_4 in solution increases with increasing loading because of a greater concentration of carbamate and protonated amine in the system. The solubility of the sulfate also increases with the temperature of the solution. The solubility of K_2SO_4, however, is lower in PZ than in MEA. This is because the ring structured PZ is more organic in nature than MEA. A solvent reclaiming process ideally requires a large difference in solubility at different loadings. Xu (2008) correlated her experimental results for K_2SO_4 solubility in MEA with an empirical equation shown in Figure 4. The results obtained for 8 m PZ from experiments 1, 2, and 3 were fitted to this empirical equation and plotted in Figure 4.

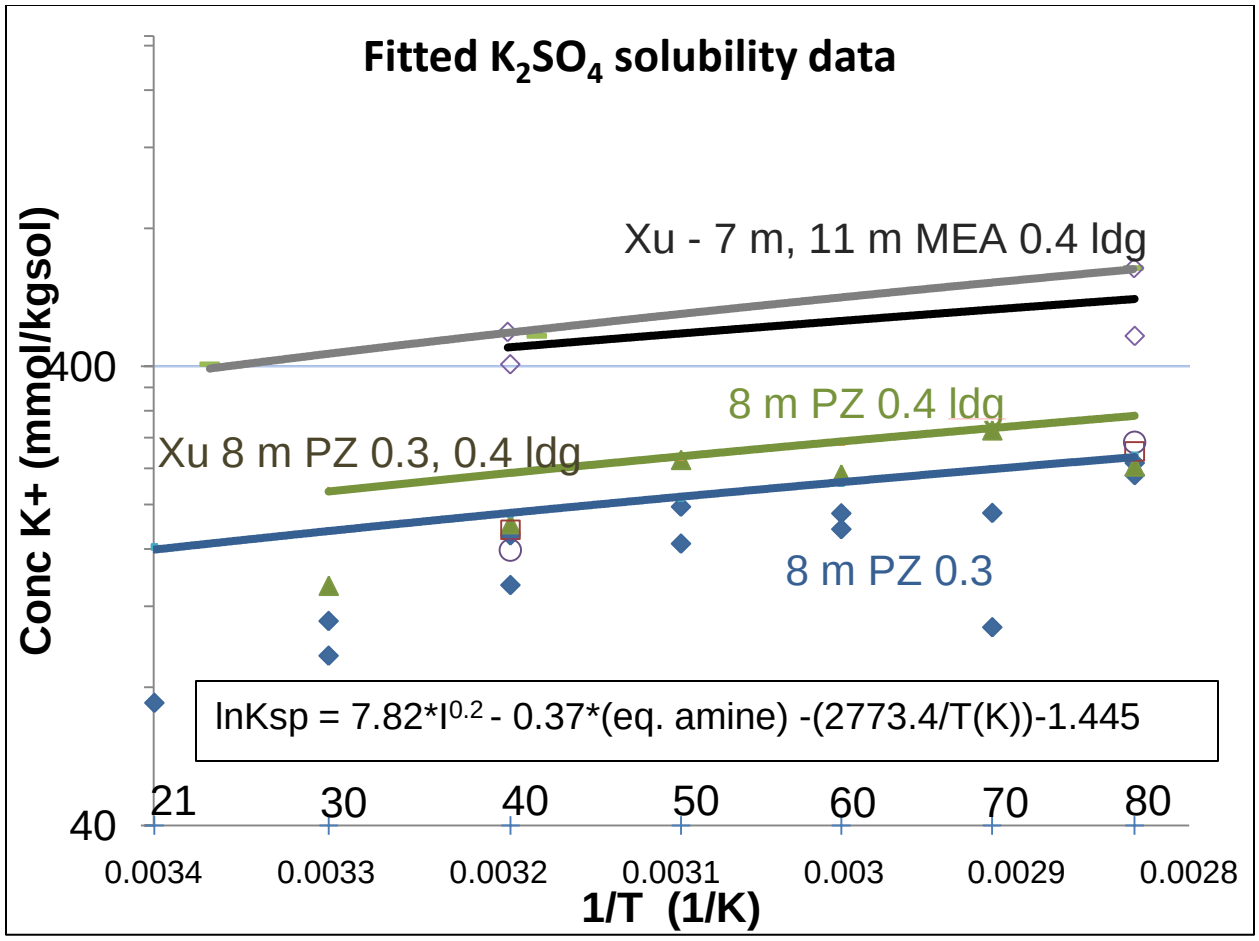

Figure 4: Fitted K_2SO_4 solubility data

It can be seen from Figure 4 that the empirical equation obtained by Xu (2008) for varying MEA concentrations does not relate very well to PZ solutions. As more solubility data are collected for PZ solutions, an empirical equation will be formed using the solid solubility method.

The concentration of CO_2 in solution at the various sampling temperatures was also analyzed using the TIC analysis method. The raw data obtained were translated into mmol/kgsol and plotted against the inverse of temperature in Figure 5 below.

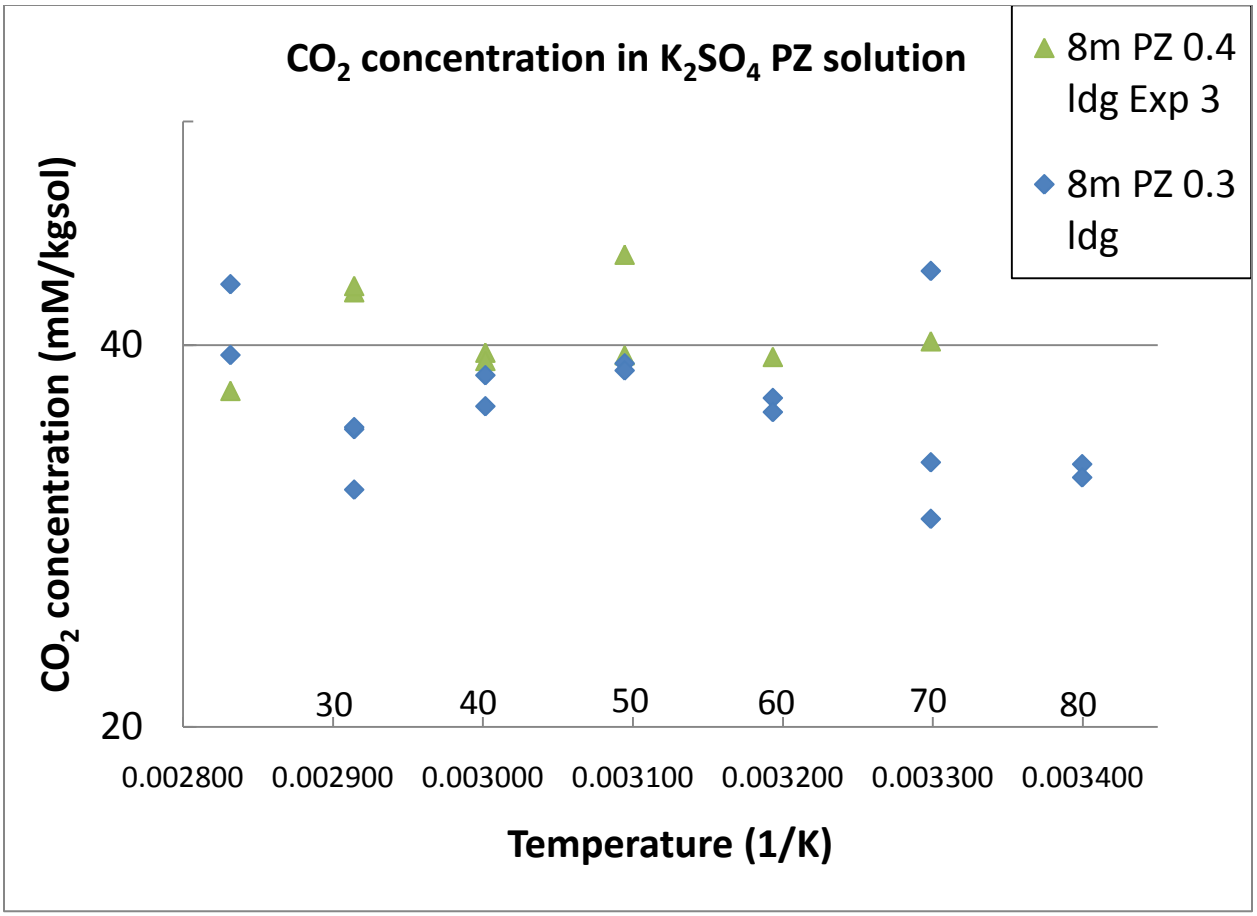

Figure 5: Concentration of CO_2 in K_2SO_4 solution

The reason for analyzing for CO_2 in PZ solutions is to determine if CO_2 was lost during the solid solubility experimental procedure. From Figure 5, a general observation can be made that at higher temperatures, some loss of CO_2 in solution does occur. For future experiments, a change in experimental procedures is being investigated to reduce heat loss in the solid solubility system.

PZ solubility - Another set of experiments that have been started this quarter are in continuation of Hilliard's work (2008) and Freeman's CO_2 solubility in PZ measurement (Freeman, 2009). Freeman studied the solubility window for CO_2 in PZ solutions. The analysis for 8 m PZ and 10 m PZ is shown in Figure 6 below.

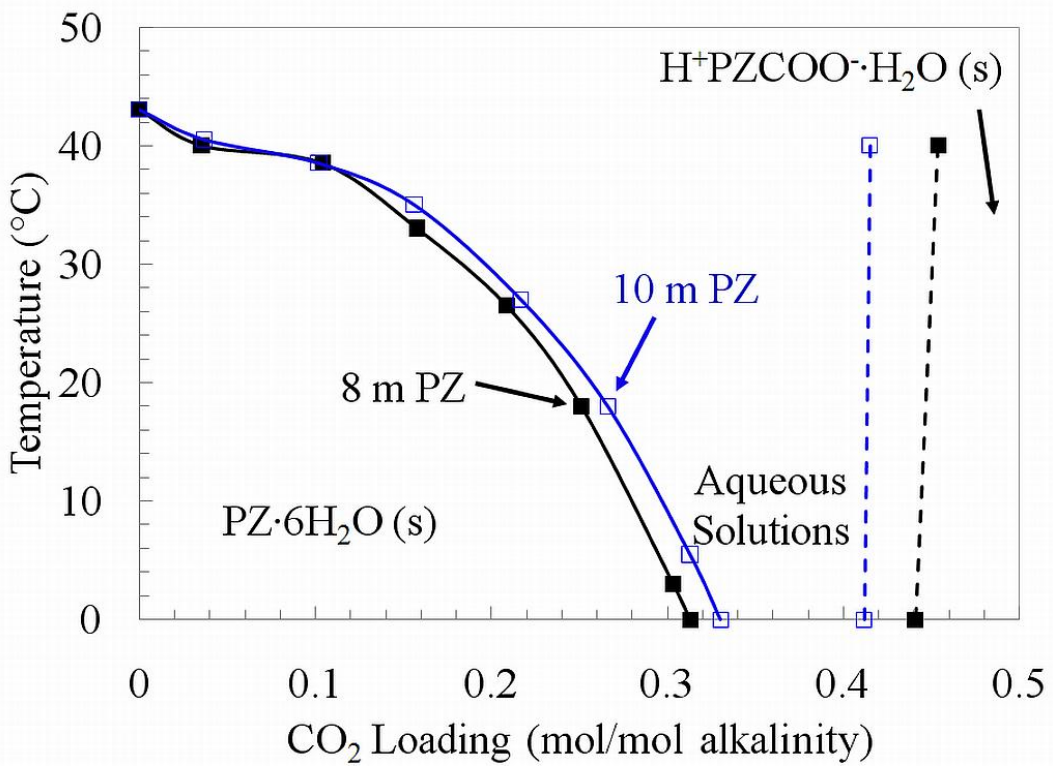

Figure 6: Solid-Liquid Transition Temperatures for Aqueous PZ

For 8 m PZ, a CO_2 loading of approximately 0.25 mole CO_2 per mole of alkalinity is required to maintain a liquid solution without precipitation at room temperature (20 °C) (Freeman, 2009). The points on the dotted lines show the CO_2 loading at which hydrated protonated PZ carbamate (H+PZCOO-.H_2O) is soluble in the PZ solution. It is predicted that beyond the 0.46 loading points H+PZCOO-.H_2O is precipitated. The trend of this solubility is predicted by the dotted lines. The actual trend for temperatures from 0 °C to beyond 50 °C is being determined from solid solubility experiments similar to those performed for determining the solubility of K_2SO_4 in PZ solutions. The crystals are first produced by loading the PZ solutions to above 0.46. If the precipitate is not formed during loading, the solution is stirred after loading until solids are seen. The solids are then air dried and solid solubility experiments performed to determine the amount of precipitate expected at a given loading.

Conclusions

It can be determined from comparing the solid solubility experiments performed this quarter for PZ and the results obtained by Xu (2008) for MEA that the solubility of sulfate decreases in organic solutions as the solution becomes more organic in nature. The solubility of sulfate also decreases with a decrease in temperature. As CO_2 is loaded in solution, the concentration of carbamate and protonated amine in the system increases, resulting in an increase in the solubility of the potassium sulfate. The concentration of K^+ in 8 m PZ solution with 0.3 CO_2 loading at 40 °C and 80 °C were within 2–5% of the results obtained by Xu (2008). However, the concentration of K^+ in 8 m PZ solution with 0.4 CO_2 loading at 40 °C and 80 °C was within 11–13%. It is expected that the concentration of K^+ obtained by analytical methods is twice the concentration of sulfate obtained by anion chromatography. Comparing the data obtained, an

average K^+ concentration/SO_4^{-2} concentration for all three experiments is 2.08 and a standard deviation of 0.276. This is small within experimental errors validating the solid solubility experimental procedure. Further solid solubility experiments at varying PZ concentrations are being performed to determine an empirical equation for the solubility of K_2SO_4 in PZ using regression of data.

Future Work

Solid solubility experiments of K_2SO_4 in 2 m, 5 m, 9 m, and 11 m PZ are being performed to determine the an empirical equation for the solubility of K_2SO_4 in PZ using regression of data. In a similar manner, Xu (2008) determined the empirical equation for the solubility of K_2SO_4 in MEA. Solubility of sulfate salts other than potassium, such as that of sodium and calcium, is also being reviewed to determine other favorable amine reclaiming materials.

For the PZ solubility experiments, 8 m PZ and 9 m PZ have been loaded to approximately 0.48 loading and crystals of hydrated protonated piperazine carbamate have been observed in the solution. The solution is being analyzed to determine the actual concentration and loading of the solutions. The crystals produced are being dried and analyzed by X-ray diffraction. They are also being prepared in bulk to determine the solubility of the carbamate in PZ solution.

References

Freeman SA, Dugas R, Van Wagener DH, Nguyen T, Rochelle GT. "Carbon dioxide capture with concentrated, aqueous piperazine". *GHGT-9.* 2009;1(1):1489–1496.

Hilliard MD. *A Predictive Thermodynamic Model for an Aqueous Blend of Potassium Carbonate, Piperazine, and Monoethanolamine for Carbon Dioxide Capture from Flue Gas.* The University of Texas at Austin. Ph.D. Dissertation. 2008.

Rochelle GT et al. "CO_2 Capture by Aqueous Absorption, Second Quarterly Progress Report 2008". Luminant Carbon Management Program. The University of Texas at Austin. 2008.

Rochelle GT et al. "CO_2 Capture by Aqueous Absorption, Fourth Quarterly Progress Report 2009". Luminant Carbon Management Program. The University of Texas at Austin. 2010.

Sexton A. *Amine Oxidation in CO_2 Capture Processes*. The University of Texas at Austin. Ph.D. Dissertation. 2008.

Söhnel O, Novotny P. *Densities of aqueous solutions of inorganic substances*. Elsevier, Amsterdam. 1985.

Xu Q. *Solvent Reclaiming by Crystallization of Potassium Sulfate*. The University of Texas at Austin. M.S. Thesis. 2008.

Degradation of MDEA When Continuously Cycled in a Thermal-Oxidative Reactor

International Technical Conference on Clean Coal & Fuel Systems - June 7, 2010

Fred Closmann

Supported by

Luminant Carbon Management Program

and

Process Science and Technology Center

Carbon Management Project

Outline of Topics

- Overview of CO_2 absorption/stripping
- Relative Performance of MDEA/PZ
- Previous results and literature
- Solvent cycling results (current work)
- Oxidative Model
- Summary/Future Work

Absorber/Stripper System for CO_2 Scrubbing in Flue Gas

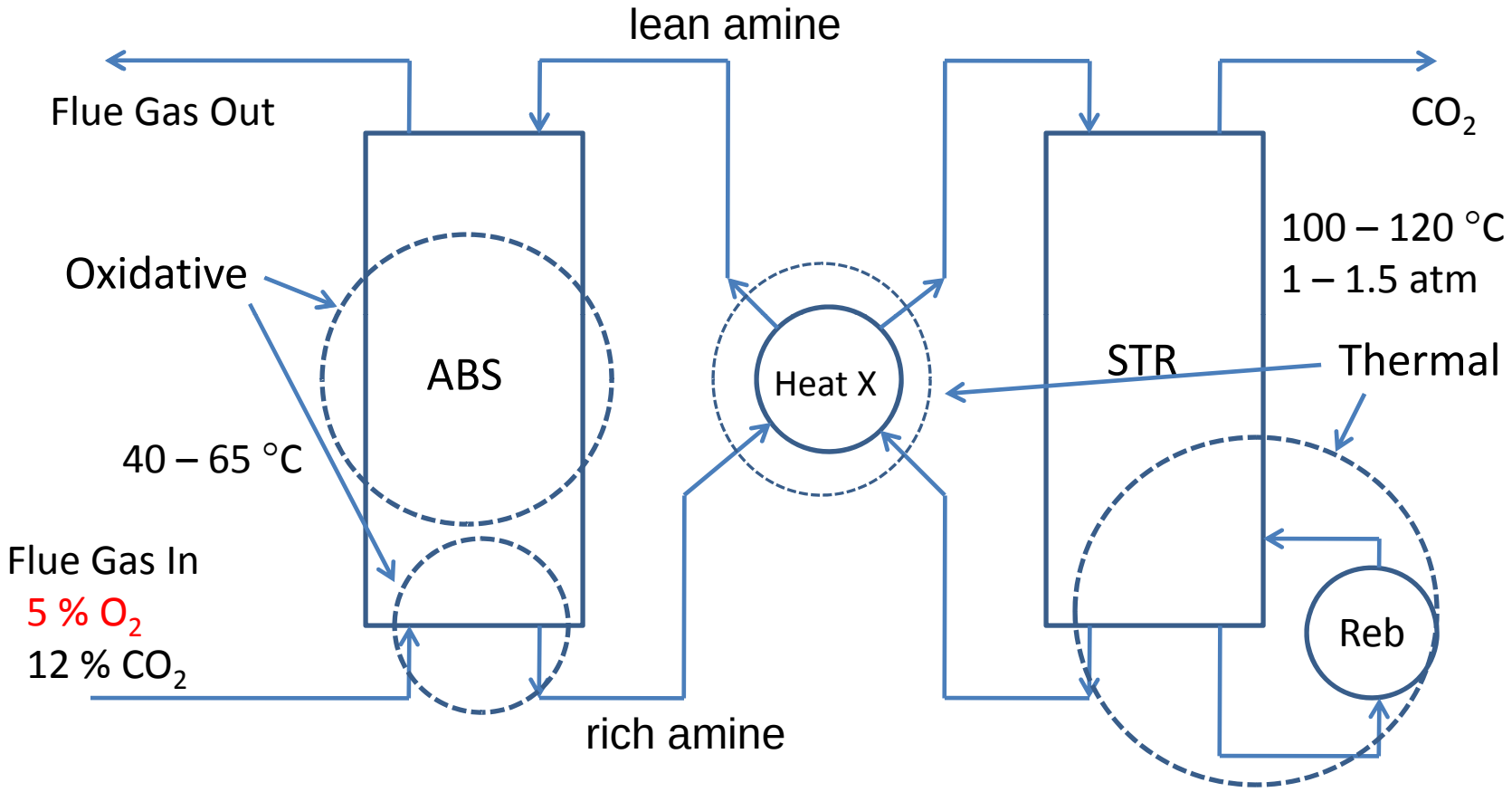

Conditions potentially leading to degradation

Solvent Performance (Fast Solvents)

Amine	Conc. (m)	CO_2 Capacity@ $P_{CO2,lean}$=0.5kPa (mol/kg (H_2O+Am))	k_g' @P_{CO2} =5kPa (×10^7mol/s·Pa·m^2)	ΔH_{abs}@P_{CO2} =1.5kPa (kJ/mol)
PZ	8	0.79	5.3	70
MDEA/PZ	7/2	0.80	5.2	68
MEA	7	0.47	3.1	82

Structures

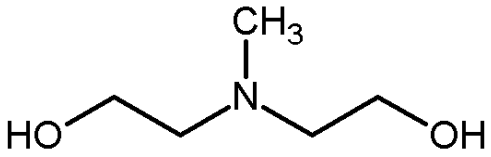

Methyldiethanolamine (MDEA)

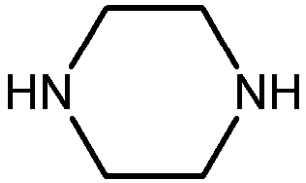

Piperazine

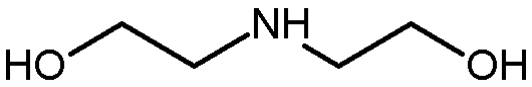

Diethanolamine (DEA)

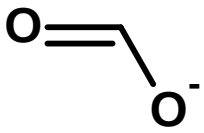

Formate

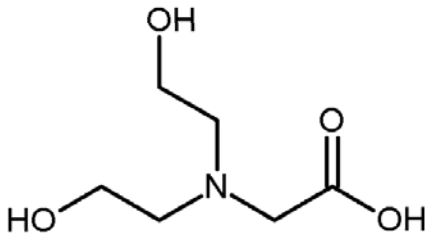

Bicine

Previous Results/Literature – MDEA, PZ and blend

- Dawodu & Meisen (1996) degraded MDEA:
  - Reported intermediates - methylamino ethanol (MAE), diethanolamine (DEA), dimethylaminoethanol (DMAE)
- MDEA/PZ systems (Bedell, 2009):
  - Disproportionation primary process; homolytic cleavage not observed
  - MDEA degrades to DMAE and triethanolamine (TEA)
  - Reported 1-methyl PZ, very little bis-hydroxyethyl piperazine (bHEP)
  - Difficult to close C-mass balance due to CO_2 evolution
- Blended systems preferentially destroyed PZ (Davis, 2008/2009)

Overview of Degradation

- MDEA oxidative degradation in simple batch expt (low-gas): formate production ~ 0.024 mM/hr
- PZ oxidative degradation (same system): formate production ~ 0.025 mM/hr
- Formate production in 7 m MDEA/2 m PZ ~ 0.013 mM/hr
- PZ thermally stable up to 175 °C (Freeman, 2009)
- Thermal degradation of blend ~ 60 mmolal/day loss for both MDEA and PZ

Solvent Cycling
Integrated Solvent Degradation Apparatus

Purpose: Simulate Cycling Effects in Absorber/Stripper system.

Why is Cycling Important?

- Continuous supply of oxygen (absorber)
- Dissolved oxygen at 120 °C+
- Entrained gas bubbles (oxygen) at 120 °C+
- Secondary effects – e.g., thermal degradation products at oxidizing conditions

Integrated Solvent Degradation Apparatus

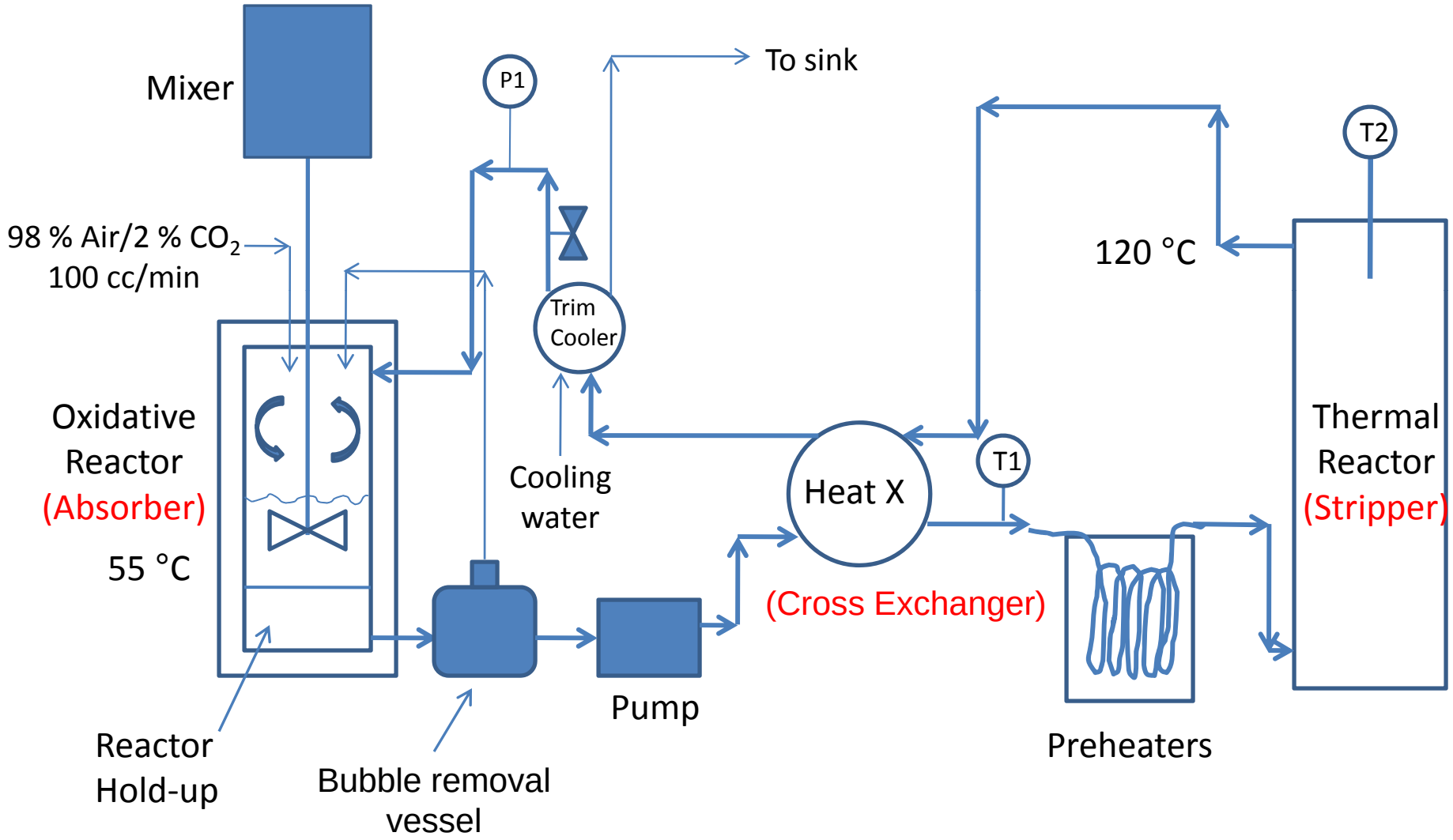

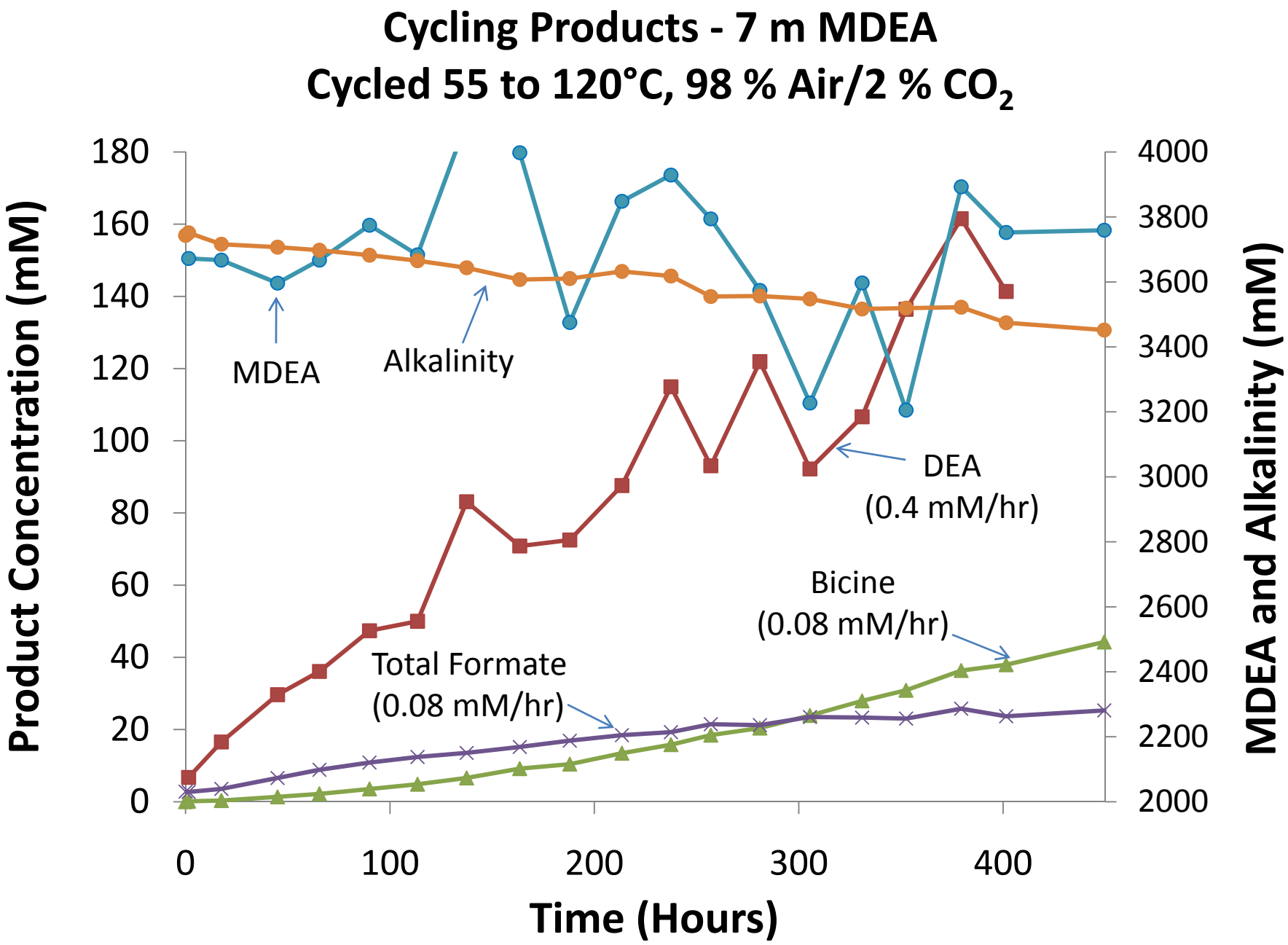
Cycling Products - 7 m MDEA
Cycled 55 to 120°C, 98 % Air/2 % CO2
Product Concentration (mM)
MDEA and Alkalinity (mM)
Time (Hours)
MDEA
Alkalinity
DEA
(0.4 mM/hr)
Bicine
(0.08 mM/hr)
Total Formate
(0.08 mM/hr)
0
20
40
60
80
100
120
140
160
180
2000
2200
2400
2600
2800
3000
3200
3400
3600
3800
4000
0
100
200
300
400

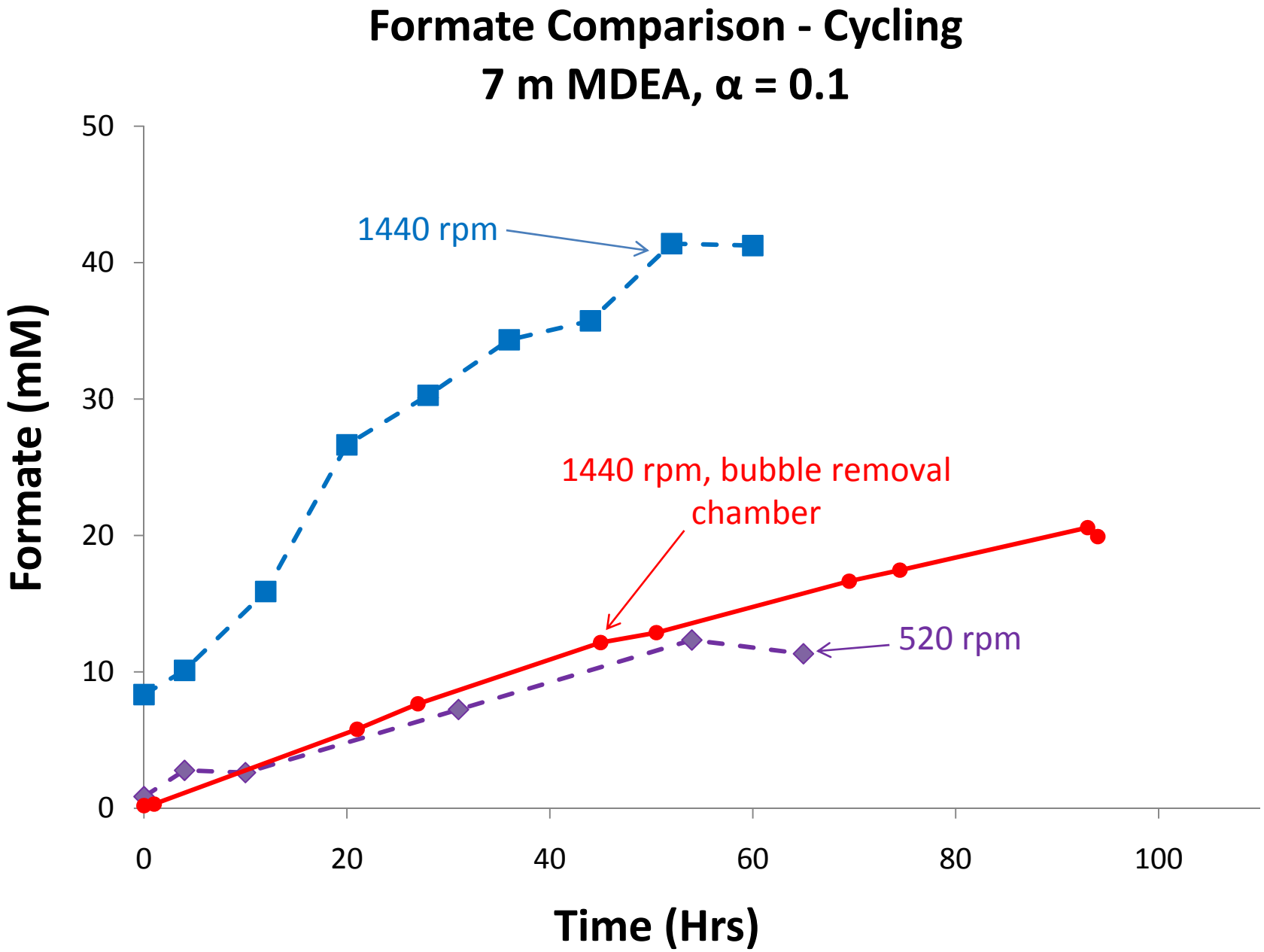
Formate Comparison - Cycling
7 m MDEA, α = 0.1
Formate (mM)
50
40
30
20
10
0
0
20
40
60
80
100
Time (Hrs)
1440 rpm
1440 rpm, bubble removal chamber
520 rpm

Formate Comparison – Inhibitor Effects
7 m MDEA, α = 0.1

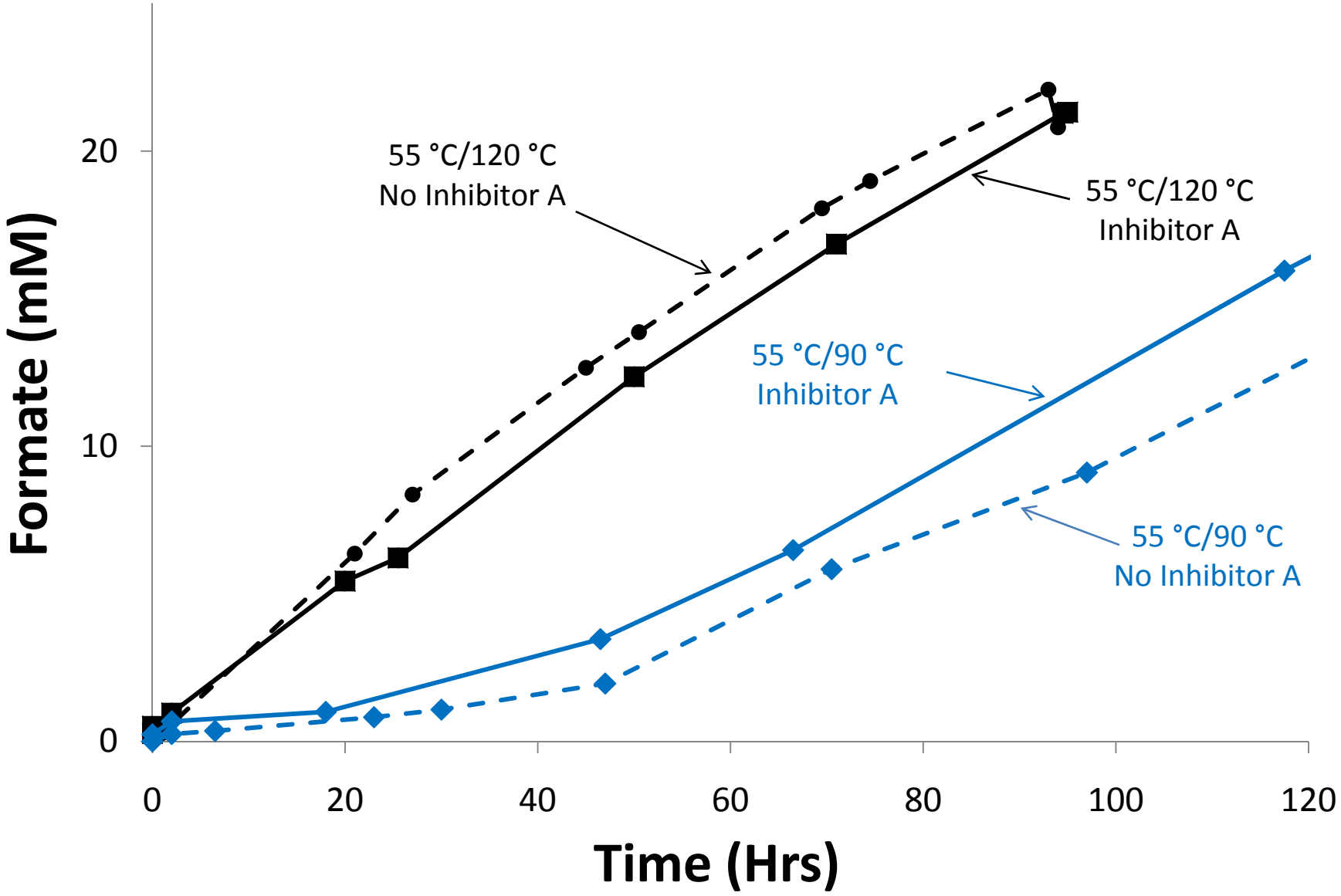

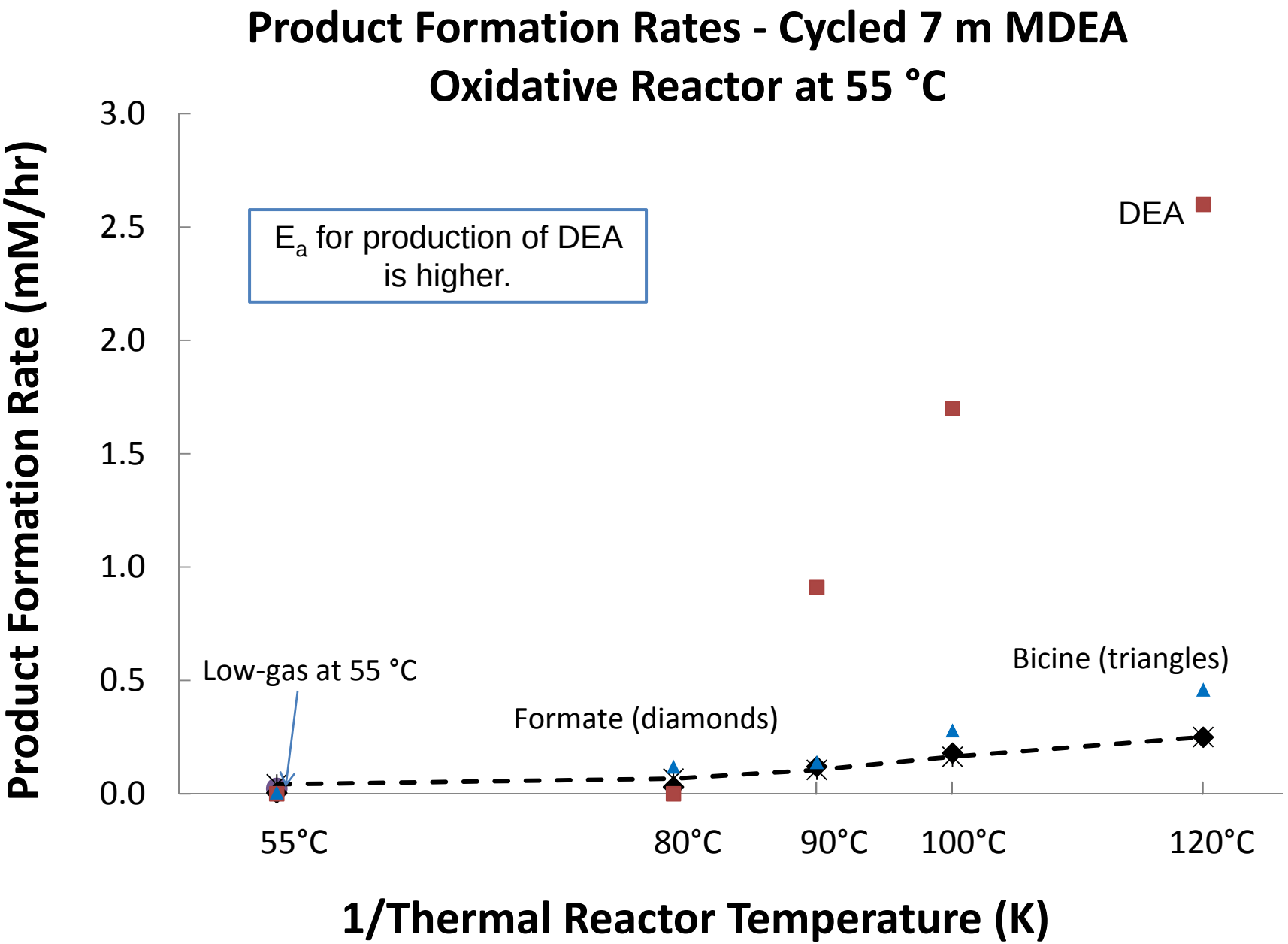
Product Formation Rates - Cycled 7 m MDEA
Oxidative Reactor at 55 °C
Product Formation Rate (mM/hr)
3.0
2.5
2.0
1.5
1.0
0.5
0.0
Ea for production of DEA is higher.
DEA
Low-gas at 55 °C
Formate (diamonds)
Bicine (triangles)
55°C
80°C
90°C
100°C
120°C
1/Thermal Reactor Temperature (K)

Oxidative Degradation Model

- Purpose: estimate oxidative degradation rates in heat exchanger and stripper
- Assume all oxidative degradation occurs in thermal reactor
- Model thermal reactor as isothermal PFR
- Rate-law over-predicts degradation due to depletion of O_2 > 100 °C
- Regress E_a, k_o, and S, where: $S = \Delta[Prod]/\Delta[DO]$ (per pass)

Product Formation Rates - Cycled 7 m MDEA
Oxidative Reactor at 55 °C

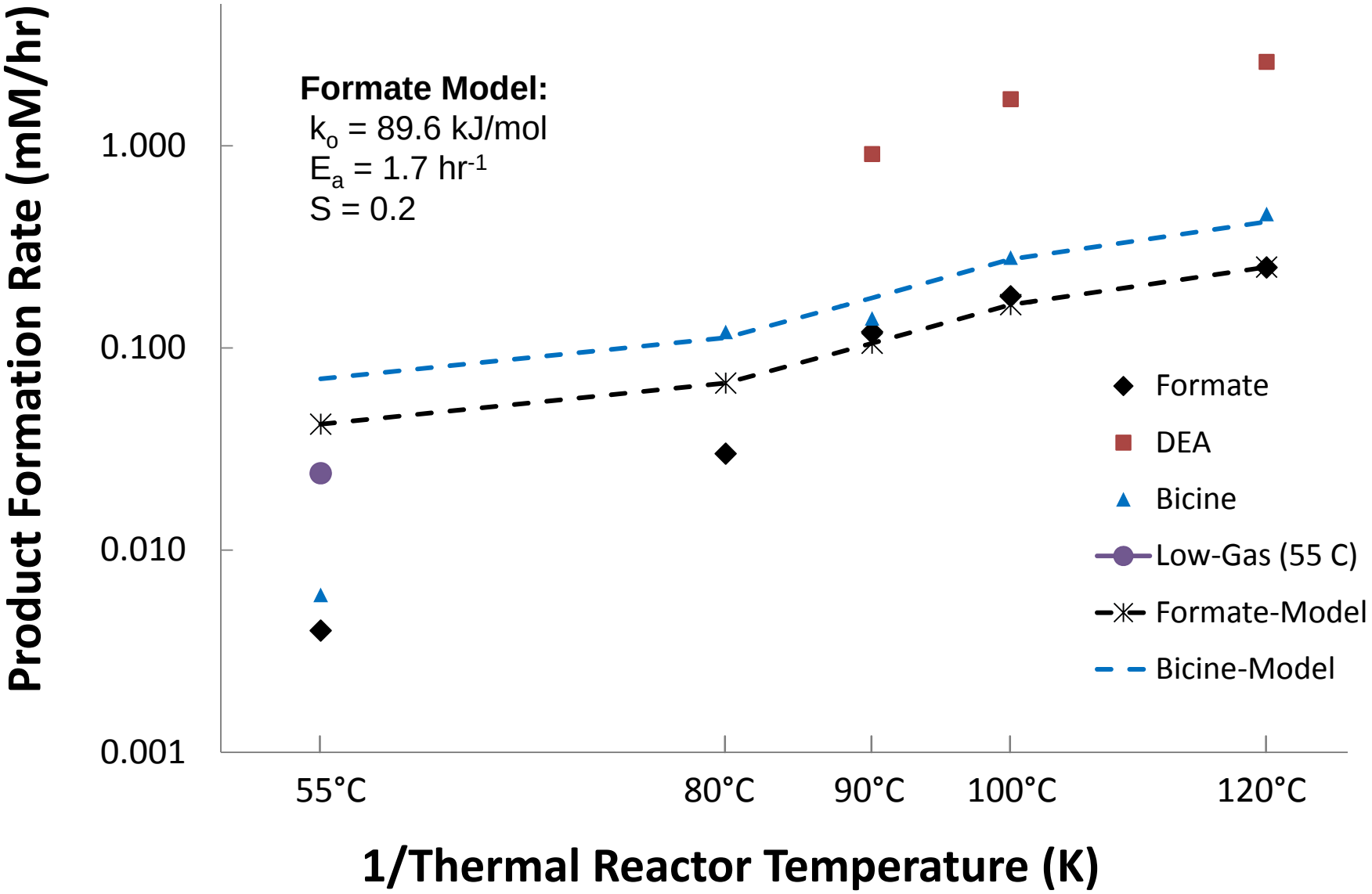

Summary

- Accelerated formate production in initial design - 0.6 mM/hr vs. 0.024 mM/hr in low-gas
- Bubble entrainment minimized, formate ~0.22 mM/hr (design implications)
- Inh A did not reduce formate production at 90 and 120 °C
- Bicine lags DEA production; bicine may be formed by DEA degradation
- When cycled from 55 to 120 °C with air, DEA production was 0.4 compared to 0.08 mM/hr for formate and bicine
- Oxidative model predicts degradation over temperature range 55 to 120 °C; over-predicts at low T
- E_a ~ 89.61 kJ/gmol, k_o ~ 1.71 hr^{-1}, and S ~ 0.2 for formate
- PZ cycling experiments are underway, followed by blend

Questions?

CO_2 Capture by Amine Scrubbing

By

Gary T. Rochelle

Luminant Carbon Management Program

Department of Chemical Engineering

The University of Texas at Austin

Clearwater

June 9, 2010

Roadmap

- The Problem and Solution
  - : CO_2 from Coal-fired Power
  - Amine Scrubbing – the Process
  - Amine scrubbing advantages
- improvements to energy Performance
  - Better solvents and processes
  - Trends in expected energy requirement
- Deployment by 2018

U.S. Electricity Generation CO_2 Emissions Forecast

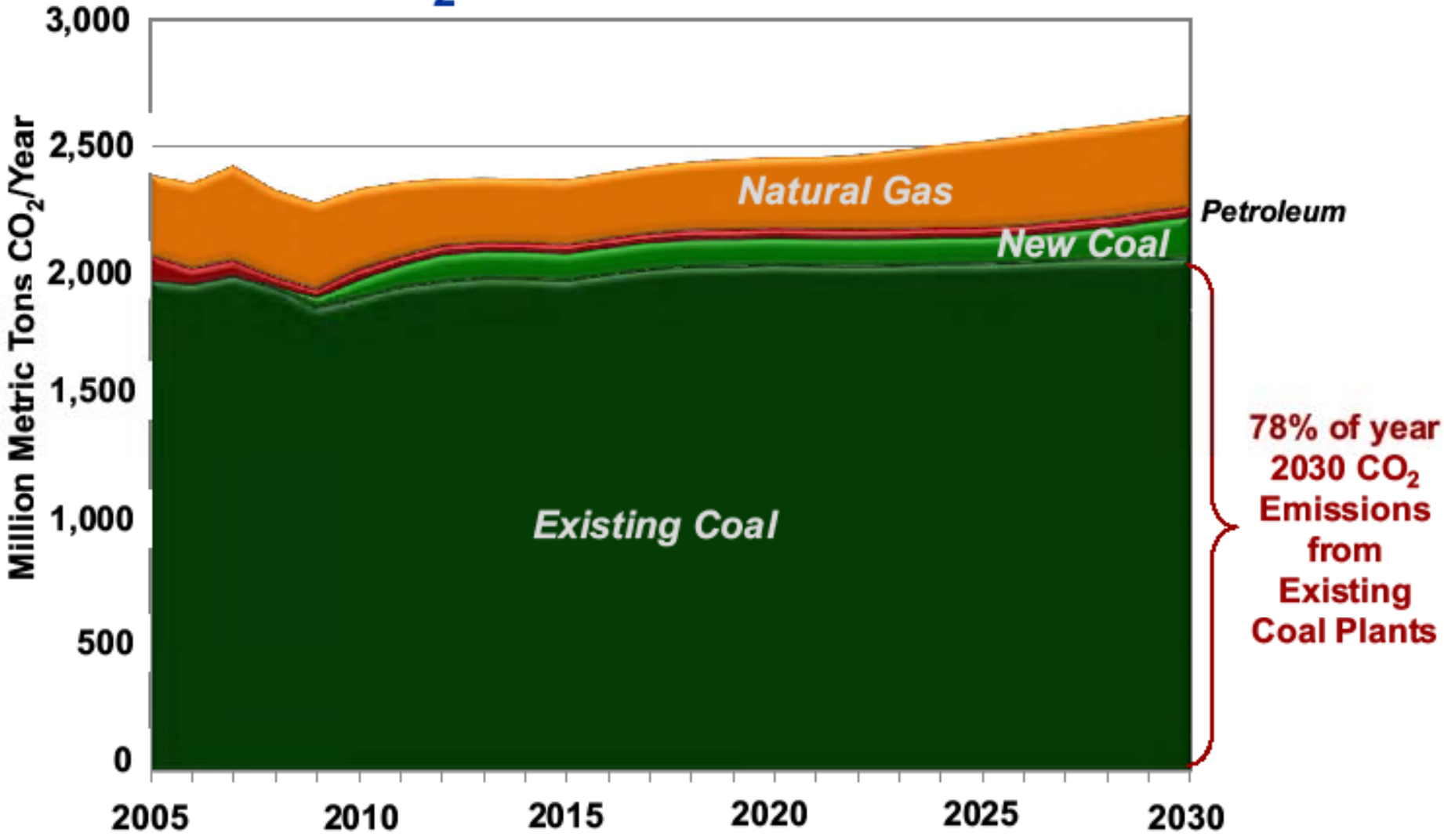

CO_2 Capture & Storage

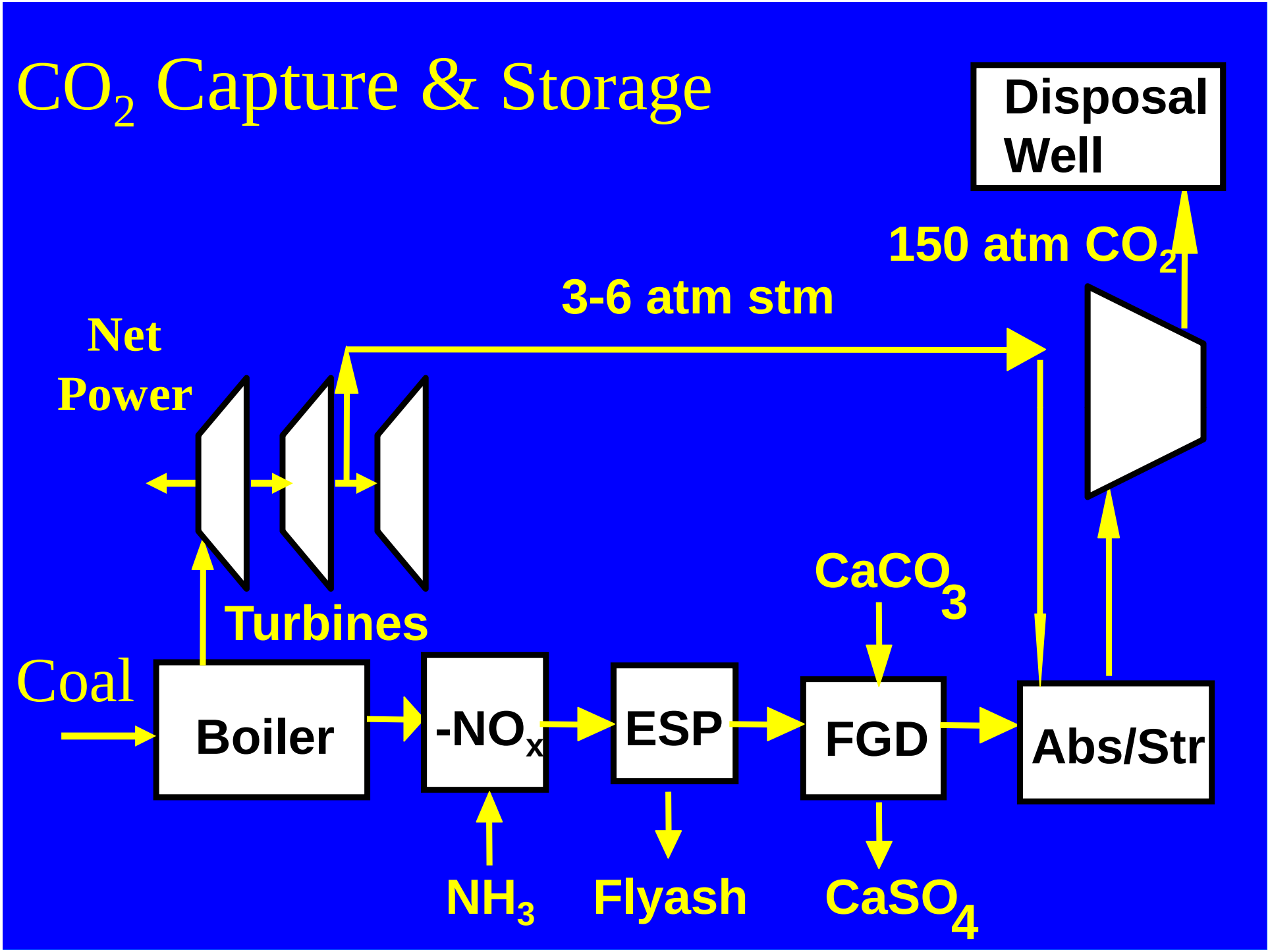

Amine Scrubbing (Bottoms, 1930)

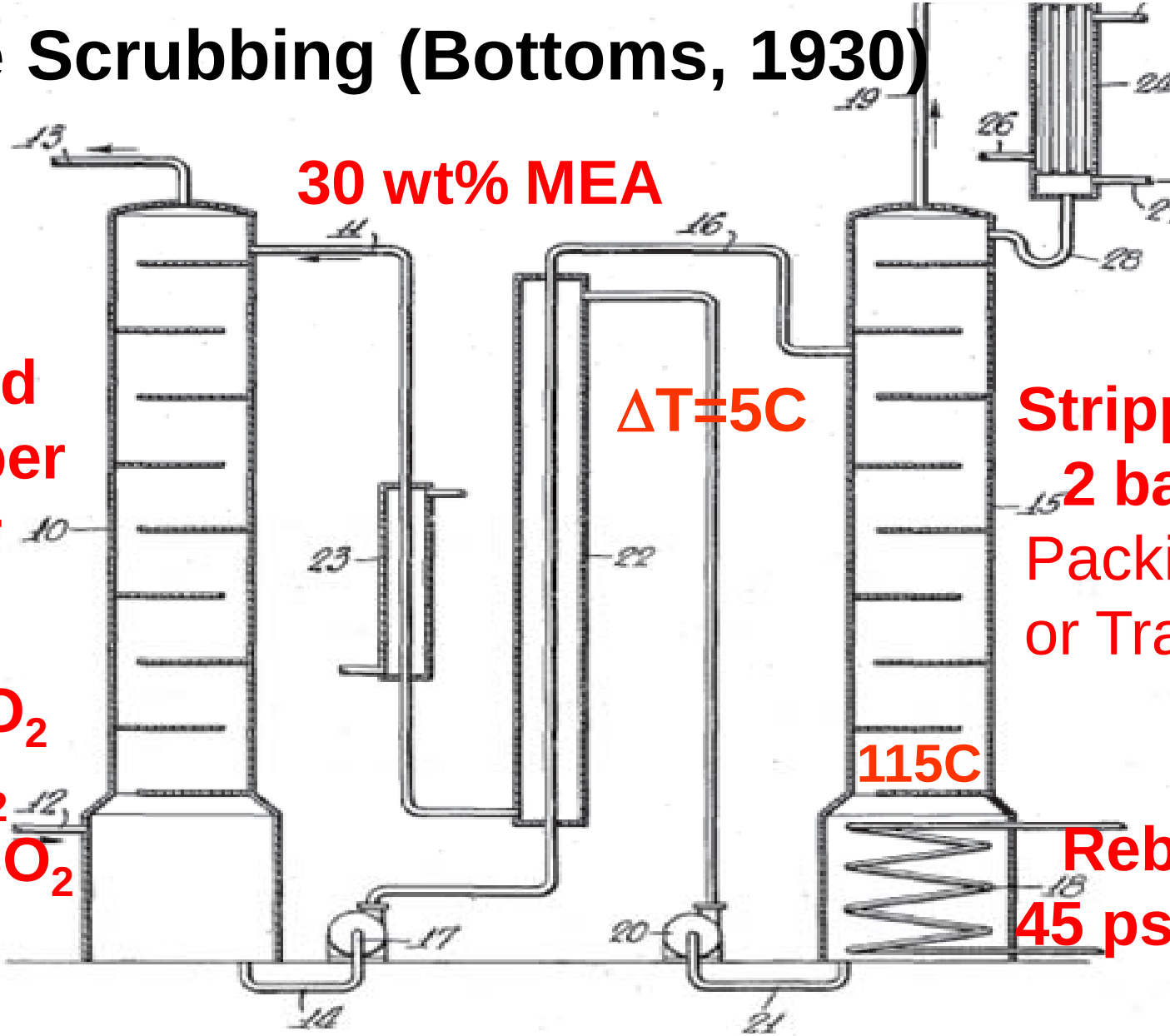

Dec. 2, 1930. R. R. BOTTOMS 1,783,901

PROCESS FOR SEPARATING ACIDIC GASES

Filed Oct. 7, 1930

Aqueous Abs/Str: Near commercial

- 100's of plants for treating H_2 & natural gas
  - MEA and other amine solvents
- 10's of plants with natural gas combustion
  - Fluor, 30% MEA
  - MHI, KS-1
- A few commercial plants with coal
  - Abb-Lummus, 20% MEA, 6, 8, & 33 MW
- Still need coal on 800 MW

Tail End Technology Ideal for Development, Demonstration, & Deployment

- Low risk
  - Independent, separable, add-on systems
  - Failures impact only Capture and Sequestration
  - Permits on/off operation to address peak load
- Low cost & less calendar time
  - Develop and demonstrate with add-on systems
  - Less demo cost than integrated systems
  - Resolve problems in small pilots with real gas
  - Demo Full-scale absorbers w 100-200 MW gas
    - Ultimately 800 MW absorbers

Other Solutions for Coal

- Oxy-Combustion
  - O_2 plant & compression require more energy
  - Gas recycle, boiler modification for high CO_2
  - Gas cleanup, compression including air leaks
- Coal Gasification / Combined Cycle
  - O_2 plant, complex gasifier, cleanup, CO_2 removal
  - Not ready for deployment
  - Relatively more expensive on PRB or lignite
  - New plants only
- Neither is Tail end: More suitable for new plants
  - Require higher development cost, time, and risk
  - Not suitable for on/off to address peaking

History Repeats
$CaCO_3$ Slurry:::Amine Scrubbing

$CaCO_3$	Event	Amine
1948	1st commercial plant	1980
1970	Too commercial for Gov. support But too costly, too dirty to use	1990
1970-82	Government funds advanced alts	1995-
1975-85	Govern. & EPRI fund test facilities	2010-
1977	Power Industry deploys 500+ MW	2016?
2009	First choice dominates	2030 ?

Practical Problem = \$41-65/ton CO_2 \$41-65/Mwh

- Energy = 20-30% of power plant output
  - \$20/ton CO_2
  - Theoretical Minimum is 11%
- Capital Cost \$500-1000/kw
  - Absorber for 500 MW:20x20x20 m
  - \$20-40/ton CO_2 for capital charges & maint
- Amine degradation/environmental impact
  - \$1-5/ton CO_2

R&D Opportunities

- Better Solvents
  - Faster Rate of Absorption
  - Greater heat of absorption
  - Greater thermal and oxidative stability
  - Greater solvent concentration and CO_2 capacity
- Better Processes
  - More heat recovery
  - Simpler configurations

Greater ΔH_{abs} & ΔT Reduce Energy

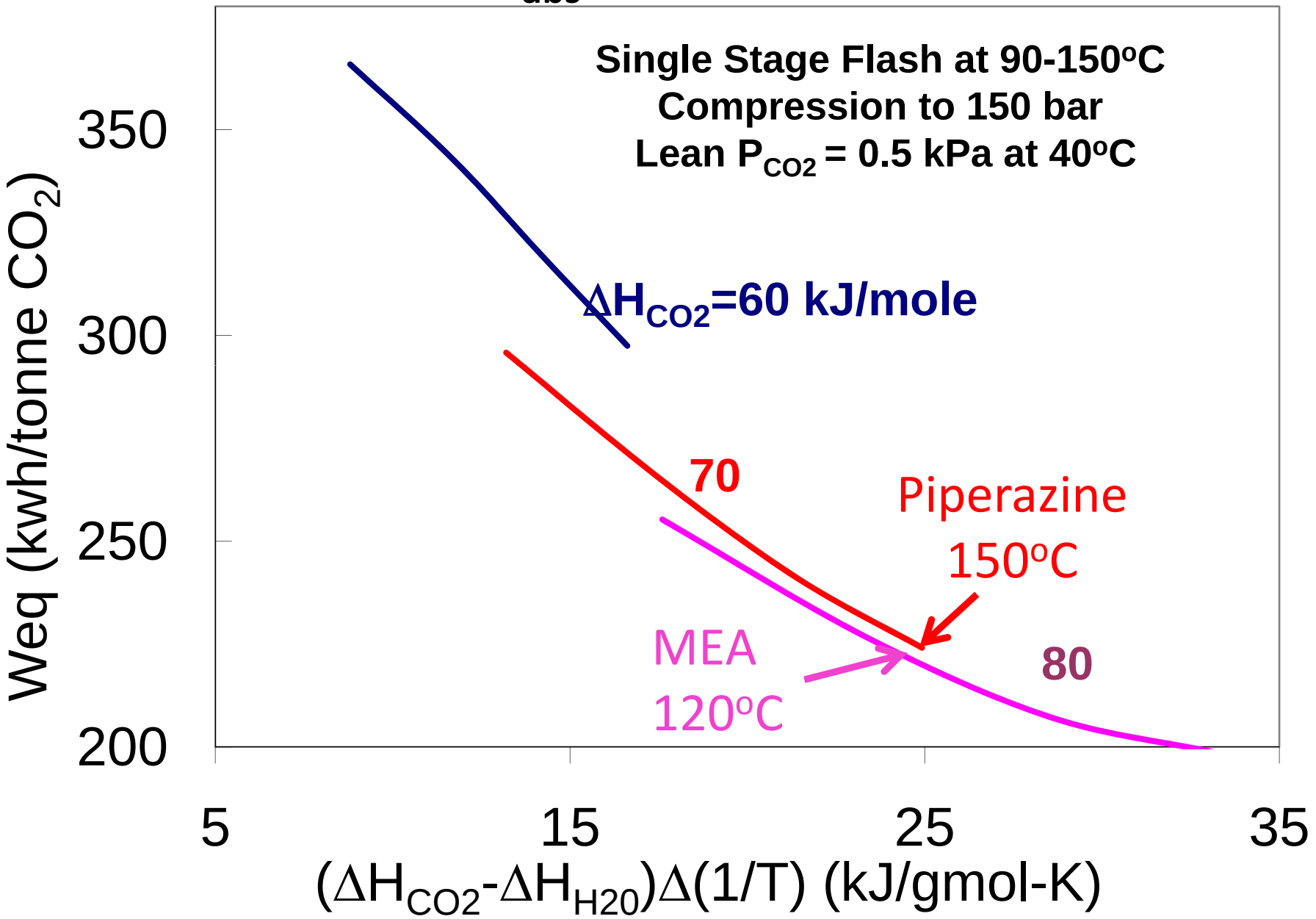

40 wt% Piperazine

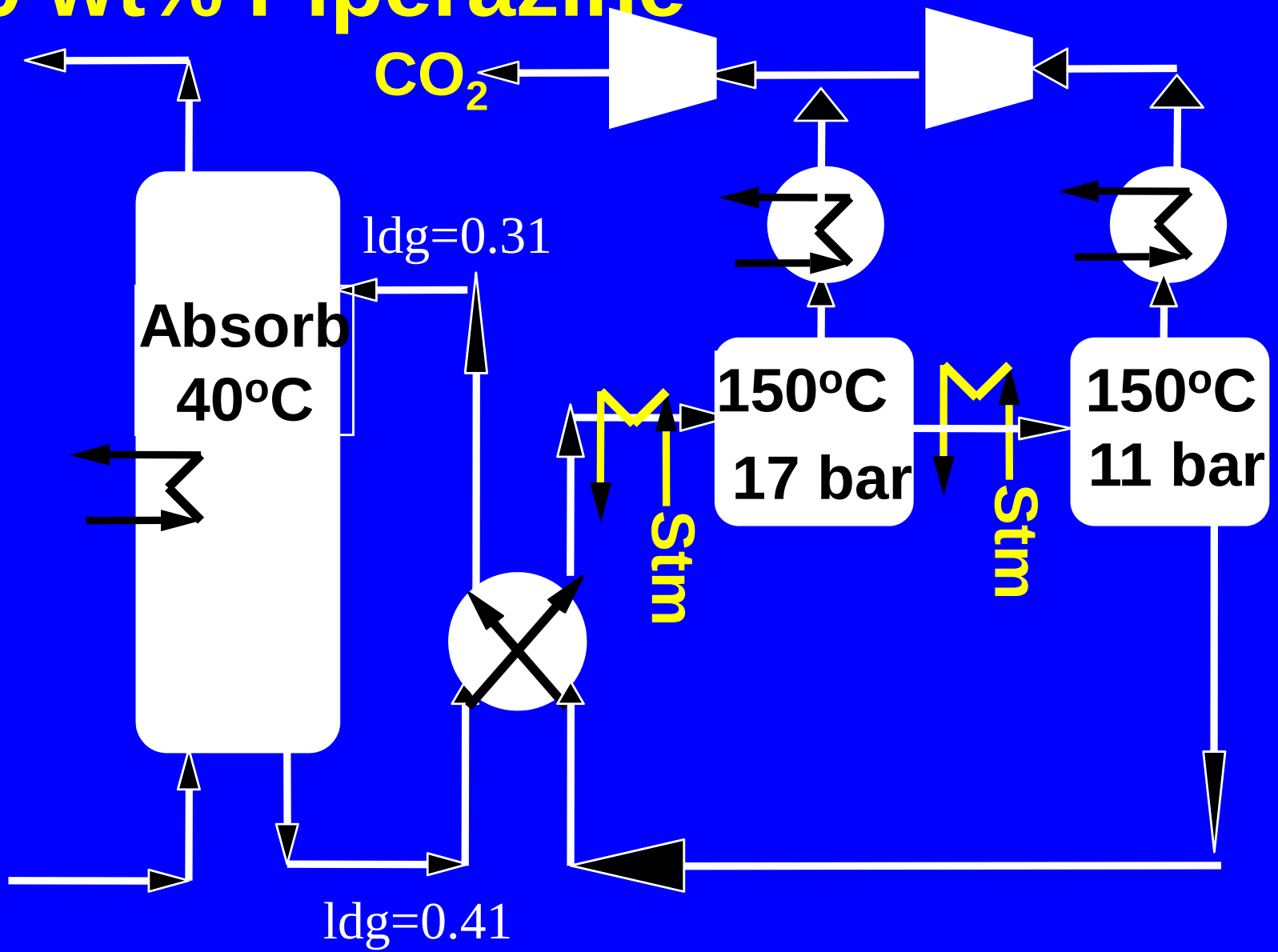

Heat Duty of Amine Scrubbing

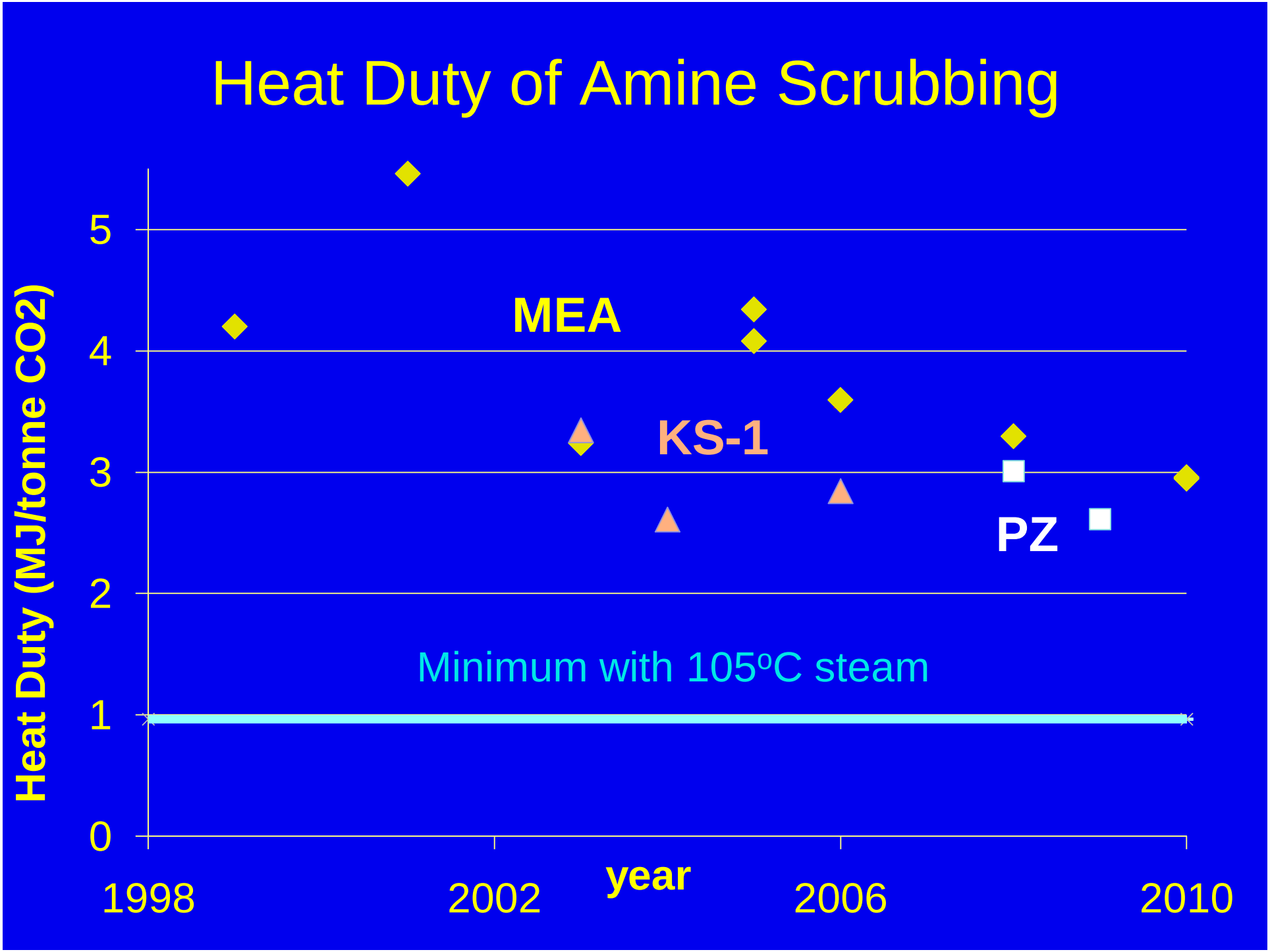

Equivalent Work of Amine Scrubbing

$$W_{equiv} = 0.75Q\frac{T_{stm} - T_{sink}}{T_{stm}} + W_{comp} + W_{pump}$$

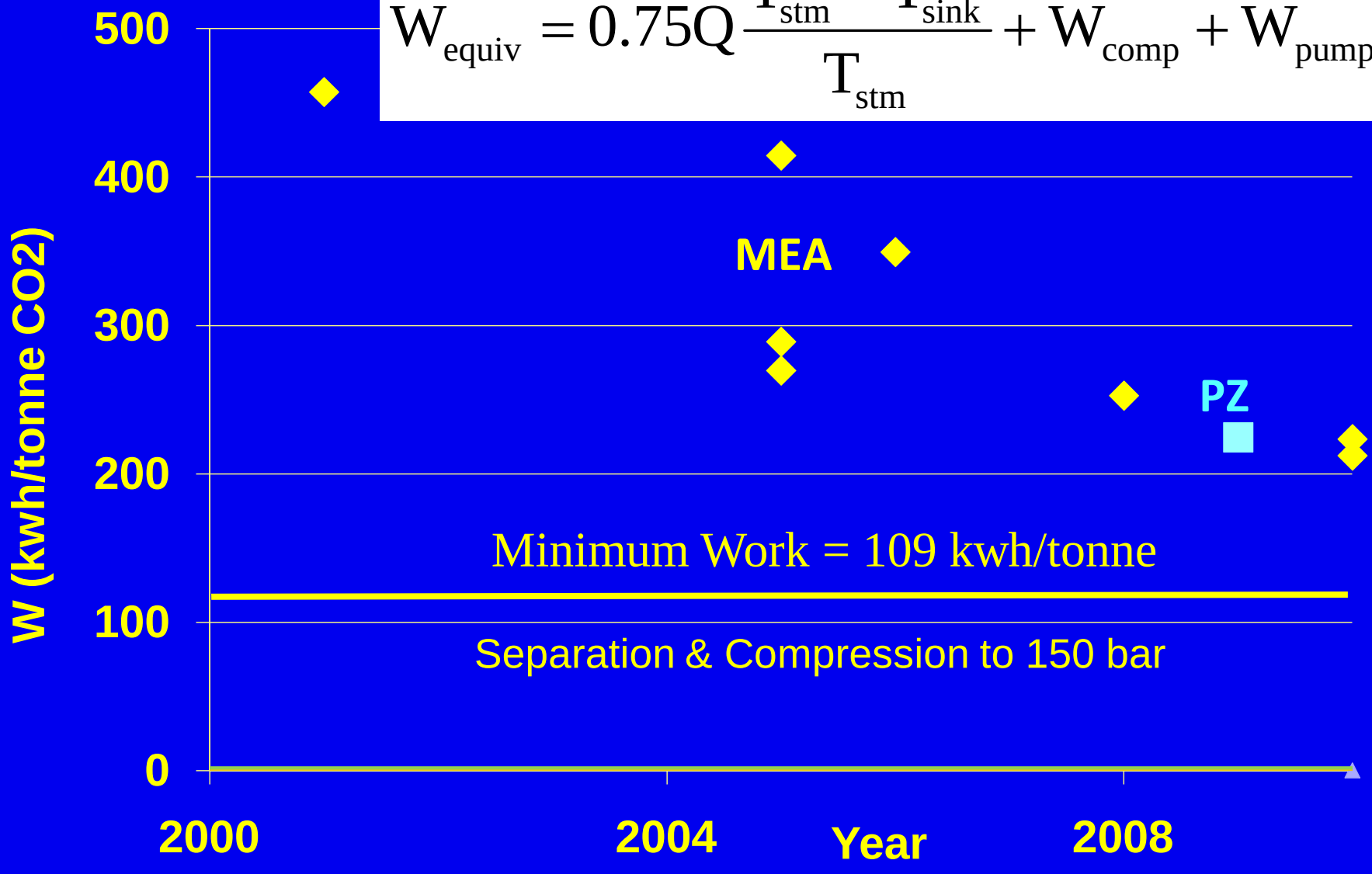

Thermodynamic Efficiency of Common Separation Processes

Process	**Efficiency (%)** $W_{minimum} / W_{actual}$
CO_2 Capture by Amine Scrubbing	50
Cryogenic Air Separation	25
Common Distillation	15-35
Water Desalination by Reverse Osmosis	21

Therefore it is improbable that we will be better than 200 kwh/ton CO_2, with any technology.

Deployment Schedule

- 2006+ 0.1-1 MW pilot plant on coal gas
  - 10+: HTC, Fluor, MHI, Castor, TNO, Dow/Alstom, Aker, CSIRO(2), Powerspan, Southern +
- 2011-12 – 6-25 MW prototype plant
  - MHI, Fluor, et al.
- 2014 – 60-250 MW Integrated module
  - SaskPower, NRG, Basin, Belchatow
- 2016 – 800 MW full-scale
- 2018 – Deployment on all plants

Conclusions

- Amine scrubbing is THE technology to reduce emissions from US coal by 50% by 2025.
  - $50/MWh, will double wholesale cost
  - $150-300 billion investment
- Total electricity required for amine scrubbing will be 200-250 kwh/tonne CO_2 removed
  - $W_{minimum}$ = 109 kwh/tonne

The University of Texas at Austin

Department of Chemical Engineering

Research Proposal

Thermodynamics of CO_2 Loaded Aqueous Amines for CO_2 Capture

Ph. D. Committee:

Supervisor: Gary T. Rochelle

Keith Johnston

Isaac Sanchez

Frank Seibert

Steven Bryant

Qing Xu

May 18, 2010

Introduction

CO_2 emissions

As climate change becomes more severe in the past decades, ways to moderate and solve the problem are being investigated by researchers over the world. The 2005 concentration of CO_2 was about 35% higher than a century and a half ago. IPCC Fourth Assessment Report – Climate Change 2007 concluded that "Most of the observed increase in global average temperature since the mid-20th century is very likely to due to the observed increase in anthropogenic greenhouse gas generations." Therefore, one approach is to manage the greenhouse gases in atmosphere, including carbon dioxide, methane, nitrous oxide and ozone.

Figure 1 shows the world CO_2 emissions in year 2007 from different sectors. The largest emission source is electricity and heat and occupies 41% of the total.

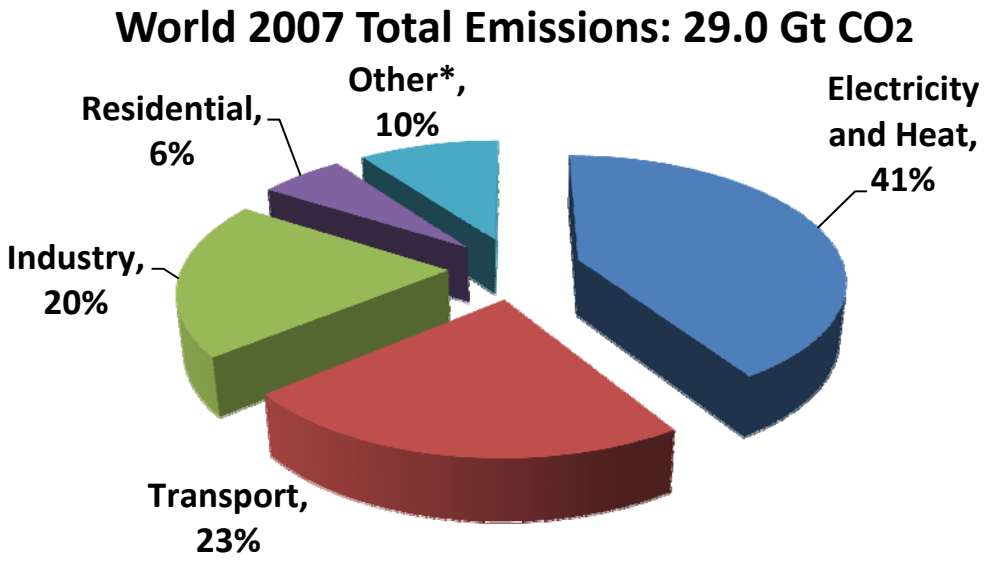

Figure 1: 2007 World CO_2 Emissions by Sector

Other* includes commercial/public services, agriculture/forestry, fishing, energy industry other than electricity and heat generation, and other emissions not specified elsewhere.
Re-plotted from Figure 11 in CO_2 emissions from fuel combustion highlights (2009 edition), International Energy Agency, 2009.

Amine based post combustion CO_2 capture

One direct approach is to capture the CO_2 and store it away from atmosphere, like underground or submarine. The captured CO_2 can also be used into chemical industry as well as enhanced oil recovery (EOR). Biological CO_2 capture refers to biochar burial, using trees and plankton to capture CO_2. Non-biological CO_2 capture from coal fired power plants and other

plants. It includes pre-combustion, oxy-combustion and amine based post combustion CO_2 capture. Among these, amine scrubbing has been investigated for decades and found as among the closest ones to commercialization. Monoethanolamine (MEA) solution serves as the baseline solvent. New solvents like piperazine (PZ) are being investigated and will be discussed in the literature review session.

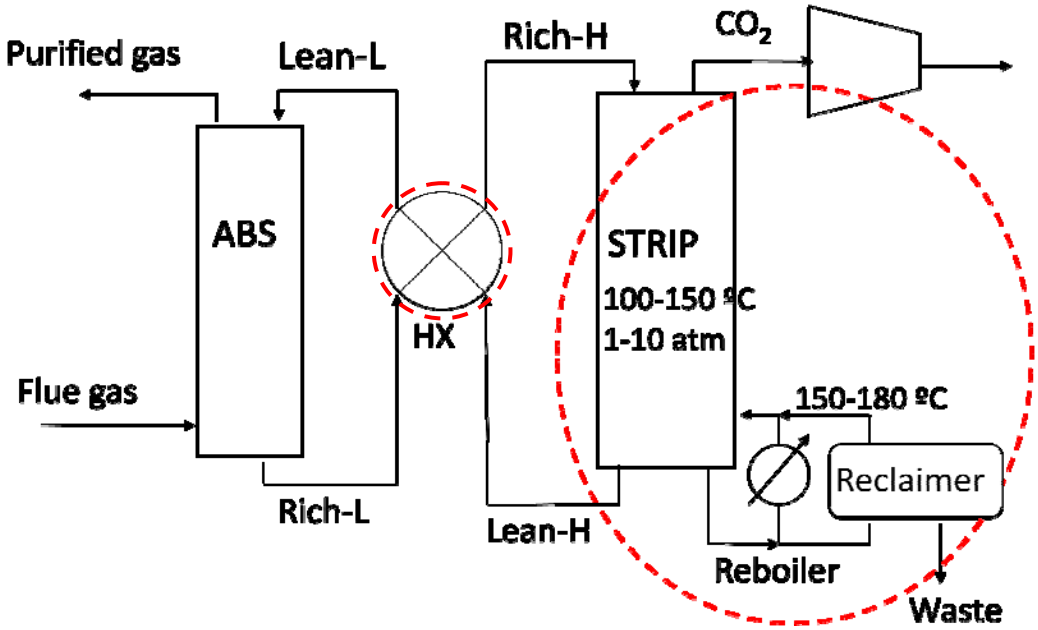

Figure 2: A Typical Amine Based CO_2 Capture Process

Figure 2 shows a typical amine based CO_2 capture process. The cooled flue gas with about 12% CO_2 enters the bottom of the absorber and counter-currently contacts the lean amine stream. After absorbing CO_2, aqueous amine becomes rich in CO_2 and flows out from the bottom. The temperature in the absorber is from 40-70 ºC. In the cross heat exchanger the cool rich stream is heated by the hot lean stream from the stripper to above 100ºC and then the hot rich solution enters the top of the stripper. In the stripper hot steam is used to heat the reboiler up to 100-150 ºC, and the pressure in the stripper can be 1.6-10 atm. A slip stream is withdrawn from the reboiler and enters a reclaimer, the temperature of which is up to 150-180ºC. CO_2 is stripped out of the solution, exits from the top and compressed to 150 bar for sequestration. The hot lean solution flows out of the bottom of the stripper and enters the absorber after cooling down to be reused. In this process, amine solution is recycled in the absorber and stripper, main energy input is in reboiler and compressors.

Needs for High temperature thermodynamics

Better energy performance can be achieved by elevating the stripper temperature and pressure. Some amines like MEA and ethylenediamine (EDA) are not thermally resistant and stripper

temperature cannot exceed 120ºC; but for thermally resistant amines like PZ, diglycolamine (DGA) and PZ derivatives the T in the stripper can be up to 150 ºC. For both cases high T thermodynamics is helpful in understanding the process at stripper and reclaimer conditions. Mid-temperature thermodynamics can also be interpolated from high temperature and low temperature data. Therefore more high temperature thermal studies will help understanding the processes inside the red dashed circles in Figure 2.

Figure 3 gives a more detailed example for the high temperature application. It is from Van Wagener's 2009 4th quarter progress report (Figure 2) and shows the 2 stage flash configuration. These units are to replace the simple stripper configuration. Hot rich solution enters a flash at a higher temperature than a simple stripper. The 2 flashes are under the same temperature but flash 1 has a higher pressure. The stripped CO_2 enters the stage in the multi-stage compressor with similar pressure; liquid stream from the 1st flash enters the 2nd flash and generates lower pressure vapor and hot lean solution. The hot lean solution will go to heat exchanger and the vapor enters the 1st stage of the multi-stage compressor. In this elevated pressure stripping process, CO_2 vapor is thermally compressed before entering the compressors. Theoretically thermal compression has higher efficiency than mechanical compression since the compression work from the later is from electricity. More flash stages can save more energy input but the capital cost will increase. According to Van Wagener's research about 0.3 and 0.5 kJ/mol CO_2 of energy can be saved by using 2 and 3 stage flash, respectively, when 9 m MEA is used as the solvent. There are also other stripping configurations with elevated temperature and pressure saving more energy than a simple stripper, e.g., double matrix flash.

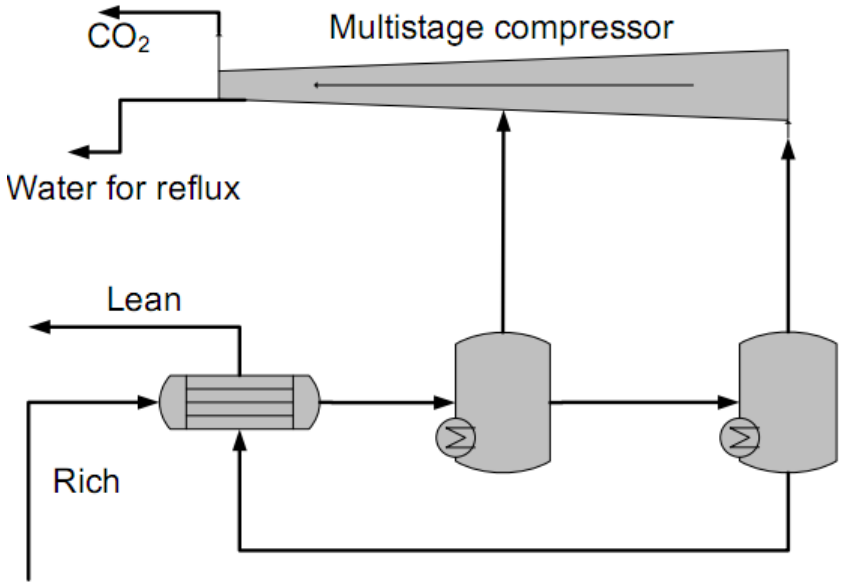

Figure 3: Two Stage Flash (D. Van Wagener, 2009 4th quarter report)

Research objectives

Thermodynamics serves as the base knowledge in the design of amine scrubbing process. CO_2 solubility, heat of CO_2 absorption, specific heat capacity and amine volatility are key thermal components to the process design. CO_2 solubility and total pressure determine how much CO_2 could be removed under certain conditions. On the other hand the heat of absorption plays an important role in the prediction of stripper energy and is critical for the process design. Specific heat capacity helps understanding the temperature dependence of heat of absorption. Amine volatility mostly involves environmental impact as well as the design of the water wash and the condenser. Investigations on the amine-water system can help understanding the more complex amine-water-CO_2 system.

These factors have interactions too. CO_2 solubility, or in other words, CO_2 partial pressure over CO_2 loaded amine, is mostly determined by temperature, amine type and the CO_2 loading (mole CO_2/mol alkalinity). For a specific amine, $\ln P_{CO2}$=f (T, loading). Amine volatility depends on amine type and concentration, temperature and CO_2 loading. Therefore for a specific amine, $\ln P_{amine}$=f (T, loading, [amine]). By taking derivatives to lnP more thermal parameters can be obtained:

According to the Gibbs-Helmholtz Equation, the CO_2 heat of absorption, $\Delta H_{abs} = -R\frac{\partial lnP_{CO2}}{\partial(\frac{1}{T})}$. In the amine-$H_2O$ system $\Delta H_{abs} = -R\frac{\partial lnP_{amine}}{\partial(\frac{1}{T})}$. R is the gas constant.

By definition, the specific heat capacity $C_p = (\frac{\partial H}{\partial T})_P$ and Cp=A+BT+CT^2+…. Thus Cp reflects the temperature dependence of ΔH. For the amine-water-CO_2 system, on a molar lean solution base, $\Delta H_{abs}(120℃) = \Delta H_{abs}(40℃) + \int_{120℃}^{40℃}[Cp(lean) + Cp_{CO2(g)}m_{CO2(g)}]dT + \int_{40℃}^{120℃} Cp(rich)\cdot(1+\frac{m_{CO2(g)}}{44.01})dT$. Please refer to the Literature Review session in this proposal for details.

MEA has been extensively studied for years and is used as the baseline solvent. There are CO_2 solubility data for MEA up to 150°C and MEA volatility data for MEA-H_2O up to 100°C. Concentrated PZ is a very promising thermally resistant solvent and its VLE data are inadequate especially at high temperature. MEA and PZ thermal models in Aspen Plus® have been developed by other group members, however the application temperature range needs to be extended.

The primary target of this project is to quantify in aqueous MEA and PZ, how the CO_2 solubility, amine volatility and heat of absorption depend on temperature, and give theoretical explanations for these behaviors. Therefore the specific objectives of this project include:

1. Validate the previous VLE data for MEA and get more adequate data at 100-160°C. This will help validating the new HPVLE methods.
2. Measure CO_2 solubility, amine volatility and specific heat capacity at 100-160°C for concentrated PZ for high temperature stripping design.
3. Identify and explain the temperature dependence of CO_2 solubility and amine volatility for both MEA and PZ systems.
4. Based on the VLE and specific heat capacity data, obtain CO_2 ΔH_{abs} in MEA and PZ, as well as amine ΔH_{abs} in aqueous MEA and PZ. Identify and explain the temperature dependence of the ΔH values.
5. Modify the existing Aspen Plus® thermal models for CO_2 loaded MEA and PZ.
6. Screen a few new thermally resistant solvents by measuring CO_2 solubility at high temperature.

Literature review

Amine solvents

Monoethanolamine (MEA) has been used in acid gas treating since 1960's and is a baseline amine for CO_2 capture. It has good properties: relative high heat of absorption, moderate reaction rate and capacity, low viscosity, low price, moderate environmentally degradability and intensive operating experiences in industry. However it degrades with O_2 in the absorber and thermally degrades at greater than 120°C.

Piperazine (PZ) has been used as a promoter for some slow amines like methyl-diethanolamine (MDEA) and 2-amino-2-methyl-1-propanol (AMP) because it accelerates reaction rate. However PZ in blends always degrades faster than only PZ. Concentrated PZ is a very promising solvent because of its high capacity, fast reaction rate, negligible oxidative and thermal degradation up to 150°C and moderate to high heat of absorption. The tolerance of high temperature gives the possibility of elevating regeneration temperature and pressure for better energy performance.

PZ derivatives, which include 1MPZ (1-methyl-piperazine) and 2MPZ (2-methyl-piperazine), are a new set of amines currently studied in Rochelle group. Preliminary results show that derivatives of PZ are also thermally resistant and react fast with CO_2. Thermodynamics related to the PZ derivatives, PZ/PZ derivative blends and comparison with that of PZ can help explaining the effect from chemical structure.

Diglycolamine (DGA®) has been used in absorbing CO_2 and H_2S from natural gas for decades. Like PZ, it is relatively thermally stable.

VLE

MEA:

Table 1 and 2 give the literature review of VLE data for unloaded and loaded aqueous MEA, respectively.

Table 1: Summary of Literature VLE Data for MEA-H_2O

Data	Pressure (kPa)	MEA (mol frac)	T (^oC)	Author
P, x	1.3-75	0-0.93	60, 78, 91.7	Nath and Bender (1983)
P, x	0.065-5.623	0.03-0.89	25, 35	Touhara (1982)
	6.8-88.5	0.27-0.81	55-140	Texaco (1989)
	6.6-69	0.23-0.96	44-95	Texaco (1989)
P, x, y	4.02-70.07		90	Tochigi (1999)
T, x, y	101.3		100-170	Park and Lee (1997)
T, x, y	66.7, 101.3			Cai (1996)
T, x, y		0.06-0.30	39.8-72.7	Hilliard (2008)
T, x, y		0-0.56	40, 60, 80, 100	Kim (2008)

Table 2: Summary of Literature CO_2 Solubility in Aqueous MEA at High TP

Author	MEA (wt%)	T (°C)	P_{CO2}(kPa)
Reed and Wood (1941)	15	100, 120, 140	138-1724
Goldman and Leibush (1959)	6, 12, 15, 30	75, 100, 120, 140	0.3-467
Jones et al. (1959)	15	40, 60, 80, 100, 120, 140	<931
Lee et al. (1974)	15, 30	40(?), 100	1.4-6620
Lawson and Garst (1976)	15	40, 60, 80, 100, 120, 134, 140	2.9-2786
Lee et al. (1976)	6, 15, 23, 30	25, 40, 60, 80, 100, 120	0.2-6616
Shen and Lee (1992)	15, 30	40, 60, 80, 100	1.1-2550
Murrieta-Guevara et al. (1993)	15, 30	30, 50, 100	1.5-2210
Robinson (1993)	20, 30	40, 70, 100, 120	0.003-6293
Jou et al. (1995)	30	0, 25, 40, 60, 80, 100, 120, 150	0.0012-19954

PZ:

Table 3 and 4 give the literature review of VLE data for unloaded and loaded aqueous MEA, respectively.

Table 3: Summary of Literature VLE Data for PZ-H_2O

Author	Data	PZ (m)	T (°C)
Wilson and Wilding (1994)	Pt	0-1 (mole frac)	113, 199
Xia (2003)	Pt	1.99, 3.97	120
Hilliard (2008)	T, P, x, y	0.9, 2, 2.5, 3.6, 5	40-60
Nguyen	T, P, x, y	2, 5, 8, 10	40-70

Table 4: Summary of Literature CO_2 Solubility in Aqueous PZ

Author	PZ (m)	T (°C)	PCO2 (kPa)
Ermatchkov et al. (2006)	2-4.2	80, 100	0.111-77.63
Hilliard (2008)	0.9-5	40, 60	0.029-51.4
Dugas (2009)	2-12	40, 60, 80, 100	0.065-39.29
Bishnoi et al. (2000)	0.6	40, 70	0.032-40
Derks et al. (2005)	0.2M, 0.6M	25, 40, 70	0.27-111
Perez-Salado Kamps et al. (2003)	2, 4	40-120	13.3-9560 (Pt)
Nguyen	8, 10	40, 60	

DGA:

Table 5: CO_2 Solubility in DGA in Literature

Author	DGA (wt%)	Data type	P_{CO2}	T (^oC)
Martin (1978)	60	P_{CO2} was calculated from analysis and a consideration of gauge, barometric and vapor pressures. (??)	1.6-5980 kPa	50, 100
Maddox (1987)	20-60	P, T, P_{CO2}=Pt-P_{H2O}	6.8-6523 kPa	25, 40, 50, 60
Dingman (1983)	65	P, T, not sure about P_{CO2}	2.9E-5~27 psia	37.8, 60, 82.2
Al-Juaied (2004)	65	P_{CO2}		23-62

<u>Specific heat capacity (Cp):</u>

Heat capacity is the derivative of CO_2 heat of absorption with respect to temperature. Thus accurate heat capacity measurement will also yield temperature dependence of heat of absorption. Differential Scanning Calorimetry (DSC) method was used in previous research by Hilliard (2008) and Nguyen for heat capacity measurement for CO_2 loaded amine. Heat capacity of amine-H_2O can help develop the model of amine-H_2O.

Table 6: Literature Summary of Specific Heat Capacity for Aqueous MEA

Author	T (°C)	Data Type
Page et al. (1993)	10, 25, 40	unloaded
Weiland (1997)	25	pure, loaded, unloaded
Chiu et al. (1999)	30-80	pure, unloaded

Table 7: Literature Summary of Specific Heat Capacity for Aqueous PZ

Author	T	Data
Hilliard (2008)	40-120	2 m and 3.6m, unloaded
Y-R Chen et al. (2010)	30-80	x_{PZ}=0.05, 0.1, 0.15, 0.2, unloaded
Nguyen	40-120	8 m, 0.21, 0.29, 0.4 CO2 loading

Heat of absorption

It is important to know the temperature dependence of heat of absorption of CO_2 into aqueous amines. In the absorber when CO_2 react with amine heat is generated, and in the stripper the heat of adsorption is needed to make the reverse reaction. According to the research by Kim at NTNU (2008), heat of absorption of CO_2 in 7m MEA increases with temperature and decreases with CO_2 loading.

Previous data are in two different types: integral and differential heat of absorption. Heat of absorption obtained from CO_2 partial pressure data are referred to as differential heat of absorption. It has been studied by Jou et al. (1994) for MEA solution. However in this approach heat of absorption is proportional to the 1^{st} derivative of logarithm CO_2 partial pressure, which requires very accurate CO_2 partial pressure measurement and cannot get temperature dependence. Integral heat of absorption could be obtained from direct measurement by calorimeter. Table 8 lists the summary of previous CO_2 heat of absorption measurement for aqueous MEA and PZ.

Table 8: Summary of CO_2 Heat of Absorption into Aqueous MEA and PZ in Literature

Author	Amine Concentration	T (°C)	P (kPa) / Loading
Mathonat et al. (1995)	30 wt% MEA	40, 80, 120	2000, 5000, 10000 kPa
Carson et al. (2000)	10, 20, 30 wt% MEA	25	
Kim (2008)	30 wt% MEA	40, 80, 120	0.04-0.72 mol CO2/mol alk.
Kim (2008)	2 m PZ	40, 80, 120	0.03-0.61 mol CO2/mol alk.
Freeman (2007?)	8 m PZ	40, 80, 120	

Theory on partial pressure, Cp and ΔH_{abs}

In the amine-H_2O-CO_2 system, the CO_2 equilibrium can be simplified as:

$$CO_2(g) \overset{K}{\Leftrightarrow} CO_2(aq)$$

CO_2 (g) is the vapor CO_2, CO_2 (aq) is the total CO_2 absorbed in the amine solution and K is the equilibrium constant of this reaction. By definition,

$$K = \frac{a_{CO_2(g)}}{a_{CO_2(aq)}} = \frac{f_{CO_2(g)}/f^o}{x_{CO_2(aq)} \cdot \gamma_{CO_2(aq)}} = \frac{f_{CO_2(g)}}{f^o \cdot x_{CO_2(aq)} \cdot \gamma_{CO_2(aq)}}$$

$$\xrightarrow{yields} lnK = lnf_{CO_2(g)} - lnf^o - lnx_{CO_2(aq)} - ln\gamma_{CO_2(aq)} \quad (1)$$

According to the Gibbs-Helmholtz Equation, $\left(\frac{\partial \frac{\Delta G}{T}}{\partial \frac{1}{T}}\right)_{P,x} = \Delta H_{abs}$ (2)

For a chemical reaction, ΔG = -RTlnK (3)

Substitute equation (3) to (2):

$$\left(\frac{\partial(-RlnK)}{\partial\left(\frac{1}{T}\right)}\right)_{P,x} = \Delta H_{abs} \xrightarrow{yields} \left(\frac{\partial lnK}{\partial \frac{1}{T}}\right)_{P,x} = -\frac{\Delta H_{abs}}{R} \quad (4)$$

Take the derivative of equation (1) with respect to 1/T:

$$\left(\frac{\partial lnK}{\partial \frac{1}{T}}\right)_{P,x} = \left(\frac{\partial(lnf_{CO_2(g)} - lnf^o - lnx_{CO_2(aq)} - ln\gamma_{CO_2(aq)})}{\partial \frac{1}{T}}\right)_{P,x}$$

$$= \left(\frac{\partial lnf_{CO_2(g)}}{\partial \frac{1}{T}} - \frac{\partial lnf^o}{\partial \frac{1}{T}} - \frac{\partial lnx_{CO_2(aq)}}{\partial \frac{1}{T}} - \frac{\partial ln\gamma_{CO_2(aq)}}{\partial \frac{1}{T}}\right)_{P,x}$$

Since lnf^o is a constant, $x_{CO_2(aq)}$ is fixed and the temperature dependence of $\gamma_{CO_2(aq)}$ can be ignored,

$$\left(\frac{\partial lnK}{\partial \frac{1}{T}}\right)_{P,x} \approx \left(\frac{\partial lnf_{CO_2(g)}}{\partial \frac{1}{T}}\right)_{P,x} \approx \left(\frac{\partial lnP_{CO_2(g)}}{\partial \frac{1}{T}}\right)_{P,x} \quad (5)$$

An assumption was made that $f_{CO_2(g)} \approx P_{CO_2(g)}$.

Compare (4) and (5), yield $\left(\frac{\partial lnP_{CO_2(g)}}{\partial \frac{1}{T}}\right)_{P,x} \approx -\frac{\Delta H_{abs}}{R}$ (6)

The absorption process at different temperature can be related with several steps shown in Figure 4. The dependence of Cp and ΔH_{abs} on pressure is ignored; the pressure in all the steps is constant. In step 1 and 3, CO_2 is absorbed into lean amine at T_1 and T_2, respectively. Cp is the specific heat capacity. For amine solution, Cp ≈ Cv and can be measured by DSC. On a molar lean solution base (other base can be chosen too):

$$\Delta H_{abs}(T_1) = \Delta H_{abs}(T_2) + Q_2 + Q_4$$

Thus $\Delta H_{abs}(T_1) - \Delta H_{abs}(T_2) = Q_2 + Q_4 = \int_{T_1}^{T_2}\left[Cp(lean) + Cp_{CO2(g)}m_{CO2(g)}\right]dT + \int_{T_2}^{T_1} Cp(rich)\cdot(1+\frac{m_{CO2(g)}}{44.01})dT.$

There are specific heat capacity data for the lean and rich amine solutions at 40-120°C. Cp for CO_2 is also available in literature. Normally $Cp=A+BT+CT^2+\ldots$.

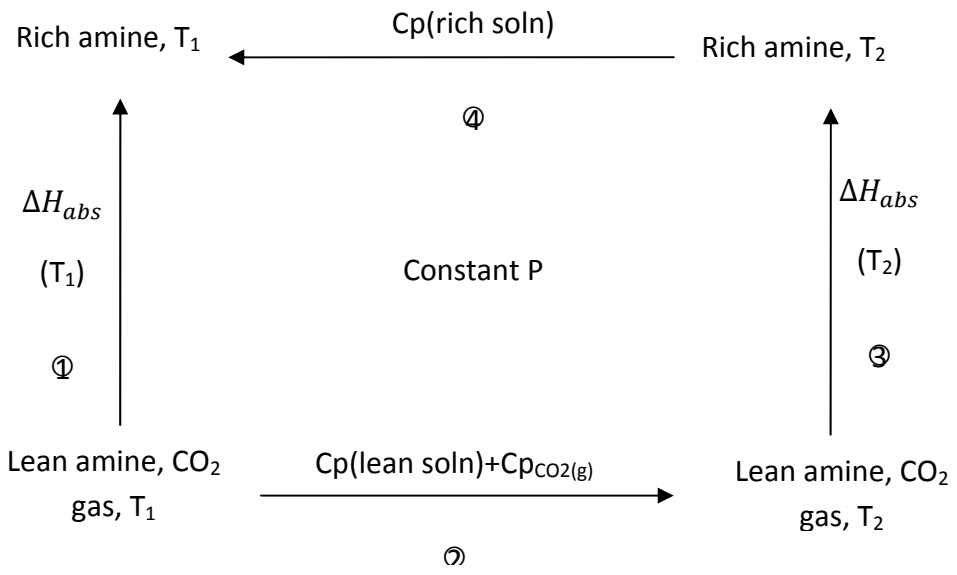

Figure 4: Illustration CO_2 Heat of Absorption at Different Temperature

Similarly, in the amine-H_2O system $\Delta H_{abs} = -R\frac{\partial lnP_{amine}}{\partial(\frac{1}{T})}$, and $\Delta H_{abs}(T_1) - \Delta H_{abs}(T_2) = \int_{T_1}^{T_2}\left[Cp(lean) + Cp_{amine(g)}m_{amine(g)}\right]dT + \int_{T_2}^{T_1} Cp(rich)\cdot(1+\frac{m_{amine(g)}}{MW_{amine}})dT$. Here lean and rich represent the relative amine concentration.

Thermal model for MEA and PZ systems

The electrolyte-Nonrandom Two-Liquid (eNRTL) theory was developed by Chen et al. (1979 and 1982), then improved by Chen and Evans (1986) and Mock et al. (1986). eNRTL is also a built-in model in Aspen Plus®, used to deal with the liquid phase non-ideality, especially for aqueous or mixed solvent electrolyte systems. The model contains a Debye-Huckel term, Born-correction for mixed solvents, and the local interaction term.

In the Rochelle group, Austgen (1989) was the first to apply the eNRTL model in Aspen Plus® to the amine-H_2O-H_2S-CO_2 system successfully. The data regression system (DRS) of Aspen Plus® was used in the rigorous thermodynamic model. After that Posey (1996), Bishnoi (2000), Dang

(2001), Freguia (2002) and Cullinane (2005) all made some contributions to the rigorous thermodynamic equilibrium/rate models. The more recent MEA-H_2O-CO_2 and PZ-H_2O-CO_2 models were by Hilliard (2008); Van Wagener modified the Hilliard PZ model in 2009 and further modification is underway by Frailie in Rochelle group. For amine-H2O-CO_2 system, vapor phase non-ideality was modeled by the SRK equation of state in most time.

With the rigorous thermodynamic models, reasonable accurate predictions should be made. Also the important parameters help interpreting and understanding thermal behaviors. Since the current models do not include much high temperature data, the temperature dependences and the high temperature predictions are not perfect.

Scope of the work

Experimental

**** Methods development***

Total pressure measurement 100-160°C (done)

CO_2-amine-H_2O VLE with continuous gas feeding and sampling above 100°C.

Amine-H_2O VLE with continuous gas feeding and sampling above 100°C.

****Total Pressure Measurement***

MEA-H_2O-CO_2 (done)

PZ-H_2O-CO_2 (done)

Amine Screening: 1MPZ, 2MPZ, PZ/1MPZ, PZ/2MPZ, DGA, each at 2 loadings.

****CO_2-amine-H_2O VLE***

MEA-H_2O-CO_2

PZ-H_2O-CO_2

****Amine-H_2O VLE***

PZ-H_2O

MEA-H_2O

****Cp***

8m PZ, unloaded, 70-150°C

Modeling

Aspen Plus®, elecNRTL framework, start from Hilliard (2008) MEA model and Frailie PZ model.

Experimental Methods and Design

Total pressure

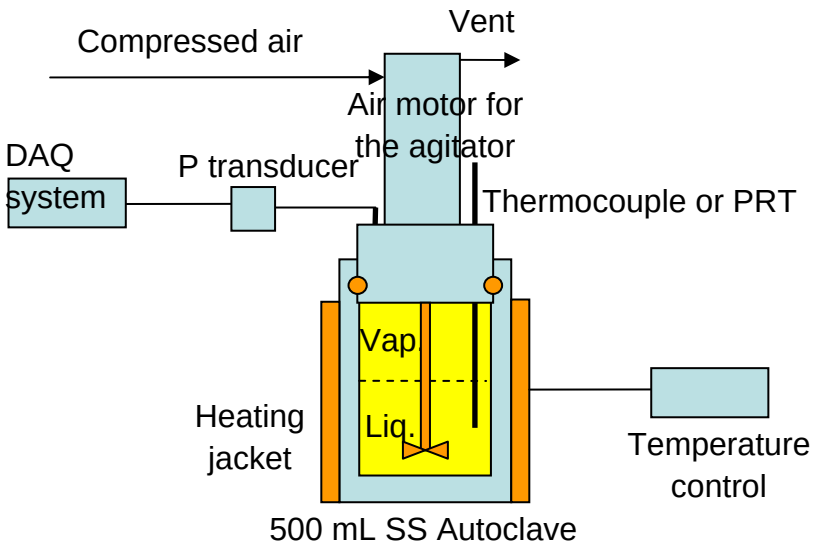

Figure 5: Total Pressure Measurement with an Autoclave

As shown in Figure 5, an autoclave (ZipperClave®, by Autoclave Engineers) was used as the equilibrium cell. Its designed operating range is up to 2000 psia and 232 ºC. The 500 mL pressure vessel is made of 316 SS stainless steel. Closure is effected by a resilient spring member inserted through a circumferential groove in the body and cover (Autoclave Engineers). A magnetic hollow shaft agitator (MAG075, MagneDrive II Series, by Autoclave Engineers) was used to get equilibrium without leaking to the atmosphere. It was driven by a compressed air motor (2AM-NCC-16, by Gast®). The agitator circulates both liquid and vapor phases.

A platinum resistance thermometer (model 5622-16, by Hart Scientific) was used for temperature measurement. It was connected to a series data logger (PT-104, by Picotech), and the temperature was recorded by Picolog software. Temperature was controlled by a Fuji Electric PXZ-4 temperature controller, with connection to a K-type thermocouple placed between the autoclave vessel wall and the heating jacket. For some runs the PRT was replaced by a K-type thermocouple, which was used for both measurement and temperature control. The results did not show difference from this change.

A pressure transducer (Validyne® DP15) was connected to a pressure indicator (Validyne® CD379). Because the indicator does not display pressure directly, calibration was performed by

heating water and correlating the readings with known vapor pressures. For the runs after 2009 summer, a new pressure transducer (Druck® PTX 611, 0-30 bar absolute pressure) was used. It was connected to a signal converter and a data logger NI USB 6009; LabView® SignalExpress® software was used for data recording. The pressure reading system was calibrated by a dead weight pressure tester (S/N 19189/278, by Budenberg Volumetrics, INC.).

Before each run, about 330 to 350 mL of the CO_2 loaded aqueous amine solution was prepared and added into the autoclave. To avoid the effects of O_2, N_2 was used to purge air out and then the cell was sealed. Initial pressure and temperature readings were recorded for later data correction. Then the cell was heated. Data recording of both temperatures and pressures started at around 100 ºC and the intervals of the data points were about 10 ºC. Liquid samples were collected before and after each experiment and analyzed by TIC and acid titration. The agitation rate varied from 1000 RPM to 2000 RPM.

Analyzing methods (FTIR, TIC and titration)

Fourier transform spectroscopy (FT-IR)

A Gasmet FT-IR (DX-4000) was used for vapor composition analysis. Calcmet software was used to do the multi-component analysis on-line. This analyzing method has been used by Hilliard (2008). The advantage over gas chromatography is that the FT-IR could get amine concentration for at ppm level; CO_2 and water could also be analyzed in wide concentration ranges.

Total Inorganic Carbon (TIC)

The concentration of CO_2 in solution was determined by TIC analysis. The liquid samples collected before and after each run were diluted by a factor of 100. About 10–15 μL diluted sample was injected into a CO_2 analyzer (Model 525, Horiba PIR 2000). Details can be found in Appendix B.2 of Hilliard's dissertation (2008).

Acid Titration

The total alkalinity of solution was determined by acid titration using a Metrohm-Peak 835 Titrando equipped with an automatic dispenser, Metrohm-Peak 801 stirrer, and 3M KCl pH probe. Details are available in Appendix A.3 of Hilliard (2008) and Appendix F of Sexton (2008).

CO_2-amine-H_2O VLE

Figure 6 gives the single vapor pass apparatus with two equilibrium cells in series. This design is improved from the present apparatus and is under construction now.

Two pressure vessels (200 and 600 mL, from Parr Instrument Co.) will be used as equilibrium cells. An oil bath will control the temperature. CO_2 under certain pressure will be sparged into the system and contact with the pre-loaded amine solution. The exiting vapor will be

depressurized to 1 atm, diluted by N_2 and analyzed by the Gasmet™ DX-4000 FT-IR. The Parker® needle valve and the dilution junction will be submerged under oil to keep the same temperature as the equilibrium cells. The N_2 stream, mixed gas and the FTIR cell will be kept at 180°C. Liquid sample will be withdrawn periodically and analyzed after the run.

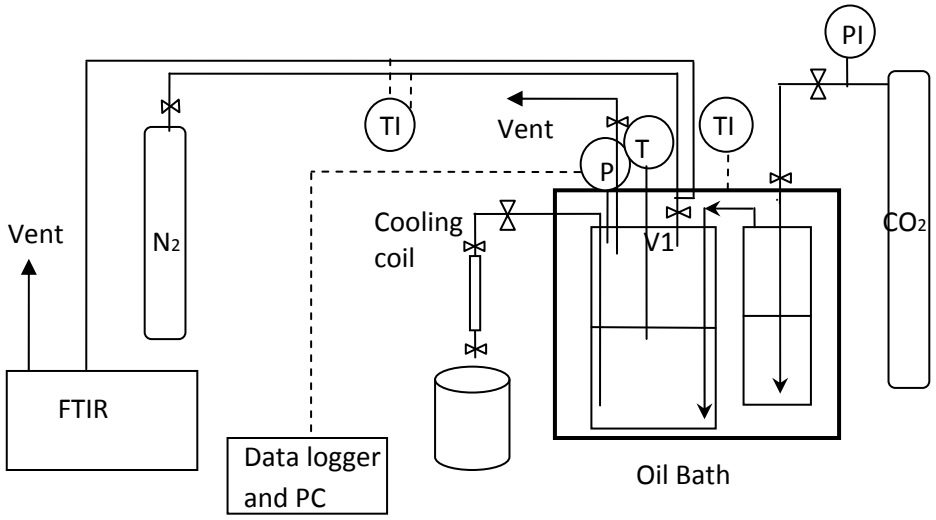

Figure 6: Single Vapor Pass HPVLE Apparatus with Oil Bath (for Amine-CO_2-H_2O)

TI: temperature controllers; PI: pressure regulator; P: pressure transducer; V1: needle valve; solid lines: actual tubes; dashed lines: electric wires.

Figure 7 shows the old apparatus used before mid April 2010. The same autoclave in the total pressure measurement was used as the equilibrium cell. The difference is that the top and surrounding of the equilibrium cell lid were covered by thermally conductive adhesive heating tapes from Clayborn Lab® and the temperature was kept between 160 and 175°C by disc thermostats from Selco Products Company. Compared with the future design, it has one equilibrium cell, but is with agitation. The needle valve and vapor sampling tube was wrapped by heating tapes from Thermo Scientific®. The temperature on the tubing surface was controlled as 148-153°C by a thermocouple and a temperature controller. The temperature control is not as good because of the various heating tapes and thermostats. Results also show that condensing might be a primary problem in this design and this will be discussed in the results session.

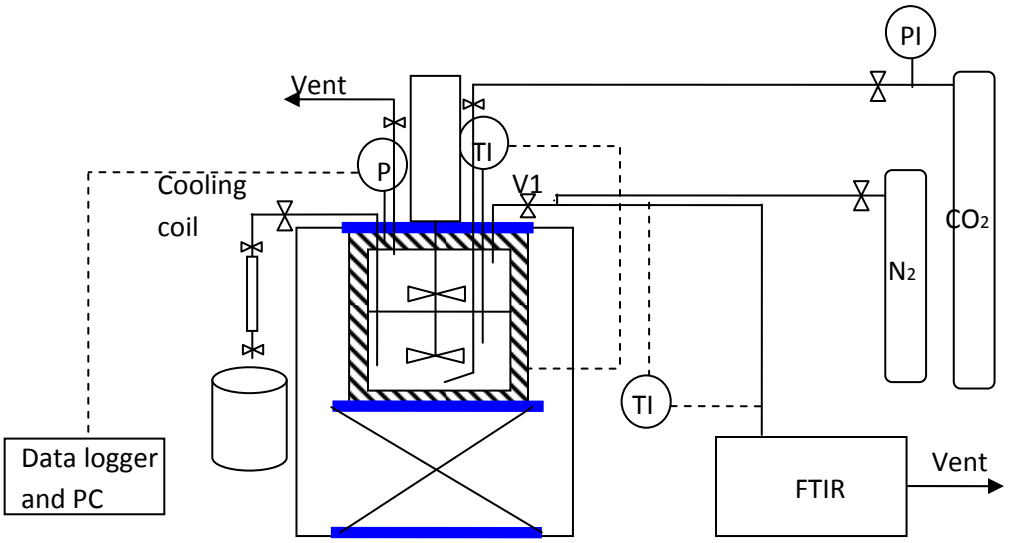

Figure 7: Single Vapor Pass HPVLE Apparatus with Autoclave (for Amine-CO_2-H_2O)

TI: temperature controller; PI: pressure regulator; P: pressure transducer; V1: needle valve; solid lines: actual tubes; dashed lines: electric wires.

The general procedures are:

350-400 mL CO_2 loaded aqueous amine was prepared and loaded into the autoclave. After purging with CO_2, the autoclave was sealed and heated to a certain temperature, with 1000-1200 RPM agitation on. When the temperature reached the target and got stable, CO_2 feeding valve was opened. The total pressure inside the equilibrium cell was controlled by the CO_2 pressure regulator. A vapor stream was continuously withdrawn from the vapor sampling line, diluted by 1.5 L/min N_2 and then analyzed by FT-IR on line. The flow rate of the vapor sample was controlled by the needle valve at 50-300 mL/min at standard pressure.

After the concentrations in FT-IR got relative constant for certain time, the CO_2 feeding, vapor sampling and agitation were stopped for 2-3 min and a liquid sample was taken. A 2 mL sampling SS bomb with valves on both ends was connected to the end of the liquid sampling line. The valves on the line were open, the high pressure liquid flushed through the line into the beaker. The bottom valve on the SS bomb was quickly closed after 20-25 mL liquid was flushed. After that the other two valves on the liquid sampling line were closed. A liquid sample was then trapped inside the SS bomb.

Amine-H_2O VLE

Amine-water VLE was measured using the same autoclave and the vapor sampling device. However no gas was fed and no liquid sample was taken during the runs. Because water was lost during the vapor sampling process, the concentration of amine kept changing and the real amine concentration in liquid was calculated from material balance.

In future by feeding inert gas like N_2O to keep high total pressure, it is possible to measure mid-temperature VLE with the same apparatus as well.

Specific heat capacity

A differential scanning calorimetry (DSC) was used to measure the specific heat capacity. Please refer to Hilliard Dissertation (2008) for calibration and operating procedures. The measuring method has been changed with the temperature range based upon aqueous PZ properties. The new data will be obtained at 70-150°C, because of the solubility issue for concentrated PZ at low temperature. The upper bond is extended from 120 to 150°C.

Preliminary Results

CO_2 solubility

Partial pressure of CO_2 was calculated by subtracting P_{N2}, P_{H2O} and P_{amine} from the total pressure, while P_{N2} was considered using ideal gas equation and the P_{H2O} and P_{amine} were estimated by Raoult's Law.

PZ-CO_2-H_2O

An empirical model was regressed based on high temperature data and previous low temperature data by Hilliard (2008), Dugas et al. (2008) and Ermatchkov et al. (2006).

$$\ln P_{CO_2} = (35.3 \pm 0.3) - \frac{91542 \pm 1069}{RT} - (18.0 \pm 3.2)\alpha^2 + (4789 \pm 435)\frac{\alpha}{T} + (9765 \pm 1436)\frac{\alpha^2}{T}$$

$r^2 = 0.993$ (7)

α is CO_2 loading in the liquid phase.

The heat of absorption of CO_2 was calculated based on Eq. (7) and Gibbs-Helmholtz Equation:

$$\Delta H_{abs} = -R\frac{\partial \ln P_{CO_2}}{\partial(\frac{1}{T})} = -R(-\frac{91542}{R} + 4789\alpha + 9765\alpha^2) \quad (J/mol\ CO_2) \qquad (8)$$

Figure 8 shows CO_2 solubility in 0.9-12 m PZ. At 0.1-0.5 CO_2 loading, ΔH is from 87-51 kJ/mol CO_2.

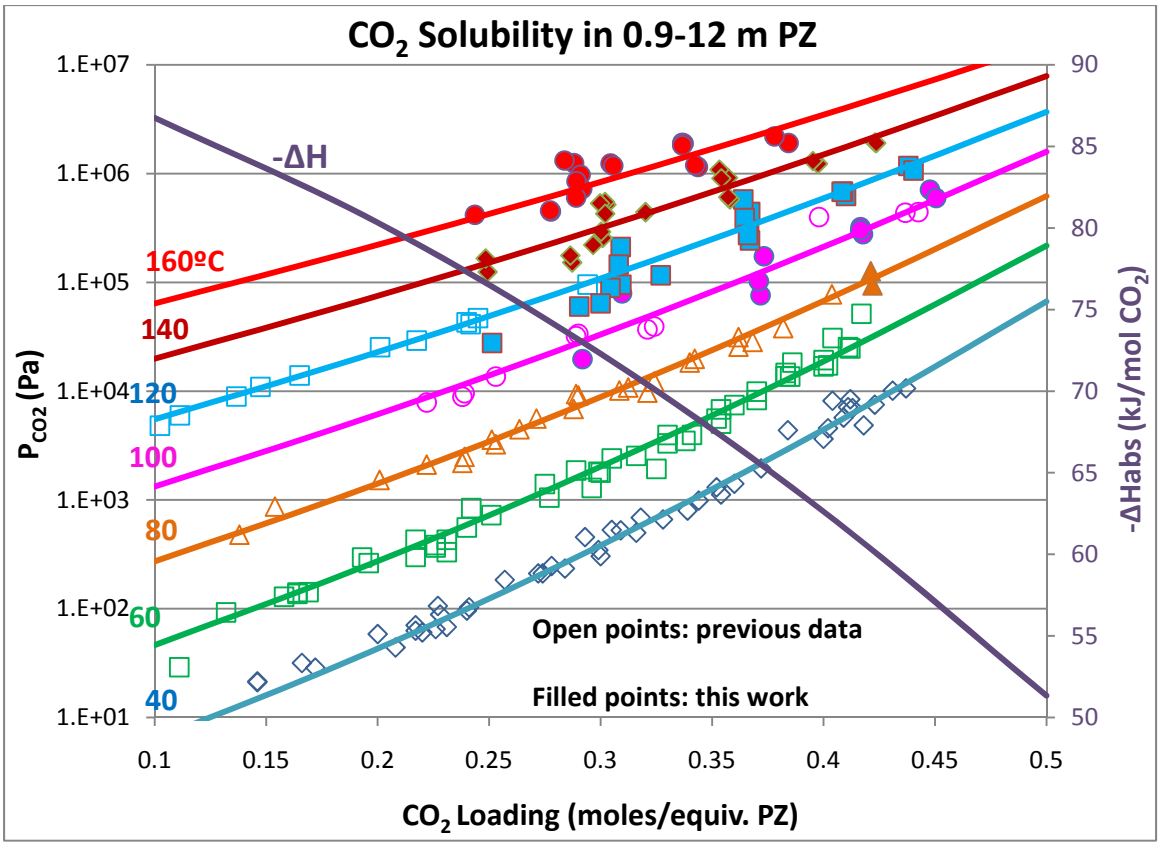

Figure 8: CO_2 Solubility in 0.9-12 m PZ

MEA-CO_2-H_2O

An empirical model was regressed based on the high temperature data and previous low temperature data by Hilliard (2008), Dugas et al. (2008) and Jou et al. (1995).

$$\ln P_{CO_2} = (39.4 \pm 0.6) - \frac{101340 \pm 1647}{RT} - (19.3 \pm 3.7)\alpha^2 + (1130 \pm 420)\frac{\alpha}{T} + (12845 \pm 1481)\frac{\alpha^2}{T}$$

$r^2 = 0.994$ (9)

α is CO_2 loading in the liquid phase.

The heat of absorption of CO_2 was calculated based on Eq. (9) and Gibbs-Helmholtz Equation:

$$\Delta H_{abs} = -R\frac{\partial \ln P_{CO_2}}{\partial(\frac{1}{T})} = -R(-\frac{101340}{R} + 1130\alpha + 12845\alpha^2) \quad (J/mol\ CO_2) \qquad (10)$$

Figure 9 shows CO_2 solubility in 3.5-13 m MEA. At 0.1-0.6 CO_2 loading, ΔH is from 99-57 kJ/mol CO_2.

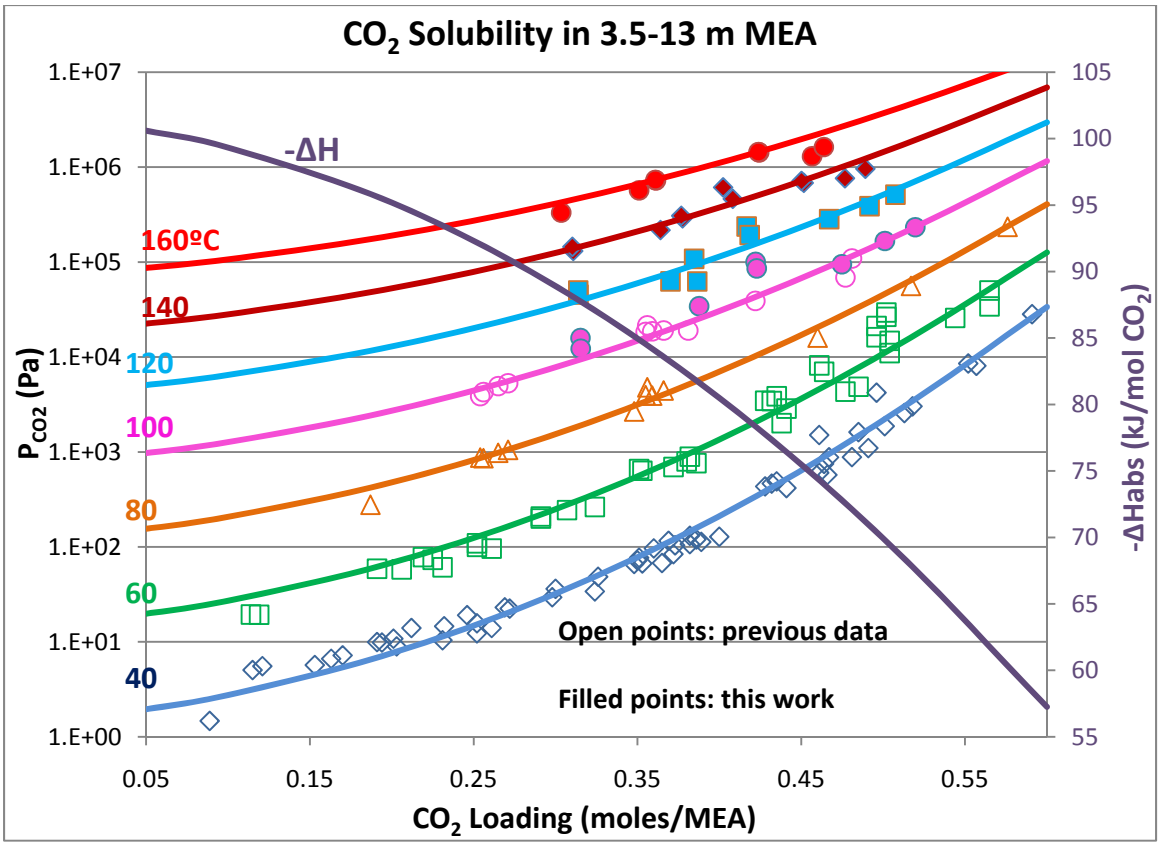

Figure 9: CO_2 Solubility in 3.5-13 m MEA

VLE method development

Amine-H_2O

An empirical model was developed based on the high temperature data in this work and low temperature data from Nguyen's work (Rochelle et al., 2009b).

$$\ln\frac{P_{PZ}}{x_{PZ}} = (-402\pm81) + (61.8\pm11.7)\ln T + \frac{16129\pm4321}{T} + (117\pm19)(x_{PZ}-0.09)^2 \qquad (11)$$

r^2=0.968

Based on Eq. (11) and the Gibbs-Helmholtz Equation, the heat of absorption of PZ is calculated:

$$\Delta H = -R\frac{\partial \ln P_{PZ}}{\partial(\frac{1}{T})} = -R(-61.8T + 16929)\ \ (J/mol\ \mathrm{PZ}) \qquad (12)$$

To give a clearer graph, the averages were taken for high temperature data and plotted in Figure 10, together with low temperature data. The purple curve in Figure 9 is the heat of absorption of PZ.

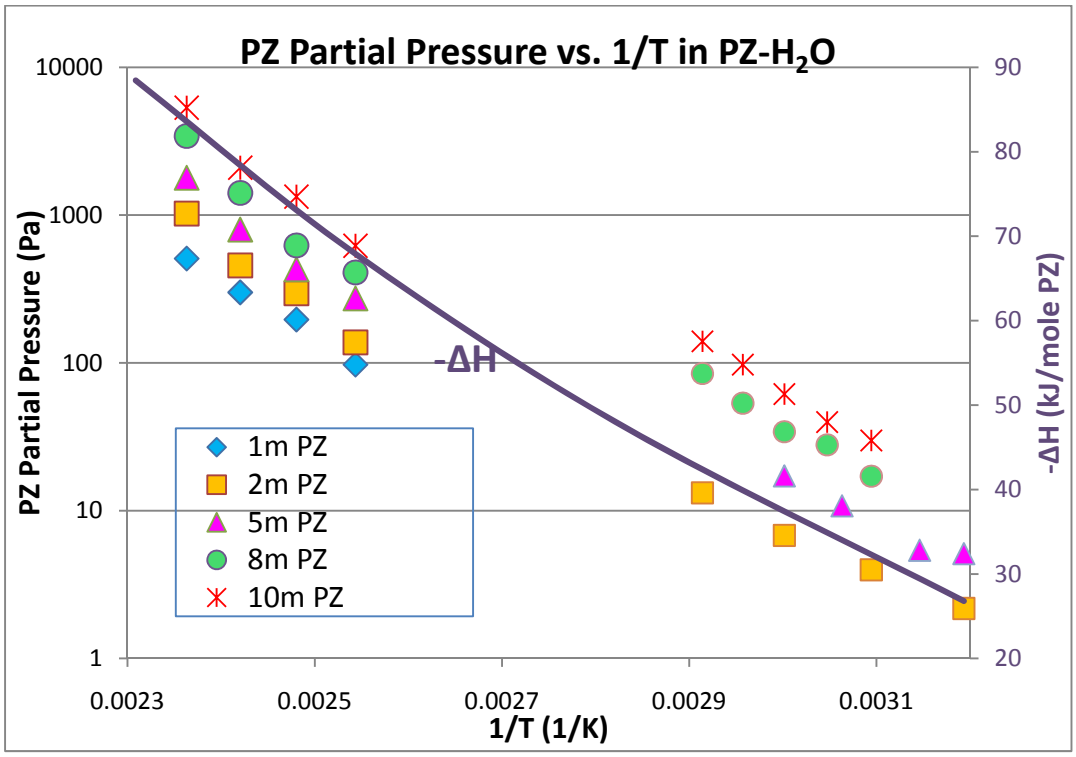

Figure 10: Temperature Dependence of PZ Partial Pressure in PZ-H_2O at 40-150ºC

Because of limited MEA data, no regression could be done to get a good empirical model. Figure 11 shows the comparison of MEA partial pressure with literature data.

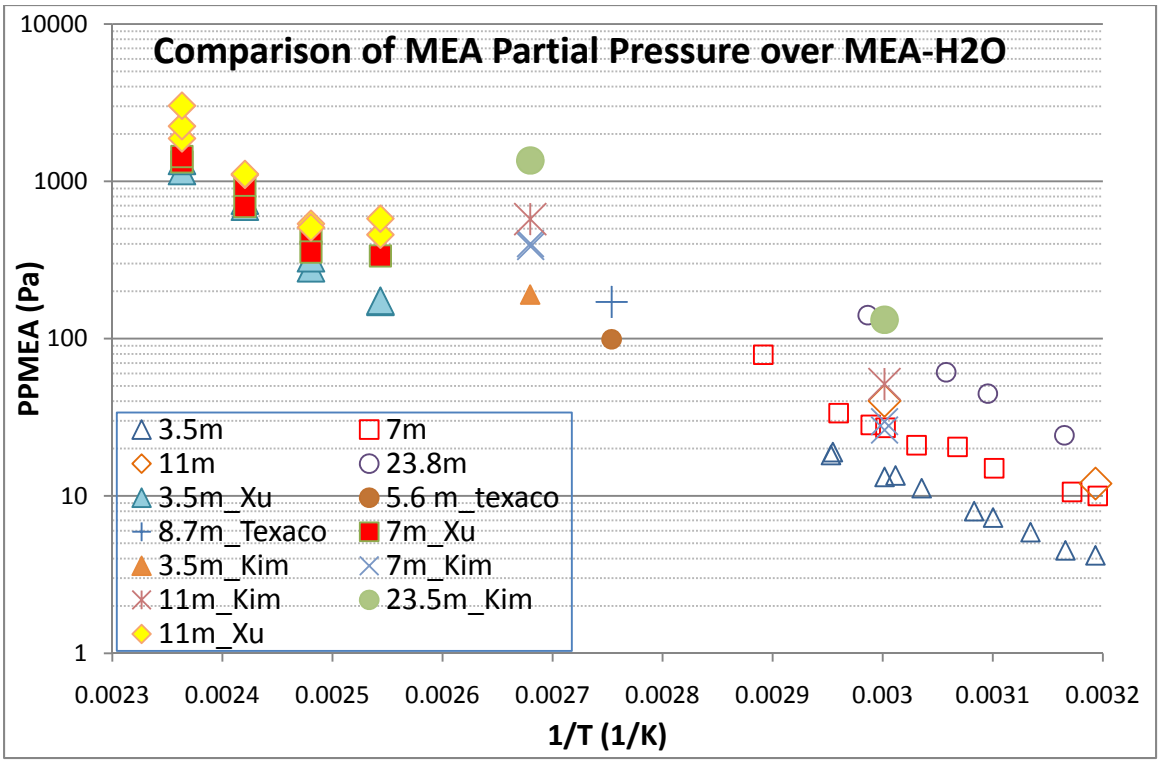

Figure 11: Comparison of MEA Volatility with Literature

Compared with low temperature data, both MEA and PZ volatilities at high temperature are low. This may result from condensing when vapor was sampled. Further discussion will be after amine-water-CO_2 results.

Amine-H_2O-CO_2

6 runs were conducted to MEA-water-CO_2. Only MEA-2, 3 and 6 are shown here.

Figure 12 gives the MEA volatility over MEA-CO_2-H_2O, compared with previous low temperature data by Hilliard (2008). The 5 points in the ellipse are from MEA-2 and 3. The vapor sample results from MEA-6 are questionable because the data are significantly smaller than the others.

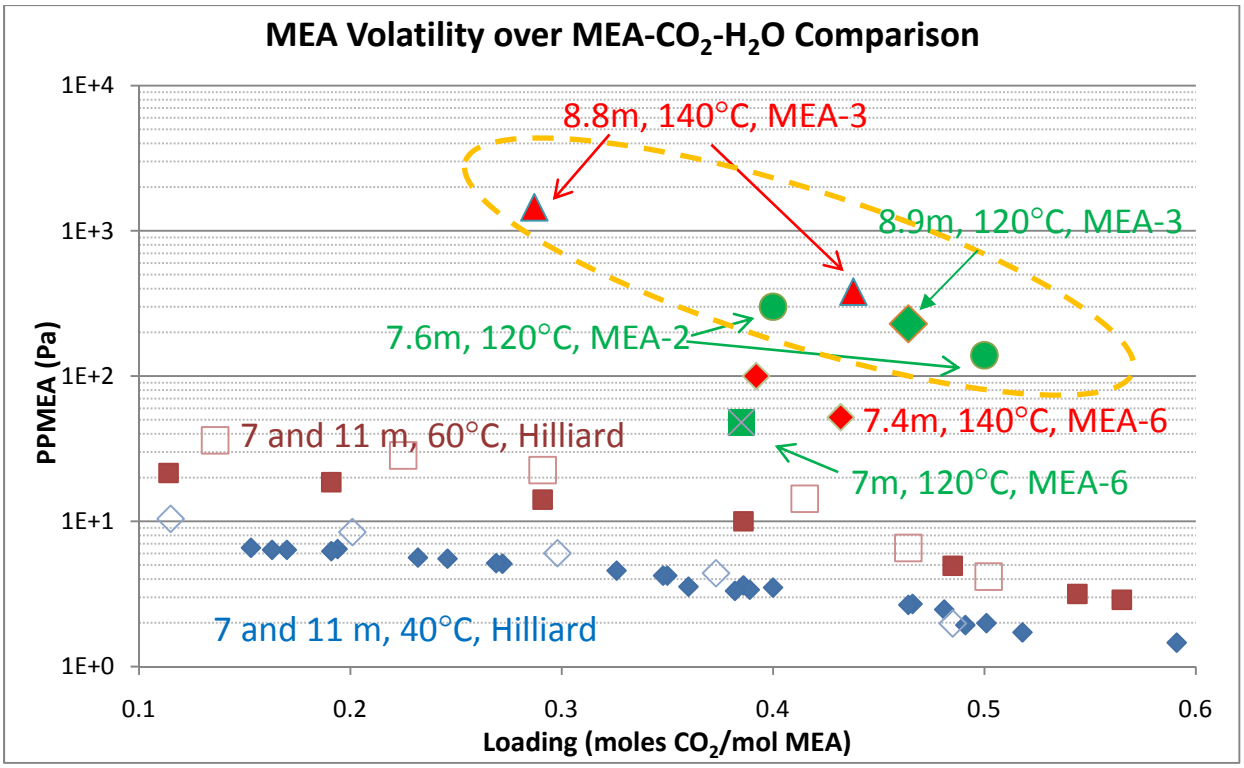

Figure 12: Comparison of MEA Volatility over MEA-CO_2-H_2O

Figure 13 compares the MEA volatility at close loadings and shows temperature dependence. Points with the same color have similar CO_2 loading. Generally lower CO_2 loading and higher MEA concentration get higher MEA volatility.

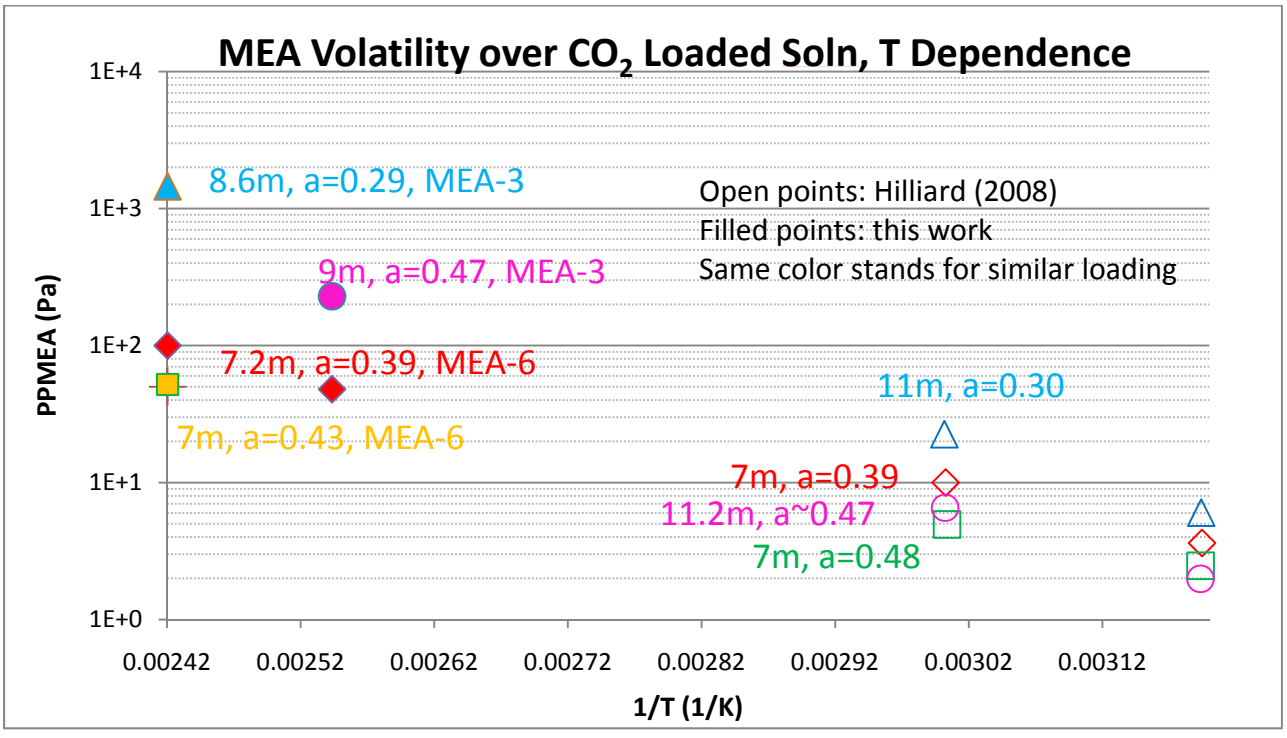

Figure 13: Comparison of MEA Volatility over MEA-CO_2-H_2O Temperature Dependence-1

Liquid Sampling Results

Figure 14 gives a comparison of total pressure of MEA-3, MEA-6 and previous data. MEA-3 has one outlier at low loading, mainly because it was the first point using the modified liquid sampling device. At higher CO_2 loading, the new total pressure data are generally higher than the previous ones, indicating flash might still happen and caused a lower CO_2 loading in the collected liquid samples. However, the previous total pressure data is only for reference because its CO_2 loading was calculated, instead of measured. Improvements need to be done to further eliminate possible flash.

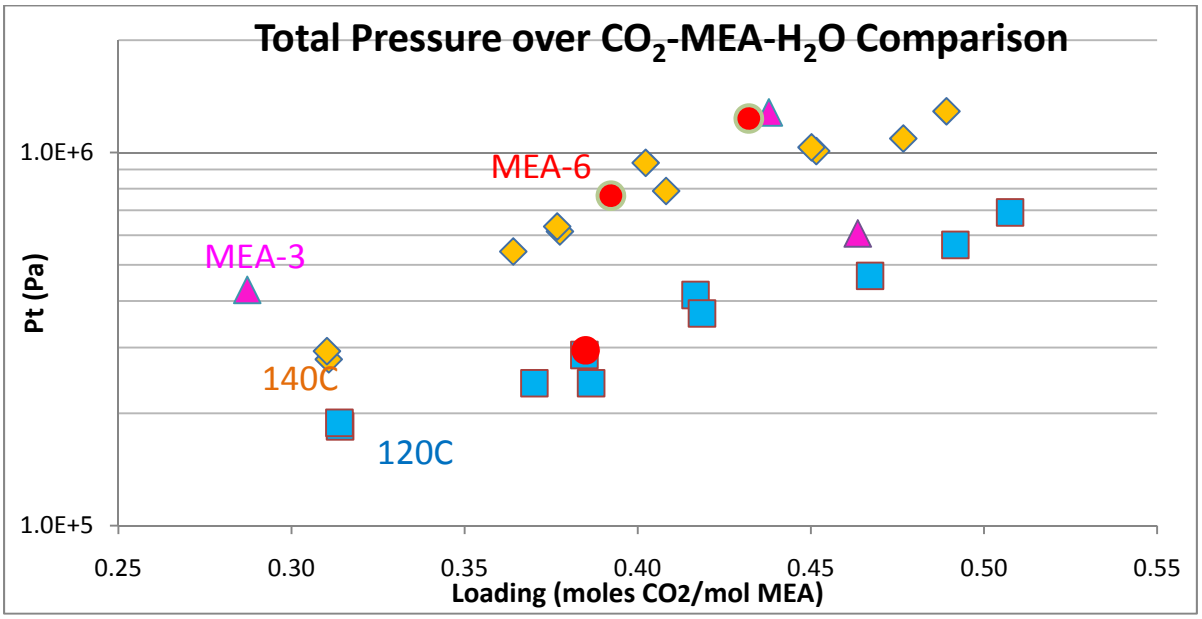

Figure 14: Comparison of Total Pressure over MEA-CO_2-H_2O at 120 and 140°C

Figure 15 gives the liquid composition analyzing results from MEA-3. Number 1 to 5 samples represent pre, A, B, C and post, taken chronologically. As the experiment went on, water got lost gradually, thus MEA became more concentrated. CO_2 concentration change relates mostly to the total pressure. Higher pressure corresponds to higher CO_2 loading at the same temperature. From these data, especially the MEA concentrations, together with the total pressure data comparison, a conclusion can be made that this liquid sample collecting and analyzing method worked well.

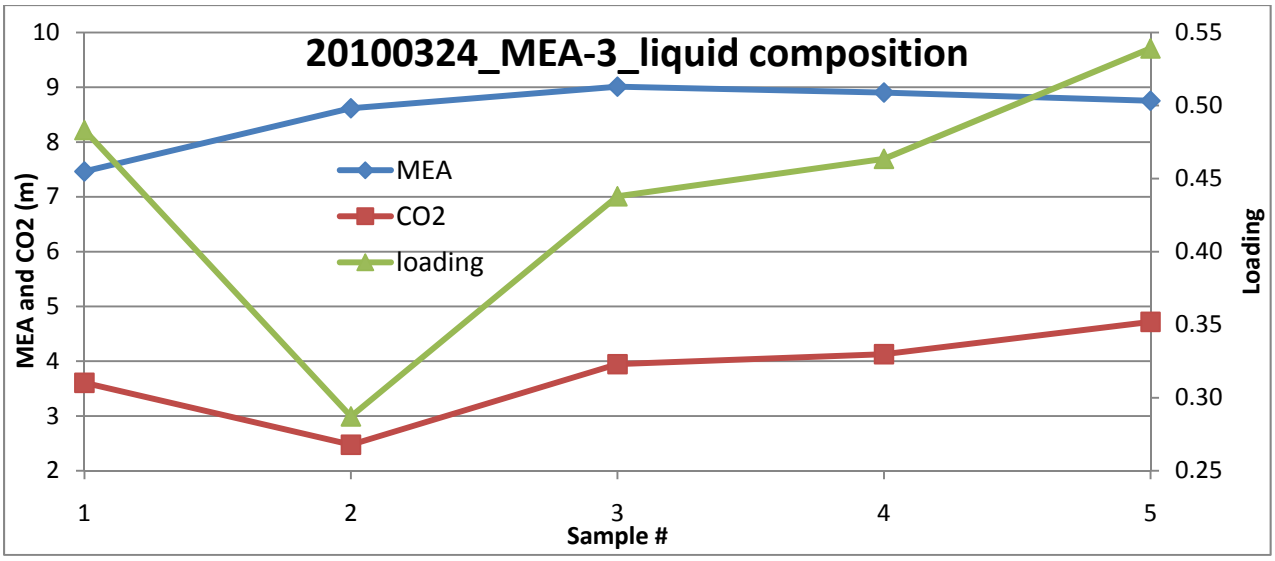

Figure 15: Liquid Composition results from MEA-3 (3/24/10)

Learnings from the amine-water and MEA-CO_2-H_2O measurements

The results show the similar problem for MEA-CO_2-H_2O and amine-water experiments, while the vapor sampling rate was from 50-270 scc/min. In both cases, the relative non-volatile component concentration shown in the FTIR was smaller than expected values. There are several possible reasons. First is condensing under the autoclave lid. Since no condensing was observed inside the vapor sampling line and there would be little condensing in the 180C heated line and the FT-IR cell, the possible condensing place will be anywhere before the gas exiting the equilibrium cell. Although the lid and its surroundings were heat traced by heating tapes and insulation, the temperature may still not be well controlled by the simple thermostats, etc. Liquid drop entrainment also affects the results by about 5%, but it is not the primary reason.

The pressure, temperature and vapor sampling rate control worked well. Liquid sampling device worked well, especially for low and mid loading solutions. To further eliminate flash, water or ice bath may need to be installed, especially at high CO_2 loading.

For the vapor sampling, the biggest problem is with condensing. In future, better temperature control over the equilibrium cell as well as the vapor sampling line will be achieved by submerging them into an oil bath.

Scientific and Engineering Contributions

This project will allow for contributions in these fields:

1. Vapor-liquid equilibrium: This project will obtain adequate CO_2 solubility and amine volatility data at 100-160°C for CO_2 loaded and unloaded MEA and PZ. By combining

with low temperature data, the temperature dependences of CO_2 solubility and amine volatility will be quantified and explained.

2. ΔH and specific heat capacity: This project will identify and explain the temperature dependence of CO_2 ΔH_{abs} in MEA and PZ, as well as amine ΔH_{abs} in aqueous MEA and PZ. More heat capacity data will be obtained for concentrated PZ over a broader temperature range to help understanding the ΔH_{abs}.
3. Thermodynamic modeling: This project will modify the thermal models for MEA and PZ systems, so that conditions and data types can be extrapolated and interpolated. The modeling also serves to interpret and understand the thermal behaviors.
4. HPVLE method: A unique versatile apparatus for HPVLE (above 1.5 bar) measurements with FT-IR will be developed.
5. New solvent screening: A few new thermal resistant solvents by measuring CO_2 solubility at high temperature.

Timeline towards PhD

Research	2009			2010			2011		
	SP	**S**	**F**	**SP**	**S**	**F**	**SP**	**S**	**F**
Total P	X	X							
VLE (1)			X	X	X	X			
VLE (2)						X	X		
Cp							X		
Modeling							X	X	
Dissertation									X

VLE (1): amine-H_2O-CO_2; VLE (2): amine-H_2O

References

Al-Juaied M. *Carbon Dioxide Removal from Natural Gas by Membranes in the Presence of Heavy Hydrocarbons and by Aqueous Diglycolamine®/Morpholine.* The University of Texas at Austin. Ph. D. Dissertation. 2004.

Al-Juaied M et al., "Thermodynamics and Equilibrium Solubility of Carbon Dioxide in Diglycolamine/Morpholine/Water." *J. Chem. Eng. Data*, 2006, 51, 708-717.

Autoclave Engineers®, Zipperclave® 500&1000 mL stirred reactor, http://www.autoclaveengineers.com/ae_pdfs/SR_500_1000_Zip.pdf

Bishnoi S et al., "Absorption of Carbon Dioxide into Aqueous Piperazine: Reaction Kinetics, Mass Transfer and Solubility." *Chem. Eng. Sci*. 55 (2000), 5531-5543.

Cai ZY et al., "Binary Isobaric Vapor-Liquid Equilibria of ethanolamines + Water." *J. Chem. Eng. Data*, 1996, 41, 1101-1103.

Chen YR et al., "Liquid Heat Capacity of the Solvent System (Piperazine + N-Methyldiethanolamine + Water)." *J. Chem. Thermodynamics*, 42 (2010), 54-59.

Chiu LF et al., "Heat Capacity of Alkanolamine Aqueous Solutions." *J. Chem. Eng. Data*, 1999, 44, 1396-1401.

Chiu LF et al., "Heat Capacity of Alkanolamines by Differential Scanning Calorimetry." *J. Chem. Eng. Data*, 1999, 44, 631-636.

Derks PWJ et al., "Solubility of Carbon Dioxide in Aqueous Piperazine Solutions." *AIChE Journal*, August 2005, Vol 51, No. 8, 2311-2327.

Dingman JC et al., *Equilibrium Data for the H2S-CO2-Dyglycolamine® Agent-Water System*, presented to the 62nd Annual Gas Process Association Convention, Mar. 14-16, 1983.

DIPPR, 1998-Provo, UT: BYU DIPPR, Thermophysical Properties Laboratory, 1998-Version 13.0.

Dugas R et al. "Absorption and desorption rates of carbon dioxide with monoethanolamine and piperazine." *GHGT-9*, Washington D.C. 2008.

Ermatchkov V et al. "Solubility of carbon dioxide in aqueous solutions of piperazine in the low gas loading region." *J. Chem. Eng. Data*, 2006, 51 (5), 1788-1796.

Freeman SA et al. "Carbon dioxide capture with concentrated, aqueous piperazine." *GHGT-9*, Washington D.C. 2008.

Hilliard MD. *A Predictive Thermodynamic Model for an Aqueous Blend of Potassium Carbonate, Piperazine, and Monoethanolamine for Carbon Dioxide Capture from Flue Gas.* The University of Texas at Austin. Ph.D. Dissertation. 2008;1083.

IPCC Fourth Assessment Report – Climate Change 2007, available at http://www.ipcc.ch.

International Energy Agency, CO_2 emissions from fuel combustion highlights (2009 edition), 2009.

Jou, F.-Y.; Mather, A. E.; Otto, F. D., "The solubility of CO_2 in a 30 mass percent monoethanolamine solution." *The Canadian Journal of Chemical Engineering*, 1995, 73, 140-146.

Jou FY et al., "Vapor-Liquid Equilibrium of CO2 in Aqueous Mixture of MEA and MDEA." *Ind. Eng. Chem. Res.* 1994, 33, 2002-2005.

Kim I et al., "Heat of Absorption of CO2 in MEA and AEEA Solutions." *Ind. Chem. Eng. Res*. 2007, 46, 5803-5809.

Kim I et al., "Ebulliometric Determination of Vapor-Liquid Equilibria for Pure Water, MEA, MDEA, 3-(Methylamino)-propylamine, and Their Binary and Ternary Solutions." *J. Chem. Eng. Data*. 2008, 2521-2531.

Kim I et al., "Enthalpy of Absorption of CO2 with Alkanolamine Solutions Predicted from Reaction Equilibrium Constants." *Chem. Eng. Sci*., 64 (2009), 2027-2038.

Maddox RN et al., *Equilibrium Solubility of Carbon Dioxide or Hydrogen Sulfide in Aqueous Solutions of Monoethanolamine, Diglycolamine, Diethanolamine and Methyldiethanolamine*. Research Report RR-104. Mar. 1987.

Martin JL et al., "Solubility of Hydrogen Sulfide and Carbon Dioxide in a Diglycolamine Solution." *J. of Chem. Eng. Data*, 1978, Vol. 23, No. 2, 163-164.

Nath A et al., "Isothermal Vapor-Liquid Equilibria of Binary and Ternary Mixtures Containing Alcohol, Alkanolamine, and Water with a New Static Device." *J. Chem. Eng. Data*, 1983, 28, 370-375.

Page et al., "A Comprehensive Thermodynamic Investigation of Water- ethanolamine Mixtures at 10, 25, and 40°C." *Can. J. Chem*. Vol. 71, 1993, 1064-1072.

Park and Lee, "Vapor-Liquid Equilibria for the Binary Monoethanolamine + Water and Monoethanolamine + Ethanol Systems." *Korean J. of Chem. Eng*., 1997, 14(2), 146-148.

Rochelle GT et al. "CO_2 Capture by Aqueous Absorption, Third Quarterly Progress Report 2008." Luminant Carbon Management Program. The University of Texas at Austin. 2008a.

Rochelle GT et al. "CO_2 Capture by Aqueous Absorption, Fourth Quarterly Progress Report 2008." Luminant Carbon Management Program. The University of Texas at Austin. 2008b.

Rochelle GT et al. "CO_2 Capture by Aqueous Absorption, Second Quarterly Progress Report 2009." Luminant Carbon Management Program. The University of Texas at Austin. 2009a.

Rochelle GT et al. "CO_2 Capture by Aqueous Absorption, Third Quarterly Progress Report 2009." Luminant Carbon Management Program. The University of Texas at Austin. 2009b.

Rochelle GT et al. "CO_2 Capture by Aqueous Absorption, Fourth Quarterly Progress Report 2009." Luminant Carbon Management Program. The University of Texas at Austin. 2010.

Sexton AJ. *Amine Oxidation in CO_2 Capture Processes*. The University of Texas at Austin. Ph.D. Dissertation. 2008.

Tochigi K et al., "Isothermal Vapor-Liquid Equilibria for Water + 2-Aminoethanol + Dimethyl Sulfoxide and Its Constituent Three Binary Systems." *J. Chem. Eng. Data*, 1999, 44, 588-590.

Touhara H et al., "Thermodynamic Properties of Aqueous Mixtures of Hydrophilic Compounds 2 Aminoethanol and Its Methyl Derivatives." *J. Chem. Thermodynamics*, 1982, 14, 145-156.

Weiland RH et al., "Heat Capacity of Aqueous Monoethanolamine, Diethanolamine, N-Methyldiethanolamine, and N- Methyldiethanolamine Based Blends with Carbon Dioxide." *J. Chem. Eng. Data*, 1997, 42, 1004-1006.

Xia JZ et al., "Solubility of H2S in (H2O + Piperazine) and in (H2O + MDEA + Piperazine)." *Fluid Phase Equilibria*, 207 (2003), 23-34.

Aqueous Piperazine as the New Standard for CO_2 Capture Technology

Gary Rochelle, Eric Chen, Stephanie Freeman, David Van Wagener, Qing Xu, Alex Voice

Abstract

Amine scrubbing will be the technology of choice for CO_2 capture from coal-fired power plants. 7 m monoethanolamine (30 wt% MEA) has been the standard solvent to represent the capability of this technology. This paper presents a new standard process that uses 8 m piperazine (40 wt% PZ) with regeneration at 150 °C by a two-stage flash. The performance data for the piperazine system is non-proprietary and available for standard comparisons. The expected energy requirement for a piperazine or other advanced amine scrubbing processes will approach 220 kWh/tonne CO_2 removed. The minimum work for this separation is 113 kWh/tonne. The major exergy losses (kWh/tonne CO_2) in the piperazine process are: condenser - 34; exchanger - 25; compressor - 22; absorber - 14. Because mechanical adiabatic compression has an overall thermodynamic efficiency of 55 to 60%, amine scrubbing with thermal swing regeneration provides better energy performance with greater heat of CO_2 absorption and maximum regeneration temperature. Piperazine can be used up to 150 °C without significant thermal degradation. This allows better energy performance and minimizes the impacts of degradation products. The piperazine solvent is resistant to oxidative degradation, has less volatility than MEA, and is not corrosive to stainless steel. It is also suitable for reclaiming by distillation and other methods already commercialized by the gas treating industry.

Keywords

Carbon dioxide, piperazine, monoethanolamine, standard, irreversibilities, equivalent work, robustness

1. Introduction and Background

1.1. Amine Scrubbing: The Technology for Post-Combustion Capture.

Amine scrubbing with absorption and stripping is the technology of choice for post-combustion CO_2 capture (***1***). The basic technology was first patented in the 1930's and has been used commercially in acid gas treating for well over 80 years (***2***). Monoethanolamine (MEA) and other proprietary amines such as Econamine (Fluor) and KS-1 (MHI) are currently used at more than 30 plants to remove CO_2 from flue gas produced by natural gas combustion. Four existing coal-fired plants in the 6 to 30 MW range use 20 wt% MEA to scrub CO_2 from the flue gas.

The evaluation of amine-based CO_2 removal technology was first conducted in 1991 and determined to be too energy intensive and costly. As a result, research and development funding from the U.S. government has primarily supported alternative technologies and amine absorption and stripping

technologies have largely been ignored. The history of limestone slurry scrubbing for flue gas desulfurization serves as a precedent for the developmental pathway of amine scrubbing.

Limestone slurry scrubbing was first identified as an effective technology by a study in 1965 (***3***), but was found to be too expensive and too commercial and did not receive government support. However, development of the technology continued and it is now the prominent technology for flue gas desulfurization. As with limestone slurry scrubbing, amine scrubbing will most likely be the preferred technology for post-combustion capture.

Amine scrubbing is a proven technology and is ready to be tested and used on large coal-fired power plants. Other advanced technologies such as membranes, pressure swing-adsorption, and ionic liquids will probably not compete with advanced amine systems that provide CO_2 at higher pressure with a heat-driven, thermal swing stripper. Implementation of the integrated coal gasification combined cycle (IGCC) requires grassroots construction of a completely new power plant. As a tail-end technology, amine scrubbing offers flexibility through implementation in scale-up, on/off operation during peak demand, and retrofit to existing utility plants. Other advanced technologies will not provide solutions as energy-efficient or as timely to decrease CO_2 emissions.

1.2. MEA as a Standard

Historically, 30 wt% MEA has served as the standard for the evaluation of processes for post-combustion capture. There are three operating systems on coal in the U.S. with 20% MEA. This solvent served as the initial process for detailed evaluations. NETL has also prepared a detailed evaluation with 30% MEA. However, these first generation evaluations have already been displaced by claims of better performance by new proprietary processes, such as KS-1 and Advanced Econamine. It will be difficult to access performance data of the proprietary processes for any detailed evaluation. Because all of the performance data are available for the concentrated piperazine process, it provides an opportunity to provide a realistic second generation standard for technology evaluations.

1.3. Previous Work on Piperazine (PZ)

Piperazine (PZ) is an advanced amine solvent that has been thoroughly characterized. Freeman et al. (***4***) summarizes much of the available data. Freeman showed that 8 m PZ (8 gmol/kg water, 40 wt%) can be used at a loading between 0.26 and 0.42 gmol CO_2/equivalent piperazine ($n_{CO2}/2n_{PZ}$) without risk of solids precipitation down to 20 °C. At 40 °C , loaded PZ has a viscosity of 12 cP.

CO_2 solubility, heat capacity, amine volatility, and speciation were measured by Ermatchkov (***5***), Hilliard (***6***), Dugas and Rochelle (***7***), Dugas (***8***), Nguyen and Rochelle (***9***). Hilliard (***6***) provided a second generation electrolyte NRTL model of these data in Aspen Plus®. The rate of CO_2 absorption/desorption in concentrated aqueous PZ was measured by Dugas and Rochelle (***7***) in a wetted wall column. Davis (***10***) and Freeman et al. (***11***) have demonstrated that PZ is can be used up to 150 °C without significant thermal degradation. Sexton (***12***) and Freeman et al. (***11***) showed that PZ is resistant to oxidative degradation. In Freeman et al. (***4***), Van Wagener provides an energy analysis of the two-stage heated flash and shows that it is competitive with MEA systems.

In this paper we will offer additional reviews of these data and their implications. Additional data are included on the solubility of CO_2 at high temperature and new and modified data are included on piperazine volatility and oxidative degradation. We add an analysis of exergy losses in this system and demonstrate that it provides much better energy performance than earlier analyses of MEA systems.

1.4. PZ Chemistry

Figure 1 shows a speciation of 5 m piperazine at 40 °C calculated with a regressed electrolyte/NRTL model by Hilliard (***6***). At low loading, CO_2 reacts with piperazine to produce PZ carbamate and protonated PZ. At the operating range of the concentrated piperazine process (0.31 – 0.41 gmol CO_2/equivalent PZ), CO_2 reacts to produce protonated PZ carbamate and PZ dicarbamate. Because there is less than 10% of the total piperazine is free piperazine over the operating range of CO_2 loading, PZ has an acceptable volatility and the precipitation of PZ–$6H_2O$ is avoided. Because the PZ carbamate still has an active amine function the operating loading, it provides for substantial enhancement of the rate of CO_2 absorption.

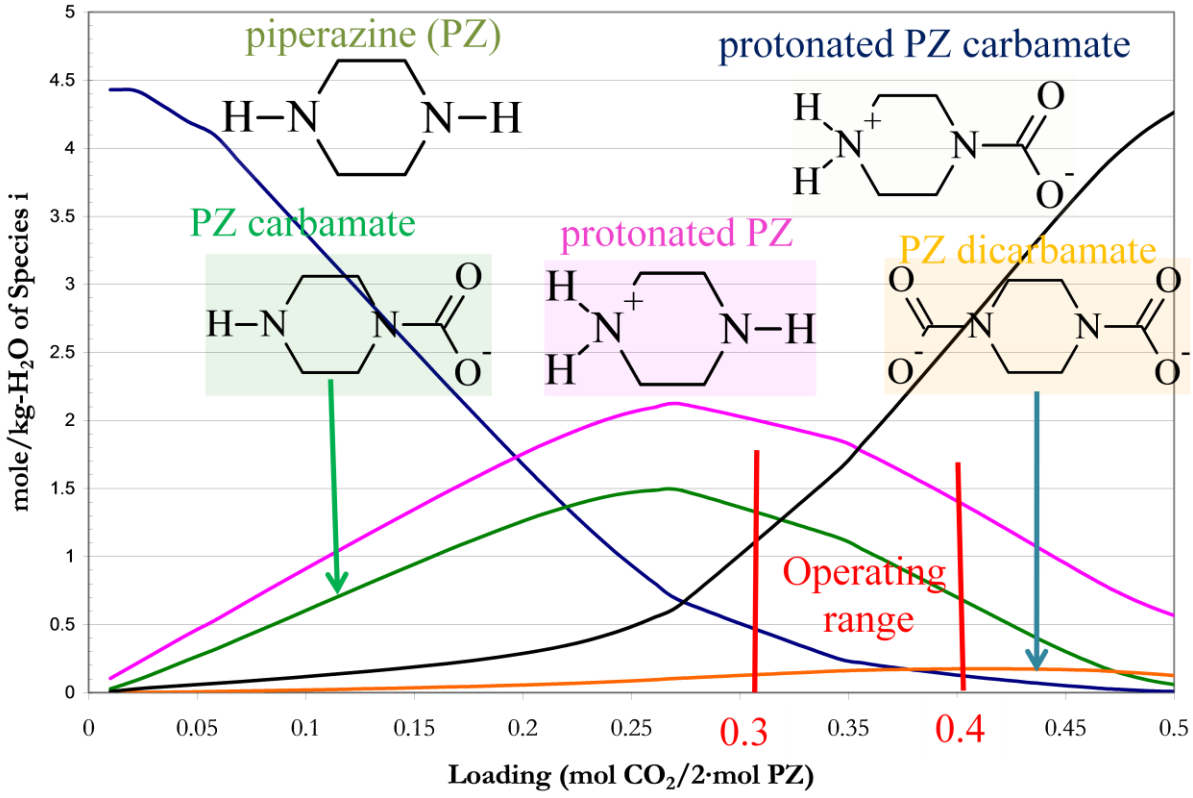

Figure 1. Speciation of 5 m PZ at 40°C (6)

2. Energy Analysis

2.1. Process Flowsheet

Figure 2 gives the flowsheet for an optimized process using 8 m PZ with regeneration by a heated two-stage flash. Solvent at 40 °C and a lean loading of 0.31 gmol CO_2/equiv PZ countercurrently contacts flue gas saturated with water at 40 °C. The packed absorber is intercooled to 40 °C to avoid deleterious effects of a maximum temperature bulge in the middle. Rich solution with a loading of 0.41 gmol CO_2/equiv PZ is heated by exchange with hot lean solution with a hot side approach T of 5 °C. It is further heated with steam to 150 °C and flashed at 17 bar. Then it is heated again to 150 °C at 11 bar. The hot lean solution is returned to the absorber through the cross-exchanger and a trim cooler. The CO_2 product is cooled to 40 °C to condense water and fed to the appropriate stage of a multistage, intercooled compressor to produce high density CO_2 at 150 bar for pipeline transportation to a storage site.

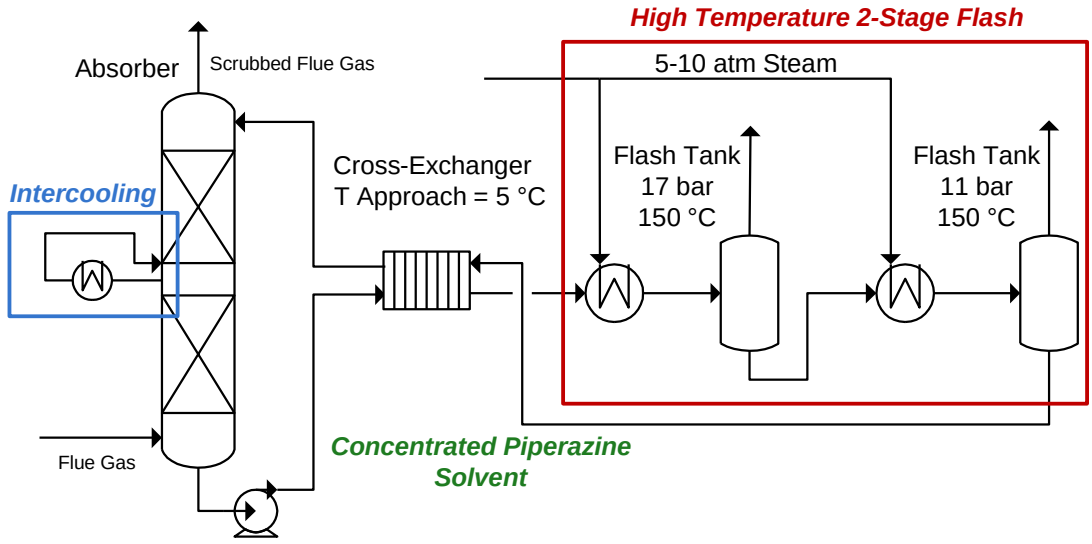

Figure 2. Flowsheet for high temperature two-stage flash process with concentrated piperazine and absorber intercooling.

The steam requirement for this process is 2.6 MJ/tonne CO_2 removed. This steam condensing at 155 °C could be used to produce electricity in the power plant with an equivalent work (W_{eq}) given by a Carnot cycle efficiency with a turbine cycle efficiency of 75%:

$$W_{stm} = 0.75Q\left(\frac{T_{stm} - 313}{T_{stm}}\right) = 145\frac{kWh}{tonne\ CO_2} \qquad \text{EQ. 1}$$

The compressor work for this process is 44 kWh/tonne CO_2. The pump work is 19 kWh/tonne CO_2. Therefore the total equivalent work or lost production of electricity is given by:

$$W_{eq} = W_{stm} + W_{comp} + W_{pump} = 208 \frac{kWh}{tonne\ CO_2} \qquad \text{EQ. 2}$$

2.2. Historical Trends of Estimated Energy Performance

Figure 3 presents the progression in time of the estimated heat duty for the stripper in amine scrubbing systems. The earliest values with 30 wt% MEA vary from 3.2 to 5.5 MJ/kg CO_2 removed (***13***,***14***,***15***). More recent estimates use 35 wt% MEA with advanced stripper configurations to get heat duties as low as 2.9 MJ/kg (***16***,***17***,***18***). The values for the KS-1 solvent by MHI have decreased from an early value of 3.3 (***19***) to a minimum value of 2.6 MJ/kg with an advanced stripper configuration (***20***,***21***). Two estimates have been published for the concentrated piperazine solvent (***4***) giving a minimum value of 2.6 MJ/kg.

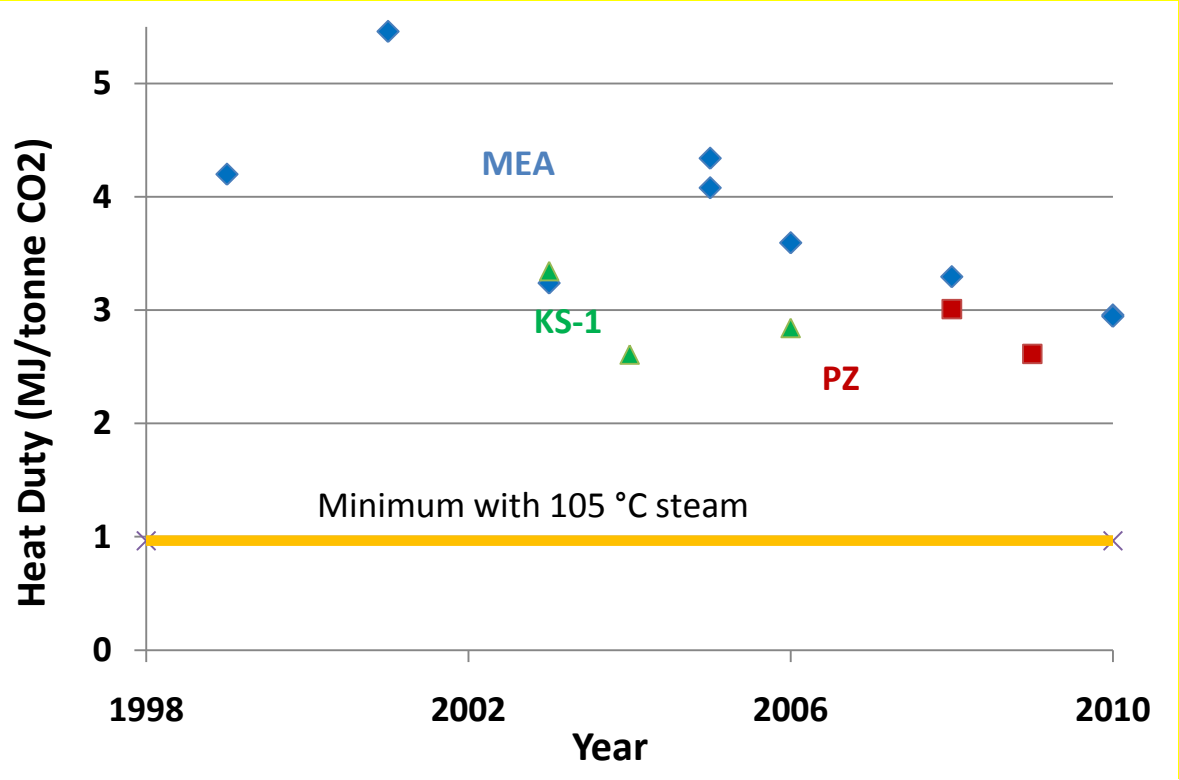

Figure 3. Literature estimates of reboiler steam for CO_2 capture by amine scrubbing

Figure 4 gives estimates of the total loss of electrical production associated with compressor work, typically to 150 bar, pump work, and with the steam use. The equivalent work requirement of early MEA designs was as high as 460 kWh/tonne CO_2 removed and is approaching 200 kWh/tonne CO_2 in recent studies. Since the typical output of a coal-fired power plant is about 1000 kWh/tonne CO_2 emitted, it should be possible to achieve an energy penalty as low as 20% of the power output to accomplish CO_2 capture.

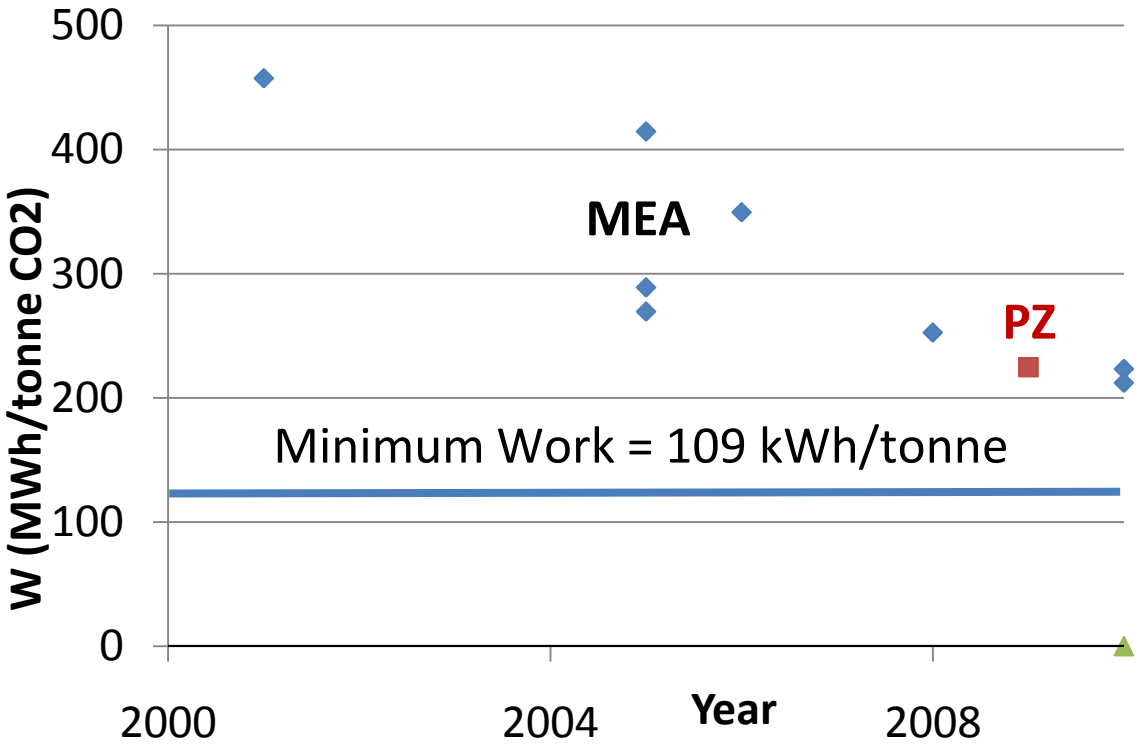

Figure 4. Estimated Total Equivalent Work (electricity derating) of Amine Scrubbing

2.3. Minimum work for CO_2 Separation and Compression

The total minimum work for post-combustion capture with compression to 150 bar is 109 kWh/tonne CO_2 removed.

The minimum work for separating 90% CO_2 from flue gas containing 12% CO_2 at 40 °C is 46 kWh/tonne CO_2 removed. Oyenekan (***22***) gives this value and more details on its calculation. Herzog et al. (***23***) report a calculated value of 43 kWh/tonne for 90% removal from 11% CO_2 at 25 °C.

Using H and S values for CO_2 from the NIST web book, the estimated work ($\Delta H - T\Delta S$) for isothermal, ideal compression at 40 °C from 1 bar to 150 bar is 63 kWh/tonne. Oyenekan (***22***) reports 64 kWh/tonne for compression at 40 °C from 1 bar to 100 bar. Herzog et al. (***23***) report 61 kWh/tonne for compression from 1 bar to 110 bar at 25 °C.

Figure 4 shows that the minimum work is about half of the most recent estimated equivalent work for amine scrubbing. It is remarkable that amine scrubbing can give an overall thermodynamic efficiency (minimum work/actual work) as high as 50%. In practice other common separation technologies are less efficient. These include: simple distillation with a relative volatility of 5 (35%), cryogenic air separation (25%), and desalination by reverse osmosis (21%).

2.3.1. Common Distillation

Separation of one gmol of a 50/50 saturated liquid feed at 40 °C has a minimum work of:

$$W_{min} = 2RTln(x_f)$$=1.8 kJ/gmol feed EQ. 3

The minimum vapor rate for such a separation in a simple refluxed distillation column with an infinite number of stages is given by:

$$V_{min}\left(\frac{moles}{mole\ feed}\right) = 0.5\frac{(1-a)}{(1+a)}$$ EQ. 4

where *a* is the relative volatility.

Heat is input at the bottoms temperature and removed at the overhead temperature. This loss of temperature in the heat can be expressed as lost work by the Carnot cycle. The change in temperature is related to the heat of absorption and relative volatility. The effective lost work accounting for the temperature difference depends on the relative volatility but not the heat of vaporization:

$$W_{loss} = V_{min}RTln(a)$$ EQ. 5

Work is also lost in the driving force for the condenser and reboiler. A minimum driving force would provide 5 °C for each exchanger, so the lost work at the minimum vapor rate is given by:

$$W_{loss} = V_{min}\ H_{vap}\left(\frac{10}{313}\right)$$ EQ. 6

A typical heat of vaporization would be 60 kJ/gmol.

Since the actual vapor rate is usually designed to be 20% more that the minimum, the total work requirement is:

$$W_{act} = 1.2 \times 0.5 \times \left(\frac{1-a}{1+a}\right)\left(8.3\frac{313}{1000}\ln(a) + 60\frac{10}{313}\right)$$ EQ. 7

The ratio of actual work to ideal work varies from a maximum of 0.35 at *a*=5 to 0.14 at *a*=1.2 and 0.33 at *a*=10.

2.3.2. Air separation

The separation of air into pure oxygen and pure nitrogen at atmospheric pressure and 40 °C would require a minimum work of 6.2 kJ/gmol O_2. Darde et al. (***24***) report an actual separation energy with cryogenic separation of 25 kJ/gmol O_2, giving an efficiency of 25%.

2.3.3. Seawater Desalination

Semiat (***25***) report the minimum work to separate fresh water from sea water with 50% recovery is 0.79 kWh/tonne of freshwater. He suggests that commercial systems are capable of 3.75 kWh/tonne, giving an efficiency of 21%. The largest RO system in the world at Ashkelon produces freshwater for 4 kWh/tonne.

2.4. Amine Scrubbing Irreversibilities

Figure 5 illustrates the unit operations that lose work in the amine scrubbing process. These include the absorber, cross-exchanger, flash tanks, condensers, and compressor stages. A lost work analysis is performed for each unit operation.

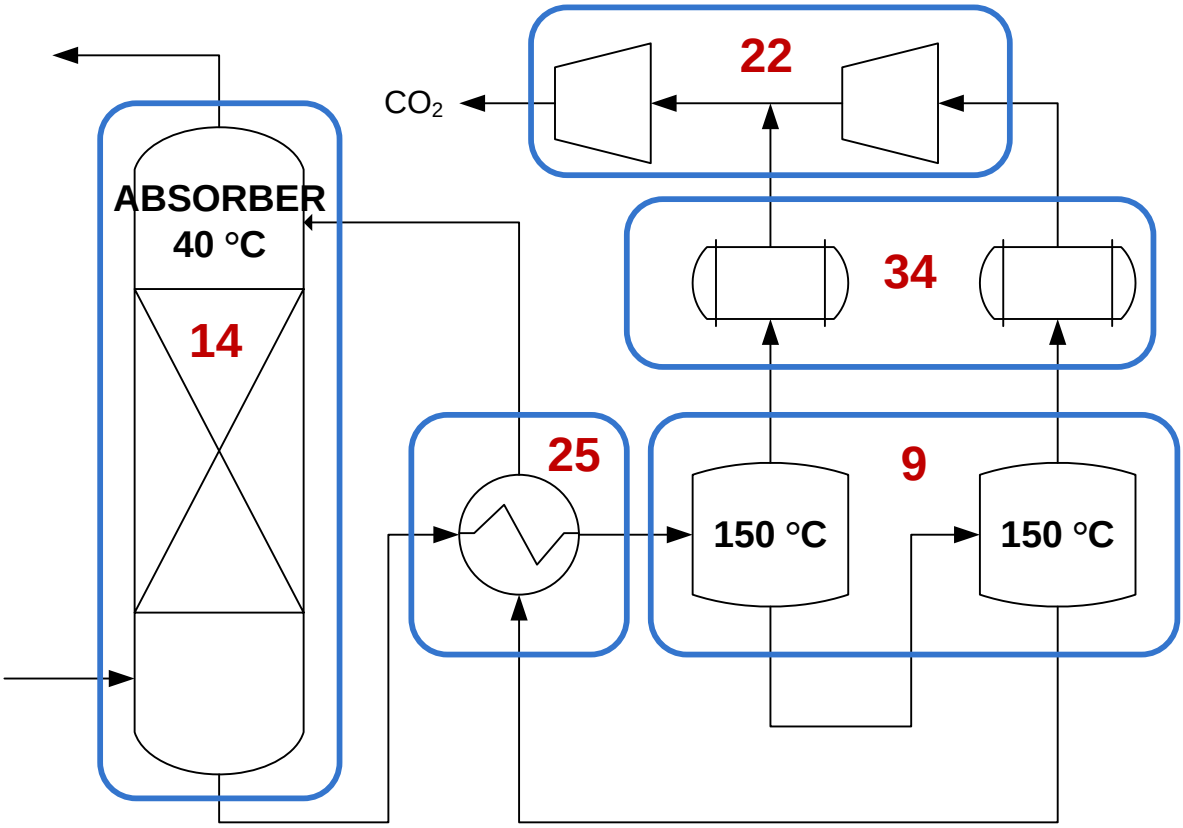

Figure 5. Irreversibilities in an absorption/stripping system where the values represent lost work in kWh/tonne CO_2

2.4.1. Absorber driving Force

CO_2 absorption by amine solutions is controlled by diffusion with fast reaction in the liquid boundary layer. The kinetics of CO_2 absorption in 8 m PZ and 7 m MEA have been measured in a wetted wall column by Dugas and Rochelle (***7***) as shown in Figure 6. The results are reported as a practical measurement of the mass transfer coefficient, k_g', defined as the ratio of the flux to the liquid film driving force expressed as a partial pressure:

$$k_g' = \frac{CO_2\ flux}{(P_{CO2,interface} - P^*_{CO2,bulk\ solution})} \qquad \text{EQ. 8}$$

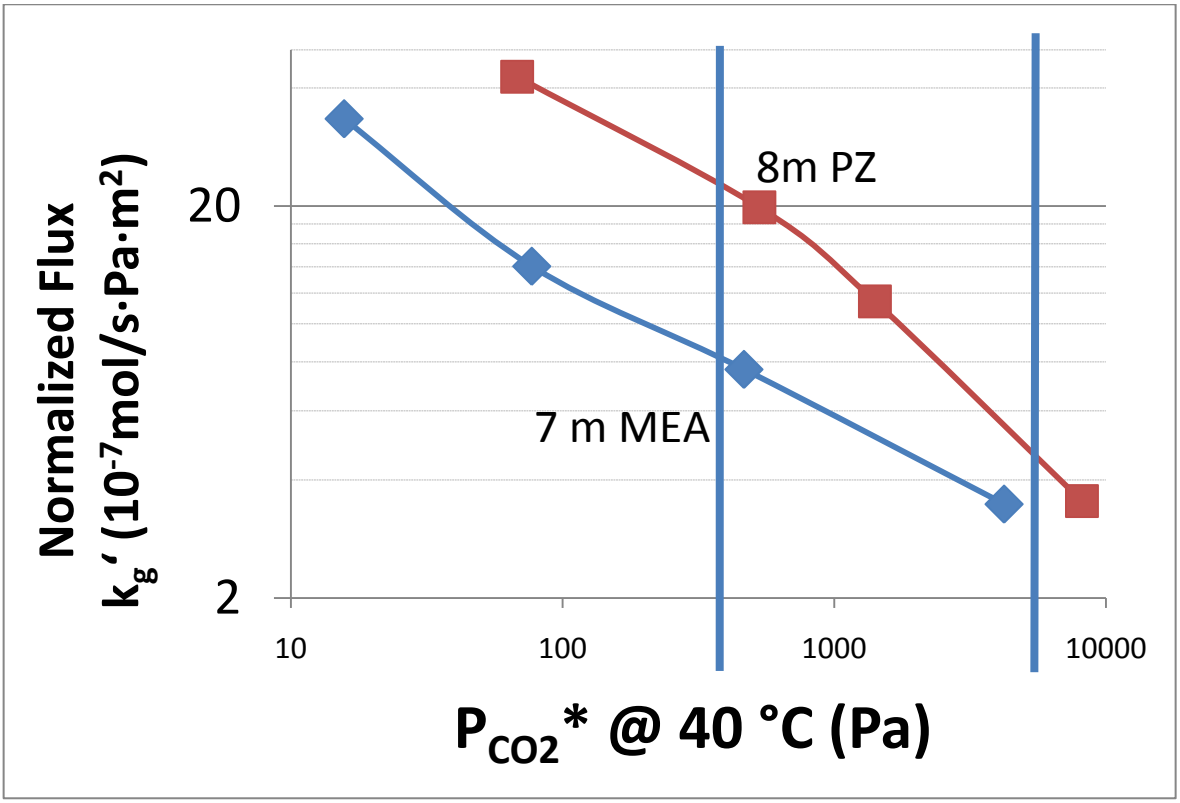

Figure 6. Normalized flux of CO_2 measured in a wetted-wall column for 7 m MEA and 8 m PZ (7)

Since the reaction kinetics of piperazine with CO_2 are much faster than MEA, PZ provides a CO_2 absorption rate that is twice as fast as MEA. Oyenekan and Van Wagener (***26***,***18***) have established that the minimum energy in the stripper is frequently achieved when the proportional driving force is the same in the top and bottom of the stripper. With 8 m PZ at 40 °C and inlet flue gas at 12% CO_2, an equilibrium partial pressure of 5 kPa in the rich solvent will give a reasonable amount of packing to get 90% removal. For this case a lean loading is selected that will give an equilibrium partial pressure of 0.5 kPa Based on Dugas (***8***), the values of k_g' at the rich and lean conditions are respectively, 2.2e-6 and 5e-7 gmol/s-m^2-Pa. The log mean average product, $k_g'\Delta P$, at the top and bottom of the absorber is 2.4e-3 gmol/s-m^2. Assuming an isothermal absorber with a linear operating curve and linear equilibrium curve, the absorber for an 800 MW coal-fired power plant would require 1900 m^3 of packing (25x25x13.5m, 1.5 m/s gas velocity, packing with 250 m^2/m^3, 0.9 tonne CO_2 removed/MWh)

With this reasonable absorber size and approach to equilibrium, the exergy lost to driving force per gmol CO_2 is given by:

$$W_{loss,abs} = RTln\left(\frac{P_g}{P^*_{bulk\ liquid}}\right) = 313R\ln\left(\frac{0.12}{0.05}\right) = 14\frac{kWh}{tonne\ CO_2} \qquad \text{EQ. 9}$$

2.4.2. Sensible Heat

Exergy is loss because of the driving force in the cross exchanger. This loss depends strongly on the working capacity of the solution. Figure 7 gives the measured CO_2 solubility in the piperazine solvent from Freeman et al. (***4***) with new data based on total pressure measurements at 120 to 160 °C. The operating range of 8 m PZ for the equilibrium partial pressures of 0.5 and 5 kPa at 40 °C is CO_2 loading of 0.31 and 0.41 gmol CO_2/equiv PZ. The working capacity of the solution is 0.88 gmol CO_2/gmol (PZ+H2O).

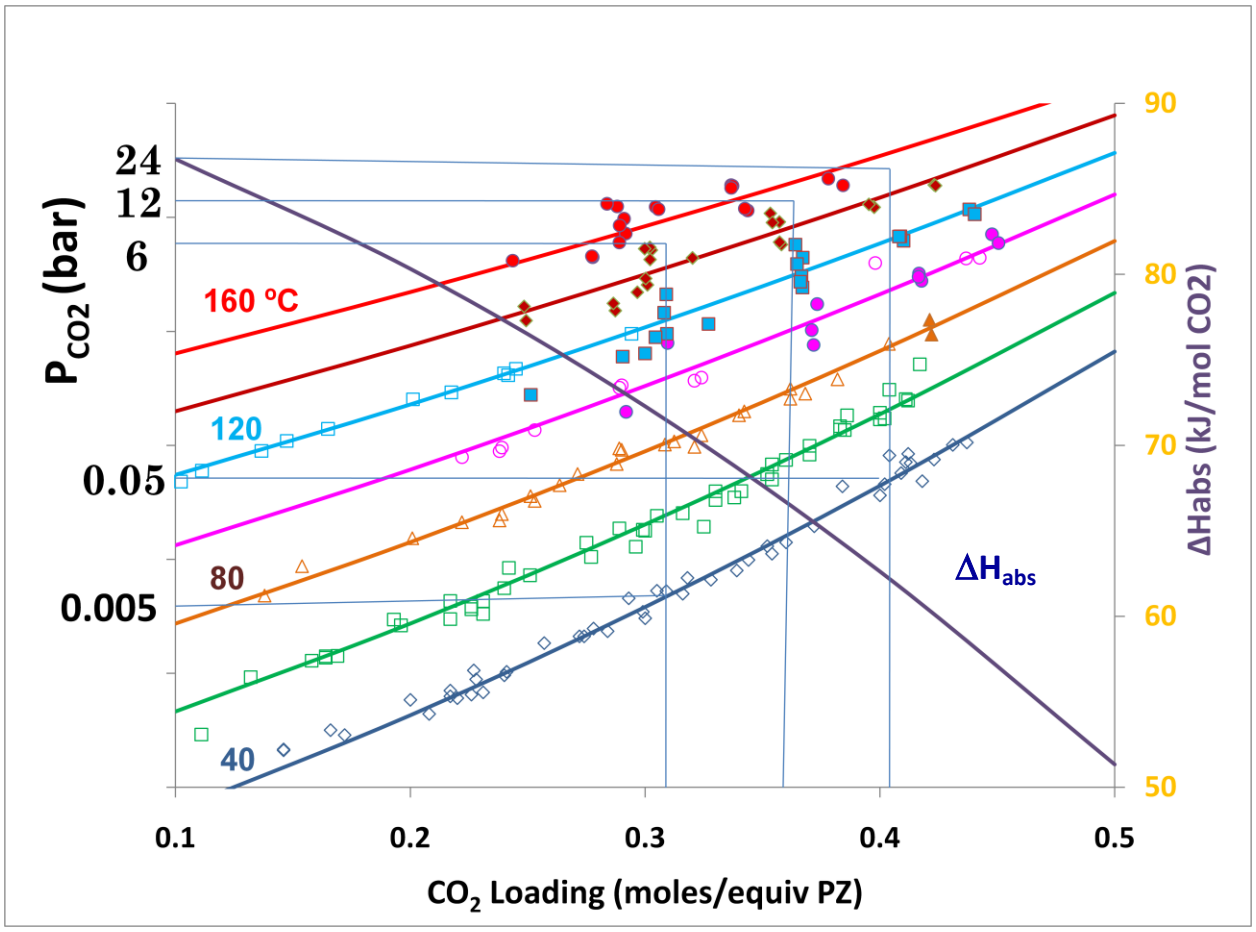

Figure 7. CO_2 solubility in 0.9 to 12 m PZ from 40 to 150 °C

The exergy loss of the cross exchanger is given approximately by the work value of the steam required to replace the sensible heat not recovered by the exchanger:

$$Q = \frac{C_p \, \Delta T}{capacity} \qquad \text{EQ. 10}$$

The heat capacity of loaded 8 m PZ as measured by differential scanning calorimetry is about 3.5 J/gmol-K, so the steam requirementis given approximately by:

$$Q_{loss} = \frac{\left(3.5\ \frac{J}{mol-K}\right) \times 5\ K}{0.88\ \frac{gmol\ CO_2}{gmol\ (PZ + H_2O)}} = 20 \frac{kJ}{gmol\ CO_2} \qquad \text{EQ. 11}$$

With steam at 155 °C, the equivalent work of the steam is given by equation 1 is 25 kWh/tonne CO_2.

2.4.3. Two-Stage Flash Regeneration

The energy requirement and exergy loss of regeneration depends in a non-intuitive way on the heat of CO_2 absorption. The equilibrium data in Figure 7 permit the calculation of ΔH_{abs} by the Gibbs-Helmholtz equation:

$$\Delta H_{abs} = -R \frac{\partial \ln\left(P^*_{CO2}\right)}{\partial\left(\frac{1}{T}\right)} \qquad \text{EQ. 12}$$

Over the operating range of the absorber the ΔH_{abs} is about -70 kJ/gmol CO_2. The heat duty of each flash includes the heat of absorption of the CO_2 and the heat of vaporization of the associated water vapor. Because the vapor pressure increases with temperature slower than that of CO_2, greater flash T and greater ΔH_{abs} results in an overall reduced heat rate with less water vapor per gmol CO_2. The exergy loss in the flash does not depend directly on the heat rate, since that is an inherent part of the separation process. However there are important secondary effects of the heat rate.

Exergy is lost in the reboiler because of the temperature driving force. The exergy loss is given by the equation:

$$W_{loss} = \frac{0.75 Q_{flash} \Delta T}{T} = \frac{0.75 \times 95 \frac{kJ}{gmol} \times 5}{423} = 0.8\ \frac{kJ}{mol\ CO_2} = 5 \frac{kWh}{tonne\ CO_2} \qquad \text{EQ. 13}$$

Exergy is lost in the condenser as the water vapor is condensed with cooling water. The loss is rated by a Carnot expression:

$$W_{loss} = \Delta H_{v,H2O} \left(\frac{n_{H2O}}{n_{CO2}}\right)\left(\frac{T_{cond} - 313}{T_{cond}}\right) = 0.625 \times 40 \times \left(\frac{125 - 40}{125 + 273}\right) = 5\ \frac{kJ}{mol} = 34 \frac{kWh}{tonne\ CO_2} \qquad \text{EQ. 14}$$

Because the flash is not conducted in infinite stages, there is pressure as a consequence of each flash. The estimate of work loss is given by

$$W_{loss} = 0.25 RT ln\left(\frac{29}{17}\right) + 0.25 RT ln\left(\frac{17}{11}\right) = 0.6 \frac{kJ}{gmol\ CO_2} = 4\ kWh/tonne \qquad \text{EQ. 15}$$

The total loss associated with these elements of the 2-stage flash and condenser is 43 kWh/tonne CO_2

2.4.4. Compressor Work and Exergy Loss

Actual Work for Mechanical, Adiabatic Compression

The actual work required with a multi-stage compressor providing CO_2 at 150 bar is given in Figure 8. The calculated work is discontinuous because of changes in the number of intercooling sections. The calculated work is effectively smoothed and approximated by the simple equation:

$$W_{comp}\left(\frac{kJ}{gmol\ CO_2}\right) = 4.35 \times ln\left(\frac{150}{P_{in}}\right) - 3.51 \qquad \text{EQ. 16}$$

The work for an ideal isothermal compressor with an ideal gas would be given by:

$$W_{comp}\left(\frac{kJ}{gmol\ CO_2}\right) = RTln\left(\frac{150}{P_{in}}\right) = 0.008314 \times 313 ln\left(\frac{150}{P_{in}}\right) = 2.6\ ln\left(\frac{150}{P_{in}}\right) \qquad \text{EQ.17}$$

The ratio of the slopes, 2.6/4.23, indicates that mechanical adiabatic compression has an overall thermodynamic "efficiency" of only 60% over the low pressure range.

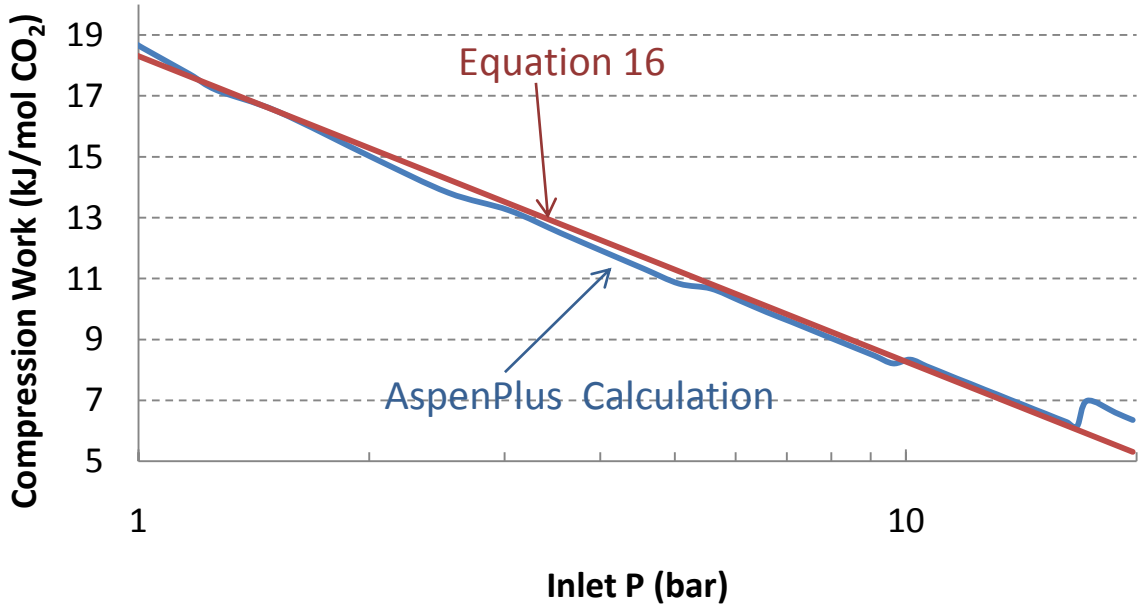

Figure 8. Compressor work calculated in AspenPlus , RKS Equation of state, maximum compression ratio/intercooling section = 2, 80% polytropic efficiency, P_{final} = 150 bar, saturated to water, intercooling to 40°C with pressure drop given by $\Delta \boldsymbol{P}(\boldsymbol{bar}) = \boldsymbol{0.2\ P_{suction}^{0.5}}$

The actual work requirement for compression from 1 bar to 150 bar is 115 kWh/tonne, compared to the minimum work for this range of 63 kWh/tonne, so the overall thermodynamic efficiency is 55%. Since the 2-stage flash operates at elevated pressure, less exergy is lost in adiabatic, mechanical compression that in a lower pressure system. The exergy loss of the compression with the 2-stage flash is the difference between the actual work and the work required for isothermal ideal compression, which is 22 kWh/tonne CO_2.

2.5. Maximizing Temperature Swing

The amine scrubbing process relies upon temperature swing regeneration to provide CO_2 separation to a greater CO_2 partial pressure than in the flue gas. The pressure of the resulting CO_2 and the energy performance is enhanced by a greater heat of CO_2 absorption and by increased regeneration temperature.

2.5.1. Model for Generic Single-Stage Flash

The lean loading is assumed to give an equilibrium CO_2 partial pressure at 40 °C of 0.005 bar. At the flash temperature, T (K), the partial pressures of CO_2 and water are estimated from their respective heats of desorption, ΔH_{CO2} (kJ/gmol), and ΔH_{H2O}(=40 kJ/gmol):

$$P_{CO2}(bar) = 0.5exp\left(\frac{1000\Delta H_{CO2}}{8.314}\left(\frac{1}{313}-\frac{1}{T}\right)\right) \quad \text{EQ. 18}$$

$$P_{H2O}(bar) = 1.01exp\left(\frac{40{,}000}{8.314}\left(\frac{1}{313}-\frac{1}{T}\right)\right) \quad \text{EQ. 19}$$

The total pressure at the flash is given by

$$P_{total} = P_{CO2} + P_{H2O} \quad \text{EQ. 20}$$

The compression work is given by EQ. 16. The sensible heat duty associated with imperfect cross exchange is given by:

$$Q_{sens}\left(\frac{kJ}{gmol\ CO_2}\right) = \frac{C_p\Delta T}{capacity} = \left(3.5\frac{kJ}{kg\ solvent - K}\right)\frac{5\ K}{1\ \frac{gmol\ CO_2}{kg\ solvent}} = 17.5\ kJ/gmol \quad \text{EQ. 21}$$

The latent heat duty is given by:

$$Q_{latent} = \Delta H_{CO2} + \left(\frac{P_{H2O}}{P_{CO2}}\right)\Delta H_{H2O} \quad \text{EQ. 22}$$

The total heat duty of the flash heater is given by:

$$Q_{flash} = Q_{latent} + Q_{sens} \quad \text{EQ. 23}$$

In order to account for loss of electrical production from use of steam the equivalent work of the steam is given by:

$$W_{equiv} = 0.75 Q_{flash} \left(\frac{T_{flash} + 5 - 313}{T_{flash} + 5} \right) \quad \text{EQ. 24}$$

The factor of 0.75 accounts for the inefficiency of the steam cycle in producing electricity from steam. The temperature ratio is the Carnot cycle efficiency with T_{stm}(K) as the condensing temperature of the steam with a 5 K driving force for the heater.

The pump work assumes an efficiency of 75% and 2 bar additional pressure drop and is given by:

$$W_{pump} \left(\frac{kJ}{gmol} \right) = 0.1 \frac{(P_{total} + 2\ bar)}{0.75\ \frac{1\ gmol\ CO2}{liter\ soln}}$$

The total work requirement of the flash system is given b y:

$$W_{total} = W_{equiv} + W_{comp} + W_{pump} \quad \text{EQ. 25}$$

This expression neglects pump work for the solvent and fan work for the flue gas.

2.5.2. Results for a Single Stage Flash

Figure 9 gives the results with a generic single stage flash. The total equivalent work is given as a function of a correlating parameter, $(\Delta H_{CO2} - \Delta H_{H2O})\Delta\left(\frac{1}{T}\right) = \left(\frac{kJ}{gmol-K}\right)$($\Delta H_{CO2}$-$\Delta H_{H20}$)$\Delta$(1/T) (kJ/gmol-K), which increases with the heat of **CO_2** absorption and the difference in temperature between the absorber and the stripper. Curves are given for ΔH_{CO2} = 60, 70, and 80 kJ/gmol with flashing from 90 to 150 °C. Over the maximum range of these conditions the equivalent work decreases from 365 to 200 kWh/tonne, because the pressure increases (reducing compressor horsepower) and because less water vapor is produced with the CO_2 at higher temperatures and greater ΔH_{CO2}.

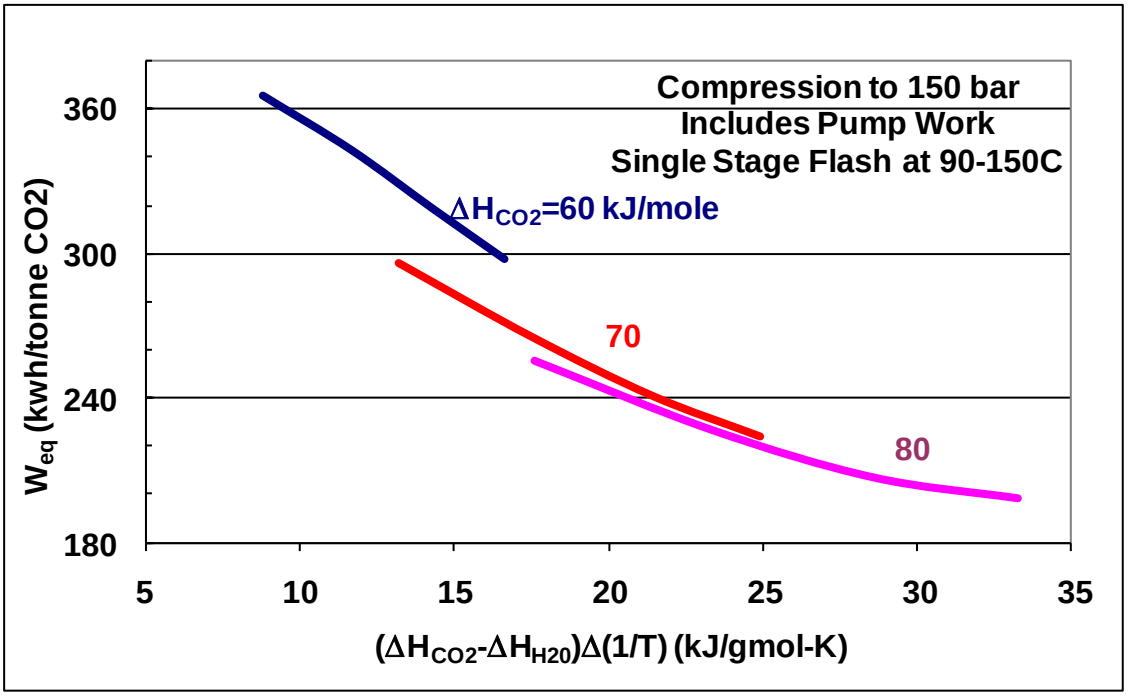

Figure 9. Total equivalent work with a single stage flash at 90-150 °C, compression to 150 bar, includes heat duty estimated as equivalent work, compressor work, and pump work (lean loading = 0.5 kPa @ 40 °C)

3. Reagent Robustness

The evaluation of a new technology for CO_2 capture must account for solvent or reagent attrition during the course of commercial operation. For solvent-based absorbents, losses may occur through thermal degradation, oxidative degradation, volatility, and corrosion. The reclaiming process represents an important pathway to remove contaminants and recover degraded solvent performance. Thermal reclaiming is a widely used method and is simple and cost effective. In lieu of reclaiming, a slipstream of the solvent would need to be purged and replaced, which could potentially be extremely expensive.

3.1. Thermal Degradation

Losses arising from thermal degradation of the solvent represent upper limits of process operations for regeneration and temperature excursions due to process upsets. Also, the equivalent work analysis has demonstrated the benefits of operating at high temperatures and pressures for thermal swing regeneration. The temperature limit for regeneration will be dictated by the rate of thermal degradation of the solvent.

Figure 10 shows the measured rate of thermal degradation as a rate constant that is first order in the amine (***11***). MEA is routinely regenerated at a temperature of 120 °C. Davis (***10***) showed that 7 m MEA with 0.4 gmol CO2/gmol MEA at 120 ^{o}C degrades at 1.7%/wk. At 135 and 150°C, loaded 7 m MEA

degrades at 8%/wk and 50%/wk, respectively. On the other hand, loaded (0.3 mol/mol alkalinity) 8 m piperazine at 150 °C degrades at 0.35%/wk. For piperazine, a 1.7%/wk degradation rate corresponds to an operating temperature of about 160 °C. However, a regeneration temperature limit of 150 °C for piperazine may represent an optimum since the cost of piperazine is approximately three times that of MEA.

Table 1 compares the thermal degradation rate constants of several other amine candidates. Piperazine is the most resistant to thermal degradation. The hindered amine, 2-amino-2-methyl-propanol, and diglycolamine are also resistant to thermal degradation.

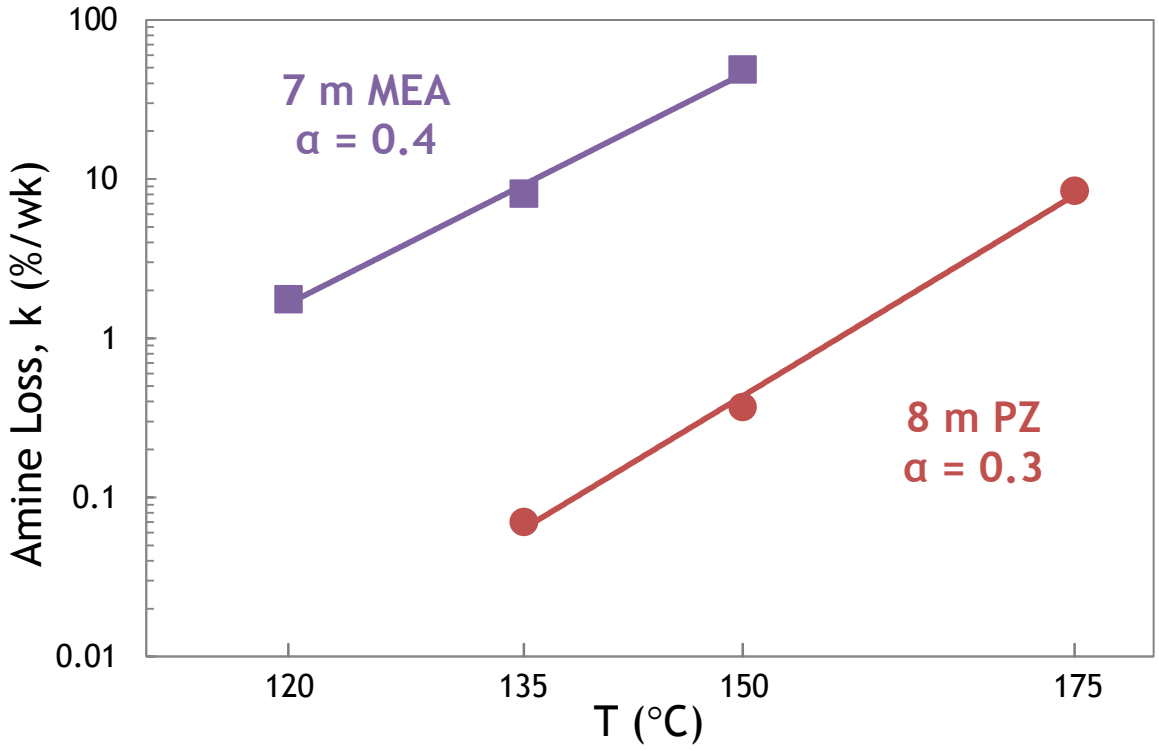

Figure 10. Thermal degradation of the 7 m MEA and 8 m PZ with CO_2 loading, α, gmol /equiv amine (data from Freeman et al.**(***11***)**).

Table 1. Molecular structure and thermal degradation rate constants of amines at 135 °C.

Amine	Structure	k(%/wk)
8 m PZ	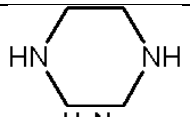	0.07
7 m 2-amino-2-methyl-propanol (AMP)	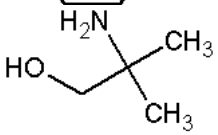	1.2
7 m Diglycolamine® (DGA)	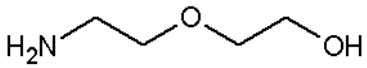	2.1
7 m N-(2-hydroxyethyl)piperazine (HEP)	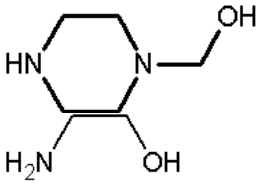	2.8
7 m MEA		8.1
8 m EDA		10.1

3.2. Oxidative Degradation

The presence of oxygen in the flue gas will cause oxidative degradation, particularly in the absorber column of a conventional thermal swing process. Oxidative degradation experiments were conducted by sparging a gas mixture of 98 mole% O_2 and 2 mole% CO_2 at 55 °C through a well-stirred (1400 rpm) solution of loaded amine by the method of Sexton (***12***). Due to the corrosive nature of aqueous amine solvents, stainless steel is expected to be used as the material of construction and will result in the dissolution of iron, chromium, and nickel into the solvent. The presence of the metals will typically catalyze oxidation reactions. Therefore, 0.4 mM Fe^{2+}, 0.1 mM Cr^{3+}, and 0.05 mM Ni^{2+} were added to simulate the catalytic effects of dissolved metals on the oxidative degradation of amines.

The figure shows that 8 m piperazine with a loading of 0.3 mole/mole alkalinity does not appreciatively degrade in the presence of Fe^{2+}, Cr^{3+}, and Ni^{2+} over a period of 600 hours. On the other hand, 7m MEA with a loading of 0.4 gmol/gmol alkalinity oxidatively degrades by more than 35% over a period of 320 hours. Concentrated piperazine offers a much stronger resistance to oxidative degradation than monoethanolamine and reduces the losses associated with oxidative degradation.

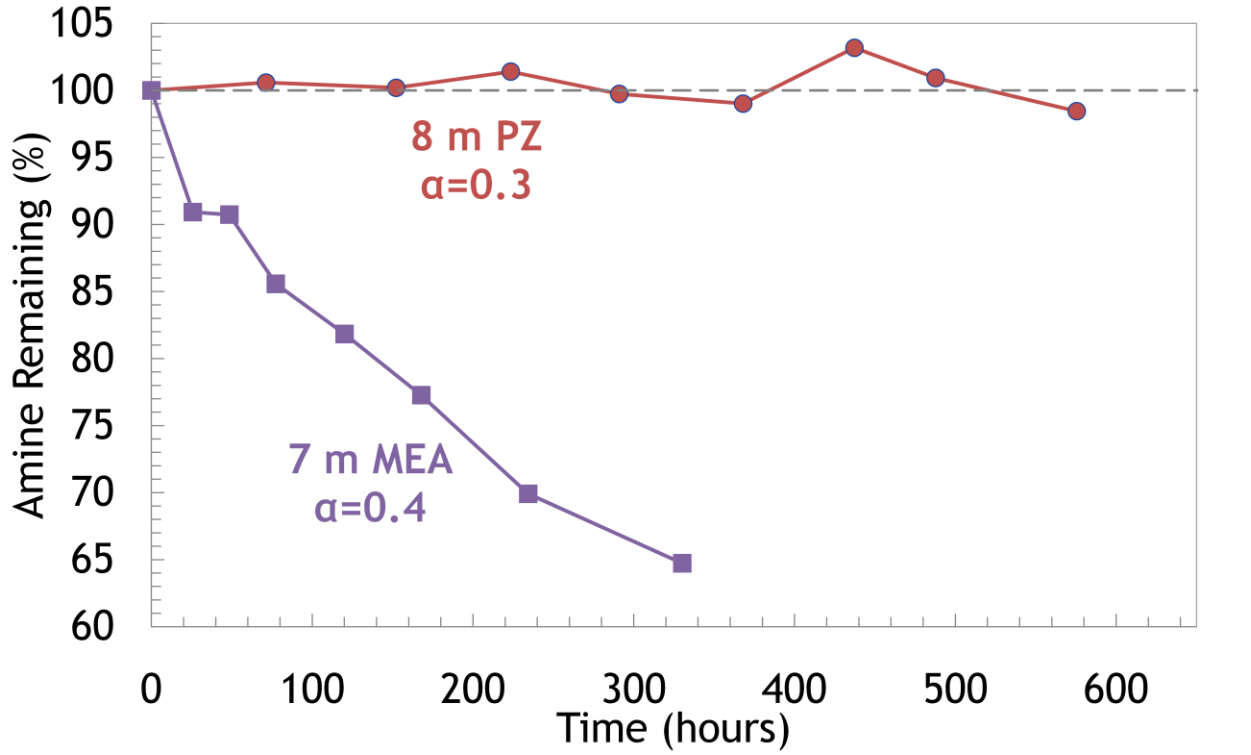

Figure 11. Oxidative degradation of loaded 7 m MEA and 8 m Piperazine with 0.4 mM Fe^{2+}, 0.1 mM Cr^{3+}, and 0.05 mM Ni^{2+} (55 °C, 98% O_2/2% CO_2, 1400 RPM)

3.3. Volatility

The CO_2 absorption process will typically be an open-loop process, with flue gas entering and leaving the absorption equipment. During the absorption process, some of the absorbents maybe transferred to the flue gas and result in solvent losses. For an amine-based aqueous solvent, volatility will determine the amount amine that is lost and would need to be added as makeup. In addition to solvent makeup, the release of amine into the atmosphere may have secondary environmental impacts in the form of air emissions, which may or may not further react with other constituents in the atmosphere.

The volatility of 7 m MEA and 8 m piperazine was measured at 40 °C over a range of loadings (***9***). At the expected lean conditions giving PCO2 =0.5 kPa at 40°C, 7 m MEA has a Co2 loading of 0.45 and a MEA volatility of 30 ppm, and 8 m PZ has a lean loading of 0.3 and a volatility of 7 ppm. Even though pure piperazine has a boiling point that is lower than pure MEA, it is significantly less volatile because it is converted to species other than free PZ at the amine concentration and lean loading of interest.

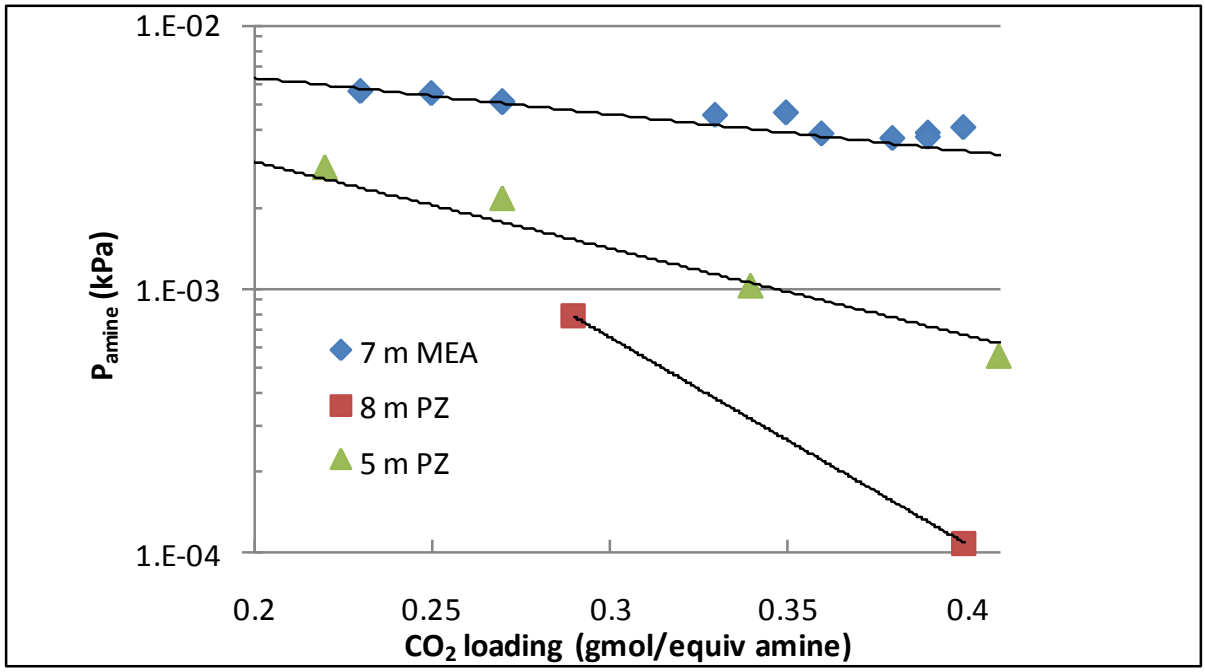

Figure 12. Amine volatility at 40 °C

3.4. Corrosion

The corrosivity of the solvent is important because it determines material selection and because it can release metals into the solvent that catalyze oxidative degradation. Figure 13 shows the accumulation of dissolved metals when solutions are in stainless steel 316 tube at extended time and elevated temperature to measure thermal degradation. The apparent corrosion rate in 7 m MEA at 135°C with a CO_2 loading of 0.4 is orders of magnitude faster than in 8 m PZ at 150°C with loading of 0.3. Therefore it is probable that 316 stainless steel or a lower cost material will be adequate for the piperazine solvent.

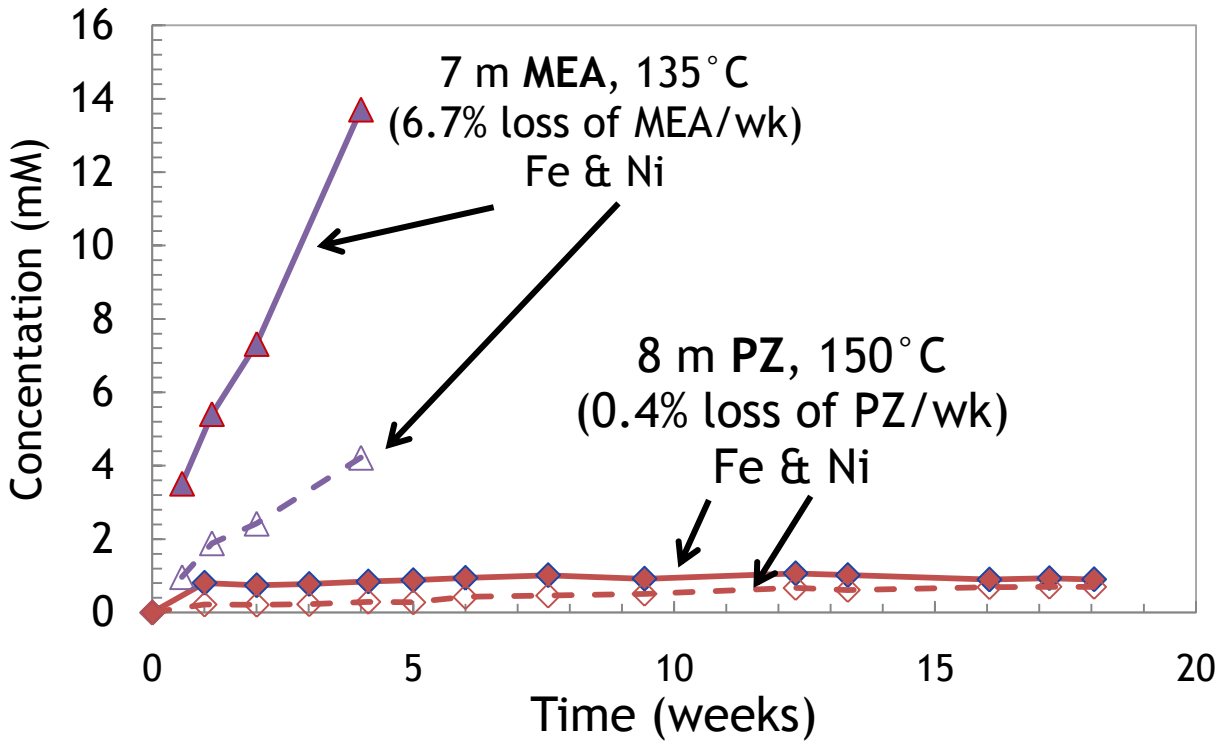

Figure 13. Metal concentrations in thermal degradation in 316 stainless steel tube containing 7 m MEA, loading=0.4 and 8 m piperazine, loading =0.3.

3.5. Reclaiming

Reclaiming of the process solvent is necessary to recover valuable amine and minimize liquid waste volume. Even with an upstream polishing scrubber, the inlet flue gas with coal combustion will contain small amounts SO_2, NOx, and fly ash and carryover of gypsum, limestone, and NH_3 from upstream gas treating. Process upsets will also introduce other unwanted products into amine solvent. Degradation and corrosion products will also accumulate in the solvent. These accumulated impurities must be removed from the solvent to maintain energy performance, minimize degradation, avoid foaming, and control corrosion.

Reclaiming of amine solvents has been routinely practiced by the gas treating industry for a number of years. Traditional thermal and distillation reclaiming is carried out at atmospheric pressure with MEA at 150°C or under vacuum with less volatile amines such as diglycolamine. There is often some additional degradation of MEA with thermal reclaiming because of the elevated temperature.

Piperazine is ideally suited for thermal reclaiming at atmospheric or elevated pressure. Pure piperazine has a lower boiling point (146 °C) than MEA (170 °C) and is thermally stable up at 150 °C. Piperazine could also be reclaimed by ion exchange or electrodialysis, which is used by the gas treating industry to remove accumulated salts.

Amine cost is an important factor, even with reclaiming. Under the best design conditions, amine will always be lost in reclaiming or by necessary purging of spent solvent. At a typical cost of $1/lb, the expected makeup cost of MEA is $2 to 5/tonne CO_2. PZ is a co-product of ethylenediamine production and can also be produced by dimerizing MEA. It is expected to have a cost of $2 to $4/lb. Reagents that are more expensive than PZ will be very sensitive to losses and reclaiming efficiency and will probably not be useful.

Finally, reclaiming will produce liquid and solid waste .Waste disposal can potentially become expensive depending on the classification. The waste classification will depend on the species of heavy metals originally present in the coal that are absorbed by the solvent and on the toxicity of degradation products that appear in the waste stream.

4. Conclusions

1. The expected energy requirement for a piperazine or other advanced amine scrubbing processes will approach 220 kWh/tonne CO_2 removed. The heat requirement will be 2.6 MJ/tonne CO_2. This represents an overall thermodynamic efficiency of 50%, comparable to or better that other common separation processes.
2. The major exergy losses (kWh/tonne CO_2) in the piperazine process are: condenser: 34; exchanger: 25; compressor: 22; absorber:14.

3. Mechanical adiabatic compression has an overall thermodynamic efficiency of 55 to 60% and will not be efficient method of providing the thermodynamic work for CO_2 separation. Aqueous amine scrubbing processes with thermal swing regeneration will provide better energy performance with greater heat of CO_2 absorption and maximum regeneration temperature. Thermal compression in this process is more efficient that mechanical compression
4. Piperazine can be used up to 150^{o}C without significant thermal degration. This allows better energy performance and minimizes the impacts of degradation products.
5. Piperazinesolvent is resistant to oxidative degradation, has less volatility than MEA, and is not corrosive to stainless steel.
6. Piperazine solvent is suitable for reclaiming by distillation and other methods already commercialized by the gas treating industry.

5. Acknowledgements

The support of the Luminant Carbon Management Program is gratefully acknowledged.

6. References

1. Rochelle, G. T. Scrubbing for CO2 Capture. *Science* **2009,** *325,* 1652-1654.

2. Bottoms, R. R. Separating Acid Gases. US Patent 1783901, 1930.

3. National Air Pollution Control Administration. *Lime/Limestone Wet Scrubbing Symposium*, Perdido Bay, FL, March 16 to 20,1970.

4. Freeman, S. A.; Dugas, R.; Van Wagener, D.; Nguyen, T.; Rochelle, G. T. Carbon dioxide capture with concentrated aqueous piperazine. *Int. J. Greenhouse Gas Control* **2010**.

5. Ermatchkov, V.; Kamps, A. P.-S.; Speyer, D.; Maurer, G. Solubility of carbon dioxide in aqueous solutions of piperazine in the low gas loading region. *J. Chem. & Eng. Data* **2006,** *51* (5), 1788-1796.

6. Hilliard, M. *A predictive thermodynamic model for an aqueous blend of potassium carbonate, piperazine, and monoethanolamine for carbon dioxide capture from flue gas;* PhD Dissertation; The University of Texas at Austin: Austin, Texas, 2008.

7. Dugas, R.; Rochelle, G. T. Absorption and desorption rates of carbon dioxide with monoethanolamine and piperazine. *Energ. Procedia* **2009,** *1* (1), 1163-1169.

8. Dugas, R. *Carbon dioxide absorption, desorption, and diffusion in aqueous piperazine and monoethanolamine;* PhD Dissertation; The University of Texas at Austin: Austin, Texas, 2009.

9. Nguyen, T.; Hilliard, M.; Rochelle, G. T. Amine volatility in CO2 capture. *Submitted to Int. J. Greenhouse Gas Control* **2010**.

10. Davis, J. *Thermal degradation of aqueous amines used for carbon dioxide capture;* PhD Dissertation; The University of Texas at Austin: Austin, Texas, 2009.

11. Freeman, S.; Davis, J.; Rochelle, G. T. Degradation of aqueous piperazine in carbon dioxide capture. *Article in press, Int. J. Greenhouse Gas Control* **2010,** *doi:10.1016/j.ijggc.2010.03.009*.

12. Sexton, A. J. *Amine oxidation in CO2 capture processes;* PhD Dissertation; The University of Texas at Austin: Austin, Texas, 2008.

13. Reddy, S. *Second National Conference on Carbon Capture and Sequestion, NETL/DOE*, May 5-8, 2003.

14. Ramezan, M. *Carbon dioxide capture from existing coal-fired power plants;* DOE/NETL-401/110907, November 2007.

15. Chapel, D. G.; Mariz, C. L.; Ernest, J. Recovery of CO2 from flue gases: commercial trends. *Canadian Society of Chemical Engineering Annual Meeting*, Saskatoon, Saskatchewan, Canada, Oct. 4-6, 1999.

16. Plaza, J. M.; Van Wagener, D.; Rochelle, G. T. Modeling CO2 capture with aqueous monoethanolamine. *IJGGC* **2010,** *4* (2), 161-166.

17. Oyenekan, B. A.; Rochelle, G. T. Alternative stripper configurations to minimize energy for CO2 capture. *in proceedings of GHGT-8*, Trondheim, Norway, June 19-22, 2006.

18. Van Wagener, D.; Rochelle, G. T. Stripper configurations for CO2 Capture by Aqueous Monoethanolamine. *submitted to Chem. Eng. J.* **2010**.

19. Imai, N. Advanced solvent to capture CO2 from flue gas. *Second Int. forum on Geologic Sequestration of CO2 in deep, unmineable Col Seams "Coal-Seq II",* March 7, 2003.

20. Yagi, Y.; Mimura, T.; Iijima, M.; Ishida, K.; Yoshiyama, R.; Kamijo, T.; Yonekaw, T. Yagi,Y., T. Mimura, M. Iijima, K. Ishida, R. YoImprovements of carbon dioxide capture technology. *GHGT-7*, 2004.

21. Yagi, Y.; Mimura, T.; Yonekawa, T.; Yoshiyama, R. Development and improvement of CO2 capture system. *Proceedings GHGT-8*, 2006.

22. Oyenekan, B. A. *Modeling of strippers for CO2 capture by aqueous amines;* PhD Dissertation; The University of Texas at Austin, 2007.

23. Herzog, H. Advanced Post-Combustion CO2 Capture, April 2009. http://sequestration.mit.edu/pdf/Advanced_Post_Combustion_CO2_Capture.pdf.

24. Darde, A.; Prabjhakar, R.; Tranier, J.-P.; Perrin, N. Air separation in flue gas compression and purification units for oxy-coal combustion systems. *Energ. Procedia* **2009,** *GHGT-9,* 572-524.

25. Semiat, R. Energy issues in desalination processes. *Env. Sci. Tech.* **2008,** *42* (22), 8193-8201.

26. Oyenekan, B. A.; Rochelle, G. T. Alternative stripper configurations for CO2 capture by aqueous amines. *AIChE J.* **2007,** *53* (12), 3144-3154.

27. Oyenekan, B. A.; Rochelle, G. T. Energy performance of stripper configurations for CO2 capture by aqueous amines. *Ind. Eng. Chem. Res.* **2006,** *45* (8), 2457-2464.

28. El-Sayed, Y. M. Designing desalination systems for higher productivity. *Desalination* **2001,** *134,* 129-158.

29. Jassim, M. S.; Rochelle, G. T. Innovative absorber/stripper configurations for CO2 capture by aqueous monoethanolamine. *Ind. Eng. Chem. Res.* **2006,** *45* (8), 2465-2472.

30. Smelser, S.C.; Booras, G.S., Fluor Daniel. *An engineering and economic evaluation of CO2 removal from fossil-fuel-fired power plants;* IE-7365; EPRI: Palo Alto, CA, 1991.